Université de Montréal

Proline et prolinol: Azacycles prototypiques pour le développement de peptidomimétiques et la synthèse d'agents médicinaux

Par

Jean-Baptiste Garsi

Département de Chimie, Faculté des Arts et des Sciences

Thèse présentée en vue de l'obtention du grade de Philosophae Doctor (Ph.D.)

en chimie

Septembre 2022

Université de Montréal

Département de Chimie, Faculté des Arts et des Sciences

Cette thèse intitulée

Proline et prolinol: Azacycles prototypiques pour le développement de peptidomimétiques et la synthèse d'agents médicinaux

Présenté par

Jean-Baptiste Garsi

A été évaluée par un jury composé des personnes suivantes

James Wuest
Président-rapporteur

Stephen Hanessian
Directeur de recherche

Richard Giasson
Membre du jury

James Gleason
Examinateur externe

Résumé

La proline est un acide aminé unique qui se caractérise par un cycle pyrrolidine qui lui confère des propriétés physiques et chimiques spécifiques comparé aux autres 20 acides aminés acycliques retrouvés de façon majoritaire dans le protéome humain. Cette différence se retrouve également dans les motifs polyproline et est utilisée par la Nature en de nombreuses façons comme le repliement des protéines, les mécanismes régulatoires liés à l'activité de certaines protéases, la formation de structures secondaires, le biomarquage de peptides substrats des oligopeptidases, et le clivage des motifs diproline par les proline-proline endopeptidases. La proline a par conséquent été un centre d'intérêt pour les chimistes médicinaux lors du développement d'agents thérapeutiques. Cette thèse se propose d'étudier plusieurs composés biologiquement actifs dérivés de la proline.

La première étude relate les avancements liés au composé SH-BC-893, un azacycle contraint dérivé de FTY720 développé au sein du groupe Hanessian. SH-BC-893 est un agent anticancéreux qui permet l'affamement des cellules cancéreuses au travers de la disruption de l'apport des nutriments cellulaires externes et internes. Par son activation de la protéine phosphatase 2A, il permet d'internaliser les récepteurs transmembranaires d'acides aminés et de glucose et de réguler à la baisse les récepteurs de lipides à faible densité. Son action permet également la perturbation de la dégradation de nutriments internes provenant de la macropinocytose et de l'autophagie en prévenant la fusion entre le lysosome et les endosomes respectifs. Afin d'augmenter l'activité de SH-BC-893, deux séries de composés ont été synthétisés et testés en vue d'une activité double. La première série a eu pour but de cibler HDAC2 suite à une étude de Spiegel au sein de laquelle son inhibition a été rapportée pour FTY720. La seconde a visé à obtenir des composés activant d'autres portions ou d'autres homologues de PP2A via l'insertion de fragments tricycliques suite aux études rapportant l'activation de PP2A par des dérivés de composés neuroleptiques tricycliques du type de la perphénazine. La synthèse et les tests biologiques de ces composés sont également décrits.

Le deuxième chapitre décrit la synthèse d'une série de morpholines pontées comportant le motif de l'acide gamma-aminobutyrique (GABA) contraint. GABA est un composant prépondérant de la

régulation du système nerveux central au travers de son action inhibitrice sur les neurorécepteurs GABA-A, GABA-B, GABA-C. De nombreux agents thérapeutiques inspirés de GABA ont été développés avec les années, notamment baclofen. Les morpholines pontées rapportées ici possèdent un centre quaternaire stéréocontrôlé pour lequel un ensemble de substituants a été varié, incluant le groupement phényle *para*-chloré du baclofen ainsi que l'*iso*-butyle de la Pregabalin, autre composé actif dans le système nerveux central dérivé de GABA. La modélisation du dérivé du baclofen a été réalisée au sein du site actif de GABA-B. L'ensemble des composés ont également été modélisés sous forme d'acides aminés au sein de la base de données LLAMA afin de déterminer leur capacité à occuper l'espace de *Lead-likeness* et confirmer qu'ils satisfont les conditions de Lipinski.

La troisième partie décrit la synthèse d'un nouveau mime de diproline, nommé ProCyp. Le dimère est composé d'un noyau pyrrolidine attaché à une unité cyclopentane à l'aide d'un pont méthylène hydroxylé. Les quatre isomères cyclopentanes *trans* dérivés de la (L)-proline ont été synthétisés et leur stéréochimie absolue a été déterminée par étude RMN et de cristallographie. Ces composés représentent la première forme de mimes de diproline de type ProCyp et peuvent être intégrés au sein de peptidomimétiques afin de mimer l'aspect structurel des diprolines ainsi que l'intermédiaire tétrahédral des ProPro endopeptidases. L'ensemble des isomères disponibles permet de choisir le plus opportun à l'appuis d'études de modélisation.

Le dernier chapitre rapporte le développement de deux séries de composés incluant le dimère ProCyp. Les motifs polyproline sont de prime importance pour de nombreux mécanismes de reconnaissance par la Nature, en particulier dans les voies de signalisation dont le dérèglement peut entrainer une myriade de troubles de santé notamment inflammatoires, immunitaires et cancéreux. La première application est centrée sur la synthèse et les tests biologiques de peptidomimétiques du motif riche en proline du peptide $p22^{phox}$, sous-unité de la NADPH oxidase 2 (NOX2) dont la reconnaissance par le domaine riche en proline de $p47^{phox}$ permet l'assemblage de NOX2 nécessaire à son activité. Lors de stress cellulaire externe, cet assemblage peut devenir excessif et engendrer un excès de production d'espèces réactives d'oxygènes, entrainant un ensemble de biomécanismes délétaires pour l'hôte. Les peptidomimétiques comportent un cœur triproline, dont deux des trois prolines ont été remplacées par le module ProCyp. Le meilleur

isomère a été sélectionné sur la base de la modélisation moléculaire afin de mimer les angles de torsion de la triproline correspondant à une hélice de type polyproline II.

La deuxième application concerne le développement de peptidomimétiques inhibiteurs de la ProPro endopeptidase (PPEP-1) de *Clostridium difficile* (C. diff). C. diff a été identifiée comme une des menaces nosocomiales majeures en raison de son caractère opportuniste lorsque la flore intestinale des patients est détruite suite à un traitement impliquant la prise soutenue d'antibiotiques. C. diff possède un arsenal de mécanismes d'évasion et de prolifération au sein de l'hôte incluant la formation de colonies recouvertes d'un biofilm protecteur sur la paroi epithéliale de l'hôte lors de la réponse immunitaire. Ces mécanismes sont complétés à l'aide de peptidases qui leurs permettent de couper les flagelles d'ancrages, dont PPEP-1. Le site de scission P1-P1' de PPEP-1 implique deux prolines, flanquées par une séquence peptidique clairement identifiée. Une série de peptides basés sur cette séquence dont la diproline centrale a été remplacée par le dimère ProCyp a été synthétisée. L'isomère ProCyp a été choisi sur la base de son recouvrement avec l'heptapeptide cristallisé au sein d'un mutant de PPEP-1 par le Pr. Baumann.

Mots-clés : Anti-cancéreux, proline, NADPH oxidase, synthèse asymétrique, *Clostridium difficile*, GABA.

Abstract

Proline is a unique amino acid characterized by a cyclic side chain that gives it specific physical and chemical properties compared to the other 20 acyclic amino acids found in the human proteome. This difference is also found in polyproline motifs and is used by Nature in many ways such as protein folding, regulatory mechanisms related to the activity of certain proteases, formation of secondary structures, biomarking of peptide substrates of oligopeptidases, and cleavage of diproline motifs by proline-proline endopeptidases. Proline has therefore been a focus of interest for medicinal chemists in the development of therapeutic agents. This thesis proposes to study several biologically active compounds derived from proline.

The first study reports on the advances related to the compound SH-BC-893, a constrained azacycle derived from FTY720 developed within the Hanessian group. SH-BC-893 is an anti-cancer agent that allows the starvation of cancer cells through the disruption of external and internal cellular nutrient supply. Through its activation of protein phosphatase 2A, it internalizes transmembrane amino acid and glucose receptors and downregulates low-density lipid receptors. Its action also allows the disruption of internal nutrient degradation from macropinocytosis and autophagy by preventing fusion between the lysosome and the respective endosomes. To enhance the activity of SH-BC-893, two series of compounds were synthesized and tested for dual activity. The first set aimed at targeting HDAC2 following a study by Spiegel in which its inhibition was reported for FTY720. The second set aimed at obtaining compounds activating other portions or homologs of PP2A via the insertion of tricyclic fragments following studies reporting PP2A activation by derivatives of tricyclic neuroleptic compounds of the perphenazine type. The synthesis and biological tests of these compounds are also described.

The second chapter describes the synthesis of a series of bridged morpholines with a constrained gamma butyric amino acid (GABA) motif. GABA is a major component of central nervous system regulation through its inhibitory action on GABA-A, GABA-B, GABA-C neuroreceptors. Many therapeutic agents inspired by GABA have been developed over the years, notably baclofen. The bridged morpholines reported here have a stereocontrolled quaternary center for which a variety of substituents have been used, including the *para*-chlorophenyl of baclofen and the *iso*-butyl of

Pregabalin, another GABA-derived compound active in the central nervous system. The baclofen derivative was modeled within the GABA-B active site. All compounds were also modeled as amino acids within the LLAMA database to determine their ability to occupy the lead-likeness space and confirm that they satisfy the Lipinski conditions.

The third part describes the synthesis of a new diproline mime, named ProCyp. The dimer is composed of a pyrrolidine ring attached to a cyclopentane unit by means of a hydroxylated methylene bridge. The four *trans* cyclopentane isomers derived from (L)-proline were synthesized and their absolute stereochemistry was determined by NMR and crystallographic studies. These compounds represent the first form of ProCyp-type diproline mimes and can be incorporated into peptidomimetics to mimic the structural aspect of diprolines as well as the tetrahedral intermediate of ProPro endopeptidases. The set of available isomers allows to choose the most appropriate one to support modeling studies.

The final chapter reports the development of two series of compounds including the ProCyp dimer. Polyproline motifs are of prime importance for many of Nature's recognition mechanisms, particularly in signaling pathways whose dysregulation can lead to a myriad of health disorders including inflammatory, immune and cancerous. The first application is focused on the synthesis and biological testing of peptidomimetics of the proline-rich motif of the peptide $p22^{phox}$, a subunit of NADPH oxidase 2 (NOX2) whose recognition by the proline-rich domain of $p47^{phox}$ allows the assembly of NOX2 necessary for its activity. During external cellular stress, this assembly can become excessive and lead to an excess of reactive oxygen species production, resulting in a series of deleterious biomechanisms for the host. The peptidomimetics comprise a triproline core, of which two of the three prolines have been replaced by the ProCyp module. The best isomer was selected on the basis of molecular modeling to mimic the torsion angles of the triproline corresponding to a polyproline II helix.

The second application concerns the development of peptidomimetics that inhibit the ProPro endopeptidase (PPEP-1) of *Clostridium difficile* (C. diff). C. diff has been identified as one of the major nosocomial threats due to its opportunistic nature when the intestinal flora of patients is destroyed following treatment with sustained antibiotics. C. diff has an arsenal of mechanisms of

escape and proliferation within the host including the formation of colonies covered by a protective biofilm on the host epithelial wall during the immune response. These mechanisms are complemented by peptidases that allow them to cleave anchoring flagella, including PPEP-1. The P1-P1' cleavage site of PPEP-1 involves two prolines, flanked by a clearly identified peptide sequence. A series of peptides based on this sequence with the central diproline replaced by the ProCyp dimer was synthesized. The ProCyp isomer was chosen on the basis of its overlap with the heptapeptide crystallized in a PPEP-1 mutant by Prof. Baumann.

Keywords : Anti-cancer, proline, NADPH oxidase, asymmetric synthesis, *Clostridium difficile*, GABA.

Table des matières

Liste des tableaux

Liste des figures

Liste des schémas

Liste des sigles et abréviations

α2AP	Sérine protéase α2-antiplasmine
δ	Déplacement chimique
Δ	Chaleur
Å	Angstrom
υ	Fréquence
(4*R*)Azp	(2S,4R)-4-azidoproline
4RHyp	(2S,4R)-4-hydroxyproline
1,2-DCE	1,2-dichloroéthane
10H-P	Phénoxazine
4F2hc/CD98hc/CD98	Chaîne lourde d'antigène de surface cellulaire 4F2
Ac	Acétyl
ACE	Enzyme de conversion de l'angiotensine
ACN	Acétonitrile
Akt	Protéine kinase B
APP	Aminopeptidases P
aq.	Aqueux
Ar	Aryle
BIR3	Répétition de l'IAP du baculovirus 3
Bn	Benzyle

BOM	Benzyloxyméthyle éther
Boc	*tert*-butoxycarbonyle
br	Large
Bu	Butyle
Bz	Benzoyle
C-ter	Terminal C
C. diff.	*Clostridioides difficile*
c-di-GMP	Diguanylate cyclique
ca.	Environ
Calcd.	Calculé
CAM	Cerium ammonium molybdate
cat.	Catalyseur
CDT	*C. diff.* transférase
CIP	Protéines qui interagissent avec le collagène
cm	Centimètre
CNA	Domaine homologique se liant au collagène
CPZ	Chlorpromazine
CTD	Domaine-terminal C
d	Doublet
DAPI	4’6-diamidino-2-phenylindole
DBU	1,8-Diazabicyclo[5.4.0]undec-7-ene
DGC	Diguanylate cyclases
DIBAL-H	Hydrure de diisobutylaluminium

DIC	Contraste interférentiel différentiel
DIPEA	Diisopropyléthylamine
DMA	Diméthylacétamide
DMEM	*Dulbecco's Modified Eagle Medium*
DMF	Diméthylformamide
DMP	Périodinane de Dess-martin
DMSO	Diméthyl sulfoxyde
DNA	Acide désoxyribonucléique
DPP	Dipeptidyl peptidase
d	Doublet
DCM	Dichlorométhane
dr	Ratio diastéréomérique
DRX	Diffraction par rayons-X
DUOX1	Oxidase double 1
E	Glu(O*t*Bu)-OH
e.g.	Par exemple
EDC	1-éthyl-3-(3-diméthylaminopropyl)carbodiimide
EGFR	Récepteur du facteur de croissance épidermique
EHT	Méthode de Hückel étendue
ENAH	Homologue de la protéine activée
eq.	Équivalent
ESI	Ionisation par électrospray

Et	Éthyle
EVH1	Drosophilia activée/Phosphoprotéine stimulée par les vasodilatateurs 1
FA	Acide formique
FACS	Cytométrie en flux
FAP	Protéine d'activation des fibroblastes
FBS	Sérum fœtal de bovin
FDA	*Food and Drug Administration*
FHA	Domaine *Forkhead-associated*
FITTED	*Flexibility Induced Through Targeted Evolutionary Description*
FL5.12	Cellules prolymphocytiques de murine
FoxO	*Forkhead box class O*
FRET	Transfert d'énergie par résonance de fluorescence
FT	Transformée de Fourier
FTY720-P	FTY720-phosphate
HOBt	Hydroxybenzotriazole
g	Gramme
GABA	Acide gamma-aminobutyrique
GIP	Peptide insulinotropique dépendant au glucose
GLUT1	Transporteur de glucose 1
GYF	Domaine glycine-tyrosine-phénylalanine
h	heures

H-bond	Liaison hydrogène
HAT	Histone acetylase
HATU	Hexafluorophosphate Azabenzotriazole Tetramethyl Uronium
HDAC	Histone déacétylase
hDT2	Domaine homologique au domaine thioester de classe 2
HEPES	4-(2-hydroxyethyl)-1-piperazineethanesulfonic acid
HIV-1	Virus d'immunodéficience humain 1
HPLC	Chromatographie liquide à haute performance
HRMS	Spectres de masse à haute résolution
Hz	Hertz
IAP	Protéine inhibitrice d'apoptose
IC50	Concentration inhibitrice médiane
i-Pr	Isopropyle
IL-3	Interleucine 3
ILV	Vésicules intraluminales
IR	Infra-rouge
J	Constante de couplage
K	Kelvin
Ka	Constante d'association
kcal	Kilocalorie
Kd	Constante de dissociation
KD	Constante d'équilibre

KHMDS	Bis(trimethylsilyl)amide de potassium
LC	Chromatographie liquide
LDA	Di-(isopropyl)amidure de lithium
LDL	Lipoprotéines à faible densité
LiHMDS	*bis*-(triméthylsilyl)amidure de lithium
LLAMA	*Lead-Likeness and Molecular Analysis*
LRMS	Spectrométrie de masse à basse résolution
m	Multiplet
M	Molarité en mol.L-1
m.p.	Point de fusion
Me	Méthyle
MEF	Fibroblaste embryonnaire de murine
mg	Milligramme
min	Minutes
MOE	Environnement opérationnel moléculaire
mol	Mole
MS	Tamis moléculaire/Spectrométrie de masse
MVB	Corps multivésiculaires
N	Normality en mol.L^{-1}
N-ter	Terminal N
NK	Neurokinine
NOE	Effet Overhauser nucléaire
NOESY	Spectroscopie nucléaire à effet Overhauser

NOX/NADPH Oxidase	Oxidase de nicotinamide adénine dinucléotide phosphate
NS3	Protéine non structurale 3
NTD	Domaine-terminal N
o	*ortho*
p	*para*
P	Fmoc-Pro-OH
P. Alvei	*Paenibacilus alvei*
PDB	*Protein Data Bank*
PBS	Solution saline tamponnée au phosphate
PDE	Phosphodiestérases
PE	Phycoérythrine
PEP	Prolyl endopeptidase
PG	Groupement protecteur
pH	Potentiel hydrogène
Ph	Phényle
PI3K	Phosphatidylinositol 3-kinase
Pin1	Protéine interagissant avec NIMA(Jamais en mitose)-1
Piv	Pivalate
pKa	Logarithme de la constante d'acidité
PMB	4-méthoxybenzyle
POP	Prolyl oligopeptidase
PPIases	Peptidyl-prolyl isomérases
PP-I	Polyproline I

PPII	Polyproline II
PP2A	Protéine phosphatase 2A
PPEP	Proline-Proline endopeptidase
PPI	Interaction protéine-protéine
ppm	Partie par million
PPP	Phosphoprotéines phosphatase
PPZ	Perphénazine
PRCP	Prolyl carboxypeptidase
PRD	Domaine riche en prolines
PRM	Motif riche en prolines
PSP	Peptidases spécifiques à la proline
PSTP	Sérine/thréonine phosphatase
PTB	Domaine liant de la phosphotyrosine
PyBOP	Benzotriazol-1-yloxytripyrrolidinophosphonium hexafluorophosphate
q	Quadruplet
quin.	Quintuplet
r.t	Température ambiante
RAS	Système rénine-angiotensine
RCM	Métathèse par fermeture de cycle
Rdt	Rendement
RIPA	Test de radio-immunoprécipitation

RMN	Résonance Magnétique Nucléaire
RNase	Endoribonucléase
ROS	Espèce réactive d'oxygène
Rx	Reflux
s	Singulet
S1P	Sphingosine-1-phosphate
SAHA	Acide hydroxamique suberoylanilide
sat.	Saturé
SCK	Cinétique à cycle unique
SDS	Système de distribution de solvant
Sem5	Protéine anormale du muscle sexuel
SH3	Src-homologique
Smac	Deuxième activateur mitochondrial des caspases
SMAP	*Small Molecule Activator of PP2A*
SNC/CNS	Système nerveux central
sol.	Solution
SphK2	Sphingosine kinase 2
SPR	Résonance plasmonique de surface
t	Triplet
T	Température
t.a	Température ambiante
TBAF	Fluorure de tétrabutylammonium
TBAI	Iodure de tétrabutylammonium

TBS = TBDMS	*tert*-butyldiméthylsilyle
TBDPS	*tert*-butyldiphénylsilyle
TBHP	*tert*-butyl hydroxyperoxide
TBTU	O-(Benzotriazol-1-yl)-N,N,N',N'-tetramethyluronium tetrafluoroborate
TcdA	Toxine A de *Clostridium difficile*
TcdB	Toxine B de *Clostridium difficile*
TFA	Acide trifluoroacétique
THF	Tétrahydrofurane
TIE	Domaines thioester, isopeptide et ester
TLC	Chromatographie sur couche mince
TMS	Triméthylsilyle
TOF	Temps de vol quantitatif
Ts	Tosyle
TSA	Trichostatine A
UEV	Variant E2 de l'ubiquitine
UV	Ultra-violet
V	Fmoc-Val-OH
w/w	Pourcentage massique
WW	Domaine rsp-5 à motif répétitif WWP
XPD	Prolidase
XS	Excès
Zmp1	Métalloprotéase de Zinc 1

À ma mère.

Remerciements

I will start by thanking Pr. Hanessian, for having always made sure to provide us with every material or financial help we may need and enabling my PhD study to become the experience it has been. Thank you for the numerous partnerships with people from all around the world; for all the projects I've been involved in through which I learned more that I would have expected; for all the students you trusted me with; for allowing me to develop my own research project and for your support when hell knocked at my door. And most importantly, thank you for having made me, through all these years, a better chemist, and a better man… Even though it may have been through fire and flames at times.

Mes pensées vont ensuite à Michèle, qui au cours de toutes ces années, a été un soutien sans faille, et a été une des personnes sur lesquelles j'ai su compter dans mes moments d'incertitudes et d'épreuves. Tu fais partie des personnes les plus chaleureuses et fortes que j'ai eu l'occasion de rencontrer, et je ne pourrais que te souhaiter le meilleur du monde pour la suite.

J'ai également un mot pour les collègues des plateformes techniques, qui ont su répondre à mes nombreuses demandes. Merci au Dr. Pedro Aguiar pour ses conseils et ses enseignements en RMN, et Cédric et Sylvie pour leur disponibilité lorsqu'il me fallait passer des expériences urgentes. Merci également à l'équipe du département de masse, Alex, Karine, Marie-Christine et Louiza. Au-delà de votre aide pour les expériences, j'ai passé de chaleureux moments à discuter avec l'ensemble d'entre vous.

Ensuite, j'aimerais remercier l'ensemble des membres du groupe Hanessian que j'ai eu l'occasion de rencontrer au cours de ces années. En particulier, ceux qui ont partagé mon laboratoire et avec lesquels j'ai passé une bonne partie de ces dernières années, comme Lorenzo, JP, Erick, et en particulier Scarlett. Je garderais le souvenir de nos discussions pour le fait que je suis rarement tombé d'accord aussi souvent avec quelqu'un sur des sujets aussi divers et profonds. Je suis heureux que l'on ait partagé le labo pour la majorité de mon doctorat, en particulier pour cette dernière année. Merci d'avoir su être disponible lorsque j'avais besoin d'une oreille attentive et pour avoir trouvé les mots. Dieu te rendra ta bienveillance. Ensuite viennent les boys du B3480,

les CPRs.. Sofiane, Edouard et Adrien. Sofiane, je te souhaite le meilleur avec Colombe. Merci pour les délires et les bonnes discussions, les solutions de gitan et les œuvres d'art intempestives trouvées au détour d'un lab. Edouard, merci pour les bons mots, les blagues non pas douteuses mais de caractère, et les moments de galère à refaire la société ou simplement à lister ce qui pourrait être mieux. Adrien, je te souhaite une bonne aventure en tant que père, et bon courage à Camille pour gérer trois gars, à moins qu'une fille ne soit prévue, qui sait. J'ai apprécié les deux-trois conseils culinaire saupoudrés au cours des dernières années, ainsi que ta bonhommie générale.

Le travail effectué dans cette thèse n'aurait également pu être possible sans l'aide des collaborateurs qui m'ont aidé à surmonter les embûches et traverser les synthèses. Merci à mes étudiants stagiaires, Catherine, Solène, Matt, et Thomas, qui se sont montrés impliqués et prêts à relever les défis auxquels ils ont eu à faire face. Merci également à Erick, Sofiane, Adrien, Lorenzo, Vito, Gregorio et Raph pour les collaborations entreprises qui se sont couronnées de succès.

En dehors de l'université, je remercie l'ensemble des amis avec lesquels j'ai pu passer des moments formidables, les Montréalais savent clairement y faire. En particulier, Matt, Kilian et JF qui ont été les piliers des quatre cents coups qu'on a pu sortir et des aventures jusqu'à pas d'heures qu'on a pu faire. Ces moments resteront gravés à travers les années.

Enfin, je remercie ma famille qui m'a toujours soutenu au travers de mes projets. Merci à ma mère et à mon père, qui ont su croire en moi lorsque beaucoup auraient renoncé, et qui ont vu la lumière au milieu de mon obscurité. Vous m'avez donné un centre de gravité, des valeurs, un amour qui est devenu une force, et me permet d'avancer sans regarder en arrière.

Chapitre 1. Introduction

Au sein de la Nature, l'acide aminé proline se distingue par son cycle pyrrolidine qui lui procure un ensemble de propriétés structurelles particulières. [1–3] Cette particularité en a fait un motif de reconnaissance structurel et fonctionnel pour les protéines et a résulté en sa conservation au travers de l'évolution du vivant. La proline a été une source d'inspiration pour les chimistes médicinaux dans de nombreux domaines thérapeutiques incluant les troubles immunologiques, oncologiques, inflammatoires, et neurologiques.

La proline est également utilisée par la Nature sous forme d'oligomères, appelés motifs riches en prolines (PRMs). [4] Ces sections protéiques sont cruciales pour la stabilité structurelle des protéines dans lesquelles on les retrouve, et peuvent adopter la forme d'hélices polyproline ou triples. [5] Ces PRMs sont également utilisés comme motifs de reconnaissance dans les mécanismes réversibles biologiques nommés interactions protéine-protéine (PPI). [4] Ces procédés sont une part importante des voies de signalisation dont dépendent la physiologie et le cycle cellulaire, et leur dérégulation est à l'origine d'un ensemble de maladies dégénératives.

Cette thèse rapporte le développement d'agents médicinaux basés sur la proline ainsi que de peptidomimétiques mimant des motifs riches en prolines pour l'inhibition de PPI et de protéases spécifiques au motif diproline.

1.1 La proline dans la Nature.

1.1.1 Structure et prévalence dans le protéome humain.

Les acides aminés représentent les éléments constitutifs de l'ensemble du protéome humain. Parmi les 900 acides aminés naturels produits par la nature, seulement 21 d'entre eux ont été sélectionnés par l'évolution et retenus de façon conséquente dont la proline. [1] Morgan a établi que sur un total de 18 666 protéines appartenant à l'Homme, 99.8% contiennent l'acide aminé proline. Au sein de ces protéines, la proline représente 6.3% de l'ensemble des acides aminés.

Bien que la plupart se retrouvent sous forme isolées au sein d'une chaine peptidique (82.1%), un pourcentage non négligeable de diproline (13.5%) et polyproline (4.4%) a également été recensé.

La proline se distingue de ses congénères par sa chaine latérale cyclique à cinq chainons et son amine secondaire, dont découle plusieurs propriétés conformationnelles (Figure 1.1). Ses angles dièdres sont contraints et l'angle φ a une valeur de -60 ° lorsque la proline est incluse dans une chaine peptidique. Les deux minima énergétiques de l'angle Ψ d'une proline isolée correspondent à Ψ = -55° et Ψ = + 145°. [2] L'angle Ψ régie l'énergie conformationnelle de la proline dans une séquence peptidique en raison de la restriction de la rotation autour de l'angle φ (N-C_α) due au cycle pyrrolidine. Il est à noter que l'amine tertiaire ne possède pas d'hydrogène susceptible de former des liaisons hydrogène comme pour le reste des acides aminés. Cependant, elle conserve son caractère accepteur de liaison hydrogène.

Lorsque trouvée au sein d'une chaine peptidique sans ordre prédéfini, la proline tend à induire une liaison peptidique de configuration *cis* (10-30%) avec l'acide aminé précédent. [3] Cette propriété contraste avec les autres acides aminés pour lesquels la configuration *cis* est presque inexistante. [6] Plusieurs effets justifient cette différence. (Figure 1.1) Dans le cas d'acides aminés autre que la proline, la répulsion stérique entre les hydrogènes portés par les C_α est plus importante dans la conformation *cis* contrairement à X-Pro où elle est équivalente. [7] Des interactions électrostatiques favorables entre O et C_β sont présentes uniquement dans le conformère *trans* contrairement à X-Pro. La perte d'entropie de la conformation *trans* vers *cis* est également plus faible pour X-Pro comparé aux autres acides aminés. L'élongation de la liaison X-Pro liée à la redistribution de charge et à la diminution de résonance générée par la perte de l'hydrogène de l'azote permet une diminution de la barrière énergétique d'activation de l'isomérisation. [2]

En raison de leur énergies conformationnelles proches, les deux isomères sont observés au sein de petits peptides, avec une proportion de conformère *cis* plus importante dans les solvants polaires. Cependant, l'isomérisation *cis/trans* reste un évènement haut en énergie (~ 20 kcal/mol) en raison du caractère partiel de double liaison de N-C_α et sa cinétique est lente (10-100 seconde). [8] Le caractère polaire du solvant peut diminuer le temps d'interconversion.[7]

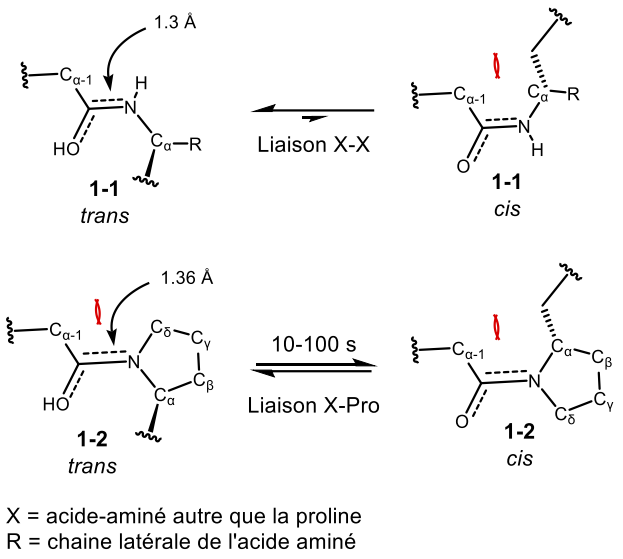

Figure 1.1 Structure de l'acide aminé proline et considérations conformationnelles.

En raison de l'énergie nécessaire pour isomériser la liaison X-Pro, celle-ci est stable lorsqu'elle se trouve au sein de protéines dans lesquelles un tel évènement induit un changement de conformation local ou global et ce processus requiert généralement une énergie d'activation. Cela permet à la Nature d'utiliser l'isomérisation de la liaison X-Pro comme commutateur moléculaire dans des mécanismes de régulation impliqués dans les voies de signalisation, et certaines protéines ont pour rôle de catalyser cette transformation. [9]

1.1.2 Fonctions dans la nature

1.1.2.1 Repliement et fonction des protéines

Le repliement des protéines leur est nécessaire afin de pouvoir fonctionner lorsqu'elles émergent du ribosome et durant leurs cycles de dépliement/repliement. [10] Ce mécanisme dynamique complexe comporte plusieurs étapes et est régi par un ensemble de paramètres liés à sa structure et son environnement immédiat, et son échec peut entrainer un ensemble de pathologies. [11] Lors de son repliement, la protéine peut être considérée comme un ensemble de segments coopératifs nommés foldons qui peuvent se déplier et se replier de manière répétée. Les interactions stabilisantes entre ces foldons peuvent par la suite générer des portions stables de protéine de plus en plus larges jusqu'au repliement final. [12]

Au sein des foldons, l'acide aminé proline joue un rôle particulier en raison de sa capacité à isomériser la liaison X-Pro. Les prolines composant les protéines peuvent être séparées en deux catégories : essentielles et non-essentielles. Les prolines essentielles sont associées aux structures secondaires que l'on trouve dans la protéine et qui sont primordiales à l'intégrité du repliement protéique (ex : Pro117 de la RNase A [13]) telle que les hélices et les tournants-β (ex : Pro55 dans la RNase T1 [14], Pro76 dans l'iso-2-cytochrome c, [15] Pro70 dans le domaine SH3 de la PI3K [16]). Ces derniers tordent la chaine protéique en épingle à cheveux à la surface de la protéine, et stabilisent indirectement le repliement protéique en favorisant l'association des résidus dont les interactions hydrophobes et les liaisons hydrogène vont permettre d'assurer la cohésion de la protéine.[17] Au contraire, les prolines non essentielles sont généralement dans des positions qui ne sont pas impliquées dans la cinétique de repliement, ou elles sont associées à des conformations neutres qui tolèrent les deux isomères. Cela se produit souvent dans les structures irrégulières et/ou labiles près de la surface de la protéine.[18] Ce type de proline semble être le plus commun et on en trouve des exemples dans la plupart des protéines. [19] Il est à noter que les phases lentes observées lors de dépliement/repliement sont parfois corrélées à l'isomérisation *cis*/*trans* de résidus proline et nécessitent l'assistance catalytique de prolyl isomérases afin de pouvoir procéder. [20]

L'isomérisation de la proline peut être exploitée de deux manières. Premièrement, les taux d'isomérisation et les rapports *cis*/*trans* à l'équilibre de prolines essentielles peuvent être utilisés pour détecter la structure locale de la protéine. [7] Deuxièmement, les isomères de proline non natifs peuvent être considérés comme mutants transitoires afin de déterminer la nature essentielle ou non-essentielle de chaque proline mutée en fonction de leurs effets sur le repliement conformationnel. Lorsqu'une proline essentielle est mutée, la modification de son angle dièdre ω vient perturber la cinétique du repliement en altérant plusieurs liaisons hydrogène peptide-peptide définissant la structure secondaire locale nécessaire au processus. La Pro93 de la ribonucléase A en est un exemple. Sa conformation X-Pro *cis* native participe à la formation d'un tournant-β qui agit comme site d'initiation pour le repliement de la chaine peptidique et la formation d'une épingle à cheveux-β à double brins. [7] Lorsqu'en conformation *trans*, Pro93 perturbe le virage du tournant-β en nécessitant la formation d'une boucle plus large. [21]

Les étapes du repliement conformationnel et d'isomérisation des liaisons prolyl sont interdépendantes. [22] Les isomères incorrects de liaison X-Pro dans une chaîne protéique ralentissent son repliement, et le repliement conformationnel peut affecter la cinétique et l'équilibre *cis*/*trans* des liaisons X-Pro. Un exemple de ce phénomène a été observé avec la RNase A. Lorsque dépliée, Garel et Baldwin ont découvert en 1973 qu'elle consistait en un mélange d'isomères dont certains permettaient un repliement rapide (U_F) et d'autres un repliement lent (U_S). [23] La cinétique de repliement de ces isomères a été liée à la configuration de quatre résidus proline dans sa forme repliée (Pro93 et Pro114 de configuration *cis*, Pro41 et Pro117 de configuration *trans*). [24] Il a été montré que la configuration des prolines composant les isomères à repliement rapide U_F était identique à celle de la configuration native alors que celle des isomères U_S diffèrent par l'état isomérique *cis*/*trans* d'une ou plusieurs liaisons peptidiques X-Pro. La cinétique lente des isomères U_S est une conséquence de la cinétique d'isomérisation de la liaison X-Pro. [8] Il est à noter que les isomères non natifs ne bloquent pas le repliement dès le début et l'isomérisation n'est pas nécessaire pour que procède la première étape du repliement. [3] Les isomères de liaison X-Pro incorrects peuvent souvent être accommodés dans des intermédiaires partiellement repliés, et dans le cas de la RNase A, un intermédiaire de repliement possédant une proline incorrecte a montré une activité catalytique partielle. [25]

L'isomérisation *cis/trans* des liaisons prolyles sert également de commutateur pour la fonction de certaines protéines et peut être catalysée par les peptidyl-prolyl isomérases (PPIases). [3] Les PPIases ont été conservées de façon ubiquitaire dans les cellules eucaryotes et procaryotes et ont pour rôle d'accélérer la conversion *cis/trans* de substrats qui leur sont spécifiques. [26] Elles sont impliquées dans de nombreux procédés cellulaires tels que la réponse immunitaire, [27] le développement neuronal [28] et la régulation du cycle cellulaire, en particulier au travers de l'activité de Pin1 (protéine interagissant avec NIMA(Jamais en mitose)-1). [9,29] La perturbation de Pin1 peut devenir la source de nombreux troubles neurodégénératifs, [30,31] cancéreux [32] et liés au système vasculaire. [33] Il est à noter que les PPIases jouent également un rôle dans le développement d'infections virales ou parasitaires, [34] notamment comme facteur de virulence de *Clostridium difficile.* [35]

1.1.2.2 Présence dans les structures secondaires

1.1.2.2.1 Tournants-β et tournants-γ

Les tournants sont les structures non-répétitives les plus communes au sein des protéines et incluent environ 25% des résidus protéiques. [36] Ils jouent un rôle crucial dans l'organisation spatiale ce celles-ci en induisant un changement directionnel impliqué dans le repliement ainsi que la reconnaissance moléculaire. Les tournants comprennent n résidus consécutifs (notés i à i+n), dans lesquels la distance entre les Cα des résidus i et i+n est inférieure à 7 Å en raison de la torsion du squelette. [37] Ils sont classés selon le nombre de résidus qui les composent dans les catégories suivantes : tournants-γ (n = 3), [38,39] tournants-β (n = 4), [40] tournants-α (n = 5) [41] et tournants-π (n = 6). [42,43]

Parmi-eux, les tournants-β ont attiré le plus d'attention en raison de leur prévalence. En plus des critères énoncés ci-avant, le tournant peut former une liaison hydrogène entre CO(i) et NH(i+3) [37] et les résidus i+1 et i+2 ne peuvent être hélicoïdaux. Les tournants-β sont classés selon les valeurs des angles dièdres φ et ψ de leur résidu central. Les classes majoritaires inclues les tournants-β de type I, II, et leurs images miroirs I', II'; VI qui sont caractérisés par la présence d'une *cis*-proline à la position i+2; VIII et IV, ce dernier regroupant l'ensemble des tournants-β qui n'ont pu être caractérisés dans l'une des classes précédentes (Tableau 1.1). de Brevern a récemment proposé plusieurs sous-catégories pour la classe IV qui a permis de classifier la moitié d'entre eux. [40]

Tableau 1.1 Classes de tournants-β et leur fréquence d'apparition. [40]

β-turn	(%)
I	38.21
II	11.81
VIII	9.84
I'	4.10
II'	2.51
VI_b	0.88
VI_{a1}	0.73
VI_{a2}	0.20
IV^{ori}	31.72
Sum	100.00

La présence de la proline n'est cependant pas limitée à la classe VI. En 2000, Guruprasad et Rajkumar ont entrepris d'identifier et classer près de 7000 tournants-β trouvés au sein de 320 chaines protéiques non-homologues. [37] Ils ont ensuite analysé quels résidus étaient favorisés à chaque position du tournant de façon globale et pour chaque classe. Au global, les acides aminés glycine et proline sont les plus communs au sein des tournants-β suivi des résidus asparagine et acide aspartiques. La proline est favorisée aux positions i et i+1 pour lesquelles elle est l'acide aminé le plus présent. Au sein des tournants de type I et II, la proline est l'acide aminé le plus présent à la position i+1 en raison de la restriction de son angle φ (-60 °). (Figure 1.2) [36] Elle fait également partie des acides aminés les plus présent à la position i. La même observation a été faite pour le type VIII, bien qu'elle soit l'acide aminé le plus présent à la position i et i+3 cette fois. Sa prépondérance à la position i+3 a été rationalisée par la contrainte d'angle qu'elle génère sur la position i+2, forçant ainsi la formation du tournant de type VIII au lieu d'un tournant de type I. [36] Les groupes I, II et VIII représentent 56% de l'ensemble des tournant-β.

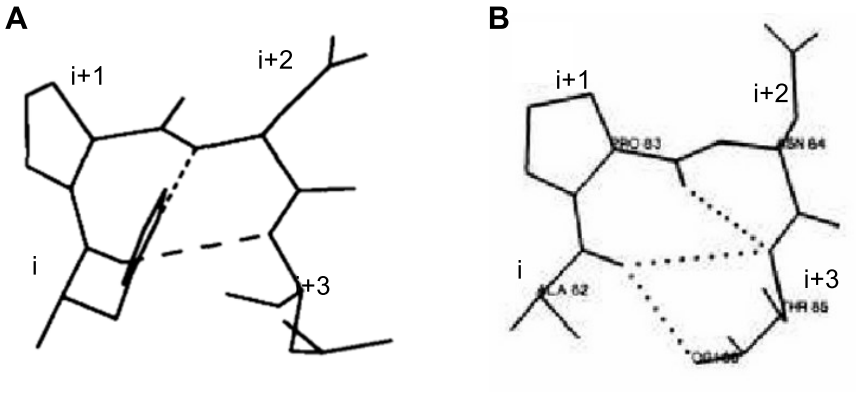

1-3
His-Pro-Asp-Leu

1-4
Ala-Pro-Asn-Thr

Figure 1.2 A. Exemple de tournant-β de type I **1-3** (His-Pro-Asp-Leu). Présence de liaisons hydrogène entre CO(i) et NH(i+2)/NH(i+3). B. Exemple de tournant-β de type II **1-4** (Ala-Pro-Asn-Thr). Présence de liaisons hydrogène entre CO(i) et NH(i+3)/NH(i+4) et CO(i+1) et NH(i+2). [36,37]

La proline est quasiment absente des groupes I' et II' (image miroir des groupes I et II) étant donné que la valeur des angles des résidus composant le tournant doit être opposée. Elle est cependant l'acide aminé le plus présent au sein du groupe IV, en particulier aux positions i, i+1 et i+3, et occupe exclusivement la position i+2 des tournants-β du groupe VI.

Guruprasad et Rajkumar ont également répertorié l'ensemble des tournants-γ. Bien que moins présents que les tournants-β, il est utile de noter que la proline est également un des acides aminés majeurs des positions i et i+1 des tournants-γ inverses. [37] Ceux-ci sont les plus retrouvés et possèdent leurs propres caractéristiques structurelles. Un point intéressant est que les virages sont souvent observés en tandem, conduisant parfois à de longues séries de γβ, βγ, ββ ou γγ [44,45]

Un certain intérêt a été porté à la stabilisation conformationnelle des protéines par le remplacement d'un acide aminé au sein de structures secondaires. [46,47] En particulier, Trevino et ses collaborateurs ont démontré que le remplacement d'acides aminés au sein de tournants-β de la RNase Sa par une glycine ou une proline peut résulter en une augmentation de la stabilité conformationnelle de la protéine (0.7-1.9 kcal/mol). [48] Leur étude a couvert une large gamme de tournants-β enfouis ou en surface, avec différentes flexibilités et incluant des doubles-tournants.

Ainsi, la proline occupe un rôle majeur au sein des tournants et le remplacement d'acides aminés moins appropriés par celle-ci est d'intérêt pour améliorer la stabilité conformationnelle des protéines au travers de leurs propriétés de repliement.

1.1.2.2.2 Hélices α

En contraste de son rôle prépondérant dans les tournants, la proline se retrouve principalement aux extrémités des hélices α en raison de l'absence d'hydrogène porté par l'azote et de sa contrainte angulaire. [49,50] Les hélices-α sont les structures secondaires les plus répandues et se caractérisent par un pitch de trois résidus et la formation de liaisons hydrogène intramoléculaires entre les résidus i et i+3. (Figure 1.3 – A) Ces structures sont longues d'environ dix acides aminés pour la plupart, soit l'équivalent de trois tours. [51] Les hélices α tournent principalement dans le sens horaire; cependant celles qui sont orientées dans le sens inverse jouent un rôle structurel ou fonctionnel important. [52] Il a été proposé par Kim et Kang que la préférence élevée pour la proline au début de l'hélice α soit due à la stabilité intrinsèque de sa conformation hélicoïdale (Figure 1.3 – B). [49] Ainsi, bien que la présence de la proline au sein de l'hélice ne soit observée qu'en rares occasions, [53] ses propriétés favorisent néanmoins leur formation. Il est également à noter que la proline joue un rôle fonctionnel au sein des hélices de certaines protéines comme l'importine-β. [54] Elle se trouve au cœur de nombreuses hélices α amphiphiles localisées à la

surface de la protéine afin de générer plus de flexibilité en leur sein (Figure 1.3 – C). Cette flexibilité est nécessaire pour le transport des importines au sein du noyau et assurer l'intégrité fonctionnelle des caryophérines.

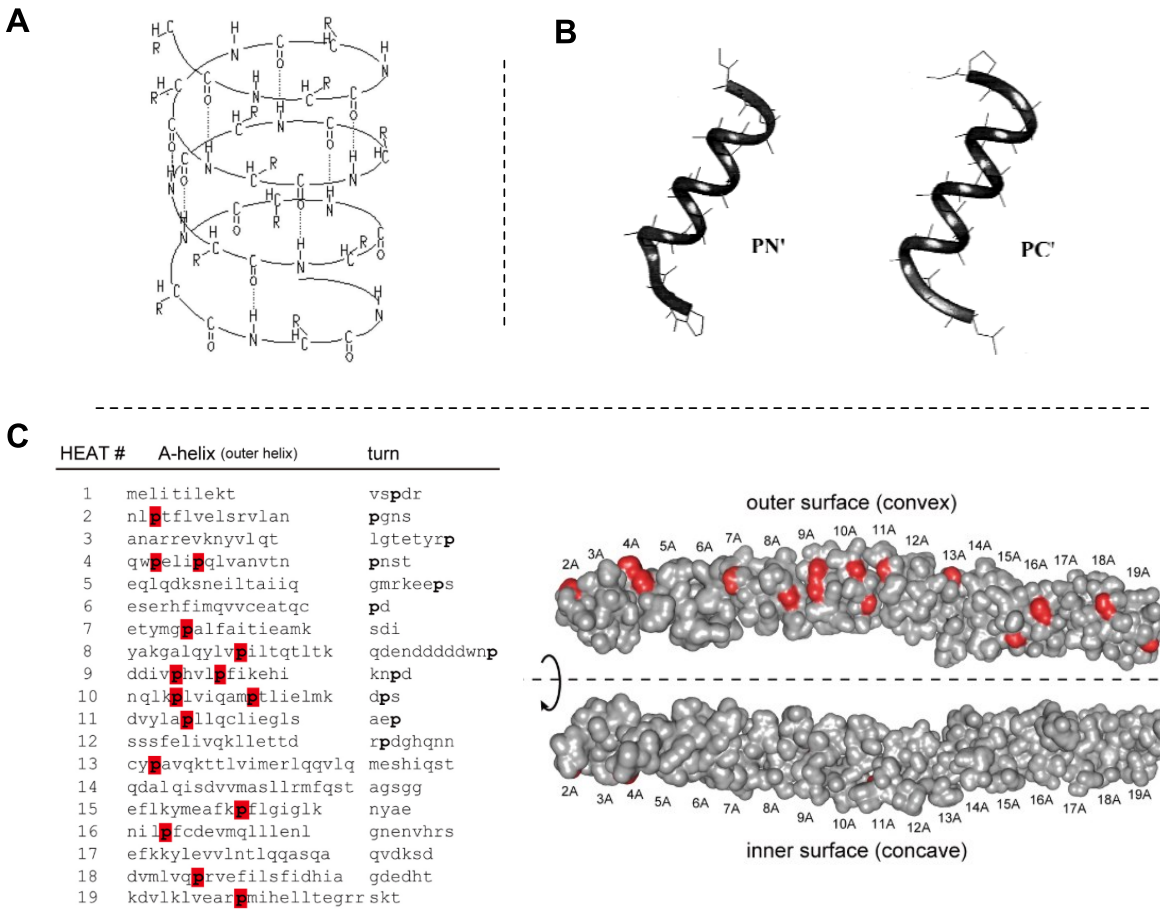

Figure 1.3 A. Représentation schématique d'une hélice α. [55] B. Exemples de types d'hélices α incluant un résidu proline à une extrémité. [49] C. Classement des hélices α de l'importine-β comportant un résidu proline dans leur cœur. [54]

Les hélices α sont également des points de nucléation important pour la formation de structures secondaires plus large comme les structures super hélicoïdales. [56]

1.1.2.3 Peptidases spécifiques à la proline

La proline occupe un rôle principal dans la protection des peptides biologiquement actifs contre la dégradation enzymatique en protégeant ceux-ci contre l'action de certaines protéases lors de l'étape post-traductionnelle. [57,58] La biosynthèse et la dégradation des peptides sont une série

d'événements dont le bon déroulement est primordial afin qu'ils puissent être fonctionnels. [59] La production d'un peptide actif implique l'action d'une endopeptidase, qui clive son précurseur à un site spécifique suivi de l'action d'exopeptidases qui réduisent la chaîne peptidique de quelques acides aminés jusqu'à obtenir la cible finale. La chaîne peptidique doit posséder un élément structurel ou biochimique qui puisse empêcher une hydrolyse excessive entraînant la perte de l'activité biologique. Les résidus proline situés dans les précurseurs polypeptidiques agissent comme des éléments structurels permettant de protéger la chaîne polypeptidique contre une activité protéolytique parasite, en particulier celle des exopeptidases. [57,58]

La spécificité structurelle de la proline lui permet également d'être reconnue par un ensemble de peptidases spécifiques à son motif, faisant d'elle un biomarqueur naturel. Lorsque trouvé au sein de la chaine peptidique, certaines protéines vont spécifiquement cliver la liaison peptidique un ou deux acides aminés précédents la proline. [60] Plus récemment, certaines protéines spécialisées dans le clivage de liaisons diproline ont également été rapportées. [61]

1.1.2.3.1 Généralités

La plupart des peptidases spécifiques à la proline (PSP) sont des exopeptidases qui peuvent hydrolyser les acides aminés situés aux deux extrémités des protéines ou des peptides. Seule la prolyl oligopeptidase (POP), aussi appelée prolyl endopeptidase (PEP), clive les peptides de moins de 30 résidus au sein de leur chaine. Les PSP sont réparties entre les peptidases à sérine et les métallopeptidases. [62] On retrouve six familles de protéases au sein des PSPs. La POP, les dipeptidyl peptidases (DPP) dont DPPII et DPPIV, la protéine d'activation des fibroblastes (FAP), et la prolyl carboxypeptidase (PRCP) appartiennent à la famille S28 des sérine peptidases. [63] Les aminopeptidases P (APP1, APP2, APP3) et la prolidase (XPD) appartiennent à la famille des métallopeptidases. De nombreuses PSP se trouvent sous formes d'isoformes résultant d'un épissage alternatif. [62] L'épissage alternatif est un élément clé de la diversité protéique et phénotypique et permet d'obtenir un système de régulation de l'expression des gènes. [64] L'épissage des PSPs a amené à une large distribution de ses fonctions parmi lesquelles on y trouve le rôle de signalisation, de régulation et trophique (digestion de protéines alimentaires riches en prolines au sein du système gastro-intestinal).

L'intérêt envers les PSPs a également été lié à leur impact dans le développement d'un ensemble de conditions pathologiques qui en ont fait des cibles de choix pour le développement de composés thérapeutiques incluant les troubles immunitaires, inflammatoires, et cancéreux. [65] Certaines PSPs telles que les PEPs, les DPPs (FAPα, DPPII, DPPIV) et la PRCP ont été particulièrement étudiées pour leurs implications dans la formation de ces conditions, et seront utilisée pour la suite afin d'illustrer le rôle des PSPs, leurs mécanismes biologiques, et comment leur disfonctionnement amène aux maladies énoncées.

1.1.2.3.2 Rôle des PSPs dans le développement de conditions pathologiques

DPPIV et FAPα appartiennent à la famille des protéines DPP4 et partagent une séquence similaire. Elles reconnaissent et clivent un dipeptide N-ter qui possèdent un résidu Pro ou Ala à l'avant-dernière position; cependant leurs localisations et substrats naturels divergent. DPPIV est une protéase de surface cellulaire possédant une vaste gamme de substrats tels que le peptide type-glucagon-1 [66] et le peptide insulinotropique dépendant au glucose (GIP) [67] dont la dérégulation est impliquée dans le diabète de type 2; le neuropeptide Y [68] dont l'altération dans le SNC peut amener au développement de maladies neurodégénératives [69] ou encore le facteur 1α/β dérivé de cellules stromales. [70,71] L'activité de DPPIV a également été liée à de nombreuses reprises au développement de cancers. [72–74] Au contraire, FAPα Fibroblast activating protein, aussi appelée séprase, est une protéine transmembranaire dont l'activité est plus spécifique. Elle est capable de cliver certaines protéines membranaires pour les relâcher dans la matrice extra- ou intracellulaire, comme par exemple la sérine protéase α2-antiplasmine (α2AP) [75] dont l'activité résulte en la suppression de la fibrinolyse et la régulation de la plasmine et de sa forme inactivée le plasminogène. α2AP est impliquée dans plusieurs pathogénèses cérébro- et cardiovasculaires. [76] FAPα possède également une activité gélatinase qui lui permet de dégrader certaines protéines de la matrice extracellulaire. Cette propriété est de première importance considérant l'impact de FAPα dans la régulation de la progression de tumeurs et métastases, [77] procédé qui dépend de la dégradation de telles matrices.

La PRCP et la DPPII partagent également une forte séquence homologique mais diffèrent dans leurs activités. [65] Alors que la PRCP hydrolyse l'acide aminé C-ter lorsque Pro ou Ala occupe l'avant-dernière position, la DPPII cible les motifs X-Pro et X-Ala du côté N-ter. La PRCP est connue

pour son rôle clé dans le système rénine-angiotensine (RAS) au travers de sa désactivation des peptides vasoactifs angiotensines II et III au travers du clivage de la Phe à la position C-ter.[78] Elle joue également un rôle important dans plusieurs autres domaines. Par exemple, elle participe à la régulation de la production de mélanocortine du SNC et a été identifiée comme cible pour le traitement de l'obésité ou du diabète de type 2, [79] ainsi que dans un ensemble de biomécanismes liés au système vasculaire. [80,81] Bien qu'aucune cible précise n'ait été identifiée dans le cas de DPPII, sa distribution subcellulaire dans de nombreuses parties du corps [82] couplée à son rôle potentiel dans les procédés cataboliques de différentiation cellulaires [60] en font une protéase d'importance. Il a également été proposé qu'elle puisse être associée avec DPPIV dans le développement de maladies auto-immunitaires et que le ratio DPPII/DPPIV puisse servir de mesure afin de détecter certaines maladies telles que la polyarthrite, l'arthrite rhumatoïde ou encore le lupus érythémateux.

POP possède une activité d'endopeptidase sélective d'oligopeptides de 30 acides aminés ou moins. POP hydrolyse les liaisons formées par le carboxyle du résidu proline au site P1. [60] Elle se trouve dans de nombreuses parties du corps telles que les muscles, le SNC, les cellules épithéliales, les fibroblastes et les lymphocytes. Son activité a aussi été liée à certaines interactions protéines-protéines, en particulier dans les mécanismes de signalisations dans lesquelles elle est impliquée, comme la croissance cellulaire, l'apoptose ou les fonctions synaptiques du SNC. [83–85] L'inhibition de PEP a été étudiée dans le contexte de maladies neurodégénératives au travers de son interaction avec la synucléine-α. Il a été montré que celle-ci promeut l'agrégation de la synucléine-α en se liant avec celle-ci. L'agrégation de synucléine-α dans le SNC a été liée au développement de la maladie de Parkinson, l'atrophie multisystémique, et la démence à corps de Lewy. [60] Myöhänen et ses collaborateurs ont montré que l'inhibition de POP réduit l'agrégation de la synucléine-α *in vivo*. [86]

Ainsi, la proline joue un rôle prépondérant pour la reconnaissance de substrat et du site de clivage d'une vaste gamme de protéases. On trouve ces dernières de manière ubiquitaire dans le corps humain et leur dérèglement est impliqué dans de nombreuses conditions dégénératives. Il est à noter que les exemples ci-dessus ne représentent qu'une fraction de l'ensemble des maladies

dans lesquelles les protéases dépendantes à la proline sont impliquées, notamment dans le système immunitaire. [65]

1.1.2.3.3 PPEP (Proline-Proline Endopeptidase 1)

En 2013, Cafardi et ses collaborateurs ont rapporté la présence d'une nouvelle protéase de zinc sécrétée par *Clostridium difficile (C. diff.)* capable de cliver spécifiquement les séquences diproline. [87] Cette nouvelle protéase a par la suite été nommée Proline-Proline Endopeptidase 1 (PPEP-1, Zmp1, CD2830) par Hensbergen et il a montré que son mode d'action est lié au clivage de protéines de surface dont l'expression permet l'adhésion bactérienne sur les parois épithéliales de l'hôte. [88] Les protéines d'adhésions, ou adhésines, sont des facteurs de virulence importants pour la survie des pathogènes afin d'assurer leur protection contre la réponse immunitaire de l'hôte. Dans le cas de *C. diff.,* les adhésines CD2831 et CD3246 lui permettent de former des colonies sur la paroi du lumen et de se recouvrir d'un biofilm pour échapper aux lymphocytes. [89,90] Une fois la phase d'incubation est terminée, *C. diff.* sécrète PPEP-1 dans le milieu extracellulaire pour se libérer de la paroi. La spécificité de PPEP-1 pour la liaison diproline est alors un atout considérable afin de pouvoir remplir son rôle de manière sélective.

Par la suite, une nouvelle PPEP a été découverte in *Paenibacillus alvei (P. alvei)*, nommée PPEP-2, qui est également une protéase d'une protéine de surface cellulaire. Cependant, PPEP-1 et PPEP-2 reconnaissent différentes séquences (VNP↓PVP et PLP↓PVP respectivement) et les substrats peptidiques de l'un n'ont pas été reconnu par l'autre lors d'une étude mécanistique d'Hensbergen. [91]

Il a été proposé que la PPEP-1 puisse être une cible d'intérêt dans le traitement d'infections de *C. diff*, cependant aucun inhibiteur n'a été rapporté jusqu'à maintenant. Un chapitre de cette thèse est dédié au développement de composés peptidomimétiques inhibiteurs de *C. diff.*

1.2 Les motifs polyproline

Les motifs polyproline sont définis comme une séquence de plusieurs prolines consécutives, souvent constitués de trois unités. Bien qu'ils se trouvent généralement au sein de protéines riches en prolines, leur corrélation n'est pas exclusive. Tout comme la proline, les polyproline

jouent un rôle majeur dans l'intégrité structurelle des protéines ainsi que comme motif de reconnaissance pour certaines fonctions protéiques. En raison de leur particularité structurelle, elles peuvent être reconnues par certaines portions protéiques afin de former des interactions réversibles avec celles-ci. Les motifs polyproline sont également impliqués dans les interactions protéines-ADN nécessaire aux mécanismes de transcription. [1,92]

1.2.1 Considérations structurelles

Au sein des motifs polyproline peuvent se former des hélices polyproline I (PP-I) ou polyproline II (PPII). Les acides aminés de PP-I sont caractérisés par des liaisons *cis* et une conformation hélicoïdale tournant dans le sens horaire, alors que les résidus des PPII sont tous en configuration *trans* et adoptent une conformation hélicoïdale anti-horaire. [7] Les hélices PPII possède une forme de prisme triangulaire et représente environ 7% de l'ensemble des résidus protéiques, qui contribuent à la formation de superstructures secondaires sous forme d'hélices enroulées (Figure 1.4). [40] Elles possèdent un tournant hélicoïdal de 9.3 Å/tour, chaque tour comportant trois résidus sous forme d'hélice étendue. Les isomères *trans* ont des valeurs de φ = -75 ° et Ψ = + 145 ° ce qui correspond aux minima énergétiques de la proline.

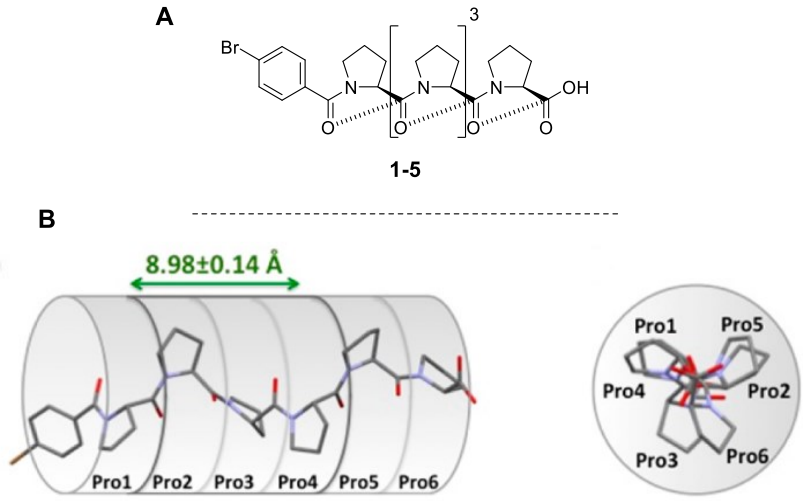

Figure 1.4 A. Structure de l'hexaproline p-Br-C_6H_4-Pro_6-OH **1-5** cristallisée sous forme d'hélice PPII. B. Structure cristalline de **1-5**. [93]

Cependant d'autres résidus peuvent également participer à la formation d'hélices PP-I et PPII. Kumar et ses collaborateurs ont montré que malgré la présence majoritaire du résidu proline au sein de ses hélices certaines positions favorisent également d'autre résidus. [5] Selon la terminaison qu'ils ont établi, *Mid* désigne un ou plusieurs résidus centraux, N1 et C1 les résidus adjacents constituant le cœur de l'hélice et Ncap et Ccap les résidus formant l'extrémité de l'hélice (Figure 1.5 – A). Pro représente une large majorité des positions *Mid* et C1, et est également majoritaire à la position N1 (Figure 1.5 – B).

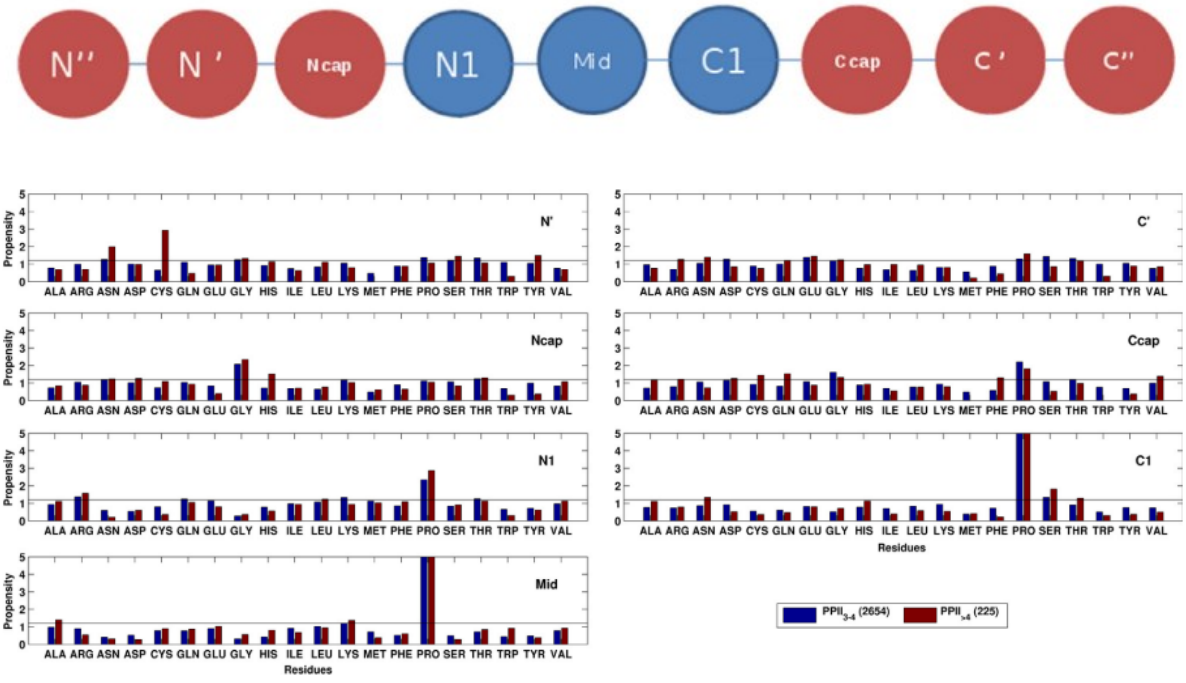

Figure 1.5 A. Dénomination des positions représentatives de l'hélice. N'', N', C', C'' : Résidus adjacents à l'hélice. Ncap, Ccap : Résidus terminaux de l'hélice. N1, C1, Mid : Résidus participant à l'hélice (Mid peut représenter plusieurs résidus pour $PPII_{\geq 4}$). B. Répartition statistique des acides aminés observée pour chaque position au sein des protéines étudiées (2879 hélices PPII au sein de 3582 chaines protéiques). [5]

Les hélices PPII ne forment pas de liaisons hydrogène au sein de la structure dû à l'azote tertiaire; cependant elles sont stabilisées par la donation n → π* de l'oxygène de l'amide vers le carbonyle de l'amide du résidu n+1. Certaines études ont montré que les effets de solvatation affectent la

conformation de l'hélice, notamment au travers des liaisons hydrogène qui peuvent être formées entre la chaine principale et le solvant. [94]

Il a été suggéré que la formation de PPII interrompe les feuillets-β qui ont une tendance à s'agréger et puisse jouer un rôle dans le repliement correct des protéines. [95] Comparée aux autres structures secondaires, on en retrouve une fraction plus importante à la surface des protéines (excepté pour les tournants-β qui marquent souvent l'extrémité d'une chaine). Cela s'explique par leur rôle dans les interactions ADN-protéines, [92] ainsi que leur prépondérance dans la formation de PPI. [92,96] Les hélices PPII sont également utilisées comme site de reconnaissance par les pathogènes afin de pouvoir interagir avec l'hôte durant les mécanismes d'infections. [97]

Les hélices PPII peuvent s'associer en trois brins pour former des triples hélices. En raison des interactions stabilisantes entre les brins qui permettent le maintien de la structure, les acides aminés les composants se doivent de former un motif régulier. Ce motif est composé de trois acides aminés démarrant par Gly. [98,99] Généralement, les deux autres acides aminés sont la proline et la 4-hydroxyproline (4RHyp) (Figure 1.6) car ils permettent une stabilisation de la structure. [98–100] L'exemple le plus commun de protéine contenant des hélices triples est le collagène, protéine structurelle principale de la matrice extracellulaire des tissus humains.

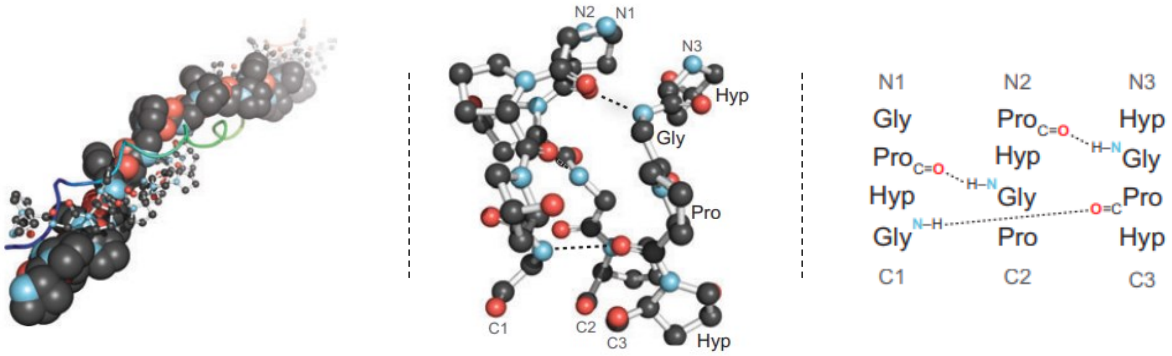

Figure 1.6 A. Vue de l'axe d'une triple hélice $(ProProHyp)_{10}$ avec les trois brins (PDB : 1k6f) représentés sous formes d'occupation de l'espace, de ruban, et d'atomes. B. Vue d'un tronçon de la triple hélice de collagène (HypProGly) (PDB : 1cag(19)). C. Représentation des trois brins de B sous forme de code des acides aminés. [99]

L'intégrité structurelle de l'hélice triple est maintenue par la présence de liaisons hydrogène intermoléculaires entre l'azote de Gly et le carbonyle du résidu X dans le motif tripeptidique (Gly-Xaa-Yaa). (Figure 1.6 – C) Des contributions additionnelles peuvent parfois émerger des chaines latérales. [97] Comme dans le cas des hélices PPII, les chaines latérales des résidus Pro et Hyp sont exposées au solvant, et forment des interactions hydrophobes entres-elles. Les hélices triples sont fortement solvatées et un réseau de liaisons hydrogène s'établit entre l'eau et le caractère donneur ou accepteur des azotes insaturés ou des carbonyles de la chaine principale. D'autres molécules d'eau peuvent également se lier à celles de la première couche et générer des réseaux capables de connecter différentes triples hélices. [101]

La spécificité structurelle du collagène et sa rigidité en font un motif de reconnaissance moléculaire différenciable des hélices PPII utilisé par les pathogènes pour la reconnaissance avec l'hôte. Son abondance au sein des mammifères en fait une cible de choix. La famille du collagène comprend 28 protéines qui contiennent toutes au moins un domaine de triple hélice. [102] La plupart se trouve dans la matrice extracellulaire ou elles forment des assemblages supramoléculaires. Le collagène est impliqué dans la régulation de nombreux mécanismes biologiques incluant la prolifération, la migration ainsi que la différentiation cellulaire au travers de protéines qui interagissent avec le collagène (CIP). [103] Les CIPs sont exprimés par les eukaryotes et les prokaryotes et procurent également des cibles pour les bactéries qui peuvent sécréter des protéines mimant le collagène afin de venir se lier aux récepteurs des CIPs de l'hôte (Figure 1.7). [97]

Ainsi, les motifs riches en prolines (PRMs) peuvent parfois s'organiser sous forme d'hélices PPII, elles-mêmes capables de former les superstructures triple hélice. Ces PRMs sont souvent impliqués dans les interactions protéines-protéines (PPI), car l'absence de stabilisation par liaisons hydrogène intramoléculaires rend la chaine plus flexible. Ces mécanismes biologiques sont cruciaux pour les voies de signalisation et toute interaction nécessitant une réversibilité. Ces interactions sont également d'intérêt pour l'étude des mécanismes infectieux de certains pathogènes ainsi que leur endiguement.

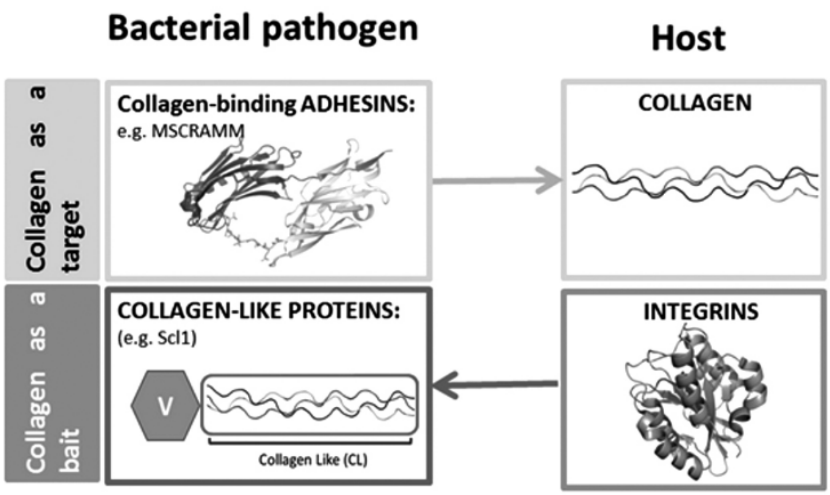

Figure 1.7 Représentation des mécanismes de reconnaissances hôte-pathogènes impliquant le collagène. [97]

1.2.2 Interactions protéine-protéine

Les interactions protéine-protéine (PPI) sont des mécanismes réversibles impliqués dans les voies de signalisation telles que la transduction, le cycle cellulaire ou l'apoptose. Elles dépendent d'interactions réversibles entre des portions spécifiques de deux protéines hautement conservées au cours de l'évolution. Afin d'assurer le succès d'une PPI, le domaine de reconnaissance protéique de la protéine A doit reconnaitre sélectivement la section peptidique de la protéine B associée à sa fonction, et l'interaction doit être réversible afin que les protéines puissent se dissocier une fois le stimulus terminé. [4] Certains domaines sont capables de reconnaitre des motifs phosphorylés comme le domaine Src-homologique 2 (SH2), [104] le domaine liant de la phosphotyrosine (PTB), [4,104] ou le domaine *Forkhead-associated* (FHA). [105] Dans le cas de la proline, ces sections protéiques sont qualifiés de domaines riches en prolines (PRDs) et motifs riches en prolines (PRMs). Les polyprolines agissent comme motif de reconnaissance pour les PPI en raison de leur spécificité structurelle décrite précédemment.

Plusieurs types de PRDs ont été recensés dans le protéome humain, chacun exerçant une fonction précise dans les voies de signalisation. Les mieux étudiés jusqu'à maintenant incluent le domaine SH3 (Src-homologique 3), [106–108] WW (domaine rsp-5 à motif répétitif WWP), [109,110] EVH1 (domaine drosophilia activée/Phosphoprotéine stimulée par les vasodilatateurs 1), [111] GYF

(domaine glycine-tyrosine-phénylalanine), [110,112] UEV (domaine variant E2 de l'ubiquitine), [113,114] et la prolifine. [115] Ball et ses collaborateurs ont recensé un ensemble de critères qui sont observés lors de PPIs. Le PRD se lie au PRM de son ligand au travers d'un ensemble d'acides aminés dont les chaines latérales aromatiques sont exposées à la surface. La liaison avec le PRM implique un ensemble de liaisons hydrogène et d'arrangements coplanaires entre les résidus proline et les cycles aromatiques. (Figure 1.8) Un résidu possédant une large chaine latérale (*e.g.* Arg, Tyr, Phe) situé à une extrémité du PRM sert de point d'ancrage à celui-ci sur le PRD et détermine son orientation. Des résidus additionnels situés sur les côtés du PRM servent à affiner l'ancrage sur le PRD. Les PRDs reconnaissent une séquence de 5-10 acides aminés contenant 3-6 prolines. [4] Il est à noter que malgré la spécificité du mécanisme de reconnaissance, certains PRDs sont capables de reconnaitre plusieurs ligands, ce qui leur permet d'effectuer plusieurs fonctions.

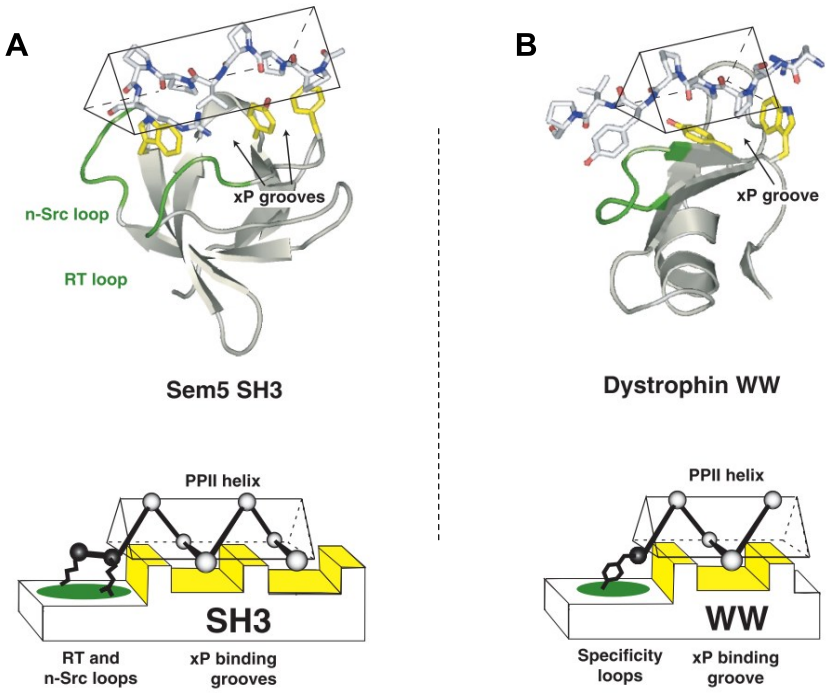

Figure 1.8 Exemples de modes de liaisons entre les PRDs SH3 de Sem5 et WW de la dystrophine et leurs ligands PRMs respectifs. [124]

En raison de leur importance dans les mécanismes de régulation de la physiologie cellulaire, le dérèglement de PPIs de certaines protéines participe à la pathogénèse de nombreuses conditions neurologiques, [116,117] immunitaires, [118] inflammatoires, [119] diabétiques, [120] et cancéreuses.

[32,121,122] Il est à noter que la hausse ou la baisse de l'activité peuvent toutes les deux engendrer de telles pathologies. Par exemple, Pin1 a été pointée pour son implication dans le développement de cancers lors de sa régulation à la hausse, et pour sa participation dans la maladie d'Alzheimer lors de sa régulation à la baisse. [123]

Un chapitre de cette thèse est dédié à la synthèse de peptidomimétiques du PRM de la sous-unité p22*phox* reconnue par le domaine SH3 p47*phox* de NOX2 (Oxidase de nicotinamide adénine dinucléotide phosphate 2) au travers d'un motif mimant la triproline de p22*phox* qui possède une conformation d'hélice PPII. [125]

1.3 La proline en chimie médicinale

La proline a eu diverses applications dans le domaine de la chimie médicinale en tant que mimes de structures secondaires, inhibiteurs de protéases dont celles spécifiques à la proline et inhibiteurs d'interactions protéine-protéine. Afin de donner une vue d'ensemble des prouesses réalisées dans ce domaine, une série d'exemples représentatifs a été sélectionnée pour cette troisième partie. Ceux-ci sont présentés dans le contexte de leur cible thérapeutique.

1.3.1 Composés initiateurs de structures secondaires

1.3.1.1 Tournants-β

En raison de la prépondérance de la proline au sein des tournants-β, plusieurs travaux ont rapporté l'utilisation de prolines modifiées au sein d'oligopeptides afin de favoriser leur formation ou d'influencer quelle classe de tournant est formée. Une des stratégies les plus employées a été l'utilisation de la diproline de configuration D-Pro-L-Pro afin de contraindre les angles (φ,Ψ) en faveur d'un tournant-β de type II'. [126] La proline est normalement inexistante dans ce type de tournant en raison de la nature de ses angles. [36] Robinson a judicieusement utilisé cette diproline comme gabarit au sein d'un peptide cyclique afin de favoriser la formation d'une épingle à cheveux-β sur la base du tournant-β formé par D-Pro-L-Pro. [127,128] Par la suite, cette stratégie a été appliquée à la formation de mimes d'épingles à cheveux-β d'une série d'anticorps. [129] Il a été montré que lorsque la même chaine peptidique que celle tirée de l'anticorps modèle était cyclisée par le gabarit diproline, plusieurs d'entre elles adoptent la conformation canonique

observée au sein des structures cristallines des anticorps (Figure 1.9). Le développement de peptidomimétiques bloqués dans la conformation native de certaines portions de protéines impliquées dans les PPI est d'importance afin de favoriser son affinité avec la cible désirée. L'utilisation de D-Pro-L-Pro a par ailleurs été appliquée avec succès afin d'augmenter la sélectivité d'heptapeptides antagonistes du récepteur NK-2 de la neurokinine. [130] Cette stratégie a été étendue à la synthèse d'analogues portant des groupements méthyle ou trifluométhyle sur différentes positions des cycles pyrrolidine afin de moduler leurs propriétés angulaires et favoriser d'autres types de tournants. [131,132]

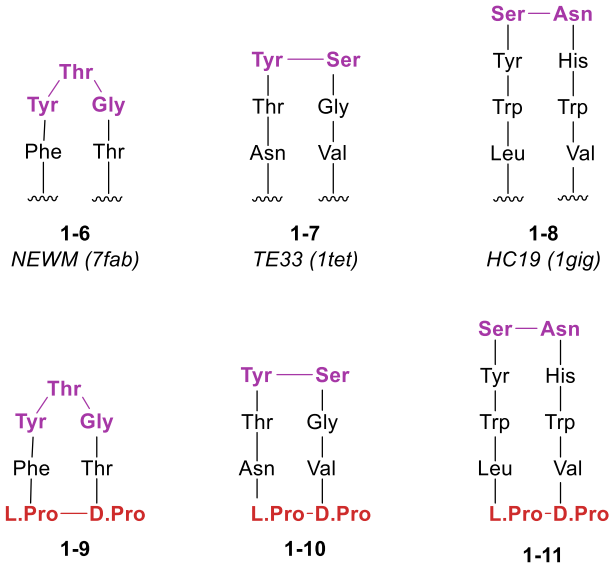

Figure 1.9 Séquences des acides aminés impliqués dans la formation des épingles à cheveux-β des anticorps (**1-6**, **1-7**, **1-8**) et structures des mimes cyclisés par la diproline L-Pro-D-Pro (**1-9**, **1-10**, **1-11**). [129]

L'idée de substituer le cycle a également été appliquée à d'autres séquences peptidiques initiatrices de tournants-β. Koskinen a comparé l'incidence du remplacement d'une Pro par une 4-Me-Pro au sein de tétrapeptides lors de la formation de tournant-β. [133] Il a observé que selon la stéréochimie associée, la présence du méthyle pouvait contrôler l'orientation de la torsion de cycle et ainsi favoriser les angles (φ,Ψ) associés à la formation de tournant-β de type II dans le cas de la (4*S*)-MePro **1-14**. (Figure 1.10 – A) Une analyse par théorie fonctionnelle de la densité (DFT)

utilisant les orbitales de liaison naturelle (NBO) leur a indiqué que la structure secondaire peut être stabilisée par une interaction $n \rightarrow \pi^*$ entre l'oxygène de la liaison amide de la (4*S*)-MePro et le carbonyle de la Gly considérant que l'angle de 107 ° est proche de la trajectoire optimale de Bürgi-Dunitz.

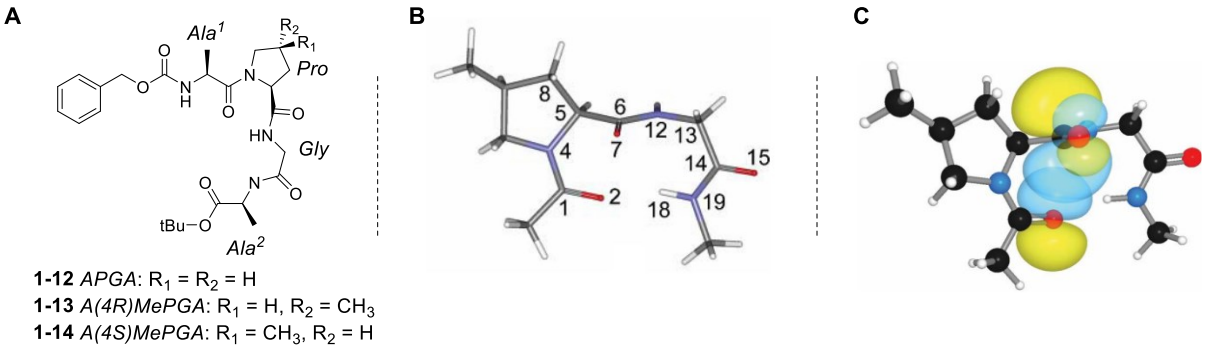

Figure 1.10 A. Structure des tétrapeptides **1-12** à **1-14** initiateurs de tournants-β de type II. B. Géométrie optimisée par B3LYP/6-311++G** du dipeptide (4S)MeProGly. C. Représentation de la contribution n → π* entre O(i) et C=O(i+1) de (4S)MeProGly. [133]

1.3.1.2 Hélices

La propriété intrinsèque des prolines à former des points de nucléation pour la formation d'hélices α a été utilisée pour la synthèse de gabarits induisant de telles structures secondaires. La formation d'hélices-3_{10} a été initialement rapportée par Balaram [134] au travers d'un tripeptide Piv-Pro-Pro-Gly-NHMe **1-15** (Figure 1.11 – A). Il a suggéré que la formation de l'hélice est promue par la présence des résidus proline contigus. Cependant, la possibilité que la chaine libre puisse s'isomériser et induire la présence de multiples conformères a poussé certains chercheurs à synthétiser des variations dont la conformation a été restreinte à l'aide d'une contrainte structurelle. Par exemple, Kemp et ses collaborateurs ont développé un gabarit synthétique **1-16** basé sur la diproline dont les deux cycles pyrrolidine sont liés par un pont sulfure (Figure 1.11 – B). [135] Ce gabarit a résulté en la formation exclusive de conformères initiateurs d'hélices-α et leur a permis d'étudier l'influence du paramètre de propagation sur la formation d'une hélice. D'autres exemples de gabarit polycycliques rigides pour la formation d'hélices ont également été documenté par d'autres groupes. [136–139]

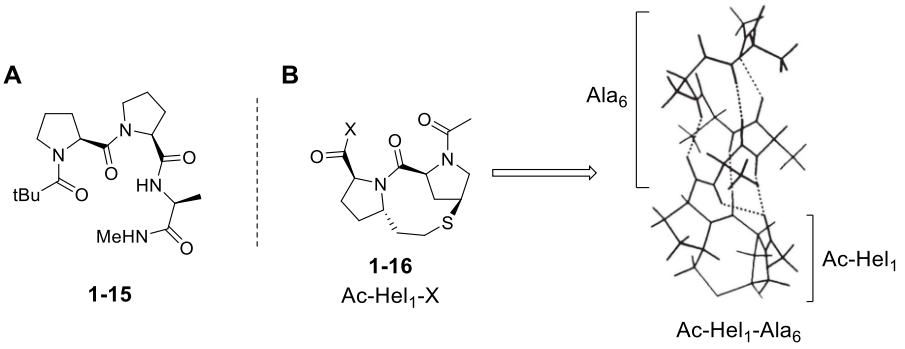

Figure 1.11 A. Piv-Pro-Pro-Ala-NHMe **1-15** utilisé pour la formation d'hélices 3_{10}. B. Gabarit tricyclique **1-16** développé par Kemp pour la formation exclusive d'hélices α. [135]

En raison de la tendance des polyprolines à former des hélices polyproline I et II, plusieurs exemples d'oligomères dérivés de polyprolines ont également été rapporté dans lesquels la nature électronique, la stéréochimie ainsi que la nature du solvant a impacté la conformation de la structure secondaire. [140,141] Un exemple rapporté par Kümin en 2007 a montré que l'insertion d'un groupement azidure en position 4 de la proline ((4*R*)Azp) a stabilisé la formation de l'hélice PPII d'oligoprolines contrairement à la configuration 4*S* (Figure 1.12 – A). [141] Les auteurs ont par la suite été capables de conserver l'hélice PPII lorsqu'ils ont fonctionnalisé ces azidures par cycloaddition [3+2] avec différents alkynes, ouvrant de nouvelles perspectives pour les stratégies associées à la synthèse de composés thérapeutiques nécessitant une conformation PPII ainsi que certains groupements fonctionnels. Un autre exemple a été rapporté par Hanessian et ses collaborateurs dans lequel des oligomères d'homo-méthanoprolines *cis* ont adopté la forme d'hélices PPII (Figure 1.12 – B). [142] Comme Koninsken, ils ont démontré la présence d'une participation $n \rightarrow \pi^*$ entre l'oxygène de la liaison amide donneur et le carbonyl de l'ester accepteur au sein des dimères et trimères avec une préférence pour l'isomère *cis/cis*. La cristallisation du tétramère **1-18** a révélé une structure hélicoïdale selon une symétrie C_3, et un pitch hélicoïdal de 9.1 Å, en accord avec les paramètres observés dans la Nature. Il est à noter que l'isomère *trans* n'a pas été capable d'adopter une telle géométrie, ce qui est redondant avec les résultats observés dans le cas de l'azidoproline.

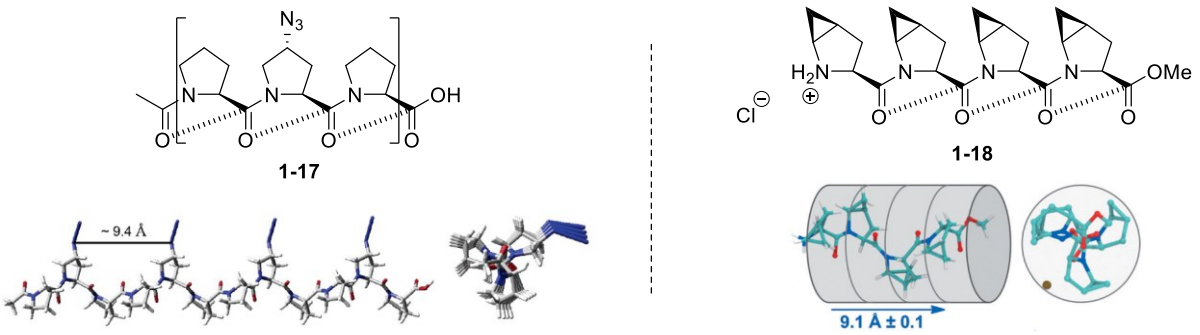

Figure 1.12 A. Motif polyproline **1-17** contenant une (4R)Azp chaque trois résidus et représentation de la forme cristalline d'un dodécamère. [141] B. Tétramère de méthanoprolines cis **1-18** et représentation de la forme cristalline. [142]

Dans les deux cas, les auteurs ont mis en avant que le réglage de la stabilisation d'hélices PPII à l'aide d'insertion de prolines stabilisantes ou déstabilisantes puisse permettre d'en apprendre plus sur l'impact des PPII dans le repliement de la protéine ou sa participation au sein d'un mécanisme biologique.

1.3.2 Composés thérapeutiques basés sur la proline

La proline a inspiré les chimistes pour le développement de composés thérapeutiques. Que ce soit sous forme de petites molécules ou de peptidomimétiques, des inhibiteurs de différentes protéases dont celles spécifiques à la proline ont été ciblés dans ce domaine, ainsi que la perturbation des interactions protéine-protéine.

1.3.2.1 Inhibiteurs de protéases

Captopril **1-19** a été découvert par Cushman et Ondetti et breveté par Bristol-Myers Squibb en 1976 comme inhibiteur de l'enzyme de conversion d'angiotensine-1 (ACE) (Figure 1.13). [143] ACE est une enzyme qui joue un rôle important dans la régulation de la pression cardiaque par catalyse du peptide angiotensine I vers l'angiotensine II, capable d'augmenter la contraction des vaisseaux sanguins. ACE catalyse aussi l'hydrolyse d'autres peptides comme la bradykinine. [144] Les inhibiteurs d'ACE sont utilisés en cas de maladies cardiovasculaires telles qu'une hausse de pression sanguine, insuffisance cardiaque, la maladie des artères coronaires et l'insuffisance rénale. ACE est composé de deux domaines (domaine N- et C-) qui peuvent être inhibés;

cependant le domaine C- est principalement responsable de la régulation de la pression sanguine. L'idée initiale de Cushman et Ondetti lors du développement de Captopril **1-19** pour l'inhibition du domaine C- était que son mécanisme d'action ressemblait celui de l'enzyme carboxypeptidase A, métalloprotéine de zinc du pancréas bovin, qui peut être inhibée avec des composés similaires à Captopril. [145,146] Par la suite, des études de cristallisation ont montré que la proline occupe une poche hydrophobe et le thiol est lié au zinc. La stéréochimie de la proline est déterminante pour une bonne orientation du cycle dans la poche hydrophobe. [147,148] D'autres composés partageant une structure similaire tels que Enalapril **1-20**, Ramipril **1-21**, Lisonopril **1-22** [149] et Fosinopril **1-23** [150] ont émergé sur le marché, dans lesquels le carboxylate ou phosphate généré *in vivo* chélate le zinc. Depuis, d'autres analogues ont été développés, [149] dont une version contrainte par Hanessian qui a obtenu une activité comparable lorsque la proline a été remplacée par une série de méthanoprolines **1-24**. [151] Les méthanoprolines ont également été utilisées dans plusieurs autres contextes médicinaux, [147] notamment pour le développement d'inhibiteurs de la DPPIV. [152,153]

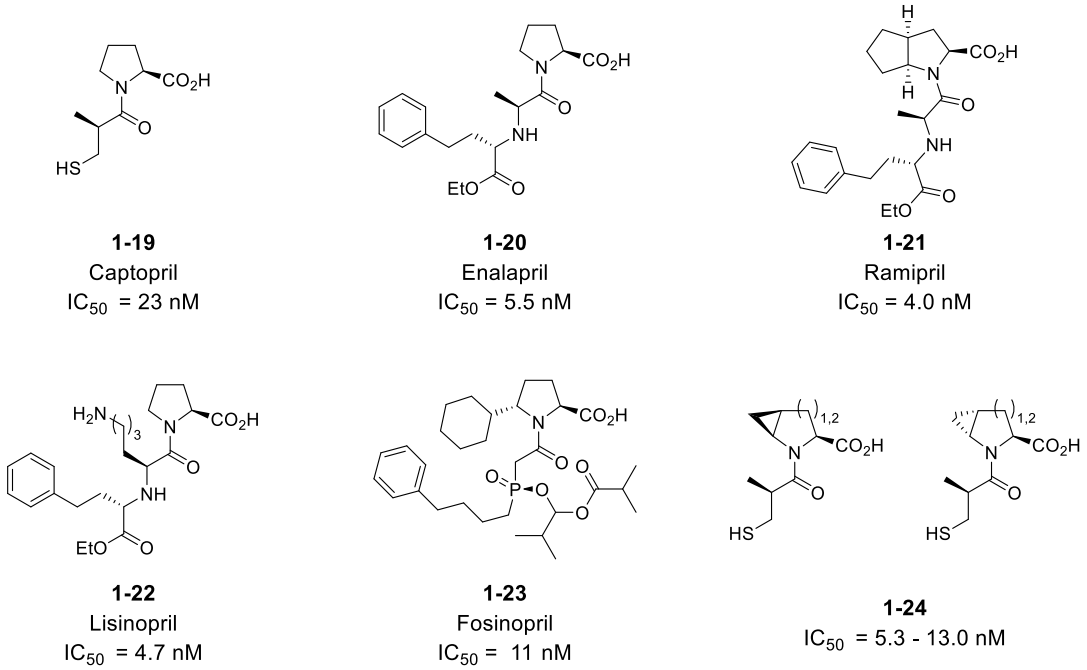

Figure 1.13 Captopril et autres inhibiteurs d'ACE. [149,151]

Plusieurs composés peptidomimétiques basés sur la proline ont également été développés. Un exemple a été rapporté par Hanessian dans lequel il a synthétisé une classe d'inhibiteurs

bicycliques de la thrombine dérivée de la triade peptidique D-Phe-Pro-Arg correspondant à celle du fibrinogène, son substrat naturel. [154] La thrombine est une protéase à sérine impliquée dans la coagulation du sang et son disfonctionnement mène à un ensemble de maladies cardiovasculaires. [155,156] L'objectif de cette étude a été de contraindre la portion gauche du peptide dans la conformation du site actif à l'aide d'un noyau indolizidone. Ces études ont culminé en la synthèse de **1-26**, qui est actif à l'ordre du nanomolaire (IC_{50} = 20 nM) (Figure 1.14 – A). Une structure cristalline a été obtenue dans laquelle la superposition de **1-26** avec D-Phe-Pro-Arg **1-25** a montré un bon recouvrement. Il est à noter que l'extrémité benzylique gauche du peptide a montré une déviation due à l'encombrement stérique généré par le cycle. [154,157] Nöteberg a également contribué dans ce domaine en synthétisant des analogues des inhibiteurs de la thrombine Inogatran **1-27** et Melagatran **1-28** (Figure 1.14 – B). [158]

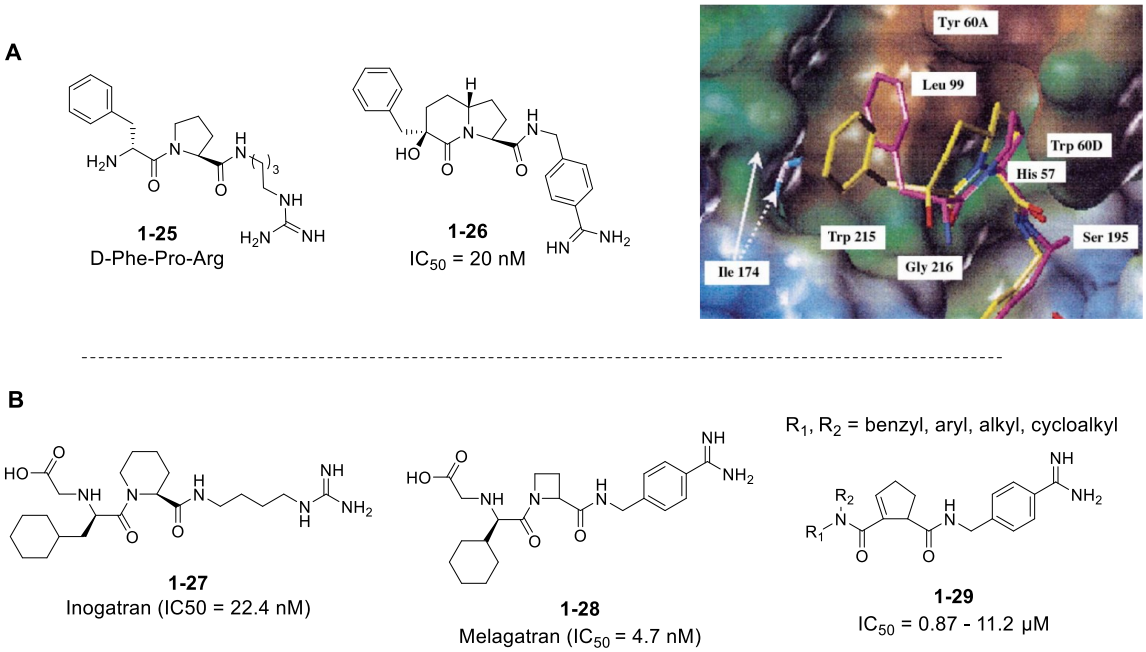

Figure 1.14 A. Inhibiteur de la thrombine **1-26** et son co-cristal avec la thrombine. [154] B. Structure des inhibiteurs Inogatran **1-27** et Melagatran **1-28** et structure générique **1-29** des analogues développés par Nöteberg. [158]

Ces composés ont été conçus sur la base de la séquence D-Phe-Pro-Arg. Dans les inhibiteurs développés par Nöteberg, différentes amines lipophiliques remplacent Phe à la position P1, un cyclopentane ou cyclopentène remplace la proline en P2 et une benzyle amidine remplace P3-Arg

(Figure 1.14 – B, **1-26**). Plusieurs de ces composés se sont révélés être actifs à l'ordre du µM et un exemple de **1-29** a été co-cristallisé dans le site actif de la thrombine. Le remplacement du cycle pyrrolidine de la proline par un cyclopentane est une stratégie qui a été utilisée à plusieurs reprises.

Etzkorn a judicieusement utilisé un cyclopentane dans la synthèse de mimes de la séquence reconnue par Pin1. [159] L'isomérase Pin1 reconnait les séquences peptidiques phosphorylées pSer-Pro et pThr-Pro qu'elle isomérise, [160] et il est d'intérêt pour la conception d'inhibiteurs de savoir si une conformation est favorisée par la protéine lors de son mode de liaison. Cependant, la proline ayant une proclivité à se trouver sous forme d'équilibre *cis*/*trans* au sein de petits peptides, il est difficile d'évaluer avec une chaine libre quelle est la participation de chaque isomère dans son mode de liaison. Par conséquent, Etzkorn et ses collaborateurs ont synthétisé deux peptidomimétiques dans lesquels la liaison amide des résidus Ser-Pro a été remplacée par un *exo*-cyclopentène dans lequel la configuration de la liaison est figée et dictée par la géométrie de l'alcène. (Figure 1.15) Les chaines latérales aromatiques N-ter et basique C-ter ont été sélectionnées sur la base de la sélectivité de Pin1. [160] Lorsque testé pour l'inhibition de Pin1, l'isomère *cis* **1-31** s'est révélé 21 fois plus actif que l'isomère *trans* **1-32**. Ce résultat a permis d'identifier quelle conformation était reconnue préférentiellement par Pin1 et valider : 1) l'intérêt d'un peptidomimétique dont la conformation est figée; 2) la validité du cyclopentane comme remplacement de l'unité proline lors de l'insertion d'un alcène.

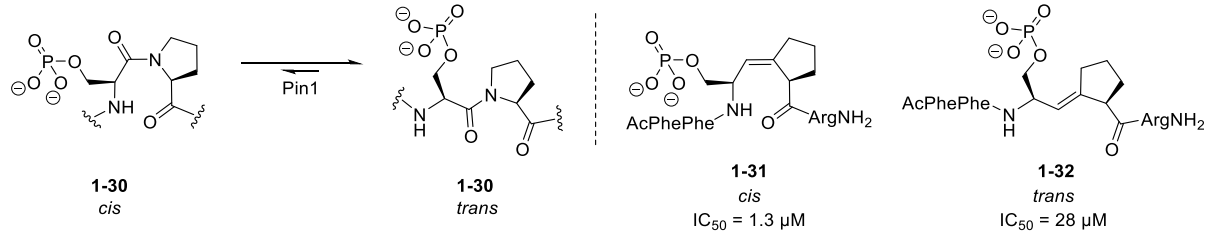

Figure 1.15 A. Conversion *cis/trans* de la liaison pSer-Pro du substrat de la Pin1 **1-30**. B. Peptidomimétiques **1-31** et **1-32** de configuration bloquée synthétisés par Etzkorn. [159]

Un des chapitres de cette thèse est dédié à la synthèse d'un nouveau dimère mime de la diproline incluant une unité cyclopentane.

Lors de la conception d'inhibiteurs de la POP, le premier exemple basé sur la proline à avoir été rapporté a été le Z-Pro-Prolinal **1-33** (Figure 1.16 – A). [161] Son affinité nanomolaire a été rationalisée sur la base de sa fonction en tant qu'inhibiteur d'état de transition de l'enzyme. L'observation de l'hémiacétal formé avec le résidu catalytique Ser554 lors de sa co-cristallisation avec la POP a confirmé le mode de liaison covalent. [162] Par la suite, plusieurs inhibiteurs ont été synthétisés sur la base de **1-33**, et certains d'entre eux ont permis d'obtenir une activité plus basse. [60] Cependant, le remplacement de la proline à la position P2 est resté difficile en raison de son rôle majeur dans la stabilisation du substrat. Sa substitution par un groupement cyclopentane à fait le sujet de plusieurs études [163,164] dont deux exemples sont présentés dans la Figure 1.16. [165,166] Wallén a rapporté une série de dipeptides dans lesquels il a fait varier plusieurs paramètres. Pour chaque paramètre, une version diproline **1-34** et une version mime **1-35** dans lequelle P2 a été remplacée par un cyclopentène ont été synthétisés (Figure 1.16). Lorsque testés pour l'inhibition de la POP, les composés des deux séries ont présenté une activité, une affinité et une lipophilicité comparables. [165] Il est à noter que la position de la double liaison du cyclopentène a influé l'activité des mimes de cyclopentène, mettant en avant l'importance de la géométrie du cycle afin de pouvoir interagir favorablement avec le site actif (Figure 1.16 – B).

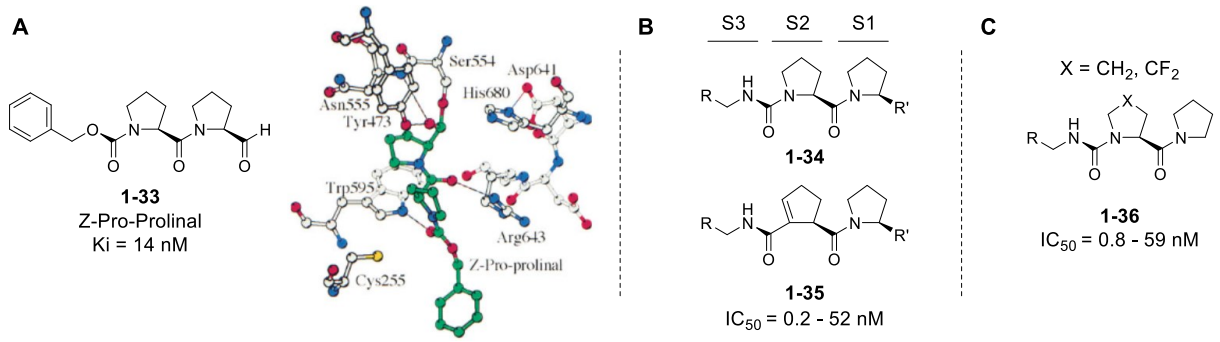

Figure 1.16 A. Structure de Z-Pro-Prolinal **1-33** et son mode de liaison dans le site actif de POP. [161] B. Structures génériques **1-34** et **1-35** des inhibiteurs développés par Wallén. [165] C. Structure générique **1-36** des inhibiteurs développés par Hermecz. [166]

Plus tard, Hermecz et ses collaborateurs ont également synthétisé des analogues de diprolines **1-36** dans lesquelles la chaine amide de la position P3 a été variée en longueur et en nature, et certains d'entre eux ont présenté une activité de l'ordre du nanomolaire. Il est à noter que suite

à la co-cristallisation de certains de leurs analogues ils ont observé que lorsque CH_2 à la position C4 est remplacé par CF_2, une liaison hydrogène faible s'établie avec Tyr473 et résulte en un mode de liaison renforcé avec le site actif (Figure 1.16 – C). [166] L'utilisation de motifs peptidomimétiques incluant une proline ou une diproline ont également été d'intérêt pour la conception d'inhibiteurs de la PRCP. [79]

L'inhibition des aminopeptidases (AP) a également été un sujet d'intérêt. Celles-ci sont une classe de protéine importantes dans le traitement des peptides par leur clivage d'un à trois acides aminés situés du côté N-ter de la chaine peptidique. [167] On les trouvent principalement dans le foie, les intestins, et le placenta. Parmi les substrats des aminopeptidases se trouvent certains neuropeptides hormonaux, l'angiotensine 3, les kinines, et certains antigènes de surface cellulaire. Les aminopeptidases sont également impliquées dans la physiologie cellulaire, la régulation de la pression sanguine, et l'angiogénèse. [168] Les aminopeptidases étant des métalloenzymes de zinc, la chélation du centre métallique a été au centre de la conception de ses inhibiteurs. [169–171] Parmi eux, la probestin **1-38** est un peptidomimétique de séquence (2*S*,3*R*)-3-amino-2-hydroxy-4-phényle-butanoyle-L-leucyl-L-prolyl-L-proline dérivé de la bestatin **1-37** qui possède une activité de 60 nM contre AP-N (Figure 1.17). [172]

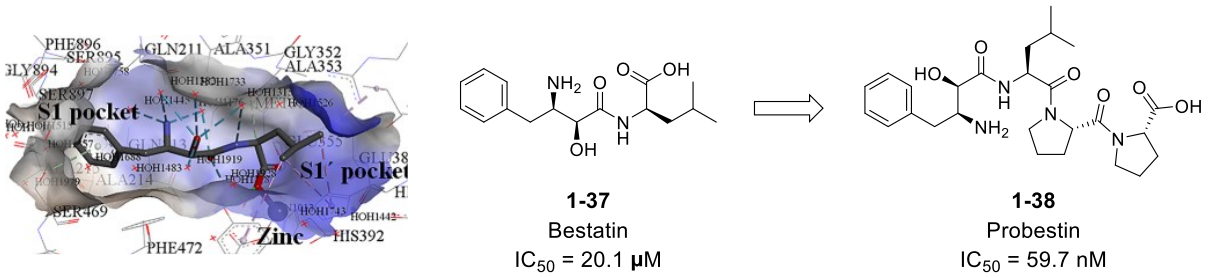

Figure 1.17 Structure de la Bestatin **1-37** et Probestin **1-38** et représentation du co-cristal de la Bestatin dans le site actif d'AP-N. [172,173]

Lorsque comparé à la structure de la Bestatin qui a été co-cristallisée avec l'enzyme, la faible IC_{50} de **1-38** vient de sa spécificité de sa chaine latérale hydrophobe qui vient occuper les poches des sites S1', S2' et S3' qui présentent des résidus hydrophobes (Phe, Leu, Val). [167] Il est à noter que Bestatin est plus active contre les aminopeptidases AP et B. [172]

De nombreuses autres classes d'inhibiteurs incluent une proline dont les propriétés structurelles sont impliquées dans la stabilité du substrat, et ce, pour diverses protéases. Celles-ci incluent les protéases à sérine NS3 (protéine non structurale 3, virus de l'hépatite C), la thrombine, l'élastase, la tryptase et la trypsine; la protéase à cystéine cathepsine B; la protéase activée au calcium calpaïne; et la protéase VIH-1 dont Leung et ses collaborateurs ont fait un rapport détaillé. [174]

1.3.2.2 Inhibiteurs de PPI

L'inhibition des PPI a suscité un intérêt ces dernières années suite à l'élucidation de leurs mécanismes et fonctions dans les voies de signalisation régulant la physiologie cellulaire. Leur dérèglement est à l'origine de nombreuses pathologies telles que des maladies génétiques dues à la mutation de domaine de reconnaissance, ainsi que certains mécanismes infectieux de virus. [175] Le développement de tels inhibiteurs présentent de nombreux défis en raison de la nature de l'interaction protéine-protéine comparée à l'inhibition d'un site actif d'une protéase; cependant certains succès ont été rapportés et plusieurs composés ont été mis sur le marché ou sont en phase clinique. [176]

Bien que les contributions de composés basés sur la proline restent éparses, quelques exemples font état de son potentiel dans ce domaine d'application. Par exemple, des composés mimes du deuxième activateur mitochondrial des caspases (Smac) en phases cliniques incorporent une unité proline (Figure 1.18 – A, GDC-0152 **1-39**, LCL-161 **1-40**, et AT-406 **1-41**). Ces composés ont un potentiel d'action pour l'apoptose des cellules cancéreuses. Celles-ci sont capables d'engendrer de multiples mutations au sein des protéines de signalisation afin d'évader les mécanismes d'apoptose, [177] qui sont régulés par un ensemble de protéines qui vont agir en amont des protéines apoptotiques. Dans le cas présent, les protéines inhibitrices d'apoptose (IAPs) nommées XIAP et cIAP1 peuvent être régulées à la hausse par les cellules oncologiques afin d'inhiber l'action des protéines apoptotiques caspases. Cependant, elles sont elles-mêmes dépendantes de Smac. Son action ou celle de ses mimétiques engendre la dégradation des cIAPs et restaure l'activité apoptotique des caspases. Smac étant un dimère capable de se lier à deux protéines IAP, des composés dimériques tels que AEG-40730 **1-42** et Birinapant **1-43** ont également été développés (Figure 1.18 – B). [175,178]

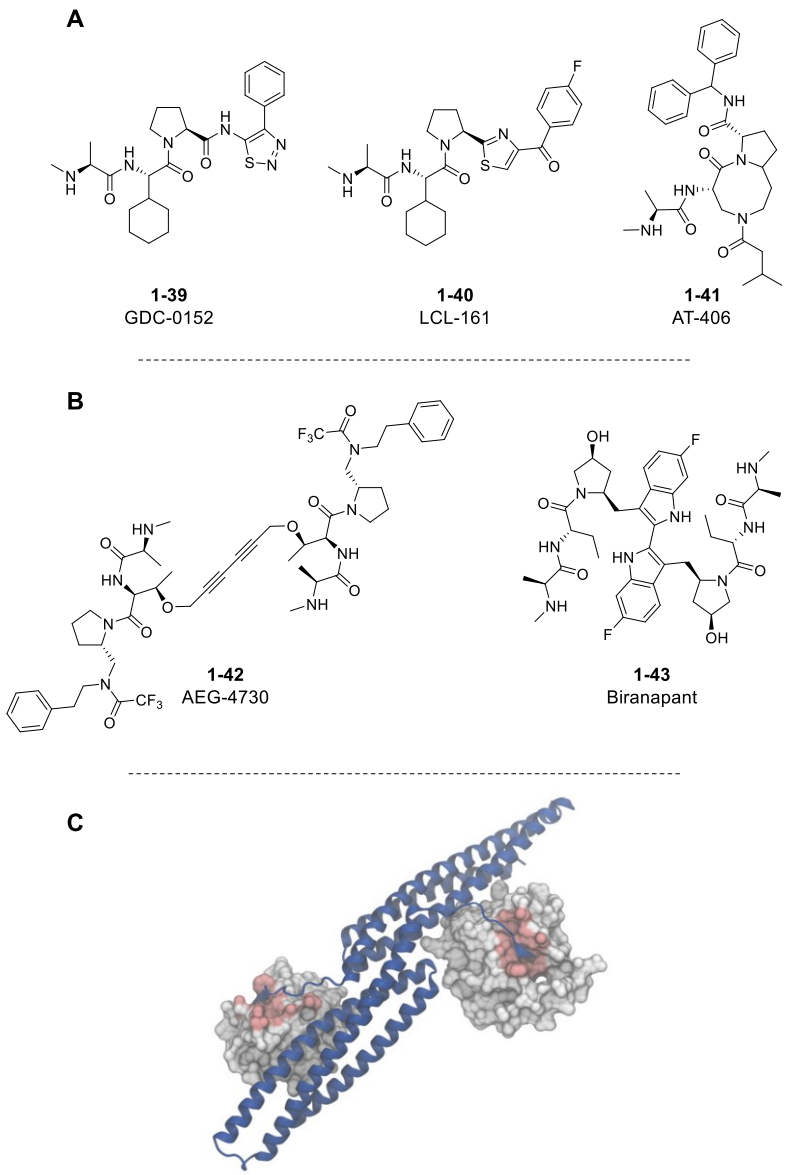

Figure 1.18 A. Structures des mimes de Smac monomériques GDC-0152 **1-39**, LCL-161 **1-40**, et AT-406 **1-41**. [175] B. Structure des mimes de Smac dimériques AEG-40730 **1-42** [175] et Birinapant **1-43**. [178] C. Structure cristalline du complexe dimérique Smac lié à deux protéines XIAP BIR3 (PDB : 1G73). [175]

Un autre exemple de design significatif a été rapporté par Schmalz. A l'aide d'un pont éthylénique, il a rigidifié un ensemble de diprolines fusionnées ou spirocycliques dans une conformation semblable à celle de l'hélice PPII (Figure 1.19 – A). Ces mimes de diprolines ont ensuite été insérés dans différentes séquences peptidiques visant à reproduire les PRMs reconnus par les PRDs Fyn-

SH3, [179] et Ena-VASP 1 (Phosphoprotéine stimulée par les vasodilatateurs Ena 1, EVH1). [180,181] Après une rigoureuse optimisation, ces travaux ont résulté en la synthèse du composé **1-48**, qui possède une affinité pour l'homologue de la protéine activée EVH1 (ENAH EVH1) à l'échelle du nanomolaire (K_d = 120 nm). [181] Qui plus est, plusieurs de ces composés ont été co-cristallisés avec la protéine ce qui a permis aux auteurs de comparer les points d'ancrages des différents peptidomimétiques avec la poche de EVH1. Ces composés se sont montrés sélectifs en faveur du domaine de EVH1 comparés aux PRDs d'autres protéines (Fyn SH3, prolifine, WW) et ont endigué l'extravasation de cellules cancéreuses du sein *in vivo*. Ces travaux pionniers mettent en valeur l'intérêt que peut receler la conception de mimes de prolines riches pour l'inhibition sélective et compétitive de PPI au travers de leurs interactions avec les PRDs ciblés.

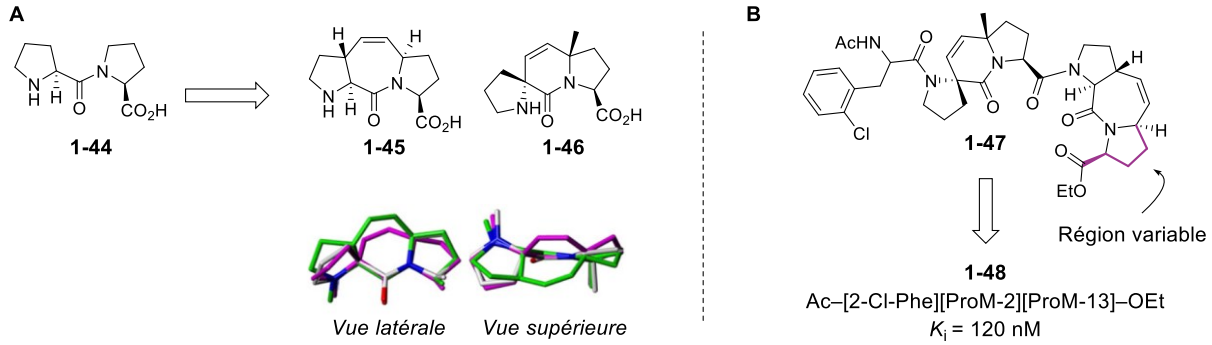

Figure 1.19 A. Représentation des mimes de diprolines contraints fusionnés **1-45** et spirocyclique **1-46** et superposition des géométries optimisées des composés **1-45** (vert) et **1-46** (violet) avec la diproline **1-44** (blanc). B. Structure générique **1-47** des inhibiteurs de ENAH EVH1 et séquence du composé de tête **1-48**. [181]

Une autre approche dans l'inhibition de PPI consiste à activer la protéine responsable de la PPI. Un exemple de cette stratégie a été rapporté par Hanessian et Edinger dans lequel une série d'études a été focalisée sur l'activation de la protéine phosphatase 2A (PP2A) par des dérivés de sphingolipides contraints. [182] Ils ont montrés qu'au travers de l'activation de PP2A, l'apport de nutriments externes et la dégradation de nutriments internes étaient interrompus, menant à l'affamement des cellules cancéreuses. [183] Bien que la façon dont PP2A est activée par SH-BC-893 **1-50** demeure élusive, il est notoire que celle-ci est un acteur principal dans les voies de signalisation et qu'un ensemble de PPIs résultent de son activation. [184] Il est à noter que dans ces

études, l'intérêt du cycle pyrrolidine sert à contraindre la structure afin de la rendre sélective pour PP2A. En effet, le composé parent FTY720 **1-49** dont est dérivé SH-BC-893 **1-50** est phosphorylé *in vivo* et provoque une bradycardie qui proscrit son utilisation à la concentration requise a pour son activité sur PP2A (Figure 1.20). [182]

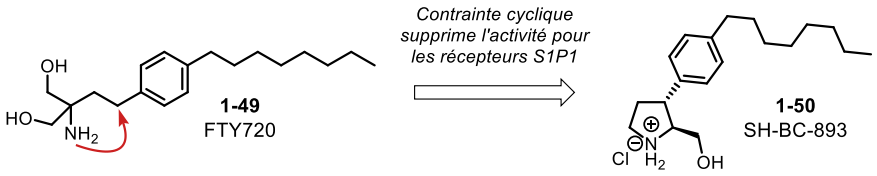

Figure 1.20 Structure du sphingolipide FTY-720 (Fingolimod) **1-49** et son analogue contraint SH-BC-893 **1-50**.

PP2A possédant plusieurs homologues responsables de son activité sur différentes voies de signalisation, il a été émis l'hypothèse que SH-BC-893 puisse être optimisé afin de cibler plusieurs isoformes et interférer avec plusieurs voies de signalisation impliquées dans le développement des cellules cancéreuses. Un chapitre de cette thèse est dédié à la conception de ses composés.

1.4 Conclusions

La proline se distingue des autres acides aminés en raison de ses propriétés structurelles. Aussi bien au sein des protéines que des peptides, elle impacte leur conformation ainsi que leur fonction. Son application en chimie médicinale est large et continue de s'étendre au travers des efforts réalisés dans divers domaines.

Au sein de cette thèse, un ensemble d'applications ont été étudiées et sont rapportées. Les deux premiers chapitres sont centrés sur l'utilisation de la proline au sein de petites molécules. Le premier chapitre est dédié à l'utilisation du prolinal dans la conception de composés modulant les voies de signalisation résultant de l'activation de PP2A. Le deuxième chapitre présente une libraire de prolines bicycliques pontées recelant un motif acide gamma-aminobutyrique.

Les deux chapitres suivants focalisent sur l'aspect peptidomimétique de la proline. Le troisième chapitre présente la synthèse d'un nouveau module dimérique mime de la diproline dans lequel un noyau pyrrolidine a été remplacé par un cyclopentane et la liaison amide a été substituée par

un groupement hydroxylé. L'étude structurelle par RMN du proton est rapportée. Le quatrième chapitre décrit deux applications au travers de cibles biologiques. La première décrit la conception de peptidomimétiques mimant le PRM de la sous-unité $p22^{phox}$ de NOX2 impliqué dans l'assemblage de la protéine au travers d'une PPI avec le PRD de la sous-unité $p47^{phox}$. La deuxième concerne la synthèse de peptidomimétiques pour l'inhibition de la protéine de virulence PPEP-1 sécrétée par *C. diff.*.

Chapitre 2. SH-BC-893 : Un mime de FTY720 contraint comme agent anticancéreux

2.1 Introduction

La lutte contre le cancer est un des défis majeurs des sciences médicinales et cette maladie continue de représenter une des causes principales de décès chez l'Homme. [185] Malgré les moyens considérables déployés pour le développement de thérapies curatives, les traitements actuels restent lourds pour les patients et peuvent engendrer un ensemble de réactions secondaires chez l'hôte, notamment immunologiques. [186] Le coût engendré par les soins est également une préoccupation pour les patients des pays développés, [187] et peut les rendre inaccessibles dans les pays en voie de développement. [188–190] Un des obstacles majeurs rencontrés lors du développement de nouvelles thérapies contre les cellules malignes réside dans leur diversité et leurs génomes prompts aux mutations qui favorisent le développement de mécanismes d'évasion et de résistance. [191,192] Par conséquent, les traitements actuels tels que la radiothérapie visent souvent à détruire un ensemble de cellules d'une région ciblée, avec des conséquences graves pour le patient. [193–197] Plus récemment, des solutions alternatives comme l'immunothérapie [198] ou les thérapies moléculaires ciblant le métabolisme forcé des cellules oncologiques [199–201] ont été proposées, ces dernières présentant l'avantage de tirer profit d'une propriété partagée par l'ensemble des tumeurs.

La capacité des cellules malignes à se répliquer à un rythme effréné réside dans la nature de leur métabolisme. [202] Afin d'alimenter leur division cellulaire, les mutations favorisent l'expression des gènes impliqués dans l'acquisition de nutriments comme ceux des transporteurs de glucose et d'acides aminés, [203–205] ou des récepteurs de lipoprotéines à faible densité (LDL). [206,207] Les tumeurs à Ras activé peuvent également acquérir de la biomasse via macropinocytose. [208] Lors d'un stress énergétique important, les cellules mutées puisent dans la dégradation de matériel cellulaire par autophagie comme source additionnelle de nutriments. Si de multiples interférences surviennent durant les processus de recrutement, elles ne peuvent pas subvenir à

leur rythme métabolique accru et périssent. Par conséquent, le ciblage de l'apport de ces nutriments comme apex de la cascade anabolique nécessaire à leur survie ainsi qu'à leur réplication représente une approche générale recelant le potentiel de surmonter la résistance associée à leur diversité ainsi qu'à leur génome mutatif. [209,210]

Ce concept a été étudié par Edinger à l'aide de sphingolipides dont le médicament FTY720 (Fingolimod, Gilenya). [205,211] Ces derniers ont provoqué l'internalisation de récepteurs d'acides aminés et de glucose au travers de l'activation de la protéine phosphatase 2A (PP2A) et entrainé l'affamement des cellules ciblées. Cependant, la concentration requise pour l'activité antitumorale de FTY720 induit également un état bradycardiaque au travers de l'activation des récepteurs S1P. [212] En effet, FTY720 est une prodrogue commerciale prescrite contre la sclérose en plaque dont l'effet immunosuppressif désiré est lié à l'activation de ces récepteurs. [213] Lorsque consommé, FTY720 va être phosphorylé par la sphingosine kinase 2 (SphK2) et diminuer l'expression du récepteur S1P1. (Figure 2.1 – A) Cela va engendrer la séquestration des lymphocytes dans les nodules lymphatiques et réduire l'inflammation causée par la réponse excessive du système immunitaire. [214] Etant donné que ces deux effets ne dépendent pas du même récepteur, des études d'optimisation de FTY720 ont été réalisées afin de proposer un composé dénué d'affinité pour les récepteurs S1P qui ont culminé dans la synthèse du composé SH-BC-893.

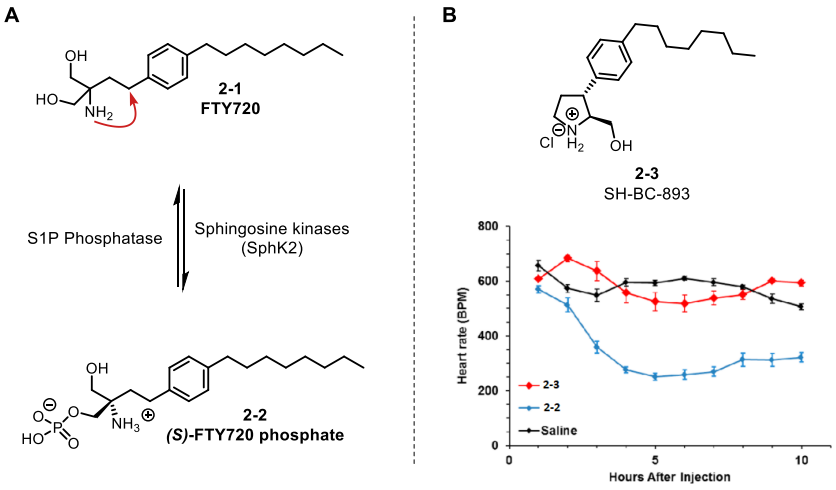

Figure 2.1 A. FTY720 **2-1** est une prodrogue stéréosélectivement phosphorylé par la sphingosine kinase 2. B. Structure de SH-BC-893 **2-3** et impact de sa contrainte tridimensionnelle sur l'effet bradycardiaque de FTY720. [182]

(Figure 2.1 – B) [182,215–217] SH-BC-893 est un dérivé azacyclique dans lequel la tête polaire de FTY720 a été contrainte à l'aide d'un cycle pyrrolidine et où l'un des deux alcools a été supprimé. Ces modifications structurelles ont eu pour conséquences de le rendre inerte aux récepteurs S1P et d'éliminer l'effet bradycardiaque de FTY720 tout en maintenant son activité envers PP2A. [182] PP2A est une serine/threonine phosphatase (PSTP) hétérotrimérique impliquée dans la régulation de divers processus physiologiques et cellulaires tels que la stabilisation neuronale, la fonction cardiaque et le cycle cellulaire. [184,218] La famille des PSTPs représente 98% de l'activité de phosphorylation du corps humain et est divisée en trois catégories selon le mécanisme observé. [219] Chaque catégorie possède une structure qui est conservée au travers de l'ensemble des phosphatases qui la compose. Les phosphoprotéines phosphatases (PPPs) représentent la catégorie la plus large des trois, [184] incluant sept classes dont PP2A. PP2A peut effectuer sélectivement ses diverses fonctions biologiques au sein du corps humain en raison de son ample variété d'holoenzymes hétérotrimériques ($\simeq$400), [220] et son activité dans les processus de signalisation cellulaire est régulée par son activation au travers de l'assemblage de ses sous-unités. [184] Récemment, PP2A est devenu une cible pour le développement de thérapies ciblées contre le cancer en raison de son rôle dans la régulation de l'activité de protéines de signalisation oncologiques. [221–225]

Hanessian et Edinger ont montré que SH-BC-893 provoque l'internalisation des récepteurs d'acide aminés 4F2hc et de glucose GLUT1 ainsi qu'une diminution des récepteurs de LDL via l'activation de PP2A. (Figure 2.2) [183,205,211] La présence de vacuoles contenant des vésicules intraluminales (ILVs) a également été observée dans les cellules traitées. [183] Ces ILVs sont formées à partir de corps multivésiculaires (MVBs) qui émergent lorsque les fusions endosome-lysosome impliquées dans la dégradation de nutriments intracellulaires ne peuvent se produire. Ces vacuoles résultent de l'effet de SH-BC-893, qui lors de son activation de PP2A, va délocaliser la protéine PI(3,5)P2 nécessaire au déroulement du mécanisme de fusion membranaire des macropinosomes et autophagosomes avec le lysosome. Cette restriction de nutriments internes

et externes a conduit à l'inhibition de la croissance ou l'apoptose de plusieurs types de cellules cancéreuses, notamment de la prostate. Il est à noter qu'en raison de leur propriété de quiescence, les cellules saines sont capables de surmonter la déprivation énergétique. Par conséquent, cibler le métabolisme constitutif des cellules oncologiques au travers de la disruption du trafic membranaire a été avancé comme solution potentielle au manque de traitements curatifs pouvant viser une large variété de cancers et faire face aux mutations associées au développement de résistances.

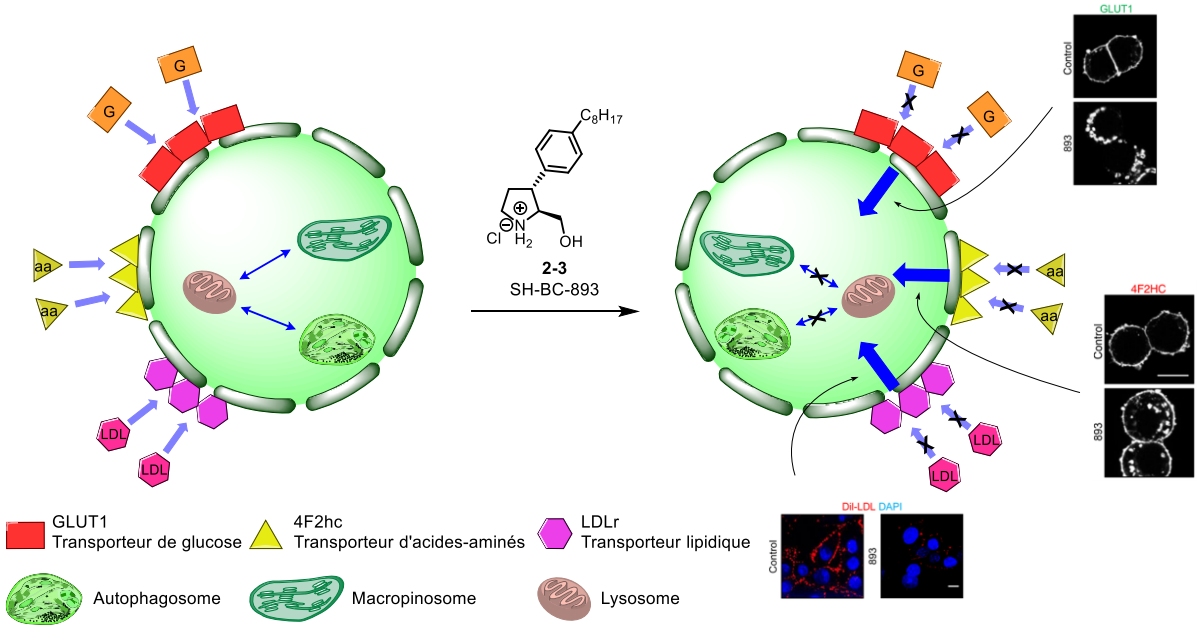

Figure 2.2 Mécanisme simplifié de la perturbation du trafic endocytique par SH-BC-893.

2.2 Développement d'analogues C2 pour l'activation de PP2A et l'inhibition parallèle de HDAC2.

2.2.1 Objectifs de projet

Les histones déacétylases (HDACs) sont un ensemble de métalloprotéines de zinc conservées au travers de l'ensemble des eucaryotes. [226] Onze ont été répertoriées dans le génome humain, et elles sont réparties au sein de quatre classes (HDAC I – IV) de la superfamille des histones. Leur fonction principale est liée à la régulation de l'expression des gènes. [227] Elles sont capables de réprimer l'accessibilité de la chromatine aux facteurs de transcription via le clivage d'un groupement acétyle porté principalement par des groupements lysine. Avec l'action combinée des histones acétyltransférases capable d'acétyler ces mêmes résidus, leur rôle est primordial pour de nombreux processus physiologiques, [228–231] et leur dysfonction a été liée à de nombreuses pathogénies [232–235] incluant le cancer. [230,234,236]

Par conséquent, cibler HDAC pour le développement de thérapeutiques est une stratégie qui a été amplement développée au cours des dernières années. [237–243] Parmi ces efforts, Yoshida a montré que le produit naturel *(R)*-trichostatine A produit une accumulation d'histones acétylées *in vivo* via l'inhibition de HDAC. [244] Breslow et ses collaborateurs se sont inspirés de cette structure pour développer l'acide hydroxamique suberoylanilide (SAHA) **2-4**, un agent anticancéreux approuvé par la FDA et commercialisé sous le nom de Zolinza (Vorinostat). (Figure 2.3) [245]

Récemment, Spiegel et ses collaborateurs ont rapportés sur l'activité inhibitrice intracellulaire de sphingosine-1-phosphate (S1P) **2-5** contre HDAC après avoir observé l'association de Sphk2 avec HDAC3. [246] Ils ont montré que S1P est un inhibiteur des histones HDAC1 et HDAC2. Dans une étude subséquente, ils ont prouvé que FTY720 **2-1** peut également être phosphorylé par la Sphk2 localisée dans le nucleus afin d'opérer la même fonction. [247] Son accumulation au sein du noyau amène à une inhibition des HDACs de classe I. Lorsque testé *in vivo,* l'administration de **2-1** a permis de restreindre le développement de tumeurs du sein et a eu un effet synergique avec tamoxifen plus important que SAHA **2-4**. [248]

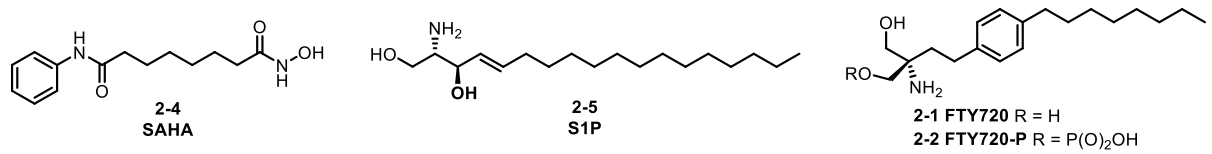

Figure 2.3 Structures des inhibiteurs de HDACs: S1P **2-4**, SAHA **2-5**, et FTY720 **2-1** et sa version phosphatée **2-2**.

En raison des similarités structurelles de FTY720 et SH-BC-893, il a été proposé que cette classe de composés puissent également agir comme inhibiteurs de HDACs de classe I après optimisation. L'objectif de ce projet a été de synthétiser des analogues combinant une activité anticancéreuse visant à la fois les voies d'apports de nutriments cellulaires, et la dérégulation de l'expression des gènes dans les cellules oncologiques. L'utilisation de thérapies combinatoires afin d'obtenir des activités synergiques ou additives est une stratégie essentielle de la lutte contre le cancer. [249,250]

Dans leur étude de 2014, Spiegel et ses collaborateurs ont avancé par étude de modélisation que FTY720-P **2-2** possède un mode de liaison similaire à celui de SAHA et S1P dans le site actif de HDAC2. [247] En particulier, la fonction amine et alcool forment un chélate bidente avec l'atome de zinc, le cycle phénylique est stabilisé par Phe151 et Phe206 et le phosphate forme une liaison hydrogène avec Arg35. (Figure 2.4) [247] La chaine octyle est accommodée dans la poche tubulaire du site actif.

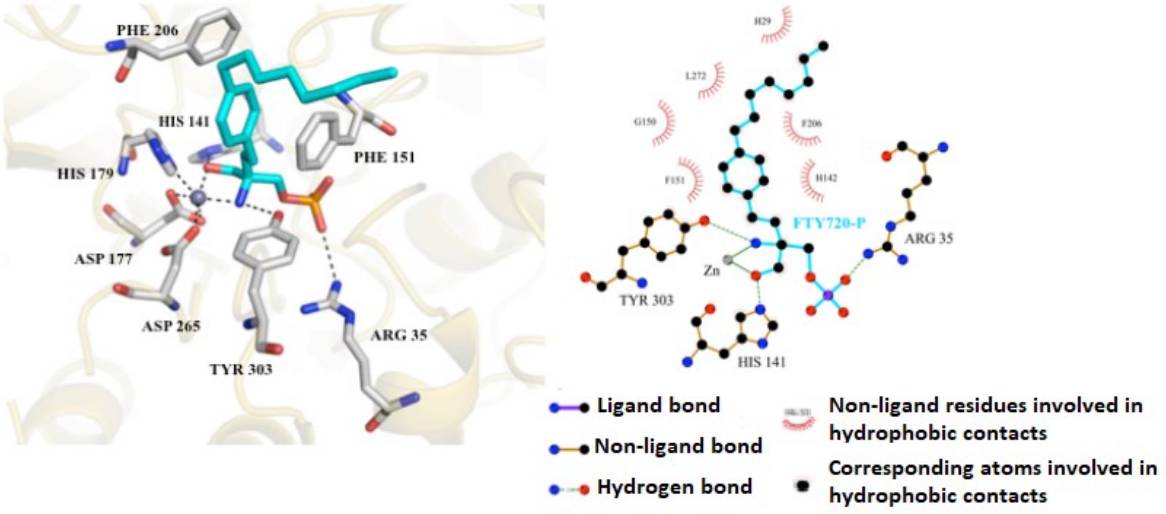

Figure 2.4 Modélisation de FTY720-P **2-2** par Spiegel dans le site actif de HDAC2 (PDB : 3MAX). [247]

Afin de tester notre hypothèse, la nouvelle classe de composés dérivés de SH-BC-893 a été conceptualisée avec pour but de pouvoir mimer le mode de liaison de FTY720-P **2-2** (Figure 2.5 – A). La chaine aryle octyle a été déplacée sur le carbone C2 et une fonction carbonylée a été ajoutée en position beta ou gamma afin de former un chélate avec l'atome de zinc. Une fonction alcool phosphorylable a également été introduite sur différentes positions du cycle afin de générer une liaison hydrogène avec Arg35. Lorsque FTY720-P **2-2** a été modélisé dans le site actif de HDAC2 à l'aide du logiciel FITTED, [251,252] une pose retenant l'ensemble des interactions rapportées par Spiegel a été obtenue. Par la suite, la structure **2-9** s'est révélée être la plus prometteuse et a été sélectionnée pour la synthèse des inhibiteurs doubles (Figure 2.5 – B). L'ensemble des interactions observées avec FTY720-P **2-2** ont été maintenues.

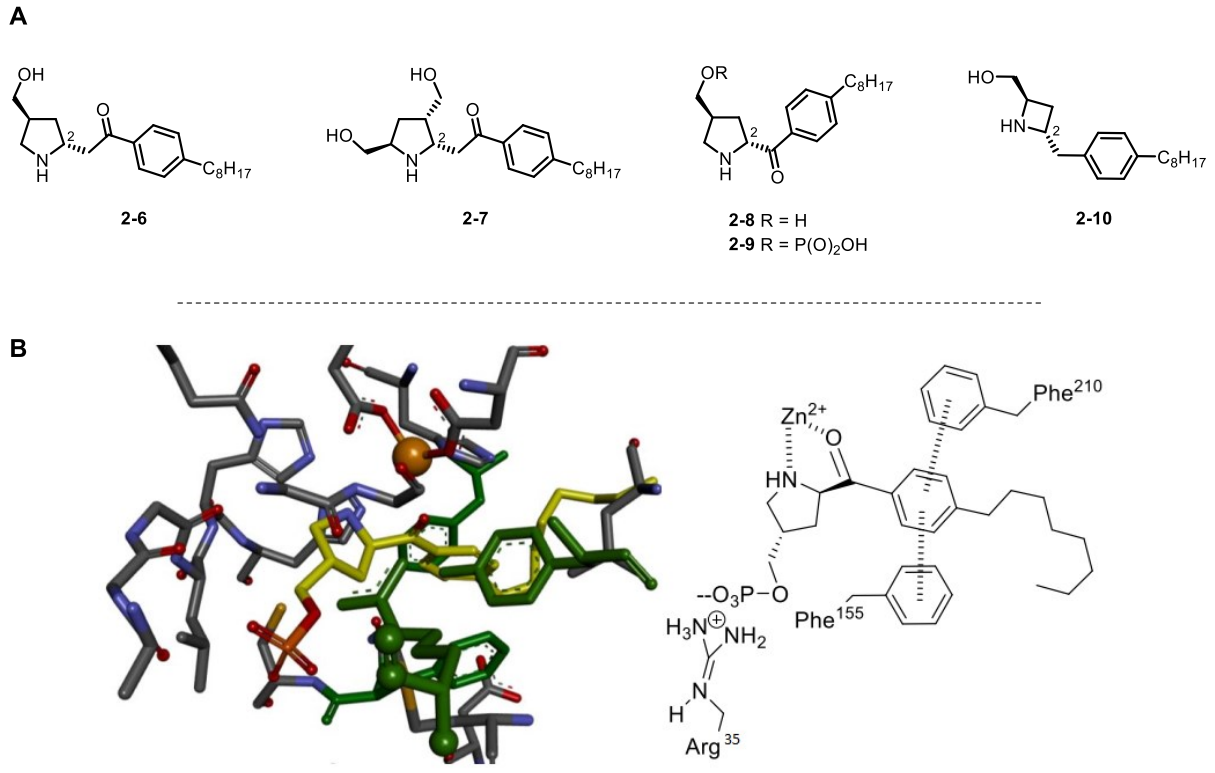

Figure 2.5 A. Structures représentatives de la série C2 de SH-BC-893 sélectionnées pour l'étude de modélisation. B. Modélisation de **2-9** dans le site actif de HDAC2 (PDB : 3MAX) à l'aide du logiciel FITTED.

Une librairie de composés portant la chaine aryle octyle à la position C2 incluant **2-9** a été synthétisée et testée contre PP2A afin d'étudier l'impact de cette variation sur l'activité de SH-

BC-893. Les tests d'inhibition de HDAC2 avec plusieurs dérivés de **2-9** utilisant SAHA et FY720-P comme contrôles ont ensuite été menés.

Ce projet décrit la conception, la synthèse et les tests biologiques contre PP2A et HDAC2 de ces nouveaux analogues. La modélisation de FTY720-P **2-2** et **2-9** est rapportée.

2.2.2 *Article 1*: In search of constrained FTY720 and phytosphingosine analogs as dual acting anticancer agents targeting metabolic and epigenetic pathways

Jean-Baptiste Garsi[a], Lorenzo Sernissi[a], Vito Vece[a], Stephen Hanessian[a,], Alison N. McCracken[b], Grigor Simitian[b], Aimee L. Edinger[b,**]*

[a] *Department of Chemistry, Université de Montréal, PO Box 6128, Station Centre-Ville, Montréal, QC, H3C 3J7, Canada*

[b] *Department of Developmental and Cell Biology, University of California, Irvine, 2128 Natural Sciences 1, CA, 92697-2300, USA*

Contributions :

- Jean-Baptiste Garsi a participé à la synthèse, la modélisation, la rédaction de l'article et de la partie expérimentale.
- Lorenzo Sernissi a participé à la synthèse, la rédaction de l'article et de la partie expérimentale.
- Vito Vece a participé à la synthèse et la rédaction de la partie expérimentale.
- Alison N. McCracken a réalisé les tests biologiques et participé à la rédaction de l'article et de la partie expérimentale.
- Grigor Simitian a travaillé en tant que stagiaire sous la supervision d'Alison N. McCracken.
- Pr. Stephen Hanessian a initié, coordonné le projet et participé à la rédaction de l'article en tant que principal investigateur.
- Pr. Aimee L. Edinger a initié, coordonné le projet et participé à la rédaction de l'article en tant que principal investigateur.

Garsi, J.-B.; Sernissi, L.; Vece, V.; Hanessian, S.; McCracken, A. N.; Simitian, G.; Edinger, A. L. In Search of Constrained FTY720 and Phytosphingosine Analogs as Dual Acting Anticancer Agents Targeting Metabolic and Epigenetic Pathways. *Eur. J. Med. Chem.* **2018**, *159*, 217–242. DOI : 10.1016/j.ejmech.2018.09.043

2.2.2.1 Abstract

A series of compounds containing pyrrolidine and pyrrolizidine cores with appended hydrophobic substituents were prepared as constrained analogs of FTY720 and phytosphingosine. The effect of these compounds on the viability of cancer cells, on downregulation of the nutrient transport systems, and on their ability to cause vacuolation was studied. An attempt to inhibit HDACs with some phosphate esters of our analogs was thwarted by our failure to reproduce the reported inhibitory action of FTY720-phosphate.

2.2.2.2 Introduction

Cancer chemotherapy remains an enigmatic and challenging endeavor. In spite of heroic efforts and impressive advances on many fronts, major obstacles such as resistance and toxicity plague the search for effective drugs. [186,191,192,200] Compounds that exploit the metabolic differences between cancer and normal cells provide an alternative to toxic systemic chemotherapies or therapies targeting oncogenic signal transduction cascades. [199,201,253] FTY720 (Gilenya, fingolimod), an approved drug for the treatment of multiple sclerosis [213] is also known to have a cytotoxic effect against cancer cells. [254] However, when phosphorylated it exerts profound cardiovascular effects at higher doses. [212] We have previously shown that pyrrolidines related to ring-constrained analogs of synthetic sphingolipids such as FTY720 **1** (Fig. 2.6) and natural phytosphingosine **2** kill cancer cells by interfering with one or more nutrient transport systems required for sustenance. [216,217,255] This strategy of "starving cancer cells to death" has been effectively demonstrated in vitro and in vivo with the analog **3**,[183] which unlike FTY720, is not phosphorylated *in vivo* and avoids the cardiovascular effects induced by FTY720-phosphate through its interaction with sphingosine-1-phosphate receptors. [205,211,256–259]

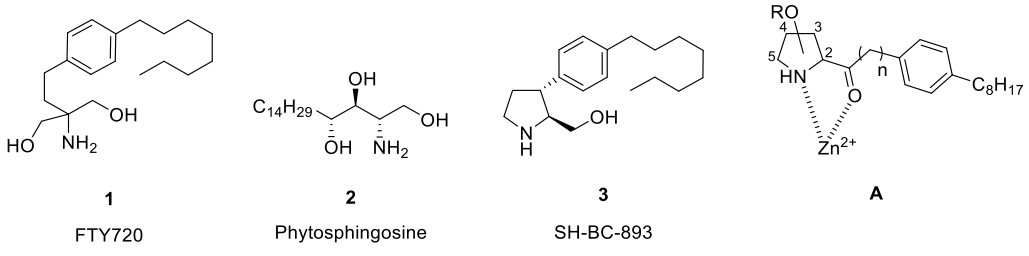

Figure 2.6 Reported anticancer compounds and a new proposed congener **A**

We have shown that four of the nutrient acquisition mechanisms used by mammalian cells, namely transporter-mediated import of amino acids and glucose, receptor-mediated LDL uptake and processing, autophagy, and macropinocytosis, are inhibited by analog **3**. [183] Remarkably, cytotoxicity is selective for cancer cells, most likely because non-transformed cells can adapt to the stress caused by nutrient deprivation by altering their metabolic program. The ability of analog **3** to kill cancer cells at ca.2-5 μM doses is attributed in part to PP2A activation which restricts access to nutrients by down-regulating amino acid and glucose transporters from the cell surface and blocks lysosomal fusion (visualized as extensive vacuolation, Figure 9.1). [183] Variations of chain length, stereochemistry, and functional group manipulations were also performed to establish thresholds of activity for each of three phenotypes: viability, transporter loss, and vacuolation. [217] The favorable activity profile and promising pharmacological properties of analog **3**, including water solubility, encouraged us to study related analogs with a view to better understanding the role of the structural and functional features that contribute to cancer cell killing. As a first objective, we were particularly interested to find new structural variants of the original analog **3** that were differentiated with regard to down-regulation and/or vacuolation, the latter property being an indication of a compound's ability to block lysosomal fusion. We initially prepared analogs in which the extremity of the C-3-aryloctyl chain was modified. As a second objective, we considered transposing the C-3-aryloctyl chain in analog **3** to the C-2 position of the pyrrolidine ring and including polar substituents within geometric proximity to the nitrogen atom. A third objective was to determine if these new analogs now carrying the aryloctyl chain containing polar groups but branched at the C-2-position of the pyrrolidine ring could inhibit histone deacetylases (HDACs). [237,242,243] Considering the position of the nitrogen atom in the pyrrolidine ring, we speculated that placing a proximal keto group could possibly result in bidentate metal coordination in a cellular environment to target zinc-dependent metalloenzymes, thereby leading to a dual mode of anti-proliferative activity on cancer cells in addition to activation of PP2A. Following this notion, we were encouraged that in 2014 Hait et al. had reported that FTY720-phosphate was an inhibitor of HDACs using cell-based and in vitro assays. [247,248] While Gardner et al. were unable to see FTY720 increase acetylation of the lysine residues reported by Hait et al., they did find histone marks that were responsive to FTY720 in

their cell type. [260] We therefore considered a generic compound represented by structure A as a constrained C-2-substituted pyrrolidine variant of FTY720 that would combine the attributes of the lead compound **3** while also having the potential to function as an inhibitor of HDACs (Fig. 2.6).

2.2.2.3 Results and discussion

*2.2.2.3.1 New C-3 arylchain-modified variants of analog **3***

As previously reported, constrained analog **3** was similarly active to FTY720 (Tableau 2.1) while lacking the dose-limiting cardiotoxicity associated with FTY720. [183,216,217,255] In an effort to further probe the structural characteristics of analog **3** vis-a-vis cytotoxicity, nutrient transporter down-regulation, and vacuolation, we first turned our attention to the hydrophobic aryloctyl appendage.

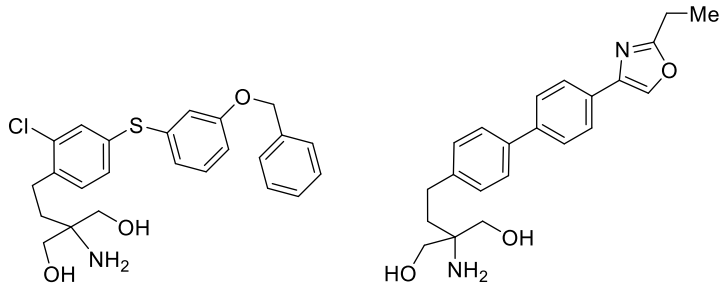

KRP203 SYL927

Figure 2.7 Immunosuppressant KRP-203 and S1P1 agonist SYL927

Inspired by the structure of the immunosuppressant KRP-203 (Fig. 2.7) [261] we wanted to investigate the effect of inserting a benzyl ether moiety at the extremity of the aryloctyl chain as shown in compound **4** (Tableau 2.1) (see Experimental Section). Next, we introduced a 2-methyl oxazoline moiety at the extremity of the octyl chain, as found in the selective S1P1 agonist SYL927 [262] to obtain analogs **5** and **6**. Cytotoxicity assays measured as IC_{50} showed a 4-7 fold reduction in potency for compounds **4**, **5**, **6** and **7** compared to analog **3** (Tableau 2.1). The loss of activity of the 2-octylketone **7** indicated that polar groups at the extremity of the octyl chain are detrimental to activity. These analogs downregulated the nutrient transporter-associated protein CD98 at high concentrations, but failed to vacuolate cells even at 40 µM, a dose where CD98 down-

regulation and cell killing were robust, suggesting that they lacked the ability to block lysosomal fusion. In view of these results, we decided not to pursue further modifications within the 3-aryloctyl appendage of the lead compound **3**.

Tableau 2.1 Cytotoxicity, CD98 down-regulation and vacuolation profiles of the new C-3-arylalkyl chain variants of analog **3**

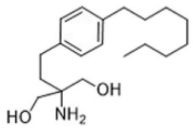

1 FTY720

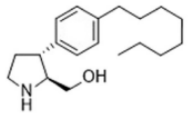

3

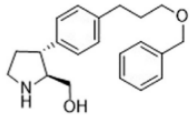

4

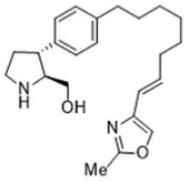

5

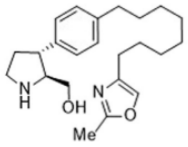

6

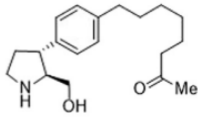

7

Comp.	IC50 (μM) [95% CI]		%CD98 down-regulation			Vacuolation score		
			2.5 μM	10 μM	40 μM	2.5 μM	10 μM	40 μM
1	2.1	[1.9, 2.4]	30	63	n.d.	+++	+++	n.d.
3	2.1	[2.0, 2.2]	41	66	n.d.	++	+++	n.d.
4	10.9	[8.7, 13.7]	11	14	51	n.d.	0	0
5	10.2	[8.7, 12.0]	5	18	61	n.d.	0	0
6	8.4	[7.0, 10.1]	5	33	61	n.d.	0	0
7	15.1	[11.2, 20.3]	−15	−8	23	n.d.	0	0

2.2.2.3.2 Extended C-2 modified variants of analog 3

Being cognizant that the pyrrolidine core had to maintain its basic character for cytotoxicity, [183,216,217,255] we next sought to probe the positioning of the aryloctyl side chain within the pyrrolidine ring. To this end, we considered branching at C-2 to generate a series of 2-substituted pyrrolidines with extended chains. Anticipating the need for a polar group within the chain for possible metal chelation and HDAC inhibition, we initially considered placing a ketone at the beta and gamma positions next to the pyrrolidine ring (Tableau 2.2). We were pleased that the modified variants in this new series exhibited cytotoxicity similar to analog **3**. They also down-regulated nutrient transporters and vacuolated at concentrations near their IC_{50}, suggesting that they most likely share the same mechanism of action as analog **3** (Tableau 2.2). Compounds **8**, **9**, and **10** were prepared from the Weinreb amide derivative of L-homoproline **8a** previously reported by Georg et al. (Schéma 2.1). [263] Treatment of **8a** with 3.0 equivalents of octyl-

phenylmagnesium bromide in Et_2O at 0 °C led to benzylic ketone **8b** as a versatile common intermediate.

Tableau 2.2 Cytotoxicity, CD98 down-regulation and vacuolation profiles of the C-2 modified variants of analog **3** (as HCl salts)

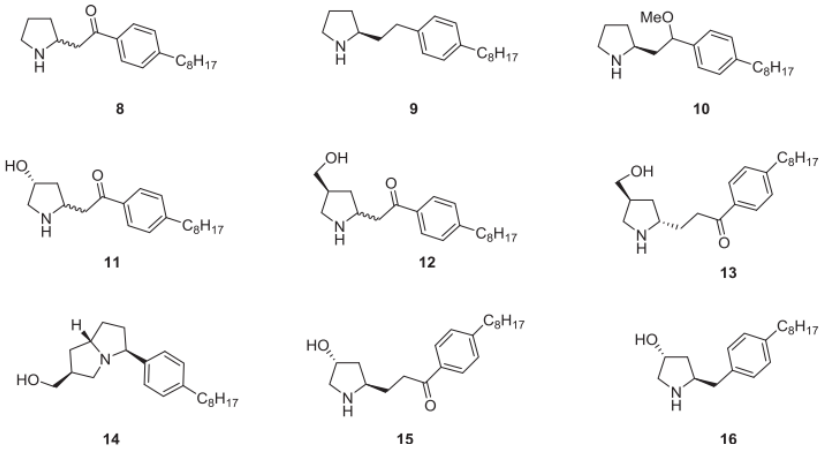

Comp.	IC50 (μM) [95% CI]		%CD98 down-regulation			Vacuolation score		
			2.5 μM	10 μM	40 μM	2.5 μM	10 μM	40 μM
3	2.1	[2.0, 2.2]	42	66	n.d.	++	+++	n.d.
8	2.5	[2.3, 2.8]	28	57	n.d.	+	+++	n.d.
9	2.8	[2.6, 3.0]	41	63	n.d.	++	+++	n.d.
10	3.0	[2.7, 3.3]	16	58	n.d.	0	+++	n.d.
11	2.1	[1.5, 2.8]	22	46	n.d.	+++	+++	n.d.
12	2.0	[1.6, 2.6]	44	60	n.d.	++	+++	n.d.
13	4.0	[3.5, 4.6]	8	46	n.d.	0	+++	n.d.
14	12.2	[11.4, 13.0]	0	32	68	0	0	+
15	2.1	[1.9, 2.3]	15	52	n.d.	++	+++	n.d.
16	2.2	[2.1, 2.3]	40	63	n.d.	++	+++	n.d.

The presence of by-products from the reagent necessitated careful chromatography of the crude reaction product affording 62% yield of pure **8b**. Removal of the N-Boc group with 4 N HCl in dioxane afforded **8** as a mixture of enantiomers due to rapid racemization in methanol or water (*vide infra*). Ketone **8b** was reduced with $NaBH_4$ to give the corresponding benzylic alcohol **8c** as a 4:1 diastereomeric mixture that could be easily separated by column chromatography. Although the stereochemistry of each diastereomer was not determined, the major diastereomer was converted to the methyl ether, then deprotected to afford product **10**. The crude diastereomeric mixture of **8c** was also catalytically hydrogenated at atmospheric pressure in ethanol, affording product **9** after final removal of the N-Boc protective group. Products **11** and **12** were obtained starting from the 4-substituted homoprolines **11a** and **12a** respectively (Schéma 2.2) (see Supporting Information Schéma 8.3 for the syntheses of **11a** and **12a**). The corresponding

Weinreb amides **11b** and **12b** were treated with octylphenylmagnesium bromide to give ketones **11c** and **12c** with acceptable yields.

Schéma 2.1 Synthesis of 2-substituted pyrrolidines

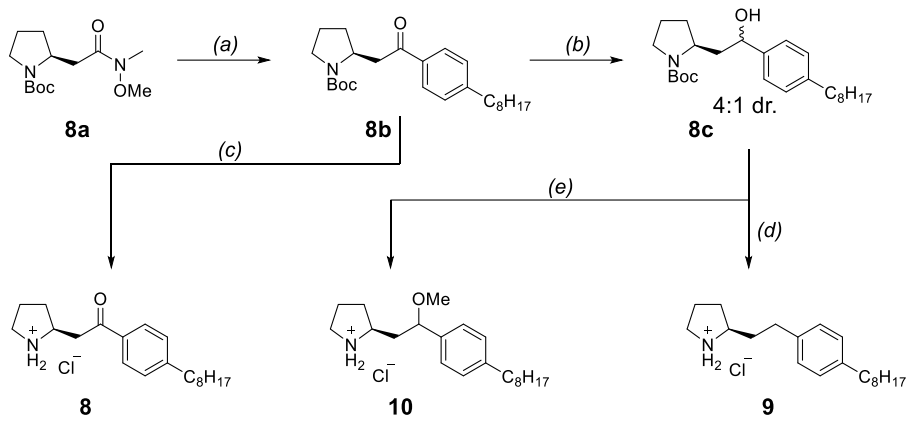

Conditions. (a) OctylPhenylMgBr, Et_2O, 0 °C to r.t., 62% *(b)* $NaBH_4$, MeOH, 0 °C to r.t, 99%. *(c)* HCl (4M), Dioxane, 99%. *(d)* **1.** H_2, Pd/C, EtOH; **2.** HCl (4M), Dioxane, 73% over 2 steps.*(e)* **1.** Diastereomeric FCC Separation; **2.** NaH, MeI, THF; **3.** HCl (4M), Dioxane, 38% over 2 steps.

Schéma 2.2 Synthesis of 2- and 4-substituted pyrrolidines

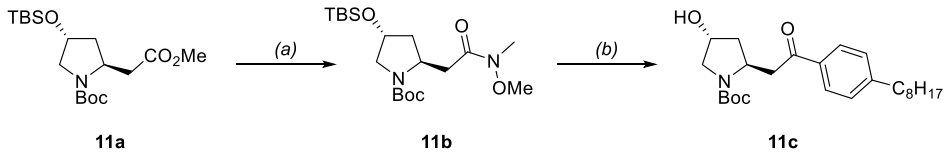

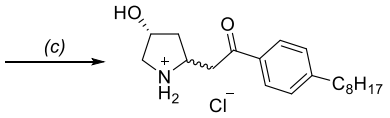

Conditions. (a) N,O-dimethylhydroxylamine-HCl, *i*PrMgCl, THF, -20 °C, 81%. *(b)* **1**. OctylphenylMgBr, Et_2O, 0 °C to rt.; **2.** TBAF, THF, 63% over 2 steps *(c)* HCl (4M), Dioxane, 75%.

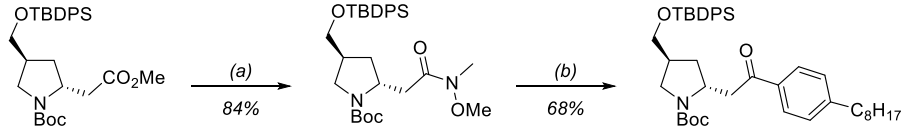

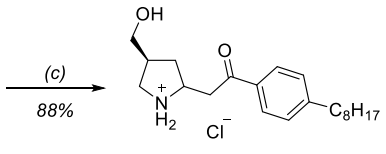

Conditions. (a) N,O-dimethylhydroxylamine-HCl, *i*PrMgCl, THF, -20 °C, 84%. *(b)* OctylphenylMgBr, Et_2O, 0 °C to rt, 68%. *(c)* **1.** TBAF, THF; **2**. HCl (4M), Dioxane, 88% over 2 steps.

Careful chromatographic purification to separate by-products resulting from the Grignard reagent followed by treatment with TBAF and acid led to products **11** and **12**. Products **13** and **15** were prepared starting from **13a** (Schéma 2.3) (see Supporting Information Schéma 8.3 for the synthesis of **13a**) and commercially available 1-(*tert*-butyl) 2-methyl (2S,4R)-4-((*tert*-butyldimethylsilyl)oxy)pyrrolidine-1,2-dicarboxylate. Reduction of the ester group to the corresponding aldehyde with DIBAL-H, followed by a Wittig reaction with methyl(triphenylphosphoranylidene)acetate, and catalytic hydrogenation afforded the ester intermediates **13b** and **15a**. The corresponding Weinreb amides were subsequently reacted with octylphenylmagnesium bromide to give ketones **13c** and **15b**, in 37% and 54% yield respectively. Removal of the OTBDPS and N-Boc groups afforded products **13** and **15**.

Schéma 2.3 Synthesis of C-2 substituted extended pyrrolidines

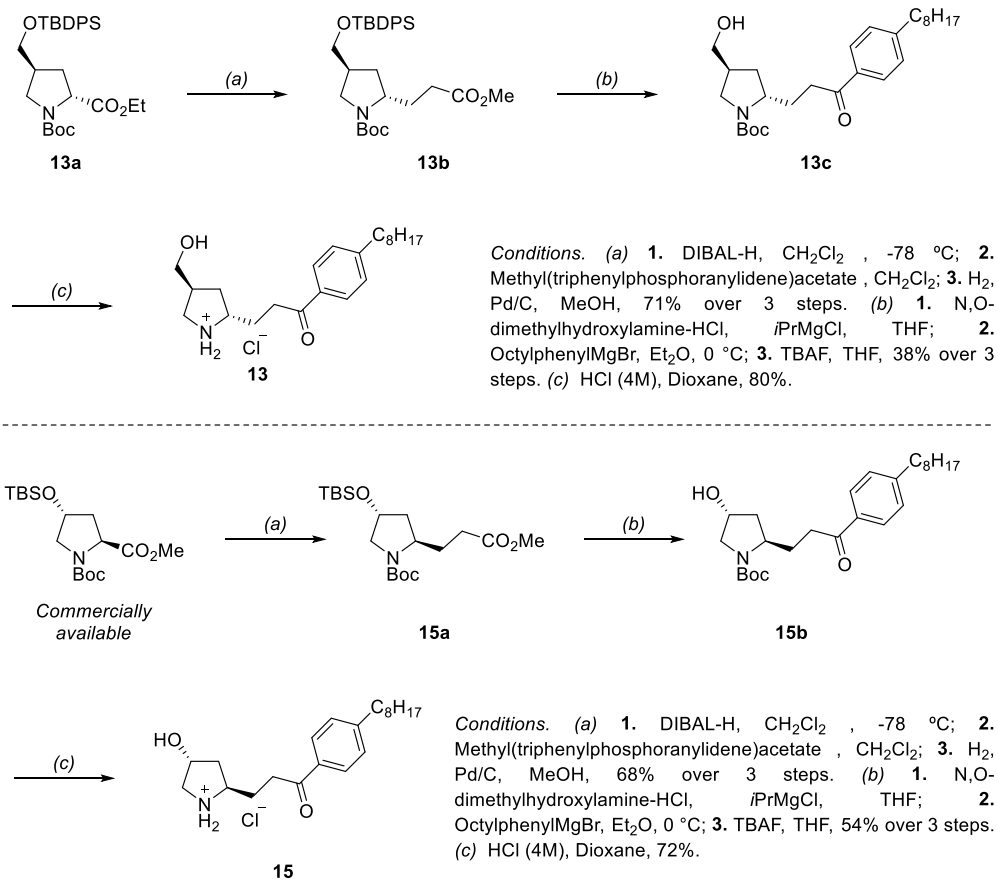

We observed that **11** and **12** epimerized at the C-2 position when dissolved in protic solvents. In the presence of D_2O at room temperature, deuterium was incorporated at C-2 confirming a fast

enolization followed by β-elimination and ring closure. Keto pyrrolidine **12** was stable only in very acidic conditions (pH ≤ 3 H2O), while epimerization was extremely fast in basic conditions. The incorporation of deuterium is complete in 30 min at pH = 10, and in 3 h at pH = 7. A similar behavior had already been observed for the chlorpromazine-like central nervous system depressant Su17595A, [264] the muscle relaxant tolperisone, [265] and the antiarrhythmic drug moricizine, [266] albeit at a slower rate.

Schéma 2.4 Epimerization and cyclisation processes observed

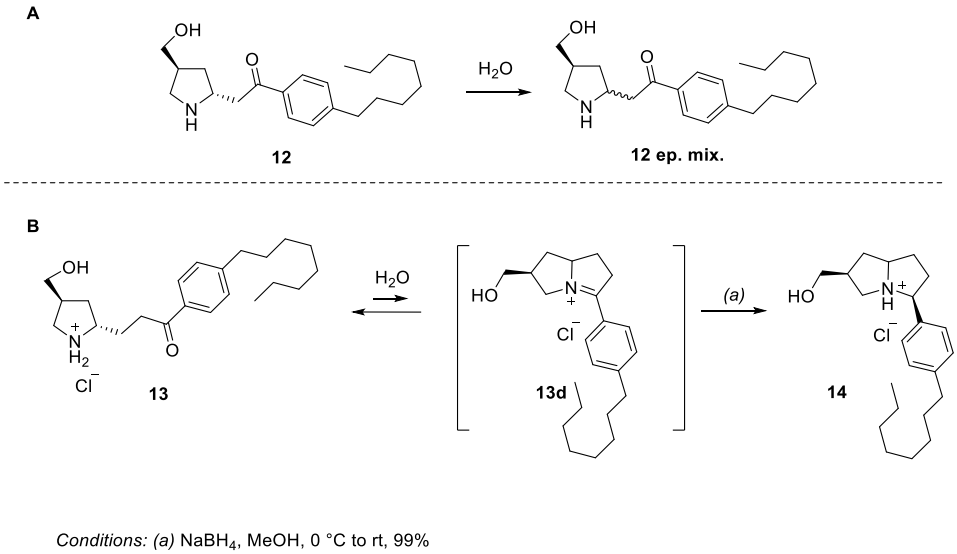

Conditions: (a) $NaBH_4$, MeOH, 0 °C to rt, 99%

When the keto group was further removed from the pyrrolidine ring by extending the chain length as in **13**, the desired ketone was found to be in equilibrium with an azabicyclic salt resulting from intramolecular iminium ion formation (2:1 mixture in H_2O) **13d**, which upon reduction with $NaBH_4$ led to **14** (Schéma 2.4, B). The same behavior was observed in the case of compound **15**.

Surprisingly the new bicyclic derivative **14** maintained a reasonable cytotoxic activity (IC_{50} 12.2 µM). We therefore decided to further investigate this new structural analog and we prepared the bicyclic enantiopure pyrrolizidine **17** bearing the aryloctyl appendage on C-3, in analogy with our lead compound **3**, as well as the monocyclic variant **18**, to check the effect of the substituent position and the nature of the azacycles (Schéma 2.5).

We started the synthesis from the readily available (*S*)-prolinal which was arylated and reoxidized to the corresponding ketone since the addition of the corresponding aryl Grignard on the Weinreb

amide resulted in decomposition of the reagent without conversion of the substrate (Schéma 2.5). Subsequent addition of the lithium enolate of ethyl acetate delivered **17c** as a mixture of diastereomers that could not be separated at this stage. The ester was further reduced to the alcohol and tosylated, which when warmed up to 105 °C in toluene, underwent a spontaneous deprotection/cyclisation, leading to the formation of the bicyclic structure **17e** and its epimer (epi-**17e**) as tosylate salts in a ratio of 2:1.

Schéma 2.5 Pyrrolizidine and pyrrolidine syntheses

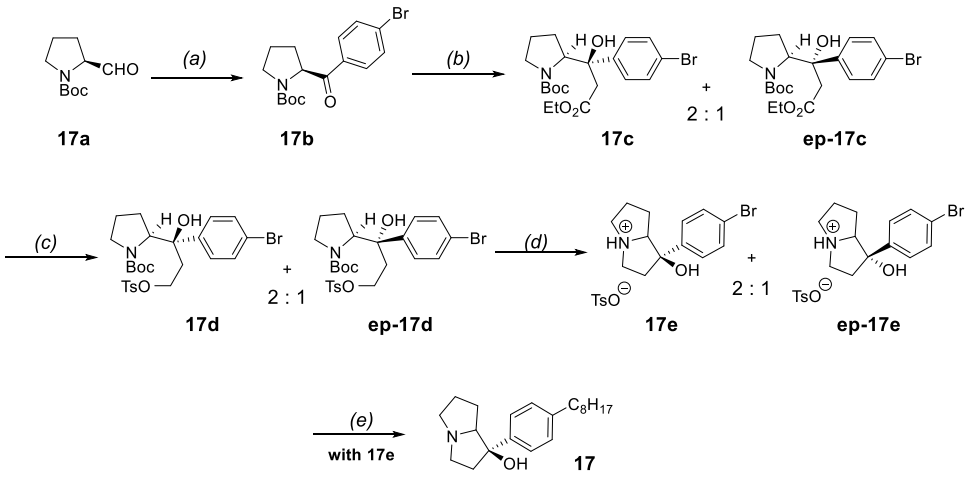

Conditions: *(a)* 1. 1,4-dibromobenzene, *n*-BuLi, THF, -78 °C; 2. DMP, CH_2Cl_2, 41% over 2 steps. *(b)* LDA, EtOAc, THF, -78 °C, 76%. *(c)* 1.$LiBH_4$, THF, 0°C to rt; 2. Ts_2O, Pyridine, CH_2Cl_2, 52% over 2 steps. *(d)* PhMe, 105 °C, 55%. *(e)* 1. Octyne, catecholborane, $NaHCO_3$, $Pd(PPh_3)_4$, DME; 2. H_2, Pd/C, EtOAc, *then* HCl, 29% over 2 steps.

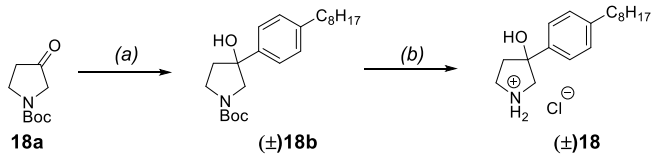

Conditions: *(a)* OctylphenylGrignard, Et_2O, 61%. *(b)* HCl (4M), dioxane, 45%

The diastereomers were separated at this stage, delivering the major product **17e** in 38% yield. Suzuki coupling of **17e** followed by hydrogenation of the resulting alkene and acid treatment delivered **17**. The moderate yield over the two last steps was attributed to the highly sensitive benzylic alcohol decomposing easily under acidic conditions. The racemic compound **18** was easily accessed from N-Boc 3-pyrrolidinone which was arylated with the octylphenylmagnesium bromide and deprotected under acidic conditions.

Interestingly, compound **17** proved to be more active than **14** with an IC_{50} in the same range as the monocyclic C-2 substituted variants while **18** was less active than **17** (Fig. 2.8), indicating that the increased steric hindrance generated by the pyrrolizidine was tolerated.

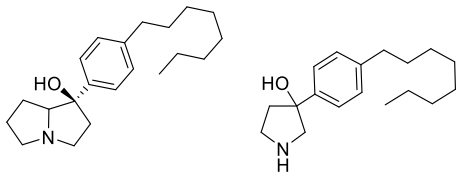

17 IC_{50} 4.2 μM

(±)**-18** IC_{50} 8.1 μM

Figure 2.8 Pyrrolizidine and pyrrolidine analogs

2.2.2.3.3 Repositioning the keto group in extended C-2 modified variants of analog 3

In considering an alternative position of the keto group in the chain, we placed it on the *α*-position of the C-2 branched aryloctyl pyrrolidine analogs (Tableau 2.3). This would avoid the issues of partial chain, we placed it on the *α*-position of the C-2 branched aryloctyl epimerization encountered due to beta elimination and ring closure as described above, although the basicity of the pyrrolidine nitrogen could be diminished due to the inductive effect of the carbonyl group.[267]

Tableau 2.3 Cytotoxicity, CD98 down-regulation and vacuolation profiles of the C-2 substituted α-keto and α-hydroxy pyrrolidines

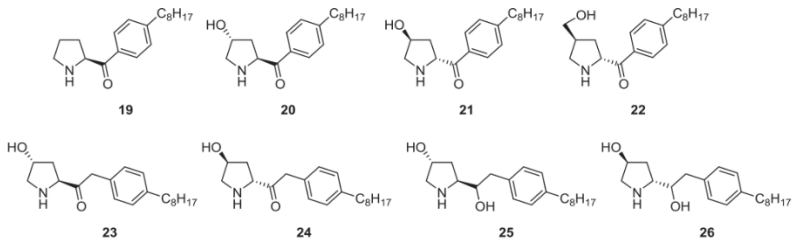

Comp.	IC50 (μM) [95% CI]		%CD98 down-regulation			Vacuolation score		
			2.5 μM	10 μM	40 μM	2.5 μM	10 μM	40 μM
3	2.1	[2.0. 2.2]	42	66	n.d.	++	+++	n.d.
19	>40		−21	−4	33	0	0	+++
20	28.1	[26.1, 30.2]	2	9	48	0	0/+	+++
21	15.3	[14.6, 15.9]	12	51	41	0	+++	+++
22	19.6	[18.7, 20.5]	0	19	61	0	0	+++
23	18.6	[15.5, 22.3]	13	23	59	0	0	+++
24	17.1	[14.5, 20.2]	11	16	54	0	0	+++
25	3.0	[2.6, 3.5]	19	62	n.d.	+	+++	n.d.
26	1.8	[1.7, 2.0]	9	62	n.d.	0	++	n.d.

In general, the cytotoxic activity of the C-2 ketoaryl compounds was significantly reduced compared to **3** and to the corresponding extended keto variants (compare Tableau 2.2 and 2.3). This indicated that a carbonyl group adjacent to the pyrrolidine nitrogen atom on a chain at C-2 was not well tolerated, whereas alcohols **25** and **26** retained activity similar to the lead compound **3**.

Nevertheless, all of the C-2 keto compounds were able to downregulate nutrient transporters at elevated concentrations. The same trend held for vacuolation, as **21** reached maximum vacuolation at 10 µM (Tableau 2.3). The negative influence of the α-keto group in the chain was further seen by the 5-10 folds decrease in cytotoxicity when comparing compounds **20** and **21** to **16**. It is also notable that, at the concentration where compound **26** kills 50% of cells, no down-regulation of nutrient transporter proteins or vacuolation was observed, suggesting an alternative mode of action. Compounds **20**, **22** and **23**, as well as the corresponding reduction products **16** and **25** were synthetised as single enantiomers from the intermediates **20b** and **22b** (Schéma 2.6). The Weinreb amides **20b** and **22b** were reacted with octylphenylmagnesium bromide to give the corresponding ketones, which were deprotected to give **20c** and **22c**. Treatment with acid afforded the pyrrolidines **20** and **22** respectively.

Pd/C catalyzed hydrogenation of the keto group in **22c** followed by N-Boc deprotection led to **16** in modest yield. Following a similar protocol, we prepared the extended ketone intermediate **23a** that was transformed to **23** and **25**, the latter consisting of a 4:1 mixture of diastereomers (Schéma 2.6). As previously stated, we proposed to prepare constrained C-2 substituted *α*-hydroxy pyrrolidine analogs of FTY720 bearing a phosphate group to test them as HDAC inhibitors. To this end we prepared phosphate esters **29** and **31** as well as their enantiomers **30** and **32** (not shown) by standard methods (Schéma 2.6).

Schéma 2.6 Syntheses of the α-keto and α-hydroxy C2-substituted pyrrolidines and their phosphate esters

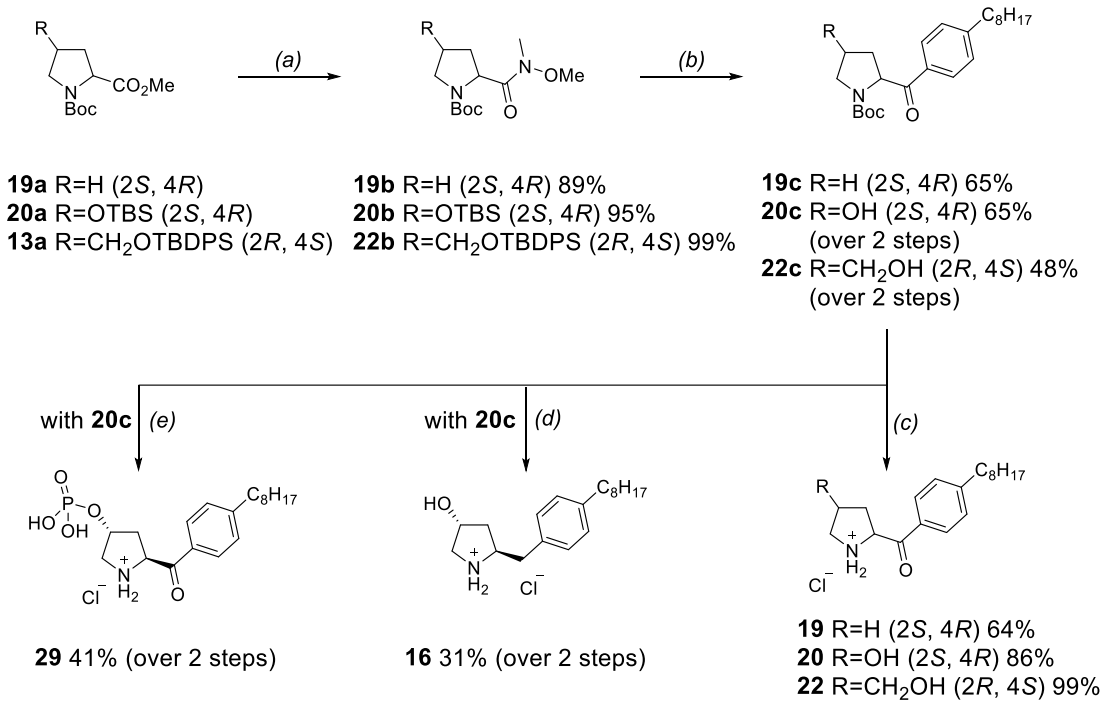

Conditions. (a) N,O-dimethylhydroxylamine-HCl, *i*PrMgCl, THF, -20 °C. *(b)* **1.** OctylphenylMgBr, Et_2O, 0 °C; **2.** TBAF, THF *(c)* HCl (4M), Dioxane. *(d)* **1.** H_2, Pd/C, EtOH; **2.** HCl (4M), Dioxane. *(e)* **1.** $P(OtBu)_2NEt_2$, tetrazole, THF, 0 °C *then* *t*BuOOH; **2.** HCl (4M), Dioxane

---

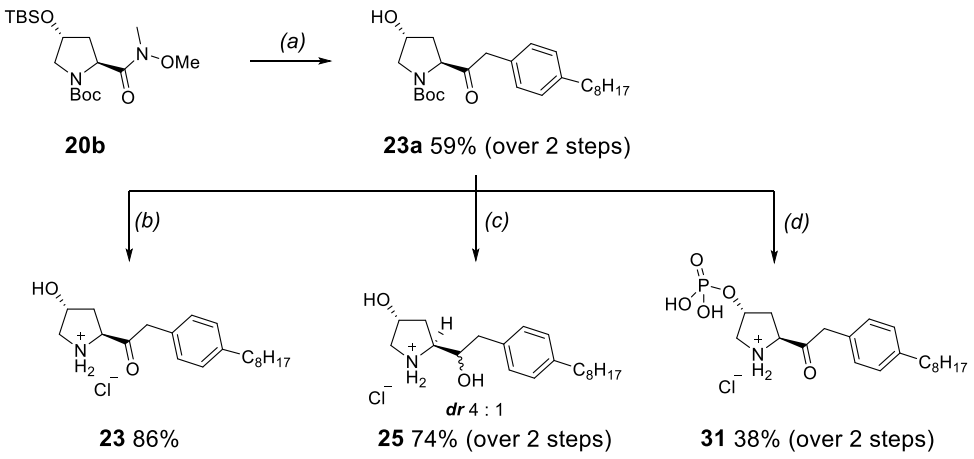

Conditions. (a) **1.** OctylphenylMgBr, Et_2O, 0 °C; **2.** TBAF, THF *(b)* HCl (4M), Dioxane. *(c)* **1.** $NaBH_4$, MeOH; **2.** HCl (4M), Dioxane. *(d)* **1.** $P(OtBu)_2NEt_2$, tetrazole, THF, 0 °C *then* *t*BuOOH; **2.** HCl (4M), Dioxane

2.2.2.3.4 Anticipated HDAC activity presents a conundrum

The nuclear zinc-dependent metalloprotease enzymes known as histone deacetylases have been the subject of extensive studies over the past decades due to their major role in regulating gene expression. [236] Chromatin remodeling affects the accessibility of DNA to transcription factors and thus plays a central role in controlling gene expression and determining cellular phenotypes. The acetylation and deacetylation of N-acetyl lysine residues catalyzed by histone acetylases (HATs) and histone deacetylases (HDACs) respectively, is a tightly controlled process that, if perturbed, can lead to cancer [34]. [236] Consequently, the search for HDAC inhibitors as drugs to combat cancer has been of considerable interest.[237,242,243] Inspired by the structure of the natural product trichostatin A (TSA) (**27**), [244] Breslow and coworkers [245] developed the simple suberoylanilide hydroxamic acid (SAHA) (**28**), which is marketed under the trade name Zolinza (Vorinostat) (Fig. 2.9).

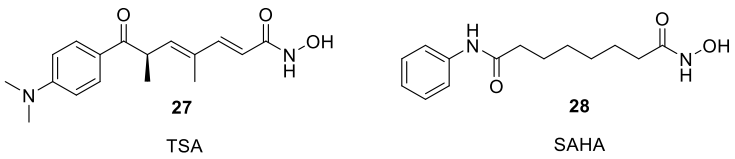

Figure 2.9 Classical HDAC inhibitors

Previous studies from our laboratory have focused on exploring the importance of the chain length and incorporation of an α-alkoxy chain as well as stereochemical features on a SAHA motif on HDAC inhibitory activity. [238,268] Relying on molecular modeling and the crystal structure of HDAC 8 [269] we reported on a series of macrocyclic inhibitors with a nanomolar activity profile against a number of class I and class II HDACs. [239]

As previously mentioned, we were intrigued by the reports by Spiegel and coworkers [247,248] that FTY720-phosphate and sphingosine-1-phosphate [246] are inhibitory toward HDACs. In these studies, nuclear SphK2 was required to observe FTY720- and sphingosine-1-phosphate-dependent increases in several histone acetylation marks. The (*S*)-phosphate formed in vivo from FTY720 would mimic the natural sphingosine phosphate intracellularly and act as a 'synthetic' inhibitor. Their results showed that FTY720-P inhibited recombinant HDACs 1, 2, 3 and 8, approaching the activity of SAHA. Using the reported crystal structure of HDAC 2, the Spiegel

group conducted molecular docking studies of FTY720-P on the active site and concluded that the binding mode was very similar to SAHA and sphingosine-1-phosphate. They hypothesized that the juxtaposition of the primary amino group and the hydroxymethyl group bearing the (*S*)-configured phosphate in FTY720 might act similarly to the hydroxamic acid group in SAHA and the phosphate in S1P. They further invoked a favorable π-π interaction of the phenyl group in FTY720-P with Phe206 and Phe151 (Fig. 2.10).

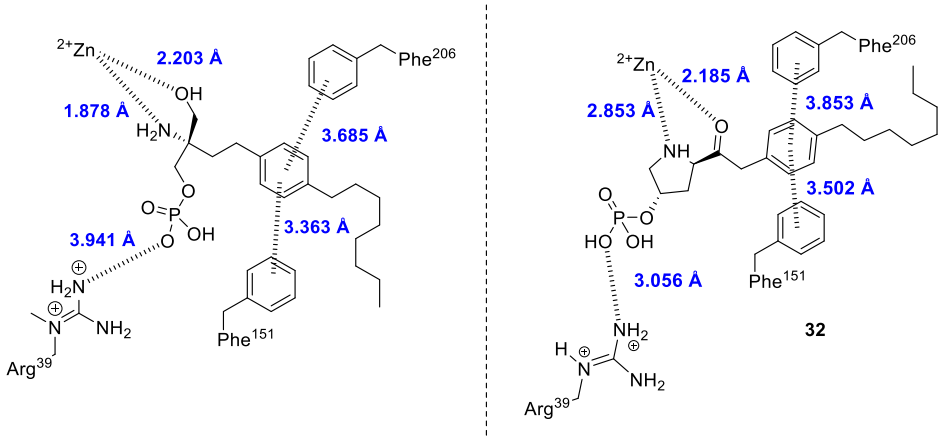

Figure 2.10 Proposed binding mode of FTY720-phosphate (Spiegel) and a hypothetical pose for a synthetic C-2-keto arylalkyl pyrrolidine 3-phosphate (**32**)

Encouraged by these highly intriguing results from the Spiegel group, we were poised to test phosphate analogs **29**-**32** sharing similar interactions as suggested by a docking study using FITTED against HDACs. [251,252] However, prior to undertaking this initiative, we wanted to see if these phosphates exhibited any cytotoxic activity. While it was not surprising that the phosphate esters **29**, **30**, **31**, and **32** were totally inactive in down-regulation and vacuolation tests compared to their hydroxy pyrrolidine ketone progenitors **20**, **21**, **23** and **24**, as the charged phosphate should not be able to enter the cell, we were surprised to find that these analogs were cytotoxic at IC_{50} 12.9 µM, 12.8 µM, 25.0 µM and 25.3 µM respectively (Tableau 2.4). The increased cytotoxicity of the phosphate esters **29** and **30** over the unphosphorylated progenitors despite the absence of transporter loss or vacuolation suggests that they could act through a distinct mechanism, possibly targeting a receptor on the cell surface.

Tableau 2.4 Cytotoxicity, CD98 down-regulation and vacuolation profiles of phosphate ester analogs

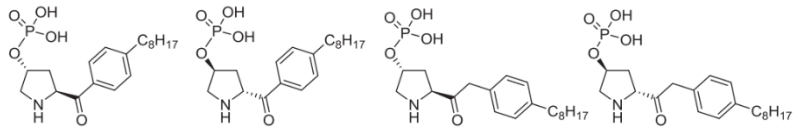

29 30 31 32

Comp.	IC50 (μM) [95% CI]		%CD98 down-regulation			Vacuolation score		
			2.5 μM	10 μM	40 μM	2.5 μM	10 μM	40 μM
3	2.1	[2.0, 2.2]	42	66	n.d.	++	+++	n.d.
29	12.9	[11.9, 14.0]	n.d.	3	−8	0	0	0
30	12.8	[11.7, 14.0]	n.d.	−9	0	0	0	0
31	25.0	[18.1, 34.4]	n.d.	3	0	n.d.	0	0
32	25.3	[19.5, 32.9]	n.d.	5	8	n.d.	0	0

We then focused on establishing the parameters to test HDAC activity. Pleasingly, the reported activity of SAHA was confirmed in both our in vitro and cell-based test systems (85% inhibition at 2 μM concentration). However, FTY720-P, reported to exhibit 60-75% inhibition at 5 μM by Spiegel, [247,248] was inactive up to 20 μM in our hands despite the fact that its integrity and phosphorylation were confirmed by UPLC-ESI-MS/MS (Figure 9.2 – A, B and Figure 9.3 and data not shown). Assays performed using **12**, **25**, **26**, **31**, and **32** that employed SAHA as a positive control failed to detect HDAC inhibition (Figure 9.2 – B, C). Examination of histone acetylation in intact cells also failed to confirm a role for FTY720-P as an HDAC inhibitor (Figure 9.3). Since other groups have reported difficulty detecting increased acetylation of specific lysine residues, [260] we utilized antibodies against multiple acetylation sites on both H3 and H4; however, no changes in histone acetylation were detected in cells treated with FTY720-P despite consistent and robust increases in acetylation in cells treated with SAHA. Clearly, this disappointing outcome presented an unexplained conundrum that led us to refrain from conducting further HDAC inhibition tests with additional compounds in this series. Given that the parent compound FTY720-P did not inhibit HDAC activity, our intended objective of achieving dual-action inhibitors was not realized.

2.2.2.4 3. Conclusions

In conclusion, we have reported that placing the aryloctyl group found in the anticancer analog **3** in the C-2 position of the pyrrolidine maintains cytotoxic activity. However, introduction of a carbonyl group in between the aryloctyl appendage and the pyrrolidine ring resulted in variable levels of activity depending on its position along the chain. Placing the carbonyl group two or

three carbon atoms removed from the pyrrolidine ring was generally better tolerated with an activity profile only slightly diminished compared to the lead analog **3**, whereas attempts to bring it closer were detrimental to the activity, likely due to a decrease of the nitrogen basicity. Our attempts to mimic the HDAC inhibiting activity of FTY720-phosphate as reported by Spiegel and coworkers with a series of constrained C-2 keto pyrrolidine analogs and their phosphate esters were thwarted by the fact that in our hands FTY720-phosphate did not act as an inhibitor. Thus, our search for a dual-action anticancer agent derived from a synthetic pyrrolidine- based sphingolipid was only partially validated with a new series of C-2 alkyl and C-2 ketoalkyl aryloctyl pyrrolidines. Gratifyingly, these maintained cytotoxicity, nutrient transporter downregulation, and vacuolation activity profiles equal to that of the lead analog **3** with the notable exception of **4**, **5**, **6**, and **7**, which do not vacuolate even at high concentrations, and **26**, which triggers changes in endolysosomal trafficking at elevated doses but appears to kill cells by binding to an additional target. Our efforts also uncovered pyrrolizidines with appended aryloctyl chains as new cytotoxic agents. Studies are in progress to better understand the anti-neoplastic actions of synthetic sphingolipids and to identify their direct protein targets in cells.

2.3 Synthèses d'analogues de SH-BC-893 O-fonctionnalisés par des hétérocycles.

2.3.1 Objectifs de projet

Dans la recherche de nouveaux agents thérapeutiques efficaces contre les tumeurs malignes, la modulation de procédés de signalisations cellulaires a été l'objet de nombreuses investigations, [121,270,271] et plusieurs classes de composés visant à interférer avec leurs activités ont été développées. [272–274] Parmi elles, les molécules incorporant un fragment tricyclique tel que la phénothiazine ont démontré un potentiel d'action contre certaines protéines de signalisation, [275–278] notamment PI3K-Akt et Ras-Erk. [279–281] Ces analogues ont été dérivés d'antipsychotiques tels que la chlorpromazine (CPZ) [282] et la perphénazine (PPZ) [283], drogues commerciales initialement prévues comme neuroleptiques. Leur activité anti-cancéreuse a été identifiée depuis les années 1990; cependant les effets secondaires toxiques pour le système nerveux central (SNC) entrainés par leur concentration effective les ont exclu de tout traitement curatif. [223]

En 2014, Ohlmeyer et ses collaborateurs ont rapporté que l'effet apoptotique de la perphénazine **2-11** (Figure 2.11 – A) contre les cellules leucémiques lymphoblastiques T-ALL est lié à l'activation de PP2A. [284] Lorsque traitées avec PPZ ou certains analogues comportant un fragment tricyclique apparenté à PPZ, les cellules T-ALL ont régressé *in vivo*. Les auteurs ont proposé que l'activation de PP2A puisse réguler à la baisse les mécanismes de signalisation d'un ensemble de récepteurs de surface dont la protéine phosphatidylinositol 3-kinase (PI3K) et la protéine kinase B (Akt). [285] Par la suite, ils ont développé une série d'analogues nommés SMAPs au sein desquels l'amine basique a été transformée en un sulfonamide neutre, et dont la nature du connecteur central et du tricycle a été variée (**2-12**, Figure 2.11 – B). [286]

Ils ont montré que la perte de la basicité de l'amine permet l'élimination de la pharmacologie associée au SNC et que le mécanisme d'action de ces composés est également lié au processus de signalisation de PI3K-Akt et Ras-Erk. L'activité des analogues les plus actifs RTC-5 **2-13** et RTC-30 **2-14** a demeuré dans l'ordre du micromolaire contre le modèle xénographique de cancer du poumon EGFR (Figure 2.11 – C). [287]

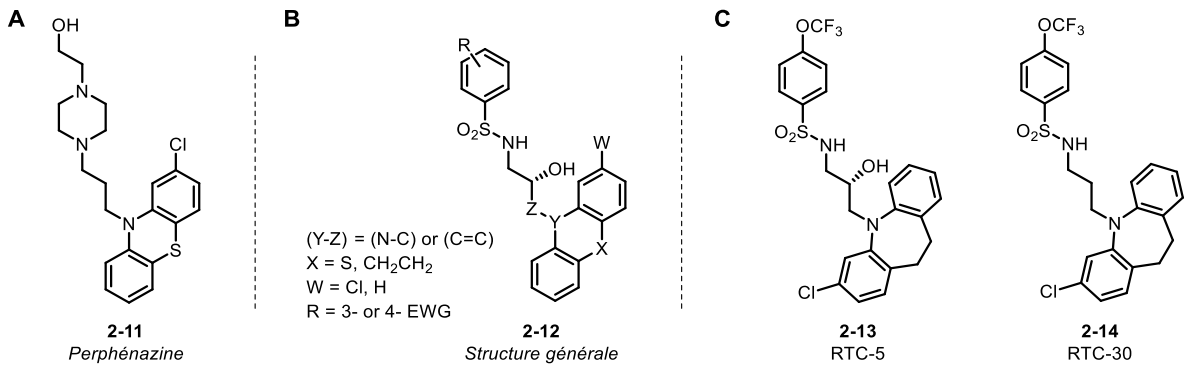

2-11 *Perphénazine* **2-12** *Structure générale* **2-13** RTC-5 **2-14** RTC-30

Figure 2.11 A. Structure du neuroleptique commercial perphénazine (Trilafon). Structure générale des dérivés tricycliques développés par Ohlmeyer. [286] Analogues tricycliques activateurs de PP2A dérivés de la perphénazine. [286]

2-13 et **2-14** ont également été actifs à l'ordre du micromolaire contre les tumeurs de type KRAS. [223,288] Certains dérivés tricycliques ont été brevetés comme effecteurs de la délocalisation de la protéine facteur de transcription *Forkhead box class O* FoxO1 dans le noyau par activation de PP2A. [289–293]

Les protéines FoxO sont des facteurs de transcription impliqués dans les processus cellulaires tels que le cycle cellulaire, la différentiation, la prolifération et l'apoptose. [294–296] Leur régulation est contrôlée par plusieurs protéines de signalisation, dont Akt et PI3K. [297,298] Leur dérégulation peut entrainer de nombreuses pathologies immunologiques, [299] cancéreuses [300] ou diabétiques. [295,296,301] Les quatre protéines FoxO principales répertoriées dans les cellules humaines (FoxO 1, 3, 4 and 6) sont contrôlées par un ensemble de biomécanismes, notamment leur délocalisation du cytosol vers le noyau cellulaire et inversement. [294] En particulier, la délocalisation de FoxO1 et FoxO3a est régulée par leur déphosphorylation. Celle-ci peut être provoquée par plusieurs phosphatases dont PP2A et il a été avancé que l'inhibition de PP2A au sein des cellules oncologiques puisse permettre d'éviter l'apoptose cellulaire engendrée par FoxO1. [302] Par conséquent, les auteurs ont proposé que l'activité antitumorale de **2-15** (Figure 2.12) puisse être renforcée par la délocalisation de FoxO1 dans le noyau suite à sa déphosphorylation par PP2A, lui permettant d'exercer sa fonction apoptotique. [293]

Etant donné la myriade d'homologues de PP2A contrôlant les divers procédés cellulaires dans

lesquels son activation est impliquée, [220] la conception de composés permettant d'agir sur plusieurs homologues impactant différents mécanismes de signalisation pouvant favoriser l'apoptose des cellules oncologiques est d'intérêt pour l'obtention d'une activité accrue. Considérant les différents effets apoptotiques résultants de l'activation de PP2A par SH-BC-893 **2-3** et les SMAPs, il a été proposé que l'insertion du pharmacophore tricyclique au sein de SH-BC-893 **2-3** puisse améliorer son activité au travers de l'activation des homologues de PP2A impliqués dans la modulation de PI3K-Akt et FoxO1. Afin de produire une série de structures hybridées, différents fragments tricycliques ont été attachés au groupement hydroxyle à l'aide d'un connecteur alkyle de 3-5 carbones (Figure 2.12). L'activité de ces composés contre PP2A a ensuite été comparée à celle de SH-BC-893 **2-3**, de la perphénazine **2-11**, et du SMAP **2-15** rapportées dans le brevet. Leur capacité à induire l'internalisation des récepteurs CD98 et la formation de vacuoles ont également été mesurées afin d'en déduire si ces composés possèdent un mécanisme d'action similaire à celui de SH-BC-893.

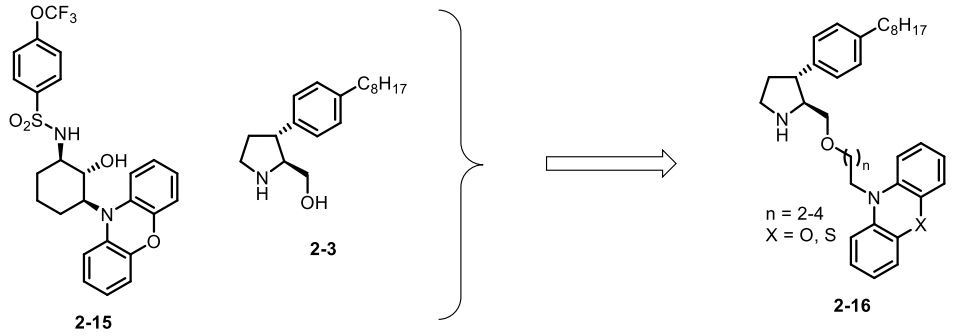

Figure 2.12 Présentation de la structure générale des analogues hybridés.

Ce projet décrit la conception, la synthèse et les tests biologiques contre PP2A de la série **2-16**. Une version optimisée de la synthèse du SMAP **2-15** ainsi que de celle d'analogues monocycliques sont également rapportées.

2.3.2 *Article 2*: Design, synthesis and anticancer activity of constrained sphingolipid- phenoxazine/phenothiazine hybrid constructs targeting protein phosphatase 2A

Jean-Baptiste Garsi[a], Vito Vece[a], Lorenzo Sernissi[a], Catherine Auger-Morin[a], Stephen Hanessian[a,], Alison N. McCracken[b], Elizabeth Selwan[b], Cuauhtemoc Ramirez[b], Amogha Dahal[b], Nadine Ben Romdhane[b], Brendan T. Finicle[b], Aimee L. Edinger[b*]*

[a] Department of Chemistry, Université de Montréal, PO Box 6128, Station Centre-Ville, Montréal, QC, H3C 3J7, Canada

[b] Department of Developmental and Cell Biology, University of California, Irvine, 2128 Natural Sciences 1, CA, 92697-2300, USA

Contributions :

- Jean-Baptiste Garsi a participé à la synthèse, la rédaction de l'article et la partie expérimentale.
- Lorenzo Sernissi a participé à la synthèse, la rédaction de l'article et de la partie expérimentale.
- Vito Vece a participé à la synthèse et la rédaction de la partie expérimentale.
- Catherine Auger-Morin a travaillé en tant que stagiaire sous la supervision de Jean-Baptiste Garsi.
- Pr. Stephen Hanessian a initié, coordonné le projet, participé à la rédaction de l'article et supervisé la rédaction de la partie expérimentale en tant que principal investigateur.
- Alison N. McCracken a réalisé les tests biologiques et participé à la rédaction de l'article et de la partie expérimentale.
- Elizabeth Selwan, Cuauhtemoc Ramirez, Amogha Dahal, Nadine Ben Romdhane et Brendan T. Finicle, ont travaillé en tant que stagiaires sous la supervision d'Alison N. McCracken.
- Pr. Aimee L. Edinger a initié, coordonné le projet et participé à la rédaction de l'article en tant que principal investigateur.

Garsi, J.-B.; Vece, V.; Sernissi, L.; Auger-Morin, C.; Hanessian, S.; McCracken, A. N.; Selwan, E.; Ramirez, C.; Dahal, A.; Romdhane, N. Ben; Finicle, B. T.; Edinger, A. L. Design, Synthesis and Anticancer Activity of Constrained Sphingolipid-Phenoxazine/Phenothiazine Hybrid Constructs Targeting Protein Phosphatase 2A. *Bioorg. Med. Chem. Lett.* **2019**, *29*, 2681–2685. DOI : 10.1016/j.bmcl.2019.07.023

2.3.2.1 Abstract

Inspired by the cytotoxicity of perphenazine toward cancer cells and its ability to activate the serine/threonine protein phosphatase 2A (PP2A), we prepared series of ether-carbon linked analogs of a constrained synthetic sphingolipid analog **3**, known for its cytotoxicity, nutrient transporter down-regulation and vacuolation properties, incorporating the tricyclic neuroleptics phenoxazine and phenothiazine to represent hybrid structures with possible synergistic cytotoxic activity. While the original activity of the lead compound **3** was diminished by fusion with the phenoxazine or phenothiazine tethered moieties, the corresponding 3-pyridyltetryl ether analog **10** showed cytotoxicity and nutrient transporter down-regulation similar to the lead compound **3**, although it separated these PP2A-dependent phenotypes from that of vacuolation.

2.3.2.2 Introduction

Endogenous sphingolipids including ceramides and sphingosine-1-phosphate are natural components of mammalian cells that have both pro-growth and pro-apoptotic functions. [303] Sphingolipids modulate a number of signaling processes that regulate the life cycle of cells. [303–305] Among the effects of sphingolipids is their ability to regulate the activity of the serine/threonine protein phosphatase 2A (PP2A). [303] The potential of small molecules to restore the tumor suppressor ability of functionally altered PP2A in cancer cells is of great interest. [183,306,307]

Sphingolipids such as ceramide (**1**) contribute to cell death in part by removing nutrient transporters from the cell surface downstream of PP2A activation, leading to death by starvation (Fig. 2.13). [183,205,211,253,255] In normal cells, nutrient stress triggers adaptive quiescence, prolonging their survival, while cancer cells that are locked in a rapidly proliferating state by oncogenic mutations experience bioenergetic crisis when they fail to undergo growth arrest.

While biologically active and tumor suppressive, ceramide is difficult to apply clinically due to its insolubility in water and ready metabolism. [303] The synthetic sphingolipid analogue FTY720 (**2**), originally conceived as an immunosuppressant and currently marketed for the treatment of multiple sclerosis under the trade name Gilenya (Fig. 2.13), was found to possess anticancer activity *in vitro* and *in vivo*. [205,213,308–311] However, FTY720 induces severe bradycardia at the anticancer dose, which has been attributed to activation of $S1P_1$ and $S1P_3$ receptors. [212,255,312,313]

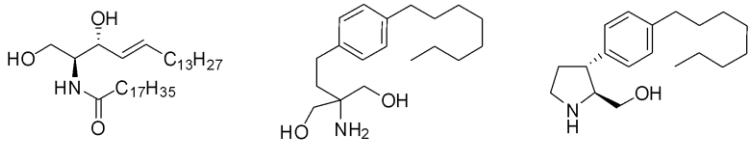

1 Ceramide **2** FTY720 **3** SH-BC-893

Figure 2.13 Structures of natural and synthetic anti-proliferative compounds

In previous reports from our laboratory we described constrained analogs of FTY720 with remarkable selectivity toward sphingosine-1-phosphate receptors ($S1P_{1\text{-}5}$). [215] More recently, we have reported structurally related 2-hydroxymethyl-3-aryloctylpyrrolidines, represented by a pharmacologically viable analog (**3**), which possesses highly favorable properties as an anticancer agent *in vitro* and *in vivo*. [183,255] This water soluble, orally bioavailable compound efficiently downregulates nutrient transporters, kills cells at single-digit μM doses, and even when phosphorylated, does not activate $S1P_1$ or induce bradycardia in mice, avoiding the dose-limiting toxicity that precludes repurposing of FTY720 for cancer. [183,255] An added feature is the ability of the lead compound **3** to cause a PP2A-dependent disruption in lysosomal fusion, visualized as extensive cytosolic vacuolation (Fig. 2.14). Preventing degradation of endosomally delivered macromolecules in the lysosome restricts cellular access to nutrients gained by processes such as macropinocytosis and autophagy and contributes to the anticancer activity of **3** *in vitro* and *in vivo*. [183,314] Furthermore, both nutrient transporter loss and vacuolation phenotypes are reversed by known inhibitors of PP2A such as Calyculin A, okadaic acid, LB100, and the protein inhibitor SV40 small t (Calyculin A data shown in Figs. 2.14 and 2.17). [183,255,314,315]

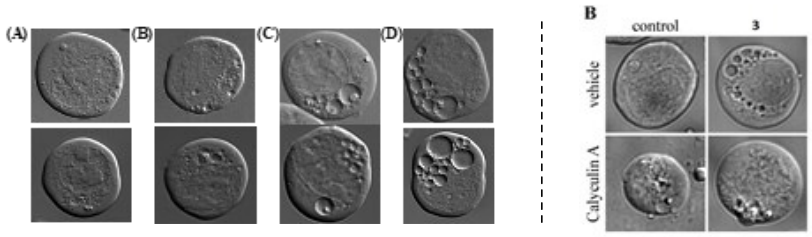

Figure 2.14 Vacuolation in FL5.12 cells. (A) Two representative vacuolation images of FL5.12 cells with vacuolation scores of: (i) 0 (no vacuoles); (ii) 1 (a few small vacuoles); (iii); 2 (multiple vacuoles); (iv) 3 (multiple large vacuoles). (B) Calyculin A protects from vacuolation caused by **3**

As would be expected for a key phosphatase, PP2A inhibition kills cells within several h, precluding direct assessment of PP2A's role in cytotoxicity. However, it is clear that the metabolic effects of PP2A-dependent vacuolation and nutrient transporter loss are an important part of the mechanism of action of **3**, as cells can be protected from death by the addition of cell-permeant nutrients. [44] Activation of PP2A has also been reported with a series of tricyclic neuroleptics such as perphenazine (**4**) [284] and by a synthetic compound incorporating a phenoxazine moiety lacking a basic nitrogen (**5**) (SMAP) [286] (Fig. 2.15). We were intrigued that a functionally important cellular enzyme such as PP2A was activated by compounds with such diverse chemical structures as **3** and the tricyclic neuroleptic **4** in which a piperazine unit was linked to a phenothiazine via a three carbons chain. With the likely premise that the lead compound **3** and perphenazine **4** were interacting at different sites within PP2A, we considered the synthesis of hybrid molecules in which the C-2 hydroxymethyl group in **3** was extended with 3–5 carbon alkyl ether chain tethers containing terminally situated phenoxazine and phenothiazine cores (Fig. 2.16).

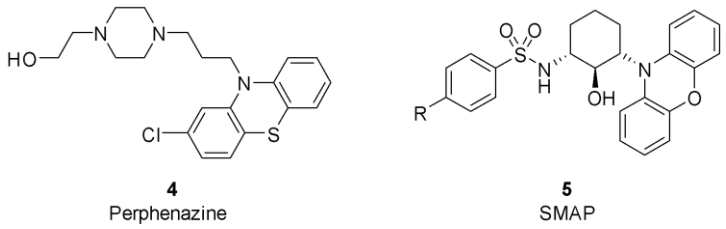

4
Perphenazine

5
SMAP

Figure 2.15 Structures of known PP2A activators

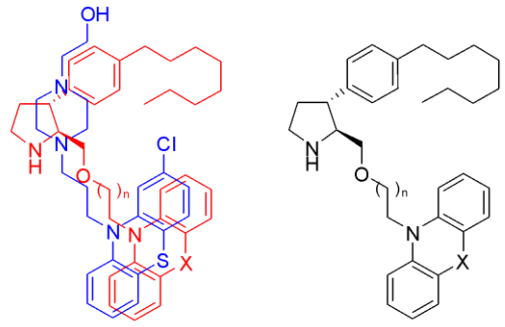

A

Expression A is the overlay of the intended hybrid (red) and perphenazine (blue).

6: n = 2, X = O
7: n = 3, X = O
8: n = 4, X = O
9: n = 4, X = S

Figure 2.16 Structures of synthetic hybrid compounds **6**-**9**

If these compounds bind PP2A at different sites, linking these two activators could potentially increase avidity above either parent compound alone, enhancing potency. We have previously shown that the positively charged nitrogen is critical for the activity of **3**. [217,255] A simple overlay of the structures of perphenazine on the intended hybrid shown as in Fig. 2.16 **A** indicated a spatially viable possible juxtaposition of the basic nitrogen atoms. It remained to be determined if the hydrophobic aryloctyl appendage, which is an important component of the lead compound **3**, would also be beneficial for the intended hybrid structures. To this end we prepared compounds **6**–**9** containing phenoxazine and phenothiazine appended units with varying chain lengths (Fig. 2.16).

We were curious to see if the presence of the phenoxazine or phenothiazine moiety in such hybrids would enhance the activity of **3** in a synergistic manner. As potential markers for the anticancer activity of these novel hybrid compounds, we would determine their cytotoxicity and monitor the PP2A-dependent phenotypes of nutrient transporter down-regulation and cytoplasmic vacuolation. [183,315]

2.3.2.3 Results and Discussion

Given that our lead compound **3**, perphenazine (**4**), and SMAP (**5**) have all been reported to activate PP2A, [183,255,284,286] we first sought to compare their ability to kill murine hematopoietic FL5.12 cells, which exhibit a rapid, cancer-like metabolism when supplied with high levels of the cytokine IL-3. While all of the compounds tested were less cytotoxic than **3**, the SMAP compound **5** was at least 8-fold less active, with an IC_{50} value of 15 μM (Fig. 2.17 and Tableau 2.5).

We next determined the degree to which these compounds could induce surface nutrient transporter loss and vacuolation. Transporter loss was evaluated by measuring surface levels of the amino acid transporter-associated protein CD98 in cells treated with 10 μM compound, a concentration at which **3** achieves maximum downregulation. Despite its slightly higher IC_{50}, perphenazine (**4**) matched the activity of **3** in CD98 down-regulation assays, while SMAP (**5**) did not reduce surface CD98 at 10 μM, consistent with its lower potency (Fig. 2.17 – A, Tableau 2.5). However, all three compounds down-regulated CD98 similarly at concentrations equal to twice the IC_{50}, suggesting an overlap in mechanism of action.

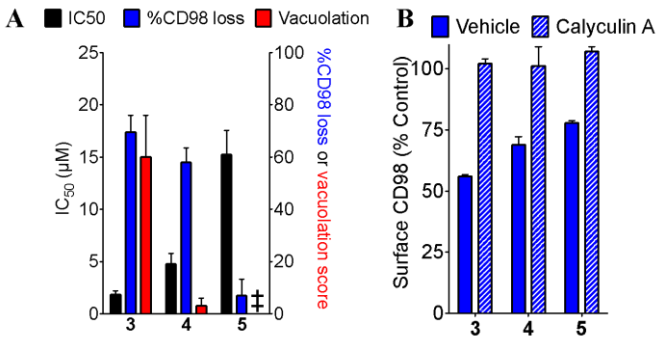

Figure 2.17 Perphenazine (**4**) and SMAP (**5**) are less potent than 3 but share PP2A dependence. (A) IC_{50}, nutrient transporter loss, and vacuolation of PP2A activators **3**-**5**. ‡Denotes a score of 0. (B) Nutrient transporter loss at 2x IC_{50} of PP2A activators shown in (A) ± pretreatment with 5 nM Calyculin A. Data in (A) are means ± S.D. and data in (B) are means ± range.

Furthermore, this phenotype was PP2A-dependent, as the PP2A inhibitor Calyculin A protected from CD98 loss in all three cases (Fig. 2.17 – B). Interestingly, neither perphenazine nor SMAP vacuolated this cell line at 10 μM (Fig. 2.17 – A, Tableau 2.5). We have previously reported that the endogenous PP2A activator ceramide also fails to produce vacuolation and in fact protects from **3**-induced vacuoles.[315] Incorporation of the phenoxazine or phenothiazine moiety as in compounds **6**–**9** decreased the activity of the parent **3**. The degree to which the phenoxazine moiety reduced activity depended on the length of the alkyl chain. Compounds with a 3–4 carbon linker such as **6** and **7** had IC_{50} values approximately 2–3 times higher than **3** and induced modest nutrient transporter down-regulation at 10 μM. Increasing the chain length as in **8** and **9** was even more detrimental to CD98 loss and cytotoxicity (Fig. 2.18, Tableau 2.5). It was evident that appending tricyclic heterocycles such as phenoxazine and phenothiazine as hybrid structures was not beneficial to the intrinsic activity of the lead compound **3**. In a previous study involving modifications of the octyl aryl appendage, [316] we realized the importance of maintaining its hydrophobic character, since the introduction of polar groups resulted in substantial loss of cytotoxicity. However, it now appears that appending ether-linked heterocyclic units at the 2-hydroxymethyl group as in compounds **6**–**7** in the current series, resulted in only a 2–4 folds loss of cytoxicity and modest downregulation at 10 μM compared to the lead compound **3**.

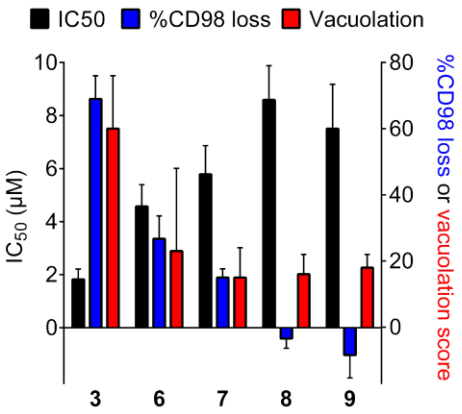

Figure 2.18 IC_{50}, nutrient transporter loss and vacuolation of synthetic hybrid compounds with increasing linker length. Data shown are means ± S.D

Tableau 2.5 IC_{50}, nutrient transporter down-regulation, and vacuolation scores in FL5.12 cells

Comp	IC_{50}(μM) ± SD	%CD98 down-regulation ± SD			Vacuolation score ± SD		
		2.5 μM	10 μM	40 μM	2.5 μM	10 μM	40 μM
3	1.8 ± 0.4	32 ± 6	69 ± 7	n.d.	46 ± 12	60 ± 16	n.d.
4	4.8 ± 1.1	19 ± 5	58 ± 6	n.d.	1 ± 2	3 ± 3	n.d.
5	15.2 ± 2.3	n.d.	7 ± 6	31 ± 8	n.d.	0 ± 0	11 ± 1
6	4.6 ± 0.8	4 ± 5	27 ± 7	n.d.	2 ± 2	23 ± 25	n.d.
7	5.8 ± 1.1	5 ± 3	15 ± 3	n.d.	7 ± 11	15 ± 9	n.d.
8	8.6 ± 1.3	n.d.	−3 ± 3	38 ± 4	n.d.	16 ± 6	66 ± 8
9	7.5 ± 1.7	n.d.	−8 ± 7	29 ± 6	n.d.	18 ± 4	42 ± 20
10	2.1 ± 0.5	40 ± 1	64 ± 3	n.d.	12 ± 10	11 ± 8	n.d.
11	2.4 ± 0.5	24 ± 5	51 ± 13	n.d.	8 ± 5	17 ± 10	n.d.
12	2.7 ± 0.5	10 ± 1	60 ± 2	n.d.	8 ± 4	15 ± 6	n.d.

This result encouraged us to probe the tolerance of side-chain appendages with less rigid and spatially more favorable monocyclic heteroaromatics containing a basic nitrogen atom. To test the hypothesis, we chose to attach 3-pyridyltetryl and 5-pyrimidinyl tetryl units to the extremity of the 2- hydroxymethyl group as first generation probes. Compounds **10**–**12** were easily prepared from a 4-carbon chain aldehyde derived from N- Boc **3** and Grignard reagents prepared *in situ* from the corresponding heteroaromatic iodides (see Schéma 8.6). Interestingly, compounds **10**–**12** maintained low micromolar cytotoxicity and good downregulation, but lacked the ability to vacuolate, indicating that this phenotype was sensitive to functional variations compared to the lead compound **3** (Figs. 2.19 and 2.20, Tableau 2.5). Of further relevance, removal of the benzylic hydroxyl group as in the 3-pyridyltetryl ether analog **10** in particular, maintained good cytotoxicity

and nutrient transporter downregulation compared to **3**. As with **3** and the other reported PP2A activators, Calyculin A successfully protected from nutrient transporter loss (Figure 9.4).

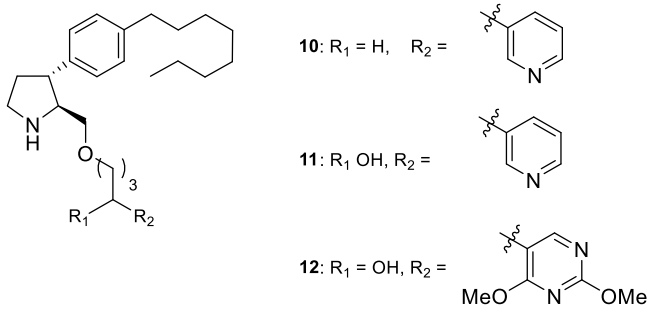

Figure 2.19 Structures of heteroaromatic linked analogs of **3**

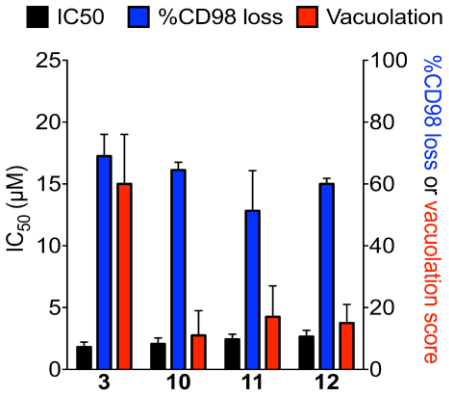

Figure 2.20 IC50, nutrient transporter loss, and vacuolation of heteroaromatic linker analogs of **3**. Data shown are means ± S.D.

2.3.2.4 Conclusions

Inspired by the anticancer activity of perphenazine and its activation of PP2A, we synthesized series of analogs of the synthetic constrained cytotoxic sphingolipid **3** in which tricyclic neuroleptic heterocycles phenoxazine and phenothiazine were appended to the hydroxymethyl group as ether linked moieties. Cytotoxicity was at best maintained and often dramatically decreased compared to **3**, suggesting that the incorporation of flat tricyclic heteroaromatic moieties as hybrid constructs with the aim of achieving synergistic cytotoxicity by combining structural elements of multiple PP2A activators was not a viable strategy. However, appending monocyclic heteroaromatics such as a 3- pyridyl unit attached by a 4-carbon chain as an ether linkage exemplified by compound **10**, maintained excellent levels of cytotoxicity and nutrient

down-regulation at lower doses than **11** or **12**. This augur well for diversification of the lead compound **3** with other heterocyclic entities attached as alkyl ethers and the prospects of improved potency and nutrient transport down-regulation as anticancer agents. Moreover, the selective loss of vacuolation capability may render compound **10** a useful tool to study the cellular factors involved in producing this phenotype.

Chapitre 3. Synthèse du motif 2-oxa-5-azabicyclo[2.2.1]heptane et extension à la formation d'analogues de l'acide gamma-aminobutyrique contraints

3.1 Objectifs de Projet

La majorité des composés pharmaceutiques développés au cours des dernières décennies possèdent une structure planaire comportant une faible fraction de carbon sp^3, principalement en raison de considération de praticabilité de synthèse. [317] Les limitations pour la découverte de nouveaux espaces chimiques générés par de telles contraintes ont été le sujet de discussions au sein du milieu industriel et académique, et la collaboration entre ces derniers pourrait détenir une des clés vers plus de diversité synthétique. [318] Ainsi, le développement de nouvelles méthodologies pour l'accès à des motifs tridimensionnels d'intérêts facilement insérable au sein de structures plus larges est considéré de première importance afin d'étendre le champ des possibles des chimistes médicinaux. [319–321] Parmi ces structures se trouve le cycle morpholine qui figure parmi les 20 hétérocycles saturés les plus recensés par la Food and Drug Administration (FDA), [322] et brevets et publications font état de l'impact positif de ce fragment lorsqu'inséré au sein de composés médicinaux. [323–326] L'ajout d'une contrainte structurelle au sein du cycle permet également d'ajouter un cran de diversité supplémentaire en générant de nouvelles espèces avec des propriétés physico-chimiques modulables, [327] et qui peuvent assurer une pré-organisation spatiale de substrat en raison de l'immobilisation de leur conformation. [180,328] Cette stratégie a été appliquée dans le passé au travers de l'insertion d'un pont à un ou deux carbones avec plusieurs succès notables. [329–336]

Une des limitations de l'appendice morpholine réside dans sa restriction de liaison par l'azote avec le reste de la molécule. Cette nécessité implique une orientation du cycle et des doublets non-liants de l'azote qui, à terme, peut l'empêcher d'interagir avec l'environnement immédiat du composé. Le développement de méthodologies de synthèse incluant de nouveaux points de fonctionnalisation sur le cycle saturé est d'intérêt afin de proposer une alternative à ce problème.

Lors de telles considérations, le contrôle et l'élucidation de la stéréochimie des groupements fonctionnels sont cruciaux afin d'assurer une orientation du cycle appropriée.

Le premier objectif de ce projet consiste à développer une méthodologie de synthèse pour l'accès à des structures 2-oxa-5-azabicyclo[2.2.1]heptane telles que **3-1** et **3-2**, dans lesquelles le noyau morpholine a été contraint à l'aide d'un pont à un carbone entre les positions C2 et C5, et où le carbone quaternaire à la position C3 inclut la présence de deux substituants introduits stéréosélectivement (Figure 3.1). Ainsi, ces composés représentent une nouvelle classe de dérivés morpholine adressant à la fois le besoin d'exploration de nouveaux espaces chimiques, et le développement de composés substitués accroissant les possibilités d'orientations spatiales lors de leur insertion dans des cibles d'intérêts thérapeutiques.

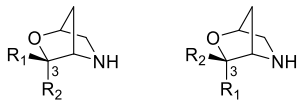

3-1 **3-2**

Figure 3.1 Structures génériques **3-1** et **3-2** des analogues 2-oxa-5-azabicyclo[2.2.1]heptane d'intérêt.

Lorsque le substituant est un groupement acide acétique, **3-4** et **3-5** peuvent également être considérés comme des versions contraintes de l'acide gamma-aminobutyrique (GABA) **3-3** (Figure 3.2 – A) ou de ses analogues β-substitués baclofen (Lioresal) **3-6** et pregabalin (Lyrica) **3-7**. (Figure 3.2 – B) Les récepteurs neuronaux de GABA sont un élément clé de la biochimie du système nerveux central (SNC) et leur dérèglement est impliqué dans la formation de troubles neurologiques. [337–339] Trois récepteurs GABAergiques majeurs sont présents dans le SNC (GABA-A, [340] GABA-B, [341] et GABA-C [342,343]), et le développement d'inhibiteurs sélectifs de chaque récepteur est amplement documenté. [344–349] Parmi eux, le développement de mimes de GABA et de baclofen (Lioresal) contraints a été étudié [350–355] et l'intérêt principal a résidé dans l'amélioration de la sélectivité du récepteur visé. [356–360] Par conséquent, les structures **3-4** et **3-5** représentent également une nouvelle classe de composés ayant le potentiel de moduler les récepteurs GABAergiques au travers d'interactions mimant celles de GABA, baclofen ou pregabalin.

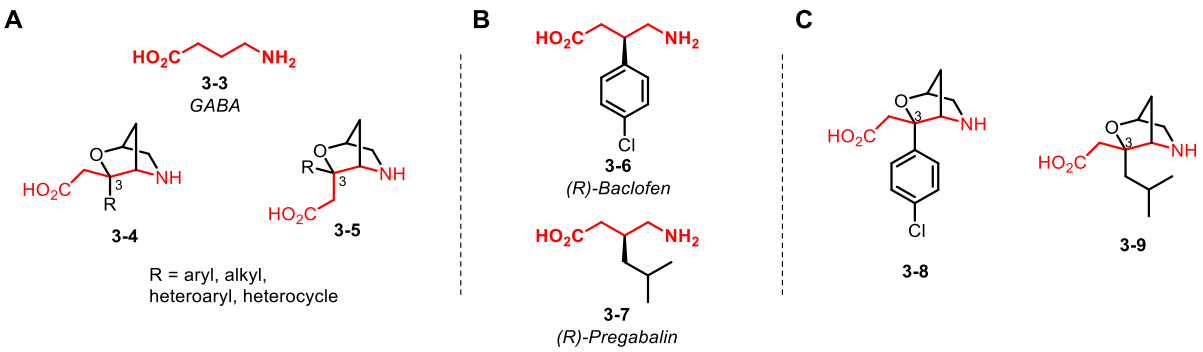

Figure 3.2 A. Motif GABA **3-3** et structures des analogues morpholines contraints contenant un motif acide aminé gamma **3-4** et **3-5**. B. Structures de baclofen (Lioresal) **3-6** et pregabalin (Lyrica) **3-7**. C. Structure des analogues contraints de baclofen **3-8** et pregabalin **3-9**.

Afin de sonder la validité de cette hypothèse, le mime contraint de baclofen **3-8** (Figure 3.2 – C) a été modélisé dans le site actif du récepteur de baclofen (GABA-B) sur la base de la co-cristallisation rapportée par Geng et ses collaborateurs. [361] Lorsque comparés, **3-8** a conservé l'orientation dans le site actif ainsi que l'ensemble des interactions de baclofen avec les résidus acides aminés environnants. (Figure 3.3)

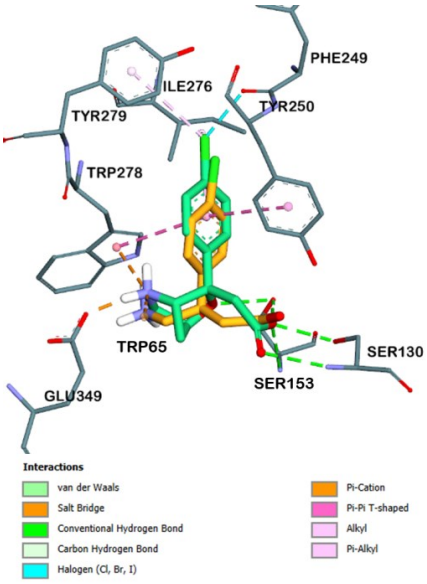

Figure 3.3 Pose d'arrimage de l'analogue contraint de baclofen **3-8** (vert) superposé au baclofen **3-6** (orange) dans le site actif de GABA-B.

Une interaction supplémentaire a également été observée entre le doublet non-liant de l'oxygène du cycle 2-oxa-5-azabicyclo[2.2.1]heptane et Ser153, mettant en avant le potentiel résidant dans la présence et l'orientation convenable de la fonction éther.

Des résultats satisfaisants ayant été obtenus, le second objectif de ce projet a été l'utilisation du groupement α-ester éthylique comme substituant au carbone C3 afin de proposer la synthèse d'un nouveau motif GABA contraint. Lorsque substitué par un phényle *para*-chloré (**3-8**) ou *iso*-butyle (**3-9**), ce dernier représente alors un mime des médicaments baclofen **3-6** et pregabalin **3-7**. Il est à noter que l'insertion de motifs GABA dans des composés carbocycliques est également d'intérêt dans d'autres contextes. [362,363]

Porthogese a été pionnier dans la synthèse du cœur 2-oxa-5-azabicyclo[2.2.1]heptane (Schéma 3.1). [364]

Schéma 3.1 Voies de synthèses vers les dérivés 2-oxa-5-azabicyclo[2.2.1]heptane.

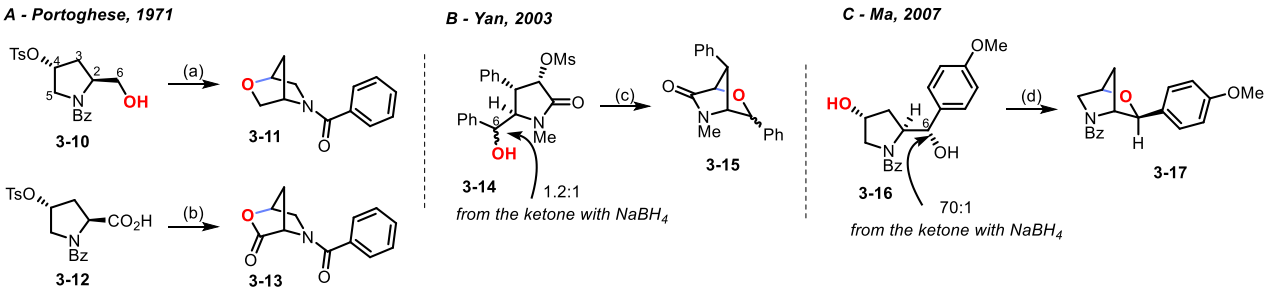

Conditions: (a) Na_2CO_3 (2.0 eq.), 2-butanone, rx, 70%. *(b)* NaOMe (1.0 eq.), MeOH:EtOH (6:1), rx, 90%. *(c)* $NaBH_4$, THF, rt, 99%. *(d)* $BF_3.OEt_2$, (7.2 eq.), Et_3SiH (8.0 eq.), CH_2Cl_2, 0°C, 82%

Depuis, plusieurs études ont été rapportées, impliquant la formation du bicycle ponté par cyclisation intramoléculaire d'un noyau pyrrolidine. [365,366]

Par conséquent, cette approche a été privilégiée lors de l'analyse rétrosynthétique. (Figure 3.4) Il a été suggéré que les morpholines pontées **3-18** et **3-19** puissent être formées par substitution du groupement tosyle par l'alcool tertiaire contenu dans **3-20** et **3-21**, lui-même résultant de l'addition de l'énolate lithié d'acétate d'éthyle sur la cétone **3-22**. La libraire de cétones aurait été à son tour obtenue par l'addition de réactifs de Grignard sur l'amide de Weinreb qui serait synthétisée à partir du dérivé 4-hydroxy-proline **3-23** en deux étapes. [316]

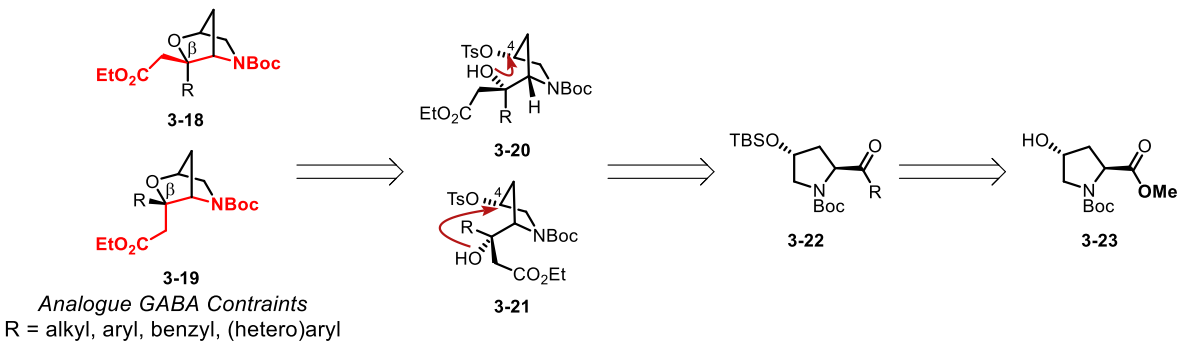

Figure 3.4 Analyse rétrosynthétique des analogues morpholines contraints contenant un motif acide aminé butyrique gamma.

L'article suivant décrit la conception et la synthèse d'une libraire de 17 exemples de 2-oxa-5-azabicyclo[2.2.1]heptane disubstitués en position C3 par un groupement α-ester éthylique et divers substituants alkyliques, benzyliques et (hétéro)aryliques. L'étude par modélisation de la position de **3-8** et de ses interactions dans le site actif de GABA-B est rapportée.

3.2 *Article 3*: 2-Oxa-5-azabicyclo[2.2.1]heptane as a Platform for Functional Diversity: Synthesis of Backbone-Constrained γ-Amino Acid Analogues

Jean-Baptiste Garsi, Solène Guggari, Thomas Deis, Myles Ma, Sofiane Hocine, Stephen Hanessian*

[a] *Department of Chemistry, Université de Montréal, 1375 Ave. Thérèse-Lavoie-Roux, Montréal, H2V 0B3 QC, Canada*

Contributions:

- Jean-Baptiste Garsi a réalisé le travail de synthèse, écrit la partie expérimentale, participé au développement du projet et à la rédaction de l'article.
- Solène Guggari, Thomas Deis et Myles Ma ont participé au travail de synthèse en tant que stagiaires.
- Sofiane Hocine a réalisé la modélisation.
- Pr. Stephen Hanessian a initié et supervisé le projet, et participé à la rédaction de l'article en tant que principal investigateur.

Garsi, J.; Guggari, S.; Deis, T.; Myles, M.; Hocine, S.; Hanessian, S. 2-Oxa-5-Azabicyclo[2.2.1]Heptane as a Platform for Functional Diversity: Synthesis of Backbone-Constrained Γ-Amino Acid Analogues. *J. Org. Chem.* **2022**. DOI : 10.1021/acs.joc.2c01338

3.2.1 Abstract

We communicate a versatile synthetic approach to C-3 disubstituted 2-oxa-5-azabicyclo[2.2.1]heptanes as carbon-atom bridged morpholines, starting with 4R-hydroxy-L-proline as a chiron. Attaching an acetic acid moiety on the C-3 carbon of the 2-oxa-5-azabicyclo[2.2.1]heptane core reveals the framework of an embedded γ-amino butyric acid (GABA). Variations in the nature of the substituent on the tertiary C-3 atom with different alkyls or aryls led to backbone-constrained analogues of the U.S. Food and Drug Administration-approved drugs baclofen and pregabalin.

3.2.2 Introduction

The morpholine ring system is a prominent component of a large number of medicinally relevant compounds. [323–326,367] It has been ranked in the top 20 most prevalent saturated nitrogen heterocycles in U.S. Food and Drug Administration-approved drugs.[322] Replacing the morpholine motif with a constrained bridged morpholine resulted in marked improvements in selectivity and activity in a number of compounds. [329–332] There are also a number of patent claims for biologically active compounds with appended N-bonded bridged morpholines. [333–336,368] Carbon-bridged morpholines confer enhanced lipophilicity when attached to drug entities. [327] Elegant approaches to a variety of bridged bicyclic amines have been recently reported by Wang and Bode [369] and Sarpong. [370] A frequently encountered one-carbon bridged morpholine is 2-oxa-5-azabicyclo[2.2.1]heptane **A**, which was first reported by Portoghese in 1971 (Figure 3.5).[364] Conformationally constrained morpholines containing one- or two-carbon bridging atoms such as compounds **A**–**C** have gained increased importance due to their unique three-dimensional topologies. [332,364,371–373] We recently reported chimeric analogues of bridged morpholine and proline units in which the lone pairs of oxygen and nitrogen atoms occupy spatially different orientations (Figure 3.5, **D** and **E**). [374] The introduction of an acetic acid unit on C-3 in the core motif **A** and further diversification with substituents of a stereodefined character would lead to novel oxazabicyclic γ-amino acids endowed with unique three-dimensional architectures. [328] Incorporating stereogenic centers in molecules of potential biological interest imparts favorable properties, especially in the context of probing the three-dimensional space of enzymes and receptors. [375,376] Introducing a carboxylic acid group in conjunction with the secondary amine in

A would constitute a new constrained γ-amino acid in the context of activities related to the CNS.[323,331,333,377]

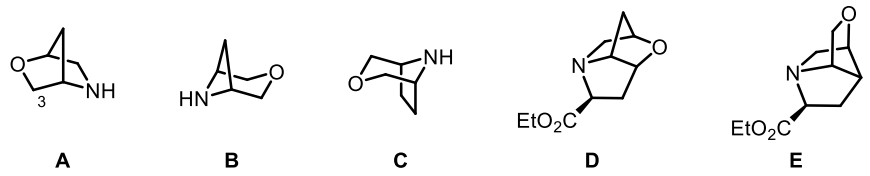

Figure 3.5 A-C Morpholines with one or two bridging carbon atoms. **D** and **E** Morpholine-proline chimeras.

Herein, we report the synthesis of a series of 2-oxa-5-azabicyclo[2.2.1]heptanes containing combinations of an acetic acid moiety and diversely appended groups on C-3, which are represented by the generic structures **F** and **G** (Figure 3.6 – B). Such compounds can be viewed as backbone-constrained examples of the venerable CNS-active compound γ-amino butyric acid (GABA), [378–382] or its β-substituted congeners baclofen and pregabalin (Lyrica) (Figure 3.6 – A). [341,347,383–388]

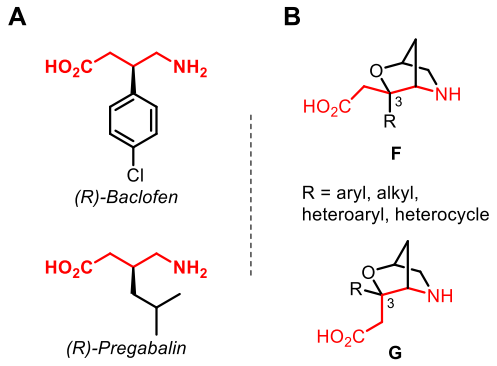

Figure 3.6 A. Structures of baclofen and pregabalin (Lyrica) B. Backbone constrained γ-amino acid-morpholine analogues **F** and **G**.

3.2.3 Results and Discussion

A well-known strategy for developing new agonists of GABA receptors lies in constraining the butyric acid backbone of GABA .[351,352,354,355,357–359,389,390] Among these compounds, some carbocyclic structures that retained the main features of GABA have been reported to be selective

inhibitors of the betaine or GABA transporter-1 [358] or the GABA-B receptor (Figure 3.7 – A). [356] This indicates that the GABA receptor can accommodate carbocyclic and azacyclic analogues.

However, bicyclic compounds such as **J** [357] and **K** [351] were devoid of GABA-receptor-binding activity even though a crystal structure of **K** adopted a conformation that matched that of GABA in the receptor (Figure 9.10).

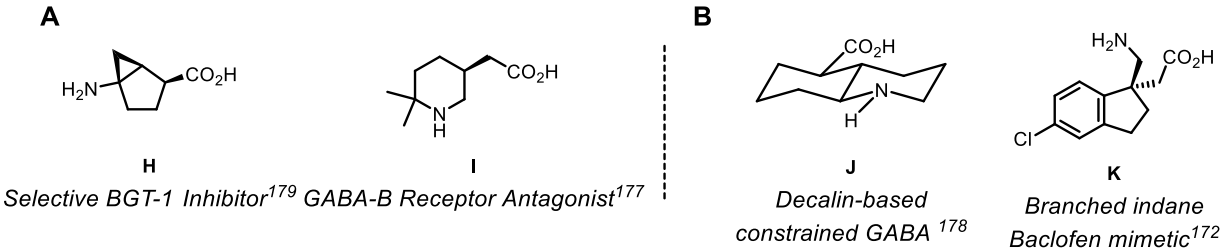

Figure 3.7 A. Constrained GABA analogues selective for specific GABA receptors. B. Examples of bicyclic analogues of GABA (**J**) and baclofen (**K**).

Incorporating the γ-amino acid motif within carbocyclic compounds is of interest in other contexts. For example, constrained γ-amino acids such as 3-amino-cyclopentanecarboxylic acid amides form parallel extended sheets. [362] They are also used as a rigid γ-amino acid spacers within macrocyclic analogues of the Arg−Gly−Asp (RDG) tripeptide in conjunction with integrin receptor activity. [363]

With this in mind, we decided to model compound **F** as a constrained analogue of baclofen (Figure 3.8, R = p- chlorophenyl) in the cocrystal structure of the GABA-B receptor with baclofen (PDB ID 4MS4).[361] The nitrogen and carbonyl of the butyric motif in **F** exhibited conserved orientations and interactions. Like with GABA and baclofen, the carboxyl unit in **F** was engaged in hydrogen bonding with Ser130 and Ser153, and the nitrogen found on the opposite side retained its interactions with Glu349, Trp65, and Trp278. (Figure 3.8, Figure 9.5 and Figure 9.7) Aromatic ring stacking similar to that reported for baclofen was found with both Tyr250 and Trp278. In addition to the expected interactions seen with baclofen, the ether function in **F** forms a hydrogen bond with Ser153, and the chlorine atom is now closer to and more stabilized by Phe249 (Figure 3.8). Interestingly, molecular modeling showed that the C-3 epimeric analogue **G** was also

accommodated within the receptor, with the orientation of the C-3 substituents being maintained (Figure 9.8). [391,392]

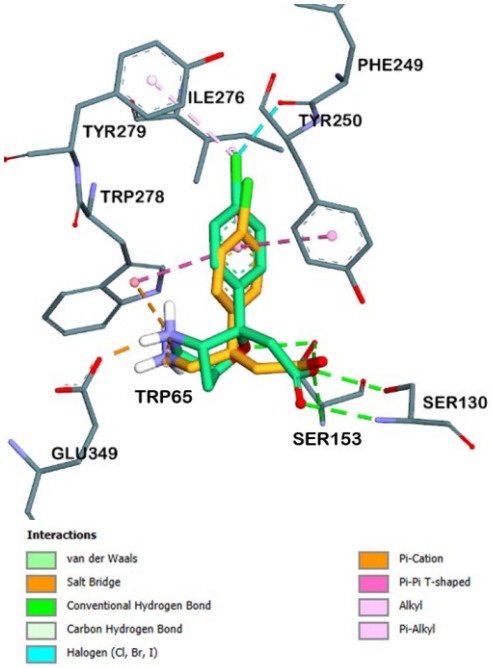

Figure 3.8 Docking pose of constrained baclofen analogue **F** (green) superimposed onto the co-crystal structure of (R)-baclofen (orange) within the GABA-B receptor. Trp65 residue was hidden for better readability.

Since the synthesis of **A** by Portoghese,[364] only scant reports describing the synthesis of analogues containing C-substituents at defined positions in the 2-oxa-5-azabicyclo[2.2.1]heptane core structure have been communicated (Schéma 3.2 – A).[333,377,393,394] Portoghese pioneered the synthesis of **A** by recognizing the value of 3-hydroxy-L-prolinol as a versatile chiron upon which an intramolecular cyclization could be effected, which led to the synthesis of the intended N-Boc 2-oxa-5-azabicyclo[2.2.1]heptane core in a 70% yield.[364] (Schéma 3.2 – A) In 2003, Yan effected an intramolecular cyclization of an α-mesyloxy lactam from a benzylic hydroxyl group to give a mixture of epimeric C-phenyl morpholinones (Schéma 3.2 – B). [365] Ma showed the successful cyclization of a secondary benzylic alcohol to give a C-aryl bridged morpholine (Schéma 3.2 – C). [366]

Schéma 3.2 Synthetic routes to 2-oxa-5-azabicyclo[2.2.1]heptanes.

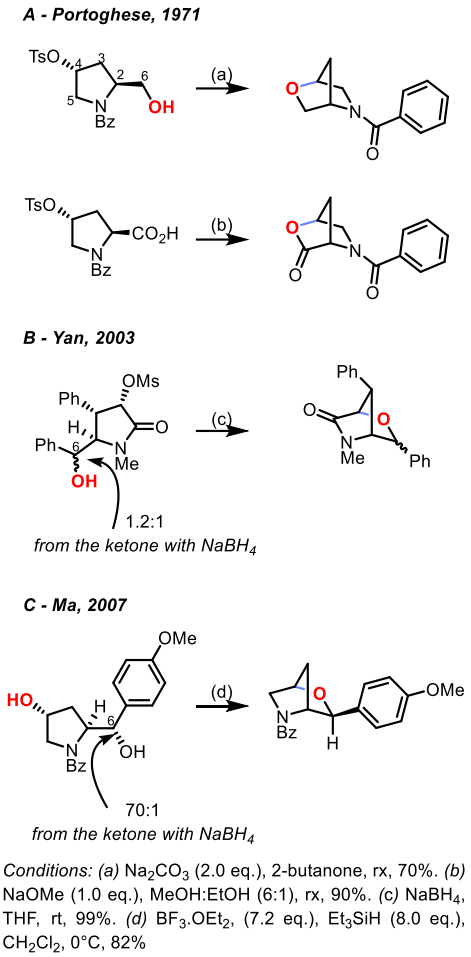

A logical approach toward C-3-functionalized 2-oxa-5-azabicyclo[2.2.1]heptanes would involve the generation of tertiary alcohols from the addition of carbon nucleophiles to ketones derived from the methyl ester of 4-hydroxy-L-proline, followed by the tosylation of the C-4 hydroxyl group and intramolecular cycloetherification (Figure 3.9). [377,395]

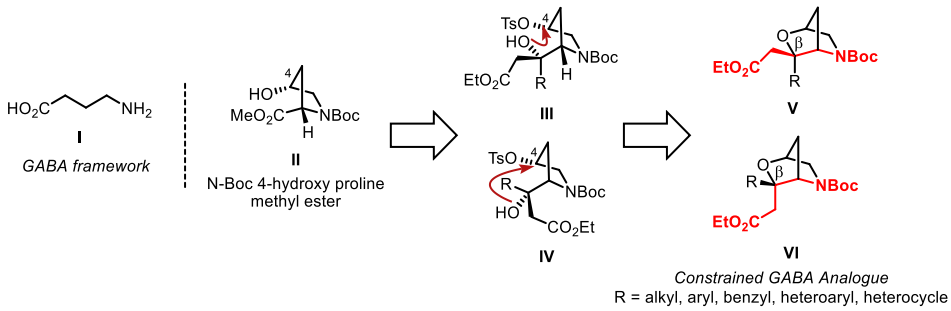

Figure 3.9 Retrosynthetic approach toward constrained ϒ-amino acid-morpholine analogues.

We used the readily available Weinreb amide **1** [316] to obtain a series of ketones **2a**–**k**, which were reacted with the Li enolate prepared from ethyl acetate to afford the corresponding tertiary alcohols (Tableau 3.1). Treatment with tosic anhydride in pyridine resulted in the selective tosylation of the secondary alcohol. After gradually being heated to 100 °C in pyridine, the corresponding bridged morpholines were obtained in good yields as pure diastereomers or were separated by silica gel chromatography. The stereochemistry at the tertiary center was assigned from NOESY measurements.

Tableau 3.1 Access to functionalized 2-oxa-5-azabicyclo[2.2.1]heptanes.

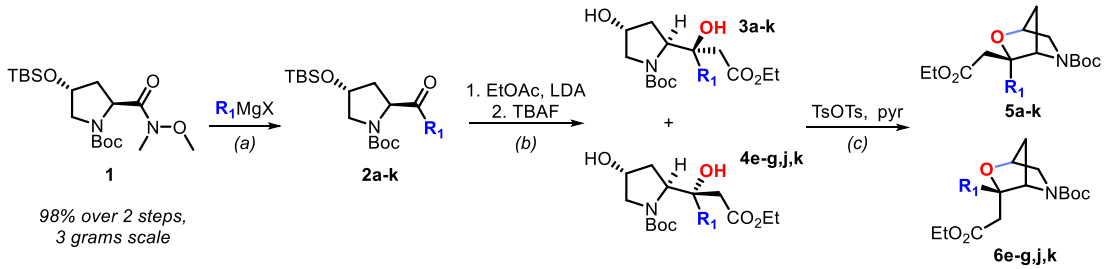

Entry	R_1MgX	Solv.	Yield	Ratio (**3**:**4**)[a]	Yield	Yield **5-6**
1	BnMgCl	THF	**2a**, 59%	**3a**/**4a** (92:8)	83%	**5a**, 74%[b]
2	3,5-$(OMe)_2$BnMgCl	THF	**2b**, 82%	**3b**/**4b** (94:6)	78%	**5b**, 66%[b]
3	3-BrBnMgCl	Et_2O	**2c**, 74%	**3c**/**4c** (96:4)	71%	**5c**, 60%[b]
4	4-FBnMgBr	Et_2O	**2d**, 65%	**3d**/**4d** (97:3)	77%	**5d**, 60%[b]
5	PhMgBr	Et_2O	**2e**, 53%	**3e**/**4e** (2:1)[d]	66%	**5e**, 49% / **6e**, 42%
6	4-ClPhMgBr	Et_2O	**2f**, 68%	**3f**/**4f** (2:1)[d]	55%	**5f**, 31% / **6f**, 35%
7	4-OMePhMgBr	Et_2O	**2g**, 74%	**3g**/**4g** (2:1)[d]	54%	**5g**, 47% / **6g**, 56%
8	EtMgBr	Et_2O	**2h**, 73%	**3h**[c]	90%	**5h**, 63%
9	*i*BuMgBr	THF	**2i**, 27%	**3i**[c]	79%	**5i**, 65%
10	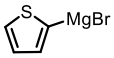	THF	**2j**, 54%	**3j**/**4j** (3:1)	68%	**5j**/**6j**, 20% (3:1)
11		THF	**2k**, 51%	**3k**/**4k** (3:1)	69%	**5k**/**6k** 54% (3:1)[e]

Conditions: (a) R_1MgX (3.0-5.0 eq.), solvent, rt. *(b)* **1.** EtOAc (3.4 eq.), LDA (3.0 eq.), THF, -78 °C; **2.** TBAF (1.1 eq.), THF. *(c)* TsOTs (3.0 eq.), pyr, rt to 100°C. [a]*Ratio determined by* ^{1}*H NMR.* [b]*The minor isomer was discarded.* [c]*Only one isomer was observed.* [d]*Isomers separated by column chromatography.* [e]*Isomers separated by preparative HPLC*

In general, good yields were obtained when the Weinreb amide **1** was subjected to a series of organomagnesium nucleophiles (Tableau 3.1, **2a**–**k**) except for the addition of *iso*-butyl MgBr to give **2i**, which was attributed to steric hindrance (Tableau 3.1, entry 9). Interestingly, an excess of the R_1MgX reagent was needed to reach full conversion in all cases, which is consistent with previous observations of **1**.[316] Excellent stereochemical control was conserved in the additions of the enolate anion to benzylic ketones **2a**–**d** (Tableau 3.1, entries 1–4). The aryl series led to ca.

2:1 mixture of diastereomeric tertiary alcohols, which favored the R-isomer (Tableau 3.1, entries 5−7). Highly stereoselective additions were observed in the reactions with the ethyl and *iso*-butyl ketones **2h** and **2i**, respectively (Tableau 3.1, entries 8 and 9, respectively). The heteroaryl ketones **2j** and **2k** completed the series with ratios similar to the aryl series favoring the (*R*) isomer albeit in poor to modest yields (Tableau 3.1, entries 10 and 11, respectively). Deprotection of the TBS group, followed by chromatographic separation, led to the individual isomers of the tertiary alcohols except for the benzyl and heteroaryl series, which were carried through as mixtures to the next step. Tosylation of each isomer, followed by intramolecular cyclization, afforded the corresponding products **5a**–**k** and **6e**-**g**, **6j**, and **6k** in moderate yields. The structures of the crystalline hydrochloride salt **7f** and the free base **7f'** derived from **6f** were determined by single-crystal X-ray analysis (Tableau 9.4, Tableau 9.5).

The highly stereoselective addition of the lithio anion of ethyl acetate to the ketones in the benzyl, ethyl, and *iso*-butyl series can be rationalized on the basis of a Felkin−Ahn model in accordance with similar cases. [396,397] A pro-*R* approach may be favored from the least hindered *Re* side in a Newman projection (Figure 3.10 – A). A similar consideration for additions to the aryl and heteroaryl ketones is less evident (Figure 3.10 – B). Based on the NOESY analysis, the assignment of the stereochemistry after cyclization confirmed the disposition of the equatorial orientation of the acetic acid ester group in the major isomers (Figure 3.10 – C).

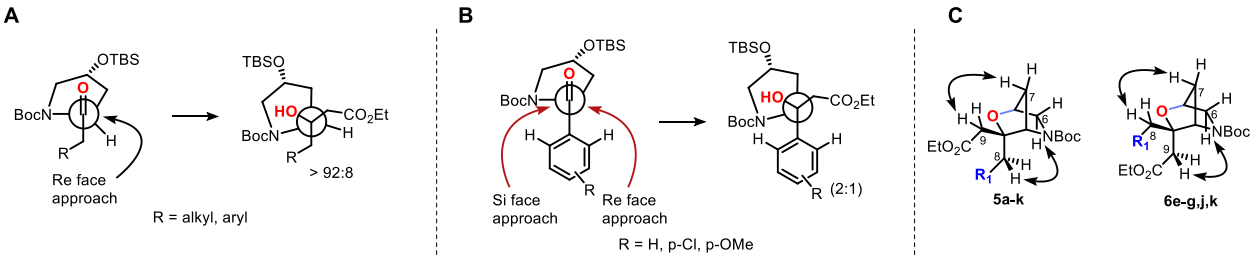

Figure 3.10 A. Felkin-Anh model for the selectivity of the ethyl acetate enolate onto ketones **2a**-**2d**, **2h**, **2i**. B. Felkin-Ahn model for the selectivity of the ethyl acetate enolate anion onto (hetero)aryl ketones **2e**-**2g**, **2j**, **2k**. C. NOESY correlations observed in analogues **5a**-**5K** and **6e**-**g**, **6j**, **6k**

Marsden, Nelson, and Foley recently disclosed LLAMA (Lead-Likeness and Molecular Analysis),[320] an open-access platform in which the novelty and viability of synthetic compounds as therapeutic agents that follow Lipinski's rule can be assessed. When modeled as free amino acids, the C-3-substituted 2-oxa-5-azabicyclo[2.2.1]heptanes **5a**–**k**, **6e**–**g**, **6j**, were found in Lipinski's space. Except for **5h**, all analogues were accommodated in the lead-like space (Figure 9.11). Their low topological polar surface areas indicated that they could cross the blood-brain barrier, and the principal moment of inertia (PMI) of these compounds was shifted toward the three-dimensional axis (Figure 9.12).

3.2.4 Conclusions

In conclusion, we report the synthesis of a series of 2-oxa-5-azabicyclo[2.2.1]heptanes substituted at C-3 with an acetic acid moiety as enantioenriched compounds that can be considered conformationally constrained analogues of γ- amino acids. Compounds substituted at C-3 with an acetic acid moiety and a p-chlorophenyl group represent bridged analogues of baclofen embedded in a morpholine core. Molecular modeling studies revealed that the bridged baclofen analogues **F** and **G** were favorably accommodated within the GABA-B receptor. We hope that the synthesis of constrained γ-amino acids based on a 3,3′-substituted 2-oxa-5-azabicyclo[2.2.1]heptane motif will be of interest in the context of medicinal chemistry projects.

Chapitre 4. Développement et applications d'un nouveau mime de diproline : Le module ProCyp

4.1 Objectifs de Projet

Au sein de la Nature, la proline se distingue des autres acides aminés en raison de son cycle azoté porté par l'amine secondaire. Sa structure de pyrrolidine la contraint à une restriction angulaire à la liaison N-Cα qui résulte en une conformation dépendant principalement de la valeur Ψ. [2] Les minima énergétiques d'une proline isolée correspondent aux valeurs d'angles Ψ = -55° et Ψ = + 145°. Lorsqu'impliquée au sein de séquences peptidiques, la proline à la capacité d'induire la formation de liaisons amide de configuration *cis*, qui jouent un rôle structurel dans l'établissement de structures secondaires comme les tournants bêtas. [398,399] Leur isomérisation *cis-trans* est également impliquée dans l'arrangement structurel des protéines, [7] et les mécanismes de contrôle de leur fonction nécessitant l'identification d'un motif de reconnaissance tels que les procédés de signalisations moléculaires. [400–402] De nombreux motifs polyproline appelés motifs riches en prolines sont également impliqués dans de tels mécanismes au travers d'interactions protéine-protéine. [4,124,402] Le développement de peptidomimétiques de ces oligomères proline est d'importance pour les maladies dégénératrices résultant de la dérégulation de ces interactions. [118]

L'acide aminé proline agit également comme biomarqueur pour certaines endopeptidases. Ces dernières nécessitent la présence d'une ou plusieurs prolines dans l'environnement immédiat du site de scission afin de procéder à leur activité hydrolytique. [60,63] Plus récemment, une nouvelle classe de ProPro endopeptidases (PPEP) a été recensée au sein des espèces Bacilli et Clostridia de la classe des Firmicutes. [61] Ces hydrolases sont capables de reconnaitre et scinder spécifiquement un motif diproline au sein de séquences peptidiques bactériennes. [403] Leur activité a été liée à la scission des adhésines lors des cycles de prolifération des pathogènes, [88,404] en faisant une cible biologique importante pour le développement de nouvelles classes de composés thérapeutiques pouvant faire face aux résistances bactériennes associées à la prise d'antibiotiques. [405,406] Pour

ces raisons, la conception de mimes du motif diproline a été un centre d'intérêt dont les succès notables se retrouvent dans plusieurs aspects de la chimie médicinale. [158,159,165,179,407,408]

L'objectif de ce projet est centré sur la conception et la synthèse d'un nouveau mime de diproline (Figure 4.1). Les éléments clés du module moléculaire repose sur trois éléments : le remplacement du second cycle pyrrolidine par un cyclopentane; la substitution de la fonction amide liant les deux unités proline par un groupement méthylène hydroxylé; l'accès stéréocontrolé aux quatre diastéréoisomères *trans*-cyclopentane partant de la L-proline dont la configuration absolue a été déterminée sans équivoque.

4-1
Motif diproline

4-2
Dimère ProCyp

Figure 4.1 Comparaison du motif diproline **4-1** avec le dimère ProCyp **4-2**.

Le cyclopentane est un mime structurel de la pyrrolidine qui a été utilisé avec succès au sein d'études antérieures. En 2000, Samuelsson a montré que le motif usuel pour la synthèse d'inhibiteurs de la thrombine D-Phe-Pro-Arg pouvait être substitué pour une triade non naturelle incluant un cyclopentane ou cyclopentene à la position P2 (Figure 4.2 – A). Ces inhibiteurs se sont montrés actifs à l'ordre du micromolaire et l'un d'entre-eux (**4-4**) a été co-cristallisé avec la thrombine. [158] Etzkorn a rapporté la synthèse de mimes du dimère Ser-Pro dans lesquels un pont alcénique a établi la jonction entre la sérine et un cyclopentane. En raison de la configuration figée de l'alcène, le composé **4-6** de configuration *cis* s'est révélé 23 fois plus actif que le composé *trans* **4-5**, mettant en lumière la configuration active préférée de Pin1 au sein de son site actif. Cette corrélation a pu être retrouvée lorsque les composés ont été testés comme agent d'antiprolifération contre des cellules cancéreuses ovariennes humaines A2780. (Figure 4.2 – B) [159] Un autre exemple a été rapporté par Wallén, dans lequel la synthèse d'inhibiteurs de la prolyl oligopeptidase (POP) a impliqué la substitution de la proline à la position P2 par un cyclopentène. [165] Ces derniers se sont révélés équipotents comparés à leur équivalent proline avec une lipophilicité accrue (Figure 4.2 – C). Le groupement hydroxyle de la position C6 dans le dimère ProCyp **4-2** remplace la fonction amide afin de simuler un intermédiaire tétraédrique résistant à

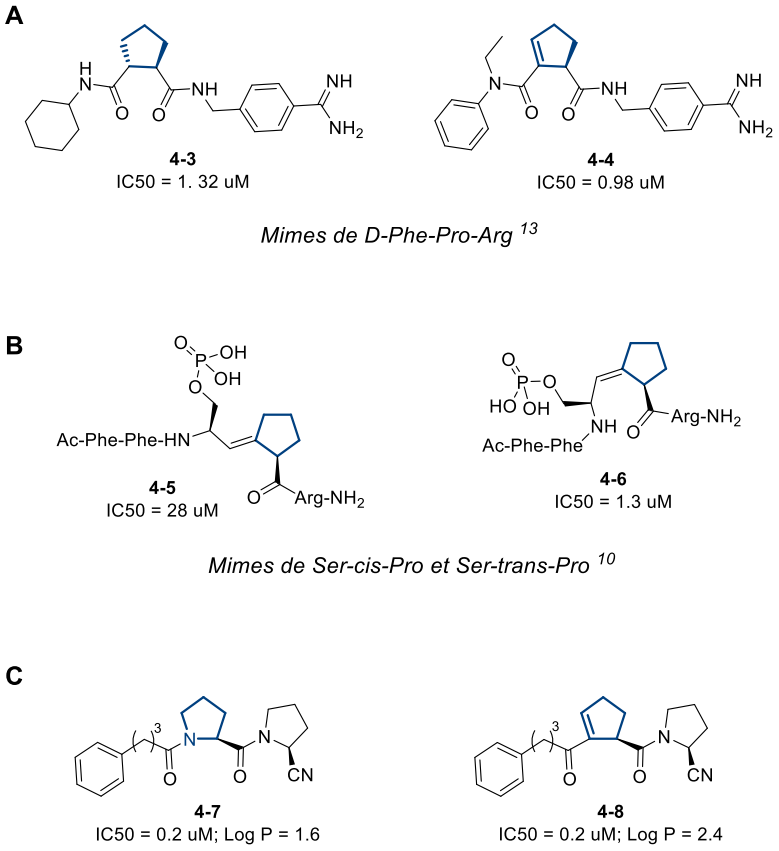

Figure 4.2 Exemples sélectionnés de composés mimétiques incluant un cyclopentane.

l'activité protéolytique de certaines protéases. Cette stratégie a été utilisée pour le développement d'inhibiteurs de la protéase aspartate et HIV-1, [174,409] menant à la co-cristallisation de la protéine avec **4-9** dans le cas de cette dernière. (Figure 4.3 – A) [410] Il est à noter que d'autres exemples de co-cristallisations de la protéase HIV-1 avec des peptidomimétiques contenant un groupement hydroxyle au cœur de leur structures ont été rapportés. [411,412] Dans chaque cas, le groupement hydroxyle s'est révélé être au contact de la triade catalytique symétrique Asp25(25')-Thr26(26')-Gly27(27'). [413] La formation de liaisons faibles avec les résidus catalytiques Asp25(25') a été observée, et il a été proposé que l'hydroxyle puisse mimer l'intermédiaire tétraédrique du mécanisme protéolytique et ainsi favoriser l'activité inhibitrice de ces composés. La flexibilité plus importante du groupement hydroxyle comparé à la liaison amide s'est également montrée d'intérêt pour la préorganisation conformationnelle des substrats en solution. [414] Lorsqu'introduit au sein d'une structure adéquate, le groupement hydroxyle peut

ainsi engendrer la formation de liaisons hydrogène intramoléculaires. Lubell a montré que la formation de tournants bêtas a été favorisée par un tel évènement en présence d'un groupement hydroxyle à la position P2 d'un tripeptide **4-10** (Figure 4.3 – B). [415] Par conséquent, l'objectif second de ce projet a été l'étude de telles liaisons au sein des dimères ProCyp.

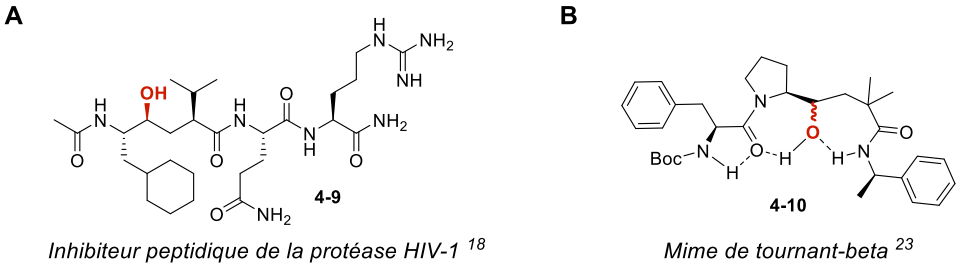

Inhibiteur peptidique de la protéase HIV-1 [18] *Mime de tournant-beta* [23]

Figure 4.3 Exemples de peptidomimétiques possédant un groupement hydroxyle.

L'accès contrôlé à différents isomères des positions C6, C7, C8 (Figure 4.1) permet de choisir l'isomère le plus prometteur pour de futures applications. Le choix de la stéréochimie à C6 peut favoriser la formation de liaisons faibles intra- et intermoléculaires avec les résidus acide aminés proches, et permettre de mimer la formation de l'intermédiaire tétraédrique lors de la conception d'inhibiteurs de protéases. La stéréochimie des carbones C7 et C8 peut être sélectionnée selon la conformation naturelle de la proline native afin de favoriser la sélection du composé par la protéine. Plusieurs exemples dénotant l'importance de la stéréochimie pour la conformation des modules diproline ou de leurs mimes ont été rapportés par Schmalz. (Figure 4.4) Sa stratégie de contrainte de dimères par la formation d'un pont éthylène a permis de les restreindre sous forme d'hélices. [139,179,416,417] Lorsqu'inclus au sein de séquences peptidiques mimant des motifs riches en prolines (PRMs), ces modules se sont montrés déterminants pour leur affinité avec un ensemble de domaines riches en prolines (PRDs) (SH3, WW, EVH1, GYF). [179,180] Ces PRDs sont impliqués dans les mécanismes de reconnaissance des interactions protéine-protéine et considérés comme des cibles difficiles d'accès pour le développement d'agents thérapeutiques. [4,118,124] Bien que le dimère ProCyp ne soit pas figé dans une conformation particulière, le choix d'un diastéréoisomère précis à l'appui d'études *in silico* peut s'avérer pertinent pour la conception d'agents thérapeutiques, en particulier pour l'inhibition d'interactions protéine-protéine.

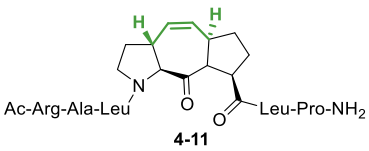

4-11

Mime de ProCyp 'verrouillé' initiateur d'hélice alpha [14]

Figure 4.4 Exemple de mime de diproline avec une conformation forcée.

L'article suivant décrit la conception, la synthèse et l'étude structurelle du dimère ProCyp en solution ainsi qu'à l'état cristallin pour certains de ses isomères.

4.2 *Article 4*: Design of Pseudodiproline Dimers as Mimetics of Pro-Pro Units: Stereocontrolled Synthesis, Configurational Relevance, and Structural Properties

Jean-Baptiste Garsi[a], Pedro M. Aguiar[a], Stephen Hanessian[a]*

[a] *Department of Chemistry, Université de Montréal, 1375 Ave. Thérèse-Lavoie-Roux, Montréal, H2V 0B3 QC, Canada*

Contributions:

- Jean-Baptiste Garsi a effectué le travail de synthèse, participé au développement du projet et à la rédaction de l'article.
- Pedro Aguiar a développé, supervisé le protocole associé à la partie expérimentale de RMN et contrôlé l'exploitation des résultats.
- Stephen Hanessian a initié, supervisé le projet et participé à la rédaction de l'article en tant que principal investigateur.

Garsi, J. B.; Aguiar, P. M.; Hanessian, S. Design of Pseudodiproline Dimers as Mimetics of Pro-Pro Units: Stereocontrolled Synthesis, Configurational Relevance, and Structural Properties. *J. Org. Chem.* **2021**, *86*, 16834–16847. DOI : 10.1021/acs.joc.1c02061

4.2.1 Abstract

Stereocontrolled methods are described for the synthesis of hitherto unreported pseudodiproline dimers in which a cyclopentanecarboxylic acid is linked to a pyrrolidine residue by a stereochemically defined hydroxymethylene tether. These proline-cyclopentane (Pro-Cyp) dimers have interesting structural characteristics as seen in their X-ray crystal structures as well as their nuclear magnetic resonance (NMR) spectra in CDCl3. They can be considered to be novel Pro-Pro mimetics, which can be used to replace natural diproline sequences with potential applications in medicinal chemistry. They also represent a new concept in the peptidomimetic design of chimeric proline-based amino acids as carbocyclic hydroxyethylene isosteres of inhibitor molecules, in which the stereodefined bridging hydroxyl group can simulate a tetrahedral intermediate in an enzyme complex.

4.2.2 Introduction

In their own unique capacity, the 20 proteinogenic amino acids represent nature's enabling toolbox to write the alphabet of life.[418] Among these, proline is the only cyclic amino acid harboring an α-substituted carboxylic acid side chain and a secondary amine, both of which engage in amide bond formation with other amino acids to generate proteins that populate the proteome and engage in a myriad of essential physiological processes.[2,419] As if ordained by evolutionary selection, proline plays a primordial role as the quintessential cornerstone amino acid in such proteins. Proline residues have a propensity to induce a cis-amide bond conformation within a peptide sequence consisting of three consecutive amino acids.[3,7] A consequence of its five-membered pyrrolidine ring structure is the imposition of conformational properties defined by the restricted torsion angle of the N−Cα bond. In effect, proline can be found in two conformations which correspond to Ψ minima of −15 and +155°.[420] Proline is one of nature's many gifts to the life sciences, manifesting its versatile properties and uses across several subdisciplines. Prominent examples of simple proline-containing drugs and natural products are shown in Figure 4.5. Captopril (N-3-mercapto 2R-methyl acetyl L-proline) was the first rationally designed drug marketed to treat hypertension targeting angiotensin-converting enzyme (ACE), a pivotal component of the blood coagulation cascade.[143] (Figure 4.5, A). Currently used modifications such as enalapril and ramipril consist of a proline amide derivative and a proline

encompassed in a bicyclic octahydroindole core structure, respectively.[421,422] Vildagliptin, featuring a pyrrolidine nitrile, is a dipeptidyl peptidase 4 (DPP4) inhibitor used for the treatment of type-2 diabetes.[423] Proline figures prominently in the repertoire of natural products, as exemplified by the neuroexcitatory kainic acid and acromelic acid.[424–426] (Figure 4.5, B).

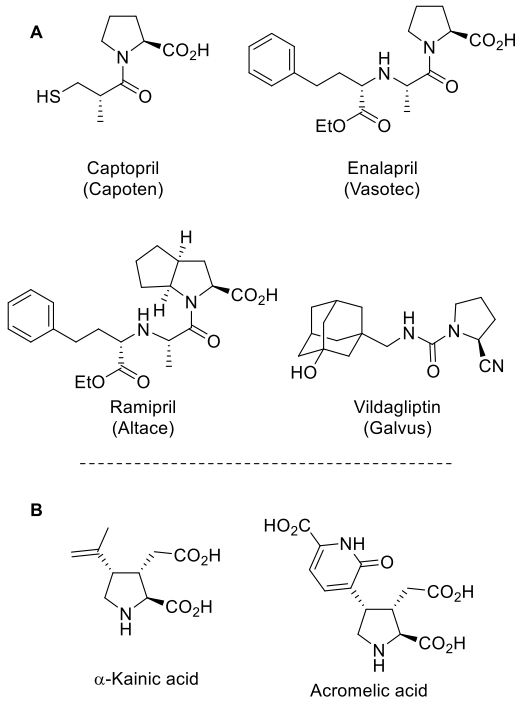

Figure 4.5 Occurrence of proline in (A) small-molecule therapeutics and (B) natural products.

Perhaps the most consequential property of proline is related to its ubiquitous occurrence in proteins, thereby conferring unique three-dimensional conformational features that are manifested in the performance of specific physiological or biophysical functions.[427] This is particularly evident in proteins that are rich in proline and in 4-hydroxy-proline residues such as in collagen.[427–430] Proteins consisting of multiple proline residues in sequence are exemplified by the polyproline II (PPII) architecture, whose structure and function in biology are widely documented.[5,92,96,431] Proline-rich motifs (PRMs) play a key role in protein−protein interactions (PPI), currently recognized as a popular target for drug action.[4] PRMs consist of several proline units which can be sequential or spaced.[427,431] The particular topology of the PRM and its flanking residues makes it recognizable by proline recognition domains (PRD).[4,124,432] This phenomenon has been exploited for the development of peptidomimetics as inhibitors of PRDs linked to

immune disorders.[116,433] Some of these active compounds involve a modification in the amino acid sequence while retaining structural features of the PRM required for recognition.[116] Of interest is a study by Lim which demonstrated that the proline residue in proline-rich sequences of peptides binding to SRC homology 3 (SH3) domain and rsp5-domain (WW) can be exchanged for an unnatural N-substituted amino acid, showing that the proline residue is most likely the main recognition feature in PRD binding grooves.[432] Mimicking a Pro-X motif also proved useful toward the development of prolyl oligopeptidase (POP) inhibitors as well as to induce specific secondary structures.[131,165,416]

Engineering new pseudodiproline Pro-X dimers as isosteres to mimic Pro-Pro units in peptide sequences of relevance to medicinal chemistry is a conceptually and practically challenging task. In this regard, there are only a handful of reports where a proline residue was replaced with a carbocyclic entity. The first example was reported by Hoppe in 1991, involving a cyclopentanecarboxylic acid ester bearing a phenylalaninol unit at C2, for the development of potential protease inhibitors that are resilient to hydrolytic activity (Figure 4.6 – A).[434] Samuelsson used cyclopentane and cyclopentene dicarboxylic acids as proline mimics of a Pro-Arg unit and achieved the cocrystallization of bioactive amide analogues with thrombin (Figure 4.6 – B).[158] Related examples have been reported with cyclohexane dicarboxylic acids as replacements for proline units and intended as enzyme inhibitors.[435–437] A strategy aimed at prolyl isomerase Pin1 inhibitors was reported by Etzkorn, in which *cis*- and *trans*-aminoethyl-alkylidene branched cyclopentanecarboxylic acid amides were intended to be Ser-Pro surrogates (Figure 4.6 – C).[438] Both units were inserted in peptidomimetics of the Pin1 ligand, and the *cis*- isomer proved to be 23 times more potent than the *trans*-isomer, thereby highlighting the preference of the enzyme for the native Ser-cis-Pro conformer and showing the value of locking conformations. [159] Etzkorn also reported the synthesis of an isostere of Gly-Pro-Hyp replacing the proline unit with a cyclopentanecarboxylic acid bearing a *trans*-alkene. However, insertion into a tripeptide unit destabilized the collagen triple-helix conformation (Figure 4.6 – D).[407]

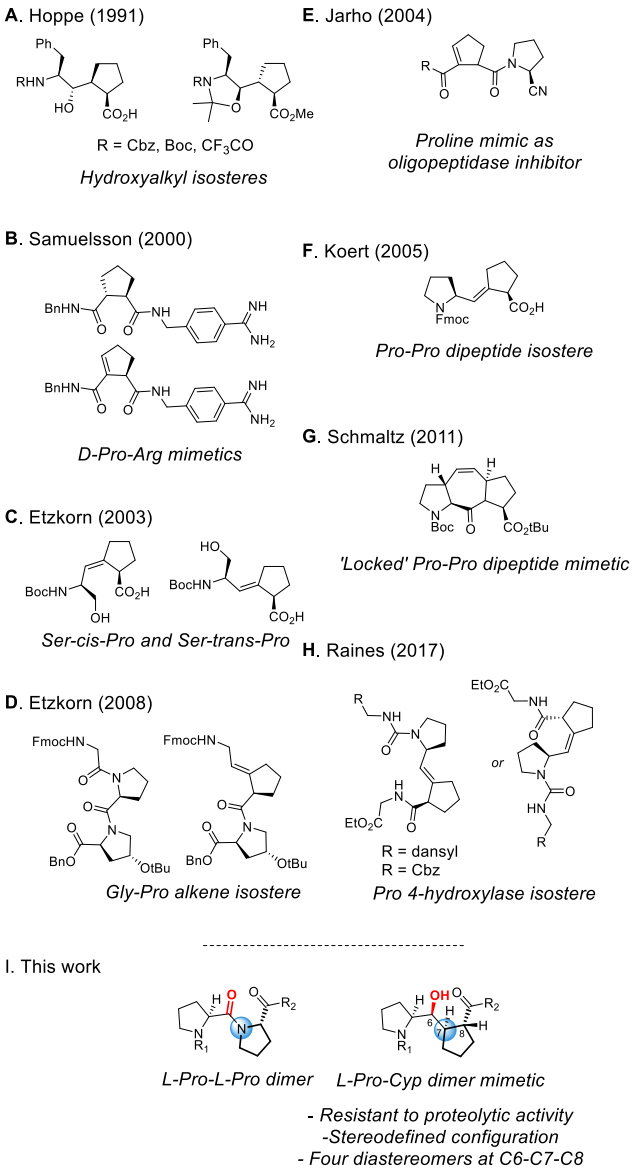

Figure 4.6 (A-H) Selected examples of *cyclopentanecarboxylic* acids as Pro-X mimetics – (I) Access to four Pro-Cyp dimers.

Jarho used a 1,2-cyclopentene-carboxylic acid as a proline mimetic to prepare a series of amide analogues as potential oligopeptidase inhibitors. This substitution increased the lipophilicity compared to the parent diproline and did not interfere with its activity as a POP inhibitor.[165] (Figure 4.6 – E). Koert extended the use of an alkene cyclopentanecarboxylic acid motif as a diproline isostere aiming at a locked *trans*-configuration of the native diprolyl amide bond (Figure 4.6 – F). The dimeric motif was readily adaptable to solid-phase peptide synthesis.[439] Schmaltz and co-workers designed and synthesized tricyclic Pro-Pro mimics by bridging two

prolines at C-3 and C-5 with a cis-ethylene linker (Figure 4.6 – G).[179] They further demonstrated that the proline units were locked with the correct angle as seen in PPII helixes. When introduced as a Pro-Pro replacement in a peptidic sequence capable of binding SH3 PRD, the binding properties were retained. Following this study, they successfully extended the strategy to the synthesis of related analogs.[139,416,417,440,441] Finally, Raines synthesized cis- and *trans*-diproline isosteres and showed which conformation of the native peptidyl bond is preferentially recognized by collagen prolyl 4-hydroxylase. It also strengthened the idea that alkenes could be made use of as replacements for peptide bonds (Figure (Figure 4.6 – H).[408]

Inspired by these elegant examples of diproline mimetics and our own interest in peptidomimetic design, [442–445] we conceived an isostere of a Pro-Pro dimer in which the C-terminal proline unit is replaced by a saturated cyclopentanecarboxylic acid with an intervening secondary hydroxy- methylene group that could simulate the amide carbonyl oxygen in a typical diproline unit (Figure 4.6 – I). It was important to devise synthetic strategies that would lead to isosteres of the natural L-Pro-L-Pro dimer among other non-natural congeners. Given the correct spatial orientation, the C6 hydroxyl group of the L-prolinol unit in these Pro-Cyp pseudodiproline isosteres could possibly mimic the tetrahedral intermediate found in proteolytic mechanisms.[446] They could also be elaborated into end-differentiated amide analogues encompassing hydrolytically stable carbocyclic hydroxyethylene isosteres. Insertion of acyclic hydroxyethylene and hydroxyethyleneamino units as isosteres in protease inhibitors has been a successful strategy.[174] Several examples of human immunodeficiency virus 1 (HIV-1) protease crystal structures complexed with hydroxyethylene-based peptidomimetic inhibitors have been reported.[410–412] Martin and co-workers introduced a hydroxyethylene group into a macrocyclic peptidomimetic inhibitor of HIV-1 protease.[409] Of importance is that the stereochemistry of the carbon atom bearing the hydroxyl group was of critical importance for binding, highlighting the value of accessing diverse stereodefined isomers. Lubell has reported on the merits of replacing the amide bond with a hydroxyl group as Pro-Aib hydroxyethylene isosteres of *β* turns.[415]

4.2.3 Results and Discussion

4.2.3.1 Retrosynthesis.

As our main objective, we devised a strategy that would provide access to four enantiomerically distinct pseudodiproline Pro-Cyp dimers linked to a *trans*-configured cyclopentanecarboxylic acid via an *R*- or *S*-hydroxymethylene tether starting with L-proline as a common progenitor. Toward this end, we envisaged that generic Pro- Cyp structure **I** could be derived through ring-closing metathesis (RCM) from bis-alkene **II**, which would result from a sequential Michael addition and the enolate allylation of unsaturated ester **III**. The secondary hydroxyl group at C6 in **IV** would be generated via addition of a propiolate ester anion to commercially available N-Boc prolinal **V** (Figure 4.7 – A). On the basis of previous reports from our laboratory and applications to natural product synthesis,[447–450] we anticipated that the intended Michael reaction and subsequent enolate alkylations shown in Figure 4.7 – A would be sufficiently stereocontrolled, leading to two enantiomerically pure Pro-Cyp amino acids **A** and **C**, from which the remaining duo of **B** and **D** could be prepared by functional group transformations as their orthogonally protected N-Boc methyl esters.

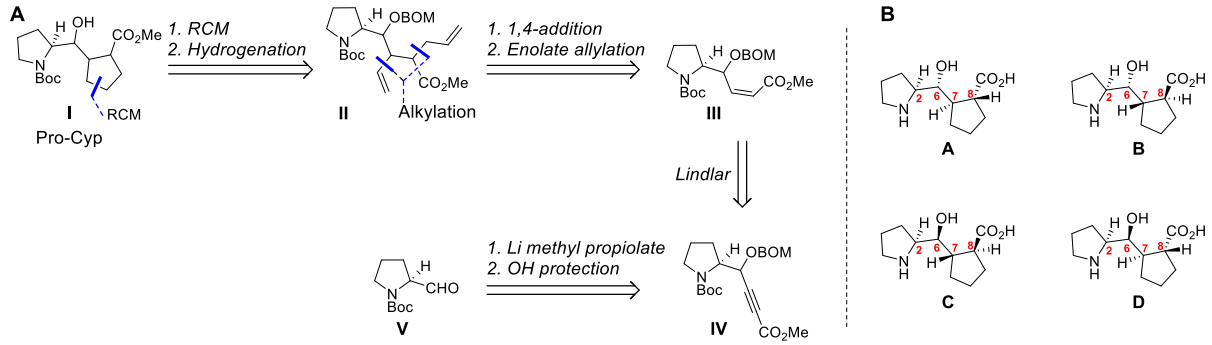

Figure 4.7 (A) Retrosynthesis toward pseudodiproline (Pro-Cyp) dimer units. (B) Isosteres of L-Pro-L-Pro (**A** and **D**) and unnatural congeners (**B** and **C**).

4.2.3.2 Synthesis of Pseudodiproline (Pro-Cyp) Dimer Units.

The addition of (3-methoxy-3-oxoprop-1-yn-1-yl)lithium to *N*-Boc prolinal **1** led to a quantitative yield of diasteromers **2** and **3** in a 1:2 ratio (Schéma 4.1, A Series). [444,445] This was acceptable because both compounds were easily separated by column chromatography and used in parallel as two linear series. A single-crystal X-ray structure identified **3** as the major isomer resulting from

a *Re* addition to the aldehyde. Protection of the hydroxyl group in **3** as the (benzyloxy)methyl ether (BOM) followed by a reduction with the Lindlar catalyst gave *cis* unsaturated ester **4**.

Schéma 4.1 Synthesis of Pro-Cyp Acyclic Precursors **5** and **6** (A Series).

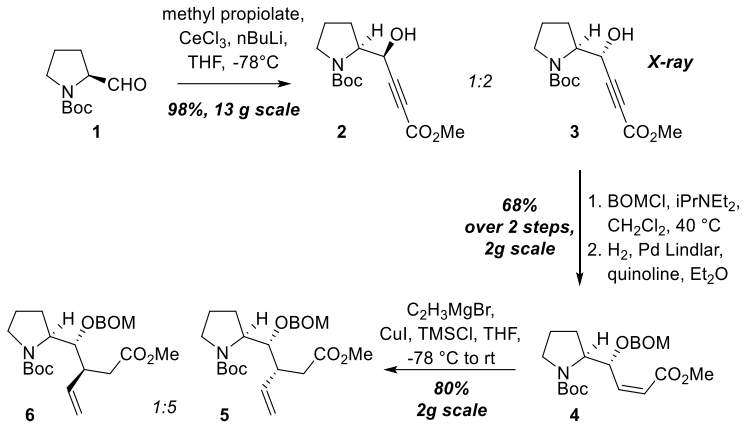

Treatment of 4 with a mixed vinyl magnesiocuprate reagent at −78 °C in the presence of trimethylsilyl chloride (TMSCl) led to an inseparable 5:1 mixture of *syn*- and *anti*-diastereomers **5** and **6** in 80% yield.[450] (Schéma 4.2).

Schéma 4.2 Synthesis of Pro-Cyp Dimers **9** and **10**

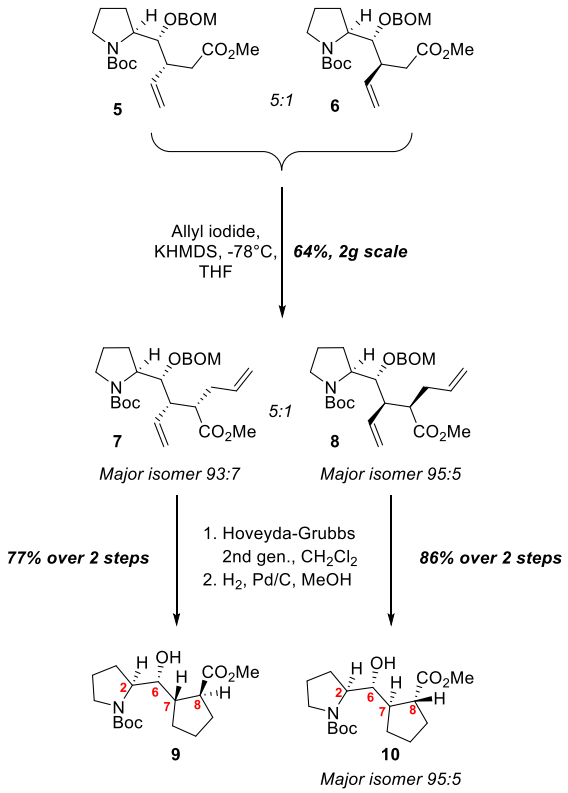

The generation of the K enolate from the mixture of **5** and **6** with potassium bis(trimethylsilyl)amide (KHMDS) followed by the addition of allyl iodide and chromatographic separation on silica gel gave both **7** and **8** as major isomers in 93:7 and 95:5 ratios, respectively. A ring-closing metathesis reaction with **7** and **8** using the second-generation Hoveyda-Grubbs catalyst [451] followed by catalytic hydrogenation led to the pseudodiproline Pro-Cyp dimers **9** and **10**, respectively.

A single crystal X-ray structure of **9** confirmed the structure, and the *syn-/ anti*-6*R*,7*S*,8*S* stereochemistry (vide infra). It also validated the proposed *anti-/ syn*-6*R*,7*R,*8*R* stereochemistry of **10**. We then turned our attention toward C6 *S*-isomer **2**, which was converted to **11** following the same protocol described above for **4** (Schéma 4.3, B Series). However, in this case, the vinyl magnesiocuprate addition to **11** led to *anti*-isomer **13** as the major isomer with only traces of the *syn*-isomer (<2%, not isolated). Addition to the *trans*-ester **12** led to the same result.[452] Allylation of the K enolate generated from **13** led to the *α*,*β*-disubstituted ester **14.** Ring-closing metathesis and hydrogenation afforded the 6*S*,7*S*,8*S* pseudodiproline Pro-Cyp dimer **15** in 49% yield over three steps (Schéma 4.3, B Series).

Schéma 4.3 Synthesis of the Pro-Cyp dimer **15** (B Series)

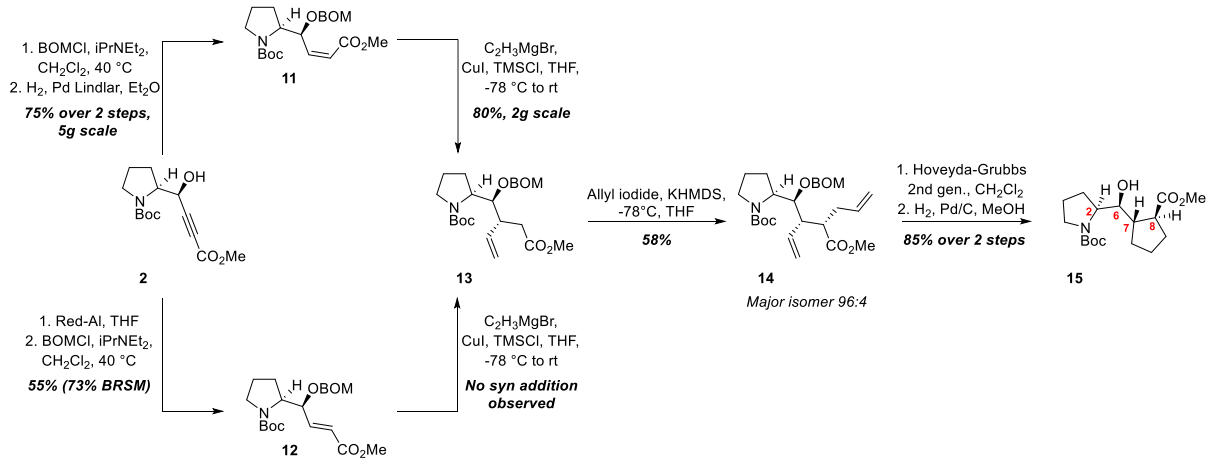

To obtain the fourth pseudodiproline Pro-Cyp dimer **D** (Figure 4.7 – B), we adopted a classical oxidation/reduction protocol. Thus, **10** was oxidized with Dess-Martin periodinane (DMP) and the resulting ketone was reduced with sodium borohydride (NaBH4), delivering **16** as the major product in a 5:1 ratio (Schéma 4.4). Other reducing agents such as L-Selectride did not

improve the selectivity. The X-ray structure of **16** confirmed the *syn- /anti*-6*S*,7*R*,8*R* stereochemistry and revealed an intramolecular H-bond between the C6 hydroxyl group and the N-Boc carbonyl which was not observed in the structure of isomeric **9** (Schéma 4.4). Application of this two-step oxidation−reduction protocol to **9** afforded a 1:3 mixture of starting material as an alternative approach to **15**. Thus, four orthogonally protected pseudodiproline Pro-Cyp dimers were synthesized in enantiomerically pure form, and the structures of **9** and **16** were confirmed by X-crystallography and corroborated by NMR analysis. Cleavage of the N-Boc and ester groups led to diastereomeric L-Pro-L-Pro isosteres **A** and **D** as the free amino acids in addition to their unnatural congeners **B** and **C** (Figure 4.7 – B, Schéma 8.7).

Schéma 4.4 Access to Pro-Cyp **15** and **16** via a two-step oxidation/reduction sequence

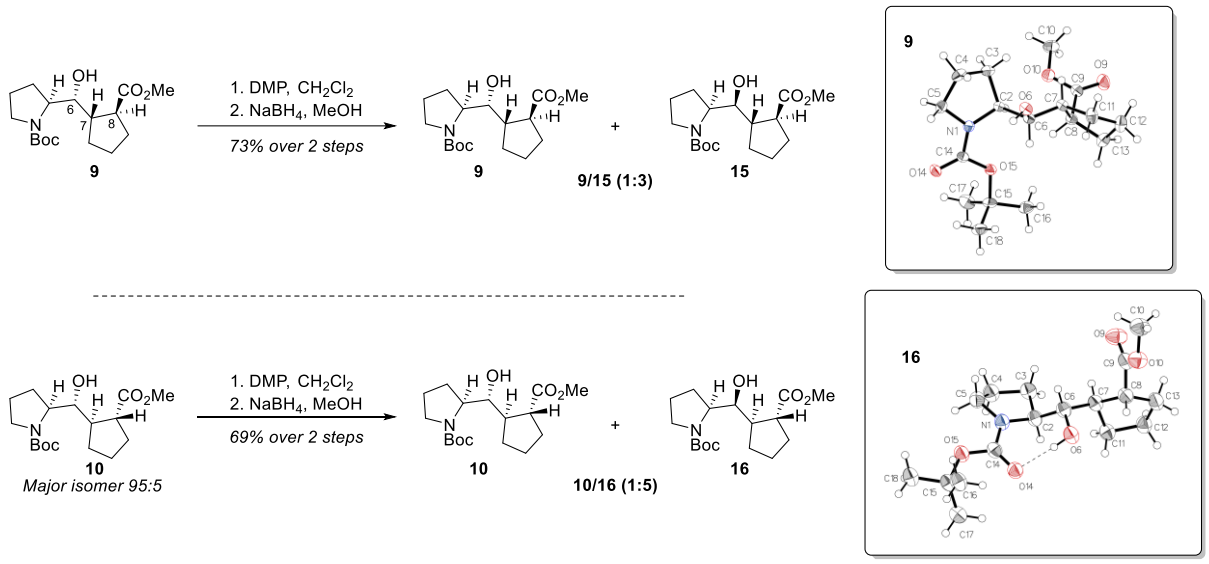

4.2.3.3 Stereoselective Cuprate Addition.

The origin of the observed diastereoselectivity in cuprate conjugate addition reactions of enoate esters remain somewhat enigmatic. In 1987, Yamamoto first reported a study in which the geometry of the unsaturated ester determined the stereochemical outcome.[453] Soon after, a report by Dorigo and Morokuma rationalized the stereoselectivity based on steric and electronic effects which were substantiated by ab initio molecular orbital studies.[454] Their results were in close agreement with the experimental data of Yamamoto favoring the formation of *anti*-products from *trans*-esters and *syn*-products from *cis*-esters as major isomers. However, later

studies showed that *syn*-or *anti*- adducts could be obtained regardless of the *cis*- or *trans*-geometry of the unsaturated ester.[455–457]

We have previously reported that the addition of lithium dimethylcuprate to methyl (*S*,*E*)-4-((benzyloxy)methoxy)-5- ((tert-butyldiphenylsilyl)oxy)pent-2-enoate in the presence of TMSCl afforded the corresponding 3-C-methyl adduct in high yield and 14:1 *anti*- /*syn*-selectivity.[447] These results were in accordance with previous studies in which the *γ*-substituent dictated the stereochemical outcome.[448,450,455,456] In considering various stereocontrolled approaches to the four pseudodiproline Pro-Cyp dimers (Figure 4.7 – B), we chose to proceed with the *cis*-unsaturated esters for the convenience of synthesis, being cognizant that the presence of the *N*-Boc L-pyrrolidinyl unit, the *R*-or *S*-OBOM group, and the ester could dictate the stereoselectivity of the cuprate addition to different extents. In the case of **11** involving a C6 *S*-alkoxy group, the major product arising from the cuprate addition was *anti*-isomer **13**, and only traces of the *syn*-isomer were observed (<2%, not isolated). To evaluate the importance of the *cis*-or *trans*-geometry of the unsaturated esters, we performed the cuprate addition on *trans*-ester **12**, which also led to *anti*-isomer **13** as the only isolable product. (Schéma 4.3). However, cuprate addition to **4** incorporating a C6 *R*-alkoxy group led to *syn*-adduct **5** as a 5:1 mixture with *anti*-isomer **6**. In fact, both *syn*- and *anti*-adducts would be used in the synthesis of the intended dimers.

In previous studies, cuprate additions to unsaturated esters bearing a *γ*-ether [447-450] or acetal [455,456] led to *anti*-products. However, the presence of a *γ*-*N*-Boc group substituent [447] or *N*-Boc/*O*-acetal groups [457] afforded *syn*-products. Considering that the *δ*-*N*-Boc L-pyrrolidinyl unit and the ester group are common in both A and B series, it appears that the *R*-or *S*-configuration of the C6 OBOM group is the only variable. Although the formation of major products in both series can be rationalized on the basis of the Felkin–Ahn transition-state models, [447,455,456] another study carried out with computational methods to better understand the role of the *δ*-*N*-Boc pyrrolidinyl unit in combination with the OBOM and ester groups leading to the formation of *syn*- or *anti*-products may be of interest. In their seminal studies, Yamamoto[453] and Morokuma[454] did not address the influence of the configuration of the carbon carrying the *γ*-alkoxy group on the stereoselectivity of conjugate additions to enoate esters.

4.2.3.4 NMR Studies.

Analysis of the X-ray crystal structures and correlations with NMR spectral data revealed interesting insights into the three-dimensional structures of the four diastereomeric pseudodiproline Pro-Cyp dimers **9**, **10**, **15**, and **16**. In the crystalline state, dimer **16** with a C6 *S*-hydroxyl group forms an intramolecular H-bond with the *N*-Boc carbonyl group, resulting in a seven-membered ring. The unit cell consists of two antiparallel Pro-Cyp units with no intermolecular H-bonds. The well-resolved ^{1}H NMR spectrum of **16** in $CDCl_3$ at 25 °C also involves a H-bond between the C6 *S*-hydroxyl group and the *N*-Boc carbonyl, which results in a relatively well-ordered structure (Figure 4.8 – A). The stability of the H-bond was low as evidenced by the rapid exchange with 5% D_2O (Figure 9.15, p. 382). The ^{1}H NMR spectrum of dimer **15** also harbors a C6 *S*-hydroxyl group and an intramolecular H-bond with the *N*-Boc group is evidenced by the lower field resonance of the hydroxyl (OH) group. (Figure 4.8 – B) The change in chemical shifts observed between the spectra in $CDCl_3$ and DMSO-d_6 was consistent with the presence of an H-bond in **9, 15** and **16** (Figure 9.13, p.380 and Figure 9.16, p. 383). Interestingly, the X-ray of dimer **9** bearing a C6 *R*-hydroxyl group revealed no intramolecular H-bonding (Figure 4.8 – C). Instead, a network of intermolecular H-bonds was present in the crystal lattice (see Section 9.4.2.1). Its ^{1}H NMR spectrum consisted of time-averaged broadened signals as a 2:1 mixture of rotamers which could also be observed in the proton-decoupled carbon ($^{13}C\{^{1}H\}$) spectrum. By and large, the ^{1}H and $^{13}C\{^{1}H\}$ NMR spectra for dimers **9**, **15**, and **16** were similar, showing minor variations in the chemical shifts of the OH group. Interestingly, variations at C2 and C6 were distinguishable between the C6-*R* and the C6-*S* isomers (Figure 4.8). The ^{1}H NMR spectrum in $CDCl_3$ at 25°C of dimer **10** with a C6 *R*-hydroxyl group (as in the crystalline dimer **9**), showed time-averaged broadened peaks in contrast to the two congeners **15** and **16**. However, a notable feature in the ^{1}H NMR spectrum of **10** was the significant upfield shift of the C6 *R*-hydroxyl resonance (Figure 4.8 – D). The resonance of the C6 hydroxyl group in dimers **15** and **16** respectively occurred at lower field and showed a progressive shift to higher field in dimers **9** and **10**, possibly reflecting their respective positions relative to the *N*-Boc (or ester carbonyl) group. This was also evidenced in the ^{13}C NMR spectra of the four dimers (Supporting (Figure 9.14, p.381).

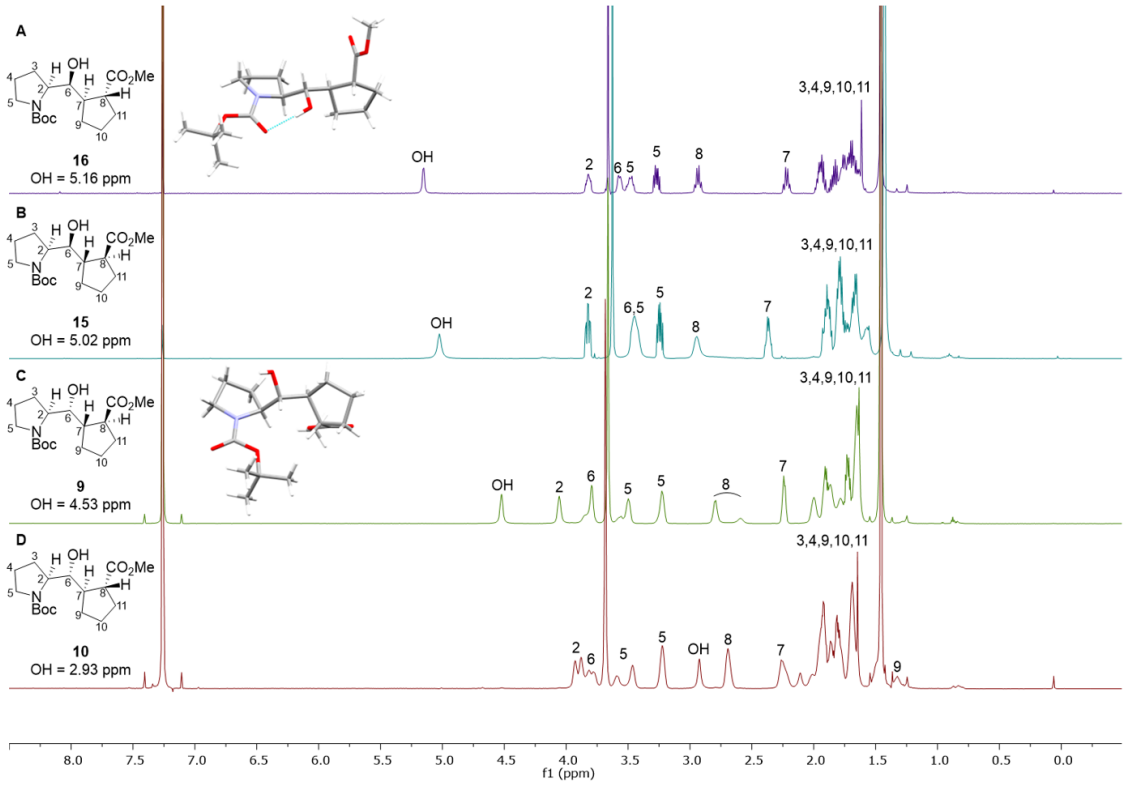

Figure 4.8 ^{1}H NMR spectra of the four Pro-Cyp dimers at 25 °C

Excellent resolution was observed at −50 °C for all four isomers, and the rate of exchange was slow enough to observe *J* coupling of the hydroxyl hydrogen for H-bonded isomers **9**, **15**, and **16** in contrast to the unchanged broad signal of **10** (Figure 9.17, p. 384). The *trans*-relationship at C7-C8 in **9** and **15** was confirmed by a nuclear Overhauser effect (NOE) study (see Section 9.4.1.2). To override intramolecular H-bonding effects, we recorded the ^{1}H NMR spectra of the four dimers in pyridine-d_5 and in DMSO-d_6 which resulted in a downfield shift of the OH signals. (Figure 9.16, p. 383 and Figure 9.18, p. 385) Interestingly, similar spectral profiles could be observed depending on the stereochemistry of the hydroxyl group. The similarity of structures seen by X-ray analysis in the solid state and by ^{1}H NMR in solution is not uncommon in the design of inhibitor molecules in medicinal chemistry.[414] These observations may have relevance when considering the replacement of a L-Pro-L-Pro unit with isosteric Pro-Cyp mimetics such as **10** and **16**. It is of interest that the infrared frequencies of the hydroxyl group in the H-bonded pair **15** and **16** (neat in CHCl3) were shifted lower ($\simeq$ 3350 cm^{-1}) compared to those for **9** and **10** ($\simeq$ 3450 cm^{-1}), which supports the presence of an H-bond in the series carrying a C6 *S*-hydroxyl group, in contrast to

their C6 *R*-hydroxyl congeners.[458] This behavior is also in agreement with the lack of H-bonding observed in the X-ray structure of **9**.

4.2.4 Conclusions

We have developed stereocontrolled methodologies to prepare novel L-Pro-L-Pro mimetics consisting of an L-pyrrolidinyl unit and a cyclopentanecarboxylic acid (Pro-Cyp unit), linked by a hydroxymethylene tether. Four diastereomers with defined stereochemistries at four contiguous stereogenic centers are accessible, starting with L-proline as a chiral progenitor. The key reactions relied on the stereocontrolled conjugate addition of a vinyl magnesiocuprate reagent to *γ*-alkoxy *cis*-*α*,*β* unsaturated esters, followed by highly stereoselective *α*-allylation of the ester via enolate chemistry to generate three contiguous stereogenic centers. Ring-closing metathesis followed by catalytic reduction led to the intended pseudodiproline Pro-Cyp dimers in enantiomerically pure form, whose structures were also confirmed by X-ray crystallography and detailed NMR analysis. Remarkably, three of the four Pro-Cyp dimers engage in intramolecular H-bonding with the *N*-Boc carbonyl, resulting in pseudotricyclic structures in $CDCl_3$ solution. This structural feature was clearly observed in the crystalline solid state of one of the dimers. Two of the four prototypical pseudodiproline Pro-Cyp dimers (**A** and **D** in Figure 4.7 – B) can be considered to be isosteres of the natural L-Pro-L-Pro dimer unit found in segments of biologically relevant proteins. The incorporation of mimetics of natural L-Pro-L-Pro dimers such as **A** and **D** (or oligomers derived from their union) with extensions at the L- pyrrolidinyl *N*- and Cyp-*C* terminal positions, aided by molecular modeling or X-ray crystallography, can have interesting applications in the inhibition of protein−protein interactions in which contiguous proline residues are sites of recognition for biological function.

Chapitre 5. Application du dimère ProCyp à la synthèse de peptidomimétiques médicinaux

5.1 Conception de mimes de triprolines pour l'inhibition de l'interaction protéine-protéine p22^{phox}-p47^{phox} de NOX2.

5.1.1 Objectifs de Projet

Au sein du protéome humain, un nombre important d'enzymes et de protéines est dédié à la protection de l'hôte contre l'invasion de pathogènes. [459–461] Parmi elles, la nicotinamide adénine dinucléotide phosphate oxydase (NOX) est responsable de la production d'espèces réactives d'oxygène (ROS), et se trouve de façon prévalente dans le corps humain. [125] Sept isoformes de la protéine NOX (NOX1-5, DUOX1 and 2) ont été recensées jusqu'à maintenant. L'isoforme majeure NOX2 se trouve principalement au sein des cellules neutrophiles contrairement aux autres isoformes qui sont localisées dans différents tissus. [462] Le rôle principal de NOX2 réside dans la production de l'anion superoxyde O_2•- lors du piégeage d'organismes par les leucocytes phagocytiques afin de favoriser leur activité antimicrobienne. Cependant, l'activité de NOX2 ainsi que celle de ses homologues a également été liée à certains mécanismes de signalisation impliqués dans la fonction cellulaire et l'apoptose. [463,464]

La régulation de la production de ROS réside dans l'assemblage des sous-unités composant NOX au travers de mécanismes de phosphorylation et d'interaction protéine-protéine (PPI). [125] Ces mécanismes sont déclenchés sous l'influence de stimuli physiologiques ou bien par la présence de particules phagocytiques dans le cas de NOX2. Cependant, certains signaux pathologiques comme le stress cellulaire peuvent entrainer une dérégulation de l'activation de NOX et générer une surproduction de ROS. [465] Lorsque l'excès de ROS ne peut pas être neutralisé par l'hôte, NOX devient alors un facteur de stress oxydant. La présence de ROS libres au sein du corps peut résulter en un ensemble de biomécanismes délétères incluant l'endommagement de l'ADN,

l'apoptose, ainsi que la détérioration de mécanismes de signalisation pouvant amener à divers problèmes inflammatoires, notamment diabétiques et cancéreux. [466–469] De nombreux troubles liés aux dommages sur le système nerveux central peuvent également émerger. [470–474] En raison de sa présence dans les cellules inflammatoires, l'isoforme NOX2 est associée à la plupart des développements de telles conditions dégénératives.

Le complexe NOX2 est composé de plusieurs sous-unités dont l'assemblage est nécessaire pour sa fonction. L'hétérodimère gp91-phox/p22^{phox} compose le flavocytochrome transmembranaire b_{558} qui est supporté par trois protéines facteurs cytosoliques (p40^{phox}, p47^{phox} et p67^{phox}) ainsi qu'une protéine GTPase de type Rac, principalement Rac2. [462] La protéine membranaire gp91-phox contient le site catalytique nécessaire à la production de ROS et p22^{phox} assure l'intégrité structurelle du complexe au travers de sa liaison avec p47^{phox} lors de son activation. Au repos, la triade cytosolique est unie par p67^{phox} qui ponte les unités p40^{phox} et p47^{phox}. (Figure 5.1) [475]

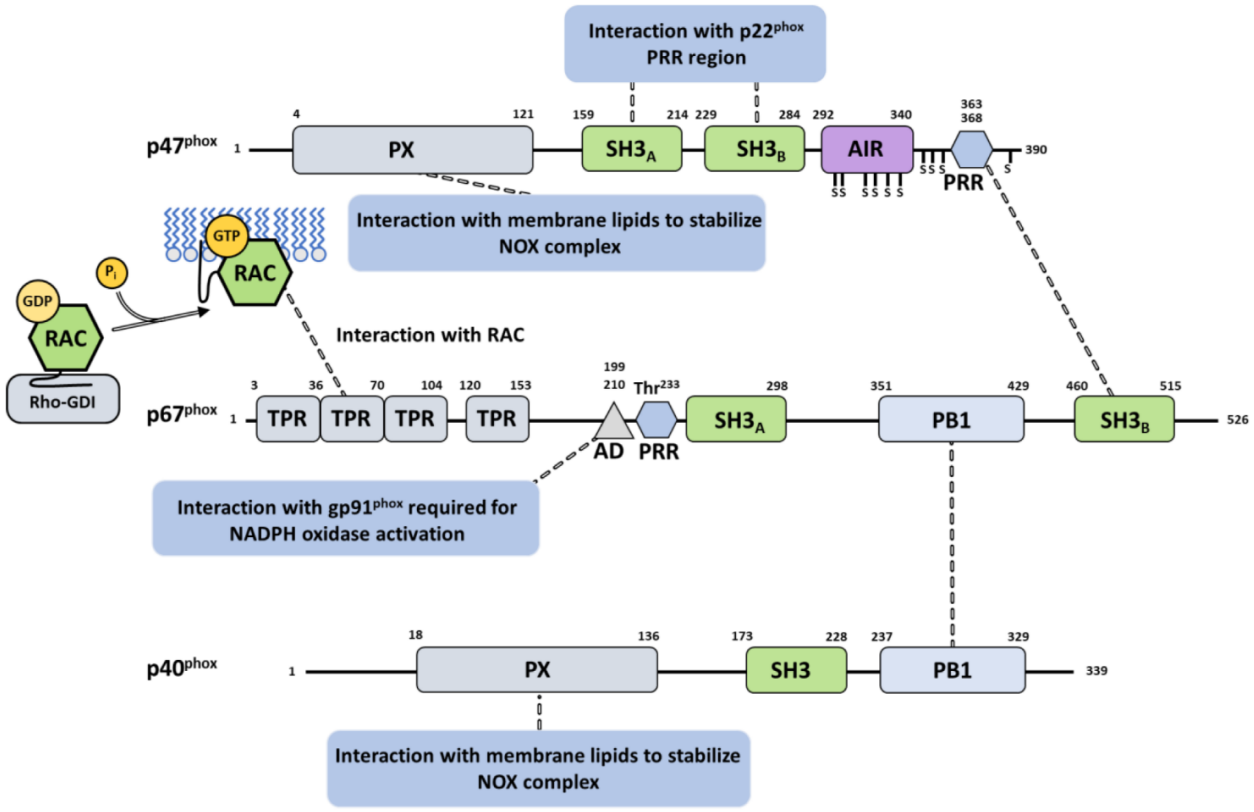

Figure 5.1 Diagramme d'interactions entre les protéines facteurs cytosoliques p47^{phox}-p67^{phox}-p40^{phox} lors de l'assemblage du complexe activé NOX2. [462]

Sous l'influence d'un stimulus externe, la phosphorylation de p47^{phox} révèle certaines portions protéiques lui permettant de translocaliser l'hétérotrimère p47^{phox}-p67^{phox}-p40^{phox} via l'interaction protéine-protéine de son domaine riche en proline (PRD) Src Homologique 3 (SH3) avec le motif riche en prolines (PRM) de p22^{phox}. [476,477] Au cours de la phosphorylation, la protéine GTPase est également libérée de son inhibiteur RhoGDI et vient s'associer au complexe membranaire via p67^{phox} afin de compléter la formation de l'espèce NOX activée. [462] L'implication de NOX2 dans les maladies liées à sa dérégulation en a fait une cible d'intérêt pour le développement de composés thérapeutiques liés à son inhibition. [119,478] Au sein des molécules brevetées pour leur action contre NOX2, certaines d'entre elles interfèrent dans l'assemblage de ses sous-unités, [479] notamment au travers de l'interaction protéine-protéine p22^{phox}-p47^{phox} en raison de son rôle clé dans l'activation du complexe. Parmi elles, on trouve des petites molécules comme le composé sélénié Ebselen [480] ou le produit naturel apocynine avec certains succès pour le traitement de maladies cérébrales *in vivo*. [481,482] Des dérivés peptidiques tels que le peptide antibactérien PR-39 [483] et gp91ds-tat [484] ont également été rapportés comme inhibiteurs de l'interaction p22^{phox}-p47^{phox}.

Ogura a étudié par RMN la structure du domaine SH3 de p47^{phox} complexé à un peptide mimant la partie riche en proline de p22^{phox} en solution. (Figure 5.2 – A) [485] Son étude a révélé que p22^{phox} (en rouge) est stabilisé par les zones C- et N-terminales (en bleu et en vert) du domaine SH3. La séquence peptidique exacte du site de reconnaissance de p22^{phox} s'étend sur seize acides aminés incluant sept prolines dont un motif ProProPro central (**5-1**) qui possède une conformation gauche polyproline de type II. (Figure 5.2 – B) Cette observation a également été faite lors de l'étude cristalline de Rittinger entre le domaine SH3 de p47^{phox} et le peptide p22^{phox}. [486]

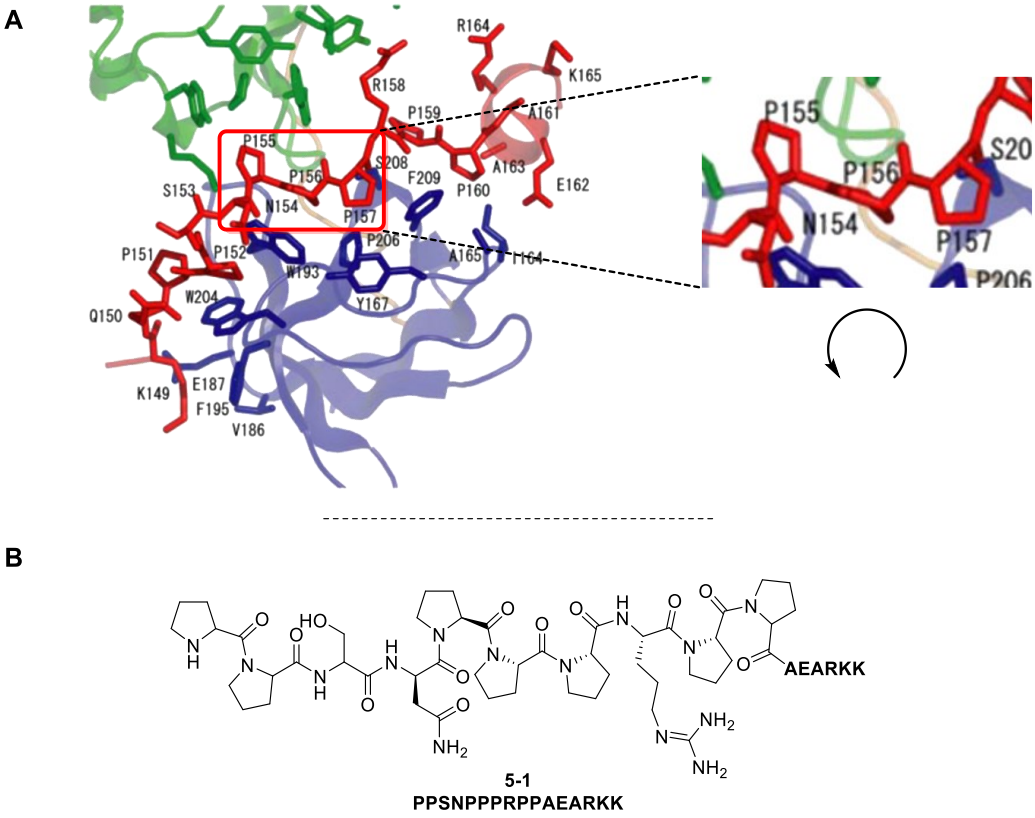

Figure 5.2 A. Site de reconnaissance du motif riche en proline de p22^{phox} (rouge) par le domaine riche en proline de p47^{phox} (bleu : partie N-terminale, vert : partie C-terminale). [27] B. Séquence hexadécapeptidique de p22^{phox} reconnu par le domaine SH3 de p47^{phox}.

Au cours d'études préalables, nos collaborateurs chez Servier ont effectué des études structurales de l'interaction p22^{phox}-p47^{phox} afin de proposer une nouvelle classe de peptidomimétiques. La séquence hexadécapeptidique de p22^{phox} a été décomposée en trois parties lors de leur conception. La partie gauche concerne les résidus PPSN, la partie centrale le motif ProProPro et la partie droite les résidus RPPA. Les résidus EARKK ont été supprimés lors du design en raison de leur caractère facultatif. Après optimisation des fragments gauche et droit, le composé de tête **5-2** a été obtenu pour l'étude du trimère ProProPro central. (Figure 5.3)

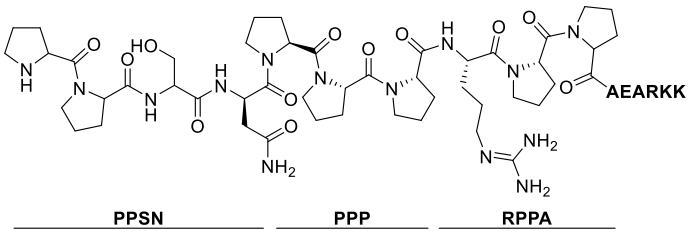

5-1
PPSNPPPRPPAEARKK
SPR Kd = 0.214 µM

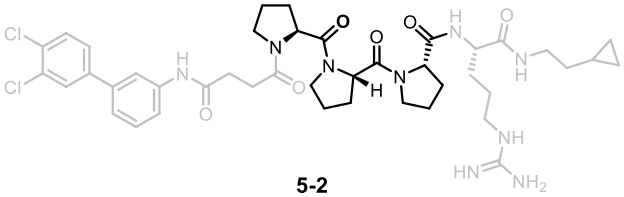

5-2
Peptidomimétique ProProPro
SPR Kd = 0.043 µM

Figure 5.3 Peptidomimétique ProProPro **5-2** dérivé de l'héxadécapeptide PPSNPPPRPPAEARKK **5-1** reconnu par le domaine riche en prolines SH3 de p47.

L'objectif de ce projet a été le remplacement du motif central ProProPro **5-3** par les triades ProCypPro **5-4** et ProProCyp **5-5** dans lesquelles une diproline a été remplacée par le dimère ProCyp. (Figure 5.4 – A) Bien que le protéome humain ne recense pas de proline-proline endopeptidase, la réduction du nombre de liaisons amide présente un intérêt pour la stabilité des peptides en milieu physiologique. Le groupement hydroxyle peut également mimer ou former des interactions supplémentaires avec les résidus peptidiques environnants. Dans les deux cas, le recouvrement spatial de la triproline native a été observé par modélisation moléculaire. (Figure 5.4 – B) La plupart des interactions avec le domaine SH3 de p47^{phox} ont été conservées, dont la liaison hydrogène avec Trp263. [487]

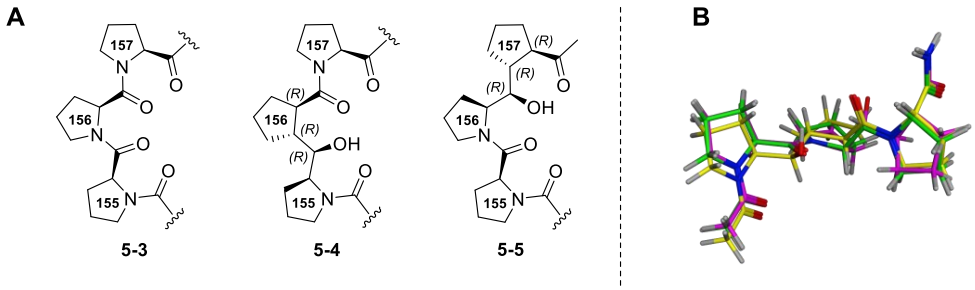

Figure 5.4 A. Structures des trimères Pro-Pro-Pro **5-3**, Pro-Cyp-Pro **5-4**, et Pro-Pro-Cyp **5-5**. B. Géométries optimisées en phase gazeuse de **5-3** (vert), **5-4** (jaune), et **5-5** (magenta). Les atomes d'oxygène sont indiqués en rouge et ceux d'azote en bleu. [487]

Lorsque inséré dans les peptidomimétiques **5-6** (ProCypPro) et **5-7** (ProProCyp), seulement **5-7** s'est révélé actif. L'abrogation d'affinité observée lors du remplacement de Pro156 (**5-6**) a montré l'importance de la position du groupement Cyp lors de la conception de mimes structuraux. L'affinité de **5-7** a mis en avant le potentiel qui réside dans le développement de mimes de motifs riches en prolines impliquant la substitution d'une proline par un cyclopentane.

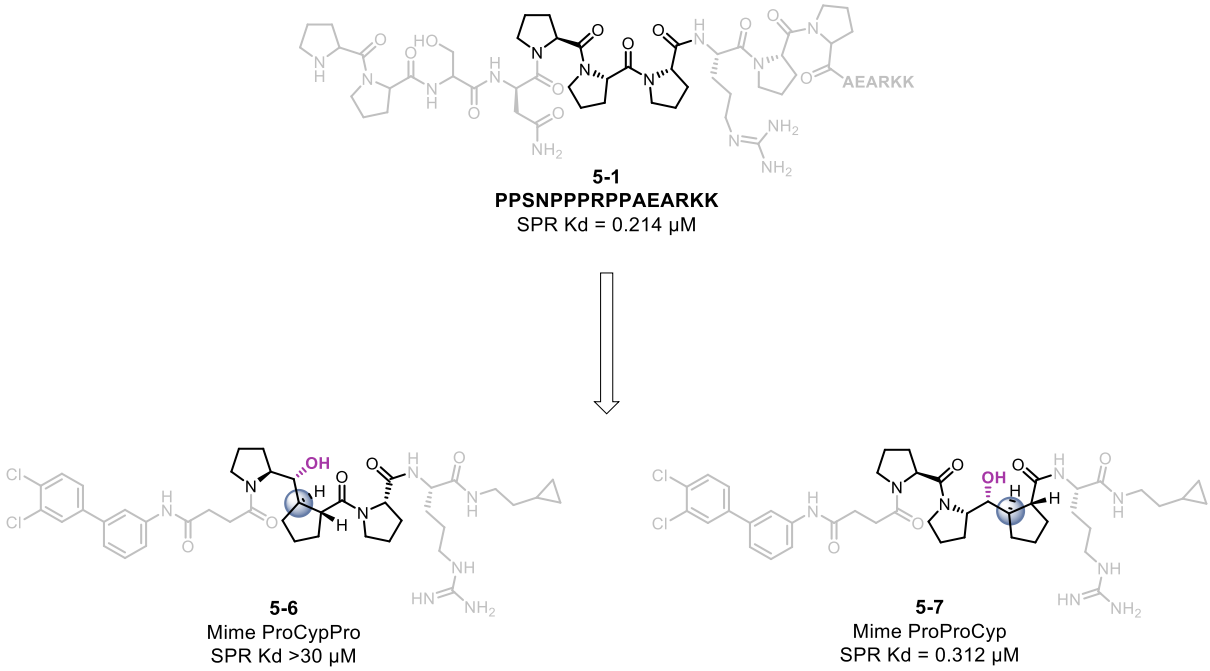

Figure 5.5 Cibles peptidomimétiques ProCypPro **5-6** et ProProCyp **5-7** dérivées de l'héxadécapeptide PPSNPPPRPPAEARKK **5-1** reconnu par le domaine riche en prolines SH3 de p47.

Ce projet décrit l'étude structurale de l'interaction p22^{phox}-p47^{phox} ainsi que la conception, la synthèse et les tests biologiques des peptidomimétiques incorporant les triades ProCypPro (**5-2**) et ProProCyp (**5-3**) dans leur partie centrale. (Figure 5.5).

5.1.2 *Article 5*: Targeting NOX2 via p47/phox-p22/phox inhibition with novel triproline mimetics

Jean-Baptiste Garsi[a], Balázs Komjáti[b], Gregorio Cullia[a], Imre Fejes[b], Melinda Sipos[b], Zoltán Sipos[b], Eszter Fördős[b], Piroska Markacz[b], Barbara Balázs[b], Nathalie Lancelot[c], Sylvie Berger[c], Eric Raimbaud[c], David Brown[c], Laurent-Michel Vuillard[c], Laure Haberkorn[c], Cyprian Cukier[d], Zoltán Szlávik[b], Stephen Hanessian[a]*

[a] *Department of Chemistry, Université de Montréal, 1375 Ave. Thérèse-Lavoie-Roux, Montréal, H2V 0B3 QC, Canada*

[b]*Servier Research of Medicinal Chemistry, 1031 Záhony utca 7 Mb, Budapest, Hungary*

[c]*Institut de Recherche Servier, 125 Chemin de la Ronde, 78290 Croissy, France*

[d]*Selvita S.A., ul. Bobrzyńskiego 14, 30-348 Kraków, Poland*

Contributions :

- Jean-Baptiste Garsi a participé à la synthèse, à la rédaction de l'article et à la partie expérimentale.
- Gregorio Cullia a participé à la synthèse et la rédaction de la partie expérimentale.
- Stephen Hanessian a initié, supervisé le projet et participé à la rédaction de l'article en tant que principal investigateur.
- Les membres de l'institut de recherche Servier ont effectué les tests biologiques, les études de cristallisation et de modélisation et participé à la rédaction de l'article et la partie expérimentale.
- Zoltan Szlavik a coordonné le projet et participé à la rédaction de l'article en tant que principal investigateur.
- Cyprian Cukier a participé à l'étude de cristallisation de la protéine en partenariat avec l'institut de recherche Servier.

Garsi, J.-B.; Komjáti, B.; Cullia, G.; Fejes, I.; Sipos, M.; Sipos, Z.; Fördős, E.; Markacz, P.; Balázs, B.; Lancelot, N.; Berger, S.; Raimbaud, E.; Brown, D.; Vuillard, L.-M.; Haberkorn, L.; Cukier, C.; Szlávik, Z.; Hanessian, S. Targeting NOX2 via P47/Phox-P22/Phox Inhibition with Novel Triproline Mimetics. *ACS Med. Chem. Lett.* **2022**, *13* (6), 949–954. DOI : 10.1021/acsmedchemlett.2c00094

5.1.2.1 Abstract

On the basis of the knowledge that the proline-rich hot spot **PPP**RPP region of P(151)PSNPPPRPP(160), an oligopeptide derived from the cytosolic portion of $p22^{phox}$ (p22), binds to the single functional bis-SH3 domain of the regulatory protein $p47^{phox}$ (p47), we designed a mimetic of the tripeptide **PPP** based on NMR and X-ray crystallographic data for the p22(151−161) peptide PPSN**PPP**RPPA with a peptide construct. Incorporation of the synthetic pseudo-triproline mimetic Pro-Pro-Cyp in a molecule derived from molecular modeling studies led to only a 7-fold diminution in activity in a surface plasmon resonance assay relative to the same molecule containing the natural Pro-Pro-Pro tripeptide. The alternative sequence corresponding to a Pro-Cyp-Pro insertion was inactive. This is a first example of the use of a triproline mimetic to interfere with the formation of the p47−p22 complex, which is critical for the activation of NOX, leading to the production of reactive oxygen species as superoxide anions.

5.1.2.2 Introduction

The NADPH oxidases (reduced forms of nicotinamide adenine dinucleotide phosphate oxidases) are a family of membrane-associated multicomponent enzymes present in phagocytes and macrophages.[119,488–491] Also known as NOX, they are widely distributed in eukaryotic organisms and play a crucial role in maintaining the delicate balance of physiological redox processes responsible for the maintenance of host defense mechanisms against invading pathogens as well as in recruiting inflammatory cells to the site of infection.[492–494] This is accomplished through reduction of molecular oxygen across membranes and release of reactive oxygen species (ROS) in the form of superoxide anions ($O2^{\bullet-}$) that destroy the biochemical machinery of invading microorganisms. [495] Among the seven isoforms of these enzymes, NOX2 (NADPH 2, or $gp91^{phox}$), a phagocystic oxidase, has garnered much attention because of its ubiquitous presence in tissues and organs, where ROS production can trigger physiological responses that ultimately lead to innate and adaptive immunity.[496]

NADPH oxidase comprises six subunits, including the trans membrane p22 and NOX2, which in combination with flavocytochrome becomes the catalytic site of the oxidase complex. Regulatory cytosolic proteins such as p47 undergo a series of phosphorylations, eventually forming reversible contacts with other multidomain proteins.[125]

NOX2 becomes catalytically active in vivo when transmembrane protein p22 binds to the single functional bis-SH3 domain of the regulatory protein p47, leading to an enzyme complex that enhances the production of ROS. [497–499] Under normal physiological conditions, ROS production mediated by NOX2 is highly regulated to defend against invading pathogens without causing damage to host tissue. Upon the action of external stimuli, the dormant or resting-state form of NADPH oxidase is activated through a series of reversible protein− protein interactions (PPIs) among its regulatory proteins to produce ROS in such a manner that host tissue is not damaged.[500] However, the beneficial gatekeeper role of NOX2 toward external harmful stimuli can be jeopardized by the overproduction of ROS under certain pathological conditions, causing oxidative stress and a cascade of physiological events resulting in serious diseases such as cancer, cystic fibrosis, schizophrenia, Alzheimer's disease, and a host of cardiac- and lung-related diseases.[1,466,469,473,501] Since the activation of the catalytic site of the NOX2 enzyme complex involves the interaction of the essential regulatory p47 and p22 proteins to produce ROS in an inducible manner, it has been suggested that interfering with this specific PPI can be exploited to render NOX2 as a druggable target.[119,479,480]

Developing small-molecule inhibitors of p47 presents obvious challenges because of the relatively large surfaces of the interacting proteins at the site of contact.[485] Interestingly, a number of natural products such as apocynin, celastrol, and glyotoxin have been reported as NOX2 inhibitors.[119,479] Among the synthetic compounds, ebselen, a selenoindazole discovered by high-throughput screening, continues to attract attention.[480] PR-39, a peptide of bacterial origin, has been reported to inhibit NADPH oxidase activity by binding to the Src homology domains of p47.[502] A series of pyrazolopyridinediones showed selective NOX4 activity but were inert toward NOX2. [503] Recently, dimeric 2-aminoquinolines bridged by a ethylenedioxa ether linker exhibiting in vitro K_i activity in the 20 μM range were obtained using a fragment-based approach.[504]

Interfering with PPIs through the use of small peptides or peptidomimetics has been a successful strategy in drug discovery. [505] In such cases, identifying so-called "hot spots" in protein partners engaged in PPIs has been the norm. Given the available structural information related to NOX, we considered a peptidomimetic approach to interfere with the PPI of p47 with p22 as a proof of concept.

5.1.2.3 Results and Discussion

The structure of p47 has been investigated by elegant X-ray crystallographic studies [506] and in solution by NMR spectroscopy. [485] Valuable insights into the conformation of p47 have identified critical regions for recognition, and relevant amino acid sequences, including proline-rich domains (PRDs), have been proposed. The structure of a p47−p22 complex comprising the conserved tandem SH3 domain of p47 bound to an oligopeptide P(151)PSN**PPP**RPP(160) derived from the cytosolic portion of p22 shows that binding involves the proline-rich sequence **PPP**RPP of p22. [486] The prospects of developing a small-molecule inhibitor of the PPIs between p47 and the hotspots in p22 to control overproduction of ROS represents a major challenge because of the enormous conformational change of the cytosolic p47 component. In fact, p47 needs to adopt an activated conformation by phosphorylation of serine residues in order to bind to p22 prior to translocation of the complex from the cytosol to the membrane.[486] As a rule, developing peptidomimetics of peptides with fewer than six residues is a good starting point, whereas peptide sequences consisting of 6−15 residues are considered challenging. [507,508]

To optimize the bioactive peptide sequence, the hot spots in the 16 amino acid sequence in p22(151−166) that would potentially interact with regions of p47 were identified using X-ray crystallography, surface plasmon resonance (SPR), and an Ala scan. A cocrystal structure of the extended conformation of p47 with the truncated undecapeptide PPSN**PPP**RPPA (**1**) is shown in Figure 5.6 (PDB: 7YXW).

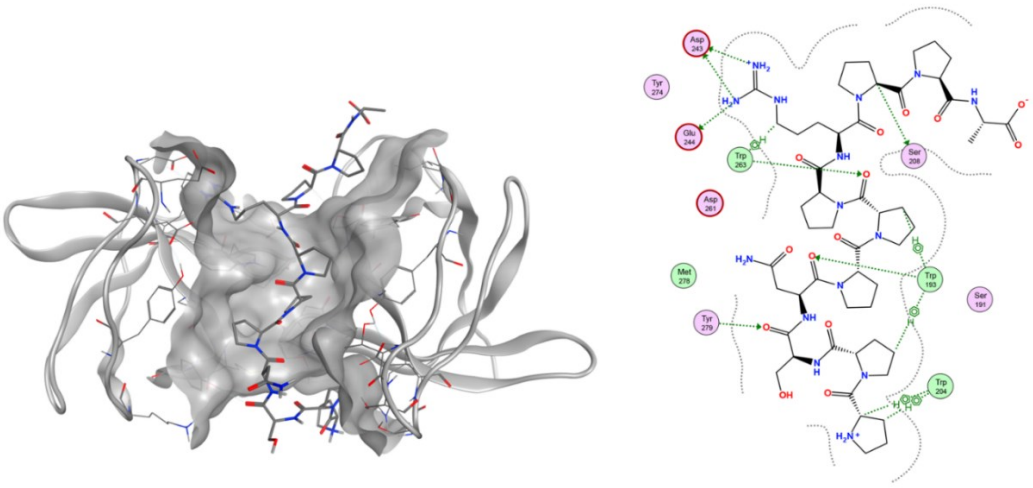

Figure 5.6 Structure of p22(151−161) peptide PPSN**PPP**RPPA (**1**) cocrystallized with a tandem protein construct.

To improve the crystallizability of the protein and to avoid the domain swap observed by Rittinger, [486] a single A200G mutation was introduced. The N-terminal Pro-Pro (151−152) is involved in a hydrophobic interaction with Trp(204) and Trp(193), while the Ser-Asn (153−154) residue acts more like a linker to the central triproline unit. Of particular interest is the spatial alignment of the **Pro-Pro-Pro** (155−157) triad, which is engaged in hydrophobic and hydrogen-bonding interactions with Trp(193) and Trp(263), respectively.

To determine the individual roles of the nine central amino acids in the 16 amino acid sequence PPSN**PPP**RPPAEARKK, we conducted an Ala scan from Ser(153) to Glu(162) in conjunction with binding affinity and free enthalpy changes. We were pleased to find that the **PPP**R(155−158) sequence was the hot spot of p22, and hence, it was considered as a suitable candidate for peptidomimetic design. Furthermore, the spatial disposition of the central Pro(156) within the triproline triad and the ionic interaction of Arg(158) with Asp(243) and Glu(244) were critical in the conceptual design of the intended triproline mimetic. The Ala scan revealed that replacement of Pro(159) in the C-terminal part of PPSN**PPP**RPPAEARKK has no impact on binding, while Pro(160) has an important role in occupying a hydrophobic region. Taken together, these studies indicated that the pentapeptide EARKK could be removed, leaving the proline-rich undecapeptide PPSN**PPP**RPPA (**1**) representing p22(151−161) as a truncated construct. Having garnered sufficient structural information from the X-ray and Ala scan studies, we considered undecapeptide **1** to be a starting point in search of truncated analogues and potential small-molecule peptidomimetics. The main challenge was to replace the natural amino acid sequence of the **PPP**R(155−158) hot spot involved in most of the essential interactions with p47 with a mimetic molecule that would adopt a well-defined geometry in the binding groove comprising two SH3 domains.

On the basis of these results and our understanding of the role of each amino acid, the following structural optimizations were performed to design a truncated peptidomimetic (data not shown): Pro(151) and Pro(152) were replaced by lipophilic groups; Ser(153) and Asp(154) were replaced by a suitable linker; Arg(158) was truncated or left unmodified; and Pro(159) and Pro(160) were replaced by lipophilic side chains. Two of the optimized triproline peptidomimetics are presented as **I** and **II** in Figure 5.7. The substantial reduction of molecular weight and the maintained affinity

of **II** resulted in a significantly better ligand efficiency compared with the p22(151−166) peptide (vide infra). Compound **II** was chosen as a surrogate for further modifications.

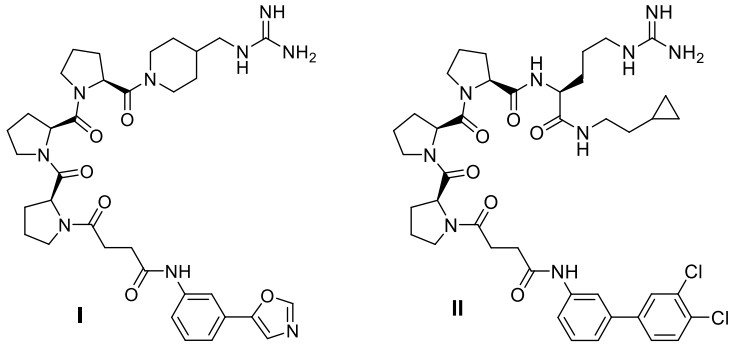

Figure 5.7 Structure of triproline mimetics **I** and **II**.

As part of our ongoing interest in the design and synthesis of proline-derived motifs and peptidomimetics,[142,147,374,509,510] we recently reported the stereocontrolled synthesis of a series of diastereomeric diproline (Pro-Pro) mimetics represented by a generic pseudo-diproline dimeric Pro-Cyp structure (Figure 5.8). [511]

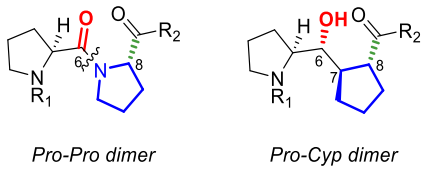

Figure 5.8 Pro-Pro and pseudodiproline Pro-Cyp motifs.

The conceptual design element considered replacing the second Pro in the Pro-Pro dimer with a cyclopentanecarboxylic acid (Cyp) in which the stereochemical combinations of three contiguous stereogenic centers were unambiguously established. The use of Cyp as a proline surrogate has been previously reported sporadically as an effort to simulate a diproline motif, but seldom in the context of a medicinally relevant target. [159,165,407,408,434,438,439,441] For the purposes of a triproline mimetic for the **Pro-Pro-Pro** (155−157) sequence in undecapeptide **1** representing p22 (Figure 5.6), we envisaged two variants, one in which the Cyp unit would replace the C-terminal Pro(157) (**B**) and another in which the Cyp unit would replace the central Pro(156) (**C**) (Figure 5.9 – A). Superposition of the Pro-Pro-Pro subunit (**A**) representing the natural PPP segment with the two pseudo-triproline motifs **B** and **C** showed excellent overlap (Figure 5.9 – B).

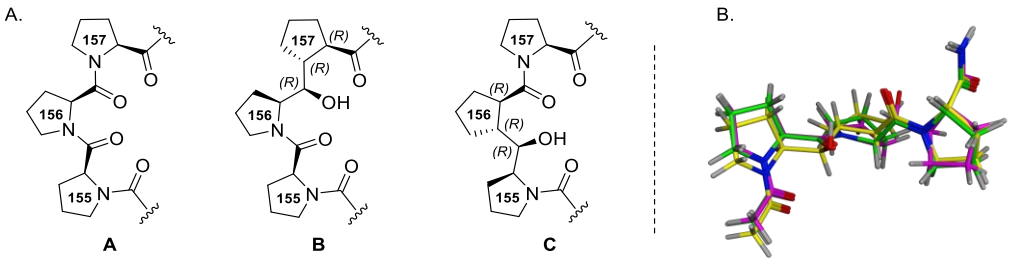

Figure 5.9 (A) Structures of Pro-Pro-Pro trimer **A**, Pro-Pro-Cyp trimer **B**, and Pro-Cyp-Pro trimer **C**. (B) Gas-phase optimized geometries of **A** (green), **B** (magenta), and **C** (yellow). Oxygen atoms ares shown in red and nitrogen atoms in blue.

The appropriate stereoisomer of Cyp was selected on thebasis of docking the candidate compounds into p47 protein. The Cyp diproline unit was placed in the two possible positions corresponding to the triproline core of compound **II**. All possible diastereomers were modeled, and thus, a total of 16 isomers were docked. Compound **II** maintains all of the specific and necessary hydrogen bonds and salt bridges as p22(151−161). The cyclopropylethyl chain in **II** replacing the last proline in undecapeptide **1** sits on a hydrophobic surface. The succinamide moiety takes the place of the first four amino acids of the undecapeptide, while the appended 3,4-dichlorobiphenyl ring is well-positioned relative to the hydrophobic surface formed by Trp(204) and Trp(193). The Pro-Pro-Cyp 2*S*,6*R*,7*R*,8*R* isomer **III**, replacing both **Pro-Pro**(155−156) and **Pro-Pro**(156−157), maintained the helical structure and most of the specific interactions with the protein. It was therefore chosen for synthesis and evaluation. When **Pro-Pro**(155−156) was replaced, rotation of the amide bond between Cyp and the linker was observed in some of the docking poses as a result of the subtle conformation change of Cyp compared with diproline, causing strain on the linker. In either case, the Cyp-containing pseudotriproline unit would expose a hydrophobic surface similarly to proline and provide possible polar interactions with the stereodefined OH group replacing an amide carbonyl. Preliminary data on the two pseudo-triproline analogues **I** and **II** as internal reference compounds revealed that the latter would be a better analogue to use as a control. Pro-Pro-Cyp **B** and Pro-Cyp-Pro **C** motifs were elaborated to include an N-terminal 3,4-dichlorobiphenyl succinamide and a C-terminal hydrophobic cyclopropylethylarginine amide, leading to the fully decorated analogues **III** and **IV**, respectively

(Figure (Figure 5.10), each having a 6*R*,7*R*,8*R* stereochemistry comprising three contiguous stereogenic centers.

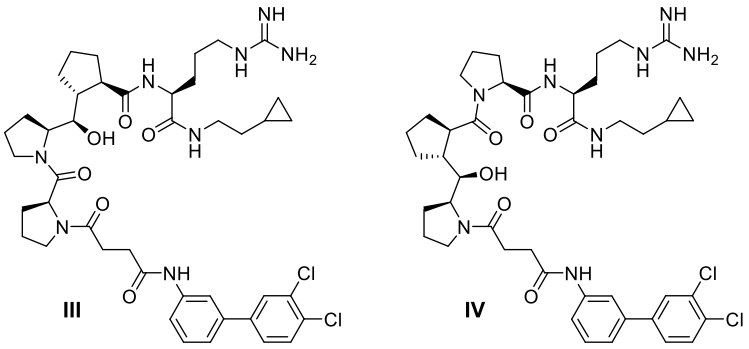

Figure 5.10 Structures of triproline mimetics **III** and **IV**.

We were pleased to find that analogue **III**, in which **Pro**(157) was replaced by a cyclopentanecarboxamide, was only 7 times less active in the SPR assay relative to triproline analogue **II**. The SPR ligand efficiencies (SPR LEs) of control analogue **II** and triproline mimetic analogue **III** were comparable to that of p22(151−166). In contrast, analogue **IV** was totally inactive. Thus, replacement of the pivotal Pro(157) in undecapeptide model **1**, a surrogate for p22, with a cyclopentanecarboxamide in the form of synthetic mimetic **III** does not negatively affect the PPI with p47. Moreover, it appears that the presence of the middle Pro(156) in the Pro-Pro-Cyp triad in **III** is essential for activity (Figures 5.10, 5.11 and Tableau 5.1).

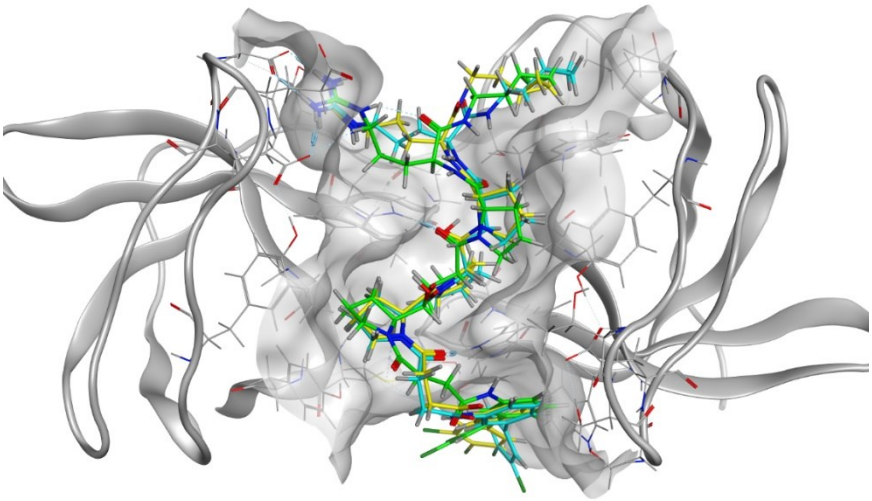

Figure 5.11 Superimposition of pseudopeptides **II**-**IV** in p47 SH3 domain.

The replacement of the Pro(156) amide carbonyl in the **PPPR** segment of undecapeptide **1** with an *R*-configured secondary alcohol facing the solvent in the active analogue **III** is beneficial, since it does not disrupt the specific hydrogen-bonding interactions in the complex.

Tableau 5.1 Experimental Affinities of Triproline Mimetic Analogues.

Compound	SPR Kd (μM)	SPR LE
p22(151-168)	0.214	0.08
I	5.71	0.15
II	0.043	0.18
III	0.312	0.15
IV	>30	NA

The side chains of peptidomimetic **III** could potentially be further optimized to improve the affinity and drug-likeness. The arginine amino acid or the guanidine derivatives seem to be a bottleneck for cellular penetration. Because of their strong basic character, they are invariably in a protonated state under physiological conditions, which may disfavor membrane penetration. The lipophilic side chain and linker connected to the N-terminal unit in **III** could be optimized to reduce the flexibility. [512]

Although the proline side chains in undecapeptide 1 are only capable of hydrophobic interactions and the backbone forms two hydrogen bonds with p47, the essential helical structure is difficult to mimic perfectly. Further studies are required to develop better di- or triproline mimetics in proline-rich polypeptides to achieve higher affinity while improving drug-likeness.

5.1.2.4 Conclusions

In conclusion, inasmuch as the design and synthesis of pseudo-triproline mimetic **III** was part of a proof-of-concept study, the result represents a first example of a rationally designed and novel synthetic triproline mimetic to exhibit submicromolar in vitro activity against the binding of p47 with p22, two critical proteins involved in the activation of NOX1 and NOX2 in relation to regulation of ROS overproduction. Large numbers of biologically relevant PPIs in eukaryotic cells [486] involve linear motifs [513] in which proline-rich domains encompassed within structurally distinct polyproline type II helices play critical roles in recognition and specificity with other proteins acting as partners. [124,514] Incorporation of our Pro-Cyp dipeptide mimetic as a pseudo-diproline or

extended versions of it with Pro-Cyp combinations with optimized N- and C-terminal residues to simulate the action of natural oligoproline sequences in designated proteins would augur well for the development of new drug prototypes as modulators of PPIs in medicinally relevant projects.[176,180,402]

5.2 Application au développement d'agents inhibiteurs de la bactérie Clostridium difficile (collaboration avec le groupe du Pr. Baumann de l'Université de Cologne (Universität zu Köln) et Erick Ivan Martinez Toto)

5.2.1 Introduction

5.2.1.1 Présentation de *Clostridium Difficile*

Clostridium difficile (*C. diff.*) est une bactérie anaérobique capable de générer des spores, et classée parmi les bactéries de type Gram-positive. [515,516] La transmission du pathogène s'effectue par les spores qui peuvent persister dans l'environnement en raison de leur résistance à l'oxygène ainsi qu'aux désinfectants et gaz stérilisants. [517] En particulier, la propagation au sein des complexes hospitaliers au travers de patients infectés ou du personnel soignant a été pointée comme responsable de la majorité des cas. [518] *C. diff.* est impliquée dans le développement d'infections diarrhéique nosocomiales associées à la prise d'antibiotiques ou différentes conditions immunologiques, [519–521] et elle a été associée au cours de la dernière décennie à l'inflammation du côlon [522] pouvant mener à la colite pseudomembranaire [523,524] ainsi qu'au mégacolon toxique. [525,526] *C. diff.* sévie principalement au sein des patients hospitalisés de 65 ans et plus d'Amérique du Nord et d'Europe suivant un traitement antimicrobien. [527–529] En cas d'infection, les traitements privilégiés consistent en la prise de Vancomycine et de Fidaxomicine, selon la sévérité encontrée.[530] De nouvelles voies thérapeutiques telles que la prise d'anticorps monoclonaux (Bezlotoxumab) ou la transplantation de microbiotes fécales ont également été développées en cas d'infections récurrentes. Les recommandations sanitaires basées sur la collection d'informations évoluent régulièrement. [531]

L'émergence de nouvelles souches hyper-virulentes telles que NAP1/B1/027 a mené à une recrudescence du nombre d'infections entraînant des complications pouvant engendrer le décès du patient. [525,528,532] En raison d'une forte récurrence et d'un taux de mortalité pouvant aller de 30% à 60% pour les cas aigus, [533] *C. diff.* est devenue un problème majeur dans les hôpitaux et

maisons de retraites. [534] Son impact financier est également devenu une charge financière préoccupante pour les systèmes de santé des pays occidentaux considérant que le nombre de cas devrait augmenter au cours des prochaines décennies.[529,535] En effet, les cas d'infections liées à la transmission au sein de communautés de populations saines a été en recrudescence aux cours des dernières années, en particulier chez les enfants. [520,526,536] L'hyper-virulence des souches émergentes telles que NAP1/B1/027 a été attribuée à leur résistance à la fluoroquinolone, [537–540] à un taux de sporulation plus élevé [541] ainsi qu'à une production de toxines glucosylantes (l'entérotoxine *Clostridium difficile* Toxin A (TcdA) et la cytotoxine *Clostridium difficile* Toxin B (TcdB)) [542] environ vingt fois supérieure aux autres souches. [543] Il a également été rapporté que la cytotoxicité des toxines glucosylantes TcdB produites par NAP1/B1/027 est plus importante, [544,545] et qu'une troisième toxine, binaire, appelée *C. diff.* transférase (CDT) pourrait rehausser leur pathogénicité. [546,547]

Le processus de contamination par *C. diff.* nécessite une exposition de l'hôte aux spores présentes dans l'environnement aérien immédiat, [548,549] sur les surfaces, ou par contact avec le personnel soignant ou autre sujet contaminé. [550] L'ingestion de spores par l'organisme se produit par voie orale et fécale. La germination des spores commence lorsqu'elles se trouvent exposées à la bile primaire de l'intestin. Après avoir migré dans le côlon, les cellules végétatives sont exposées à un environnement hostile lorsqu'elles se trouvent au sein d'un sujet sain. [515,526] La flore microbienne de l'hôte, les réponses immunitaires ainsi que la présence de peptides antimicrobiens spécialisés agissent contre le développement de l'infection. [551] Par exemple, certains microorganismes du côlon convertissent la bile primaire nécessaire à la germination des spores en bile secondaire qui inhibe le développement des cellules végétatives de *C. diff*.. [552–554] Cependant, dans le cas de patients dont le microbiote du côlon a été significativement réduit, et ce combiné à la présence de facteurs de virulence qui permettent l'évasion de la réponse immunitaire, et promeuvent l'adhésion et l'invasion des tissus cellulaires, l'infection peut persister. [526,532] Le processus de colonisation requiert l'adhésion de *C. diff.* aux cellules épithéliales du côlon. (Figure 5.12) [515] Ce phénomène est principalement contrôlé par la libération de protéines qui vont permettre l'adhérence de la bactérie aux colonocytes. [89] Les cellules bactériennes forment alors des colonies et produisent un biofilm qui diminue leur susceptibilité à la réponse immunitaire de l'hôte et à

l'utilisation d'antibiotiques. [555,556] Il est à noter que le pathogène peut également former des agrégats protégés par un biofilm au sein du lumen avant de venir s'attacher à la paroi épithéliale. Les colonies produisent alors divers facteurs de virulence tels que TcdA et TcdB qui désactivent les GTPases de la famille Rho (Rho, Rac et Cdc42). [557] Cela entraine la perturbation du cytosquelette des cellules de surface, amène à la destruction de la barrière épithéliale intestinale et génère la production de cytokines inflammatoires. [542] Les cytotoxines peuvent par la suite accéder au système sanguin et renforcer la réponse inflammatoire. Il a également été supposé que la relaxation de la barrière épithéliale contribue à l'exsudation de nutriments cellulaires. [88] Lors de la production des toxines, les cellules coloniales vont également générer des spores qui permettent la transmission aux nouveaux hôtes et des cellules filles qui pourront propager l'infection en répétant le cycle de colonisation sur de nouveaux sites. (Figure 5.12) [555]

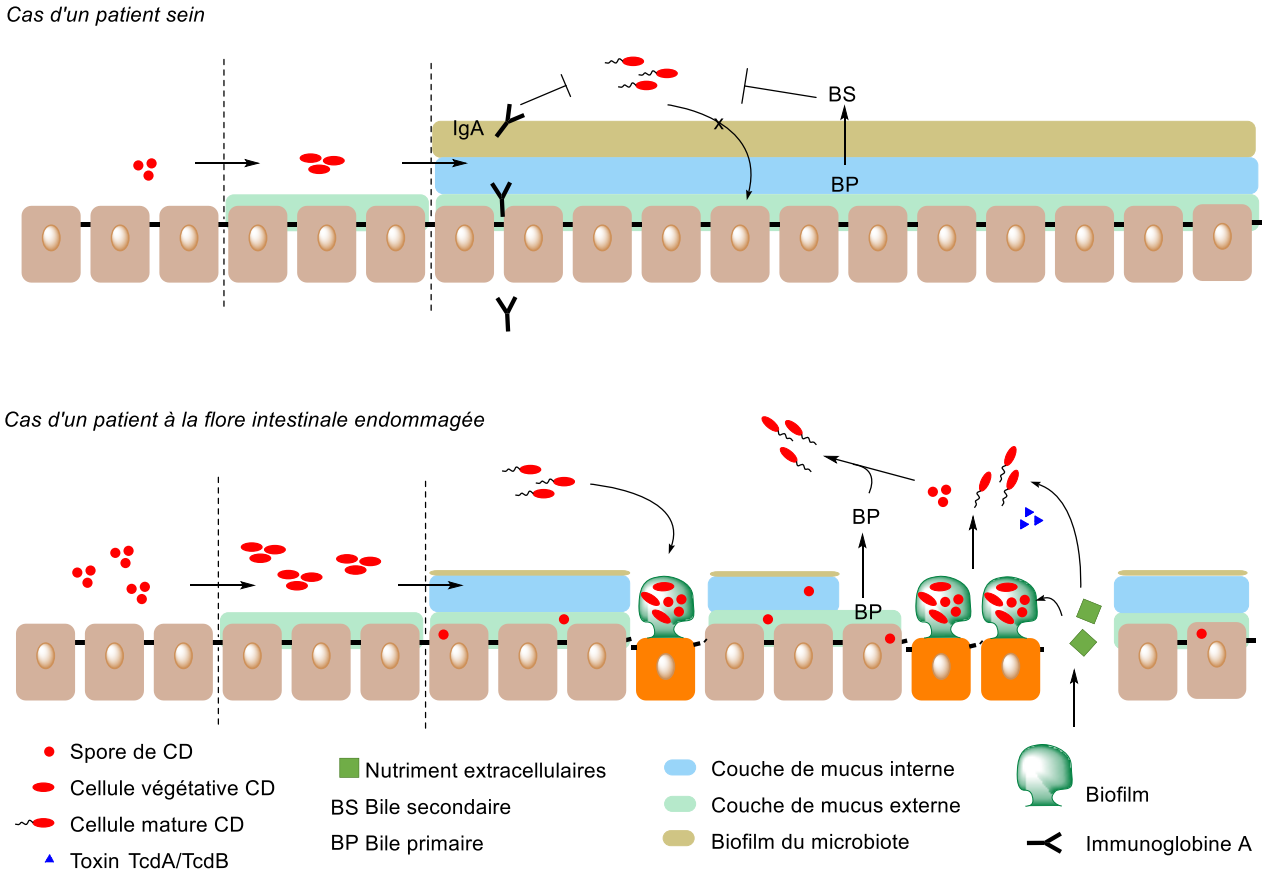

Figure 5.12 Mécanisme infectieux de C. diff..

Les rechutes chroniques d'infection de *C. diff.* ont été associées à des mécanismes de survie de la bactérie tels que l'encapsulation de spores par les cellules épithéliales ou les couches de mucus. L'ensemble de ces facteurs de virulence permettent à *C. diff.* d'envahir l'hôte rapidement et persister face aux réponses immunitaires. La présence d'éléments génétiques mobiles lui permettent également d'acquérir divers gènes supplémentaires impliqués dans la résistance antimicrobienne, la virulence, les interactions avec l'hôte ou encore la production d'éléments protéiques de surface.[558] La production de CDT observée au sein des nouvelles souches hyper-virulentes telles que NAP027 en est un exemple. Les facteurs associés à la mobilité et à l'adhésion aux cellules épithéliales de l'hôte tels que la production de flagelles ou de protéines d'adhésines sont également impliquées dans l'internalisation cellulaire des toxines ainsi que la formation de biofilm. [89,559] Par conséquent, l'inhibition de ces mécanismes a été considérée pour le développement de nouvelles cibles thérapeutiques. [560] Parmi eux, l'adhésion du pathogène aux colonocytes est de premier intérêt considérant que cette étape est cruciale pour l'invasion et la survie de *C. diff.*. [89]

5.2.1.2 L'adhésine, une cible potentielle pour une nouvelle génération de thérapeutiques.

Certaines protéines de surface extracellulaires sécrétées par les bactéries envahissantes jouent un rôle dans les mécanismes d'invasion et de propagation. [560–563] Elles sont exprimées sous l'influence de signaux biologiques générés par l'hôte ou la bactérie, [561,564] et possèdent différentes fonctions qui permettent la survie, la propagation ou la toxicité du pathogène. Parmi elles, les protéines d'adhésines permettent aux bactéries de se lier aux cellules cibles de l'hôte, principalement via la formation d'interactions faibles avec les matrices extracellulaires telles que le collagène, le fibrinogène ou la fibronectine. [565] L'adhésion du bacterium à la paroi cellulaire de l'hôte joue un rôle primordial pour la libération efficace des toxines. La proximité pathogène-hôte permet entre autres une attaque séquentielle des cellules épithéliales lorsque nécessaire [566] ou bien de générer une concentration locale de toxine précise. [567] L'arrimage de la bactérie s'effectue en plusieurs phase. (Figure 5.13) L'attraction initiale entre la bactérie et la cellule de l'hôte est régie par la présence d'interactions faibles non spécifiques, résultant en un processus d'adsorption réversible. [568] Une fois dans l'environnement immédiat de l'épithélium, il a été montré par Anderson que l'adhésion initiale peut impliquer la formation de liaisons à faible

affinité. [569] Cette faible affinité permet alors à la bactérie de conserver une certaine mobilité afin de trouver le meilleur point d'ancrage pour la formation de liaisons présentant une forte affinité. Ces liaisons impliquent la formation de paires entre des sucres, des protéines ou des lipides. [565]

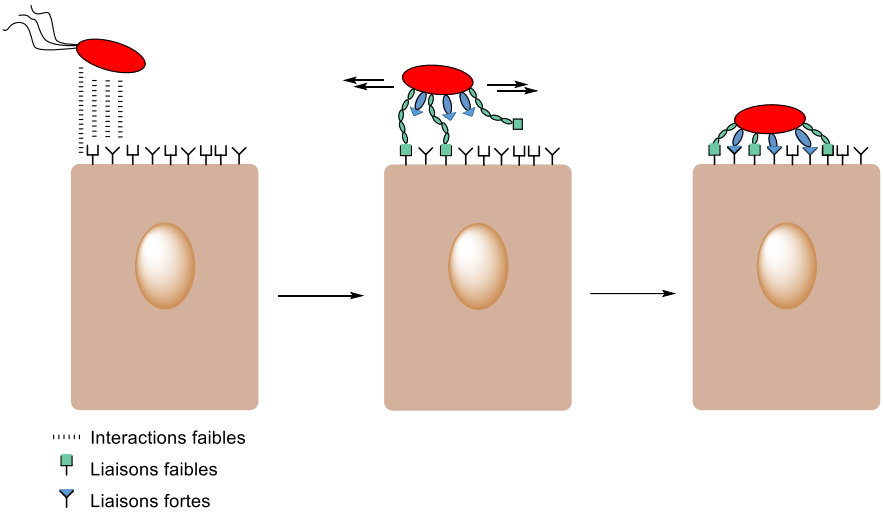

Figure 5.13 Mécanisme d'adhésion aux cellules épithéliales.

Les protéines d'adhésines ont également d'autres fonctions une fois la bactérie ancrée à la paroi cellulaire. De nombreux exemples ont fait état de leur implication dans les mécanismes d'évasions de réponse immunitaire, [570] de la formation de biofilm, [89,570,571] d'internalisation, [572,573] et d'inflammation. [574,575]

La récente recrudescence de nouvelles souches de bactéries résistante aux antibiotiques est une conséquence directe de mutations associées à leur utilisation au cours du dernier siècle, et le ciblage de nouveaux mécanismes biologiques liés aux processus d'infection est primordial pour le développement de futures thérapies. [405,576,577] La thérapie par anti-adhésion représente une alternative potentielle pour plusieurs raisons. Etant donné que leur mécanisme d'action implique la formation d'interactions spécifiques avec les cellules de l'hôte, les mutations associées au développement de résistance seraient néfastes à leur mécanisme d'action et le gène correspondant deviendrait probablement récessif. [565] Ces composés ayant un mécanisme d'action extra-cellulaire, il n'est pas nécessaire qu'ils puissent traverser la paroi membranaire du pathogène qui requiert parfois des propriétés physicochimiques moléculaires allant à l'encontre du milieu physiologique. Ils permettent également d'éviter la libération d'endotoxines et de

toxines bactériennes associées à l'utilisation de composés bactéricides. [578,579] A la place, l'hôte est exposé à la bactérie inactive, ce qui lui permet de susciter une réponse immunitaire qui puisse le protéger d'infections récurrentes et supprimer rapidement les bactéries qui n'ont pas été éliminées mécaniquement. [580] En raison de leur omniprésence au sein des cycles de propagation bactériens, plusieurs stratégies ont été développées pour leur inhibition, [581] avec certains succès notables *in vitro* et *in vivo*. [582–588] Cependant, inhiber le processus d'adhésion présente certaines limitations. Les bactéries produisent différents types de macromolécules complémentaires, et ce de façon spécifique selon le moment et le tissu ciblé. De plus, la présence d'inhibiteurs de récepteurs des cellules hôtes engendre la possibilité d'interférer avec les mécanismes de signalisation. [589]

Une solution alternative consiste à cibler les protéases responsables de la libération du pathogène par scission des macromolécules ancrées aux parois cellulaires de l'hôte. Un exemple récent a été rapporté par Hensbergen en 2015, dans lequel il a montré qu'il était capable d'inhiber la virulence de la bactérie *Clostridium difficile in vivo* lorsque le gène de la diproline endopeptidase CD2830/Zmp1/PPEP-1, une protéase des adhésines CD2831 et CD3246, était supprimé. [403] Dans le contexte hospitalier actuel, l'inhibition du cycle d'adhésion de *C. diff.* représente une solution potentielle afin de réduire sa virulence lorsque le patient reçoit un traitement antibiotique réduisant sa flore intestinale et l'exposant aux symptômes liés à la colonisation.

5.2.1.3 Rôle de l'enzyme PPEP-1 dans le cycle de colonisation de *C. diff.*

Comme pour beaucoup de bactéries, le cycle de colonisation de *C. diff.* est régulé par le taux intracellulaire de diguanylate cyclique (c-di-GMP). [590] Le rôle de c-di-GMP est de contrôler la physiologie du pathogène ainsi que sa réponse à un stimuli externe, [591] principalement en interchangeant entre son mode motile et sessile. [592] Dans le cas de *C. diff.*, le taux intracellulaire de c-di-GMP régule la production de certaines protéines à l'aide de commutateurs ribosomiques (ribocommutateurs) localisés en amont des gènes ciblés. La production de CD2831 et CD3246 est positivement régulée par un fort taux de c-di-GMP via un ribocommutateur de type II. (Figure 5.14) Un fort taux de c-di-GMP a également été associé à la production des toxines TcdA et TcdB et à la formation de biofilm indiquant qu'il correspond à la forme sessile. Au contraire, la production de PPEP-1 est régulée de façon négative par le taux de c-di-GMP via un

ribocommutateur de type I, ce qui est en accord avec son rôle de peptidase des adhésines CD2831/CD3246. [89] Il est à noter que la production de c-di-GMP a été liée à l'activité de diguanylate cyclases (DGC) and phosphodiestérases (PDE) présentes en grand nombre dans *C. diff.*. Ces dernières sont attendues d'être régulées par des facteurs externes, comme la disponibilité de phosphate dans le milieu extracellulaire environnant. [564]

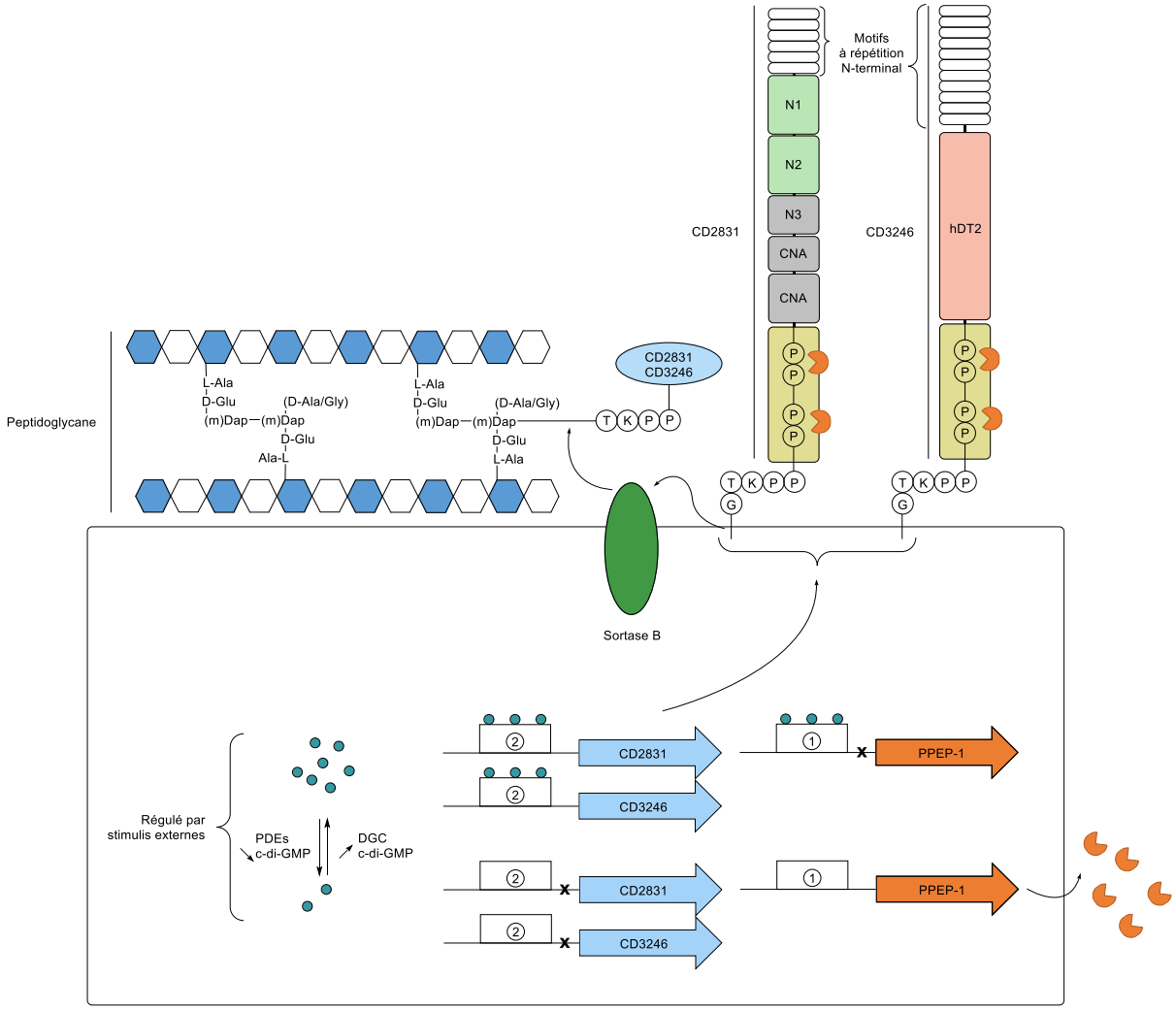

Figure 5.14 Mécanisme général d'adhésion de C. diff..

CD2831 et CD3246 sont des substrats de l'enzyme sortase B qui possèdent un motif LPXTG (PPKTG) à l'extrémité C-terminale servant de point d'ancrage à la membrane cellulaire de la bactérie par liaison covalente (Figure 5.14). [88,564] La région riche en proline contenant les sites de scission de PPEP-1 se trouve à la suite du point d'ancrage. Les domaines qui suivent les régions riches en proline sont responsable des interactions avec l'hôte. [61] Dans le cas de CD2831, il est

composé de deux domaines homologiques à la protéine se liant au collagène (CNA) et trois domaines N-terminal (N1/N2/N3). Les domaines CNA ainsi que N3 ont été supposés agir comme connecteurs afin de maintenir une certaine distance entre le pathogène et le collagène. Les domaines N1 et N2 sont responsables de l'interaction avec le collagène via la formation de 'collagen hug'. Ce mode d'interaction a été rapporté précédemment au sein de *Staphylococcus aureus* par Zong. [593] Le domaine central de CD3246 est homologique au domaine thioester de classe 2 (hDT2) et structurellement proche de celui des adhésines putatives de *Enterococcus faecium* TIE86 et *Bacillus anthracis* BaTIE. Bien que la liaison entre le collagène et CD3246 n'ait été prouvée expérimentalement, il a été montré que les protéines de surfaces bactériennes contenant un domaine thioester interne se lient aux cellules épithéliales par réticulation. [594] Les régions N-terminales sont constituées dans les deux cas de motifs à répétitions qui varient selon les souches et leur fonction n'a pas été élucidée. [61] Lors de la formation de colonies, la production de c-di-GMP augmente, CD2831 et CD3246 sont sécrétées dans le milieu extracellulaire et servent de point d'ancrage à *C. diff.* avec les matrices de collagène. Arato a également montré que CD2831 était impliqué dans la sécrétion de biofilm et l'évasion immunitaire de l'hôte par inhibition de la formation du complexe C1. [89] Lors du transfert de la forme sessile à la forme mobile, la production de c-di-GMP diminue, PPEP-1 est excrétée dans le milieu extracellulaire et hydrolyse CD2831/CD3246 dans la région riche en proline, permettant à *C. diff.* de retrouver sa mobilité et d'aller former de nouveaux sites de colonisation. [564]

PPEP-1 est une métalloprotéase dont l'activité est catalysée par un atome de zinc. Les métalloprotéases de zinc sont présentes de façon ubiquitaire au sein du protéome humain[595] et répertoriées sous formes de familles définies selon le motif structural du site actif environnant l'atome de zinc. [596,597] Elles sont impliquées dans divers mécanismes biologiques liés à la physiologie cellulaire,[598–600] aux processus de signalisation cellulaire, [598,601] à l'homéostasie des tissus, [601] à la plasticité neuronale, [602–604] et au développement de maladies dégénératives et cancéreuses. [598,600,603,605] Elles jouent également un rôle crucial dans les mécanismes de virulence de pathogènes. [606–611] Le gène des PPEPs se retrouve principalement au sein des espèces *Bacilli* et *Clostridia* de la classe des *Firmicutes*. [61] Les domaines protéiques de PPEP ont été découverts au cours de la dernière décennie et seulement deux d'entre elles, PPEP-1 et PPEP-2, ont été

étudiées jusqu'à maintenant. [87,91] Elles appartiennent aux domaines protéiques de *Clostridium difficile* et *Paenibacilus alvei* (*P. Alvei*) et il a été montré que les deux protéases, bien que reconnaissant différents motifs peptidiques, partagent des rôles similaires dans la scission de protéines de surfaces impliquées dans l'adhésion des bactéries. [61]

Hensbergen a décrit le motif de scission préférentiel reconnu par PPEP-1 sur la base des sites de clivages observés au sein de CD2831 et CD3246. [403] (Figure 5.15 – A) Ce motif a été confirmé à l'aide d'un set de peptides FRET comportant des permutations sélectives d'acides aminés sur l'ensemble des positions P3 à P3'. La vitesse d'hydrolyse par PPEP-1 a ensuite été mesurée par fluorescence et comparée à celle du motif préférentiel VNPPVP (P3-P3') (Figure 5.15 – B-G). La position P3 a montré une préférence pour les groupements aliphatiques (Figure 5.15 – B). Le remplacement de la valine (V) par l'isoleucine (I) ou la leucine (L) a été toléré, bien que cette dernière ait réduit la cinétique de moitié. Les acides aminés hydrophiles ont abrogé l'activité. Au contraire, la position P2 a démontré une spécificité pour le résidu asparagine, et toute déviation a résulté en une perte presque totale de l'activité (Figure 5.15 – C). Le remplacement d'une proline (P) au site de clivage P1-P1' par une hydroxyproline (O) a mené à une baisse conséquente de la vitesse d'hydrolyse, et l'activité a été supprimée lors du remplacement des deux prolines (Figure 5.15 – D). Le même effet a été observé en présence d'un motif bis-alanine (AA). La position P2' a démontré une affinité pour les groupements hydrophobes. En particulier, l'insertion d'une proline a accru la vitesse d'hydrolyse du peptide initial (Figure 5.15 – E). L'absence de résidu proline à cette position dans les séquences natives de CD2831/CD3246 semble indiquer qu'une autre raison puisse prévenir son inclusion. Les auteurs n'ont pas commenté cette observation. La position P3' s'est révélée sensible au remplacement de la proline par l'ensemble des acides aminés testés (Figure 5.15 – F).

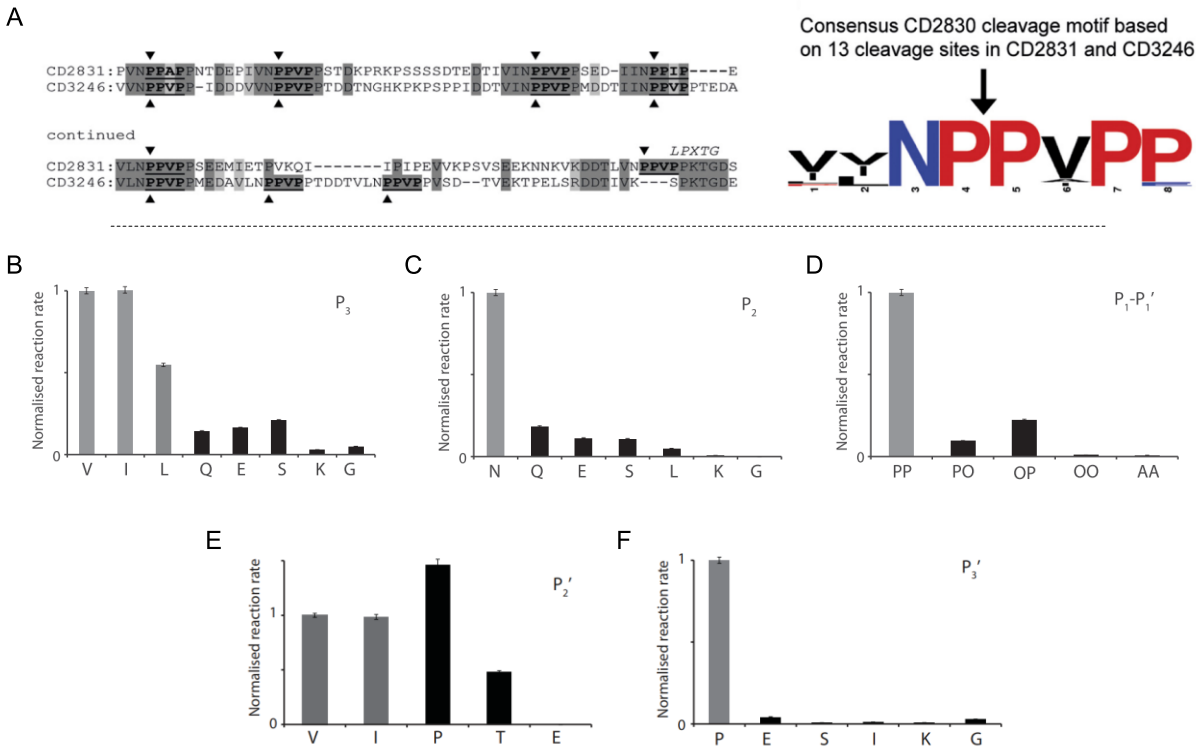

Figure 5.15 A. Sites de clivages observés dans les régions riches en proline de CD2831 et CD3246 et motif de scission proposé sur la base des acides aminés trouvés aux sites de clivages. B-F. Diagrammes de la vitesse d'hydrolyse du peptide FRET modifié à la position P3 (B), P2 (C), P1-P1' (D), P2' (E) et P3' (F). [88,403]

Il peut être conclut de l'ensemble des informations que le motif de scission préférentiel de PPEP-1 (CD2830/Zmp1) est composé des résidus (VIL)NP↓P(VIP)P de la position P3 à P3'. [88,403] Au sein du protéome de *C. diff.*, seulement quatre protéines contiennent ce motif de façon conséquente, en particulier les protéines d'adhésines CD2831 et CD3246 (Figure 5.15 – A).

Baumann a résolu la structure d'un cristal d'un mutant structurel de PPEP-1 lié à l'heptapeptide Ac-EVNPPVP-NH_2 dans lequel l'activité protéolytique a été supprimée, mettant en lumière les aspects structuraux impliqués dans l'hydrolyse du motif diproline. [404] La structure en solution de PPEP-1 libre a également été établie, et il a été montré que sa conformation est similaire à celle observée dans l'état cristallin. [612] Les sections peptidiques les plus importantes pour la reconnaissance du substrat et l'activité protéolytique sont la boucle divergente (diverting loop), le boucle-S (S-loop), l'hélice-α4 contenant le site actif et l'atome de zinc. (Figure 5.16) [404] La

boucle-S possède une conformation ouverte et fermée impliquée dans l'activité catalytique du site actif.

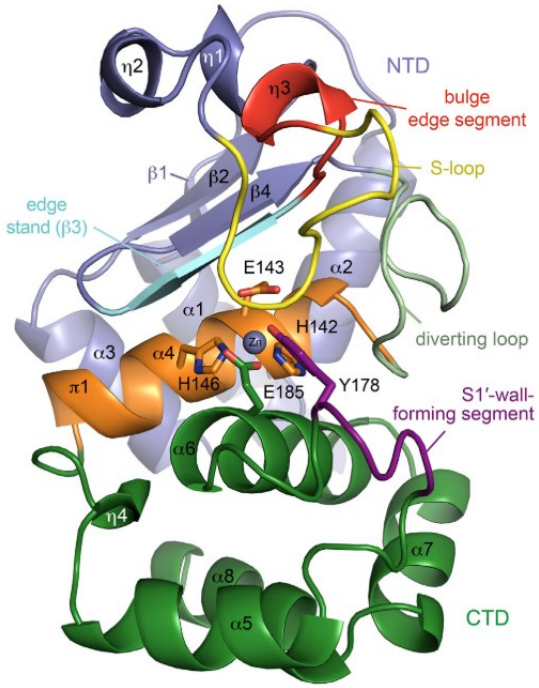

Figure 5.16 Diagramme en ruban de PPEP-1 – Bleu ardoise: Domaine-terminal N (NTD); Jaune: Boucle-S (S-loop); Vert clair: Boucle divergente (diverting loop); Orange: Hélice-α4 contenant le site actif; Vert: Domaine-terminal C (CTD); Violet: Segment de fermeture facial du site actif (contient Tyr178 pour la catalyse) (S1'-wall-forming segment), fait partie de CTD. [404]

Lors de la reconnaissance, la conformation spatiale du peptide facilite son insertion dans le site actif où il interagit avec plusieurs acide aminés aromatiques et aliphatiques de la boucle-S. Ces interactions démarrent le mécanisme de repliement de la conformation ouverte au cours duquel Lys101 (K) de la boucle-S interagit avec l'asparagine (N) à la position P2. [404] (Figure 5.17) L'interaction K-N permet d'approcher Lys101 des résidus Glu184 et Glu185 portés par l'hélice gluzincique afin de former l'interface nommée KEEN (Arg(P2)-Glu184-Glu185-Lys101). [613] La formation de l'interface KEEN est nécessaire à l'activité protéolytique, le changement de conformation permettant de restreindre l'espace dans le site actif et induire la conformation active du peptide. La nouvelle proximité de Lys101 permet également d'augmenter la réactivité de l'ion catalytique de zinc en modifiant sa sphère de coordination secondaire.

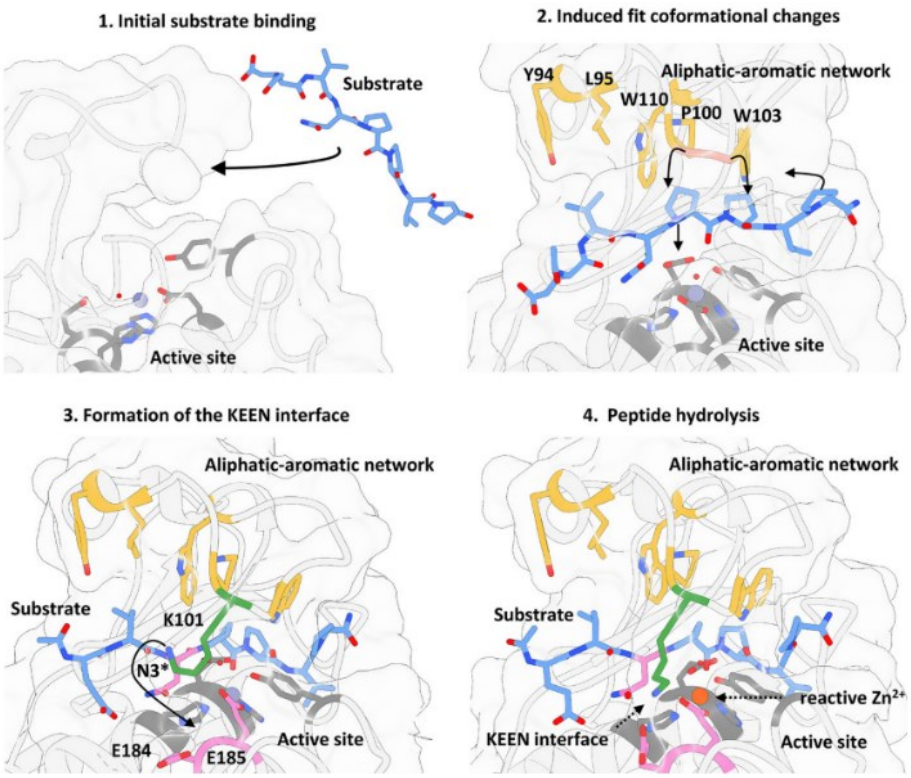

Figure 5.17 Modèle proposé pour le mécanisme d'hydrolyse. [404,613]

Le site actif présente alors une poche hydrophobe accommodante pour les acides aminés Pro-Pro P1-P1' ainsi que les motifs aliphatiques possible de la position P2' (alanine, valine ou isoleucine). La prominence des acides aminés aliphatiques à la position P3 est favorisée par la présence du réseau aliphatique-aromatique composé des résidus Tyr94, Leu95, Pro100, Trp110 et Trp103 portés par la boucle-S. Pro est conservé à la position P3' en raison de son interaction avec Trp103 et la torsion nécessaire au repliement du peptide dans la configuration fermée. [404,613] Il est à noter que la boucle divergente impacte également la conformation spatiale du peptide en générant un encombrement stérique important du côté N-terminal et que l'ablation de la boucle-S résulte en la perte complète de l'activité protéique.[404,612]

L'orientation des résidus du site actif impliqués dans le maintien de la structure et l'hydrolyse du substrat est régie par l'atome de zinc et le repliement de la boucle-S. L'atome de zinc est stabilisé par les chaines latérales des résidus Glu185, His142 et His146, ainsi qu'une molécule d'eau stabilisée par Glu143 et His142/Glu143/His146 forment un motif HEXXH typique des métalloprotéases zinciques. [404] Alors que Glu185, His142 et His146 servent à stabiliser la structure

du site actif, Glu143 et Tyr178 sont impliqués dans la fonction hydrolytique de PPEP-1. Le rôle de catalyseur de Glu143 et Tyr178 a été mis en évidence lors d'expériences de mutations dirigées, le remplacement de Glu143 et Tyr178 abolissant l'activité protéolytique mais ne compromettant pas l'intégrité structurelle de la protéine (Figure 5.18). [404]

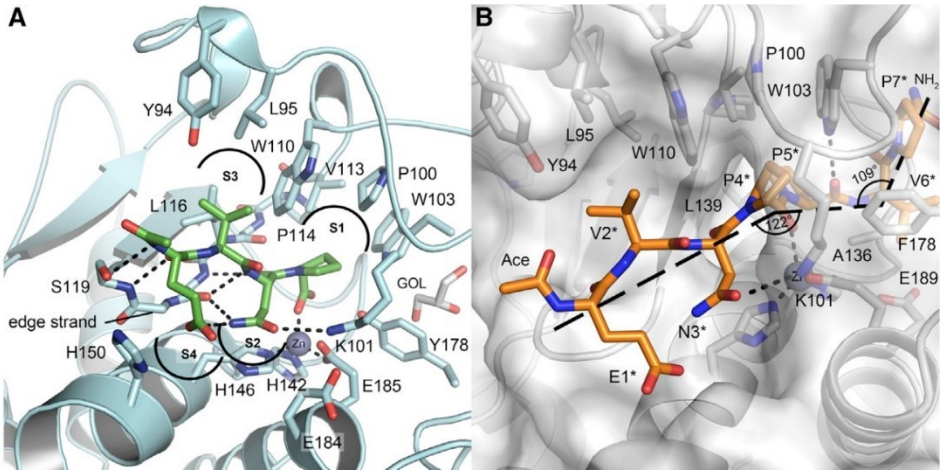

Figure 5.18 A. Co-cristal du site actif de PPEP1 avec la section N-terminale de l'heptapeptide Ac-EVNPPVP-NH_2 (Ac-EVNP-OH). B. Co-cristal du site actif de PPEP1(E143AY178F) muté avec l'heptapeptide Ac-EVNPPVP-NH_2. [404]

Il a été proposé que Glu143 agisse comme catalyseur basique par déprotonation de la molécule d'eau liée au zinc en raison de sa distance proximale (3.5 ± 0.1Å), [612] et que Tyr178 possède un effet stabilisateur de l'intermédiaire tétraédrique comme accepteur de liaison hydrogène. [404] De tels effets ont déjà été rapportés dans plusieurs métalloprotéases de zinc telles que les serralysines, [614] les astacines, [615] la thermolysine [616] et l'insulysine. [617] De même, le mécanisme général des métalloprotéases de zinc ayant été établi au cours de ces études, celui de PPEP-1 peut être proposé sur la base du consensus général. (Schéma 5.1)

Lorsqu'aucun substrat n'occupe le site actif, la sphère de coordination de l'atome de Zn (Zn^{2+}) est complétée par H142/H146/G185 et une molécule d'eau. (A) [404] Lors de l'insertion du substrat, l'atome d'oxygène de la liaison amide P1-P1' vient se coordonner à Zn^{2+} qui devient alors pseudo-pentavalent (B). [615–617] Il est à noter que Tyr178 se trouve à une distance proximale du carbonyle et que la formation d'une liaison hydrogène est possible. L'activation du carbonyle permet l'addition de la molécule d'eau sur le carbonyle et l'intermédiaire tétraédrique généré est stabilisé

par son interaction avec Tyr178 (C). [614–617] Il est possible que la protonation de l'atome d'azote soit nécessaire afin que l'intermédiaire puisse être formé. Toutefois il n'est pas exclu qu'elle soit concertée ou subséquente à l'addition (D). [615–617] La rupture de la liaison amide peut alors prendre place et générer les nouveaux fragments peptidiques sous forme pyrrolidinium et carboxylate (E).

Schéma 5.1 Mécanisme d'hydrolyse de la fonction diproline par la métalloprotéase PPEP-1.

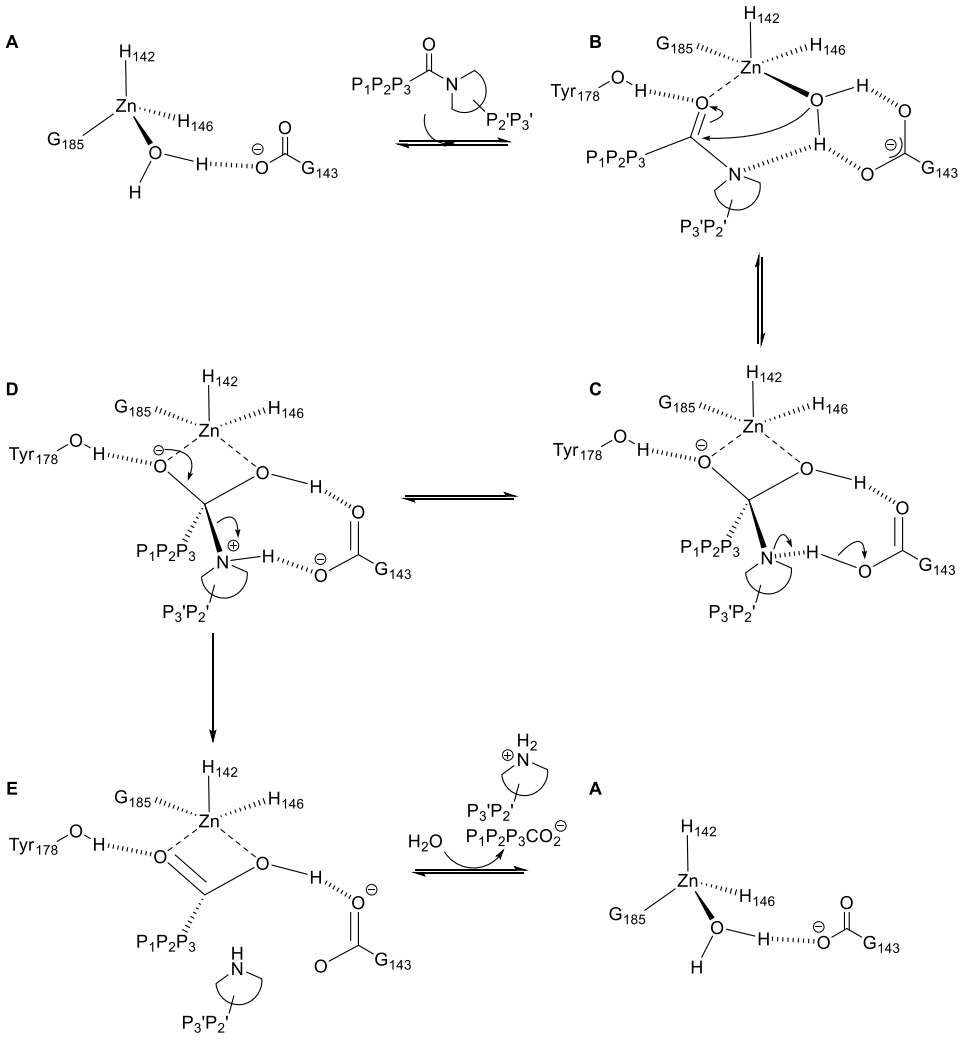

5.2.1.4 Objectifs de projet

L'élucidation de la structure, de la fonction et du mécanisme de PPEP-1 au cours des dernières années ont mis en lumière son importance dans le cycle de prolifération de *C. diff.*. En particulier, la baisse de virulence du mutant de *C. diff.* dans lequel le gène codant pour PPEP-1 a été supprimé

a confirmé son potentiel comme cible thérapeutique pour le développement de nouvelles classes de molécules composant avec la résistance acquise aux antibiotiques des nouvelles souches. [403] Il est à noter que la littérature est dépourvue d'inhibiteurs de PPEP-1. L'objectif de ce projet est de proposer et tester des inhibiteurs du site actif de PPEP-1. En raison de la spécificité de substrat imposé par la boucle-S et le mécanisme protéolytique, la conception des inhibiteurs a été focalisée sur la conservation des résidus P3, P2, P2' et P3' de la séquence peptidique reconnue par le site actif de PPEP-1 ((ILV)NP↓P(AIV)P), et le remplacement du motif diproline P1-P1' par un mime structurel résistant à l'hydrolyse. Suite au succès du Pr. Baumann lors de la cristallisation d'un double mutant de PPEP-1 avec l'heptapeptide Ac-EVNPPVP-NH_2 **5-8**, [404] le motif EVN**PX**VP **5-9** a été choisi (Figure 5.19 – A). Le dimère ProCyp a été sélectionné comme remplacement du motif diproline **PX** car il satisfait aux trois conditions principales pour le concept de l'inhibiteur. [511] Le cycle pentanoïque est un mime structurel de la seconde proline accommodant la poche hydrophobe S1' (**5-10** et **5-11**, Figure 5.19 – B). Le groupement hydroxyle en position C6 agit comme pseudo-isostère de l'intermédiaire tétraédrique lié à Tyr178 tout en étant résistant au mécanisme d'hydrolyse de la liaison amide catalysé par le zinc. La présence des trois centres asymétriques aux carbones C6-C7-C8 permet de sélectionner le stéréoisomère satisfaisant la conformation requise par le repliement de la boucle-S. [404,613]

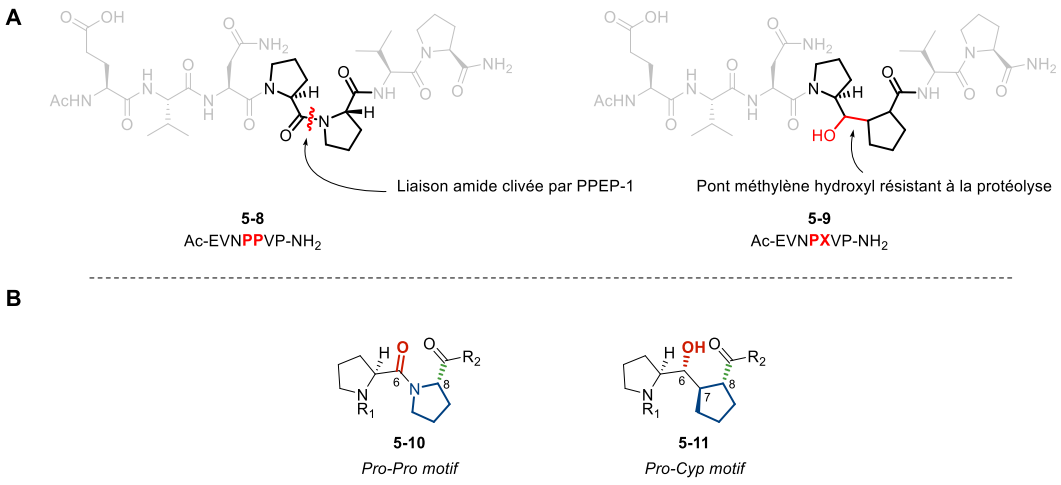

Figure 5.19 A. Structure de l'heptapeptide Ac-EVNPPVP-NH_2 **5-8** et de son mime Ac-EVNPXVP-NH_2 **5-9**. B. Motif diproline **5-10** et dimère ProCyp **5-11**.

Les isomères ProCyp ont été sélectionnés suite aux études de modélisation réalisées par le Pr. Baumann basées sur les analyses par rayons-X des isomères **5-12** et **5-13** et le co-cristal de PPEP-1 avec l'heptapeptide AcHN-EVNPPVP-NH_2 **5-8**. Comme illustré dans la Figure 5.20, le groupement hydroxyle de configuration *R* de l'isomère 4 pointe en direction de Tyr178 à une distance de 2.5 Å indiquant la formation potentielle d'une liaison faible analogue à celle de l'intermédiaire tétraédrique (Figure 5.20 – A). Au contraire, la configuration *S* de l'hydroxyle de l'isomère 5 impose une orientation orthogonale, excluant la possibilité d'une telle interaction stabilisante (Figure 5.20 – B). Afin de proposer la meilleure cible théorique, le Pr. Baumann a également modélisé les autres isomères ProCyp possibles possédant l'hydroxyle de configuration *R.* Le meilleur résultat a été obtenu pour l'isomère **5-14**, qui présente une configuration C6(*R*)- C7(*S*)-C8(*R*) (Figure 5.20 – C). La jonction *cis* du cyclopentane permet d'obtenir une orientation des unités Pro et Cyp de **5-14** comparable à celles des prolines situées au site de clivage (S1-S1') observée dans le co-cristal. La stéréochimie de C8(*R*) alloue la superposition du carbonyle de **5-14** avec la liaison peptidique de Pro(S1')-Val(S2'). Le groupement hydroxyle se trouve à une distance de 2.0 Angström de Tyr178 pour la formation potentielle de liaison hydrogène.

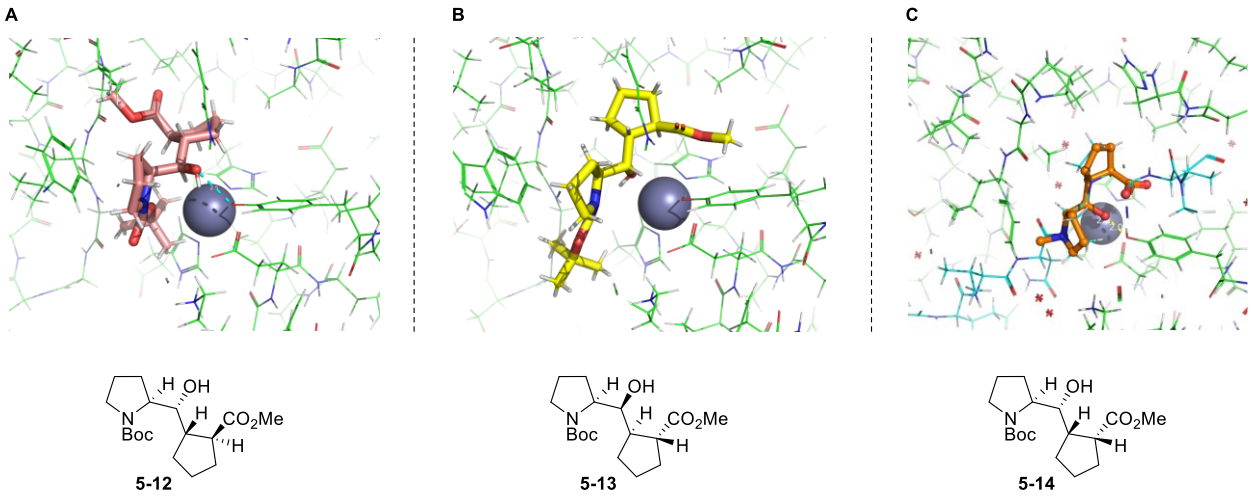

Figure 5.20 A. Modélisation de l'isomère trans ProCyp **5-12** (rose). B. Modélisation de l'isomère trans ProCyp **5-13** (jaune). C. Modélisation de l'isomère cis ProCyp **5-14** (orange) superposée au peptide de co-cristallisation (cyan).

Par conséquent, les deux isomères ProCyp **5-12** et **5-13** comportant la configuration *R* du groupement hydroxyle ont été sélectionnés pour la synthèse des cibles de PPEP-1 dans l'optique de favoriser l'interaction avec Tyr178. Le second isomère *trans* possédant la configuration C8(*R*) **5-11** a également été considéré dans l'optique de réunir une gamme de résultats plus large.

Une fois synthétisés, ces trois isomères ont été évalués au travers d'expériences de co-cristallisation et de compétition au sein du site actif de PPEP-1. Bien qu'il soit attendu que **5-14** présente le meilleur profil d'inhibition, il n'est pas exclu que **5-11** et **5-12** puissent également être actifs.

5.2.2 Résultats et discussion

5.2.2.1 Analyse rétrosynthétique

Bien que la synthèse peptidique s'effectue généralement sur support solide par itération de C-ter vers N-ter, [618,619] une synthèse en ballon a été choisie dans le cas des heptapeptides afin de minimiser le nombre d'étapes impliquant le dimère ProCyp. Dans cette optique, la structure heptapeptidique a été divisée en trois fragments représentant la partie N-ter Ac-EVN (**A**), le module central ProCyp PX (**B**), et la partie C-ter VP-NH_2 (**C**). (Figure 5.21) La stratégie a consisté à synthétiser les trois fragments au préalable puis à les assembler avant l'étape de déprotection finale. Etant donné que la stéréochimie des diastéréomères de **B** ne devrait pas avoir d'impact sur la synthèse, une stratégie générale a été conçue pour les trois cibles. Le groupement acétyle à la position N-ter a été choisi afin de pouvoir mener les études de co-cristallisation et de compétition. [404] L'heptapeptide **5-9** est obtenu suite au couplage entre **5-15-AB** et **5-21-C** et hydrolyse des groupements protecteurs. (Figure 5.217 – A) **5-15-AB** est directement formé par couplage entre **5-16-A** et l'isomère ProCyp **B** choisi suivi de l'hydrolyse de l'ester méthylique. Cette stratégie de synthèse convergente permet ainsi de limiter de façon avantageuse le nombre d'étapes impliquant le groupement ProCyp **B**. Les fragments **5-16-A** et **5-21-C** sont synthétisés de manière linéaire. **5-16-A** est dérivé de **5-17** après échange du groupement Fmoc pour la fonction acétyle et hydrolyse de l'ester méthylique. Le tripeptide **5-17** est obtenu après deux cycles de couplage/déprotection du dérivé asparagine **5-18**, d'abord avec la Fmoc-Val-OH puis le Fmoc-Glu-

O(tBu)-OH. La synthèse de **5-21-C** implique le couplage entre Fmoc-Val-OH **5-19** et le dérivé de la proline **5-20**, lui-même synthétisé en deux étapes depuis Fmoc-Pro-OH. (Figure 5.21 – B)

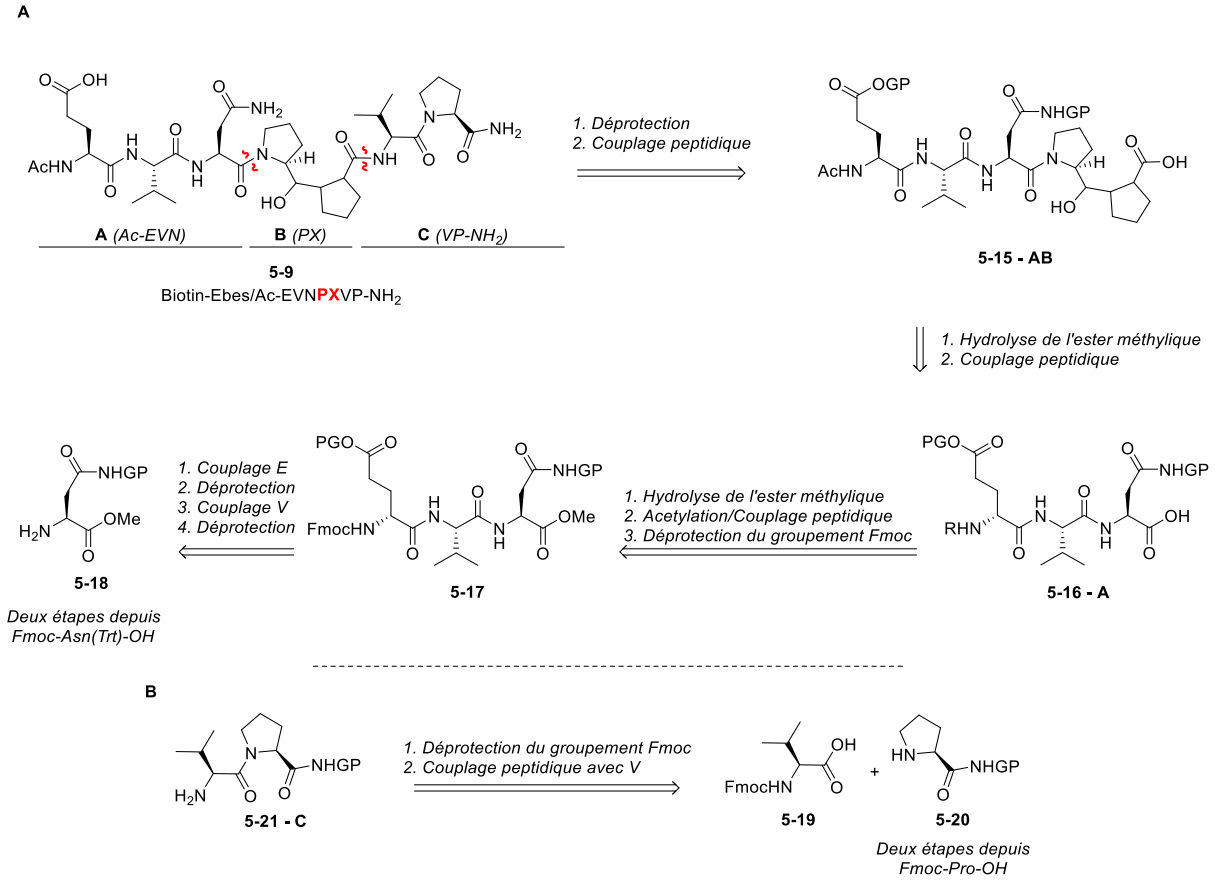

Figure 5.21 Stratégie rétrosynthétique de l'heptapeptide.

Dans cette stratégie de synthèse, la protection du groupement hydroxyle du fragment **B** n'a pas été considérée car il a été observé expérimentalement au sein des études précédentes qu'il était inerte, ce qui a été imputé à l'encombrement stérique généré par les deux cycles environnants. Le choix des groupements protecteurs des autres fonctions a été pensé afin d'être orthogonal aux conditions de déprotection des groupements Fmoc et ester méthylique tout en présentant des conditions d'hydrolyses communes.

5.2.2.2 Synthèse des fragments A et C

La préparation de **5-23** par estérification du groupement carboxylique suivi de la déprotection du groupement Fmoc de l'asparagine (N) a permis son obtention avec des rendements quantitatifs

sur une échelle de treize millimoles. (Schéma 5.2) Le couplage entre **5-23** et le fragment Fmoc-Val-OH (V) **5-22** a résulté en la formation de la dicétopipérazine qui a pu être évitée lorsque la réaction a été accomplie à 0 °C dans le dichlorométhane. La déprotection du groupement Fmoc a amené à la formation de **5-25** avec un rendement de 90% sur deux étapes. Le cœur du tripeptide EVN a été forgé lors du couplage suivant entre **5-25** et Glu(O*t*Bu)-OH (E) **5-24**, et **5-16** a été formé avec 70% de rendement après hydrolyse du groupement Fmoc. Les groupements protecteurs des chaînes latérales de E et N ont été choisis afin de pouvoir être déprotégés en milieu acide. Après avoir réalisé l'acétylation de l'amine primaire, l'étape d'hydrolyse de l'ester méthylique s'est révélée plus délicate. L'utilisation d'hydroxyde de lithium a résulté en l'hydrolyse partielle de l'ester *tert*-butylique et la promotion d'une épimérisation partielle à température ambiante et à 0 °C. La structure de l'épimère n'a pas été élucidée mais il a été convenu que l'épimérisation se produit en position alpha de l'ester en raison de l'acidité du proton. L'utilisation d'hydroxyde de triméthylétain dans le dichloroéthane [620] a permis d'éviter le problème et a résulté en la formation du fragment **5-27-A** avec un rendement quantitatif. La synthèse de ce fragment à l'échelle millimolaire a permis de générer une quantité confortable de précurseur pour la seconde partie de la synthèse. La synthèse du fragment **5-29-C** a démarré par le couplage peptidique de la Fmoc-Pro-OH (P) avec l'amine tritylée suivi de la déprotection du groupement Fmoc pour délivrer **5-28** avec 54% de rendement sur deux étapes. Le groupement protecteur trityle a été choisi afin de pouvoir être déprotégé de façon concomitante avec les groupements protecteurs des chaînes latérales du fragment **5-27-A**. Le couplage suivant avec Fmoc-Val-OH **5-19** suivi de la déprotection du groupement Fmoc de l'amine a mené à l'obtention du fragment **5-29-C** avec 67% de rendement. Comme pour le fragment **5-27-A**, plusieurs grammes de ce fragment ont été préparés en prévision de la seconde partie de la synthèse des trois isomères.

Schéma 5.2 Synthèse des fragments **5-27-A** et **5-29-C**.

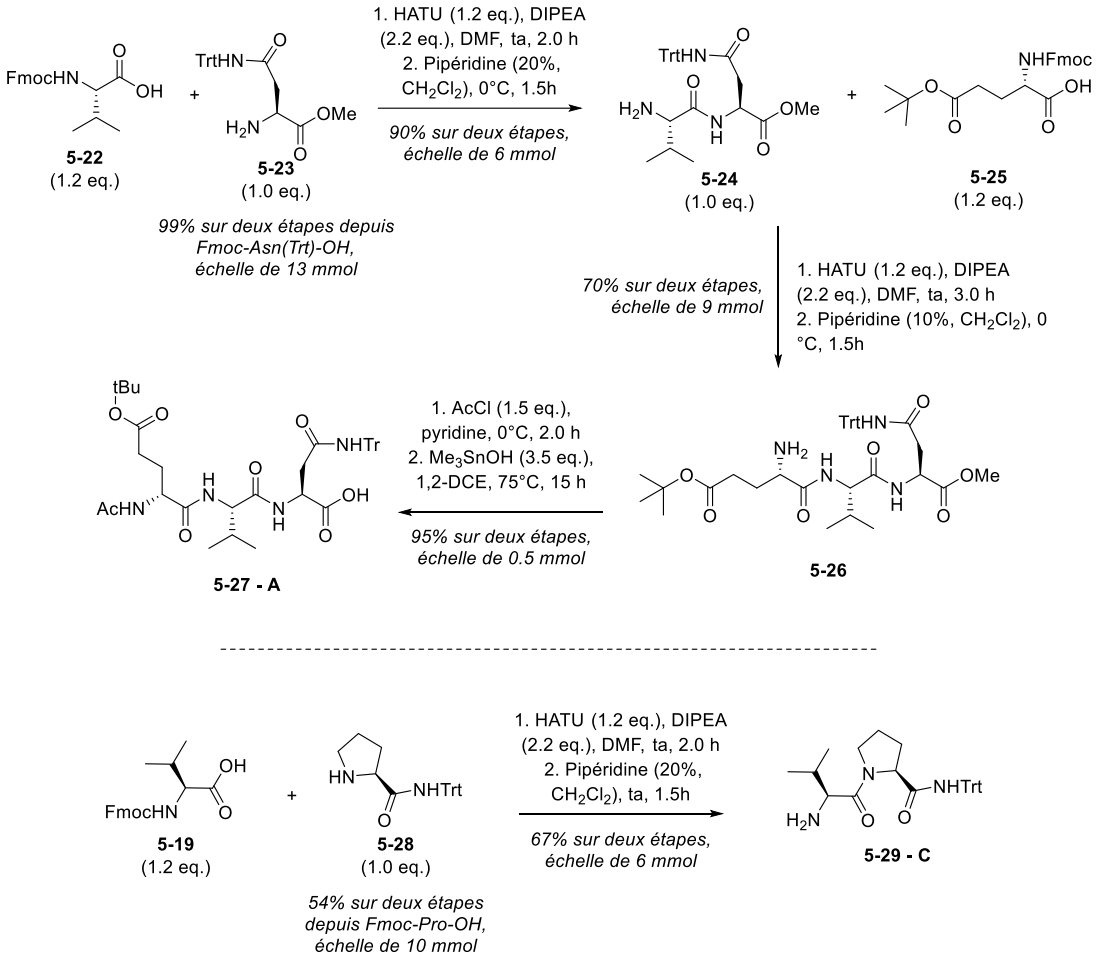

5.2.2.3 Synthèse des heptapeptides des isomères ProCyp **5-11** et **5-12**.

Le premier heptapeptide synthétisé a été celui du ProCyp **5-12**. Lors du couplage avec le fragment **5-27-A**, un mélange d'épimères a été formé avec un ratio de 2:1 (Schéma 5.3). Bien que la structure n'ait été élucidée, il a été proposé que l'épimère soit formé à la position α de l'acide carboxylique via la formation de l'oxazolone. [621,622] La formation de l'épimère a pu être réduite lorsque la réaction a été conduite à -50 °C et un ratio de 83:17 a été obtenu avec 57% de rendement. L'utilisation de différents agents de couplage n'a pas réussi à améliorer le ratio. L'hydrolyse de l'ester méthylique a été effectuée en utilisant le réactif d'hydroxyde de triméthylétain comme lors de la synthèse du fragment **5-27-A**. Dans ces conditions, le produit de départ n'a pu être entièrement solubilisé et la conversion partielle vers l'acide carboxylique **5-31**

a résulté en un faible rendement. Le solvant a alors été échangé pour le toluène, [623,624] et la solubilisation complète de l'ester a été observée lorsque le mélange réactionnel a été chauffé à 60 °C. Il est à noter que dans ces conditions, un ajout régulier d'hydroxyde de triméthylétain a été nécessaire afin d'améliorer la conversion de la réaction. Ce phénomène a également été observé au cours d'études précédentes. [625] Les isomères ont pu être séparés à cette étape et **5-31** a été obtenu avec 49% de rendement. Le couplage suivant avec le fragment **5-29-C** a été réalisé dans des conditions standards et l'heptapeptide a été formé avec 82% de rendement.

Schéma 5.3 Synthèse de l'heptapeptide **5-32.**

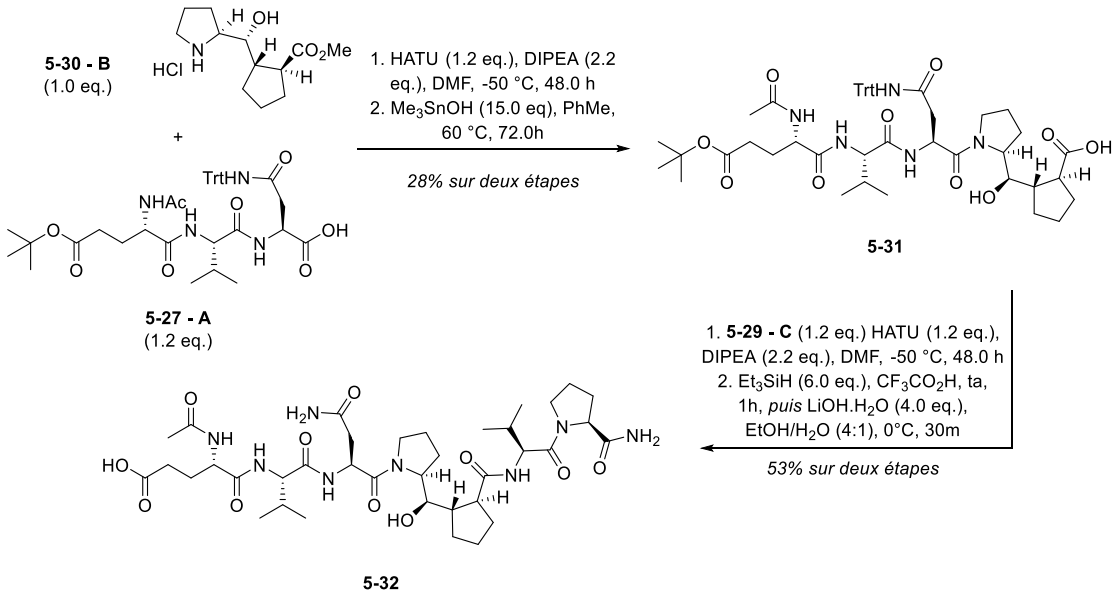

Afin de pouvoir éliminer l'ensemble des groupes protecteurs du peptide final, des conditions acides ont été privilégiées considérant que le composé ne possédait pas de fonctions sensibles à ce système hormis les groupements tritylés et l'ester *tert*-butylique. En effet, la dissolution de l'heptapeptide dans un volume d'acide trifluoroacétique suivi par l'addition d'hydrure de triméthylsilane a résulté en la déprotection totale de l'heptapeptide. Il est à noter que la formation d'une faible quantité de trifluoroacétate a été observée par spectrométrie de masse au cours de la réaction. Cependant, le produit secondaire a pu être facilement hydrolysé et le produit final **5-32** a été obtenu avec 65% de rendement et 100% de pureté après purification par HPLC préparative.

Une fois la synthèse établie à l'aide de **5-32**, la même approche a été appliquée à l'isomère ProCyp **5-11**. Le couplage entre le fragment **5-27-A** et le module ProCyp **5-11-B** a permis l'obtention du pentapeptide avec des rendements et ratio d'isomères similaires à ceux observés pour la série **5-12** (55%, *dr* 82:18). (Schéma 5.4) Le mélange d'isomères a ensuite été hydrolysé à l'aide d'hydroxyde de triméthylétain, bien que l'isomère mineur n'ai pu être séparé dans ce cas. Néanmoins, le couplage entre **5-34** et **5-29-C** a délivré l'heptapeptide avec un excellent rendement, et l'isomère mineur a alors été séparé par HPLC préparative. Enfin, la déprotection finale a permis l'obtention de l'heptapeptide **5-35** avec 66% de rendement et 95% de pureté.

Schéma 5.4 Synthèse de l'heptapeptide **5-35**.

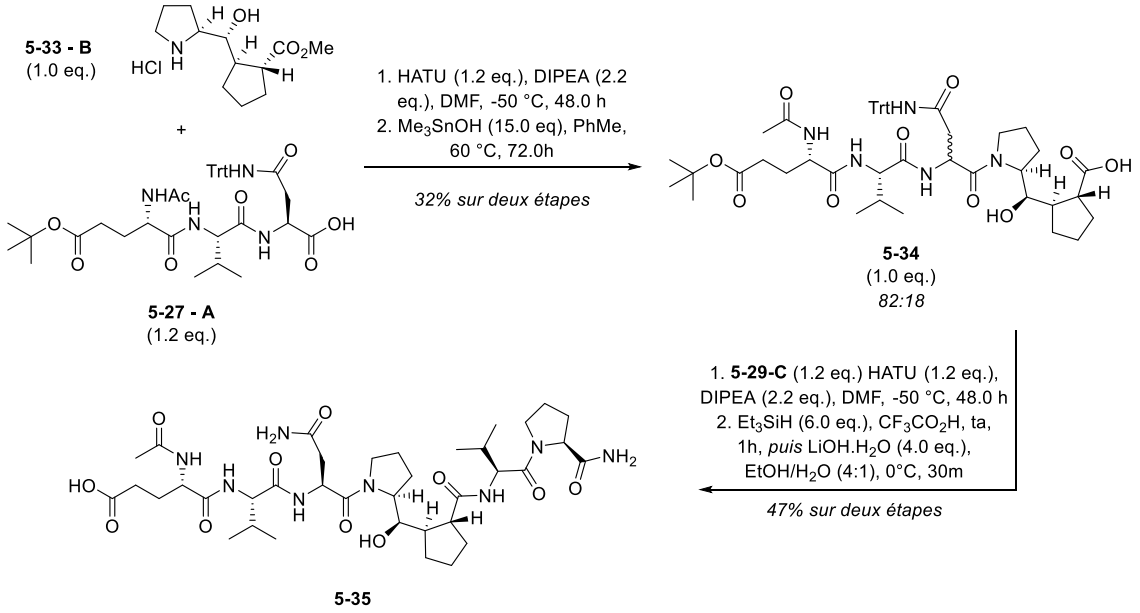

5.2.2.4 Synthèse de l'isomère ProCyp **5-14**

La synthèse de l'isomère ProCyp **5-14** pouvant être dérivé de l'isomérisation du carbone C8 de **5-12** (Tableau 5.2), sa formation a été considérée pré et post cyclisation du cyclopentane, étant conscient que la géométrie du cycle une fois formé défavoriserait la formation de l'isomère *cis*. Considérant que **5-12** fournirait directement le cyclopentane **5-14**, la première tentative a été de déprotoner **5-12** en conditions cinétiques en présence du bis-hexaméthylsilylamidure de potassium (KHMDS) afin de favoriser la formation potentielle de l'isomère *cis*. Cependant, la

déprotonation du groupement hydroxyle a entrainé son addition sur le carbamate du groupement protecteur Boc, résultant en la formation de **5-36** par cyclisation intramoléculaire (entrée 1). Aucun produit d'épimérisation n'a été détecté. Bien que la protection du groupement hydroxyle aurait permis d'éviter la cyclisation parasite, cette stratégie a été écartée. En effet, les précédents synthétiques ont prouvé que la manipulation du groupement hydroxyle pour l'installation d'un groupement protecteur après cyclisation relevait du défi compte tenu de l'encombrement stérique. Par conséquent, le substrat fut changé pour **5-37**, qui présente l'avantage de toujours posséder le groupement BOM. Considérant que la présence du substrat initial après la réaction puisse être due à un manque de conversion ou bien à la sélectivité faciale de l'énolate lors de la protonation, la réaction a été arrêtée par ajout d'eau deutérée. Lorsque les mêmes conditions cinétiques ont été appliquées, aucune conversion n'a été observée (entrée 2). L'échange de la base pour l'amidure de lithium diisopropylé (LDA) n'a pas permis d'améliorer ce résultat, et le produit de départ a été récupéré sans que l'épimère **5-38** n'ait pu être observé. (entrée 3) L'augmentation de la température s'est également révélée infructueuse dans le cas de KHMDS, et l'apparition de dégradation du produit de départ a été observée. (entrée 4) Le produit a finalement pu être observé sous forme de traces lorsque le produit de départ a été mis en présence de LDA à température ambiante; cependant la quantité importante de dégradation formée a proscrit son utilisation (entrée 5). Suite aux difficultés de conversion rencontrées, notre attention s'est tournée vers l'épimérisation de la chaîne allylique de **5-39** avant d'effectuer la cyclisation par réaction de métathèse. Bien que le même manque de réactivité ait été constaté lors de l'utilisation d'une base lithiée en conditions cinétiques (entrées 6,7), l'utilisation de conditions thermodynamiques s'est révélée fructueuse. Ainsi, lorsqu'en présence d'une solution de méthanoate de sodium à température ambiante pendant 15h, le nouvel épimère **5-40** a été formé avec un ratio de 9:1 en faveur de **5-39**. (entrée 8) Afin d'améliorer le ratio, la réaction a été accomplie à 65 °C et l'épimérisation complète de C8 a pu être obtenue après 48h de réaction avec un rendement de 94%. (entrée 9) Ces conditions réactionnelles n'ont produit aucune conversion pour **5-12** et a résulté en la dégradation de **5-37** sur le temps, confirmant la nécessité de la présence de la chaîne libre lorsque des conditions thermodynamiques sont utilisées.

Tableau 5.2 Optimisation des conditions d'épimérisation du carbone C8.

	Substrat	*Conditions*	*Ratio du produit obtenu*		
1	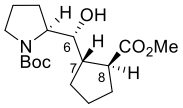 **5-12**	KHMDS, THF, -78°C, 30m	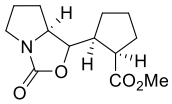 **5-36** 100%		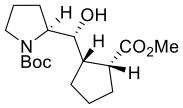 **5-14** Non observé
2	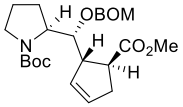 **5-37**	KHMDS, THF, -78°C, 30m *puis* D_2O, -78C à ta	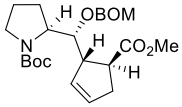 **5-37** 100%		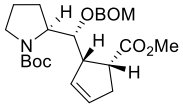 **5-38** Non observé
3	**5-37**	LDA, THF, -78°C, 30m *puis* D_2O, -78C à ta	**5-37** Récupéré		**5-38** Non observé
4	**5-37**	KHMDS, THF, -78°C à ta, 30m *puis* D_2O	**5-37** Récupéré		**5-38** Non observé
5	**5-37**	LDA, THF, -78°C à ta, 30m *puis* D_2O	**5-37** Récupéré		**5-38** Traces
6	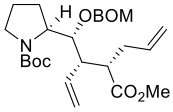 **5-39**	KHMDS, THF, -78°C, 30m *puis* D_2O, -78C à ta	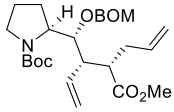 **5-39** Récupéré		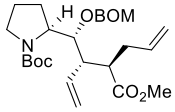 **5-40** Non observé
7	**5-39**	LDA, THF, -78°C, 30m *puis* D_2O, -78C à ta	**5-39** Récupéré		**5-40** Non observé
8	**5-39**	MeONa, THF, ta, 16h	**5-39**	9:1	**5-40**
9	**5-39**	MeONa, THF, 65°C, 48h	**5-39**	1:1	**5-40**

Bien que les isomères n'aient pu être isolés à cette étape, le mélange a pu être directement utilisé dans l'étape de cyclisation par métathèse, (Schéma 5.5) et le nouvel isomère **5-42** s'est révélé prompt à l'isomérisation de la double liaison formée. Ce phénomène n'est pas étranger aux mécanismes de métathèse et a été documenté à de nombreuses occasions. [626,627] Les deux isomères ont pu être isolés et caractérisés, et l'hypothèse que **5-43** était un isomère de position de **5-42** a été confirmé lors de l'étape d'hydrogénolyse qui a résulté en la formation de **5-14**. Aucun parachèvement aqueux n'a été impliqué au cours de ces deux étapes afin d'éviter

l'épimérisation du carbone C8. La stéréochimie de **5-14** a été confirmée par analyse aux rayons-X après déprotection du groupement Boc et lactonisation concomitante. La formation de la lactone **5-44** a été conservée pour la suite des étapes, protégeant le centre C8 de potentielles épimérisations en milieu acidobasique.

Schéma 5.5 Synthèse de l'isomère ProCyp **5-14**.

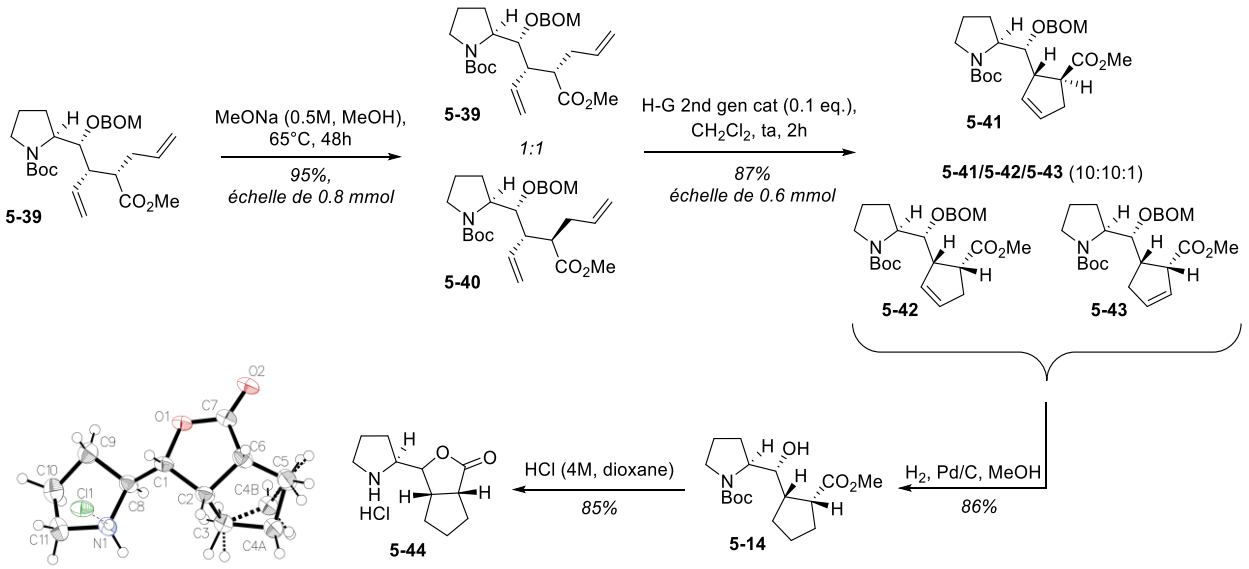

Une fois la lactone **5-44** formée, notre attention s'est tournée vers l'assemblage des fragments **A**, **B** et **C**. Un ratio de 71:25:4 et un rendement de 66% ont été obtenus lors du couplage de **5-44** avec le fragment **5-27-A**, ce qui est consistant avec les deux autres séries. (Schéma 5.6) Bien que la structure n'ait pas été élucidée, il a été proposé que l'isomère mineur à 4% soit dû à la présence résiduelle de l'isomère *trans* **5-12**. Le mélange n'a pas pu être séparé à cette étape et a été soumis à l'hydrolyse de la lactone en tant que tel. L'ouverture de la lactone a été réalisée à l'aide d'hydroxyde de lithium et a permis d'obtenir la formation de **5-45** avec 46% de rendement sur deux étapes. La partie finale de la synthèse consistant en la manipulation de l'acide carboxylique pour son couplage avec le fragment **5-29-C**, il a été anticipé qu'un mécanisme de lactonisation parasite puisse affecter l'efficacité de la réaction. En effet, la réaction de couplage a délivré un mélange de 3:1 en faveur de la lactone **5-46**. (Schéma 5.6) La présence d'un large excès de fragment **5-29-C**, la baisse de la température ou l'addition lente de l'agent de couplage n'ont pas réussi à améliorer le ratio.

Schéma 5.6 Synthèse de l'heptapeptide: Approche par couplage peptidique.

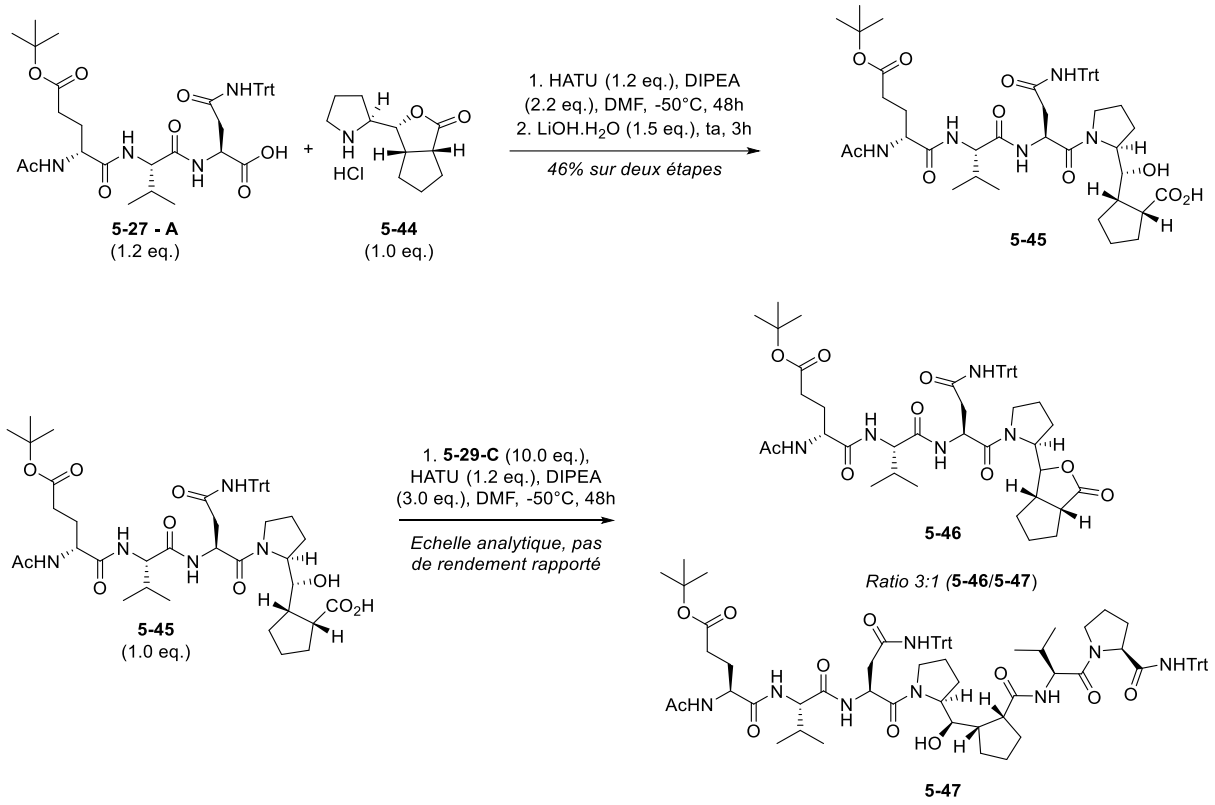

Bien que la lactone puisse être recyclée, une autre approche a été considérée pour des raisons d'économies de matériel et de temps. Dans le cadre de la synthèse d'inhibiteurs de la β-secrétase, l'ouverture d'un dérivé de la butyrolactone par une butylamine activée par le triméthyle d'aluminium a été rapportée par des membres du groupe. [628] Bien que l'encombrement stérique de l'amine secondaire de la proline soit plus important, il a été considéré que sa plus grande nucléophilie combinée à l'activation par le triméthyle d'aluminium puisse permettre d'obtenir une réactivité similaire. Un essai préliminaire entre **5-29-C** et la butyrolactone **5-48** a confirmé ce résultat avec 79% de rendement, bien que le produit n'ait pas pu être séparé de l'excès de **5-29-C**. (Schéma 5.7 – A) La réaction a ensuite été testée sur la lactone **5-44**, et la conversion complète du produit a été observée avec 66% de rendement. Un premier essai sur une échelle analytique a alors été conduit avec la lactone **5-51**, et l'analyse HPLC du brut réactionnel a confirmé la présence du produit désiré avec 75% de conversion. La réaction s'est montrée reproductible lors de la montée en échelle, et un rendement final de 46% de l'heptapeptide **5-47** avec 17% du produit de départ **5-46** a été isolé après séparation par HPLC préparative. (Schéma 5.7 – B) Le

produit de départ a pu être recyclé pour effectuer un deuxième cycle. L'étape de déprotection finale a été effectuée selon le même protocole que pour les séries précédentes. Comme dans le cas de **5-32**, une estérification partielle du groupement hydroxyle a été observée, et le trifluoroacétate a pu être hydrolysé sans incident majeur.

Schéma 5.7 Synthèse de l'heptapeptide **5-52** : Approche par transamidification. A – Essais méthodologiques. B – Fin de la synthèse.

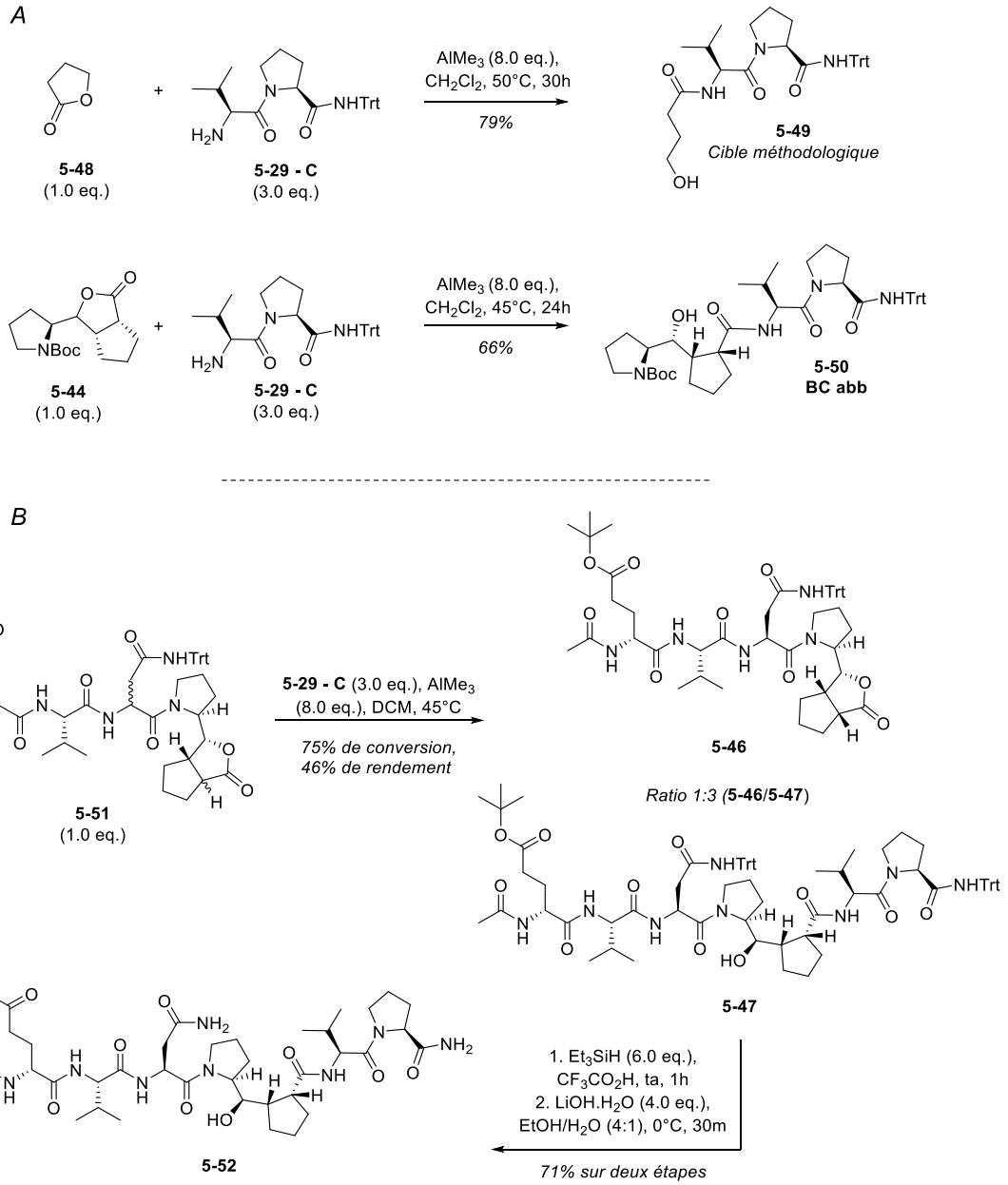

L'heptapeptide final **5-52** a été obtenu avec 71% de rendement sur les deux étapes et 99% de pureté après purification par HPLC préparative, complétant ainsi la synthèse du troisième isomère à être testé contre le peptide FRET pour l'inhibition de PPEP-1.

5.2.3 Conclusions

Suite à l'élucidation du co-cristal de PPEP-1 avec un peptidomimétique de sa séquence native EVNPPVP, un ensemble de peptides basés sur la même séquence et incluant le dimère ProCyp ont été synthétisés. Les isomères ProCyp ont été sélectionnés sur la base de la modélisation moléculaire réalisée par le Pr. Baumann lors de cette collaboration. Afin d'obtenir le meilleur isomère, le carbone C8 a été isomérisé et le cyclopentane *cis* a été obtenu. Les trois peptides cibles ont été synthétisés et sont en cours d'études biologiques. Celles-ci sont composée d'une part d'études de compétition afin de déterminer l'affinité de chaque peptide avec PPEP-1, et d'autre part d'essais de co-cristallisation avec la protéine.

Chapitre 6. Conclusion générale et perspectives

6.1 Conclusions

La proline est un acide aminé unique en raison de son cycle pyrrolidine. Celui-ci lui confère des propriétés structurelles particulières dont la Nature a su tirer parti pour l'établissement de la structure des protéines ainsi que certaines de leurs fonctions. De même, les chimistes médicinaux se sont inspirés de cette particularité au travers de diverses applications dans la conception de petites molécules bioactives ou de peptidomimétiques. Cette thèse a été dédiée à l'étude de tels composés, et ce, à travers différentes applications.

Le chapitre deux fait part de deux projets d'extension du composé activateur de PP2A, SH-BC-893. Le premier projet décrit la synthèse et les tests biologiques d'une nouvelle série de composés dans laquelle la chaine aryloctyle a été déplacée en position C-2. Certains de ces composés ont été phosphatés afin d'être testés contre HDAC2. Bien que les tests de HDAC2 n'aient été concluants, l'activation de PP2A a été maintenue excepté lors de la présence d'une cétone en position β. Au sein du deuxième projet, un des composés de tête des SMAPs a été synthétisé et son activité a été comparée avec SH-BC-893. Puis, une nouvelle série de composés dans laquelle un fragment (tri)cyclique a été attaché à la fonction hydroxyle de SH-BC-893 a été synthétisée afin d'améliorer son activité envers PP2A en activant d'autres sites actifs ou homologues agissant sur les voies de signalisation de FoxO1.

Le chapitre trois décrit la méthodologie de synthèse de nouveaux composés bicycliques issus de la proline, dans lesquels est contenu un motif GABA. La synthèse permet également la formation stéréocontrôlée d'un centre quaternaire sur la proline pontée formé à l'aide de l'addition successive de substituants sur une fonction carbonylée. Lorsque le substituant ajouté est un phényle *para*-chloré ou un *iso*-butyle, les composés formés représentent une version contrainte des drogues du SNC baclofen et pregabalin. Lorsque modélisé au sein du site actif du récepteur GABA-B co-cristallisé avec baclofen, l'analogue contraint a montré un bon recouvrement. Leur modélisation dans la plateforme LLAMA a également montré que leur lipophilie devrait leur permettre de traverser la barrière du SNC, ce qui suggère que ces composés puissent détenir un

potentiel pour le développement de drogues neuronales liés à la modulation des récepteurs GABA.

Le quatrième chapitre rapporte la conception et la synthèse d'un nouveau module synthétique de la diproline, nommé ProCyp. Dans celui-ci, le second cycle pyrrolidine a été remplacé par un cyclopentane et la fonction amide par un pont hydroxylé. Au cours de la synthèse, l'ensemble des isomères *trans* du cyclopentane ont été synthétisé et leur stéréochimie absolue a été déterminée à l'aide d'une combinaison d'expériences RMN et de diffraction par rayons-X. De plus, il a été montré que trois de ces isomères possède une liaison hydrogène intramoléculaire en solution entre l'oxygène donneur du groupement carbamate et l'hydrogène accepteur de la fonction hydroxylée. Ce module ProCyp a ensuite été utilisé au sein de différents projets.

Le chapitre six présente deux applications du module ProCyp. La première est centrée sur le développement de peptidomimétiques du peptide de la sous-unité $p22^{phox}$ de NOX2 dans laquelle son PRM est reconnu par le PRD de la sous-unité $p47^{phox}$. Cette interaction régule l'activité de NOX2 au travers de son assemblage. La séquence peptidique a été établie à l'aide d'une étude de co-cristallisation couplée à un Ala scan puis les flancs gauche et droite de la triproline formant le PRM ont été optimisés. L'isomère ProCyp possédant la stéréochimie permettant un bon recouvrement avec la conformation PPII de la triproline a ensuite été inséré aux positions P155-P156 et P156-P157. Lorsque ProCyp a remplacé P156-P157, le peptide a présenté une activité comparable à la séquence native de $p22^{phox}$ et a été sept fois moins actif que son parent triproline.

La deuxième application a visé à développer des inhibiteurs de la protéine facteur de virulence de PPEP-1. Dans ce projet, la séquence peptidique naturelle des sites de scission des adhésines CD2830 et CD3241 a été utilisée et la diproline centrale du site de scission S1-S1' a été remplacée par plusieurs isomères de ProCyp. Les isomères ont été sélectionnés sur la base de l'étude de modélisation réalisée par le Pr. Baumann. Suite à cette étude, un nouvel isomère ProCyp portant un cyclopentane de configuration *cis* a été synthétisé. Ces composés sont actuellement en cours d'étude pour établir leur affinité avec PPEP-1. Leur co-cristallisation avec PPEP-1 est également à l'essai.

6.2 Perspective

Les projets liés à SH-BC-893 sont désormais terminés et il n'est pas prévu de nouvelles extensions sur ces travaux étant donné que plusieurs brevets ont été déposés et qu'une entreprise a été créée pour les développements futurs.

Bien que cela n'ait pas été présenté au sein de l'article sur les prolines pontées, il est également possible d'additionner d'autres types de nucléophiles sur la cétone au lieu de l'énolate d'acétate d'éthyle, amenant à une nouvelle diversité chimique (Schéma 6.1 – A). Lorsqu'un groupement allylique a été implémenté, l'octahydroindolizine **6-8** qui s'apparente à l'alcaloïde loline a pu être synthétisée (Schéma 6.1 – B). Par conséquent, il est envisageable d'étendre cette stratégie à de nouvelles structures d'intérêts pour la synthèse de produits naturels ou médicinaux.

Schéma 6.1 A. Approche par addition séquentielle de réactifs de Grignard pour la formation de 2-oxa-5-azabicyclo[2.2.1]heptanes. B. Post-fonctionnalisation vers le composé octahydroindolizine **6-8**.

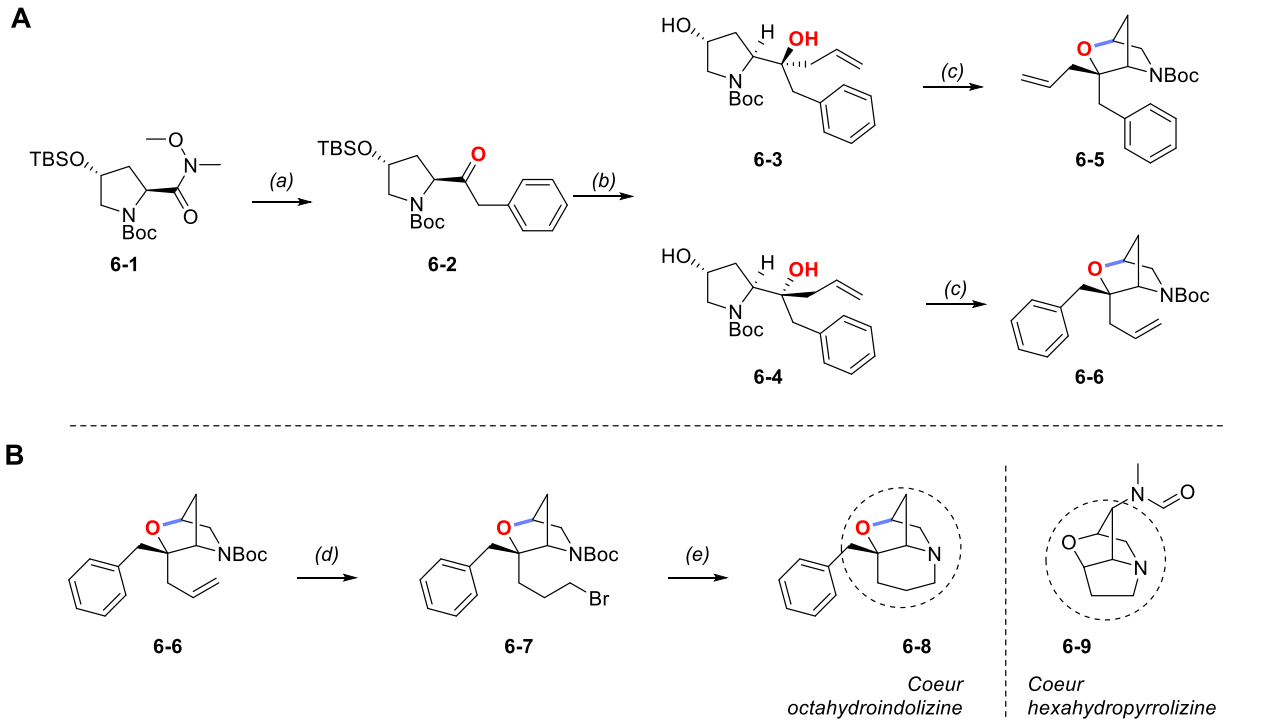

Conditions: (a) BnMgCl (3.0 eq.), THF, 65%. *(b)* **1.** C_3H_5MgBr, THF, 0°C à ta; **2.** TBAF (1.1 eq.), THF, 78% sur 2 étapes, 2:1 (**6-3**/**6-4**). *(c)* TsOTs (3.0 eq.), pyridine, ta à 100°C, **6-5**: 82%, **6-6**: 90%; *(d)*1. BH_3.DMS, THF *puis* NaOH, H_2O_2; 2. PPh_3, CBr_4, DCM, 61% sur 2 étapes. *(e)* 1. TFA/DCM (1:1); 2. Et_3N, MeOH, 80% sur 2 étapes.

Les perspectives pour le motif ProCyp sont plus larges. Il est envisageable qu'elles puissent s'étendre à un ensemble d'applications impliquant un PRM au sein d'une PPI impliquée dans une voie de signalisation, ainsi qu'à d'autres membres des PPEPs lorsqu'elles seront découvertes. Il est également possible que ce dimère recèle un potentiel pour la formation ou le maintien de structures secondaires telles que les tournants-β ou les hélices. Récemment, plusieurs homo-oligomères ont été synthétisés au laboratoire dans lesquels l'organisation spontanée sous forme d'hélice est à l'étude (Figure 6.1 – A). En effet, la formation de structures secondaires a été observée par dichroïsme circulaire au sein d'une série d'octamères (Figure 6.1 – B). Un cristal du tétramère **6-14** a également montré la formation d'une hélice dont le pitch hélicoïdal est de 9.6 Å/tour et les angles φ = - 84 ° et Ψ = + 178 ° (Figure 6.1 – C).

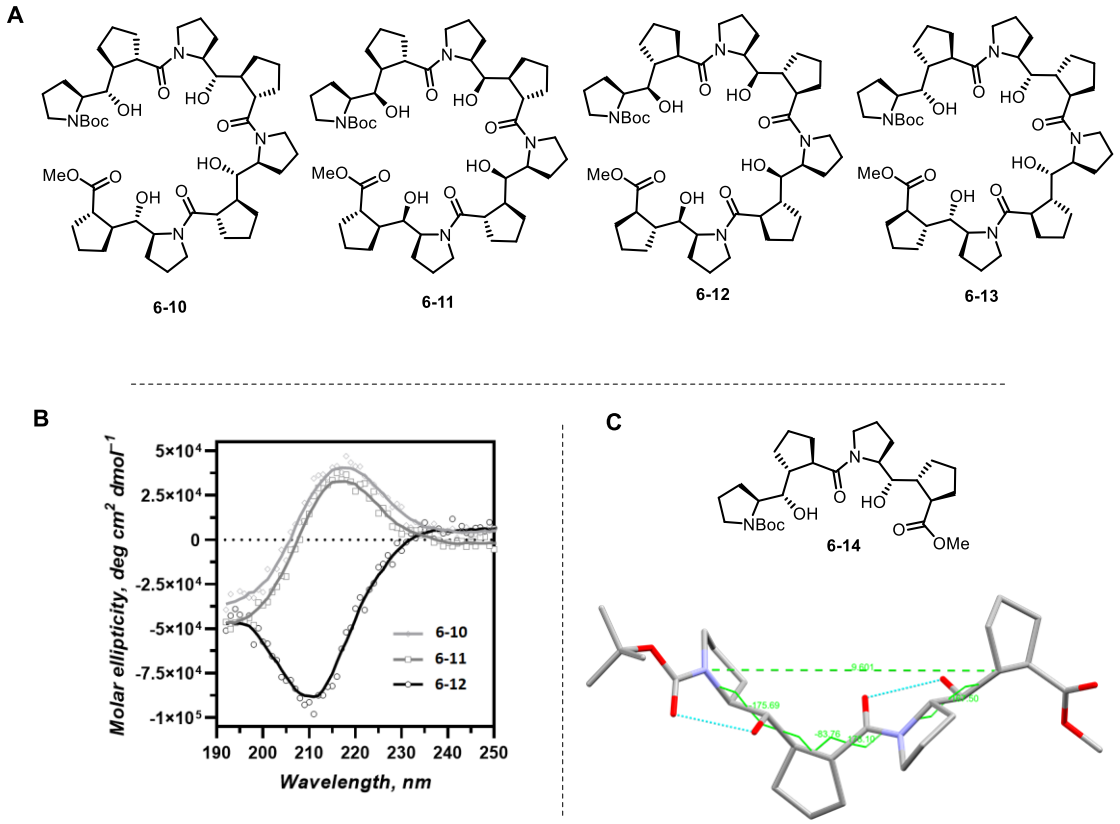

Figure 6.1 A. Structure des octamères de ProCyp (**6-10** – **6-13**). B. Graphes de dichroïsme circulaire des composés **6-10**, **6-11**, et **6-12**. C. Cristal du tétramère **6-14**.

Ceux-ci s'approchent des valeurs des PPII et peuvent indiquer que la formation d'une telle structure secondaire est applicable aux oligomères de ProCyp. Les spectres RMN du proton des tétramères et octamères indiquent que le maintien des liaisons hydrogène et de la structure hélicoïdale puisse être conservé en raison des similarités observées entre les signaux de dimères contenus au sein de chaque oligomère.

Chapitre 7. Références bibliographiques

(1) Morgan, A. A.; Rubenstein, E. Proline: The Distribution, Frequency, Positioning, and Common Functional Roles of Proline and Polyproline Sequences in the Human Proteome. *PLoS One* **2013**, *8*, 1–9. https://doi.org/10.1371/journal.pone.0053785.

(2) MacArthur, M. W.; Thornton, J. M. Influence of Proline Residues on Protein Conformation. *J. Mol. Biol.* **1991**, *218*, 397–412. https://doi.org/10.1016/0022-2836(91)90721-H.

(3) Schmidpeter, P. A. M.; Schmid, F. X. Prolyl Isomerization and Its Catalysis in Protein Folding and Protein Function. *J. Mol. Biol.* **2015**, *427*, 1609–1631. https://doi.org/10.1016/j.jmb.2015.01.023.

(4) Ball, L. J.; Kühne, R.; Schneider-Mergener, J.; Oschkinat, H. Recognition of Proline-Rich Motifs by Protein-Protein-Interaction Domains. *Angew. Chemie - Int. Ed.* **2005**, *44*, 2852–2869. https://doi.org/10.1002/anie.200400618.

(5) Kumar, P.; Bansal, M. Structural and Functional Analyses of PolyProline-II Helices in Globular Proteins. *J. Struct. Biol.* **2016**, *196*, 414–425. https://doi.org/10.1016/j.jsb.2016.09.006.

(6) Ramachandran, G. N.; Mitra, A. K. An Explanation for the Rare Occurrence of Cis Peptide Units in Proteins and Polypeptides. *J. Mol. Biol.* **1976**, *107*, 85–92. https://doi.org/10.1016/S0022-2836(76)80019-8.

(7) Wedemeyer, W. J.; Welker, E.; Scheraga, H. A. Proline Cis-Trans Isomerization and Protein Folding. *Biochemistry* **2002**, *41*, 14637–14644. https://doi.org/10.1021/bi020574b.

(8) Brandts, J. F.; Halvorson, H. R.; Brennan, M. Consideration of the Possibility That the Slow Step in Protein Denaturation Reactions Is Due to Cis-Trans Isomerism of Proline Residues. *Biochemistry* **1975**, *14*, 4953–4963. https://doi.org/10.1021/bi00693a026.

(9) Yeh, E. S.; Means, A. R. PIN1, the Cell Cycle and Cancer. *Nat. Rev. Cancer* **2007**, *7*, 381–388. https://doi.org/10.1038/nrc2107.

(10) Bai, Y.; Englander, S. W. Future Directions in Folding: The Multi-State Nature of Protein Structure. *PROTEINS Struct. Funct. Genet.* **1996**, *24*, 145–151.

(11) Chaudhuri, T. K.; Paul, S. Protein-Misfolding Diseases and Chaperone-Based Therapeutic Approaches. *FEBS J.* **2006**, *273*, 1331–1349. https://doi.org/10.1111/j.1742-4658.2006.05181.x.

(12) Englander, S. W.; Mayne, L. The Nature of Protein Folding Pathways. *Proc. Natl. Acad. Sci. U. S. A.* **2014**, *111*, 15873–15880. https://doi.org/10.1073/pnas.1411798111.

(13) Raines, R. T. Rinonuclease A. *Chem. Rev.* **1998**, *98*, 1045–1065.

(14) Odefey, C.; Mayr, L. M.; Schmid, F. X. Non-Prolyl Cis-Trans Peptide Bond Isomerization as a Rate-Determining Step in Protein Unfolding and Refolding. *J. Mol. Biol.* **1995**, *245*, 69–78. https://doi.org/10.1016/S0022-2836(95)80039-5.

(15) Wood, L. C.; White, T. B.; Ramdas, L.; Nall, B. T. Replacement of a Conserved Proline Eliminates the Absorbance-Detected Slow Folding Phase of Iso-2-Cytochrome C. *Biochemistry* **1988**, *27*, 8562–8568. https://doi.org/10.1021/bi00423a009.

(16) Guijarro, J. I.; Morton, C. J.; Plaxco, K. W.; Campbell, I. D.; Dobson, C. M. Folding Kinetics of the SH3 Domain of PI3 Kinase by Real-Time NMR Combined with Optical Spectroscopy. *J. Mol. Biol.* **1998**, *276*, 657–667. https://doi.org/10.1006/jmbi.1997.1553.

(17) Lewis, P. N.; Momany, F. A.; Scheraga, H. A. Folding of Polypeptide Chains in Proteins: A Proposed Mechanism for Folding. *Proc. Natl. Acad. Sci. U. S. A.* **1971**, *68*, 2293–2297. https://doi.org/10.1073/pnas.68.9.2293.

(18) Krebs, H.; Schmid, F. X.; Jaenicke, R. Folding of Homologous Proteins. *J. Mol. Biol.* **1983**, *169*, 619–635. https://doi.org/10.1016/s0022-2836(83)80067-9.

(19) Creighton, T. E. Possible Implications of Many Proline Residues for the Kinetics of Protein Unfolding and Refolding. *J. Mol. Biol.* **1978**, *125*, 401–406. https://doi.org/10.1016/0022-2836(78)90411-4.

(20) Schmid, F. X. Prolyl Isomerase: Enzymatic Catalysis of Slow Protein-Folding Reactions.

Annu. Rev. Biophys. Biomol. Struct. **1993**, *22*, 123–143. https://doi.org/10.1146/annurev.bb.22.060193.001011.

(21) Udgaonkar, J. B.; Baldwin, R. L. Early Folding Intermediate of Ribonuclease A. *Proc. Natl. Acad. Sci. U. S. A.* **1990**, *87*, 8197–8201. https://doi.org/10.1073/pnas.87.21.8197.

(22) Schmidpeter, P. A. M.; Koch, J. R.; Schmid, F. X. Control of Protein Function by Prolyl Isomerization. *Biochim. Biophys. Acta* **2015**, *1850*, 1973–1982. https://doi.org/10.1016/j.bbagen.2014.12.019.

(23) Garel, J. R.; Baldwin, R. L. Both the Fast and Slow Refolding Reactions of Ribonuclease A Yield Native Enzyme. *Proc. Natl. Acad. Sci. U. S. A.* **1973**, *70*, 3347–3351. https://doi.org/10.1073/pnas.70.12.3347.

(24) Kim, P. S.; Baldwin, R. L. Specific Intermediates in the Folding Reactions of Small Proteins and the Mechanism of Protein Folding. *Annu. Rev. Biochem.* **1982**, *51*, 459–489. https://doi.org/10.1146/annurev.bi.51.070182.002331.

(25) Schmid, F. X.; Blaschek, H. A Native-Like Intermediate on the Ribonuclease A Folding Pathway: 2. Comparison of Its Properties to Native Ribonuclease A. *Eur. J. Biochem.* **1981**, *114*, 111–117. https://doi.org/10.1111/j.1432-1033.1981.tb06179.x.

(26) Schiene-Fischer, C.; Aumüller, T.; Fischer, G. Peptide Bond Cis/Trans Isomerases: A Biocatalysis Perspective of Conformational Dynamics in Proteins. *Top. Curr. Chem.* **2013**, *328*, 35–68.

(27) Nath, P. R.; Isakov, N. Insights into Peptidyl-Prolyl Cis-Trans Isomerase Structure and Function in Immunocytes. *Immunol. Lett.* **2015**, *163*, 120–131. https://doi.org/10.1016/j.imlet.2014.11.002.

(28) Fagiani, F.; Govoni, S.; Racchi, M.; Lanni, C. The Peptidyl-Prolyl Isomerase Pin1 in Neuronal Signaling: From Neurodevelopment to Neurodegeneration. *Mol. Neurobiol.* **2021**, *58*, 1062–1073. https://doi.org/10.1007/s12035-020-02179-8.

(29) Rizzolio, F.; Lucchetti, C.; Caligiuri, I.; Marchesi, I.; Caputo, M.; Klein-Szanto, A. J.; Bagella,

L.; Castronovo, M.; Giordano, A. Retinoblastoma Tumor-Suppressor Protein Phosphorylation and Inactivation Depend on Direct Interaction with Pin1. *Cell Death Differ.* **2012**, *19*, 1152–1161. https://doi.org/10.1038/cdd.2011.202.

(30) Blair, L. J.; Baker, J. D.; Sabbagh, J. J.; Dickey, C. A. The Emerging Role of Peptidyl-Prolyl Isomerase Chaperones in Tau Oligomerization, Amyloid Processing, and Alzheimer's Disease. *J. Neurochem.* **2015**, *133*, 1–13. https://doi.org/10.1111/jnc.13033.

(31) Wang, L.; Zhou, Y.; Chen, D.; Lee, T. H. Peptidyl-Prolyl Cis/Trans Isomerase Pin1 and Alzheimer's Disease. *Front. Cell Dev. Biol.* **2020**, *8*, 1–12. https://doi.org/10.3389/fcell.2020.00355.

(32) Yu, J. H.; Im, C. Y.; Min, S.-H. Function of PIN1 in Cancer Development and Its Inhibitors as Cancer Therapeutics. *Front. Cell Dev. Biol.* **2020**, *8*, 1–12. https://doi.org/10.3389/fcell.2020.00120.

(33) Perrucci, G. L.; Gowran, A.; Zanobini, M.; Capogrossi, M. C.; Pompilio, G.; Nigro, P. Peptidyl-Prolyl Isomerases: A Full Cast of Critical Actors in Cardiovascular Diseases. *Cardiovasc. Res.* **2015**, *106*, 353–364. https://doi.org/10.1093/cvr/cvv096.

(34) Ünal, C. M.; Steinert, M. Microbial Peptidyl-Prolyl Cis/Trans Isomerases (PPIases): Virulence Factors and Potential Alternative Drug Targets. *Microbiol. Mol. Biol. Rev.* **2014**, *78*, 544–571. https://doi.org/10.1128/mmbr.00015-14.

(35) Ünal, C. M.; Berges, M.; Smit, N.; Schiene-Fischer, C.; Priebe, C.; Strowig, T.; Jahn, D.; Steinert, M. PrsA2 (CD630_35000) of Clostridioides Difficile Is an Active Parvulin-Type PPiase and a Virulence Modulator. *Front. Microbiol.* **2018**, *9*, 1–13. https://doi.org/10.3389/fmicb.2018.02913.

(36) Hutchinson, E. G.; Thornton, J. M. A Revised Set of Potentials for B-turn Formation in Proteins. *Protein Sci.* **1994**, *3*, 2207–2216. https://doi.org/10.1002/pro.5560031206.

(37) Guruprasad, K.; Rajkumar, S. β- and γ-Turns in Proteins Revisited: A New Set of Amino Acid Turn-Type Dependent Positional Preferences and Potentials. *J. Biosci.* **2000**, *25*, 143–156. https://doi.org/10.1007/bf03404909.

(38) Matthews, B. W. The γ Turn. Evidence for a New Folded Conformation in Proteins. **1972**, *5*, 818–819.

(39) Milner-White, E. J. Situations of Gamma-Turns in Proteins. Their Relation to Alpha-Helices, Beta-Sheets and Ligand Binding Sites. *J. Mol. Biol.* **1990**, *216*, 385–397. https://doi.org/10.1016/S0022-2836(05)80329-8.

(40) De Brevern, A. G. Extension of the Classical Classification of β-Turns. *Sci. Rep.* **2016**, *6*, 1–15. https://doi.org/10.1038/srep33191.

(41) Pavone, V.; Gaeta, G.; Lombardi, A.; Nastri, F.; Maglio, O.; Isernia, C.; Saviano, M. Discovering Protein Secondary Structures: Classification and Description of Isolated α-Turns. *Biopolymers* **1996**, *38*, 705–721. https://doi.org/10.1002/(SICI)1097-0282(199606)38:6<705::AID-BIP3>3.0.CO;2-V.

(42) Dasgupta, B.; Chakrabarti, P. Pi-Turns: Types, Systematics and the Context of Their Occurrence in Protein Structures. *BMC Struct. Biol.* **2008**, *8*, 1–14. https://doi.org/10.1186/1472-6807-8-39.

(43) Rajashankar, K. R.; Ramakumar, S. π-Turns in Proteins and Peptides: Classification, Conformation, Occurrence, Hydration and Sequence. *Protein Sci.* **1996**, *5*, 932–946. https://doi.org/10.1002/pro.5560050515.

(44) Guruprasad, K.; Prasad, M. S.; Kumar, G. R. Analysis of Γβ, Bγ, Γγ, Bβ Multiple Turns in Proteins. *J. Pept. Res.* **2000**, *56*, 250–263. https://doi.org/10.1034/j.1399-3011.2000.00739.x.

(45) Guruprasad, K.; Prasad, M. S.; Kumar, G. R. Analysis of γ,β, Bγ, Γγ Bβ Continuous Turns in Proteins. *J. Pept. Res.* **2001**, *57*, 292–300. https://doi.org/10.1046/j.1397-002X.2000.00822.x.

(46) Predki, P. F.; Agrawal, V.; Brcmger, A. T.; Regan, L. Amino-Acid Substitutions in a Surface Turn Modulate Protein Stability. *Nat. Struct. Biol.* **1996**, *3*, 54–58.

(47) Kimura, S.; Kanaya, S.; Nakamura, H. Thermostabilization of Escherichia Coli Ribonuclease

HI by Replacing Left-Handed Helical Lys95 with Gly or Asn. *J. Biol. Chem.* **1992**, *267*, 22014–22017. https://doi.org/10.1016/s0021-9258(18)41628-6.

(48) Trevino, S. R.; Schaefer, S.; Scholtz, J. M.; Pace, C. N. Increasing Protein Conformational Stability by Optimizing β-Turn Sequence. *J. Mol. Biol.* **2007**, *373*, 211–218. https://doi.org/10.1016/j.jmb.2007.07.061.

(49) Kim, M. K.; Kang, Y. K. Positional Preference of Proline in α-Helices. *Protein Sci.* **1999**, *8*, 1492–1499. https://doi.org/10.1110/ps.8.7.1492.

(50) Wang, J.; Feng, J.-A. Exploring the Sequence Patterns in the α-Helices of Proteins. *Protein Eng.* **2003**, *16*, 799–807. https://doi.org/10.1093/protein/gzg101.

(51) Barlow, D. J.; Thornton, J. M. Helix Geometry in Proteins. *J. Mol. Biol.* **1988**, *201*, 601–619. https://doi.org/10.1016/0022-2836(88)90641-9.

(52) Sidorova, A. E.; Malyshko, E. V.; Lutsenko, A. O.; Shpigun, D. K.; Bagrova, O. E. Protein Helical Structures: Defining Handedness and Localization Features. *Symmetry (Basel).* **2021**, *13*, 1–17. https://doi.org/10.3390/sym13050879.

(53) Piela, L.; Nemethy, G.; Harold, A. Proline-Induced Constraints in a-Helices. *Biopolymers* **1987**, *26*, 1587–1600.

(54) Kumeta, M.; Konishi, H. A.; Zhang, W.; Sakagami, S.; Yoshimura, S. H. Prolines in the α-Helix Confer the Structural Flexibility and Functional Integrity of Importin-β. *J. Cell Sci.* **2018**, *131*, 1–11. https://doi.org/10.1242/jcs.206326.

(55) Fu, J.; Su, J.; Wang, P.; Yu, Y.; Wang, Q.; Cavaco-Paulo, A. Enzymatic Processing of Protein-Based Fibers. *Appl. Microbiol. Biotechnol.* **2015**, *99*, 10387–10397. https://doi.org/10.1007/s00253-015-6970-x.

(56) Lupas, A. N.; Bassler, J.; Dunin-Horkawicz, S. The Structure and Topology of α-Helical Coiled Coils. In *Fibrous Proteins: Structures and Mechanisms*; Parry, D. A. D., Squire, J. M., Eds.; Springer, 2017; pp 95–130.

(57) Yaron, A. The Role of Proline in the Proteolytic Regulation of Biologically Active Peptides.

Biopolymers **1987**, *26*, S215–S222. https://doi.org/10.1002/bip.360260019.

(58) Mentlein, R. Proline Residues in the Maturation and Degradation of Peptide Hormones and Neuropeptides. *FEBS Lett.* **1988**, *234*, 251–256. https://doi.org/10.1016/0014-5793(88)80092-9.

(59) Chen, L.; Kashina, A. Post-Translational Modifications of the Protein Termini. *Front. Cell Dev. Biol.* **2021**, *9*, 1–14. https://doi.org/10.3389/fcell.2021.719590.

(60) Cunningham, D. F.; O'Connor, B. Proline Specific Peptidases. *Biochim. Biophys. Acta* **1997**, *1343*, 160–186. https://doi.org/10.1016/S0167-4838(97)00134-9.

(61) van Leeuwen, H. C.; Roelofs, D.; Corver, J.; Hensbergen, P. Phylogenetic Analysis of the Bacterial Pro-Pro-Endopeptidase Domain Reveals a Diverse Family Including Secreted and Membrane Anchored Proteins. *Curr. Res. Microb. Sci.* **2021**, *2* (January), 100024. https://doi.org/10.1016/j.crmicr.2021.100024.

(62) Dunaevsky, Y. E.; Tereshchenkova, V. F.; Oppert, B.; Belozersky, M. A.; Filippova, I. Y.; Elpidina, E. N. Human Proline Specific Peptidases: A Comprehensive Analysis. *Biochim. Biophys. Acta - Gen. Subj.* **2020**, *1864*, 1–18. https://doi.org/10.1016/j.bbagen.2020.129636.

(63) Gass, J.; Khosla, C. Prolyl Endopeptidases. *Cell. Mol. Life Sci.* **2007**, *64*, 345–355. https://doi.org/10.1007/s00018-006-6317-y.

(64) Wright, C. J.; Smith, C. W. J.; Jiggins, C. D. Alternative Splicing as a Source of Phenotypic Diversity. *Nat. Rev. Genet.* **2022**, 1–14. https://doi.org/10.1038/s41576-022-00514-4.

(65) Waumans, Y.; Baerts, L.; Kehoe, K.; Lambeir, A.-M.; De Meester, I. The Dipeptidyl Peptidase Family, Prolyl Oligopeptidase and Prolyl Carboxypeptidase in the Immune System and Inflammatory Disease, Including Atherosclerosis. *Front. Immunol.* **2015**, *6*, 1–18. https://doi.org/10.3389/fimmu.2015.00387.

(66) MacDonald, P. E.; El-kholy, W.; Riedel, M. J.; Salapatek, A. M. F.; Light, P. E.; Wheeler, M. B. The Multiple Actions of GLP-1 on the Process of Glucose-Stimulated Insulin Secretion.

Diabetes **2002**, *51*, S434–S442. https://doi.org/10.2337/diabetes.51.2007.s434.

(67) Holst, J. J.; Rosenkilde, M. M. GIP as a Therapeutic Target in Diabetes and Obesity: Insight from Incretin Co-Agonists. *J. Clin. Endocrinol. Metab.* **2020**, *105*, e2710–e2716. https://doi.org/10.1210/clinem/dgaa327.

(68) Frerker, N.; Wagner, L.; Wolf, R.; Heiser, U.; Hoffmann, T.; Rahfeld, J. U.; Schade, J.; Karl, T.; Naim, H. Y.; Alfalah, M.; Demuth, H. U.; von Hörsten, S. Neuropeptide Y (NPY) Cleaving Enzymes: Structural and Functional Homologues of Dipeptidyl Peptidase 4. *Peptides* **2007**, *28*, 257–268. https://doi.org/10.1016/j.peptides.2006.09.027.

(69) Duarte-Neves, J.; Pereira de Almeida, L.; Cavadas, C. Neuropeptide Y (NPY) as a Therapeutic Target for Neurodegenerative Diseases. *Neurobiol. Dis.* **2016**, *95*, 210–224. https://doi.org/10.1016/j.nbd.2016.07.022.

(70) Christopherson, K. W.; Hangoc, G.; Broxmeyer, H. E. Cell Surface Peptidase CD26/Dipeptidylpeptidase IV Regulates CXCL12/Stromal Cell-Derived Factor-1α-Mediated Chemotaxis of Human Cord Blood CD34 + Progenitor Cells. *J. Immunol.* **2002**, *169*, 7000–7008. https://doi.org/10.4049/jimmunol.169.12.7000.

(71) Takashima, S.; Fujita, H.; Fujishima, H.; Shimizu, T.; Sato, T.; Morii, T.; Tsukiyama, K.; Narita, T.; Takahashi, T.; Drucker, D. J.; Seino, Y.; Yamada, Y. Stromal Cell–Derived Factor-1 Is Upregulated by Dipeptidyl Peptidase-4 Inhibition and Has Protective Roles in Progressive Diabetic Nephropathy. *Kidney Int.* **2016**, *90*, 783–796. https://doi.org/10.1016/j.kint.2016.06.012.

(72) Stulc, T.; Sedo, A. Inhibition of Multifunctional Dipeptidyl Peptidase-IV: Is There a Risk of Oncological and Immunological Adverse Effects? *Diabetes Res. Clin. Pract.* **2010**, *88*, 125–131. https://doi.org/10.1016/j.diabres.2010.02.017.

(73) Yu, D. M. T.; Yao, T.-W.; Chowdhury, S.; Nadvi, N. A.; Osborne, B.; Church, W. B.; McCaughan, G. W.; Gorrell, M. D. The Dipeptidyl Peptidase IV Family in Cancer and Cell Biology. *FEBS J.* **2010**, *277*, 1126–1144. https://doi.org/10.1111/j.1742-4658.2009.07526.x.

(74) Bušek, P.; Malík, R.; Šedo, A. Dipeptidyl Peptidase IV Activity and/or Structure Homologues (DASH) and Their Substrates in Cancer. *Int. J. Biochem. Cell Biol.* **2004**, *36*, 408–421. https://doi.org/10.1016/S1357-2725(03)00262-0.

(75) Lee, K. N.; Jackson, K. W.; Christiansen, V. J.; Lee, C. S.; Chun, J. G.; McKee, P. A. Antiplasmin-Cleaving Enzyme Is a Soluble Form of Fibroblast Activation Protein. *Blood* **2006**, *107*, 1397–1404. https://doi.org/10.1182/blood-2005-08-3452.

(76) Singh, S.; Saleem, S.; Reed, G. L. Alpha2-Antiplasmin: The Devil You Don't Know in Cerebrovascular and Cardiovascular Disease. *Front. Cardiovasc. Med.* **2020**, *7*, 1–10. https://doi.org/10.3389/fcvm.2020.608899.

(77) Kotačková, L.; Balážiová, E.; Šedo, A. Expression Pattern of Dipeptidyl Peptidase IV Activity and/or Structure Homologues in Cancer. *Folia Biol. (Praha).* **2009**, *55*, 77–84.

(78) Odya, C. E.; Marinkovic, D. V.; Hammon, K. J.; Stewart, T. A.; Erdös, E. G. Purification and Properties of Prolylcarboxypeptidase (Angiotensinase C) from Human Kidney. *J. Biol. Chem.* **1978**, *253*, 5927–5931. https://doi.org/10.1016/s0021-9258(17)34557-x.

(79) Jeong, J. K.; Diano, S. Prolyl Carboxypeptidase and Its Inhibitors in Metabolism. *Trends Endocrinol. Metab.* **2013**, *24*, 61–67. https://doi.org/10.1016/j.tem.2012.11.001.

(80) De Hert, E.; Bracke, A.; Pintelon, I.; Janssens, E.; Lambeir, A. M.; Van der Veken, P.; De Meester, I. Prolyl Carboxypeptidase Mediates the C-Terminal Cleavage of (Pyr)-Apelin-13 in Human Umbilical Vein and Aortic Endothelial Cells. *Int. J. Mol. Sci.* **2021**, *22*, 1–18. https://doi.org/10.1016/j.bcp.2021.114738.

(81) Adams, G. N.; Stavrou, E. X.; Fang, C.; Merkulova, A.; Alaiti, M. A.; Nakajima, K.; Morooka, T.; Merkulov, S.; LaRusch, G. A.; Simon, D. I.; Jain, M. K.; Schmaier, A. H. Prolylcarboxypeptidase Promotes Angiogenesis and Vascular Repair. *Blood* **2013**, *122*, 1522–1531. https://doi.org/10.1182/blood-2012-10-460360.

(82) Maes, M. B.; Scharpé, S.; De Meester, I. Dipeptidyl Peptidase II (DPPII), a Review. *Clin. Chim. Acta* **2007**, *380*, 31–49. https://doi.org/10.1016/j.cca.2007.01.024.

(83) Di Daniel, E.; Glover, C. P.; Grot, E.; Chan, M. K.; Sanderson, T. H.; White, J. H.; Ellis, C. L.; Gallagher, K. T.; Uney, J.; Thomas, J.; Maycox, P. R.; Mudge, A. W. Prolyl Oligopeptidase Binds to GAP-43 and Functions without Its Peptidase Activity. *Mol. Cell. Neurosci.* **2009**, *41*, 373–382. https://doi.org/10.1016/j.mcn.2009.03.003.

(84) Männistö, P. T.; García-Horsman, J. A. Mechanism of Action of Prolyl Oligopeptidase (PREP) in Degenerative Brain Diseases: Has Peptidase Activity Only a Modulatory Role on the Interactions of PREP with Proteins? *Front. Aging Neurosci.* **2017**, *9*, 1–10. https://doi.org/10.3389/fnagi.2017.00027.

(85) Matsuda, T.; Sakaguchi, M.; Tanaka, S.; Yoshimoto, T.; Takaoka, M. Prolyl Oligopeptidase Is a Glyceraldehyde-3-Phosphate Dehydrogenase-Binding Protein That Regulates Genotoxic Stress-Induced Cell Death. *Int. J. Biochem. Cell Biol.* **2013**, *45*, 850–857. https://doi.org/10.1016/j.biocel.2013.01.009.

(86) Myöhänen, T. T.; Hannula, M. J.; Van Elzen, R.; Gerard, M.; Van Der Veken, P.; García-Horsman, J. A.; Baekelandt, V.; Männistö, P. T.; Lambeir, A. M. A Prolyl Oligopeptidase Inhibitor, KYP-2047, Reduces α-Synuclein Protein Levels and Aggregates in Cellular and Animal Models of Parkinson's Disease. *Br. J. Pharmacol.* **2012**, *166*, 1097–1113. https://doi.org/10.1111/j.1476-5381.2012.01846.x.

(87) Cafardi, V.; Biagini, M.; Martinelli, M.; Leuzzi, R.; Rubino, J. T.; Cantini, F.; Norais, N.; Scarselli, M.; Serruto, D.; Unnikrishnan, M. Identification of a Novel Zinc Metalloprotease through a Global Analysis of Clostridium Difficile Extracellular Proteins. *PLoS One* **2013**, *8*, 1–14. https://doi.org/10.1371/journal.pone.0081306.

(88) Hensbergen, P. J.; Klychnikov, O. I.; Bakker, D.; Van Winden, V. J. C.; Ras, N.; Kemp, A. C.; Cordfunke, R. A.; Dragan, I.; Deelder, A. M.; Kuijper, E. J.; Corver, J.; Drijfhout, J. W.; Van Leeuwen, H. C. A Novel Secreted Metalloprotease (CD2830) from Clostridium Difficile Cleaves Specific Proline Sequences in LPXTG Cell Surface Proteins. *Mol. Cell. Proteomics* **2014**, *13*, 1231–1244. https://doi.org/10.1074/mcp.M113.034728.

(89) Arato, V.; Gasperini, G.; Giusti, F.; Ferlenghi, I.; Scarselli, M.; Leuzzi, R. Dual Role of the

Colonization Factor CD2831 in Clostridium Difficile Pathogenesis. *Sci. Rep.* **2019**, *9*, 1–12. https://doi.org/10.1038/s41598-019-42000-8.

(90) Dawson, L. F.; Peltier, J.; Hall, C. L.; Harrison, M. A.; Derakhshan, M.; Shaw, H. A.; Fairweather, N. F.; Wren, B. W. Extracellular DNA, Cell Surface Proteins and c-Di-GMP Promote Biofilm Formation in Clostridioides Difficile. *Sci. Rep.* **2021**, *11*, 1–21. https://doi.org/10.1038/s41598-020-78437-5.

(91) Klychnikov, O. I.; Shamorkina, T. M.; Weeks, S. D.; van Leeuwen, H. C.; Corver, J.; Drijfhout, J. W.; van Veelen, P. A.; Sluchanko, N. N.; Strelkov, S. V.; Hensbergen, P. J. Discovery of a New Pro-Pro Endopeptidase, PPEP-2, Provides Mechanistic Insights into the Differences in Substrate Specificity within the PPEP Family. *J. Biol. Chem.* **2018**, *293*, 11154–11165. https://doi.org/10.1074/jbc.RA118.003244.

(92) Narwani, T. J.; Santuz, H.; Shinada, N.; Melarkode Vattekatte, A.; Ghouzam, Y.; Srinivasan, N.; Gelly, J.-C.; de Brevern, A. G. Recent Advances on Polyproline II. *Amino Acids* **2017**, *49*, 705–713. https://doi.org/10.1007/s00726-017-2385-6.

(93) Wilhelm, P.; Lewandowski, B.; Trapp, N.; Wennemers, H. A Crystal Structure of an Oligoproline PPII-Helix, at Last. *J. Am. Chem. Soc.* **2014**, *136*, 15829–15832. https://doi.org/10.1021/ja507405j.

(94) Mansiaux, Y.; Joseph, A. P.; Gelly, J.-C.; de Brevern, A. G. Assignment of Polyproline II Conformation and Analysis of Sequence - Structure Relationship. *PLoS One* **2011**, *6*, 1–15. https://doi.org/10.1371/journal.pone.0018401.

(95) Darnell, G.; Orgel, J. P. R. O.; Pahl, R.; Meredith, S. C. Flanking Polyproline Sequences Inhibit β-Sheet Structure in Polyglutamine Segments by Inducing PPII-like Helix Structure. *J. Mol. Biol.* **2007**, *374*, 688–704. https://doi.org/10.1016/j.jmb.2007.09.023.

(96) Adzhubei, A. A.; Sternberg, M. J. E.; Makarov, A. A. Polyproline-II Helix in Proteins: Structure and Function. *J. Mol. Biol.* **2013**, *425*, 2100–2132. https://doi.org/10.1016/j.jmb.2013.03.018.

(97) Berisio, R.; Vitagliano, L. Polyproline and Triple Helix Motifs in Host-Pathogen Recognition.

Curr. Protein Pept. Sci. **2012**, *13*, 855–865. https://doi.org/10.2174/138920312804871157.

(98) Okuyama, K. Revisiting the Molecular Structure of Collagen. *Connect. Tissue Res.* **2008**, *49*, 299–310. https://doi.org/10.1080/03008200802325110.

(99) Shoulders, M. D.; Raines, R. T. Collagen Structure and Stability. *Annu. Rev. Biochem.* **2009**, *78*, 929–958. https://doi.org/10.1146/annurev.biochem.77.032207.120833.

(100) Bella, J. A New Method for Describing the Helical Conformation of Collagen: Dependence of the Triple Helical Twist on Amino Acid Sequence. *J. Struct. Biol.* **2010**, *170*, 377–391. https://doi.org/10.1016/j.jsb.2010.02.003.

(101) Bochicchio, B.; Tamburro, A. M. Polyproline II Structure in Proteins: Identification by Chiroptical Spectroscopies, Stability, and Functions. *Chirality* **2002**, *14*, 782–792. https://doi.org/10.1002/chir.10153.

(102) Gordon, M. K.; Hahn, R. A. Collagens. *Cell Tissue Res.* **2010**, *339*, 247–257. https://doi.org/10.1007/s00441-009-0844-4.

(103) Leitinger, B.; Hohenester, E. Mammalian Collagen Receptors. *Matrix Biol.* **2007**, *26*, 146–155. https://doi.org/10.1016/j.matbio.2006.10.007.

(104) Songyang, Z.; Shoelson, S. E.; Chaudhuri, M.; Gish, G.; Pawson, T.; Haser, W. G.; King, F.; Roberts, T.; Ratnofsky, S.; Lechleider, R. J.; Neel, B. G.; Birge, R. B.; Fajardo, J. E.; Chou, M. M.; Hanafusa, H.; Schaffhausen, B.; Cantley, L. C. SH2 Domains Recognize Specific Phosphopeptide Sequences. *Cell* **1993**, *72*, 767–778. https://doi.org/10.1016/0092-8674(93)90404-E.

(105) Yaffe, M. B.; Cantley, L. C. Grabbing Phosphoproteins. *Nature* **1999**, *402*, 30–31. https://doi.org/10.1038/46925.

(106) Yu, H.; Chen, J. K.; Feng, S.; Dalgarno, D. C.; Brauer, A. W.; Schrelber, S. L. Structural Basis for the Binding of Proline-Rich Peptides to SH3 Domains. *Cell* **1994**, *76*, 933–945. https://doi.org/10.1016/0092-8674(94)90367-0.

(107) Musacchio, A.; Saraste, M.; Wilmanns, M. High-Resolution Crystal Structures of Tyrosine

Kinase SH3 Domains Complexed with Proline-Rich Peptides. *Struct. Biol.* **1994**, *1*, 546–551.

(108) Lim, W. A.; Richards, F. M.; Fox, R. O. Structural Determinants of Peptide-Binding Orientation and of Sequence Specificity in SH3 Domains. *Nature* **1994**, *372*, 375–379.

(109) Chen, H. I.; Sudol, M. The WW Domain of Yes-Associated Protein Binds a Proline-Rich Ligand That Differs from the Consensus Established for Src Homology 3-Binding Modules. *Proc. Natl. Acad. Sci. U. S. A.* **1995**, *92*, 7819–7823. https://doi.org/10.1073/pnas.92.17.7819.

(110) Kofler, M.; Schuemann, M.; Merz, C.; Kosslick, D.; Schlundt, A.; Tannert, A.; Schaefer, M.; Lührmann, R.; Krause, E.; Freund, C. Proline-Rich Sequence Recognition: I. Marking GYF and WW Domain Assembly Sites in Early Spliceosomal Complexes. *Mol. Cell. Proteomics* **2009**, *8*, 2461–2473. https://doi.org/10.1074/mcp.M900191-MCP200.

(111) Reinhard, M.; Rüdiger, M.; Jockusch, B. M.; Walter, U. VASP Interaction with Vinculin: A Recurring Theme of Interactions with Proline-Rich Motifs. *FEBS Lett.* **1996**, *399*, 103–107. https://doi.org/10.1016/S0014-5793(96)01295-1.

(112) Freund, C.; Dotsch, V.; Nishizawa, K.; Reinherz, E. L.; Wagner, G. The GYF Domain Is a Novel Structural Fold That Is Involved in Lymphoid Signaling through Proline-Rich Sequences. *Nat. Struct. Biol.* **1999**, *6*, 656–660. https://doi.org/10.1038/10712.

(113) Pornillos, O.; Alam, S. L.; Davis, D. R.; Sundquist, W. I. Structure of the Tsg101 Uev Domain in Complex with the Ptap Motif of the Hiv-1 P6 Protein. *Nat. Struct. Biol.* **2002**, *9*, 812–817. https://doi.org/10.1038/nsb856.

(114) Pornillos, O.; Alam, S. L.; Rich, R. L.; Myszka, D. G.; Davis, D. R.; Sundquist, W. I. Structure and Functional Interactions of the Tsg101 UEV Domain. *EMBO J.* **2002**, *21*, 2397–2406. https://doi.org/10.1093/emboj/21.10.2397.

(115) Mahoney, N. M.; Janmey, P. A.; Almo, S. C. Structure of the Profilin-Poly-L-Proline Complex Involved in Morphogenesis and Cytoskeletal Regulation. *Nat. Struct. Biol.* **1997**, *4*, 953–960.

(116) Rush, T.; Roth, J. R.; Thompson, S. J.; Aldaher, A. R.; Cochran, J. N.; Roberson, E. D. A Peptide

Inhibitor of Tau-SH3 Interactions Ameliorates Amyloid-β Toxicity. *Neurobiol. Dis.* **2020**, *134*, 1–9. https://doi.org/10.1016/j.nbd.2019.104668.

(117) Tai, C.; Chang, C.-W.; Yu, G.-Q.; Lopez, I.; Yu, X.; Wang, X.; Guo, W.; Mucke, L. Tau Reduction Prevents Key Features of Autism in Mouse Models. *Neuron* **2020**, *106*, 1–17. https://doi.org/10.1016/j.neuron.2020.01.038.

(118) Srinivasan, M.; Dunker, A. K. Proline Rich Motifs as Drug Targets in Immune Mediated Disorders. *Int. J. Pept.* **2012**, 1–14. https://doi.org/10.1155/2012/634769.

(119) Diebold, B. A.; Smith, S. M. E.; Li, Y.; Lambeth, J. D. NOX2 as a Target for Drug Development: Indications, Possible Complications, and Progress. *Antioxidants Redox Signal.* **2015**, *23*, 375–405. https://doi.org/10.1089/ars.2014.5862.

(120) Sánchez-Garrido, M. A.; Habegger, K. M.; Clemmensen, C.; Holleman, C.; Müller, T. D.; Perez-Tilve, D.; Li, P.; Agrawal, A. S.; Finan, B.; Drucker, D. J.; Tschöp, M. H.; DiMarchi, R. D.; Kharitonenkov, A. Fibroblast Activation Protein (FAP) as a Novel Metabolic Target. *Mol. Metab.* **2016**, *5*, 1015–1024. https://doi.org/10.1016/j.molmet.2016.07.003.

(121) Sanchez-Vega, F.; Mina, M.; Armenia, J.; Chatila, W. K.; Luna, A.; La, K. C.; Dimitriadoy, S.; Liu, D. L.; Kantheti, H. S.; Saghafinia, S.; Chakravarty, D.; Daian, F.; Gao, Q.; Bailey, M. H.; Liang, W. W.; Foltz, S. M.; Shmulevich, I.; Ding, L.; Heins, Z.; Ochoa, A.; Gross, B.; Gao, J.; Zhang, H.; Kundra, R.; Kandoth, C.; Bahceci, I.; Dervishi, L.; Dogrusoz, U.; Zhou, W.; Shen, H.; Laird, P. W.; Way, G. P.; Greene, C. S.; Liang, H.; Xiao, Y.; Wang, C.; Iavarone, A.; Berger, A. H.; Bivona, T. G.; Lazar, A. J.; Hammer, G. D.; Giordano, T.; Kwong, L. N.; McArthur, G.; Huang, C.; Tward, A. D.; Frederick, M. J.; McCormick, F.; Meyerson, M.; Van Allen, E. M.; Cherniack, A. D.; Ciriello, G.; Sander, C.; Schultz, N. Oncogenic Signaling Pathways in The Cancer Genome Atlas. *Cell* **2018**, *173*, 321–337. https://doi.org/10.1016/j.cell.2018.03.035.

(122) Lu, Z.; Hunter, T. Prolyl Isomerase Pin1 in Cancer. *Cell Res.* **2014**, *24*, 1033–1049. https://doi.org/10.1038/cr.2014.109.

(123) Lu, K. P.; Zhou, X. Z. The Prolyl Isomerase PIN1: A Pivotal New Twist in Phosphorylation

Signalling and Disease. *Nat. Rev. Mol. Cell Biol.* **2007**, *8*, 904–916. https://doi.org/10.1038/nrm2261.

(124) Zarrinpar, A.; Bhattacharyya, R. P.; Lim, W. A. The Structure and Function of Proline Recognition Domains. *Sci. STKE* **2003**, *179*, 1–10. https://doi.org/10.1126/stke.2003.179.re8.

(125) Rastogi, R.; Geng, X.; Li, F.; Ding, Y. NOX Activation by Subunit Interaction and Underlying Mechanisms in Disease. *Front. Cell. Neurosci.* **2017**, *10*, 1–13. https://doi.org/10.3389/fncel.2016.00301.

(126) Bean, J. W.; Kopple, K. D.; Peishoff, C. E. Conformational Analysis of Cyclic Hexapeptides Containing the D-Pro-L-Pro Sequence To Fix β-Turn Positions. *J. Am. Chem. Soc.* **1992**, *114*, 5328–5334. https://doi.org/10.1021/ja00039a050.

(127) Späth, J.; Stuart, F.; Jiang, L.; Robinson, J. A. Stabilization of a β-Hairpin Conformation in a Cyclic Peptide Using the Templating Effect of a Heterochiral Diproline Unit. *Helv. Chim. Acta* **1998**, *81*, 1726–1738. https://doi.org/10.1002/(SICI)1522-2675(19980909)81:9<1726::AID-HLCA1726>3.0.CO;2-H.

(128) Chalmers, D. K.; Marshall, G. R. Pro-D-NMe-Amino Acid and D-Pro-NMe-Amino Acid : Simple , Efficient Reverse-Turn Constraints. *J. Am. Chem. Soc.* **1995**, *117*, 5927–5937.

(129) Favre, M.; Moehle, K.; Jiang, L.; Pfeiffer, B.; Robinson, J. A. Structural Mimicry of Canonical Conformations in Antibody Hypervariable Loops Using Cyclic Peptides Containing a Heterochiral Diproline Template. *J. Am. Chem. Soc.* **1999**, *121*, 2679–2685. https://doi.org/10.1021/ja984016p.

(130) McElroy, A. B.; Clegg, S. P.; Deal, M. J.; Ewan, G. B.; Hagan, R. M.; Ireland, S. J.; Jordan, C. C.; Porter, B.; Rose, B. C.; Ward, P.; Whittington, A. R. Highly Potent and Selective Heptapeptide Antagonists of the Neurokinin NK-2 Receptor. *J. Med. Chem.* **1992**, *35*, 2582–2591. https://doi.org/10.1021/jm00092a008.

(131) Gadais, C.; Van holsbeeck, K.; Moors, S. L. C.; Buyst, D.; Fehér, K.; Van Hecke, K.; Tourwé, D.; Brigaud, T.; Martin, C.; De Proft, F.; Pytkowicz, J.; Martins, J. C.; Chaume, G.; Ballet, S.

Trifluoromethylated Proline Surrogates as Part of “Pro–Pro” Turn-Inducing Templates. *ChemBioChem* **2019**, *20*, 2513–2518. https://doi.org/10.1002/cbic.201900294.

(132) Baures, P. W.; Ojala, W. H.; Gleason, W. B.; Johnson, R. L. Conformational Analysis of Homochiral and Heterochiral Diprolines as β-Turn-Forming Peptidomimetics: Unsubstituted and Substituted Models. *J. Pept. Res.* **1997**, *50*, 1–13. https://doi.org/10.1111/j.1399-3011.1997.tb00614.x.

(133) Koivisto, J. J.; Kumpulainen, E. T. T.; Koskinen, A. M. P. Conformational Ensembles of Flexible β-Turn Mimetics in DMSO-D6. *Org. Biomol. Chem.* **2010**, *8*, 2103–2116. https://doi.org/10.1039/b921794k.

(134) Venkatachalapathi, Y. V.; Balaram, P. An Incipient 3(10) Helix in Piv-Pro-Pro-Ala-NHMe as a Model for Peptide Folding. *Nature* **1979**, *281*, 83–84.

(135) Kemp, D. S.; Boyd, J. G.; Muendel, C. C. The Helical s Constant for Alanine in Water Derived from Template-Nucleated Helices. *Nature* **1991**, *352*, 451–454. https://doi.org/10.1038/255242a0.

(136) Rai, R.; Aravinda, S.; Kanagarajadurai, K.; Raghothama, S.; Shamala, N.; Balaram, P. Diproline Templates as Folding Nuclei in Designed Peptides. Conformational Analysis of Synthetic Peptide Helices Containing Amino Terminal Pro-Pro Segments. *J. Am. Chem. Soc.* **2006**, *128*, 7916–7928. https://doi.org/10.1021/ja060674v.

(137) Hanessian, S.; Papeo, G.; Fettis, K.; Therrien, E.; Viet, M. T. P. Synthesis of 310-Helix-Inducing Constrained Analogues of L-Proline. *J. Org. Chem.* **2004**, *69*, 4891–4899.

(138) Austin, R. E.; Maplestone, R. A.; Sefler, A. M.; Liu, K.; Hruzewicz, W. N.; Liu, C. W.; Cho, H. S.; Wemmer, D. E.; Bartlett, P. A. A Template for Stabilization of a Peptide α-Helix: Synthesis and Evaluation of Conformational Effects by Circular Dichroism and NMR. *J. Am. Chem. Soc.* **1997**, *119*, 6461–6472. https://doi.org/10.1021/ja964231a.

(139) Hack, V.; Reuter, C.; Opitz, R.; Schmieder, P.; Beyermann, M.; Neudörfl, J.-M.; Kühne, R.; Schmalz, H.-G. Efficient α-Helix Induction in a Linear Peptide Chain by n-Capping with a Bridged-Tricyclic Diproline Analogue. *Angew. Chemie - Int. Ed.* **2013**, *52*, 9539–9543.

https://doi.org/10.1002/anie.201302014.

(140) Horng, J.-C.; Raines, R. T. Stereoelectronic Effects on Polyproline Conformation. *Protein Sci.* **2006**, *15*, 74–83. https://doi.org/10.1110/ps.051779806.

(141) Kümin, M.; Sonntag, L. S.; Wennemers, H. Azidoproline Containing Helices: Stabilization of the Polyproline II Structure by a Functionalizable Group. *J. Am. Chem. Soc.* **2007**, *129*, 466–467. https://doi.org/10.1021/ja067148o.

(142) Berger, G.; Vilchis-Reyes, M.; Hanessian, S. Structural Properties and Stereochemically Distinct Folding Preferences of 4,5-Cis and Trans-Methano-L-Proline Oligomers: The Shortest Crystalline PPII-Type Helical Proline-Derived Tetramer. *Angew. Chemie - Int. Ed.* **2015**, *54*, 13268–13272. https://doi.org/10.1002/anie.201506208.

(143) Cushman, D. W.; Ondetti, M. A. History of the Design of Captopril and Related Inhibitors of Angiotensin Converting Enzyme. *Hypertension* **1991**, *17*, 589–592. https://doi.org/10.1161/01.HYP.17.4.589.

(144) Zhao, Y.; Xu, C. Structure and Function of Angiotensin Converting Enzyme and Its Inhibitors. *Chin. J. Biotechnol.* **2008**, *24*, 171–176. https://doi.org/10.1016/s1872-2075(08)60007-2.

(145) Cushman, D. W.; Cheung, H. S.; Sabo, E. F.; Ondetti, M. A. Design of Potent Competitive Inhibitors of Angiotensin-Converting Enzyme. Carboxyalkanoyl and Mercaptoalkanoyl Amino Acids. *Biochemistry* **1977**, *16*, 5484–5941.

(146) Cushman, D. W.; Ondetti, M. A. Design of Angiotensin Converting Enzyme Inhibitors. *Nat. Med.* **1999**, *5*, 1110–1112. https://doi.org/10.1038/13423.

(147) Vilchis-Reyes, M. A.; Hanessian, S. Proline Methanologues: Design, Synthesis, Structural Properties, and Applications in Medicinal Chemistry. In *Top Heterocycl Chem*; Lubell, W. D., Ed.; Springer International Publishing Switzerland 2015, 2017; Vol. 48, pp 51–96. https://doi.org/10.1007/7081_2015_191.

(148) Natesh, R.; Schwager, S. L. U.; Evans, H. R.; Sturrock, E. D.; Acharya, K. R. Structural Details on the Binding of Antihypertensive Drugs Captopril and Enalaprilat to Human Testicular

Angiotensin I-Converting Enzyme. *Biochemistry* **2004**, *43*, 8718–8724. https://doi.org/10.1021/bi049480n.

(149) Arora, P. K.; Chauhan, A. Ace Inhibitors: A Comprehensive Review. *Int. J. Pharm. Sci. Res.* **2013**, *4*, 532–549.

(150) Sica, D. A.; Gehr, T. W. B.; Kelleher, N.; Blumenthal, M. Fosinopril: Emerging Considerations and Implications for Angiotensin-Converting Enzyme Inhibitor Therapy. *Cardiovasc. Drug Rev.* **1998**, *16*, 319–345. https://doi.org/10.1111/j.1527-3466.1998.tb00362.x.

(151) Hanessian, S.; Reinhold, U.; Saulnier, M.; Claridge, S. Probing the Importance of Spacial and Conformational Domains in Captopril Analogs for Angiotensin Converting Enzyme Activity. *Bioorganic Med. Chem. Lett.* **1998**, *8*, 2123–2128. https://doi.org/10.1016/S0960-894X(98)00377-1.

(152) Magnin, D. R.; Robl, J. A.; Sulsky, R. B.; Augeri, D. J.; Huang, Y.; Simpkins, L. M.; Taunk, P. C.; Betebenner, D. A.; Robertson, J. G.; Abboa-Offei, B. E.; Wang, A.; Cap, M.; Xin, L.; Tao, L.; Sitkoff, D. F.; Malley, M. F.; Gougoutas, J. Z.; Khanna, A.; Huang, Q.; Han, S.-P.; Parker, R. A.; Hamann, L. G. Synthesis of Novel Potent Dipeptidyl Peptidase IV Inhibitors with Enhanced Chemical Stability: Interplay between the N-Terminal Amino Acid Alkyl Side Chain and the Cyclopropyl Group of α -Aminoacyl-L-Cis-4,5-Methanoprolinenitrile-Based Inhibitors. *J. Med. Chem.* **2004**, *47*, 2587–2598. https://doi.org/10.1021/jm049924d.

(153) Augeri, D. J.; Robl, J. A.; Betebenner, D. A.; Magnin, D. R.; Khanna, A.; Robertson, J. G.; Wang, A.; Simpkins, L. M.; Taunk, P.; Huang, Q.; Han, S.-P.; Abboa-Offei, B.; Cap, M.; Xin, L.; Tao, L.; Tozzo, E.; Welzel, G. E.; Egan, D. M.; Marcinkeviciene, J.; Chang, S. Y.; Biller, S. A.; Kirby, M. S.; Parker, R. A.; Hamann, L. G. Discovery and Preclinical Profile of Saxagliptin (BMS-477118): A Highly Potent, Long-Acting, Orally Active Dipeptidyl Peptidase IV Inhibitor for the Treatment of Type 2 Diabetes. *J. Med. Chem.* **2005**, *48*, 5025–5037. https://doi.org/10.1021/jm050261p.

(154) Hanessian, S.; Balaux, E.; Musil, D.; Olsson, L.-L.; Nilsson, I. Exploring the Chiral Space within the Active Site of α-Thrombin with a Constrained Mimic of D-Phe-Pro-Arg - Design,

Synthesis, Inhibitory Activity, and X-Ray Structure of an Enzyme-Inhibitor Complex. *Bioorganic Med. Chem. Lett.* **2000**, *10*, 243–247. https://doi.org/10.1016/S0960-894X(99)00669-1.

(155) Negrier, C.; Shima, M.; Hoffman, M. The Central Role of Thrombin in Bleeding Disorders. *Blood Rev.* **2019**, *38*, 1–8. https://doi.org/10.1016/j.blre.2019.05.006.

(156) Al-Amer, O. M. The Role of Thrombin in Haemostasis. *Blood Coagul. Fibrinolysis* **2022**, *33*, 145–148. https://doi.org/10.1097/MBC.0000000000001130.

(157) Hanessian, S.; Therrien, E.; Granberg, K.; Nilsson, I. Targeting Thrombin and Factor VIIa: Design, Synthesis, and Inhibitory Activity of Functionally Relevant Indolizidinones. *Bioorganic Med. Chem. Lett.* **2002**, *12*, 2907–2911. https://doi.org/10.1016/S0960-894X(02)00612-1.

(158) Nöteberg, D.; Brånalt, J.; Kvarnström, I.; Linschoten, M.; Musil, D.; Nyström, J.-E.; Zuccarello, G.; Samuelsson, B. New Proline Mimetics: Synthesis of Thrombin Inhibitors Incorporating Cyclopentane- and Cyclopentenedicarboxylic Acid Templates in the P2 Position. Binding Conformation Investigated by X-Ray Crystallography. *J. Med. Chem.* **2000**, *43*, 1705–1713. https://doi.org/10.1021/jm990557t.

(159) Wang, X. J.; Xu, B.; Mullins, A. B.; Neiler, F. K.; Etzkorn, F. A. Conformationally Locked Isostere of PhosphoSer-Cis-Pro Inhibits Pin1 23-Fold Better than PhosphoSer-Trans-Pro Isostere. *J. Am. Chem. Soc.* **2004**, *126*, 15533–15542. https://doi.org/10.1021/ja046396m.

(160) Yaffe, M. B.; Schutkowski, M.; Shen, M.; Zhou, X. Z.; Stukenberg, P. T.; Rahfeld, J.-U.; Xu, J.; Kuang, J.; Kirschner, M. W.; Fischer, G.; Cantley, L. C.; Lu, K. P. Sequence-Specific and Phosphorylation Dependent Proline Isomerization: A Potential Mitotic Regulatory Mechanism. *Science,* **1997**, *278*, 1957–1960. Https://doi.org/10.1126/science.278.5345.1957.

(161) Wilk, S.; Orlowski, M. Inhibition of Rabbit Brain Prolyl Endopeptidase by N-Benzyloxycarbonyl-Prolyl-Prolinal, a Transition State Aldehyde Inhibitor. *J. Neurochem.* **1983**, *41*, 69–75. https://doi.org/10.1111/j.1471-4159.1983.tb11815.x.

(162) Fülöp, V.; Böcskei, Z.; Polgar, L. Prolyl Oligopeptidase: An Unusual β-Propeller Domain Regulates Proteolysis. *Cell* **1998**, *94*, 161–170. https://doi.org/10.1016/0076-6879(94)44016-6.

(163) Faraci, W. S.; Nagel, A. A.; Spencer, R. W.; Vinick, F. J. Aromatic Pyrrolidine and Thiazolidine Amide. WO91018891, 1991.

(164) Toda, M.; Ohuchida, S.; Ohno, H. Novel Prolinal Derivatives. 0268190A1, 1987.

(165) Jarho, E. M.; Venäläinen, J. I.; Huuskonen, J.; Christiaans, J. A. M.; Garcia-Horsman, J. A.; Forsberg, M. M.; Järvinen, T.; Gynther, J.; Männistö, P. T.; Wallén, E. A. A. A Cyclopent-2-Enecarbonyl Group Mimics Proline at the P2 Position of Prolyl Oligopeptidase Inhibitors. *J. Med. Chem.* **2004**, *47*, 5605–5607. https://doi.org/10.1021/jm049503w.

(166) Kánai, K.; Arányi, P.; Böcskei, Z.; Ferenczy, G.; Harmat, V.; Simon, K.; Bátori, S.; Náray-Szabó, G.; Hermecz, I. Prolyl Oligopeptidase Inhibition by N-Acyl-pro-Pyrrolidine-Type Molecules. *J. Med. Chem.* **2008**, *51*, 7514–7522. https://doi.org/10.1021/jm800944x.

(167) Mucha, A.; Drag, M.; Dalton, J. P.; Kafarski, P. Metallo-Aminopeptidase Inhibitors. *Biochimie* **2010**, *92*, 1509–1529. https://doi.org/10.1016/j.biochi.2010.04.026.

(168) Mina-Osorio, P. The Moonlighting Enzyme CD13: Old and New Functions to Target. *Trends Mol. Med.* **2008**, *14*, 361–371. https://doi.org/10.1016/j.molmed.2008.06.003.

(169) Amin, S. A.; Adhikari, N.; Jha, T. Design of Aminopeptidase N Inhibitors as Anti-Cancer Agents. *J. Med. Chem.* **2018**, *61*, 6468–6490. https://doi.org/10.1021/acs.jmedchem.7b00782.

(170) Hitzerd, S. M.; Verbrugge, S. E.; Ossenkoppele, G.; Jansen, G.; Peters, G. J. Positioning of Aminopeptidase Inhibitors in next Generation Cancer Therapy. *Amino Acids* **2014**, *46*, 793–808. https://doi.org/10.1007/s00726-013-1648-0.

(171) Barlow, N.; Thompson, P. E. IRAP Inhibitors: M1-Aminopeptidase Family Inspiration. *Front. Pharmacol.* **2020**, *11*, 1–8. https://doi.org/10.3389/fphar.2020.585930.

(172) Aoyagi, T.; Yoshida, S.; Nakamura, Y.; Shigihara, Y.; Hamada, M.; Takeuchi, T. Probestin, a

New Inhibitor of Aminopeptidase M, Produced by Strptomyces Azureus MH663-2F6. I. Taxonomy, Production, Isolation, Physico-Chemical Properties and Biological Activities. *J. Antibiot. (Tokyo).* **1990**, *43*, 143–148.

(173) Yoshida, S.; Nakamura, Y.; Naganawa, H.; Aoyagi, T.; Takeuchi, T. Probestin, a New Inhibitor of Aminopeptidase M, Produced by Streptomyces Azureus MH663-2F6. II. Structure Determination of Probestin. *J. Antibiot. (Tokyo).* **1990**, *43*, 149–153.

(174) Leung, D.; Abbenante, G.; Fairlie, D. P. Protease Inhibitors: Current Status and Future Prospects. *J. Med. Chem.* **2000**, *43*, 305–341. https://doi.org/10.1021/jm990412m.

(175) Corbi-Verge, C.; Kim, P. M. Motif Mediated Protein-Protein Interactions as Drug Targets. *Cell Commun. Signal.* **2016**, *14*, 1–12. https://doi.org/10.1186/s12964-016-0131-4.

(176) Lu, H.; Zhou, Q.; He, J.; Jiang, Z.; Peng, C.; Tong, R.; Shi, J. Recent Advances in the Development of Protein–Protein Interactions Modulators: Mechanisms and Clinical Trials. *Signal Transduct. Target. Ther.* **2020**, *5*, 1–23. https://doi.org/10.1038/s41392-020-00315-3.

(177) Infante, J. R.; Dees, E. C.; Olszanski, A. J.; Dhuria, S. V.; Sen, S.; Cameron, S.; Cohen, R. B. Phase I Dose-Escalation Study of LCL161, an Oral Inhibitor of Apoptosis Proteins Inhibitor, in Patients with Advanced Solid Tumors. *J. Clin. Oncol.* **2014**, *32*, 3103–3110. https://doi.org/10.1200/JCO.2013.52.3993.

(178) Chang, Y.-C.; Cheung, C. H. A. An Updated Review of Smac Mimetics, LCL161, Birinapant, and GDC-0152 in Cancer Treatment. *Appl. Sci.* **2021**, *11*, 1–13. https://doi.org/10.3390/app11010335.

(179) Zaminer, J.; Brockmann, C.; Huy, P.; Opitz, R.; Reuter, C.; Beyermann, M.; Freund, C.; Müller, M.; Oschkinat, H.; Kühne, R.; Schmalz, H.-G. Addressing Protein-Protein Interactions with Small Molecules: A pro-pro Dipeptide Mimic with a PPII Helix Conformation as a Module for the Synthesis of PRD-Binding Ligands. *Angew. Chemie - Int. Ed.* **2010**, *49*, 7111–7115. https://doi.org/10.1002/anie.201001739.

(180) Opitz, R.; Müller, M.; Reuter, C.; Barone, M.; Soicke, A.; Roske, Y.; Piotukh, K.; Huy, P.;

Beerbaum, M.; Wiesner, B.; Beyermann, M.; Schmieder, P.; Freund, C.; Volkmer, R.; Oschkinat, H.; Schmalz, H.-G.; Kühne, R. A Modular Toolkit to Inhibit Proline-Rich Motif–Mediated Protein–Protein Interactions. *Proc. Natl. Acad. Sci.* **2015**, *112*, 5011–5016. https://doi.org/10.1073/pnas.1422054112.

(181) Barone, M.; Müller, M.; Chiha, S.; Ren, J.; Albat, D.; Soicke, A.; Dohmen, S.; Klein, M.; Bruns, J.; Van Dinther, M.; Opitz, R.; Lindemann, P.; Beerbaum, M.; Motzny, K.; Roske, Y.; Schmieder, P.; Volkmer, R.; Nazaré, M.; Heinemann, U.; Oschkinat, H.; Ten Dijke, P.; Schmalz, H.-G.; Kühne, R. Designed Nanomolar Small-Molecule Inhibitors of Ena/VASP EVH1 Interaction Impair Invasion and Extravasation of Breast Cancer Cells. *Proc. Natl. Acad. Sci. U. S. A.* **2020**, *117*, 29684–29690. https://doi.org/10.1073/pnas.2007213117.

(182) Chen, B.; Roy, S. G.; McMonigle, R. J.; Keebaugh, A.; McCracken, A. N.; Selwan, E.; Fransson, R.; Fallegger, D.; Huwiler, A.; Kleinman, M. T.; Edinger, A. L.; Hanessian, S. Azacyclic FTY720 Analogues That Limit Nutrient Transporter Expression but Lack S1P Receptor Activity and Negative Chronotropic Effects Offer a Novel and Effective Strategy to Kill Cancer Cells in Vivo. *ACS Chem. Biol.* **2016**, *11* (2), 409–414. https://doi.org/10.1021/acschembio.5b00761.

(183) Kim, S. M.; Roy, S. G.; Chen, B.; Nguyen, T. M.; McMonigle, R. J.; McCracken, A. N.; Zhang, Y.; Kofuji, S.; Hou, J.; Selwan, E.; Finicle, B. T.; Nguyen, T. T.; Ravi, A.; Ramirez, M. U.; Wiher, T.; Guenther, G. G.; Kono, M.; Sasaki, A. T.; Weisman, L. S.; Potma, E. O.; Tromberg, B. J.; Edwards, R. A.; Hanessian, S.; Edinger, A. L. Targeting Cancer Metabolism by Simultaneously Disrupting Parallel Nutrient Access Pathways. *J. Clin. Invest.* **2016**, *126*, 4088–4102. https://doi.org/10.1172/JCI87148.

(184) Wlodarchak, N.; Xing, Y. PP2A as a Master Regulator of the Cell Cycle. *Crit. Rev. Biochem. Mol. Biol.* **2016**, *51*, 162–184. https://doi.org/10.3109/10409238.2016.1143913.

(185) Sung, H.; Ferlay, J.; Siegel, R. L.; Laversanne, M.; Soerjomataram, I.; Jemal, A.; Bray, F. Global Cancer Statistics 2020: GLOBOCAN Estimates of Incidence and Mortality Worldwide for 36 Cancers in 185 Countries. *CA. Cancer J. Clin.* **2021**, *71*, 209–249. https://doi.org/10.3322/caac.21660.

(186) Kroschinsky, F.; Stölzel, F.; von Bonin, S.; Beutel, G.; Kochanek, M.; Kiehl, M.; Schellongowski, P. New Drugs, New Toxicities: Severe Side Effects of Modern Targeted and Immunotherapy of Cancer and Their Management. *Crit. Care* **2017**, *21*, 1–11. https://doi.org/10.1186/s13054-017-1678-1.

(187) Smith, G. L.; Lopez-Olivo, M. A.; Advani, P. G.; Ning, M. S.; Geng, Y.; Giordano, S. H.; Volk, R. J. Financial Burdens of Cancer Treatment: A Systematic Review of Risk Factors and Outcomes. *JNCCN J. Natl. Compr. Cancer Netw.* **2019**, *17*, 1184–1192. https://doi.org/10.6004/jnccn.2019.7305.

(188) Samiei, M. Challenges of Making Radiotherapy Accessible in Developing Countries. *Cancer Control* **2013**, 85–96.

(189) Dos-Santos-Silva, I.; Gupta, S.; Orem, J.; Shulman, L. N. Global Disparities in Access to Cancer Care. *Commun. Med.* **2022**, *2*, 1–4. https://doi.org/10.1038/s43856-022-00097-5.

(190) Ruff, P.; Al-sukhun, S.; Blanchard, C.; Shulman, L. N. Access to Cancer Therapeutics in Low- and Middle-Income Countries. *ASCO Educ. B.* **2016**, 58–65.

(191) Holohan, C.; Van Schaeybroeck, S.; Longley, D. B.; Johnston, P. G. Cancer Drug Resistance: An Evolving Paradigm. *Nat. Rev. Cancer* **2013**, *13*, 714–726. https://doi.org/10.1038/nrc3599.

(192) Hanahan, D.; Weinberg, R. A. Hallmarks of Cancer: The Next Generation. *Cell* **2011**, *144*, 646–674. https://doi.org/10.1016/J.CELL.2011.02.013.

(193) Jairam, V.; Lee, V.; Park, H. S.; Thomas, C. R.; Melnick, E. R.; Gross, C. P.; Presley, C. J.; Adelson, K. B.; Yu, J. B. Treatment-Related Complications of Systemic Therapy and Radiotherapy. *JAMA Oncol.* **2019**, *5*, 1028–1035. https://doi.org/10.1001/jamaoncol.2019.0086.

(194) Pearce, A.; Haas, M.; Viney, R.; Pearson, S. A.; Haywood, P.; Brown, C.; Ward, R. Incidence and Severity of Self-Reported Chemotherapy Side Effects in Routine Care: A Prospective Cohort Study. *PLoS One* **2017**, *12*, 1–12. https://doi.org/10.1371/journal.pone.0184360.

(195) Oun, R.; Moussa, Y. E.; Wheate, N. J. The Side Effects of Platinum-Based Chemotherapy Drugs: A Review for Chemists. *Dalt. Trans.* **2018**, *47*, 6645–6653. https://doi.org/10.1039/c8dt00838h.

(196) van den Boogaard, W. M. C.; Komninos, D. S. J.; Vermeij, W. P. Chemotherapy Side-Effects: Not All DNA Damage Is Equal. *Cancers (Basel).* **2022**, *14*, 1–27. https://doi.org/10.3390/cancers14030627.

(197) Aslam, M. S.; Naveed, S.; Ahmed, A.; Abbas, Z.; Gull, I.; Athar, M. A. Side Effects of Chemotherapy in Cancer Patients and Evaluation of Patients Opinion about Starvation Based Differential Chemotherapy. *J. Cancer Ther.* **2014**, *5*, 817–822. https://doi.org/10.4236/jct.2014.58089.

(198) Schirrmacher, V. From Chemotherapy to Biological Therapy: A Review of Novel Concepts to Reduce the Side Effects of Systemic Cancer Treatment (Review). *Int. J. Oncol.* **2019**, *54*, 407–419. https://doi.org/10.3892/ijo.2018.4661.

(199) Luengo, A.; Gui, D. Y.; Vander Heiden, M. G. Targeting Metabolism for Cancer Therapy. *Cell Chem. Biol.* **2017**, *24*, 1161–1180. https://doi.org/10.1016/J.CHEMBIOL.2017.08.028.

(200) Huang, M.; Shen, A.; Ding, J.; Geng, M. Molecularly Targeted Cancer Therapy: Some Lessons from the Past Decade. *Trends Pharmacol. Sci.* **2014**, *35*, 41–50. https://doi.org/10.1016/J.TIPS.2013.11.004.

(201) Martinez-Outschoorn, U. E.; Peiris-Pagés, M.; Pestell, R. G.; Sotgia, F.; Lisanti, M. P. Cancer Metabolism: A Therapeutic Perspective. *Nat. Rev. Clin. Oncol.* **2017**, *14*, 11–31. https://doi.org/10.1038/nrclinonc.2016.60.

(202) Martínez-Reyes, I.; Chandel, N. S. Cancer Metabolism: Looking Forward. *Nat. Rev. Cancer* **2021**, *21*, 669–680. https://doi.org/10.1038/s41568-021-00378-6.

(203) McCracken, A. N.; Edinger, A. L. Nutrient Transporters: The Achilles' Heel of Anabolism. *Trends Endocrinol. Metab.* **2013**, *24*, 200–208. https://doi.org/10.1016/j.tem.2013.01.002.

(204) Ying, H.; Kimmelman, A. C.; Lyssiotis, C. A.; Hua, S.; Chu, G. C.; Fletcher-Sananikone, E.;

Locasale, J. W.; Son, J.; Zhang, H.; Coloff, J. L.; Yan, H.; Wang, W.; Chen, S.; Viale, A.; Zheng, H.; Paik, J. H.; Lim, C.; Guimaraes, A. R.; Martin, E. S.; Chang, J.; Hezel, A. F.; Perry, S. R.; Hu, J.; Gan, B.; Xiao, Y.; Asara, J. M.; Weissleder, R.; Wang, Y. A.; Chin, L.; Cantley, L. C.; Depinho, R. A. Oncogenic Kras Maintains Pancreatic Tumors through Regulation of Anabolic Glucose Metabolism. *Cell* **2012**, *149*, 656–670. https://doi.org/10.1016/j.cell.2012.01.058.

(205) Romero Rosales, K.; Singh, G.; Wu, K.; Chen, J.; Janes, M. R.; Lilly, M. B.; Peralta, E. R.; Siskind, L. J.; Bennett, M. J.; Fruman, D. A.; Edinger, A. L. Sphingolipid-Based Drugs Selectively Kill Cancer Cells by down-Regulating Nutrient Transporter Proteins. *Biochem. J.* **2011**, *439*, 299–311. https://doi.org/10.1042/BJ20110853.

(206) Yue, S.; Li, J.; Lee, S. Y.; Lee, H. J.; Shao, T.; Song, B.; Cheng, L.; Masterson, T. A.; Liu, X.; Ratliff, T. L.; Cheng, J. X. Cholesteryl Ester Accumulation Induced by PTEN Loss and PI3K/AKT Activation Underlies Human Prostate Cancer Aggressiveness. *Cell Metab.* **2014**, *19*, 393–406. https://doi.org/10.1016/j.cmet.2014.01.019.

(207) Guillaumond, F.; Bidaut, G.; Ouaissi, M.; Servais, S.; Gouirand, V.; Olivares, O.; Lac, S.; Borge, L.; Roques, J.; Gayet, O.; Pinault, M.; Guimaraes, C.; Nigri, J.; Loncle, C.; Lavaut, M. N.; Garcia, S.; Tailleuxi, A.; Staels, B.; Calvom, E.; Tomasini, R.; Iovanna, J. L.; Vasseur, S. Cholesterol Uptake Disruption, in Association with Chemotherapy, Is a Promising Combined Metabolic Therapy for Pancreatic Adenocarcinoma. *Proc. Natl. Acad. Sci. U. S. A.* **2015**, *112*, 2473–2478. https://doi.org/10.1073/pnas.1421601112.

(208) Palm, W.; Park, Y.; Wright, K.; Pavlova, N. N.; Tuveson, D. A.; Thompson, C. B. The Utilization of Extracellular Proteins as Nutrients Is Suppressed by MTORC1. *Cell* **2015**, *162*, 259–270. https://doi.org/10.1016/j.cell.2015.06.017.

(209) Garcia-Bermudez, J.; Williams, R. T.; Guarecuco, R.; Birsoy, K. Targeting Extracellular Nutrient Dependencies of Cancer Cells. *Mol. Metab.* **2020**, *33*, 67–82. https://doi.org/10.1016/j.molmet.2019.11.011.

(210) Fan, K.; Liu, Z.; Gao, M.; Tu, K.; Xu, Q.; Zhang, Y. Targeting Nutrient Dependency in Cancer Treatment. *Front. Oncol.* **2022**, *12*, 1–18. https://doi.org/10.3389/fonc.2022.820173.

(211) Guenther, G. G.; Peralta, E. R.; Rosales, K. R.; Wong, S. Y.; Siskind, L. J.; Edinger, A. L. Ceramide Starves Cells to Death by Downregulating Nutrient Transporter Proteins. *Proc. Natl. Acad. Sci. U. S. A.* **2008**, *105*, 17402–17407. https://doi.org/10.1073/pnas.0802781105.

(212) Camm, J.; Hla, T.; Bakshi, R.; Brinkmann, V. Cardiac and Vascular Effects of Fingolimod: Mechanistic Basis and Clinical Implications. *Am. Heart J.* **2014**, *168*, 632–644. https://doi.org/10.1016/J.AHJ.2014.06.028.

(213) Brinkmann, V.; Billich, A.; Baumruker, T.; Heining, P.; Schmouder, R.; Francis, G.; Aradhye, S.; Burtin, P. Fingolimod (FTY720): Discovery and Development of an Oral Drug to Treat Multiple Sclerosis. *Nat. Rev. Drug Discov.* **2010**, *9*, 883–897. https://doi.org/10.1038/nrd3248.

(214) Chun, J.; Hartung, H. P. Mechanism of Action of Oral Fingolimod (FTY720) in Multiple Sclerosis. *Clin. Neuropharmacol.* **2010**, *33*, 91–101. https://doi.org/10.1097/WNF.0b013e3181cbf825.

(215) Hanessian, S.; Charron, G.; Billich, A.; Guerini, D. Constrained Azacyclic Analogues of the Immunomodulatory Agent FTY720 as Molecular Probes for Sphingosine 1-Phosphate Receptors. *Bioorganic Med. Chem. Lett.* **2007**, *17*, 491–494. https://doi.org/10.1016/j.bmcl.2006.10.014.

(216) Fransson, R.; McCracken, A. N.; Chen, B.; McMonigle, R. J.; Edinger, A. L.; Hanessian, S. Design, Synthesis, and Antileukemic Activity of Stereochemically Defined Constrained Analogues of FTY720 (Gilenya). *ACS Med. Chem. Lett.* **2013**, *4*, 969–973. https://doi.org/10.1021/ml4002425.

(217) Perryman, M. S.; Tessier, J.; Wiher, T.; O'Donoghue, H.; McCracken, A. N.; Kim, S. M.; Nguyen, D. G.; Simitian, G. S.; Viana, M.; Rafelski, S.; Edinger, A. L.; Hanessian, S. Effects of Stereochemistry, Saturation, and Hydrocarbon Chain Length on the Ability of Synthetic Constrained Azacyclic Sphingolipids to Trigger Nutrient Transporter down-Regulation, Vacuolation, and Cell Death. *Bioorganic Med. Chem.* **2016**, *24*, 4390–4397.

https://doi.org/10.1016/j.bmc.2016.07.038.

(218) Heijman, J.; Dewenter, M.; El-Armouche, A.; Dobrev, D. Function and Regulation of Serine/Threonine Phosphatases in the Healthy and Diseased Heart. *J. Mol. Cell. Cardiol.* **2013**, *64*, 90–98. https://doi.org/10.1016/j.yjmcc.2013.09.006.

(219) Shi, Y. Serine/Threonine Phosphatases: Mechanism through Structure. *Cell* **2009**, *139*, 468–484. https://doi.org/10.1016/j.cell.2009.10.006.

(220) Virshup, D. M.; Shenolikar, S. From Promiscuity to Precision: Protein Phosphatases Get a Makeover. *Mol. Cell* **2009**, *33*, 537–545. https://doi.org/10.1016/j.molcel.2009.02.015.

(221) Seshacharyulu, P.; Pandey, P.; Datta, K.; Batra, S. K. Phosphatase: PP2A Structural Importance, Regulation and Its Aberrant Expression in Cancer. *Cancer Lett.* **2013**, *335*, 9–18. https://doi.org/10.1016/j.canlet.2013.02.036.

(222) Mumby, M. PP2A: Unveiling a Reluctant Tumor Suppressor. *Cell* **2007**, *130*, 21–24. https://doi.org/10.1016/j.cell.2007.06.034.

(223) Sangodkar, J.; Perl, A.; Tohme, R.; Kiselar, J.; Kastrinsky, D. B.; Zaware, N.; Izadmehr, S.; Mazhar, S.; Wiredja, D. D.; O'Connor, C. M.; Hoon, D.; Dhawan, N. S.; Schlatzer, D.; Yao, S.; Leonard, D.; Borczuk, A. C.; Gokulrangan, G.; Wang, L.; Svenson, E.; Farrington, C. C.; Yuan, E.; Avelar, R. A.; Stachnik, A.; Smith, B.; Gidwani, V.; Giannini, H. M.; McQuaid, D.; McClinch, K.; Wang, Z.; Levine, A. C.; Sears, R. C.; Chen, E. Y.; Duan, Q.; Datt, M.; Haider, S.; Ma'Ayan, A.; DiFeo, A.; Sharma, N.; Galsky, M. D.; Brautigan, D. L.; Ioannou, Y. A.; Xu, W.; Chance, M. R.; Ohlmeyer, M.; Narla, G. Activation of Tumor Suppressor Protein PP2A Inhibits KRAS-Driven Tumor Growth. *J. Clin. Invest.* **2017**, *127*, 2081–2090. https://doi.org/10.1172/JCI89548.

(224) McClinch, K.; Avelar, R. A.; Callejas, D.; Izadmehr, S.; Wiredja, D.; Perl, A.; Sangodkar, J.; Kastrinsky, D. B.; Schlatzer, D.; Cooper, M.; Kiselar, J.; Stachnik, A.; Yao, S.; Hoon, D.; McQuaid, D.; Zaware, N.; Gong, Y.; Brautigan, D. L.; Plymate, S. R.; Sprenger, C. C. T.; Oh, W. K.; Levine, A. C.; Kirschenbaum, A.; Sfakianos, J. P.; Sears, R.; DiFeo, A.; Ioannou, Y.; Ohlmeyer, M.; Narla, G.; Galsky, M. D. Small-Molecule Activators of Protein Phosphatase

2A for the Treatment of Castration-Resistant Prostate Cancer. *Cancer Res.* **2018**, *78*, 2065–2080. https://doi.org/10.1158/0008-5472.CAN-17-0123.

(225) Tohmé, R.; Izadmehr, S.; Gandhe, S.; Tabaro, G.; Vallabhaneni, S.; Thomas, A.; Vasireddi, N.; Dhawan, N. S.; Ma'ayan, A.; Sharma, N.; Galsky, M. D.; Ohlmeyer, M.; Sangodkar, J.; Narla, G. Direct Activation of PP2A for the Treatment of Tyrosine Kinase Inhibitor–Resistant Lung Adenocarcinoma. *JCI Insight* **2019**, *4*, 1–11. https://doi.org/10.1172/jci.insight.125693.

(226) Milazzo, G.; Mercatelli, D.; Di Muzio, G.; Triboli, L.; De Rosa, P.; Perini, G.; Giorgi, F. M. Histone Deacetylases (HDACs): Evolution, Specificity, Role in Transcriptional Complexes, and Pharmacological Actionability. *Genes (Basel).* **2020**, *11*, 1–49. https://doi.org/10.3390/genes11050556.

(227) Eberharter, A.; Becker, P. B. Histone Acetylation: A Switch between Repressive and Permissive Chromatin. Second in Review on Chromatin Dynamics. *EMBO Rep.* **2002**, *3*, 224–229. https://doi.org/10.1093/embo-reports/kvf053.

(228) Karpac, J.; Jasper, H. Metabolic Homeostasis: HDACs Take Center Stage. *Cell* **2011**, *145*, 497–499. https://doi.org/10.1016/j.cell.2011.04.017.

(229) Ellmeier, W.; Seiser, C. Histone Deacetylase Function in CD4+ T Cells. *Nat. Rev. Immunol.* **2018**, *18*, 617–634. https://doi.org/10.1038/s41577-018-0037-z.

(230) Sun, X. J.; Man, N.; Tan, Y.; Nimer, S. D.; Wang, L. The Role of Histone Acetyltransferases in Normal and Malignant Hematopoiesis. *Front. Oncol.* **2015**, *5*, 1–11. https://doi.org/10.3389/fonc.2015.00108.

(231) Shvedunova, M.; Akhtar, A. Modulation of Cellular Processes by Histone and Non-Histone Protein Acetylation. *Nat. Rev. Mol. Cell Biol.* **2022**, *23*, 329–349. https://doi.org/10.1038/s41580-021-00441-y.

(232) Chuang, D. M.; Leng, Y.; Marinova, Z.; Kim, H. J.; Chiu, C. T. Multiple Roles of HDAC Inhibition in Neurodegenerative Conditions. *Trends Neurosci.* **2009**, *32*, 591–601. https://doi.org/10.1016/j.tins.2009.06.002.

(233) Villagra, A.; Sotomayor, E. M.; Seto, E. Histone Deacetylases and the Immunological Network: Implications in Cancer and Inflammation. *Oncogene* **2010**, *29*, 157–173. https://doi.org/10.1038/onc.2009.334.

(234) Falkenberg, K. J.; Johnstone, R. W. Histone Deacetylases and Their Inhibitors in Cancer, Neurological Diseases and Immune Disorders. *Nat. Rev. Drug Discov.* **2014**, *13*, 673–691. https://doi.org/10.1038/nrd4360.

(235) Haberland, M.; Montgomery, R. L.; Olson, E. N. The Many Roles of Histone Deacetylases in Development and Physiology: Implications for Disease and Therapy. *Nat. Rev. Genet.* **2009**, *10*, 32–42. https://doi.org/10.1038/nrg2485.

(236) Chen, H. P.; Zhao, Y. T.; Zhao, T. C. Histone Deacetylases and Mechanisms of Regulation of Gene Expression (Histone Deacetylases in Cancer). *Crit. Rev. Oncog.* **2015**, *20*, 35–47. https://doi.org/10.1615/CritRevOncog.2015012997.

(237) Zhang, L.; Fang, H.; Xu, W. Strategies in Developing Promising Histone Deacetylase Inhibitors. *Med. Res. Rev.* **2010**, *30*, 585–602. https://doi.org/10.1002/med.20169.

(238) Hanessian, S.; Auzzas, L.; Giannini, G.; Marzi, M.; Cabri, W.; Barbarino, M.; Vesci, L.; Pisano, C. ω-Alkoxy Analogues of SAHA (Vorinostat) as Inhibitors of HDAC: A Study of Chain-Length and Stereochemical Dependence. *Bioorg. Med. Chem. Lett.* **2007**, *17*, 6261–6265. https://doi.org/10.1016/J.BMCL.2007.09.014.

(239) Auzzas, L.; Larsson, A.; Matera, R.; Baraldi, A.; Deschênes-Simard, B.; Giannini, G.; Cabri, W.; Battistuzzi, G.; Gallo, G.; Ciacci, A.; Vesci, L.; Pisano, C.; Hanessian, S. Non-Natural Macrocyclic Inhibitors of Histone Deacetylases: Design, Synthesis, and Activity. *J. Med. Chem.* **2010**, *53*, 8387–8399. https://doi.org/10.1021/jm101092u.

(240) Marks, P. A.; Rifkind, R. A.; Richon, V. M.; Breslow, R.; Miller, T.; Kelly, W. K. Histone Deacetylases and Cancer: Causes and Therapies. *Nat. Rev. Cancer* **2001**, *1*, 194–202. https://doi.org/10.1038/35106079.

(241) Bolden, J. E.; Peart, M. J.; Johnstone, R. W. Anticancer Activities of Histone Deacetylase Inhibitors. *Nat. Rev. Drug Discov.* **2006**, *5*, 769–784. https://doi.org/10.1038/nrd2133.

(242) Körner, M.; Tibes, U. 5 Histone Deacetylase Inhibitors: A Novel Class of Anti-Cancer Agents on Its Way to the Market. *Prog. Med. Chem.* **2008**, *46*, 205–280.

(243) Atadja, P. W. HDAC Inhibitors and Cancer Therapy. In *Epigenetics and Disease. Progress in Drug Research*; Gasser, S., Li, E., Eds.; Springer, Basel, 2011; p 67.

(244) Yoshida, M.; Kijima, M.; Akita, M.; Beppu, T. Potent and Specific Inhibition of Mammalian Histone Deacetylase Both in Vivo and in Vitro by Trichostatin A. *J. Biol. Chem.* **1990**, *265*, 17174–17179. https://doi.org/10.1016/s0021-9258(17)44885-x.

(245) Marks, P. A.; Breslow, R. Dimethyl Sulfoxide to Vorinostat: Development of This Histone Deacetylase Inhibitor as an Anticancer Drug. *Nat. Biotechnol.* **2007**, *25*, 84–90. https://doi.org/10.1038/nbt1272.

(246) Hait, N. C.; Allegood, J.; Maceyka, M.; Strub, G. M.; Harikumar, K. B.; Singh, S. K.; Luo, C.; Marmorstein, R.; Kordula, T.; Milstien, S.; Spiegel, S. Regulation of Histone Acetylation in the Nucleus by Sphingosine-1-Phosphate. *Science* **2009**, *325*, 1254–1257. https://doi.org/10.1126/science.1176709.

(247) Hait, N. C.; Wise, L. E.; Allegood, J. C.; O'Brien, M.; Avni, D.; Reeves, T. M.; Knapp, P. E.; Lu, J.; Luo, C.; Miles, M. F.; Milstien, S.; Lichtman, A. H.; Spiegel, S. Active, Phosphorylated Fingolimod Inhibits Histone Deacetylases and Facilitates Fear Extinction Memory. *Nat. Neurosci.* **2014**, *17*, 971–980. https://doi.org/10.1038/nn.3728.

(248) Hait, N. C.; Avni, D.; Yamada, A.; Nagahashi, M.; Aoyagi, T.; Aoki, H.; Dumur, C. I.; Zelenko, Z.; Gallagher, E. J.; Leroith, D.; Milstien, S.; Takabe, K.; Spiegel, S. The Phosphorylated Prodrug FTY720 Is a Histone Deacetylase Inhibitor That Reactivates ERα Expression and Enhances Hormonal Therapy for Breast Cancer. *Oncogenesis* **2015**, *4*, 1–11. https://doi.org/10.1038/oncsis.2015.16.

(249) Mokhtari, R. B.; Homayouni, T. S.; Baluch, N.; Morgatskaya, E.; Kumar, S.; Das, B.; Yeger, H. Combination Therapy in Combating Cancer. *Oncotarget* **2017**, *8*, 38022–38043.

(250) Mazhar, S.; Taylor, S. E.; Sangodkar, J.; Narla, G. Targeting PP2A in Cancer: Combination Therapies. *Biochim. Biophys. Acta - Mol. Cell Res.* **2019**, *1866*, 51–63.

https://doi.org/10.1016/j.bbamcr.2018.08.020.

(251) Moitessier, N.; Pottel, J.; Therrien, E.; Englebienne, P.; Liu, Z.; Tomberg, A.; Corbeil, C. R. Medicinal Chemistry Projects Requiring Imaginative Structure-Based Drug Design Methods. *Acc. Chem. Res.* **2016**, *49*, 1646–1657. https://doi.org/10.1021/acs.accounts.6b00185.

(252) Pottel, J.; Therrien, E.; Gleason, J. L.; Moitessier, N. Docking Ligands into Flexible and Solvated Macromolecules. 6. Development and Application to the Docking of HDACs and Other Zinc Metalloenzymes Inhibitors. *J. Chem. Inf. Model.* **2014**, *54*, 254–265. https://doi.org/10.1021/ci400550m.

(253) Selwan, E. M.; Finicle, B. T.; Kim, S. M.; Edinger, A. L. Attacking the Supply Wagons to Starve Cancer Cells to Death. *FEBS Lett.* **2016**, *590*, 885–907. https://doi.org/10.1002/1873-3468.12121.

(254) Zhang, L.; Wang, H.-D.; Ji, X.-J.; Cong, Z.-X.; Zhu, J.-H.; Zhou, Y. FTY720 for Cancer Therapy (Review). *Oncol. Rep.* **2013**, *30*, 2571–2578. https://doi.org/10.3892/or.2013.2765.

(255) Chen, B.; Roy, S. G.; McMonigle, R. J.; Keebaugh, A.; McCracken, A. N.; Selwan, E.; Fransson, R.; Fallegger, D.; Huwiler, A.; Kleinman, M. T.; Edinger, A. L.; Hanessian, S. Azacyclic FTY720 Analogues That Limit Nutrient Transporter Expression but Lack S1P Receptor Activity and Negative Chronotropic Effects Offer a Novel and Effective Strategy to Kill Cancer Cells in Vivo. *ACS Chem. Biol.* **2016**, *11*, 409–414. https://doi.org/10.1021/acschembio.5b00761.

(256) Chung, N.; Mao, C.; Heitman, J.; Hannun, Y. A.; Obeid, L. M. Phytosphingosine as a Specific Inhibitor of Growth and Nutrient Import in Saccharomyces Cerevisiae. *J. Biol. Chem.* **2001**, *276*, 35614–35621. https://doi.org/10.1074/jbc.M105653200.

(257) Skrzypek, M. S.; Nagiec, M. M.; Lester, R. L.; Dickson, R. C. Inhibition of Amino Acid Transport by Sphingoid Long Chain Bases in Saccharomyces Cerevisiae. *J. Biol. Chem.* **1998**, *273*, 2829–2834. https://doi.org/10.1074/jbc.273.5.2829.

(258) Welsch, C. A.; Roth, L. W. A.; Goetschy, J. F.; Movva, N. R. Genetic, Biochemical, and Transcriptional Responses of Saccharomyces Cerevisiae to the Novel Immunomodulator

FTY720 Largely Mimic Those of the Natural Sphingolipid Phytosphingosine. *J. Biol. Chem.* **2004**, *279*, 36720–36731. https://doi.org/10.1074/jbc.M406179200.

(259) Barthelemy, C.; Barry, A. O.; Twyffels, L.; André, B. FTY720-Induced Endocytosis of Yeast and Human Amino Acid Transporters Is Preceded by Reduction of Their Inherent Activity and TORC1 Inhibition. *Sci. Rep.* **2017**, *7*, 1–16. https://doi.org/10.1038/s41598-017-14124-2.

(260) Gardner, N. M.; Riley, R. T.; Showker, J. L.; Voss, K. A.; Sachs, A. J.; Maddox, J. R.; Gelineau-van Waes, J. B. Elevated Nuclear and Cytoplasmic FTY720-Phosphate in Mouse Embryonic Fibroblasts Suggests the Potential for Multiple Mechanisms in FTY720-Induced Neural Tube Defects. *Toxicol. Sci.* **2016**, *150*, 161–168. https://doi.org/10.1093/toxsci/kfv321.

(261) Shimizu, H.; Takahashi, M.; Kaneko, T.; Murakami, T.; Hakamata, Y.; Kudou, S.; Kishi, T.; Fukuchi, K.; Iwanami, S.; Kuriyama, K.; Yasue, T.; Enosawa, S.; Matsumoto, K.; Takeyoshi, I.; Morishita, Y.; Kobayashi, E. KRP-203, a Novel Synthetic Immunosuppressant, Prolongs Graft Survival and Attenuates Chronic Rejection in Rat Skin and Heart Allografts. *Circulation* **2005**, *111*, 222–229. https://doi.org/10.1161/01.CIR.0000152101.41037.AB.

(262) Xiao, Q.; Jin, J.; Wang, X.; Hu, J.; Xi, M.; Tian, Y.; Yin, D. Synthesis, Identification, and Biological Activity of Metabolites of Two Novel Selective S1P1 Agonists. *Bioorg. Med. Chem.* **2016**, *24*, 2273–2279. https://doi.org/10.1016/J.BMC.2016.03.059.

(263) Kimball, F. S.; Turunen, B. J.; Ellis, K. C.; Himes, R. H.; Georg, G. I. Enantiospecific Synthesis and Cytotoxicity of 7-(4-Methoxyphenyl)-6-Phenyl-2,3,8,8a-Tetrahydroindolizin-5(1H)-One Enantiomers. *Bioorg. Med. Chem.* **2008**, *16*, 4367–4377. https://doi.org/10.1016/J.BMC.2008.02.073.

(264) Mollica, J. A.; Smith, J. B.; Nunes, I. M.; Govan, H. K. The Decomposition of a Mannich Base. *J. Pharm. Sci.* **1971**, *59*, 1770–1774.

(265) Orgován, G.; Tihanyi, K.; Noszál, B. NMR Analysis, Protonation Equilibria and Decomposition Kinetics of Tolperisone. *J. Pharm. Biomed. Anal.* **2009**, *50*, 718–723. https://doi.org/10.1016/J.JPBA.2009.05.036.

(266) King, S. P.; Sigvardson, K. W.; Dudzinski, J.; Torosian, G. Degradation Kinetics and Mechanisms of Moricizine Hydrochloride in Acidic Medium. *J. Pharm. Sci.* **1992**, *81*, 586–591. https://doi.org/10.1002/jps.2600810625.

(267) Morgenthaler, M.; Schweizer, E.; Hoffmann-Röder, A.; Benini, F.; Martin, R. E.; Jaeschke, G.; Wagner, B.; Fischer, H.; Bendels, S.; Zimmerli, D.; Schneider, J.; Diederich, F.; Kansy, M.; Müller, K. Predicting and Tuning Physicochemical Properties in Lead Optimization: Amine Basicities. *ChemMedChem* **2007**, *2*, 1100–1115. https://doi.org/10.1002/cmdc.200700059.

(268) Hanessian, S.; Auzzas, L.; Larsson, A.; Zhang, J.; Giannini, G.; Gallo, G.; Ciacci, A.; Cabri, W. Vorinostat-Like Molecules as Structural, Stereochemical, and Pharmacological Tools. *ACS Med. Chem. Lett.* **2010**, *1*, 70–74. https://doi.org/10.1021/ml100028g.

(269) Vannini, A.; Volpari, C.; Gallinari, P.; Jones, P.; Mattu, M.; Carfí, A.; De Francesco, R.; Steinkühler, C.; Di Marco, S. Substrate Binding to Histone Deacetylases as Shown by the Crystal Structure of the HDAC8–Substrate Complex. *EMBO Rep.* **2007**, *8*, 879–884. https://doi.org/10.1038/sj.embor.7401047.

(270) Yip, H. Y. K.; Papa, A. Signaling Pathways in Cancer: Therapeutic Targets, Combinatorial Treatments, and New Developments. *Cells* **2021**, *10*, 1–30. https://doi.org/10.3390/cells10030659.

(271) Sever, R.; Brugge, J. S. Signal Transduction in Cancer. *Cold Spring Harb Perspect Med* **2015**, *5*, 1–21.

(272) Espinosa-Sánchez, A.; Suárez-Martínez, E.; Sánchez-Díaz, L.; Carnero, A. Therapeutic Targeting of Signaling Pathways Related to Cancer Stemness. *Front. Oncol.* **2020**, *10*, 1–32. https://doi.org/10.3389/fonc.2020.01533.

(273) Juliano, R. L. Addressing Cancer Signal Transduction Pathways with Antisense and SiRNA Oligonucleotides. *NAR Cancer* **2020**, *2*, 1–14. https://doi.org/10.1093/narcan/zcaa025.

(274) Yang, Y.; Li, X.; Wang, T.; Guo, Q.; Zheng, L. Emerging Agents That Target Signaling Pathways in Cancer Stem Cells. *J. Hematol. Oncol.* **2020**, 1–18.

(275) Kamgar-Dayhoff, P.; Brelidze, T. I. Multifaceted Effect of Chlorpromazine in Cancer: Implications for Cancer Treatment. *Oncotarget* **2021**, *12*, 1406–1426. https://doi.org/10.18632/oncotarget.28010.

(276) Wu, C.-H.; Bai, L.-Y.; Tsai, M.-H.; Chu, P.-C.; Chiu, C.-F.; Chen, M. Y.; Chiu, S.-J.; Chiang, J.-H.; Weng, J.-R. Pharmacological Exploitation of the Phenothiazine Antipsychotics to Develop Novel Antitumor Agents-A Drug Repurposing Strategy. *Sci. Rep.* **2016**, *6*, 1–11. https://doi.org/10.1038/srep27540.

(277) Yang, C.-E.; Lee, W.-Y.; Cheng, H.-W.; Chung, C.-H.; Mi, F.-L.; Lin, C.-W. The Antipsychotic Chlorpromazine Suppresses YAP Signaling, Stemness Properties, and Drug Resistance in Breast Cancer Cells. *Chem. Biol. Interact.* **2019**, *302*, 28–35. https://doi.org/10.1016/j.cbi.2019.01.033.

(278) Singh, V.; Bhoir, S.; Chikhale, R. V.; Hussain, J.; Dwyer, D.; Bryce, R. A.; Kirubakaran, S.; De Benedetti, A. Generation of Phenothiazine with Potent Anti-TLK1 Activity for Prostate Cancer Therapy. *iScience* **2020**, *23*, 1–13. https://doi.org/10.1016/j.isci.2020.101474.

(279) Choi, J. H.; Yang, Y. R.; Lee, S. K.; Kim, S.-H.; Kim, Y.-H.; Cha, J.-Y.; Oh, S.-W.; Ha, J.-R.; Ryu, S. H.; Suh, P.-G. Potential Inhibition of PDK1/Akt Signaling by Phenothiazines Suppresses Cancer Cell Proliferation and Survival. *Ann. N. Y. Acad. Sci.* **2008**, *1138*, 393–403. https://doi.org/10.1196/annals.1414.041.

(280) Kau, T. R.; Schroeder, F.; Ramaswamy, S.; Wojciechowski, C. L.; Zhao, J. J.; Roberts, T. M.; Clardy, J.; Sellers, W. R.; Silver, P. A. A Chemical Genetic Screen Identifies Inhibitors of Regulated Nuclear Export of a Forkhead Transcription Factor in PTEN-Deficient Tumor Cells. *Cancer Cell* **2003**, 463–476. https://doi.org/10.1016/S1535-6108(03)00303-9.

(281) Rho, S. B.; Kim, B.-R.; Kang, S. A Gene Signature-Based Approach Identifies Thioridazine as an Inhibitor of Phosphatidylinositol-3'-Kinase (PI3K)/AKT Pathway in Ovarian Cancer Cells. *Gynecol. Oncol.* **2011**, *120*, 121–127. https://doi.org/10.1016/j.ygyno.2010.10.003.

(282) Adams, C. E.; Rathbone, J.; Thornley, B.; Clarke, M.; Borrill, J.; Wahlbeck, K.; Awad, A. G. Chlorpromazine for Schizophrenia: A Cochrane Systematic Review of 50 Years of

Randomised Controlled Trials. *BMC Med.* **2005**, *3*, 1–7. https://doi.org/10.1186/1741-7015-3-15.

(283) Hartung, B.; Sampson, S.; Leucht, S. Perphenazine for Schizophrenia (Review). *Cochrane Database Syst. Rev.* **2015**, 1–365. https://doi.org/10.1002/14651858.CD003443.pub3.

(284) Gutierrez, A.; Pan, L.; Groen, R. W. J.; Baleydier, F.; Kentsis, A.; Marineau, J.; Grebliunaite, R.; Kozakewich, E.; Reed, C.; Pflumio, F.; Poglio, S.; Uzan, B.; Clemons, P.; Verplank, L.; An, F.; Burbank, J.; Norton, S.; Tolliday, N.; Steen, H.; Weng, A. P.; Yuan, H.; Bradner, J. E.; Mitsiades, C.; Look, A. T.; Aster, J. C. Phenothiazines Induce PP2A-Mediated Apoptosis in T Cell Acute Lymphoblastic Leukemia. *J. Clin. Invest.* **2014**, *124*, 644–655. https://doi.org/10.1172/JCI65093.644.

(285) Hemmings, B. A.; Restuccia, D. F. PI3K-PKB/Akt Pathway. *Cold Spring Harb. Perspect. Biol.* **2012**, *4*, 1–3.

(286) Kastrinsky, D. B.; Sangodkar, J.; Zaware, N.; Izadmehr, S.; Dhawan, N. S.; Narla, G.; Ohlmeyer, M. Reengineered Tricyclic Anti-Cancer Agents. *Bioorganic Med. Chem.* **2015**, *23*, 6528–6534. https://doi.org/10.1016/j.bmc.2015.07.007.

(287) Li, X.-Y.; Huang, L.-T.; Wu, J.-Q.; He, M.-F.; Zhu, S.-H.; Zhan, P.; Lv, T.-F.; Song, Y. Zebrafish Xenograft Model of Human Lung Cancer for Evaluating Osimertinib Resistance. *Biomed Res. Int.* **2019**, 1–10. https://doi.org/10.1155/2019/3129748.

(288) Kauko, O.; O'Connor, C. M.; Kulesskiy, E.; Sangodkar, J.; Aakula, A.; Izadmehr, S.; Yetukuri, L.; Yadav, B.; Padzik, A.; Laajala, T. D.; Haapaniemi, P.; Momeny, M.; Varila, T.; Ohlmeyer, M.; Aittokallio, T.; Wennerberg, K.; Narla, G.; Westermarck, J. PP2A Inhibition Is a Druggable MEK Inhibitor Resistance Mechanism in KRAS-Mutant Lung Cancer Cells. *Sci. Transl. Med.* **2018**, *10*, 1–12. https://doi.org/10.1126/scitranslmed.aaq1093.

(289) Ohlmeyer, M.; Narla, G.; Dhawan, N.; Kastrinsky, D. B. Tricyclic Compounds as Anticancer Agents. WO2013025882A2, 2013.

(290) Ohlmeyer, M.; Kastrinsky, D. B. Constrained Tricyclic Sulfonamides. WO2015138496A1, 2015.

(291) Ohlmeyer, M.; Kastrinsky, D. B. Sulfonamides Derived from Tricyclyl-2-Aminocycloalkanols as Anticancer Agents. WO2015138500A1, 2015.

(292) Ohlmeyer, M.; Zaware, N. Heterocyclic Constrained Tricyclic Sulfonamides as Anti-Cancer Agents. WO2017044569A1, 2017.

(293) Ohlmeyer, M.; Kastrinsky, D. Sulfonamides Derived from Tricyclyl-2-Aminocycloalkanols as Anticancer Agents. US 2017/0015625 A1, 2017.

(294) Calnan, D. R.; Brunet, A. The FoxO Code. *Oncogene* **2008**, *27*, 2276–2288. https://doi.org/10.1038/onc.2008.21.

(295) Tuteja, G.; Kaestner, K. H. SnapShot: Forkhead Transcription Factors I. *Cell* **2007**, *130*, 1160-1160.e1. https://doi.org/10.1016/j.cell.2007.09.005.

(296) Tuteja, G.; Kaestner, K. H. SnapShot: Forkhead Transcription Factors II. *Cell* **2007**, *131*, 192-192.e1. https://doi.org/10.1016/j.cell.2007.09.016.

(297) Zhang, X.; Tang, N.; Hadden, T. J.; Rishi, A. K. Akt, FoxO and Regulation of Apoptosis. *Biochim. Biophys. Acta - Mol. Cell Res.* **2011**, *1813*, 1978–1986. https://doi.org/10.1016/j.bbamcr.2011.03.010.

(298) Tzivion, G.; Dobson, M.; Ramakrishnan, G. FoxO Transcription Factors; Regulation by AKT and 14-3-3 Proteins. *Biochim. Biophys. Acta - Mol. Cell Res.* **2011**, *1813*, 1938–1945. https://doi.org/10.1016/j.bbamcr.2011.06.002.

(299) Xu, S.; Ma, Y.; Chen, Y.; Pan, F. Role of Forkhead Box O3a Transcription Factor in Autoimmune Diseases. *Int. Immunopharmacol.* **2021**, *92*, 1–10. https://doi.org/10.1016/j.intimp.2020.107338.

(300) Yadav, R. K.; Chauhan, A. S.; Zhuang, L.; Gan, B. FoxO Transcription Factors in Cancer Metabolism. *Semin. Cancer Biol.* **2018**, *50*, 65–76. https://doi.org/10.1016/j.semcancer.2018.01.004.

(301) Lee, S.; Dong, H. H. FoxO Integration of Insulin Signaling with Glucose and Lipid Metabolism. *J. Endocrinol.* **2017**, *233*, R67–R79. https://doi.org/10.1530/JOE-17-0002.

(302) Yan, L.; Lavin, V. A.; Moser, L. R.; Cui, Q.; Kanies, C.; Yang, E. PP2A Regulates the Pro-Apoptotic Activity of FOXO1. *J. Biol. Chem.* **2008**, *283*, 7411–7420. https://doi.org/10.1074/jbc.M708083200.

(303) Hannun, Y. A.; Obeid, L. M. Sphingolipids and Their Metabolism in Physiology and Disease. *Nat. Rev. Mol. Cell Biol.* **2018**, *19*, 175–191. https://doi.org/10.1038/nrm.2017.107.

(304) Ogretmen, B. Sphingolipid Metabolism in Cancer Signalling and Therapy. *Nat. Rev. Cancer* **2018**, *18*, 33–50. https://doi.org/10.1038/nrc.2017.96.

(305) Liao, J.; Tao, J.; Lin, G.; Liu, D. Chemistry and Biology of Sphingolipids. *Tetrahedron* **2005**, *61*, 4715–4733. https://doi.org/10.1016/j.tet.2005.02.075.

(306) O'Connor, C. M.; Perl, A.; Leonard, D.; Sangodkar, J.; Narla, G. Therapeutic Targeting of PP2A. *Int. J. Biochem. Cell Biol.* **2018**, *96*, 182–193. https://doi.org/10.1016/j.biocel.2017.10.008.

(307) Perrotti, D.; Neviani, P. Protein Phosphatase 2A: A Target for Anticancer Therapy. *Lancet Oncol.* **2013**, *14*, e229–e238. https://doi.org/10.1016/S1470-2045(12)70558-2.

(308) Sanford, M. Fingolimod: A Review of Its Use in Relapsing-Remitting Multiple Sclerosis. *Drugs* **2014**, *74*, 1411–1433. https://doi.org/10.1007/s40265-014-0264-y.

(309) Neviani, P.; Santhanam, R.; Oaks, J. J.; Eiring, A. M.; Notari, M.; Blaser, B. W.; Liu, S.; Trotta, R.; Muthusamy, N.; Gambacorti-Passerini, C.; Druker, B. J.; Cortes, J.; Marcucci, G.; Chen, C.-S.; Verrills, N. M.; Roy, D. C.; Caligiuri, M. A.; Bloomfield, C. D.; Byrd, J. C.; Perrotti, D. FTY720, a New Alternative for Treating Blast Crisis Chronic Myelogenous Leukemia and Philadelphia Chromosome-Positive Acute Lymphocytic Leukemia. *J. Clin. Invest.* **2007**, *117*, 2408–2421. https://doi.org/10.1172/JCI31095.

(310) Azuma, H.; Takahara, S.; Horie, S.; Muto, S.; Otsuki, Y.; Katsuoka, Y. Induction of Apoptosis in Human Bladder Cancer Cells in Vitro and in Vivo Caused by FTY720 Treatment. *J. Urol.* **2003**, *169*, 2372–2377.

(311) Azuma, H.; Takahara, S.; Ichimaru, N.; Wang, J. D.; Itoh, Y.; Otsuki, Y.; Morimoto, J.; Fukui,

R.; Hoshiga, M.; Ishihara, T.; Nonomura, N.; Suzuki, S.; Okuyama, A.; Katsuoka, Y. Marked Prevention of Tumor Growth and Metastasis by a Novel Immunosuppressive Agent, FTY720, in Mouse Breast Cancer Models. *Cancer Res.* **2002**, *62*, 1410–1419.

(312) Sanna, M. G.; Liao, J.; Jo, E.; Alfonso, C.; Ahn, M.-Y.; Peterson, M. S.; Webb, B.; Lefebvre, S.; Chun, J.; Gray, N.; Rosen, H. Sphingosine 1-Phosphate (S1P) Receptor Subtypes S1P1 and S1P3, Respectively, Regulate Lymphocyte Recirculation and Heart Rate. *J. Biol. Chem.* **2004**, *279*, 13839–13848. https://doi.org/10.1074/jbc.M311743200.

(313) Kono, M.; Tucker, A. E.; Tran, J.; Bergner, J. B.; Turner, E. M.; Proia, R. L. Sphingosine-1-Phosphate Receptor 1 Reporter Mice Reveal Receptor Activation Sites in Vivo. *J. Clin. Invest.* **2014**, *124*, 2076–2086. https://doi.org/10.1172/JCI71194.

(314) Finicle, B. T.; Jayashankar, V.; Edinger, A. L. Nutrient Scavenging in Cancer. *Nat. Rev. Cancer* **2018**, *18*, 619–633. https://doi.org/10.1038/s41568-018-0048-x.

(315) Kubiniok, P.; Finicle, B. T.; Piffaretti, F.; McCracken, A. N.; Perryman, M.; Hanessian, S.; Edinger, A. L.; Thibault, P. Dynamic Phosphoproteomics Uncovers Signaling Pathways Modulated by Anti-Oncogenic Sphingolipid Analogs*□S. *Mol. Cell. Proteomics* **2019**, *18*, 408–422. https://doi.org/10.1074/mcp.RA118.001053.

(316) Garsi, J.-B.; Sernissi, L.; Vece, V.; Hanessian, S.; McCracken, A. N.; Simitian, G.; Edinger, A. L. In Search of Constrained FTY720 and Phytosphingosine Analogs as Dual Acting Anticancer Agents Targeting Metabolic and Epigenetic Pathways. *Eur. J. Med. Chem.* **2018**, *159*, 217–242. https://doi.org/10.1016/j.ejmech.2018.09.043.

(317) Brown, D. G.; Boström, J. Analysis of Past and Present Synthetic Methodologies on Medicinal Chemistry: Where Have All the New Reactions Gone? *J. Med. Chem.* **2016**, *59* (10), 4443–4458. https://doi.org/10.1021/acs.jmedchem.5b01409.

(318) Michaudel, Q.; Ishihara, Y.; Baran, P. S. Academia-Industry Symbiosis in Organic Chemistry. *Acc. Chem. Res.* **2015**, *48*, 712–721. https://doi.org/10.1021/ar500424a.

(319) Lovering, F.; Bikker, J.; Humblet, C. Escape from Flatland: Increasing Saturation as an Approach to Improving Clinical Success. *J. Med. Chem.* **2009**, *52*, 6752–6756.

https://doi.org/10.1021/jm901241e.

(320) Foley, D. J.; Nelson, A.; Marsden, S. P. Evaluating New Chemistry to Drive Molecular Discovery: Fit for Purpose? *Angew. Chemie - Int. Ed.* **2016**, *55*, 13650–13657. https://doi.org/10.1002/anie.201604193.

(321) Cox, B.; Booker-Milburn, K. I.; Elliott, L. D.; Robertson-Ralph, M.; Zdorichenko, V. Escaping from Flatland: [2 + 2] Photocycloaddition; Conformationally Constrained Sp3-Rich Scaffolds for Lead Generation. *ACS Med. Chem. Lett.* **2019**, *10*, 1512–1517. https://doi.org/10.1021/acsmedchemlett.9b00409.

(322) Vitaku, E.; Smith, D. T.; Njardarson, J. T. Analysis of the Structural Diversity, Substitution Patterns, and Frequency of Nitrogen Heterocycles among U.S. FDA Approved Pharmaceuticals. *J. Med. Chem.* **2014**, *57*, 10257–10274. https://doi.org/10.1021/jm501100b.

(323) Lenci, E.; Calugi, L.; Trabocchi, A. Occurrence of Morpholine in Central Nervous System Drug Discovery. *ACS Chem. Neurosci.* **2021**, *12*, 378–390. https://doi.org/10.1021/acschemneuro.0c00729.

(324) Kumari, A.; Singh, R. K. Morpholine as Ubiquitous Pharmacophore in Medicinal Chemistry: Deep Insight into the Structure-Activity Relationship (SAR). *Bioorg. Chem.* **2020**, *96*, 1–33. https://doi.org/10.1016/j.bioorg.2020.103578.

(325) Arshad, F.; Khan, M. F.; Akhtar, W.; Alam, M. M.; Nainwal, L. M.; Kaushik, S. K.; Akhter, M.; Parvez, S.; Hasan, S. M.; Shaquiquzzaman, M. Revealing Quinquennial Anticancer Journey of Morpholine: A SAR Based Review. *Eur. J. Med. Chem.* **2019**, *167*, 324–356. https://doi.org/10.1016/j.ejmech.2019.02.015.

(326) Kourounakis, A. P.; Xanthopoulos, D.; Tzara, A. Morpholine as a Privileged Structure: A Review on the Medicinal Chemistry and Pharmacological Activity of Morpholine Containing Bioactive Molecules. *Med. Res. Rev.* **2020**, *40*, 709–752. https://doi.org/10.1002/med.21634.

(327) Degorce, S. L.; Bodnarchuk, M. S.; Cumming, I. A.; Scott, J. S. Lowering Lipophilicity by

Adding Carbon: One-Carbon Bridges of Morpholines and Piperazines. *J. Med. Chem.* **2018**, *61*, 8934–8943. https://doi.org/10.1021/acs.jmedchem.8b01148.

(328) Komarov, I. V.; Grigorenko, A. O.; Turov, A. V.; Khilya, V. P. Conformationally Rigid Cyclic α-Amino Acids in the Design of Peptidomimetics, Peptide Models, and Biologically Active Compounds. *Russ. Chem. Rev.* **2004**, *73*, 785–810. https://doi.org/10.1070/rc2004v073n08abeh000912.

(329) Pasquier, B.; El-Ahmad, Y.; Filoche-Rommé, B.; Dureuil, C.; Fassy, F.; Abecassis, P.-Y.; Mathieu, M.; Bertrand, T.; Benard, T.; Barrière, C.; El Batti, S.; Letallec, J.-P.; Sonnefraud, V.; Brollo, M.; Delbarre, L.; Loyau, V.; Pilorge, F.; Bertin, L.; Richepin, P.; Arigon, J.; Labrosse, J. R.; Clément, J.; Durand, F.; Combet, R.; Perraut, P.; Leroy, V.; Gay, F.; Lefrançois, D.; Bretin, F.; Marquette, J. P.; Michot, N.; Caron, A.; Castell, C.; Schio, L.; McCort, G.; Goulaouic, H.; Garcia-Echeverria, C.; Ronan, B. Discovery of (2 S)-8-[(3 R)-3-Methylmorpholin-4-yl]-1-(3-methyl-2-oxobutyl)-2-(trifluoromethyl)-3,4-dihydro-2 H -pyrimido[1,2-a]pyrimidin-6-one: A Novel Potent and Selective Inhibitor of Vps34 for the Treatment of Solid Tumors. *J. Med. Chem.* **2015**, *58*, 376–400. https://doi.org/10.1021/jm5013352.

(330) Zask, A.; Verheijen, J. C.; Richard, D. J.; Kaplan, J.; Curran, K.; Toral-Barza, L.; Lucas, J.; Hollander, I.; Yu, K. Discovery of 2-Ureidophenyltriazines Bearing Bridged Morpholines as Potent and Selective ATP-Competitive MTOR Inhibitors. *Bioorganic Med. Chem. Lett.* **2010**, *20*, 2644–2647. https://doi.org/10.1016/j.bmcl.2010.02.045.

(331) Rageot, D.; Bohnacker, T.; Melone, A.; Langlois, J.-B.; Borsari, C.; Hillmann, P.; Sele, A. M.; Beaufils, F.; Zvelebil, M.; Hebeisen, P.; Löscher, W.; Burke, J.; Fabbro, D.; Wymann, M. P. Discovery and Preclinical Characterization of 5-[4,6-Bis({3-oxa-8-azabicyclo[3.2.1]octan-8-yl})-1,3,5-triazin-2-yl]-4-(difluoromethyl)pyridin-2-amine (PQR620), a Highly Potent and Selective MTORC1/2 Inhibitor for Cancer and Neurological Disorders. *J. Med. Chem.* **2018**, *61*, 10084–10105. https://doi.org/10.1021/acs.jmedchem.8b01262.

(332) Zask, A.; Kaplan, J.; Verheijen, J. C.; Richard, D. J.; Curran, K.; Brooijmans, N.; Bennett, E. M.; Toral-Barza, L.; Hollander, I.; Ayral-Kaloustian, S.; Yu, K. Morpholine Derivatives Greatly

Enhance the Selectivity of Mammalian Target of Rapamycin (MTOR) Inhibitors. *J. Med. Chem.* **2009**, *52*, 7942–7945. https://doi.org/10.1021/jm901415x.

(333) Cecere, G.; Galley, G.; Hu, Y.; Norcross, R.; Pflieger, P.; Shen, H. 5-Oxa-2-azabicyclo[2.2.2]octan-4-yl and 5-Oxa-2-azabicyclo[2.2.1]heptan-4-yl Derivatives as TAAR1 Modulators. WO 2015181061 A1, 2015.

(334) Davenport, A. J.; Braeuer, N.; Fischer, O. M.; Rotgeri, A.; Rottmann, A.; Neagoe, I.; Nagel, J.; Godin-Ho-Coelho, A.-M. 1, 3-Thiazol-2-yl Substituted Benzamides. WO 2016091776 A1, 2016.

(335) Lynch, R.; Cansfield, A. D.; Hardy, D. P.; Feutrill, J. T.; Adrego, R.; Ellard, K.; Ladduwahetty, T. Morpholino Substituted Bicyclic Pyrimidine Urea or Carbamate Derivatives as MTOR Inhibitors. WO 2013050508 A1, 2013.

(336) Fabbro, D.; Hebeisen, P.; Hillmann-Wuellner, P.; Stuetz, A.; Seykora, John, T.; Beaufils, F. Treatment of Skin Lesions. WO 2017198347 A1, 2017.

(337) Deidda, G.; Bozarth, I. F.; Cancedda, L. Modulation of GABAergic Transmission in Development and Neurodevelopmental Disorders: Investigating Physiology and Pathology to Gain Therapeutic Perspectives. *Front. Cell. Neurosci.* **2014**, *8*, 1–23. https://doi.org/10.3389/fncel.2014.00119.

(338) Braat, S.; Kooy, R. F. The GABAA Receptor as a Therapeutic Target for Neurodevelopmental Disorders. *Neuron* **2015**, *86*, 1119–1130. https://doi.org/10.1016/j.neuron.2015.03.042.

(339) Bettler, B.; Kaupmann, K.; Mosbacher, J.; Gassmann, M. Molecular Structure and Physiological Functions of GABAB Receptors. *Physiol. Rev.* **2004**, *84*, 835–867. https://doi.org/10.1152/physrev.00036.2003.

(340) Sarto-Jackson, I.; Sieghart, W. Assembly of GABAA Receptors (Review). *Mol. Membr. Biol.* **2008**, *25*, 302–310. https://doi.org/10.1080/09687680801914516.

(341) Evenseth, L. S. M.; Gabrielsen, M.; Sylte, I. The GABAB Receptor—Structure, Ligand Binding and Drug Development. *Molecules* **2020**, *25*, 1–19.

https://doi.org/10.4324/9780429320712-13.

(342) Zhang, D.; Pan, Z.-H.; Awobuluyi, M.; Lipton, S. A. Structure and Function of GABAC Receptors: A Comparison of Native versus Recombinant Receptors. *Trends Pharmacol. Sci.* **2001**, *22*, 121–132. https://doi.org/10.1016/S0165-6147(00)01625-4.

(343) Enz, R.; Cutting, G. R. Molecular Composition of GABA(C) Receptors. *Vision Res.* **1998**, *38*, 1431–1441. https://doi.org/10.1016/S0042-6989(97)00277-0.

(344) Chebib, M.; Johnston, G. A. R. The "ABC" of GABA Receptors: A Brief Review. *Clin. Exp. Pharmacol. Physiol.* **1999**, *26*, 937–940. https://doi.org/10.1046/j.1440-1681.1999.03151.x.

(345) Froestl, W. GABA Receptors. *Biotrend Rev.* **2011**, *7*, 1–15.

(346) Froestl, W. An Historical Perspective on GABAergic Drugs. *Future Med. Chem.* **2011**, *3*, 163–175.

(347) Brown, K. M.; Roy, K. K.; Hockerman, G. H.; Doerksen, R. J.; Colby, D. A. Activation of the γ-Aminobutyric Acid Type B (GABAB) Receptor by Agonists and Positive Allosteric Modulators. *J. Med. Chem.* **2015**, *58*, 6336–6347. https://doi.org/10.1021/jm5018913.

(348) Rudolph, U.; Knoflach, F. Beyond Classical Benzodiazepines: Novel Therapeutic Potential of GABA A Receptor Subtypes. *Nat. Rev. Drug Discov.* **2011**, *10*, 685–697. https://doi.org/10.1038/nrd3502.

(349) Bartholini, G. GABA Receptor Agonists: Pharmacological Spectrum and Therapeutic Actions. *Med. Res. Rev.* **1985**, *5*, 55–75. https://doi.org/10.1002/med.2610050103.

(350) Qiu, J.; Pingsterhaus, J. M.; Silverman, R. B. Inhibition and Substrate Activity of Conformationally Rigid Vigabatrin Analogues with γ-Aminobutyric Acid Aminotransferase. *J. Med. Chem.* **1999**, *42*, 4725–4728. https://doi.org/10.1021/jm990271o.

(351) Mann, A.; Boulanger, T.; Brandau, B.; Durant, F.; Evrard, G.; Heaulme, M.; Desaulles, E.; Wermuth, C. G. Synthesis and Biochemical Evaluation of Baclofen Analogues Locked in the Baclofen Solid-State Conformation. *J. Med. Chem.* **1991**, *34*, 1307–1313.

https://doi.org/10.1021/jm00108a011.

(352) Qiu, J.; Silverman, R. B. A New Class of Conformationally Rigid Analogues of 4-Amino-5-Halopentanoic Acids, Potent Inactivators of γ-Aminobutyric Acid Aminotransferase. *J. Med. Chem.* **2000**, *43*, 706–720. https://doi.org/10.1021/jm9904755.

(353) Shuto, S.; Shibuya, N.; Yamada, S.; Ohkura, T.; Kimura, R.; Matsuda, A. Synthesis of Conformationally Restricted Analogs of Baclofen, a Potent GABAB Receptor Agonist, by the Introduction of a Cyclopropane Ring. *Chem. Pharm. Bull.* **1991**, *47*, 1188–1192.

(354) Melnykov, K. P.; Volochnyuk, D. M.; Ryabukhin, S. V.; Rusanov, E. B.; Grygorenko, O. O. A Conformationally Restricted GABA Analogue Based on Octahydro-1H-Cyclopenta[b]Pyridine Scaffold. *Amino Acids* **2019**, *51*, 255–261. https://doi.org/10.1007/s00726-018-2660-1.

(355) Chebib, M.; Duke, R. K.; Allan, R. D.; Johnston, G. A. R. The Effects of Cyclopentane and Cyclopentene Analogues of GABA at Recombinant GABAC Receptors. *Eur. J. Pharmacol.* **2001**, *430*, 185–192. https://doi.org/10.1016/S0014-2999(01)01390-5.

(356) Bolser, D. C.; Blythin, D. J.; Chapman, R. W.; Egan, R. W.; Hey, J. A.; Rizzo, C.; Kuo, S.-C.; Kreutner, W. The Pharmacology of SCH 50911 : A Novel, Orally-Active GABA-B Receptor Antagonist. *J. Pharmacol. Exp. Ther.* **1995**, *274*, 1393–1398.

(357) Witiak, D. T.; Patch, R. J.; Enna, S. J.; Fung, Y. K. Stereoselective Syntheses of the Trans-Decahydroquinoline-5-carboxylic Acid Epimers. Diastereomeric Zwitterionic Probes of γ-Aminobutyric Acid Related Biological Properties in Vitro and in Vivo. *J. Med. Chem* **1986**, *29*, 1–8.

(358) Kobayashi, T.; Suemasa, A.; Igawa, A.; Ide, S.; Fukuda, H.; Abe, H.; Arisawa, M.; Minami, M.; Shuto, S. Conformationally Restricted GABA with Bicyclo[3.1.0]hexane Backbone as the First Highly Selective BGT-1 Inhibitor. *ACS Med. Chem. Lett.* **2014**, *5*, 889–893. https://doi.org/10.1021/ml500134k.

(359) Steffan, T.; Renukappa-Gutke, T.; Höfner, G.; Wanner, K. T. Design, Synthesis and SAR Studies of GABA Uptake Inhibitors Derived from 2-Substituted Pyrrolidine-2-yl-acetic Acids.

Bioorganic Med. Chem. **2015**, *23*, 1284–1306. https://doi.org/10.1016/j.bmc.2015.01.035.

(360) Nakada, K.; Yoshikawa, M.; Ide, S.; Suemasa, A.; Kawamura, S.; Kobayashi, T.; Masuda, E.; Ito, Y.; Hayakawa, W.; Katayama, T.; Yamada, S.; Arisawa, M.; Minami, M.; Shuto, S. Cyclopropane-Based Conformational Restriction of GABA by a Stereochemical Diversity-Oriented Strategy: Identification of an Efficient Lead for Potent Inhibitors of GABA Transports. *Bioorganic Med. Chem.* **2013**, *21*, 4938–4950. https://doi.org/10.1016/j.bmc.2013.06.063.

(361) Geng, Y.; Bush, M.; Mosyak, L.; Wang, F.; Fan, Q. R. Structural Mechanism of Ligand Activation in Human GABA B Receptor. *Nature* **2013**, *504*, 254–259. https://doi.org/10.1038/nature12725.

(362) Woll, M. G.; Lai, J. R.; Guzei, I. A.; Taylor, S. J. C.; Smith, M. E. B.; Gellman, S. H. Parallel Sheet Secondary Structure in γ -Peptides. *J Am Chem Soc* **2001**, *123*, 11077–11078.

(363) Casiraghi, G.; Rassu, G.; Auzzas, L.; Burreddu, P.; Gaetani, E.; Battistini, L.; Zanardi, F.; Curti, C.; Nicastro, G.; Belvisi, L.; Motto, I.; Castorina, M.; Giannini, G.; Pisano, C. Grafting Aminocyclopentane Carboxylic Acids onto the RGD Tripeptide Sequence Generates Low Nanomolar Avβ3/ Avβ5 Integrin Dual Binders. *J. Med. Chem.* **2005**, *48*, 7675–7687. https://doi.org/10.1021/jm050698x.

(364) Portoghese, P. S.; Turcotte, J. G. Bicyclic Bases: Synthesis and Nuclear Magnetic Resonance Investigation of Some Chiral 2-Oxa-5-azabicyclo[2.2.1]heptane Derivatives. *Tetrahedron* **1971**, *27*, 961–967. https://doi.org/10.1016/S0040-4020(01)92495-0.

(365) Yan, Z.; Wang, J.; Tian, W. A Concise Total Synthesis of (-)-Dehydroclausenamide Utilizing the Novel Formation of Cis-Epoxide as the Key Step. *Tetrahedron Lett.* **2003**, *44*, 9383–9384. https://doi.org/10.1016/j.tetlet.2003.09.229.

(366) Ma, Z.; Hu, H.; Xiong, W.; Zhai, H. Formal Syntheses of (-)- and (+)-Aphanorphine from (2S,4R)-4-Hydroxyproline. *Tetrahedron* **2007**, *63*, 7523–7531. https://doi.org/10.1016/j.tet.2007.05.059.

(367) Taylor, R. D.; Maccoss, M.; Lawson, A. D. G. Rings in Drugs. *J. Med. Chem.* **2014**, *57*, 5845–

5859. https://doi.org/10.1021/jm4017625.

(368) Malojcic, G.; Daniels, Matthew, H.; Williams, Brett, D.; Yu, M.; Ledeboer, Mark, W.; Harmange, Jean-Christophe, P.; Wang, Jenna, L. Substituted 1,6-Naphthyridine Inhibitors of CDK5. WO 2022011274 A1, 2022.

(369) Wang, Y. Y.; Bode, J. W. Olefin Amine (OLA) Reagents for the Synthesis of Bridged Bicyclic and Spirocyclic Saturated N-Heterocycles by Catalytic Hydrogen Atom Transfer (HAT) Reactions. *J. Am. Chem. Soc.* **2019**, *141*, 9739–9745. https://doi.org/10.1021/jacs.9b05074.

(370) Lux, M. C.; Jurczyk, J.; Lam, Y.-H.; Song, Z. J.; Ma, C.; Roque, J. B.; Ham, J. S.; Sciammetta, N.; Adpressa, D.; Sarpong, R.; Yeung, C. S. Synthesis of Bridged Bicyclic Amines by Intramolecular Amination of Remote C-H Bonds: Synergistic Activation by Light and Heat. *Org. Lett.* **2020**, *22*, 6578–6583. https://doi.org/10.1021/acs.orglett.0c02345.

(371) Walker, D. P.; Eklov, B. M.; Bedore, M. W. Practical Synthesis of 3-Oxa-6-azabicyclo[3.1.1]heptane Hydrotosylate; A Novel Morpholine-Based Building Block. *Synthesis (Stuttg).* **2012**, *44*, 2859–2862. https://doi.org/10.1055/s-0032-1316748.

(372) Zaytsev, A. V.; Pickles, J. E.; Harnor, S. J.; Henderson, A. P.; Alyasiri, M.; Waddell, P. G.; Cano, C.; Griffin, R. J.; Golding, B. T. Concise Syntheses of Bridged Morpholines. *RSC Adv.* **2016**, *6*, 53955–53957. https://doi.org/10.1039/c6ra08737j.

(373) Venkatesan, A. M.; Chen, Z.; Dos Santos, O.; Dehnhardt, C.; Santos, E. D.; Ayral-Kaloustian, S.; Mallon, R.; Hollander, I.; Feldberg, L.; Lucas, J.; Yu, K.; Chaudhary, I.; Mansour, T. S. PKI-179: An Orally Efficacious Dual Phosphatidylinositol-3-Kinase (PI3K)/Mammalian Target of Rapamycin (MTOR) Inhibitor. *Bioorganic Med. Chem. Lett.* **2010**, *20*, 5869–5873. https://doi.org/10.1016/j.bmcl.2010.07.104.

(374) Hocine, S.; Berger, G.; Hanessian, S. Design and Synthesis of Backbone-Fused, Conformationally Constrained Morpholine-Proline Chimeras. *J. Org. Chem.* **2020**, *85*, 4237–4247. https://doi.org/10.1021/acs.joc.9b03413.

(375) Aldeghi, M.; Malhotra, S.; Selwood, D. L.; Chan, A. W. E. Two- and Three-Dimensional Rings in Drugs. *Chem. Biol. Drug Des.* **2014**, *83*, 450–461. https://doi.org/10.1111/cbdd.12260.

(376) Cox, B.; Duffy, J.; Zdorichenko, V.; Bellanger, C.; Hurcum, J.; Laleu, B.; Booker-Milburn, K. I.; Elliott, L. D.; Robertson-Ralph, M.; Swain, C. J.; Bishop, S. J.; Hallyburton, I.; Anderson, M. Escaping from Flatland: Antimalarial Activity of sp3-Rich Bridged Pyrrolidine Derivatives. *ACS Med. Chem. Lett.* **2020**, *11*, 2497–2503. https://doi.org/10.1021/acsmedchemlett.0c00486.

(377) Norcross, R.; Galley, G.; Cecere, G.; Pflieger, P.; Shen, H.; Hu, Y. 2-Oxa-5-azabicyclo[2.2.1]heptan-3-yl Derivatives. WO 2016015333 A1, 2016.

(378) Engin, E.; Benham, R. S.; Rudolph, U. An Emerging Circuit Pharmacology of GABAA Receptors. *Trends Pharmacol. Sci.* **2018**, *39*, 710–732. https://doi.org/10.1016/j.tips.2018.04.003.

(379) Owens, D. F.; Kriegstein, A. R. Is There More to GABA than Synaptic Inhibition? *Nat. Rev. Neurosci.* **2002**, *3*, 715–727. https://doi.org/10.1038/nrn919.

(380) Borden, L. A. GABA Transporter Heterogeneity: Pharmacology and Cellular Localization. *Neurochem. Int.* **1996**, *29*, 335–356. https://doi.org/10.1016/0197-0186(95)00158-1.

(381) Farrant, M.; Nusser, Z. Variations on an Inhibitory Theme: Phasic and Tonic Activation of GABA A Receptors. *Nat. Rev. Neurosci.* **2005**, *6*, 215–229. https://doi.org/10.1038/nrn1625.

(382) Ngo, D. H.; Vo, T. S. An Updated Review on Pharmaceutical Properties of Gamma-Aminobutyric Acid. *Molecules* **2019**, *24*, 1–23. https://doi.org/10.3390/molecules24152678.

(383) Kerr, D. I. .; Ong, J. Metabotropic GABAB Receptors: New Challenges in Drug Design. *Curr. Med. Chem. Nerv. Syst. Agents* **2001**, *1*, 27–42. https://doi.org/10.2174/1568015013358653.

(384) Taylor, C. P.; Angelotti, T.; Fauman, E. Pharmacology and Mechanism of Action of Pregabalin: The Calcium Channel A2-δ (Alpha2-Delta) Subunit as a Target for Antiepileptic Drug Discovery. *Epilepsy Res.* **2007**, *73*, 137–150. https://doi.org/10.1016/j.eplepsyres.2006.09.008.

(385) Kent, C. N.; Park, C.; Lindsley, C. W. Classics in Chemical Neuroscience: Baclofen. *ACS Chem. Neurosci.* **2020**, *11*, 1740–1755. https://doi.org/10.1021/acschemneuro.0c00254.

(386) Herdeis, C.; Hubmann, H. P. Synthesis of Homochiral R-Baclofen from S-Glutamic Acid. *Tetrahedron: Asymmetry* **1992**, *3*, 1213–1221. https://doi.org/10.1016/S0957-4166(00)82107-2.

(387) Hayashi, Y.; Sakamoto, D.; Okamura, D. One-Pot Synthesis of (S)-Baclofen via Aldol Condensation of Acetaldehyde with Diphenylprolinol Silyl Ether Mediated Asymmetric Michael Reaction as a Key Step. *Org. Lett.* **2016**, *18*, 4–7. https://doi.org/10.1021/acs.orglett.5b02839.

(388) Attia, M. I.; Herdeis, C.; Bräuner-Osborne, H. GABAB-Agonistic Activity of Certain Baclofen Homologues. *Molecules* **2013**, *18*, 10266–10284. https://doi.org/10.3390/molecules180910266.

(389) Yashin, N. V.; Chmovzh, T. N.; Averina, E. B.; Kuznetsova, T. S.; Zefirov, N. S. Synthesis of Conformationally Restricted Analogs of γ-Aminobutyric Acid. *Rev. J. Chem.* **2014**, *4*, 253–275. https://doi.org/10.1134/s2079978014040049.

(390) Field, M. J.; Li, Z.; Schwarz, J. B. Ca2+ Channel A2-δ Ligands for the Treatment of Neuropathic Pain. *J. Med. Chem.* **2007**, *50*, 2569–2575. https://doi.org/10.1021/jm060650z.

(391) Naumenko, A. M.; Shapoval, L. M.; Nyporko, A. Y.; Voiteshenko, M. I.; Tsymbalyuk, A. V.; Sagach, V. F.; Davydovska, T. L. Computer Simulation of Molecular Interaction between Baclofen and the GABAB Receptor. *Neurophysiology* **2017**, *49*, 2–7. https://doi.org/10.1007/s11062-017-9623-0.

(392) Bernard, P.; Guedin, D.; Hibert, M. Molecular Modeling of the GABA/GABAB Receptor Complex. *J. Med. Chem.* **2001**, *44*, 27–35. https://doi.org/10.1021/jm000915o.

(393) Zhang, Y. M.; Peng, X. J.; Hu, L. H.; Wang, X.; Dong, J. C.; Wu, H.; Ma, R. J.; Chen, S. H. 3-Trifluoromethyl-5-tert-butoxycarbonyl-2,5-(two heterobicyclic rings)[2.2.1]heptane and Preparation Method. CN 10216770 A, 2010.

(394) Kou, B.; Zhu, W.; Liu, H.; Shen, H. C.; Wu, J.; Hu, T. Synthesis of Bridged Bicyclic Morpholine Amino Acids as Compact Modules for Medicinal Chemistry. *Chem. Lett.* **2017**, *46*, 566–568. https://doi.org/10.1246/cl.170011.

(395) Portoghese, P. S.; Sepp, D. T. Bicyclic Base (1,2). Ambident Anions as Intramolecular Nucleophiles in the Formation of 2-Oxa-5-azabicyclo[2.2.1]heptane Derivatives. *J. Heterocycl. Chem.* **1971**, *8*, 531–535.

(396) Toda, N.; Ori, M.; Takami, K.; Tago, K.; Kogen, H. Total Synthesis of (+)-Benzastatin E via Diastereoselective Grignard Addition to 2-Acylindoline. *Org. Lett.* **2003**, *5*, 269–271. https://doi.org/10.1021/ol027215t.

(397) Wei, H.; Qiao, C.; Liu, G.; Yang, Z.; Li, C. Stereoselective Total Syntheses of (-)-Flueggine A and (+)-Virosaine B. *Angew. Chemie - Int. Ed.* **2013**, *52*, 620–624. https://doi.org/10.1002/anie.201208261.

(398) Gunasekaran, K.; Ramakrishnan, C.; Balaram, P. β-Hairpins in Proteins Revisited: Lessons for de Novo Design. *Protein Eng.* **1997**, *10*, 1131–1141. https://doi.org/10.1093/protein/10.10.1131.

(399) Yarava, J. R.; Nishiyama, Y.; Raghothama, S.; Ramanathan, K. V. Conformational Investigation of Peptides Using Solid-State NMR Spectroscopy—A Study of Polymorphism of β-Turn Peptides Containing Diprolines. *Chem. Biol. Drug Des.* **2020**, *95*, 394–407. https://doi.org/10.1111/cbdd.13649.

(400) Andreotti, A. H. Native State Proline Isomerization: An Intrinsic Molecular Switch. *Biochemistry* **2003**, *42*, 9515–9524. https://doi.org/10.1021/bi0350710.

(401) Sarkar, P.; Reichman, C.; Saleh, T.; Birge, R. B.; Kalodimos, C. G. Proline Cis-Trans Isomerization Controls Autoinhibition of a Signaling Protein. *Mol. Cell* **2007**, *25*, 413–426. https://doi.org/10.1016/j.molcel.2007.01.004.

(402) Kay, B. K.; Williamson, M. P.; Sudol, M. The Importance of Being Proline: The Interaction of Proline-Rich Motifs in Signaling Proteins with Their Cognate Domains. *FASEB J.* **2000**, *14*, 231–241. https://doi.org/10.1096/fasebj.14.2.231.

(403) Hensbergen, P. J.; Klychnikov, O. I.; Bakker, D.; Dragan, I.; Kelly, M. L.; Minton, N. P.; Corver, J.; Kuijper, E. J.; Drijfhout, J. W.; Van Leeuwen, H. C. Clostridium Difficile Secreted Pro-Pro Endopeptidase PPEP-1 (ZMP1/CD2830) Modulates Adhesion through Cleavage of the Collagen Binding Protein CD2831. *FEBS Lett.* **2015**, *589*, 3952–3958. https://doi.org/10.1016/j.febslet.2015.10.027.

(404) Schacherl, M.; Pichlo, C.; Neundorf, I.; Baumann, U. Structural Basis of Proline-Proline Peptide Bond Specificity of the Metalloprotease Zmp1 Implicated in Motility of Clostridium Difficile. *Structure* **2015**, *23*, 1632–1642. https://doi.org/10.1016/j.str.2015.06.018.

(405) Ventola, C. L. The Antibiotic Resistance Crisis. *Pharm. Ther.* **2015**, *40*, 277–283. https://doi.org/10.1016/B978-1-4831-9711-1.50022-3.

(406) Aslam, B.; Wang, W.; Arshad, M. I.; Khurshid, M.; Muzammil, S.; Rasool, M. H.; Nisar, M. A.; Aslam, M. A.; Qamar, M. U.; Salamat, M. K. F.; Baloch, Z. Antibiotic Resistance: A Rundown of a Global Crisis. *Infect. Drug Resist.* **2018**, *11*, 1645–1658.

(407) Dai, N.; Wang, X. J.; Etzkorn, F. A. The Effect of a Trans-Locked Gly-Pro Alkene Isostere on Collagen Triple Helix Stability. *J. Am. Chem. Soc.* **2008**, *130*, 5396–5397. https://doi.org/10.1021/ja711021m.

(408) Vasta, J. D.; Choudhary, A.; Jensen, K. H.; McGrath, N. A.; Raines, R. T. Prolyl 4-Hydroxylase: Substrate Isosteres in Which an (E)- or (Z)-Alkene Replaces the Prolyl Peptide Bond. *Biochemistry* **2017**, *56*, 219–227. https://doi.org/10.1021/acs.biochem.6b00976.

(409) Martin, J. L.; Begun, J.; Schindeler, A.; Wickramasinghe, W. A.; Alewood, D.; Alewood, P. F.; Bergman, D. A.; Brinkworth, R. I.; Abbenante, G.; March, D. R.; Reid, R. C.; Fairlie, D. P. Molecular Recognition of Macrocyclic Peptidomimetic Inhibitors by HIV-1 Protease. *Biochemistry* **1999**, *38*, 7978–7988. https://doi.org/10.1021/bi990174x.

(410) Hong, L.; Treharne, A.; Hartsuck, J. A.; Foundling, S.; Tang, J. Crystal Structures of Complexes of a Peptidic Inhibitor with Wild-Type and Two Mutant HIV-1 Proteases. *Biochemistry* **1996**, *35*, 10627–10633. https://doi.org/10.1021/bi960481s.

(411) Tie, Y.; Boross, P. I.; Wang, Y.-F.; Gaddis, L.; Hussain, A. K.; Leshchenko, S.; Ghosh, A. K.;

Louis, J. M.; Harrison, R. W.; Weber, I. T. High Resolution Crystal Structures of HIV-1 Protease with a Potent Non-Peptide Inhibitor (UIC-94017) Active against Multi-Drug-Resistant Clinical Strains. *J. Mol. Biol.* **2004**, *338*, 341–352. https://doi.org/10.1016/j.jmb.2004.02.052.

(412) Yedidi, R. S.; Liu, Z.; Wang, Y.; Brunzelle, J. S.; Kovari, I. A.; Woster, P. M.; Kovari, L. C.; Gupta, D. Crystal Structures of Multidrug-Resistant HIV-1 Protease in Complex with Two Potent Anti-Malarial Compounds. *Biochem. Biophys. Res. Commun.* **2012**, *421*, 413–417. https://doi.org/10.1016/j.bbrc.2012.03.096.

(413) Mager, P. P. The Active Site of HIV-1 Protease. *Med. Res.* **2001**, *21*, 348–353.

(414) Vidal, P.; Timm, D.; Broughton, H.; Chen, S.-H.; Martín, J. A.; Rivera-Sagredo, A.; McCarthy, J. R.; Shapiro, M. J.; Espinosa, J. F. Preorganization of the Hydroxyethylene Dipeptide Isostere: The Preferred Conformation in Solution Resembles the Conformation Bound to BACE. *J. Med. Chem.* **2005**, *48*, 7623–7627. https://doi.org/10.1021/jm050631+.

(415) Lama, T.; Del Valle, S. E.; Genest, N.; Lubell, W. D. Alcohols as Replacements of the Central Amide in β-Turns, Synthesis of Pro-Aib Hydroxyethylene Isostere and Analysis in Model β-Turn Peptides. *Int. J. Pept. Res. Ther.* **2007**, *13*, 355–366. https://doi.org/10.1007/s10989-007-9093-0.

(416) Reuter, C.; Kleczka, M.; De Mazancourt, S.; Neudörfl, J. M.; Kühne, R.; Schmalz, H. G. Stereoselective Synthesis of Proline-Derived Dipeptide Scaffolds (Prom-3 and Prom-7) Rigidified in a PPII Helix Conformation. *European J. Org. Chem.* **2014**, 2664–2667. https://doi.org/10.1002/ejoc.201301875.

(417) Reuter, C.; Opitz, R.; Soicke, A.; Dohmen, S.; Barone, M.; Chiha, S.; Klein, M. T.; Neudörfl, J.-M.; Kühne, R.; Schmalz, H.-G. Design and Stereoselective Synthesis of ProM-2: A Spirocyclic Diproline Mimetic with Polyproline Type II (PPII) Helix Conformation. *Chem. - A Eur. J.* **2015**, *21*, 8464–8470. https://doi.org/10.1002/chem.201406493.

(418) Berg, J. M.; Tymoczko, J. L.; Stryer, L. *Biochemistry. 5th Edition.*; New York: W H Freeman., 2002.

(419) Vanhoof, G.; Goossens, F.; De Meester, I.; Hendriks, D.; Scharpé, S. Proline Motifs in Peptides and Their Biological Processing. *FASEB J.* **1995**, *9*, 736–744.

(420) Etzkorn, F. A.; Ware, R. I.; Pester, A. M.; Troya, D. Conformational Analysis of N→π∗ Interactions in Collagen Triple Helix Models. *J. Phys. Chem. B* **2019**, *123*, 496–503. https://doi.org/10.1021/acs.jpcb.8b08384.

(421) Todd, P. A.; Heel, R. C. Enalapril. A Review of Its Pharmacodynamic and Pharmacokinetic Properties, and Therapeutic Use in Hypertension and Congestive Heart Failure. *Drugs* **1986**, *31*, 198–248. https://doi.org/10.1016/B978-008055232-3.61678-2.

(422) Frampton, J. E.; Peters, D. H. Ramipril: An Updated Review of Its Therapeutic Use in Essential Hypertension and Heart Failure. *Drugs* **1995**, *49*, 440–466. https://doi.org/10.2165/00003495-199549030-00008.

(423) Keating, G. M. Vildagliptin : A Review of Its Use in Type 2 Diabetes Mellitus. *Drugs* **2014**, *74* (5), 587–610. https://doi.org/10.1007/s40265-014-0199-3.

(424) Konno, K.; Hashimoto, K.; Ohfune, Y.; Shirahama, H.; Matsumoto, T. Acromelic Acids A and B. Potent Neuroexcitatory Amino Acids Isolated from Clitocybe Acromelalga. *J. Am. Chem. Soc.* **1988**, *110*, 4807–4815. https://doi.org/10.1021/ja00222a044.

(425) Moloney, M. G. Excitatory Amino Acids. *Nat. Prod. Rep.* **1998**, 205–219. https://doi.org/10.1016/B978-012373947-6.00151-3.

(426) Mauger, A. B. Naturally Occurring Proline Analogues. *J. Nat. Prod.* **1996**, *59*, 1205–1211. https://doi.org/10.1021/np9603479.

(427) Williamson, M. P. The Structure and Function of Proline-Rich Regions in Proteins. *Biochem. J.* **1994**, *297*, 249–260. https://doi.org/10.1042/bj2970249.

(428) Holt, M. R.; Koffer, A. Cell Motility: Proline-Rich Proteins Promote Protrusions. *Trends Cell Biol.* **2001**, *11*, 38–46. https://doi.org/10.1016/S0962-8924(00)01876-6.

(429) Chow, W. Y.; Forman, C. J.; Bihan, D.; Puszkarska, A. M.; Rajan, R.; Reid, D. G.; Slatter, D. A.; Colwell, L. J.; Wales, D. J.; Farndale, R. W.; Duer, M. J. Proline Provides Site-Specific

Flexibility for in Vivo Collagen. *Sci. Rep.* **2018**, *8*, 1–13. https://doi.org/10.1038/s41598-018-31937-x.

(430) Karna, E.; Szoka, L.; Huynh, T. Y. L.; Palka, J. A. Proline-Dependent Regulation of Collagen Metabolism. *Cell. Mol. Life Sci.* **2020**, *77*, 1911–1918. https://doi.org/10.1007/s00018-019-03363-3.

(431) Siligardi, G.; Drake, A. F. The Importance of Extended Conformations and, in Particular, the Pll Conformation for the Molecular Recognition of Peptides. *Biopolymers* **1995**, *37*, 281–292.

(432) Nguyen, J. T.; Turck, C. W.; Cohen, F. E.; Zuckermann, R. N.; Lim, W. A. Exploiting the Basis of Proline Recognition by SH3 and WW Domains: Design of N-Substituted Inhibitors. *Science.* **1998**, *282* (5396), 2088–2092. https://doi.org/10.1126/science.282.5396.2088.

(433) Cunningham, A. D.; Qvit, N.; Mochly-Rosen, D.; Opin Struct Biol Author manuscript, C. PM for PPI 1 - Peptides and Peptidomimetics as Regulators of Protein-Protein Interactions HHS Public Access Author Manuscript. *Curr Opin Struct Biol* **2017**, *44*, 59–66. https://doi.org/10.1016/j.sbi.2016.12.009.

(434) Hanko, R.; Rabe, K.; Dally, R.; Hoppe, D. Stereoselektive Synthese von Cyclischen N,N-dialkylcarbamidsäure-2-alkenylester. *Angew. Chemie* **1991**, *12*, 1725–1727. https://doi.org/https://doi.org/10.1002/ange.19911031242.

(435) Turbanti, L.; Cerbai, G.; Di Bugno, C.; Giorgi, R.; Garzelli, G.; Criscuoli, M.; Renzetti, A. R.; Subissi, A.; Bramanti, G.; Depriest, S. A. 1,2-Cyclomethylenecarboxylic Monoamide Hydroxamic Derivatives. A Novel Class of Non-Amino Acid Angiotensin Converting Enzyme Inhibitors. *J. Med. Chem.* **1993**, *36*, 699–707.

(436) Sample, J. E.; Rowley, D. C.; Brunck, T. K.; Ripka, W. C. Synthesis and Biological Activity of P2-P4 Azapeptidomimetic P1-Argininal and P1-Ketoargininamide Derivatives: A Novel Class of Serine Protease Inhibitors. *Bioorganic Med. Chem. Lett.* **1997**, *7*, 315–320. https://doi.org/10.1016/S0960-894X(97)00005-X.

(437) Harmat, N. J. S.; Di Bugno, C.; Criscuoli, M.; Giorgi, R.; Lippi, A.; Martinelli, A.; Monti, S.;

Subissi, A. 1, 2-Disubstituted Cyclohexane Derived Tripeptide Aldehydes as Novel Selective Thrombin Inhibitors. *Bioorganic Med. Chem. Lett.* **1998**, *8*, 1249–1254. https://doi.org/10.1016/S0960-894X(98)00200-5.

(438) Wang, X. J.; Hart, S. A.; Xu, B.; Mason, M. D.; Goodell, J. R.; Etzkorn, F. A Serine-Cis-Proline and Serine-Trans-Proline Isosteres: Stereoselective Synthesis of (Z)- and (E)-Alkene Mimics by Still-Wittig and Ireland-Claisen Rearrangements. *J. Org. Chem.* **2003**, *68*, 2343–2349. https://doi.org/10.1021/jo026663b.

(439) Bandur, N. G.; Harms, K.; Koert, U. First Stereoselective Synthesis of a Pro-Pro E -Alkene Dipeptide Isostere. *Synlett* **2004**, *5*, 773–776. https://doi.org/10.1055/s-2005-863731.

(440) Soicke, A.; Reuter, C.; Winter, M.; Neudörfl, J.-M.; Schlörer, N.; Kühne, R.; Schmalz, H.-G. Stereoselective Synthesis of Tricyclic Diproline Analogues That Mimic a PPII Helix: Structural Consequences of Ring-Size Variation. *European J. Org. Chem.* **2014**, 6467–6480. https://doi.org/10.1002/ejoc.201402737.

(441) Maassen, A.; Gebauer, J. M.; Abraham, E. T.; Grimm, I.; Neudörfl, J.-M.; Kühne, R.; Neundorf, I.; Baumann, U.; Schmalz, H.-G. Triple-Helix-Stabilizing Effects in Collagen Model Peptides Containing PPII-Helix-Preorganized Diproline Modules. *Angew. Chemie - Int. Ed.* **2020**, *59*, 2–11. https://doi.org/10.1002/anie.201914101.

(442) Hanessian, S.; Yun, H.; Hou, Y.; Yang, G.; Bayrakdarian, M.; Therrien, E.; Moitessier, N.; Roggo, S.; Veenstra, S.; Tintelnot-Blomley, M.; Rondeau, J.-M.; Ostermeier, C.; Strauss, A.; Ramage, P.; Paganetti, P.; Neumann, U.; Betschart, C. Structure-Based Design, Synthesis, and Memapsin 2 (BACE) Inhibitory Activity of Carbocyclic and Heterocyclic Peptidomimetics. *J. Med. Chem.* **2005**, *48*, 5175–5190. https://doi.org/10.1021/jm050142+.

(443) Hanessian, S.; Moitessier, N.; Wilmouth, S. Tetrahydrofuran as a Scaffold for Peptidomimetics. Application to the Design and Synthesis of Conformationally Constrained Metalloproteinase Inhibitors. *Tetrahedron* **2000**, *56*, 7643–7660. https://doi.org/10.1016/S0040-4020(00)00687-6.

(444) Hanessian, S.; Yang, G.; Rondeau, J.-M.; Neumann, U.; Betschart, C.; Tintelnot-Blomley, M. Structure-Based Design and Synthesis of Macroheterocyclic Peptidomimetic Inhibitors of the Aspartic Protease β-Site Amyloid Precursor Protein Cleaving Enzyme (BACE). *J. Med. Chem.* **2006**, *49*, 4544–4567. https://doi.org/10.1021/jm060154a.

(445) Hanessian, S.; Chénard, E. A New Approach to the Synthesis of Peptidomimetic Renin Inhibitors: Palladium-Catalyzed Asymmetric Allylation of Acyclic Alkyl Aryl Ketones. *Org. Lett.* **2012**, *14* (12), 3222–3225. https://doi.org/10.1021/ol301332f.

(446) Klein, T.; Eckhard, U.; Dufour, A.; Solis, N.; Overall, C. M. Proteolytic Cleavage - Mechanisms, Function, and "Omic" Approaches for a Near-Ubiquitous Posttranslational Modification. *Chem. Rev.* **2018**, *118*, 1137–1168. https://doi.org/10.1021/acs.chemrev.7b00120.

(447) Hanessian, S.; Sumi, K. On the Stereochemical Divergence in the Conjugate Addition of Lithium Dimethylcuprate/Trimethylsilyl Chloride to γ-Alkoxy and γ-Ureido α,β-Unsaturated Esters. *Synthesis (Stuttg).* **1991**, 1083–1089.

(448) Hanessian, S.; Gai, Y.; Wang, W. Stereocontrolled Sequential Functionalization in Acyclic Systems by Exploiting Internal 1,2-Asymmetric Induction - Generation of Symmetry-Related Polypropionate and Related Motifs. *Tetrahedron Lett.* **1996**, *37*, 7473–7476. https://doi.org/10.1016/0040-4039(96)01754-6.

(449) Hanessian, S.; Ma, J.; Wang, W. One- and Two-Directional Iterative 1,2-Asymmetric Induction in Acyclic Systems - Easy Access to Anti,Anti and Anti,Syn Dipropionate and Diphenylacetate Stereotriads. *Tetrahedron Lett.* **1999**, *40*, 4627–4630. https://doi.org/10.1016/S0040-4039(99)00783-2.

(450) Hanessian, S.; Wang, W.; Gai, Y.; Olivier, E. A General and Stereocontrolled Strategy for the Iterative Assembly of Enantiopure Polypropionate Subunits: Synthesis of the C19-C28 Segment of Rifamycin S from a Single Chiron. *J. Am. Chem. Soc.* **1997**, *119*, 10034–10041. https://doi.org/10.1021/ja970251g.

(451) Boal, A. K.; Guryanov, I.; Moretto, A.; Crisma, M.; Lanni, E. L.; Toniolo, C.; Grubbs, R. H.; O'Leary, D. J. Facile and E-Selective Intramolecular Ring-Closing Metathesis Reactions in

310-Helical Peptides: A 3D Structural Study. *J. Am. Chem. Soc.* **2007**, *129*, 6986–6987. https://doi.org/10.1021/ja071148m.

(452) Meta, C. T.; Koide, K. Trans-Selective Conversions of γ-Hydroxy-α,β-alkynoic Esters to γ-Hydroxy-α,β-alkenoic Esters. *Org. Lett.* **2004**, *6*, 1785–1787. https://doi.org/10.1021/ol0495366.

(453) Yamamoto, Y.; Nishii, S.; Ibuka, T. Diastereoselectivity of Conjugate Addition to γ-Alkoxy-α,β-unsaturated Esters via Organocopper-Lewis Acids and Related Reagents. Importance of the Double Bond Geometry in Controlling the Selectivity. *Chem. Commun.* **1987**, 464–466.

(454) Dorigo, A. E.; Morokuma, K. Stereoselectivity of the Nucleophilic Addition of Organocopper Reagents to Chiral α, β-Unsaturated Carbonyl Compounds. Ab Initio Molecular Orbital Studies of Steric and Electronic Effects. *J. Am. Chem. Soc.* **1989**, *111*, 6524–6536. https://doi.org/10.1021/ja00199a008.

(455) Nicolaou, K. C.; Pavia, M. R.; Seitz, S. P. Synthesis of 16-Membered-Ring Marcolide Antibiotics. 4. Carbomycin B and Leucomycin A3: Total Synthesis of Cyclic Key Intermediate. *J. Am. Chem. Soc.* **1981**, *103* (5), 1224–1226.

(456) Roush, W. R.; Lesur, B. M. Stereochemistry of Vinyl Cuprate Additions to Carbohydrate-Derived Enones and α,β-Unsaturated Esters. *Tetrahedron Lett.* **1983**, *24*, 2231–2234.

(457) Jako, I.; Uibera, P.; Mann, A.; Taddei, M.; Wermuth, C.-G. Diastereoselectivity in Conjugate Addition of Alkylcuprates to Vinylogous Ester of N,O-Diprotected Serinal. *Tetrahedron Lett.* **1990**, *31* (7), 1011–1014. https://doi.org/10.1016/S0040-4039(00)94416-2.

(458) Jiang, S.; Kong, X.; Wang, C.; Zang, X.; Su, M.; Zheng, H.; Zhang, B.; Li, G.; Xie, H.; Yang, X.; Liu, Z.; Liu, Z.; Jiang, L. Infrared Spectroscopy of Hydrogen-Bonding Interactions in Neutral Dimethylamine-Methanol Complexes. *J. Phys. Chem. A* **2019**, *123*, 10109–10115. https://doi.org/10.1021/acs.jpca.9b08630.

(459) Nathan, C.; Shiloh, M. U. Reactive Oxygen and Nitrogen Intermediates in the Relationship between Mammalian Hosts and Microbial Pathogens. *Proc. Natl. Acad. Sci. U. S. A.* **2000**,

97, 8841–8848. https://doi.org/10.1073/pnas.97.16.8841.

(460) Sadler, A. J.; Williams, B. R. G. Interferon-Inducible Antiviral Effectors. *Nat. Rev. Immunol.* **2008**, *8*, 559–568. https://doi.org/10.1038/nri2314.

(461) Flannagan, R. S.; Cosío, G.; Grinstein, S. Antimicrobial Mechanisms of Phagocytes and Bacterial Evasion Strategies. *Nat. Rev. Microbiol.* **2009**, *7*, 355–366. https://doi.org/10.1038/nrmicro2128.

(462) Vermot, A.; Petit-Härtlein, I.; Smith, S. M. E.; Fieschi, F. Nadph Oxidases (Nox): An Overview from Discovery, Molecular Mechanisms to Physiology and Pathology. *Antioxidants* **2021**, *10*, 1–55. https://doi.org/10.3390/antiox10060890.

(463) D'Autréaux, B.; Toledano, M. B. ROS as Signalling Molecules: Mechanisms That Generate Specificity in ROS Homeostasis. *Nat. Rev. Mol. Cell Biol.* **2007**, *8*, 813–824. https://doi.org/10.1038/nrm2256.

(464) Nordzieke, D. E.; Medraño-Fernandez, I. The Plasma Membrane: A Platform for Intra-and Intercellular Redox Signaling. *Antioxidants* **2018**, *7*, 1–34. https://doi.org/10.3390/antiox7110168.

(465) Jiang, F.; Zhang, Y.; Dusting, G. J. NADPH Oxidase-Mediated Redox Signaling: Roles in Cellular Stress Response, Stress Tolerance, and Tissue Repair. *Pharmacol. Rev.* **2011**, *63*, 218–242. https://doi.org/10.1124/pr.110.002980.

(466) Cave, A. C.; Brewer, A. C.; Narayanapanicker, A.; Ray, R.; Grieve, D. J.; Walker, S.; Shah, A. M. NADPH Oxidases in Cardiovascular Health and Disease. *Antioxid. Redox Signal.* **2006**, *8*, 691–728.

(467) Wiktorin, H. G.; Aydin, E.; Hellstrand, K.; Martner, A. Nox2-Derived Reactive Oxygen Species in Cancer. *Oxid. Med. Cell. Longev.* **2020**, 1–15. https://doi.org/10.1155/2020/7095902.

(468) Li, J.-M.; Fan, L. M.; Christie, M. R.; Shah, A. M. Acute Tumor Necrosis Factor Alpha Signaling via NADPH Oxidase in Microvascular Endothelial Cells: Role of P47phox Phosphorylation and Binding to TRAF4. *Mol. Cell. Biol.* **2005**, *25*, 2320–2330.

https://doi.org/10.1128/mcb.25.6.2320-2330.2005.

(469) Costa, A.; Scholer-Dahirel, A.; Mechta-Grigoriou, F. The Role of Reactive Oxygen Species and Metabolism on Cancer Cells and Their Microenvironment. *Semin. Cancer Biol.* **2014**, *25*, 23–32. https://doi.org/10.1016/j.semcancer.2013.12.007.

(470) Tang, X. N.; Cairns, B.; Kim, J. Y.; Yenari, M. A. NADPH Oxidase in Stroke and Cerebrovascular Disease. *Neurol. Res.* **2012**, *34*, 338–345. https://doi.org/10.1179/1743132812Y.0000000021.

(471) Tang, X. N.; Zheng, Z.; Giffard, R. G.; Yenari, M. A. Significance of Marrow-Derived Nicotinamide Adenine Dinucleotide Phosphate Oxidase in Experimental Ischemic Stroke. *Ann. Neurol.* **2011**, *70*, 606–615. https://doi.org/10.1002/ana.22476.

(472) Braunersreuther, V.; Montecucco, F.; Ashri, M.; Pelli, G.; Galan, K.; Frias, M.; Burger, F.; Quinderé, A. L. G.; Montessuit, C.; Krause, K. H.; Mach, F.; Jaquet, V. Role of NADPH Oxidase Isoforms NOX1, NOX2 and NOX4 in Myocardial Ischemia/Reperfusion Injury. *J. Mol. Cell. Cardiol.* **2013**, *64*, 99–107. https://doi.org/10.1016/j.yjmcc.2013.09.007.

(473) Hernandes, M. S.; D'Avila, J. C.; Trevelin, S. C.; Reis, P. A.; Kinjo, E. R.; Lopes, L. R.; Castro-Faria-Neto, H. C.; Cunha, F. Q.; Britto, L. R. G.; Bozza, F. A. The Role of Nox2-Derived ROS in the Development of Cognitive Impairment after Sepsis. *J. Neuroinflammation* **2014**, *11*, 1–12. https://doi.org/10.1186/1742-2094-11-36.

(474) Park, L.; Zhou, P.; Pitstick, R.; Capone, C.; Anrather, J.; Norris, E. H.; Younkin, L.; Younkin, S.; Carlson, G.; McEwen, B. S.; Iadecola, C. Nox2-Derived Radicals Contribute to Neurovascular and Behavioral Dysfunction in Mice Overexpressing the Amyloid Precursor Protein. *Proc. Natl. Acad. Sci. U. S. A.* **2008**, *105*, 1347–1352. https://doi.org/10.1073/pnas.0711568105.

(475) Lapouge, K.; Smith, S. J. M.; Groemping, Y.; Rittinger, K. Architecture of the P40-P47-P67phox Complex in the Resting State of the NADPH Oxidase. A Central Role for P67phox. *J. Biol. Chem.* **2002**, *277*, 10121–10128. https://doi.org/10.1074/jbc.M112065200.

(476) Ago, T.; Kuribayashi, F.; Hiroaki, H.; Takeya, R.; Ito, T.; Kohda, D.; Sumimoto, H. Phosphorylation of P47phox directs Phox Homology Domain from SH3 Domain toward

Phosphoinositides, Leading to Phagocyte NADPH Oxidase Activation. *Proc. Natl. Acad. Sci. U. S. A.* **2003**, *100*, 4474–4479. https://doi.org/10.1073/pnas.0735712100.

(477) Takeshige, K.; Ito, T.; Sumimoto, H. Activation of the Phagocyte NADPH Oxidase. *J. Toxicol. Sci.* **1996**, *21*, 291–292. https://doi.org/10.1074/jbc.271.36.22152.

(478) Williams, H. C.; Griendling, K. K. NADPH Oxidase Inhibitors: New Antihypertensive Agents? *J. Cardiovasc. Pharmacol.* **2007**, *50*, 9–16. https://doi.org/10.1097/FJC.0b013e318063e820.

(479) Kim, J. A.; Neupane, G. P.; Lee, E. S.; Jeong, B. S.; Park, B. C.; Thapa, P. NADPH Oxidase Inhibitors: A Patent Review. *Expert Opin. Ther. Pat.* **2011**, *21*, 1147–1158. https://doi.org/10.1517/13543776.2011.584870.

(480) Smith, S. M. E.; Min, J.; Ganesh, T.; Diebold, B.; Kawahara, T.; Zhu, Y.; McCoy, J.; Sun, A.; Snyder, J. P.; Fu, H.; Du, Y.; Lewis, I.; Lambeth, J. D. Ebselen and Congeners Inhibit NADPH Oxidase 2-Dependent Superoxide Generation by Interrupting the Binding of Regulatory Subunits. *Chem. Biol.* **2012**, *19*, 752–763. https://doi.org/10.1016/j.chembiol.2012.04.015.

(481) Tang, X. N.; Cairns, B.; Cairns, N.; Yenari, M. A. Apocynin Improves Outcome in Experimental Stroke with a Narrow Dose Range. *Neuroscience* **2008**, *154*, 556–562. https://doi.org/10.1016/j.neuroscience.2008.03.090.

(482) Wang, Q.; Tompkins, K. D.; Simonyi, A.; Korthuis, R. J.; Sun, A. Y.; Sun, G. Y. Apocynin Protects against Global Cerebral Ischemia-Reperfusion-Induced Oxidative Stress and Injury in the Gerbil Hippocampus. *Brain Res.* **2006**, *1090*, 182–189. https://doi.org/10.1016/j.brainres.2006.03.060.

(483) Shi, J.; Ross, C. R.; Leto, T. L.; Blecha, F. PR-39, a Proline-Rich Antibacterial Peptide That Inhibits Phagocyte NADPH Oxidase Activity by Binding to Src Homology 3 Domains of P47phox. *Proc. Natl. Acad. Sci. U. S. A.* **1996**, *93*, 6014–6018. https://doi.org/10.1073/pnas.93.12.6014.

(484) Rey, F. E.; Cifuentes, M. E.; Kiarash, A.; Quinn, M. T.; Pagano, P. J. Novel Competitive Inhibitor of NAD(P)H Oxidase Assembly Attenuates Vascular O_2^- and Systolic Blood Pressure

in Mice. *Circ. Res.* **2001**, *89*, 408–414. https://doi.org/10.1161/hh1701.096037.

(485) Ogura, K.; Nobuhisa, I.; Yuzawa, S.; Takeya, R.; Torikai, S.; Saikawa, K.; Sumimoto, H.; Inagaki, F. NMR Solution Structure of the Tandem Src Homology 3 Domains of P47 Phox Complexed with a P22phox-Derived Proline-Rich Peptide. *J. Biol. Chem.* **2006**, *281*, 3660–3668. https://doi.org/10.1074/jbc.M505193200.

(486) Groemping, Y.; Lapouge, K.; Smerdon, S. J.; Rittinger, K. Molecular Basis of Phosphorylation-Induced Activation of the NADPH Oxidase. *Cell* **2003**, *113*, 343–355. https://doi.org/10.1016/S0092-8674(03)00314-3.

(487) Garsi, J.-B.; Komjáti, B.; Cullia, G.; Fejes, I.; Sipos, M.; Sipos, Z.; Fördős, E.; Markacz, P.; Balázs, B.; Lancelot, N.; Berger, S.; Raimbaud, E.; Brown, D.; Vuillard, L.-M.; Haberkorn, L.; Cukier, C.; Szlávik, Z.; Hanessian, S. Targeting NOX2 via P47/Phox-P22/Phox Inhibition with Novel Triproline Mimetics. *ACS Med. Chem. Lett.* **2022**, *13*, 949–954. https://doi.org/10.1021/acsmedchemlett.2c00094.

(488) Babior, B. M.; Lambeth, J. D.; Nauseef, W. The Neutrophil NADPH Oxidase. *Arch. Biochem. Biophys.* **2002**, *397*, 342–344. https://doi.org/10.1006/abbi.2001.2642.

(489) Vignais, P. V. The Superoxide-Generating NADPH Oxidase: Structural Aspects and Activation Mechanism. *Cell. Mol. Life Sci.* **2002**, *59*, 1428–1459. https://doi.org/10.1007/s00018-002-8520-9.

(490) Babior, B. M. NADPH Oxidase: An Update. *Blood* **1999**, *93*, 1464–1476.

(491) Groemping, Y.; Rittinger, K. Activation and Assembly of the NADPH Oxidase: A Structural Perspective. *Biochem. J.* **2005**, *386*, 401–416. https://doi.org/10.1042/BJ20041835.

(492) Bedard, K.; Krause, K. H. The NOX Family of ROS-Generating NADPH Oxidases: Physiology and Pathophysiology. *Physiol. Rev.* **2007**, *87*, 245–313. https://doi.org/10.1152/physrev.00044.2005.

(493) Lambeth, J. D. NOX Enzymes and the Biology of Reactive Oxygen. *Nat. Rev. Immunol.* **2004**, *4*, 181–189. https://doi.org/10.1038/nri1312.

(494) Sumimoto, H. Structure, Regulation and Evolution of Nox-Family NADPH Oxidases That Produce Reactive Oxygen Species. *FEBS J.* **2008**, *275*, 3249–3277. https://doi.org/10.1111/j.1742-4658.2008.06488.x.

(495) Rada, B.; Leto, T. L. Oxidative Innate Immune Defenses by Nox/Duox Family NADPH Oxidases. *Contrib Microbiol. Basel, Karger* **2008**, *15*, 164–187.

(496) Augsburger, F.; Filippova, A.; Rasti, D.; Seredenina, T.; Lam, M.; Maghzal, G.; Mahiout, Z.; Jansen-Dürr, P.; Knaus, U. G.; Doroshow, J.; Stocker, R.; Krause, K. H.; Jaquet, V. Pharmacological Characterization of the Seven Human NOX Isoforms and Their Inhibitors. *Redox Biol.* **2019**, *26* (May), 101272. https://doi.org/10.1016/j.redox.2019.101272.

(497) Sumimoto, H.; Kage, Y.; Nunoi, H.; Sasaki, H.; Nose, T.; Fukumaki, Y.; Ohno, M.; Minakami, S.; Takeshige, K. Role of Src Homology 3 Domains in Assembly and Activation of the Phagocyte NADPH Oxidase. *Proc. Natl. Acad. Sci. U. S. A.* **1994**, *91*, 5345–5349. https://doi.org/10.1073/pnas.91.12.5345.

(498) Leto, T. L.; Adams, A. G.; De Mendez, I. Assembly of the Phagocyte NADPH Oxidase: Binding of Src Homology 3 Domains to Proline-Rich Targets. *Proc. Natl. Acad. Sci. U. S. A.* **1994**, *91*, 10650–10654. https://doi.org/10.1073/pnas.91.22.10650.

(499) Sumimoto, H.; Hata, K.; Mizuki, K.; Ito, T.; Kage, Y.; Sakaki, Y.; Fukumaki, Y.; Nakamura, M.; Takeshige, K. Assembly and Activation of the Phagocyte NADPH Oxidase. *J. Biol. Chem.* **1996**, *271*, 22512–22158.

(500) Dröge, W. Free Radicals in the Physiological Control of Cell Function. *Physiol. Rev.* **2002**, *82*, 47–95. https://doi.org/10.1152/physrev.00018.2001.

(501) Quinn, M. T.; Ammons, M. C. B.; DeLeo, F. R. The Expanding Role of NADPH Oxidases in Health and Disease: No Longer Just Agents of Death and Destruction. *Clin. Sci.* **2006**, *111*, 1–20. https://doi.org/10.1042/CS20060059.

(502) Shi, J.; Ross, C. R.; Leto, T. L.; Blecha, F. PR-39, a Proline-Rich Antibacterial Peptide That Inhibits Phagocyte NADPH Oxidase Activity by Binding to Src Homology 3 Domains of P47phox. *Proc. Natl. Acad. Sci. U. S. A.* **1996**, *93*, 6014–6018.

(503) Laleu, B.; Gaggini, F.; Orchard, M.; Fioraso-Cartier, L.; Cagnon, L.; Houngninou-Molango, S.; Gradia, A.; Duboux, G.; Merlot, C.; Heitz, F.; Szyndralewiez, C.; Page, P. First in Class, Potent, and Orally Bioavailable NADPH Oxidase Isoform 4 (Nox4) Inhibitors for the Treatment of Idiopathic Pulmonary Fibrosis. *J. Med. Chem.* **2010**, *53*, 7715–7730. https://doi.org/10.1021/jm100773e.

(504) Solbak, S. M. Ø.; Zang, J.; Narayanan, D.; Høj, L. J.; Bucciarelli, S.; Softley, C.; Meier, S.; Langkilde, A. E.; Gotfredsen, C. H.; Sattler, M.; Bach, A. Developing Inhibitors of the P47phox-P22phox Protein-Protein Interaction by Fragment-Based Drug Discovery. *J. Med. Chem.* **2020**, *63*, 1156–1177. https://doi.org/10.1021/acs.jmedchem.9b01492.

(505) Sillerud, L. O.; Larson, R. S. Design and Structure of Peptide and Peptidomimetic Antagonists of Protein-Protein Interaction. *Curr. Protein Pept. Sci.* **2005**, *6*, 151–169.

(506) Yuzawa, S.; Suzuki, N. N.; Fujioka, Y.; Ogura, K.; Sumimoto, H.; Inagaki, F. Crystallization and Preliminary Crystallographic Analysis of the Autoinhibited Form of the Tandem SH3 Domain of P47phox. *Acta Crystallogr. - Sect. D Biol. Crystallogr.* **2003**, *59*, 1479–1480. https://doi.org/10.1107/S0907444903011636.

(507) Lau, J. L.; Dunn, M. K. Therapeutic Peptides: Historical Perspectives, Current Development Trends, and Future Directions. *Bioorganic Med. Chem.* **2018**, *26*, 2700–2707. https://doi.org/10.1016/j.bmc.2017.06.052.

(508) Hummel, G.; Reineke, U.; Reimer, U. Translating Peptides into Small Molecules. *Mol. Biosyst.* **2006**, *2*, 499–508. https://doi.org/10.1039/b611791k.

(509) Hanessian, S.; Auzzas, L. The Practice of Ring Constraint in Peptidomimetics Using Bicyclic and Polycyclic Amino Acids. *Acc. Chem. Res.* **2008**, *41*, 1241–1251. https://doi.org/10.1021/ar8000052.

(510) Hanessian, S. Structure-Based Organic Synthesis of Drug Prototypes: A Personal Odyssey. *ChemMedChem* **2006**, *1*, 1300–1330. https://doi.org/10.1002/cmdc.200600203.

(511) Garsi, J. B.; Aguiar, P. M.; Hanessian, S. Design of Pseudodiproline Dimers as Mimetics of Pro-Pro Units: Stereocontrolled Synthesis, Configurational Relevance, and Structural

Properties. *J. Org. Chem.* **2021**, *86*, 16834–16847. https://doi.org/10.1021/acs.joc.1c02061.

(512) Flaten, G. E.; Kottra, G.; Stensen, W.; Isaksen, G.; Karstad, R.; Svendsen, J. S.; Daniel, H.; Svenson, J. In Vitro Characterization of Human Peptide Transporter HPEPT1 Interactions and Passive Permeation Studies of Short Cationic Antimicrobial Peptides. *J. Med. Chem.* **2011**, *54*, 2422–2432. https://doi.org/10.1021/jm1015704.

(513) Davey, N. E.; Van Roey, K.; Weatheritt, R. J.; Toedt, G.; Uyar, B.; Altenberg, B.; Budd, A.; Diella, F.; Dinkel, H.; Gibson, T. J. Attributes of Short Linear Motifs. *Mol. Biosyst.* **2012**, *8*, 268–281. https://doi.org/10.1039/c1mb05231d.

(514) Freund, C.; Schmalz, H. G.; Sticht, J.; Kuhne, R. Proline Rich Sequence Recognition Domain (PRD): Ligands, Function and Inhibition. *Handb. Exp. Pharmacol.* **2008**, *186*, 407–429.

(515) Schäffler, H.; Breitrück, A. Clostridium Difficile - From Colonization to Infection. *Front. Microbiol.* **2018**, *9* (APR), 1–12. https://doi.org/10.3389/fmicb.2018.00646.

(516) Kuijper, E. J.; Coignard, B.; Tüll, P.; Poxton, I.; Brazier, J.; Duerden, B.; Delmée, M.; Mastrantonio, P.; Gastmeier, P.; Barbut, F.; Rupnik, M.; Suetens, C.; Collignon, A.; McDonald, C.; Gerding, D. N.; Tjallie van der Kooi, I.; van den Hof, S.; Notermans, D. W.; Pearson, A.; Nagy, E.; Colville, A.; Wilcox, M.; Borriello, P.; Pituch, H.; Minton, N. Emergence of Clostridium Difficile-Associated Disease in North America and Europe. *Clin. Microbiol. Infect.* **2006**, *12* (12 SUPPL. 6), 2–18. https://doi.org/10.1111/j.1469-0691.2006.01580.x.

(517) Kuipers, E. J.; Surawicz, C. M. Clostridium Difficile Infection. *Lancet* **2008**, *371*, 1486–1488.

(518) Martin, J. S. H.; Monaghan, T. M.; Wilcox, M. H. Clostridium Difficile Infection: Epidemiology, Diagnosis and Understanding Transmission. *Nat. Rev. Gastroenterol. Hepatol.* **2016**, *13*, 206–216. https://doi.org/10.1038/nrgastro.2016.25.

(519) Lessa, F. C.; Mu, Y.; Bamberg, W. M.; Beldavs, Z. G.; Dumyati, G. K.; Dunn, J. R.; Farley, M. M.; Holzbauer, S. M.; Meek, J. I.; Phipps, E. C.; Wilson, L. E.; Winston, L. G.; Cohen, J. A.; Limbago, B. M.; Fridkin, S. K.; Gerding, D. N.; McDonald, L. C. Burden of Clostridium Difficile Infection in the United States. *N. Engl. J. Med.* **2015**, *372*, 825–834.

https://doi.org/10.1056/nejmoa1408913.

(520) Fu, Y.; Luo, Y.; Grinspan, A. M. Epidemiology of Community-Acquired and Recurrent Clostridioides Difficile Infection. *Therap. Adv. Gastroenterol.* **2021**, *14*, 1–11. https://doi.org/10.1177/17562848211016248.

(521) Abad, C. L. R.; Safdar, N. A Review of Clostridioides Difficile Infection and Antibiotic-Associated Diarrhea. *Gastroenterol. Clin. N. Am.* **2021**, *50*, 323 — 340.

(522) George, W. L.; Sutter, V. L.; Finegold, S. M. Antimicrobial Agent-Induced Diarrhea - A Bacterial Disease. *J. Infect. Dis.* **1977**, *136*, 822–828.

(523) George, R. H.; Symonds, J. M.; Dimock, F.; Brown, J. D.; Arabi, Y.; Shinagawa, N.; Keighley, M. R. B.; Alexander-Williams, J.; Burdon, D. W. Identification of Clostridium Difficile as a Cause of Pseudomembranous Colitis. *Br. Med. J.* **1978**, 695. https://doi.org/10.1136/bmj.1.6114.695.

(524) Bartlett, J. G.; Chang, T. W.; Gurwith, M.; Gorbach, S. L.; Onderdonk, A. B. Antibiotic-Associated Pseudomembranous Colitis Due to Toxin-Producing Clostridia. *New English J. Med.* **1978**, *298*, 531 — 534.

(525) Bartlett, J. G. Narrative Review: The New Epidemic of Clostridium Difficile - Associated Enteric Disease. *Ann. Intern. Med.* **2006**, *145*, 758 — 764.

(526) Rupnik, M.; Wilcox, M. H.; Gerding, D. N. Clostridium Difficile Infection: New Developments in Epidemiology and Pathogenesis. *Nat. Rev. Microbiol.* **2009**, *7*, 526–536. https://doi.org/10.1038/nrmicro2164.

(527) Thomas, C.; Stevenson, M.; Riley, T. V. Antibiotics and Hospital-Acquired Clostridium Difficile-Associated Diarrhoea: A Systematic Review. *J. Antimicrob. Chemother.* **2003**, *51*, 1339–1350. https://doi.org/10.1093/jac/dkg254.

(528) O'Connor, J. R.; Johnson, S.; Gerding, D. N. Clostridium Difficile Infection Caused by the Epidemic BI/NAP1/027 Strain. *Gastroenterology* **2009**, *136*, 1913–1924. https://doi.org/10.1053/j.gastro.2009.02.073.

(529) Bouza, E. Consequences of Clostridium Difficile Infection: Understanding the Healthcare Burden. *Clin. Microbiol. Infect.* **2012**, *18*, 5–12. https://doi.org/10.1111/1469-0691.12064.

(530) Jarmo, O.; Veli-Jukka, A.; Eero, M. Treatment of Clostridioides (Clostridium) Difficile Infection. *Ann. Med.* **2020**, *52*, 12–20. https://doi.org/10.1080/07853890.2019.1701703.

(531) Chaar, A.; Feuerstadt, P. Evolution of Clinical Guidelines for Antimicrobial Management of Clostridioides Difficile Infection. *Therap. Adv. Gastroenterol.* **2021**, *14*, 1–16. https://doi.org/10.1177/https.

(532) Freeman, J.; Bauer, M. P.; Baines, S. D.; Corver, J.; Fawley, W. N.; Goorhuis, B.; Kuijper, E. J.; Wilcox, M. H. The Changing Epidemiology of Clostridium Difficile Infections. *Clin. Microbiol. Rev.* **2010**, *23*, 529–549. https://doi.org/10.1128/CMR.00082-09.

(533) McGowan, A. P.; Lalayiannis, L. C.; Sarma, J. B.; Marshall, B.; Martin, K. E.; Welfare, M. R. Thirty-Day Mortality of Clostridium Difficile Infection in a UK National Health Service Foundation Trust between 2002 and 2008. *J. Hosp. Infect.* **2011**, *77*, 11–15. https://doi.org/10.1016/j.jhin.2010.09.017.

(534) Makris, A. T.; Gelone, S. Clostridium Difficile in the Long-Term Care Setting. *J. Am. Med. Dir. Assoc.* **2007**, *8*, 290–299. https://doi.org/10.1016/j.jamda.2007.01.098.

(535) Kuijper, E. J.; Coignard, B.; Tüll, P.; Poxton, I.; Brazier, J.; Duerden, B.; Delmée, M.; Mastrantonio, P.; Gastmeier, P.; Barbut, F.; Rupnik, M.; Suetens, C.; Collignon, A.; McDonald, C.; Gerding, D. N.; Tjallie van der Kooi, I.; van den Hof, S.; Notermans, D. W.; Pearson, A.; Nagy, E.; Colville, A.; Wilcox, M.; Borriello, P.; Pituch, H.; Minton, N. Emergence of Clostridium Difficile-Associated Disease in North America and Europe. *Clin. Microbiol. Infect.* **2006**, *12*, 2–18. https://doi.org/10.1111/j.1469-0691.2006.01580.x.

(536) Sammons, J. S.; Toltzis, P.; Zaoutis, T. E. Clostridium Difficile Infection in Children. *JAMA Pediatr.* **2013**, *167*, 567–573. https://doi.org/10.1001/jamapediatrics.2013.441.

(537) McDonald, L. C.; Killgore, G. E.; Thompson, A.; Owens, R. C.; Kazakova, S. V.; Sambol, S. P.; Johnson, S.; Gerding, D. N. An Epidemic, Toxin Gene–Variant Strain of Clostridium Difficile. *N. Engl. J. Med.* **2005**, *353*, 2433–2441.

(538) Zaiß, N. H.; Witte, W.; Nübel, U. Fluoroquinolone Resistance and Clostridium Difficile, Germany. *Emerg. Infect. Dis.* **2010**, *16*, 675–677. https://doi.org/10.3201/eid1604.090859.

(539) Spigaglia, P.; Barbanti, F.; Dionisi, A. M.; Mastrantonio, P. Clostridium Difficile Isolates Resistant to Fluoroquinolones in Italy: Emergence of PCR Ribotype 018. *J. Clin. Microbiol.* **2010**, *48*, 2892–2896. https://doi.org/10.1128/JCM.02482-09.

(540) Sánchez-Somolinos, M.; Alcalá, L.; Peláez, T.; Marín, M.; Martín, A.; Catalán, P.; Bouza, E. High Levels of Resistance to Fluoroquinolones among Clostridium Difficile Isolates in a Spanish Hospital. *Clin. Infect. Dis.* **2008**, *47*, 818–822. https://doi.org/10.1086/591201.

(541) Åkerlund, T.; Persson, I.; Unemo, M.; Norén, T.; Svenungsson, B.; Wullt, M.; Burman, L. G. Increased Sporulation Rate of Epidemic Clostridium Difficile Type 027/NAP1. *J. Clin. Microbiol.* **2008**, *46*, 1530–1533. https://doi.org/10.1128/JCM.01964-07.

(542) Shen, A. Clostridium Difficile Toxins: Mediators of Inflammation. *J. Innate Immun.* **2012**, *4* (2), 149–158. https://doi.org/10.1159/000332946.

(543) Warny, M.; Pepin, J.; Fang, A.; Killgore, G.; Thompson, A.; Brazier, J.; Frost, E.; McDonald, L. C. Toxin Production by an Emerging Strain of Clostridium Difficile Associated with Outbreaks of Severe Disease in North America and Europe. *Lancet* **2005**, *366*, 1079–1084. https://doi.org/10.1016/S0140-6736(05)67420-X.

(544) Lanis, J. M.; Barua, S.; Ballard, J. D. Variations in Tcdb Activity and the Hypervirulence of Emerging Strains of Clostridium Difficile. *PLoS Pathog.* **2010**, *6*, 1–11. https://doi.org/10.1371/journal.ppat.1001061.

(545) Stabler, R. A.; Dawson, L. F.; Phua, L. T. H.; Wren, B. W. Comparative Analysis of BI/NAP1/027 Hypervirulent Strains Reveals Novel Toxin B-Encoding Gene (TcdB) Sequences. *J. Med. Microbiol.* **2008**, *57*, 771–775. https://doi.org/10.1099/jmm.0.47743-0.

(546) Gerding, D. N.; Johnson, S.; Rupnik, M.; Aktories, K. Clostridium Difficile Binary Toxin CDT. *Gut Microbes* **2013**, *5*, 15–27. https://doi.org/10.4161/gmic.26854.

(547) Cowardin, C. A.; Buonomo, E. L.; Mahmoud, M. S.; Wilson, M. G.; Burgess, S. L.; Kuehne, S. A.; Schwan, C.; Eichhoff, A. M.; Friedrich, K.-N.; Lyras, D.; Aktories, K.; Minton, N. P.; Petri Jr, W. A. The Binary Toxin CDT Enhances Clostridium Difficile Virulence by Suppressing Protective Colonic Eosinophilia. *Nat. Microbiol.* **2016**, *1*, 16108.

(548) Best, E. L.; Fawley, W. N.; Parnell, P.; Wilcox, M. H. The Potential for Airborne Dispersal of Clostridium Difficile from Symptomatic Patients. *Clin. Infect. Dis.* **2010**, *50*, 1450–1457. https://doi.org/10.1086/652648.

(549) Snelling, A. M.; Beggs, C. B.; Kerr, K. G.; Shepherd, S. J. Spores of Clostridium Difficile in Hospital Air. *Clin. Infect. Dis.* **2010**, *51*, 1104–1105. https://doi.org/10.1086/656686.

(550) Riggs, M. M.; Sethi, A. K.; Zabarsky, T. F.; Eckstein, E. C.; Jump, R. L. P.; Donskey, C. J. Asymptomatic Carriers Are a Potential Source for Transmission of Epidemic and Nonepidemic Clostridium Difficile Strains among Long-Term Care Facility Residents. *Clin. Infect. Dis.* **2007**, *45*, 992–998. https://doi.org/10.1086/521854.

(551) Muniz, L. R.; Knosp, C.; Yeretssian, G. Intestinal Antimicrobial Peptides during Homeostasis, Infection, and Disease. *Front. Immunol.* **2012**, *3*, 1–13. https://doi.org/10.3389/fimmu.2012.00310.

(552) Winston, J. A.; Theriot, C. M. Impact of Microbial Derived Secondary Bile Acids on Colonization Resistance against Clostridium Difficile in the Gastrointestinal Tract. *Anaerobe* **2016**, *41*, 44–50. https://doi.org/10.1016/j.anaerobe.2016.05.003.

(553) Theriot, C. M.; Bowman, A. A.; Young, V. B. Antibiotic-Induced Alterations of the Gut Microbiota Alter Secondary Bile Acid Production and Allow for Clostridium Difficile Spore Germination and Outgrowth in the Large Intestine. *mSphere* **2016**, *1*, 1–16. https://doi.org/10.1128/mSphere.00045-15.Editor.

(554) Buffie, C. G.; Bucci, V.; Stein, R. R.; McKenney, P. T.; Ling, L.; Gobourne, A.; No, D.; Liu, H.; Kinnebrew, M.; Viale, A.; Littmann, E.; Van Den Brink, M. R. M.; Jenq, R. R.; Taur, Y.; Sander, C.; Cross, J. R.; Toussaint, N. C.; Xavier, J. B.; Pamer, E. G. Precision Microbiome Reconstitution Restores Bile Acid Mediated Resistance to Clostridium Difficile. *Nature*

2015, *517*, 205–208. https://doi.org/10.1038/nature13828.

(555) Meza-Torres, J.; Auria, E.; Dupuy, B.; Tremblay, Y. D. N. Wolf in Sheep's Clothing: Clostridioides Difficile Biofilm as a Reservoir for Recurrent Infections. *Microorganisms* **2021**, *9* (9). https://doi.org/10.3390/microorganisms9091922.

(556) Rahmoun, L. A.; Azrad, M.; Peretz, A. Antibiotic Resistance and Biofilm Production Capacity in Clostridioides Difficile. *Front. Cell. Infect. Microbiol.* **2021**, *11* (August), 1–10. https://doi.org/10.3389/fcimb.2021.683464.

(557) Jank, T.; Aktories, K. Structure and Mode of Action of Clostridial Glucosylating Toxins: The ABCD Model. *Trends Microbiol.* **2008**, *16*, 222–229. https://doi.org/10.1016/j.tim.2008.01.011.

(558) Sebaihia, M.; Wren, B. W.; Mullany, P.; Fairweather, N. F.; Minton, N.; Stabler, R.; Thomson, N. R.; Roberts, A. P.; Cerdeño-Tárraga, A. M.; Wang, H.; Holden, M. T. G.; Wright, A.; Churcher, C.; Quail, M. A.; Baker, S.; Bason, N.; Brooks, K.; Chillingworth, T.; Cronin, A.; Davis, P.; Dowd, L.; Fraser, A.; Feltwell, T.; Hance, Z.; Holroyd, S.; Jagels, K.; Moule, S.; Mungall, K.; Price, C.; Rabbinowitsch, E.; Sharp, S.; Simmonds, M.; Stevens, K.; Unwin, L.; Whithead, S.; Dupuy, B.; Dougan, G.; Barrell, B.; Parkhill, J. The Multidrug-Resistant Human Pathogen Clostridium Difficile Has a Highly Mobile, Mosaic Genome. *Nat. Genet.* **2006**, *38*, 779–786. https://doi.org/10.1038/ng1830.

(559) Tijerina-Rodríguez, L.; Villarreal-Treviño, L.; Morfín-Otero, R.; Camacho-Ortíz, A.; Garza-González, E. Virulence Factors of Clostridioides (Clostridium) Difficile Linked to Recurrent Infections. *Can. J. Infect. Dis. Med. Microbiol.* **2019**, 1–7. https://doi.org/10.1155/2019/7127850.

(560) Demuyser, L.; Jabra-Rizk, M. A.; van Dijck, P. Microbial Cell Surface Proteins and Secreted Metabolites Involved in Multispecies Biofilms. *Pathog. Dis.* **2014**, *70*, 219–230. https://doi.org/10.1111/2049-632X.12123.

(561) Navarre, W. W.; Schneewind, O. Surface Proteins of Gram-Positive Bacteria and Mechanisms of Their Targeting to the Cell Wall Envelope. *Microbiol. Mol. Biol. Rev.* **1999**,

63, 174–229. https://doi.org/10.1128/mmbr.63.1.174-229.1999.

(562) Fischetti, V. A. Surface Proteins on Gram-Positive Bacteria. *Microbiol. Spectr.* **2019**, *7*, 1–15. https://doi.org/10.1128/9781683670131.ch2.

(563) Pickering, A. C.; Fitzgerald, J. R. The Role of Gram-Positive Surface Proteins in Bacterial Niche- and Host-Specialization. *Front. Microbiol.* **2020**, *11*, 1–9. https://doi.org/10.3389/fmicb.2020.594737.

(564) Corver, J.; Cordo', V.; van Leeuwen, H. C.; Klychnikov, O. I.; Hensbergen, P. J. Covalent Attachment and Pro-Pro Endopeptidase (PPEP-1)-Mediated Release of Clostridium Difficile Cell Surface Proteins Involved in Adhesion. *Mol. Microbiol.* **2017**, *105* (5), 663–673. https://doi.org/10.1111/mmi.13736.

(565) Krachler, A. M.; Orth, K. Targeting the Bacteria-Host Interface. *Virulence* **2013**, *4*, 284–294. https://doi.org/10.4161/viru.24606.

(566) Hayes, C. S.; Aoki, S. K.; Low, D. A. Bacterial Contact-Dependent Delivery Systems. *Annu. Rev. Genet.* **2010**, *44*, 71–90. https://doi.org/10.1146/annurev.genet.42.110807.091449.

(567) Kim, Y. R.; Lee, S. E.; Kook, H.; Yeom, J. A.; Na, H. S.; Kim, S. Y.; Chung, S. S.; Choy, H. E.; Rhee, J. H. Vibrio Vulnificus RTX Toxin Kills Host Cells Only after Contact of the Bacteria with Host Cells. *Cell. Microbiol.* **2008**, *10*, 848–862. https://doi.org/10.1111/j.1462-5822.2007.01088.x.

(568) Boland, T.; Latour, R. A.; J., S. F. Molecular Basis of Bacterial Adhesion. In *Handbook of Bacterial Adhesion*; An, Y. H., Friedman, R. J., Eds.; Humana Press, Totowa, NJ, 2000; pp 29–41.

(569) Anderson, B. N.; Ding, A. M.; Nilsson, L. M.; Kusuma, K.; Tchesnokova, V.; Vogel, V.; Sokurenko, E. V.; Thomas, W. E. Weak Rolling Adhesion Enhances Bacterial Surface Colonization. *J. Bacteriol.* **2007**, *189*, 1794–1802. https://doi.org/10.1128/JB.00899-06.

(570) Foster, T. J.; Geoghegan, J. A.; Ganesh, V. K.; Höök, M. Adhesion, Invasion and Evasion: The Many Functions of the Surface Proteins of Staphylococcus Aureus. *Nat. Rev. Microbiol.*

2014, *12*, 49–62. https://doi.org/10.1038/nrmicro3161.

(571) Crawford, R. W.; Reeve, K. E.; Gunn, J. S. Flagellated but Not Hyperfimbriated Salmonella Enterica Serovar Typhimurium Attaches to and Forms Biofilms on Cholesterol-Coated Surfaces. *J. Bacteriol.* **2010**, *192*, 2981–2990. https://doi.org/10.1128/JB.01620-09.

(572) Isberg, R. R.; Leong, J. M. Multiple B1 Chain Integrins Are Receptors for Invasin, a Protein That Promotes Bacterial Penetration into Mammalian Cells. *Cell* **1990**, *60*, 861–871. https://doi.org/10.1016/0092-8674(90)90099-Z.

(573) Heise, T.; Dersch, P. Identification of a Domain in Yersinia Virulence Factor YadA That Is Crucial for Extracellular Matrix-Specific Cell Adhesion and Uptake. *Proc. Natl. Acad. Sci. U. S. A.* **2006**, *103*, 3375–3380. https://doi.org/10.1073/pnas.0507749103.

(574) Servin, A. L. Pathogenesis of Human Diffusely Adhering Escherichia Coli Expressing Afa/Dr Adhesins (Afa/Dr DAEC): Current Insights and Future Challenges. *Clin. Microbiol. Rev.* **2014**, *27*, 823–869. https://doi.org/10.1128/CMR.00036-14.

(575) Ishijima, N.; Suzuki, M.; Ashida, H.; Ichikawa, Y.; Kanegae, Y.; Saito, I.; Borén, T.; Haas, R.; Sasakawa, C.; Mimuro, H. BabA-Mediated Adherence Is a Potentiator of the Helicobacter Pylori Type IV Secretion System Activity. *J. Biol. Chem.* **2011**, *286*, 25256–25264. https://doi.org/10.1074/jbc.M111.233601.

(576) Zur Wiesch, P. A.; Kouyos, R.; Engelstädter, J.; Regoes, R. R.; Bonhoeffer, S. Population Biological Principles of Drug-Resistance Evolution in Infectious Diseases. *Lancet Infect. Dis.* **2011**, *11*, 236–247. https://doi.org/10.1016/S1473-3099(10)70264-4.

(577) Levy, S. B.; Bonnie, M. Antibacterial Resistance Worldwide: Causes, Challenges and Responses. *Nat. Med.* **2004**, *10*, S122–S129. https://doi.org/10.1038/nm1145.

(578) Rogers, T. J.; Paton, J. C. Therapeutic Strategies for Shiga Toxin-Producing Escherichia Coli Infections. *Expert Rev. Anti. Infect. Ther.* **2009**, *7*, 683–686.

(579) Holzheimer, R. G. Antibiotic Induced Endotoxin Release and Clinical Sepsis: A Review. *J. Chemother.* **2001**, *13*, 159–172. https://doi.org/10.1179/joc.2001.13.supplement-2.159.

(580) Ghosh, S.; Chakraborty, K.; Nagaraja, T.; Basak, S.; Koley, H.; Dutta, S.; Mitra, U.; Das, S. An Adhesion Protein of Salmonella Enterica Serovar Typhi Is Required for Pathogenesis and Potential Target for Vaccine Development. *Proc. Natl. Acad. Sci. U. S. A.* **2011**, *108*, 3348–3353. https://doi.org/10.1073/pnas.1016180108.

(581) Asadi, A.; Razavi, S.; Talebi, M.; Gholami, M. A Review on Anti-Adhesion Therapies of Bacterial Diseases. *Infection* **2019**, *47*, 13–23. https://doi.org/10.1007/s15010-018-1222-5.

(582) Kelly, C. G.; Younson, J. S.; Hikmat, B. Y.; Todryk, S. M.; Czisch, M.; Haris, P. I.; Flindall, I. R.; Newby, C.; Mallet, A. I.; Ma, J. K. C.; Lehner, T. A Synthetic Peptide Adhesion Epitope as a Novel Antimicrobial Agent. *Nat. Biotechnol.* **1999**, *17*, 42–47. https://doi.org/10.1038/5213.

(583) Younson, J.; Kelly, C. The Rational Design of an Anti-Caries Peptide against Streptococcus Mutans. *Mol. Divers.* **2004**, *8*, 121–126. https://doi.org/10.1023/B:MODI.0000025655.93643.fa.

(584) Krachler, A. M.; Ham, H.; Orth, K. Turnabout Is Fair Play: Use of the Bacterial Multivalent Adhesion Molecule 7 as an Antimicrobial Agent. *Virulence* **2012**, *3*, 68–71. https://doi.org/10.4161/viru.3.1.18172.

(585) Sarshar, M.; Behzadi, P.; Ambrosi, C.; Zagaglia, C.; Palamara, A. T.; Scribano, D. FimH and Anti-Adhesive Therapeutics: A Disarming Strategy against Uropathogens. *Antibiotics* **2020**, *9*, 1–16. https://doi.org/10.3390/antibiotics9070397.

(586) Rahman, F.; Nguyen, T.-M.; Adekoya, O. A.; Campestre, C.; Tortorella, P.; Sylte, I.; Winberg, J.-O. Inhibition of Bacterial and Human Zinc-Metalloproteases by Bisphosphonate- and Catechol-Containing Compounds. *J. Enzyme Inhib. Med. Chem.* **2021**, *36*, 819–830. https://doi.org/10.1080/14756366.2021.1901088.

(587) Rahman, F.; Wushur, I.; Malla, N.; Åstrand, O. A. H.; Rongved, P.; Winberg, J. O.; Sylte, I. Zinc-Chelating Compounds as Inhibitors of Human and Bacterial Zinc Metalloproteases. *Molecules* **2022**, *27*, 1–18. https://doi.org/10.3390/molecules27010056.

(588) Wang, Z.; Rahkola, J.; Redzic, J. S.; Chi, Y. C.; Tran, N.; Holyoak, T.; Zheng, H.; Janoff, E.; Eisenmesser, E. Mechanism and Inhibition of Streptococcus Pneumoniae IgA1 Protease. *Nat. Commun.* **2020**, *11*, 1–8. https://doi.org/10.1038/s41467-020-19887-3.

(589) Stones, D. H.; Krachler, A. M. Fatal Attraction: How Bacterial Adhesins Affect Host Signaling and What We Can Learn from Them. *Int. J. Mol. Sci.* **2015**, *16*, 2626–2640. https://doi.org/10.3390/ijms16022626.

(590) Tamayo, R. Cyclic Diguanylate Riboswitches Control Bacterial Pathogenesis Mechanisms. *PLoS Pathog.* **2019**, *15* (2), 1–7. https://doi.org/10.1371/journal.ppat.1007529.

(591) Römling, U.; Galperin, M. Y.; Gomelsky, M. Cyclic Di-GMP: The First 25 Years of a Universal Bacterial Second Messenger. *Microbiol. Mol. Biol. Rev.* **2013**, *77*, 1–52. https://doi.org/10.1128/mmbr.00043-12.

(592) Purcell, E. B.; Tamayo, R. Cyclic Diguanylate Signaling in Gram-Positive Bacteria. *FEMS Microbiol. Rev.* **2016**, *40*, 753–773. https://doi.org/10.1093/femsre/fuw013.

(593) Zong, Y.; Xu, Y.; Liang, X.; Keene, D. R.; Höök, A.; Gurusiddappa, S.; Höök, M.; Narayana, S. V. L. A "Collagen Hug" Model for Staphylococcus Aureus CNA Binding to Collagen. *EMBO J.* **2005**, *24* (24), 4224–4236. https://doi.org/10.1038/sj.emboj.7600888.

(594) Walden, M.; Edwards, J. M.; Dziewulska, A. M.; Bergmann, R.; Saalbach, G.; Kan, S. Y.; Miller, O. K.; Weckener, M.; Jackson, R. J.; Shirran, S. L.; Botting, C. H.; Florence, G. J.; Rohde, M.; Banfield, M. J.; Schwarz-Linek, U. An Internal Thioester in a Pathogen Surface Protein Mediates Covalent Host Binding. *Elife* **2015**, *4* (JUNE), 1–24. https://doi.org/10.7554/eLife.06638.

(595) *Encyclopedia of Metalloproteins*, 1st ed.; Kretsinger, R. H., Uversky, V. N., Permyakov, E. A., Eds.; Springer New York, NY, 2013. https://doi.org/10.1007/978-1-4614-1533-6.

(596) Hooper, N. M. Families of Zinc Metalloproteases. **1994**, *354*, 1–6.

(597) Spyroulias, G. A.; Galanis, A. S.; Pairas, G.; Manessi-Zoupa, E.; Cordopatis, P. Structural Features of Angiotensin-I Converting Enzyme Catalytic Sites: Conformational Studies in

Solution, Homology Models and Comparison with Other Zinc Metallopeptidases. *Curr. Top. Med. Chem.* **2004**, *4*, 403–429. https://doi.org/10.2174/1568026043451294.

(598) Jones, J. C.; Rustagi, S.; Dempsey, P. J. ADAM Proteases and Gastrointestinal Function. *Annu. Rev. Physiol.* **2016**, *78*, 243–276. https://doi.org/10.1146/annurev-physiol-021014-071720.

(599) Nagase, H.; Visse, R.; Murphy, G. Structure and Function of Matrix Metalloproteinases and TIMPs. *Cardiovasc. Res.* **2006**, *69*, 562–573. https://doi.org/10.1016/j.cardiores.2005.12.002.

(600) Page-McCaw, A.; Ewald, A. J.; Werb, Z. Matrix Metalloproteinases and the Regulation of Tissue Remodelling. *Nat. Rev. Mol. Cell Biol.* **2007**, *8*, 221–233. https://doi.org/10.1038/nrm2125.

(601) Löffek, S.; Schilling, O.; Franzke, C. W. Biological Role of Matrix Metalloproteinases: A Critical Balance. *Eur. Respir. J.* **2011**, *38*, 191–208. https://doi.org/10.1183/09031936.00146510.

(602) Brzdak, P.; Nowak, D.; Wiera, G.; Mozrzymas, J. W. Multifaceted Roles of Metzincins in CNS Physiology and Pathology: From Synaptic Plasticity and Cognition to Neurodegenerative Disorders. *Front. Cell. Neurosci.* **2017**, *11*, 1–22. https://doi.org/10.3389/fncel.2017.00178.

(603) Rivera, S.; Khrestchatisky, M.; Kaczmarek, L.; Rosenberg, G. A.; Jaworski, D. M. Metzincin Proteases and Their Inhibitors: Foes or Friends in Nervous System Physiology? *J. Neurosci.* **2010**, *30*, 15337–15357. https://doi.org/10.1523/JNEUROSCI.3467-10.2010.

(604) Yong, V. W.; Power, C.; Forsyth, P.; Edwards, D. R. Metalloproteinases in Biology and Pathology of the Nervous System. *Nat. Rev. Neurosci.* **2001**, *2*, 502–511. https://doi.org/10.1038/35081571.

(605) Martin, M. D.; Matrisian, L. M. The Other Side of MMPs: Protective Roles in Tumor Progression. *Cancer Metastasis Rev.* **2007**, *26*, 717–724. https://doi.org/10.1007/s10555-007-9089-4.

(606) Breidenbach, M. A.; Brunger, A. T. Substrate Recognition Strategy for Butulinum Neurotoxin Serotype A. *Nature* **2004**, *432*, 925–929. https://doi.org/10.1038/nature03123.

(607) Teo, J. W. P.; Zhang, L. H.; Poh, C. L. Cloning and Characterization of a Metalloprotease from Vibrio Harveyi Strain AP6. *Gene* **2003**, *303*, 147–156. https://doi.org/10.1016/S0378-1119(02)01151-4.

(608) Molla, A.; Tanase, S.; Hong, Y.; Maeda, H. Interdomain Cleavage of Plasma Fibronectin by Zinc-Metalloproteinase from Serratia Marcescens. *Biochim. Biophys. Acta (BBA)/Protein Struct. Mol.* **1988**, *955*, 77–85. https://doi.org/10.1016/0167-4838(88)90181-1.

(609) Hase, C. C.; Finkelstein, R. A. Bacterial Extracellular Zinc-Containing Metalloproteases. *Microbiol. Rev.* **1993**, *57*, 823–837. https://doi.org/10.1128/mmbr.57.4.823-837.1993.

(610) Duesbery, N. S.; Webb, C. P.; Leppla, S. H.; Gordon, V. M.; Klimpel, K. R.; Copeland, T. D.; Ahn, N. G.; Oskarsson, M. K.; Fukasawa, K.; Paull, K. D.; Vande Woude, G. F. Proteolytic Inactivation of MAP-Kinase-Kinase by Anthrax Lethal Factor. *Science,* **1998**, *280*, 734–737. https://doi.org/10.1126/science.280.5364.734.

(611) Wu, J. W.; Chen, X. L. Extracellular Metalloproteases from Bacteria. *Appl. Microbiol. Biotechnol.* **2011**, *92*, 253–262. https://doi.org/10.1007/s00253-011-3532-8.

(612) Rubino, J. T.; Martinelli, M.; Cantini, F.; Castagnetti, A.; Leuzzi, R.; Banci, L.; Scarselli, M. Structural Characterization of Zinc-Bound Zmp1, a Zinc-Dependent Metalloprotease Secreted by Clostridium Difficile. *J. Biol. Inorg. Chem.* **2016**, *21*, 185–196. https://doi.org/10.1007/s00775-015-1319-6.

(613) Pichlo, C.; Juetten, L.; Wojtalla, F.; Schacherl, M.; Diaz, D.; Baumann, U. Molecular Determinants of the Mechanism and Substrate Specificity of Clostridium Difficile Proline-Proline Endopeptidase-1. *J. Biol. Chem.* **2019**, *294*, 11525–11535. https://doi.org/10.1074/jbc.RA119.009029.

(614) Hege, T.; Baumann, U. Protease C of Erwinia Chrysanthemi: The Crystal Structure and Role of Amino Acids Y228 and E189. *J. Mol. Biol.* **2001**, *314* (2), 187–193.

https://doi.org/10.1006/jmbi.2001.5124.

(615) Grams, F.; Dive, V.; Yiotakis, A.; Yiallouros, I.; Vassiliou, S.; Zwilling, R.; Bode, W.; Stocker, W. Structure of Astacin with a Transition-State Analogue Inhibitor. *Nat. Struct. Biol.* **1996**, *3* (8), 671–675. https://doi.org/10.1038/nsb0896-671.

(616) Matthews, B. W. Structural Basis of the Action of Thermolysin and Related Zinc Peptidases. *Acc. Chem. Res.* **1988**, *21* (9), 333–340. https://doi.org/10.1021/ar00153a003.

(617) Paul, T. J.; Barman, A.; Ozbil, M.; Bora, R. P.; Zhang, T.; Sharma, G.; Hoffmann, Z.; Prabhakar, R. Mechanisms of Peptide Hydrolysis by Aspartyl and Metalloproteases. *Phys. Chem. Chem. Phys.* **2016**, *18* (36), 24790–24801. https://doi.org/10.1039/c6cp02097f.

(618) Palomo, J. M. Solid-Phase Peptide Synthesis: An Overview Focused on the Preparation of Biologically Relevant Peptides. *RSC Adv.* **2014**, *4*, 32658–32672. https://doi.org/10.1039/c4ra02458c.

(619) Jaradat, D. M. M. Thirteen Decades of Peptide Synthesis: Key Developments in Solid Phase Peptide Synthesis and Amide Bond Formation Utilized in Peptide Ligation. *Amino Acids* **2018**, *50*, 39–68. https://doi.org/10.1007/s00726-017-2516-0.

(620) Nicolaou, K. C.; Estrada, A. A.; Zak, M.; Lee, S. H.; Safina, B. S. A Mild and Selective Method for the Hydrolysis of Esters with Trimethyltin Hydroxide. *Angew. Chemie - Int. Ed.* **2005**, *44* (9), 1378–1382. https://doi.org/10.1002/anie.200462207.

(621) Marra, I. F. S.; de Castro, P. P.; Amarante, G. W. Recent Advances in Azlactone Transformations. *European J. Org. Chem.* **2019**, 5830–5855. https://doi.org/10.1002/ejoc.201901076.

(622) De Castro, P. P.; Batista, G. M. F.; Dos Santos, H. F.; Amarante, G. W. Theoretical Study on the Epimerization of Azlactone Rings: Keto-Enol Tautomerism or Base-Mediated Racemization? *ACS Omega* **2018**, *3*, 3507–3512. https://doi.org/10.1021/acsomega.8b00060.

(623) Salomon, C. J.; Mata, E. G.; Mascaretti, O. A. Scope and Mechanism of Deprotection of

Carboxylic Esters by Bis(Tributyltin) Oxide. *J. Org. Chem.* **1994**, *59*, 7259–7266. https://doi.org/10.1021/jo00103a016.

(624) Furlán, R. L. E.; Mata, E. G.; Mascaretti, O. A. Cleavage of Carboxylic Esters Effected by Organotin Oxides and Hydroxides under Classical Heating and Microwave Irradiation. A Comparative Study. *Tetrahedron Lett.* **1996**, *37*, 5229–5232. https://doi.org/10.1016/0040-4039(96)01071-4.

(625) Hanessian, S.; Del Valle, J. R.; Xue, Y.; Blomberg, N. Total Synthesis and Structural Confirmation of Chlorodysinosin A. *J. Am. Chem. Soc.* **2006**, *128*, 10491–10495. https://doi.org/10.1016/j.tetlet.2012.07.121.

(626) Hong, S. H.; Sanders, D. P.; Lee, C. W.; Grubbs, R. H. Prevention of Undesirable Isomerization during Olefin Metathesis. *J. Am. Chem. Soc.* **2005**, *127*, 17160–17161. https://doi.org/10.1021/ja052939w.

(627) Lehman, S. E. J.; Schwendeman, J. E.; O'Donnell, P. M.; Wagener, K. B. Olefin Isomerization Promoted by Olefin Metathesis Catalysts. *Inorganica Chim. Acta* **2003**, *345*, 190–198. https://doi.org/10.1016/S0020-1693(02)01307-5.

(628) Hanessian, S.; Yang, G.; Rondeau, J. M.; Neumann, U.; Betschart, C.; Tintelnot-Blomley, M. Structure-Based Design and Synthesis of Macroheterocyclic Peptidomimetic Inhibitors of the Aspartic Protease β-Site Amyloid Precursor Protein Cleaving Enzyme (BACE). *J. Med. Chem.* **2006**, *49*, 4544–4567. https://doi.org/10.1021/jm060154a.

(629) Bruker. SAINT. Bruker AXS Inc.: Madison, Winsconsin, USA 2013.

(630) Krause, L.; Herbst-Irmer, R.; Sheldrick, G. M.; Stalke, D. Comparison of Silver and Molybdenum Microfocus X-Ray Sources for Single-Crystal Structure Determination. *J. Appl. Crystallogr.* **2015**, *48*, 3–10. https://doi.org/10.1107/S1600576714022985.

(631) Sheldrick, G. M. SHELXT - Integrated Space-Group and Crystal-Structure Determination. *Acta Crystallogr. Sect. A Found. Crystallogr.* **2015**, *A71*, 3–8. https://doi.org/10.1107/S2053273314026370.

(632) Sheldrick, G. M. Crystal Structure Refinement with SHELXL. *Acta Crystallogr. Sect. C Struct. Chem.* **2015**, *C71*, 3–8. https://doi.org/10.1107/S2053229614024218.

(633) Dolomanov, O. V.; Bourhis, L. J.; Gildea, R. J.; Howard, J. A. K.; Puschmann, H. OLEX2: A Complete Structure Solution, Refinement and Analysis Program. *J. Appl. Crystallogr.* **2009**, *42*, 339–341. https://doi.org/10.1107/S0021889808042726.

(634) Entwistle, D. A.; Jordan, S. I.; Montgomery, J.; Pattenden, G. Total Synthesis of Oxazole-Based Virginiamycin Antibiotics: 14,15- Anhydropristinamycin II(B). *Synthesis (Stuttg).* **1998**, 603–612. https://doi.org/10.1055/s-1998-5935.

(635) Radl, S.; Doubsky, J. A Method for the Preparation of Fingolimod. WO2013185740A1, 2006.

(636) Sharpless, K. B.; Michaelson, R. C. High Stereo- and Regioselectivities in the Transition Metal Catalyzed Epoxidations of Olefinic Alcohols by Tert-Butyl Hydroperoxide. *J. Am. Chem. Soc.* **1973**, *95*, 6136–6137.

(637) Nicolaou, K. C.; Ding, H.; Richard, J.-A.; Chen, D. Y.-K. Formal Total Synthesis of Echinopines A and B. *J. Am. Chem. Soc.* **2010**, *132*, 3815–3818. https://doi.org/10.1021/acs.orglett.5b01326.

(638) Bongini, A.; Cardillo, G.; Orena, M.; Porzi, G.; Sandri, S. Regio- and Stereocontrolled Synthesis of Epoxy Alcohols and Triols from Allylic and Homoallylic Alcohols via Iodo Carbonates. *J. Org. Chem.* **1982**, *47*, 4626–4633. https://doi.org/10.1021/jo00145a004.

(639) Calvani, F.; Crotti, P.; Gardelli, C.; Pineschi, M. Regiochemical Control of the Ring Opening of 1,2-Epoxides by Means of Chelating Processes. 8. Synthesis and Ring Opening Reactions of cis- and trans-Oxides Derived from 3-Benzyloxycyclohexene and 2-Benzyloxy-5,6-dihydro-2H-pyran. *Tetrahedron* **1994**, *50*, 12999–13022. https://doi.org/10.1016/S0040-4020(01)81219-9.

(640) Hanessian, S.; Mu, C. $Yb(OTf)_3$-Mediated Ring Opening of Functionalized Cyclopentane Epoxides with Aniline: Aspects of Regiochemistry and Stereochemistry. *Heterocycles* **2014**, *88*, 1553–1563. https://doi.org/10.1002/chin.201424058.

(641) Hudlicky, T.; Rinner, U.; Gonzalez, D.; Akgun, H.; Schilling, S.; Siengalewicz, P.; Martinot, T. A.; Pettit, G. R. Total Synthesis and Biological Evaluation of Amaryllidaceae Alkaloids: Narciclasine, Ent-7-deoxypancratistatin, Regioisomer of 7-Deoxypancratistatin, 10b-Epi-deoxypancratistatin, and Truncated Derivatives. *J. Org. Chem.* **2002**, *67*, 8726–8743. https://doi.org/10.1021/jo020129m.

(642) Yuan, Y.-A.; Lu, D.-F.; Chen, Y.-R.; Xu, H. Iron-Catalyzed Direct Diazidation for a Broad Range of Olefins. *Angew. Chemie - Int. Ed.* **2016**, *55*, 534–538. https://doi.org/10.1002/anie.201507550.

(643) Thimmaiah, K. N.; Horton, J. K.; Seshadri, R.; Israel, M.; Houghton, J. A.; Harwood, F. C.; Houghton, P. J. Synthesis and Chemical Characterization of N-Substituted Phenoxazines Directed toward Reversing Vinca Alkaloid Resistance in Multidrug-Resistant Cancer Cells Kuntebommanahalli. *J. Med. Chem.* **1992**, *35*, 3358–3364.

(644) Bello, C.; Dal Bello, G.; Cea, M.; Nahimana, A.; Aubry, D.; Garuti, A.; Motta, G.; Moran, E.; Fruscione, F.; Pronzato, P.; Grossi, F.; Patrone, F.; Ballestrero, A.; Dupuis, M.; Sordat, B.; Zimmermann, K.; Loretan, J.; Wartmann, M.; Duchosal, M. A.; Nencioni, A.; Vogel, P. Anti-Cancer Activity of 5-O-Alkyl 1,4-Imino-1,4-Dideoxyribitols. *Bioorganic Med. Chem.* **2011**, *19*, 7720–7727. https://doi.org/10.1016/j.bmc.2011.07.053.

(645) Mahender Reddy, K.; Bhimireddy, E.; Thirupathi, B.; Breitler, S.; Yu, S.; Corey, E. J. Cationic Chiral Fluorinated Oxazaborolidines. More Potent, Second-Generation Catalysts for Highly Enantioselective Cycloaddition Reactions. *J. Am. Chem. Soc.* **2016**, *138*, 2443–2453. https://doi.org/10.1021/jacs.6b00100.

(646) Ma, J. Acyclic Stereocontrol and Chemical Diversity and Application to the Total Synthesis of Bafilomycin A1, Université de Montréal, 2001.

(647) Kawade, R. K.; Liu, R.-S. Copper-Catalyzed Three-Component Annulations of Alkenes, Nitrosoarenes, and N-Hydroxyallylamines To Form Fused Oxazinane/Isoxazolidine Heterocycles. *Angew. Chemie - Int. Ed.* **2017**, *56*, 2035–2039. https://doi.org/10.1002/anie.201611388.

(648) Friesner, R. A.; Murphy, R. B.; Repasky, M. P.; Frye, L. L.; Greenwood, J. R.; Halgren, T. A.; Sanschagrin, P. C.; Mainz, D. T. Extra Precision Glide: Docking and Scoring Incorporating a Model of Hydrophobic Enclosure for Protein-Ligand Complexes. *J. Med. Chem.* **2006**, *49*, 6177–6196. https://doi.org/10.1021/jm051256o.

(649) Garsi, J.-B.; Komjáti, B.; Cullia, G.; Fejes, I.; Sipos, M.; Sipos, Z.; Fördős, E.; Markacz, P.; Balázs, B.; Lancelot, N.; Berger, S.; Raimbaud, E.; Brown, D.; Vuillard, L.-M.; Haberkorn, L.; Cukier, C.; Szlávik, Z.; Hanessian, S. Targeting NOX2 via P47/Phox-P22/Phox Inhibition with Novel Triproline Mimetics. *ACS Med. Chem. Lett.* **2022**, *13*, 949–954. https://doi.org/10.1021/acsmedchemlett.2c00094.

(650) Petermichl, M.; Loscher, S.; Schobert, R. Total Synthesis of Aurantoside G, an N-β-Glycosylated 3-Oligoenoyltetramic Acid from Theonella Swinhoei. *Angew. Chemie - Int. Ed.* **2016**, *55*, 10122–10125. https://doi.org/10.1002/anie.201604912.

(651) Abraham, M. H.; Abraham, R. J.; Acree, W. E.; Aliev, A. E.; Leo, A. J.; Whaley, W. L. An NMR Method for the Quantitative Assessment of Intramolecular Hydrogen Bonding; Application to Physicochemical, Environmental, and Biochemical Properties. *J. Org. Chem.* **2014**, *79*, 11075–11083. https://doi.org/10.1021/jo502080p.

Chapitre 8. Partie expérimentale

8.1 Informations générales

All reactions were performed in flame-dried glassware under a positive pressure of dry, oxygen free argon and in dry solvents. All flasks were flushed with three alternative cycles of vacuum/argon and sealed with Teflon. Anhydrous solvents were distilled under a positive pressure of argon before use and dried by standard methods. THF, ether, CH_2Cl_2 and toluene were dried by the SDS (Solvent Delivery System). Commercial grade reagents were used without further purification. Silica column chromatography was performed on 230-400 mesh silica gel. Reactions were monitored by mass spectrometry with positive ionization or by thin-layer chromatography carried out on a 0.25 mm aluminium-backed plate. Visualisation was effected by UV light (254 nm) or by staining with potassium permanganate solution, cerium ammonium molybdate (CAM), p-anisaldehyde or ninhydrin solution followed by heating. ^{1}H NMR and $^{13}C\{^{1}H\}$ NMR spectra were recorded on Bruker instruments with field strengths notated in the text at room temperature (298 K) with complete proton decoupling for nuclei other than ^{1}H unless otherwise stated. Chemical shifts are reported in parts per million (ppm) referenced from $CDCl_3$ (δ_H: 7.26 ppm and δ_C: 77.0 ppm) and CD_3OD (δ_H: 3.31 ppm and δ_C: 49.0 ppm). Coupling constants (J) are reported in Hertz (Hz). Multiplicities are given as multiplet (m), singlet (s), doublet (d), triplet (t), quartet (q), quintet (quin.) and broad (br.). Optical rotations were determined on an Anton Paar MCP 100 polarimeter at 589 nm at 25 °C. Specific rotations are given in units of 10^{-1} deg cm^2 g^{-1}. High Resolution Mass Spectra (HRMS) and High-Performance Liquid Chromatography (HPLC) were performed by the "Centre régional de spectroscopie de masse de l'Université de Montréal" with electrospray ionisation (ESI) coupled to a quantitative time-of-flight (TOF) detector. Infrared spectra were recorded on a FT-IR spectrometer and are reported in reciprocal centimetres (cm^{-1}). The data for the crystal was collected from a shock-cooled single crystal at 100 K on a Bruker Smart APEX three-circle diffractometer with a Microfocus Source using Quazar MX Mirror Optics as monochromator and a Bruker APEX2 CCD detector. The diffractometer was equipped with an Oxford Cryostream 700 low temperature device and used Cu K_α radiation (λ = 1.54178 Å). All data

were integrated with *SAINT* and a multi-scan absorption correction using *SADABS* was applied.[629,630] The structure were solved by dual methods using *XT* and refined by full-matrix least-squares methods against F^2 by *XL*.[631,632] Structure solution and refinement cycles were performed within the graphical user interface of *OLEX2*.[633] Ellipsoids are drawn at the 50% probability level and hydrogen atoms are shown as spheres of arbitrary size. All non-hydrogen atoms were refined with anisotropic displacement parameters. The hydrogen atoms were refined isotropically on calculated positions using a riding model with their U_{iso} values constrained to 1.2 times the U_{eq} of their pivot. Disordered moieties were refined using bond length restraints and displacement parameter restraints.

8.2 Partie expérimentale de l'article 1

8.2.1 Chemistry

8.2.1.1 Synthetic schemes

Schéma 8.1 Synthesis of compound **4**.

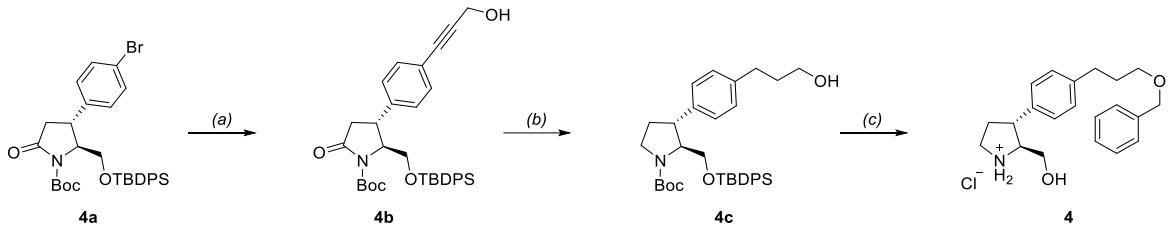

Conditions. (a) prop-2-yn-1-ol, $Pd(PPh_3)_4$, CuI, DMF/Et_3N, 70 °C. *(b)* **1.** H_2, Pd/C 10%, EtOH; **2.** BH_3-Me_2S, THF, from 0 °C to r.t. *(c)* **1.** BnBr, NaH, THF 0 °C; **2.** TBAF, THF; **3.** HCl (1M), Dioxane, CH_2Cl_2.

Schéma 8.2 Syntheses of compounds **5** and **6**.

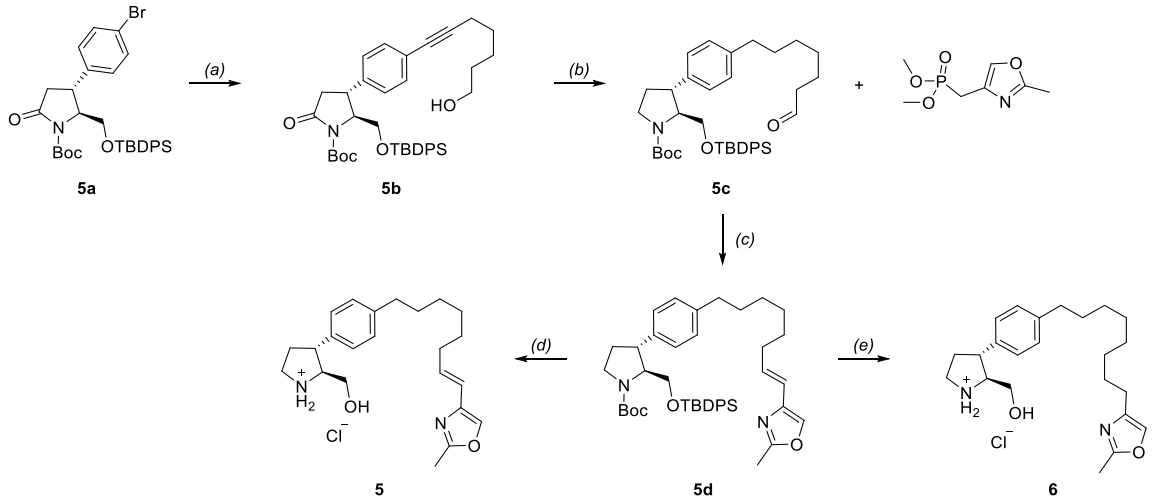

Conditions. (a) hept-6-yn-1-ol, $Pd(PPh_3)_4$, CuI, DMF/Et_3N, 70 °C. *(b)* **1.** H_2, Pd/C 10% EtOH 2. BH_3-Me_2S, THF, from 0 °C to r.t. 3. $(COCl)_2$, $DMSO/CH_2Cl_2$, -78 °C *then* Et_3N, from -78 °C to r.t. *(c)* LIHMDS, THF, from -78 °C to r.t. *(d)* **1.** TBAF, THF; **2.** HCl (1M), Dioxane, CH_2Cl_2. *(e)* **1.** H_2, Pd/C 10 %, Et_3N; **2.** TBAF, THF; **3.** HCl (1M), Dioxane, CH_2Cl_2.

Schéma 8.3 Synthesis of compound **7**.

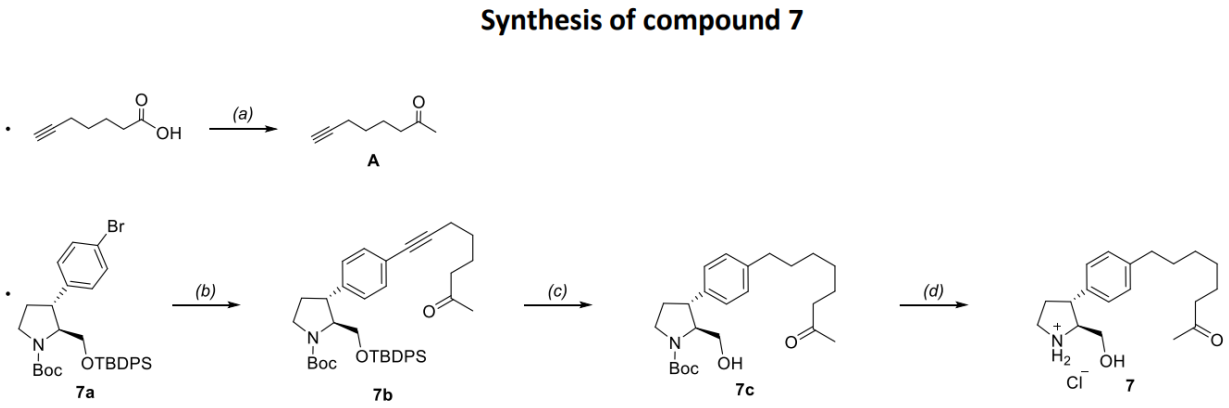

Conditions. (a) **1.** N,O-dimethylhydroxylamine-HCl, EDC-HCl , HOBT, CH_2Cl_2; **2.** MeMgBr, THF, 48%. *(b)* **A**, $Pd(PPh_3)_4$, CuI, DMF, Et_3N , 70 ºC, 52%. *(c)* 1. H_2 , Pd/C, EtOAc; 2. TBAF, THF, 98%. *(d)* HCl (4M), Dioxane, 99%.

Schéma 8.4 Synthesis of intermediates **12a** and **13a**.

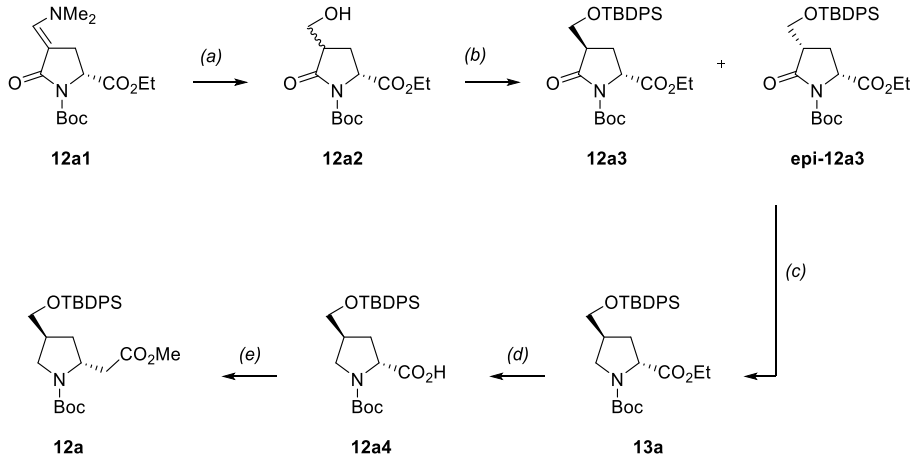

Conditions. (a) 1. MeOH, HCl*;* **2.** $NaBH_3CN$ *(b)* TBDPSCl, imidazole, DMF *(c)* **1.** $LiEt_3BH$, THF , -78 ºC**; 2.** BF_3OEt_2 , Et_3SiH, CH_2Cl_2 , -78 ºC *(d)* NaOH 1 N, MeOH *(e)* **1.** Isobutyl-chloroformate, Et_3N. THF; **2.** CH_2N_2, Et_2O; **3.** AgOBz , Et_3N, MeOH , reflux

8.2.1.2 Experimental procedures

General procedure A for N-Boc deprotection

HCl (500 µL, 4.0 M in dioxane, excess) was added to substrate in dry dioxane. The reaction mixture was stirred at rt until disappearance of the starting material by TLC analysis. The solution was then concentrated *in vacuo* in several cycles co-distilling with dry dioxane.

General procedure B for removal of silyl ethers

TBAF (1.1 eq., 1.0 M in THF) was added to a solution of substrate in dry THF (C = 60 mM). The reaction mixture was then stirred at rt until disappearance of the starting material by TLC analysis. The solution was diluted with saturated aq. $NaHCO_3$ solution and EtOAc. The aqueous layer was extracted x2 with EtOAc. The organic layers were combined, washed x1 with brine, dried over Na_2SO_4, filtered and concentrated.

General procedure C for addition of Grignard reagents

A 3-neck round-bottomed flask equipped with a thermometer and a condenser was flame-dried and flushed with Ar. The flask was then charged with Mg^0 (1.1 eq.), a single I_2 crystal and another vacuum/Ar cycle was performed. Et_2O (C = 0.65 M) was added resulting in a bright orange suspension of Mg^0 pellets. Octyl phenyl bromide (1.0 eq.) was then added in one portion and the suspension was heated *via* a heatgun until the internal temperature reached 32 °C and stabilized for 5-10 seconds, indicating that the Grignard formation had started. The reaction mixture was stirred at rt until disappearance of the starting material by ^1H NMR analysis (e.g. ≈ 1h).

The Grignard solution (3.0 eq., C = 0.65 M) was then syringed to another flask containing substrate (1.0. eq.) in dry Et_2O (C = 50 mM). The solution was stirred at rt until disappearance of the starting material by TLC analysis. Saturated aqueous NH_4Cl solution was added and the aqueous layer was extracted x2 with EtOAc. The organic layers were collected, washed sequentially x1 with HCl (1 M), $NaHCO_3$, brine, dried over Na_2SO_4, filtered and concentrated *in vacuo*.

tert-Butyl (2S,3R)-2-(((tert-butyldiphenylsilyl)oxy)methyl)-3-(4-(3-hydroxyprop-1-yn-1-yl)phenyl)-5-oxopyrrolidine-1-carboxylate **(4b)** (See Schéma 8.1)

tert-Butyl (2S,3R)-3-(4-bromophenyl)-2-(((*tert*-butyldiphenylsilyl)oxy)methyl)-5-oxopyrrolidine-1-carboxylate **4a** (0.18 g, 0.30 mmol, 1.0 equiv.) was dissolved in dry DMF (1 mL) and Et_3N (3 mL), then propargyl alcohol (0.14 mL, 2.4 mmol, 8.0 equiv.) was added. Argon was bubbled through the solution for 20 min, then CuI (17 mg, 90 µmol, 0.30 equiv.) and $Pd(PPh_3)_4$ (52 mg, 50 µmol, 1.5 equiv.) were added sequentially. The bubbling of Ar was continued for further 15 min, then the mixture was warmed to 70 °C and stirred for 18 h in a sealed flask. The mixture was extracted with an aqueous NH_4OH 1 M solution (100 mL) mixed with brine (100 mL) and EtOAc (100 mL x 4 times). The combined organic layers were dried over Na_2SO_4, filtered and the solvent was removed under reduced pressure. The crude was purified by silica gel column chromatography with hexane/EtOAc (gradient from 8:2 to 6:2) to afford the title compound **4b** as a brown oil (68 mg, 39%). R_f: 0.54 (Hexane/EtOAc 6:4). $[\alpha]^{20}_D$: +12.9° (*c* 0.5, $CHCl_3$). IR (neat), υ_{max}: 3435, 3165, 3071, 2927, 2856, 2167, 2079, 1778, 1748, 1713, 1366, 1149, 1107, 1029, 882, 700 cm^{-1}. ^1H NMR ($CDCl_3$, 500 MHz), δ: 7.70-7.60 (m, 4H), 7.48-7.36 (m, 8H), 7.09 (d, *J* = 8.2 MHz, 2H), 4.53-4.47 (m, 2H), 4.08-4.07 (m, 1H), 3.97 (dd, *J* = 10.6 MHz, *J* = 4.4 MHz, 1H), 3.80 (dd, *J* = 12.9 MHz, *J* = 2.6 MHz, 1H), 3.48 (broad d, *J* = 9.4 MHz, 1H), 3.19 (dd, *J* = 17.9 MHz, *J* = 9.4 MHz, 1H), 2.55 (dd, *J* = 17.9 MHz, *J* = 2.6 MHz, 1H), 1.85-1.75 (m, 1H), 1.42 (s, 9H), 1.08 (s, 9H) ppm. ^{13}C NMR ($CDCl_3$, 125 MHz), δ: 173.9, 149.7, 144.5, 135.7, 135.6, 133.0, 132.6, 130.1, 128.1, 128.0, 126.6, 121.7, 87.8, 85.2, 83.4, 66.6, 64.3, 51.8, 39.8, 38.7, 28.1, 27.0, 19.4, 1.2 ppm. HRMS (ESI) calcd. for $C_{35}H_{42}NO_5Si^+$ $(M+H)^+$: 584.28268, found: 584.28328.

tert-Butyl (2S,3R)-2-(((tert-butyldiphenylsilyl)oxy)methyl)-3-(4-(3-hydroxypropyl)phenyl)pyrrolidine-1-carboxylate **(4c)** (See Schéma 8.1)

tert-Butyl (2S,3R)-2-(((*tert*-butyldiphenylsilyl)oxy)methyl)-3-(4-(3-hydroxyprop-1-yn-1-yl)phenyl)-5-oxopyrrolidine-1-carboxylate **4b** (52 mg, 90 µmol) was dissolved in EtOH (0.80 mL) and Pd/C (10% w/w, 48 mg, 50 µmol, 0.5 eq.) was added. The air was pumped out of the flask and replaced by H_2. Upon completion (24 h), the reaction mixture was filtered through Celite. The solvent was removed under reduced pressure to afford a colorless oil. The crude was dissolved in dry THF (2 mL) and the solution was cooled to 0 °C. Borane dimethyl sulfide complex (50 µL, 0.53 mmol, 6.0

equiv.) was then added and the reaction mixture was allowed to reach room temperature and stirred for 18 h. The mixture was quenched with H_2O (1 mL) and the solvent was removed under reduced pressure. The residue was extracted with an aqueous $NaHCO_3$ saturated solution (50 mL) and CH_2Cl_2 (50 mL x 4 times). The combined organic layers were dried over Na_2SO_4 and filtered. The solvent was removed under reduced pressure to afford **4c** as a pale yellow oil (51 mg, 98% over two steps). R_f: 0.58 (Hexane/EtOAc 6:4). $[\alpha]^{20}_D$: -6.0° (*c* 0.5, $CHCl_3$). IR (neat), υ_{max}: 3461, 3070, 3047, 2958, 2929, 2858, 2166, 2115, 2010, 1692, 1589, 1514, 1472, 1454, 1426, 1391, 1364, 1254, 1166, 1106, 1070, 1033, 1006, 987, 923, 856, 821, 772, 737, 700, 643, 608 cm^{-1}. ^1H NMR ($CDCl_3$, 500 MHz, mixture of rotamers), δ: 7.70-762 (m, 4H), 7.46-7.34 (m, 6H), 7.15-7.06 (m, 4H), 4.20-3.35 (m, 7H), 2.74-2.64 (m, 1H), 2.59-2.52 (m, 1H), 2.31-2.17 (m, 1H), 1.95-1.83 (m, 2H), 1.68-1.55 (m, 1H), 1.50 (s, 3H), 1.33 (s, 6H), 1.06 (s, 9H), 0.98-0.92 (m, 1H) ppm. ^{13}C NMR ($CDCl_3$, 125 MHz, mixture of rotamers), δ: 154.4, 154.3, 141.1, 140.2, 135.8, 133.7, 133.5, 129.8, 129.7, 128.8, 127.9, 127.8, 127.7, 127.6, 127.4, 127.2, 79.5, 65.7, 65.5, 63.7, 62.5, 47.3, 46.6, 46.4, 45.5, 37.8, 34.3, 33.1, 32.0, 31.8, 28.7, 28.6, 27.0, 24.7, 19.5, 19.4, 14.0 ppm. HRMS (ESI) calcd. for $C_{35}H_{48}NO_4Si^+$ $(M+H)^+$: 574.33471, found: 574.33298.

(2S,3R)-3-(4-(3-(Benzyloxy)propyl)phenyl)-2-(hydroxymethyl)pyrrolidin-1-ium chloride **(4)** (See Schéma 8.1)

tert-Butyl (2S,3R)-2-(((*tert*-butyldiphenylsilyl)oxy)methyl)-3-(4-(3-hydroxypropyl)phenyl)pyrrolidine-1-carboxylate **4c** (34 mg, 60 µmol, 1.0 equiv.) was dissolved in dry THF (0.50 mL) and the solution was cooled 0 °C. To this solution NaH (60% in mineral oil, 12 mg, 0.30 mmol, 5.0 equiv.) was slowly added in one portion, then benzyl bromide (30 µL, 0.24 mmol, 4.0 equiv.) was added dropwise. The reaction mixture was stirred for 2 h, then quenched with the addition of an aqueous NH_4Cl saturated solution (1 mL) and extracted with brine (30 mL) and EtOAc (30 mL x 4 times), The combined organic layers were dried over Na_2SO_4 and filtered. The solvent was removed under reduced pressure to afford a pale yellow oil. This oil was dissolved in dry THF (1 mL) and the solution was cooled to 0 °C. Tetrabutylammonium fluoride solution (1 M in THF, 0.30 mL, 0.30 mmol, 5.0 equiv.) was added and the reaction mixture was warmed to room temperature and stirred for 18 h. The reaction mixture was quenched with an aqueous $NaHCO_3$ saturated solution (20 mL) and extracted three times with CH_2Cl_2 (30 mL). The combined

organic layers were washed with brine (30 mL), dried over Na_2SO_4 and filtered. The solvent was removed under reduced pressure to afford a pale yellow oil. To this crude a HCl 1 M solution in dioxane (0.50 mL, 0.50 mmol, 8.0 equiv.) was added. The reaction mixture was stirred at room temperature for 1 h, then the solvent was removed under reduced pressure. The crude mixture was purified by silica gel column chromatography with CH_2Cl_2/MeOH (gradient from 9:1 to 6:4) to give a pale yellow oil. This oil was dissolved in water, filtered through a plastic syringe filter (pore size: 0.45 µm) and lyophilized to afford the title compound **4** as a white solid (20 mg, 93% over three steps). R_f: 0.72 (CH_2Cl_2/MeOH 8:2). $[\alpha]^{20}_D$: -19.2° (*c* 0.1, MeOH). IR (neat), υ_{max}: 3254, 2922, 2848, 2496, 1719, 1595, 1516, 1494, 1476, 1452, 1427, 1391, 1353, 1307, 1265, 1206, 1174, 1117, 1067, 1046, 998, 920, 858, 841, 812, 791, 745, 699 cm^{-1}. ^1H NMR (MeOD, 500 MHz), δ: 7.37-7.18 (m, 9H), 4.50 (s, 2H), 3.75 (t, *J* = 5.6 MHz, 2H), 3.71-3.53 (m, 2H), 3.49 (*J* = 6.0 MHz, 2H), 3.45-3.35 (m, 1H), 3.35-3.25 (m, 1H), 2.70 (t, *J* = 7.2 MHz, 2H), 2.53-2.40 (m, 1H), 2.30-2.18 (m, 1H), 1.94-1.85 (m, 2H) ppm. ^{13}C NMR ($CDCl_3$, 125 MHz), δ: 141.5, 138.4, 135.7, 128.9, 128.0, 127.6, 127.3, 127.2, 72.6, 72.2, 71.1, 69.0, 67.1, 60.8, 58.3, 44.7, 44.6, 42.4, 32.5, 31.5, 31.2 ppm. HRMS (ESI) calcd. for $C_{21}H_{28}NO_2^+$ $(M+H)^+$: 326.21146, found: 326.21200.

tert-Butyl (2S,3R)-2-(((tert-butyldiphenylsilyl)oxy)methyl)-3-(4-(7-hydroxyhept-1-yn-1-yl)phenyl)-5-oxopyrrolidine-1-carboxylate **(5b)** (See Schéma 8.2)

tert-Butyl (2S,3R)-3-(4-bromophenyl)-2-(((*tert*-butyldiphenylsilyl)oxy)methyl)-5-oxopyrrolidine-1-carboxylate **5a** (436 mg, 720 µmol, 1.0 equiv.) was dissolved in dry DMF (3 mL) and Et_3N (1 mL), then 1-heptynol (180 µL, 1.44 mmol, 2.0 equiv.) was added. Inside the solution was bubbling a flow of Ar for 20 min before to add sequentially CuI (41 mg, 0.22 mmol, 0.3 equiv.) and $Pd(PPh_3)_4$ (125 mg, 110 µmol, 0.15 equiv.). The bubbling of Ar was continued for further 15 min, then the mixture was warmed to 70 °C and stirred for 18 h in a sealed flask. The mixture was extracted with an aqueous NH_4OH 1 M solution (100 mL) mixed with brine (100 mL) and EtOAc (100 mL x 4 times). The combined organic layers were dried over Na_2SO_4, filtered and the solvent was removed under reduced pressure. The crude was purified by silica gel column chromatography with hexane/EtOAc (gradient from 8:2 to 3:7) to afford the title compound **5b** as a brown oil. (345 mg, 75%). R_f: 0.51 (Hexane/EtOAc 5:5). $[\alpha]^{20}_D$: +12.3° (*c* 0.5, $CHCl_3$). IR (neat), υ_{max}: 3489, 3166, 2932, 2858, 2154, 1781, 1748, 1713, 1366, 1303, 1255, 1149, 1072, 822, 700 cm^{-1}. ^1H NMR ($CDCl_3$,

500 MHz), δ: 7.70-7.64 (m, 4H), 7.48-7.40 (m, 8H), 7.37 (d, *J* = 7.4 MHz, 2H), 7.10 (d, *J* = 7.4 MHz, 2H), 4.09 (broad s, 1H), 4.00 (dd, *J* = 10.6 MHz, *J* = 4.0 MHz, 1H), 3.83 (d, *J* = 10.6 MHz, 1H), 3.67 (t, *J* = 6.4 MHz, 2H), 3.51 (d, *J* = 8.9 MHz, 1H), 3.22 (dd, *J* = 17.8 MHz, *J* = 9.6 MHz, 1H), 2.58 (d, *J* = 17.8 MHz, 1H), 2.43 (t, *J* = 6.4 MHz, 2H), 1.86 (broad s, 1H), 1.68-1.50 (m, 4H), 1.44 (s, 9H), 1.11 (s, 9H) ppm. ^{13}C NMR ($CDCl_3$, 125 MHz), δ: 174.0, 149.6, 143.3, 135.6, 135.5, 132.9, 132.6, 132.2, 130.0, 128.0, 127.9, 126.3, 123.0, 90.6, 83.2, 80.2, 66.6, 64.2, 62.7, 39.7, 38.6, 32.3, 28.5, 28.0, 26.9, 25.1, 19.4, 19.2 ppm. HRMS (ESI) calcd. for $C_{39}H_{50}NO_5Si^+$ $(M+H)^+$: 640.34528, found: 640.34597.

tert-Butyl (2S,3R)-2-(((tert-butyldiphenylsilyl)oxy)methyl)-3-(4-(6 oxohexyl)phenyl)pyrrolidine-1-carboxylate **(5c)** (See Schéma 8.2)

tert-Butyl (2S,3R)-2-(((*tert*-butyldiphenylsilyl)oxy)methyl)-3-(4-(7-hydroxyhept-1-yn-1-yl)phenyl)-5-oxopyrrolidine-1-carboxylate **5b** (312 mg, 490 µmol, 1.0 equiv.) was dissolved in EtOH (2.5 mL) and Pd/C (10% w/w, 164 mg, 150 µmol, 0.3 equiv.) was added. The air was pumped out of the flask and replaced by H_2. Upon completion (18 h), the reaction mixture was filtered through Celite. The solvent was removed under reduced pressure to afford a colorless oil. The crude was dissolved in dry THF (5 mL) and the solution was cooled to 0 °C, then borane dimethyl sulfide complex (180 µL, 1.94 mmol, 4.0 equiv.) was added and the reaction mixture was allowed to warm to room temperature and stirred for 24 h. The mixture was quenched with H_2O (1 mL) and the solvent was removed under reduced pressure. The residue was extracted with an aqueous $NaHCO_3$ saturated solution (80 mL) and CH_2Cl_2 (80 mL x 4 times), The combined organic layers were dried over Na_2SO_4 and filtered. The solvent was removed under reduced pressure to afford a slight yellow oil. This crude was used directly for the next step without further purification. A solution of dimethyl sulfoxide (0.08 mL, 1.18 mmol, 2.4 equiv.) in CH_2Cl_2 (2 mL) was added dropwise, via cannula, over 10 min to a stirred solution of oxalyl chloride (50 µL, 0.59 mmol, 1.2 equiv.) in CH_2Cl_2 (2 mL) at -78 °C. The mixture was stirred at -78 °C for 15 min and then a solution of the previous alcohol in CH_2Cl_2 (3 mL) was added dropwise, via cannula, over 10 min. The mixture was stirred at -78 °C for 1 h and then Et_3N (250 µL, 1.76 mmol, 3.6 equiv.) was added dropwise over 5 min. The mixture was warmed to 0 °C over a period of 3.5 h, then quenched with an aqueous $NaHCO_3$ saturated solution (50 mL) and warmed to room temperature. The separated

aqueous layer was extracted with CH_2Cl_2 (50 mL x 3 times), and the combined organic layers were dried over Na_2SO_4 and concentrated in vacuum to leave a yellow oil which was purified by silica gel column chromatography with hexane/EtOAc (gradient from 9:1 to 8:2) to afford the title compound **5c** as a colourless oil (220 mg, 72% over three steps). R_f: 0.59 (Hexane/EtOAc 8:2). $[\alpha]^{20}_D$: -9.7° (*c* 0.3, $CHCl_3$). IR (neat), υ_{max}: 3072, 3050, 2951, 2831, 2740, 1732, 1692, 1426, 1390, 1164, 1105, 1070, 1034, 822, 701 cm^{-1}.^{1}H NMR ($CDCl_3$, 500 MHz, mixture of rotamers), δ: 9.76 (s, 1H), 7.71-7.63 (m, 4H), 7.46-733 (m, 6H), 7.16-7.06 (m, 4H), 4.20-3.35 (m, 6H), 2.62-2,55 (m, 2H), 2.42 (t, *J* = 7.2 MHz, 2H), 2.32-2.18 (m, 1H), 1.99-1.85 (m, 1H), 1.70-1,57 (m, 4H), 1.55-1.42 (m, 4H), 1.41-1.30 (m, 9H), 1.07 (s, 9H) ppm. ^{13}C NMR ($CDCl_3$, 125 MHz, mixture of rotamers), δ: 202.8, 154.3, 154.2, 141.1, 140.8, 135.6, 133.6, 133.4, 129.7, 129.6, 128.6, 127.8, 127.8, 127.7, 127.3, 127.2, 79.4, 79.1, 65.6 65.4, 63.6, 62.1, 60.4, 53.4, 47.2, 46.5, 46.3, 45.4, 43.9, 35.4, 32.9, 31.9, 31.3, 29.1, 29.0, 28.6, 28.4, 26.9, 22.0, 19.4, 19.3 ppm. HRMS (ESI) calcd. for $C_{39}H_{54}NO_4Si^+$ $(M+H)^+$: 628.38166, found: 628.38194.

tert-Butyl (2S,3R)-2-(((tert-butyldiphenylsilyl)oxy)methyl)-3-(4-((E)-7-(2-methyloxazol-4-yl)hept-6-en-1-yl)phenyl)pyrrolidine-1-carboxylate **(5d)** (See Schéma 8.2)

A solution of lithium bis(trimethylsilyl)amide (1.0 M in THF, 0.49 mL, 0.49 mmol, 2.0 equiv.) was added over 5 min via syringe to a stirred solution of dimethyl((2-methyloxazol-4-yl)methyl)phosphonate). The oxazole phosphonate derivative was prepared by using standard procedures from the known 4-hydroxymethyl-2-methyloxazole [634] (101 mg, 490 µmol, 2.0 equiv.) in dry THF (2 mL) at -78 °C. The resulting orange solution was stirred at -78 °C for 30 min and then a solution of the aldehyde derivative **5c** (154 mg, 250 µmol, 1.0 equiv.) in dry THF (2 mL) was added via cannula. The mixture was allowed to warm slowly to room temperature over 5 h, stirred overnight, and then quenched with an aqueous NH_4Cl saturated solution (20 mL) and diluted with EtOAc (50 mL). The organic extract was washed with brine (50 mL), then dried over Na_2SO_4, filtered and evaporated to dryness. The residue was purified by silica gel column chromatography with hexane/EtOAc (gradient from 9:1 to 8:2) to afford the title compound **5d** as a colourless oil (88 mg, 51%). R_f: 0.36 (Hexane/EtOAc 85:15). $[\alpha]^{20}_D$: -15.2° (*c* 0.5, $CHCl_3$). IR (neat), υ_{max}: 3072, 3045, 2956, 2855, 2032, 2022, 1692, 1654, 1516, 1488, 1447, 1410, 1391, 1270, 1070, 982, 742, 700 cm^{-1}. ^{1}H NMR ($CDCl_3$, 400 MHz, mixture of rotamers), δ: 7.79-7.66 (m, 4H), 7.46-7.25 (m, 7H),

7.15-7.05 (m, 4H), 6.40 (dt, *J* = 15.6 MHz, *J* = 7.0 MHz, 1H), 6.17 (d, *J* = 15.6 MHz, 1H), 4.25-3.35 (m, 5H), 2.63-2.52 (m, 2H), 2.44 (s, 3H), 2.35-2.15 (m, 3H), 2.00-1.85 (m, 1H), 1.70-1.25 (m, 16H), 1.08 (s, 9H) ppm. ^{13}C NMR ($CDCl_3$, 100 MHz, mixture of rotamers), δ: 161.6, 154.4, 141.2, 139.2, 135.7, 133.6, 132.9, 129.8, 128.7, 127.8, 127.2, 118.2, 79.4, 72.7, 65.7,64.7, 63.6, 48.1, 46.6, 35.6, 32.9, 32.0, 31.5, 29.3, 29.1, 28.7, 28.5, 27.0, 19.4, 14.0 ppm. HRMS (ESI) calcd. for $C_{44}H_{59}N_2O_4Si^+$ $(M+H)^+$: 707.42386, found: 707.42492.

(2S,3R)-2-(Hydroxymethyl)-3-(4-((E)-7-(2-methyloxazol-4-yl)hept-6-en-1-yl)phenyl)pyrrolidin-1-ium chloride **(5)** (See Schéma 8.2)

tert-Butyl (2S,3R)-2-(((*tert*-butyldiphenylsilyl)oxy)methyl)-3-(4-((E)-7-(2-methyloxazol-4-yl)hept-6-en-1-yl)phenyl)pyrrolidine-1-carboxylate **5d** (27 mg, 40 µmol, 1.0 equiv.), was dissolved in dry THF (1 mL) and the solution was cooled to 0 °C. Tetrabutylammonium fluoride solution (1.0 M in THF, 80 µL, 80 µmol, 2.0 equiv.) was added and the reaction mixture was warmed to room temperature and stirred for 24 h. The reaction mixture was quenched with an aqueous $NaHCO_3$ saturated solution (20 mL) and extracted with CH_2Cl_2 (30 mL x 3 times). The combined organic layers were washed with brine (50 mL), dried over Na_2SO_4 and filtered. The solvent was removed under reduced pressure to afford a pale yellow oil. To this crude a HCl 1 M solution in dioxane (0.50 mL, 0.50 mmol, 13 equiv.) was added. The reaction mixture was stirred at room temperature for 1 h, then the solvent was removed under reduced pressure. The crude mixture was purified by silica gel column chromatography with CH_2Cl_2/MeOH (gradient from 9:1 to 6:4) to give a yellow oil. This oil was dissolved in water, filtered through a plastic syringe filter (pore size: 0.45 µm) and lyophilized to afford the title compound **5** as a white solid (15 mg, 96% over two steps). R_f: 0.59 (CH_2Cl_2/MeOH 8:2). $[\alpha]^{20}_D$: -16.5° (*c* 0.2, MeOH). IR (neat), υ_{max}: 3331, 3254, 2929, 2857, 2029, 2020, 1654, 1515, 1487, 1449, 1407, 1270, 1079, 982, 742, 705, 576 cm^{-1}. ^{1}H NMR (MeOD, 500 MHz), δ: 7.63 (s, 1H), 7.27 (d, *J* = 11.0, MHz, 2H), 7.22 (d, *J* = 11.0 MHz, 2H), 6.38-6.29 (m, 1H), 6.21 (d, *J* = 15.8 MHz, 1H), 3.88-3.75 (m, 1H), 3.70-3.53 (m, 3H), 2.63 (t, *J* = 7.7 MHz, 2H) 2.53-2.42 (m, 1H), 2.45 (s, 3H), 2.30-2.15 (m, 3H), 1.70-1.57 (m, 2H), 1.55-1.30 (m, 6H) ppm. ^{13}C NMR (MeOD, 125 MHz), δ: 162.3, 142.3, 138.7, 135.5, 134.3, 132.4, 128.8, 127.1, 117.7, 67.1, 58.2, 44.7, 44.5, 35.0, 32.4, 32.3, 31.2, 28.8, 28.7, 28.6, 12.1 ppm. HRMS (ESI) calcd. for $C_{23}H_{33}N_2O_2^+$ $(M+H)^+$: 369.25365, found: 369.25509.

(2S,3R)-2-(Hydroxymethyl)-3-(4-(7-(2-methyloxazol-4-yl)heptyl)phenyl)pyrrolidin-1-ium chloride **(6)** (See Schéma 8.2)

tert-Butyl (2*S*,3*R*)-2-(((*tert*-butyldiphenylsilyl)oxy)methyl)-3-(4-((E)-7-(2-methyloxazol-4-yl)hept-6-en-1-yl)phenyl)pyrrolidine-1-carboxylate **5d** (34 mg, 50 µmol, 1.0 eq.) was dissolved in freshly distilled Et_3N (1 mL) and Pd/C (10% w/w, 20 mg, 20 µmol, 0.4 eq.) was added. The air was pumped out of the flask and replaced by H_2. Upon completion (6 h), the reaction mixture was filtered through Celite. The solvent was removed under reduced pressure to afford a colorless oil. This oil was dissolved in dry THF (1 mL) and the solution was cooled to 0 °C. Tetrabutylammonium fluoride solution (1.0 M in THF, 0.10 mL, 0.10 mmol, 2.0 equiv.) was added and the reaction mixture was warmed to room temperature and stirred for 24 h. The reaction mixture was quenched with an aqueous $NaHCO_3$ saturated solution (30 mL) and extracted with CH_2Cl_2 (30 mL x 4 times). The combined organic layers were washed with brine (60 mL), dried over Na_2SO_4 and filtered. The solvent was removed under reduced pressure to afford a pale yellow oil. To this crude a HCl solution in dioxane (1.0 M, 0.50 mL, 0.50 mmol, 10 equiv.) was added. The reaction mixture was stirred at room temperature for 1 h, then the solvent was removed under reduced pressure. The crude mixture was purified by silica gel column chromatography with CH_2Cl_2/MeOH (gradient from 9:1 to 6:4) to give a pale yellow oil. This oil was dissolved in water, filtered through a plastic syringe filter (pore size: 0.45 µm) and lyophilized to afford the title compound **6** as a white solid (17 mg, 88% over three steps). R_f: 0.59 (CH_2Cl_2/MeOH 8:2). $[\alpha]^{20}_D$: -22.9° (*c* 0.2, MeOH). IR (neat), υ_{max}: 3390, 3192, 2924, 2855, 2344, 2244, 2166, 2038, 1709, 1654, 1607, 1515, 1381, 1227, 1181, 1065, 1032, 1019, 819, 723, 599, 543 cm^{-1}. ^1H NMR (DMSO, 500 MHz), δ: 9.86 (broad s, 1H), 9.02 (broad s, 1H), 7.67 (s, 1H), 7.25 (d, *J* = 8.1 MHz, 2H), 7.16 (d, *J* = 8.1 MHz, 2H), 3.62-3.43 (m, 3H), 3.42-3.35 (m, 1H), 3.25-3.12 (m, 3H), 2.56-2.52 (m, 2H) 2.39-2.35 (m, 1H) 2.36 (s, 3H), 2.34-2.25 (m, 1H), 2.07-1.98 (m, 1H), 1.68 (m, 4H), 1.32-1.20 (m, 9H) ppm. ^{13}C NMR (DMSO, 125 MHz), δ: 160.7, 141.3, 139.7, 136.7 134.3, 128.6, 127.5, 66.5, 62.8, 58.5, 48.6, 44.3, 44.2, 34.7, 32.5, 31.0, 28.8, 28.7, 28.5, 27.7, 25.3, 13.5 ppm. HRMS (ESI) calcd. for $C_{23}H_{35}N_2O_2^+$ $(M+H)^+$: 371.26930, found: 371.26964.

tert-Butyl (2S,3R)-2-(((tert-butyldiphenylsilyl)oxy)methyl)-3-(4-(7-oxooct-1-yn-1-yl)phenyl)pyrrolidine-1-carboxylate **(7b)** (See Schéma 8.3)

A solution of commercially available oct-7-yn-2-one **A** (176 mg, 1.42 mmol, 2.0 eq.) in dry DMF (500 µL) was added to a solution of **7a** (422 mg, 710 µmol, 1.0 eq.) in dry DMF (1.2 mL) and Et_3N (727 µL). The resulting mixture was degassed by bubbling argon for 20 min, before adding CuI (41 mg, 0.23 mmol, 0.3 eq.) and $Pd(PPh_3)_4$ (82 mg, 71 µmol, 0.1 eq.). After having been degassed again for additional 15 min, the reaction mixture was stirred for 48 h at 70 °C. Afterwards, the mixture was diluted with a combination of NH_4OH 1 M (25 mL) and brine (50 mL) and the product was extracted with EtOAc (4 x 30 mL). The combined organic layers were dried over Na_2SO_4, filtered and concentrated. The residue was purified by flash column chromatography (EtOAc/hexane 1:6, R*f*: 0.09) to give **7b** as a yellow oil (236 mg, 52%). $[\alpha]^{25}_D$: -0.8 (*c* 1.55, $CHCl_3$). IR (neat), υ_{max}: 2931, 2858, 1690, 1510, 1472, 1427, 1391, 1364, 1240, 1166, 1107, 1070, 987, 823, 773, 740, 702, 605, 541, 504 cm^{-1}. ^1H NMR ($CDCl_3$, 500 MHz, mixture of rotamers), δ: 7.67-7.62 (m, 4 H), 7.42-7.35 (m, 6 H), 7.31 (t, *J* = 9.1 Hz, 2H), 7.07 (d, *J* = 7.5 Hz, 2 H), 4.13 (dd, *J* = 10.1, 3.4 Hz, 0.4 H), 3.89 (br. s, 0.4 H), 3.79-3.75 (m, 1.8 H), 3.72-3.69 (m, 1 H), 3.64-3.59 (m, 1 H), 3.56-3.52 (m, 0.4 H), 3.44-3.38 (m, 1 H), 2.49 (t, J = 7.3 Hz, 2 H), 2.42 (t, J = 6.9 Hz, 2 H), 2.30-2.22 (m, 1 H), 2.15 (s, 3 H), 1.93-1.86 (m, 1 H), 1.77-1.72 (m, 2 H), 1.63-1.58 (m, 2 H), 1.50 (s, 3.6 H), 1.33 (s, 5.4 H), 1.06 (s, 9 H) ppm. ^{13}C NMR ($CDCl_3$, 125 MHz, mixture of rotamers), δ: 208.7, 154.2, 143.3, 142.7, 135.6, 133.7, 133.5, 133.4, 133.3, 131.8, 129.7, 129.6, 127.7, 127.3, 127.1, 122.1, 89.5, 80.7, 79.5, 79.2, 65.4, 65.1, 63.5, 62.1, 47.0, 46.5, 46.4, 45.6, 43.2, 32.7, 31.7, 29.9, 28.6, 28.4, 28.1, 26.8, 23.0, 19.2 ppm. HRMS (ESI) calcd. for $C_{40}H_{52}NO_4Si$ $(M+H)^+$ 638.36601, found 638.36681.

tert-Butyl (2S,3R)-2-(hydroxymethyl)-3-(4-(7-oxooctyl)phenyl)pyrrolidine-1-carboxylate **(7c)** (See Schéma 8.3)

7b (200 mg, 0.31 mmol, 1.0 eq.) was dissolved in EtOAc (5 mL) and Pd/C (10%, 37 mg, 34 µmol, 0.11 eq.) was added to the resulting solution. The air was removed from the flask under vacuum and replaced with hydrogen (balloon). The reaction mixture was vigorously stirred overnight at room temperature. Afterwards, the mixture was filtered through a Celite pad, washing with EtOAc. The collected solution was concentrated *in vacuo*, affording the intermediate (*2S,3R*)-2-(((*tert*-butyldiphenylsilyl)oxy)methyl)-3-(4-(7-oxooctyl)phenyl)pyrrolidine-1-carboxylate a colorless oil (201 mg, 99%). $[\alpha]^{25}_D$: +8.5 (*c* 0.87, $CHCl_3$). IR (neat), υ_{max}: 2929, 2856, 1692, 1514, 1472, 1427, 1392, 1365, 1254, 1166, 1108, 987, 856, 822, 772, 740, 701, 607, 504 cm^{-1}. ^1H NMR

($CDCl_3$, 500 MHz, mixture of rotamers), δ: 7.73-7.63 (m, 4 H), 7.42-7.35 (m, 6 H), 7.15-7.08 (m, 4 H), 4.16-4.13 (m, 0.4 H), 3.90 (br. s, 0.4 H), 3.84-3.76 (m, 1.8 H), 3.72-3.69 (m, 1 H), 3.66-3.60 (m, 1 H), 3.58-3.54 (m, 0.4 H), 3.44-3.39 (m, 1 H), 2.59-2.55 (m, 2 H), 2.41 (t, J = 7.4 Hz, 2 H), 2.30-2.21 (m, 1 H), 2.13 (s, 3 H), 1.95-1.88 (m, 1 H), 1.62-1.55 (m, 4 H), 1.50 (s, 3.6 H), 1.33 (br. s, 9.4 H), 1.06 (s, 9 H) ppm. ^{13}C NMR ($CDCl_3$, 125 MHz, mixture of rotamers), δ: 209.2, 154.3, 154.2, 141.0, 140.9, 135.6, 134.8, 133.8, 133.6, 133.5, 133.4, 129.7, 129.6, 128.6, 127.7, 127.3, 127.1, 79.4, 79.0, 65.5, 65.3, 63.5, 62.1, 47.1, 46.4, 46.2, 45.3, 43.7, 35.4, 32.9, 31.9, 31.3, 29.8, 29.1, 29.0, 28.6, 28.5, 28.4, 28.0, 26.9, 26.5, 23.7, 19.4. 19.3 ppm. HRMS (ESI) calcd. for $C_{40}H_{56}NO_4Si$ $(M+H)^+$ 642.3973, found 642.40020.

(*2S,3R*)-2-(((*tert*-butyldiphenylsilyl)oxy)methyl)-3-(4-(7-oxooctyl)phenyl)pyrrolidine-1-carboxylate (50 mg, 78 µmol) was submitted to general procedure B. The crude was purified by flash column chromatography (EtOAc/hexane 1:1, R*f*: 0.29) to give **7c** as a colorless oil (31 mg, 99%). IR (neat), υ_{max}: 3402, 2928, 2855, 1690, 1666, 1514, 1454, 1394, 1365, 1251, 1165, 1115, 1084, 1054, 968, 854, 772, 535 cm^{-1}. ^1H NMR ($CDCl_3$, 500 MHz), δ: 7.15-7.11 (m, 4 H), 3.91-3.88 (m, 1 H), 3.76-3.73 (m, 2 H), 3.61 (dd, *J* = 11.5, 6.9 Hz, 1 H), 3.34 (td, *J* = 10.5, 6.4 Hz, 1 H), 2.90 (br. s, 1 H), 2.58-2.55 (m, 2 H), 2.41 (t, *J* = 7.4 Hz, 2 H), 2.13 (s, 3 H), 1.99-1.91 (m, 1 H), 1.62-1.54 (m, 4 H), 1.50 (s, 9 H), 1.34-1.30 (m, 4 H) ppm. ^{13}C NMR ($CDCl_3$, 125 MHz), δ: 209.3, 156.5, 141.6, 138.0, 128.7, 127.5, 80.5, 67.0, 65.7, 47.5, 47.1, 43.7, 35.4, 32.8, 31.2, 29.9, 29.0, 28.5, 23.7 ppm. HRMS (ESI) calcd. for $C_{24}H_{37}NO_4Na$ $(M+Na)^+$ 426.26150, found 426.26007.

8-(4-((2S,3R)-2-(hydroxymethyl)pyrrolidin-3-yl)phenyl)octan-2-one hydrochloride **(7)** (See Schéma 8.3)

Prepared according to general procedure A, starting from **7c** (20 mg, 50 µmol). The crude was recrystallized from EtOAc to give product **7** as a white solid (16 mg, 94%). For biological testing a portion of the product was dissolved in the minimum amount of HPLC grade water, filtered (pore size = 0.45 µm) and lyophilized. $[\alpha]^{25}_D$: +16.4 (*c* 0.55, $CHCl_3$). IR (neat), υ_{max}: 3277, 2922, 2848, 1707, 1589, 1517, 1464, 1401, 1367, 1332, 1216, 1161, 1110, 1064, 1020, 965, 928, 819, 775, 716, 654, 634, 591, 542, 503 cm^{-1}. ^1H NMR (CD_3OD, 500 MHz), δ: 7.27 (d, J = 8.2 Hz, 2 H), 7.22 (d, J = 8.2 Hz, 2 H), 3.77 (q, *J* = 6.2 Hz, 1 H), 3.66-3.60 (m, 2 H), 3.58 (ddd, *J* = 11.8, 8.8, 3.3 Hz, 1 H), 3.41

(ddd, *J* = 11.8, 9.9, 7.3 Hz, 1 H), 3.31-3.27 (m, 1 H), 2.64-2.61 (m, 2 H), 2.50-2.45 (m, 3 H), 2.28-2.20 (m, 1 H), 2.14 (s, 3 H), 1.66-1.60 (m, 2 H), 1.59-1.53 (m, 2 H), 1.37-1.32 (m, 4 H) ppm. ^{13}C NMR (CD_3OD, 125 MHz), δ: 210.7, 142.2, 135.5, 128.8, 127.1, 67.1, 58.2, 44.7, 44.5, 42.8, 35.0, 32.4, 31.1, 28.6, 28.4, 23.4 ppm.

tert-Butyl (S)-2-(2-(4-octylphenyl)-2-oxoethyl)pyrrolidine-1-carboxylate **(8b)**

Prepared according to general procedure C, starting from **8a** [25] (300 mg, 1.10 mmol). The crude was purified by flash column chromatography (EtOAc/hexane 1:6, R*f*: 0.17) to give **8b** as a colorless oil (274 mg, 62%). $[\alpha]^{25}_D$: -22.9 (*c* 1.3, $CHCl_3$). IR (neat), υ_{max}: 2924, 2854, 1680, 1606, 1455, 1391, 1365, 1277, 1169, 1116, 1012, 989, 772, 545 cm^{-1}. ^{1}H NMR ($CDCl_3$, 500 MHz, mixture of rotamers), δ: 7.96-7.87 (m, 2 H), 7.25 (d, *J* = 7.5 Hz, 2 H), 4.34-4.29 (m, 1 H), 3.74 (br. d, *J* = 14.8 Hz, 0.5 H), 3.47 (br. d, *J* = 15.2 Hz, 0.5 H), 3.40 (br. s, 1 H), 3.32 (br. s, 1 H), 2.85-2.73 (m, 1 H), 2.64 (br. s, 2 H), 2.03 (br. s, 1 H), 1.90-1.79 (m, 2 H), 1.75 (br. s, 1 H), 1.64-1.57 (m, 2 H), 1.45 (s, 9 H), 1.30-1.22 (m, 10 H), 0.86 (t, *J* = 7.0 Hz, 3 H) ppm. ^{13}C NMR ($CDCl_3$, 125 MHz, mixture of rotamers), δ: 198.8, 198.3, 154.4, 154.3, 149.1, 148.7, 134.6, 128.7, 128.5, 128.4, 79.7, 79.2, 54.5, 54.3, 46.7, 46.2, 43.7, 43.0, 36.0, 31.9, 31.3, 31.1, 30.3, 29.4, 29.3, 29.2, 28.6, 23.6, 22.8, 22.6, 14.1 ppm. HRMS (ESI) calcd. for $C_{25}H_{40}NO_3$ $(M+H)^+$ 402.30027, found 402.29965.

(S)-1-(4-Octylphenyl)-2-(pyrrolidin-2-yl)ethan-1-one hydrochloride **(8)**

Prepared according to general procedure A, starting from **8b** (100 mg, 250 µmol). The crude was purified by flash column chromatography ($EtOH/CH_2Cl_2$ 1:4, R*f*: 0.45) to give product **8** as a white solid (84 mg, 99%). Note: the product racemized spontaneously when dissolved in MeOH or H_2O. For biological testing a portion of this solid was dissolved in the minimum amount of HPLC grade water, filtered (pore size = 0.45 µm) and lyophilized. $[\alpha]^{25}_D$: -39.1 (*c* 0.23, $CHCl_3$). IR (neat), υ_{max}: 2921, 2852, 1678, 1605, 1589, 1466, 1377, 1222, 1188, 1032, 976, 914, 822, 770, 569 cm^{-1}. ^{1}H NMR ($CDCl_3$, 400 MHz), δ: 9.52 (br. s, 2 H), 7.86 (d, *J* = 8.1 Hz, 2 H), 7.18 (d, *J* = 7.8 Hz, 2 H), 4.17-4.09 (m, 1 H), 3.89 (dd, *J* = 18.4, 5.9 Hz, 1 H), 3.50 (dd, *J* = 18.4, 6.8 Hz, 1 H), 3.40 (t, *J* = 7.2 Hz, 2 H), 2.61-2.57 (m, 2 H), 2.37-2.29 (m, 1 H), 2.10-1.95 (m, 2 H), 1.81-1.70 (m, 1 H), 1.59-1.54 (m, 2 H), 1.30-1.24 (m, 10 H), 0.88 (t, *J* = 6.8 Hz, 3 H) ppm. ^{13}C NMR ($CDCl_3$, 125 MHz), δ: 196.8, 149.6,

133.6, 128.7, 128.4, 56.0, 45.0, 40.5, 36.0, 31.9, 31.0, 30.6, 29.7, 29.4, 29.3, 29.2, 23.6, 22.6, 14.1 ppm. HRMS (ESI) calcd. for $C_{20}H_{32}NO$ $(M)^+$ 302.24784, found 302.24782.

tert-Butyl (2S)-2-(2-hydroxy-2-(4-octylphenyl)ethyl)pyrrolidine-1-carboxylate **(8c)**

$NaBH_4$ (4.9 mg, 0.13 mmol, 1.5 eq.) was added to a solution of **8b** (35 mg, 87 µmol) in MeOH (3 mL) at 0 °C. The resulting mixture was stirred for 2 h at the same temperature. Afterwards, the reaction mixture was quenched with brine (1 mL), the MeOH was removed *in vacuo* and the product was extracted with EtOAc (4 x 4 mL). The organic layers were dried over Na_2SO_4, filtered and concentrated. The residue was purified by flash column chromatography (EtOAc/hexane 1:6, then EtOAc/hexane 1:4 R*f*: 0.38 and 0.19) to give **8c diast1** (7 mg, 20%) and **8c diast2** (28 mg, 80%) as colorless oils. **8c diast1:** $[\alpha]^{20}_D$: -8.0 (*c* 0.2, MeOH). IR (neat), υ_{max}: 3406, 2923, 2851, 1723, 1671, 1397, 1245, 1168, 1104, cm^{-1}. ^1H NMR ($CDCl_3$, 300 MHz), δ: 7.28 (d, *J* = 7.9 Hz, 2 H), 7.13 (d, *J* = 8.0 Hz, 2 H), 5.33 (br. s, 1 H), 4.64-4.57 (m, 1 H), 4.33-4.25 (m, 1 H), 3.37 (t, *J* = 6.6 Hz, 2 H), 2.60-2.54 (m, 2 H), 2.03-1.93 (m, 2 H), 1.91-1.87 (m, 2 H), 1.72-1.67 (m, 2 H), 1.62-1.54 (m, 2 H), 1.49 (s, 9 H), 1.25 (br. s, 10 H), 0.87 (t, *J* = 6.8 Hz, 3 H) ppm. ^{13}C NMR ($CDCl_3$, 75 MHz), δ: 156.7, 141.6, 141.5, 128.2, 125.6, 80.0, 69.8, 54.0, 46.6, 46.3, 35.6, 31.9, 31.5, 31.2, 29.7, 29.5, 29.3, 28.5, 23.6, 22.7, 14.1 ppm. HRMS (ESI) calcd. for $C_{25}H_{41}NO_3Na$ $(M+Na)^+$ 426.29787, found 426.29919. **8c diast2** $[\alpha]^{20}_D$: -52.5 (*c* 0.8, MeOH). IR (neat), υ_{max}: 3413, 2924, 2854, 1668, 1393, 1365, 1247, 1168, 1103, 849, 772, 557 cm^{-1}. ^1H NMR ($CDCl_3$, 300 MHz), δ: 7.26 (d, *J* = 7.8 Hz, 2 H), 7.13 (d, *J* = 7.7 Hz, 2 H), 4.74 (br. s, 1 H), 4.10 (br. s, 1 H), 3.31 (br. s, 2 H), 2.60-2.55 (m, 2 H), 2.14 (br. s, 1 H), 2.05-1.93 (m, 1 H), 1.89-1.79 (m, 2 H), 1.69 (br. s, 2 H), 1.61-1.54 (m, 2 H), 1.46 (s, 9 H), 1.30-1.26 (m, 10 H), 0.87 (t, *J* = 6.8 Hz, 3 H) ppm. ^{13}C NMR ($CDCl_3$, 75 MHz), δ: 155.4, 142.3, 141.6, 128.3, 125.5, 79.7, 72.5, 55.7, 46.4, 46.3, 35.6, 32.4, 31.9, 31.5, 29.7, 29.5, 29.3, 29.2, 28.5, 23.8, 22.6, 14.1 ppm. HRMS (ESI) calcd. for $C_{25}H_{41}NO_3Na$ $(M+Na)^+$ 426.29787, found 426.29907.

(R)-2-(4-Octylphenethyl)pyrrolidine hydrochloride **(9)**

8c (12 mg, 30 µmol, 1.0 eq.) was dissolved in EtOH (3 mL) and Pd/C (10% w/w, 7.0 mg, 6.5 µmol, 0.2 eq.) was added to the resulting solution. The air was removed from the flask under vacuum and replaced with hydrogen (balloon). The reaction mixture was vigorously stirred overnight at room temperature. Afterwards, the mixture was filtered through a Celite pad, washing with EtOH.

The collected solution was concentrated *in vacuo*, affording the intermediate *tert*-butyl (*R*)-2-(4-octylphenethyl)pyrrolidine-1-carboxylate as a colorless oil (9 mg, 78%). $[\alpha]^{20}_{D}$: -36.0 (*c* 0.45, $CHCl_3$). IR (neat), υ_{max}: 2924, 2853, 1694, 1514, 1455, 1391, 1364, 1254, 1169, 1100, 771 cm^{-1}. ^1H NMR ($CDCl_3$, 400 MHz, mixture of rotamers), δ: 7.09 (s, 4 H), 3.85 (br. s, 0.4 H), 3.75 (br. s, 0.6 H), 3.41 (br. s, 0.8 H), 3.32 (br. s, 1.2 H), 2.58-2.54 (m, 4 H), 2.14 (br. s, 0.4 H), 2.04-1.87 (m, 1.6 H), 1.85-1.80 (m, 2 H), 1.72 (br. s, 1 H), 1.63-1.55 (m, 3 H), 1.45 (s, 9 H), 1.32-1.24 (m, 10 H), 0.88 (t, *J* = 6.8 Hz, 3 H) ppm. ^{13}C NMR ($CDCl_3$, 75 MHz, major rotamer), δ: 154.6, 140.3, 139.2, 128.3, 128.1, 79.0, 56.9, 46.1, 36.4, 35.5, 32.4, 31.9, 31.6, 30.6, 29.7, 29.5, 29.4, 29.2, 28.6, 23.2, 22.7, 14.1 ppm. HRMS (ESI) calcd. for $C_{25}H_{41}NO_2K$ $(M+K)^+$ 426.27744, found 426.27543.

tert-Butyl (*R*)-2-(4-octylphenethyl)pyrrolidine-1-carboxylate (9.0 mg, 23 µmol) was submitted to general procedure A. The crude was purified by flash column chromatography (EtOH/CH_2Cl_2 1:8, R*f*: 0.16) to give product **9** as a white solid (7 mg, 93%). For biological testing a portion of this solid was dissolved in the minimum amount of HPLC grade water, filtered (pore size = 0.45 µm) and lyophilized. $[\alpha]^{25}_{D}$: -4.0 (*c* 0.35, $CHCl_3$). IR (neat), υ_{max}: 2921, 2852, 2751, 1591, 1514, 1455, 1418, 1042, 815, 722, 554 cm^{-1}. ^1H NMR ($CDCl_3$, 500 MHz), δ: 9.69 (br. s, 1 H), 9.19 (br. s, 1 H), 7.12 (d, *J* = 8.0 Hz, 2 H), 7.05 (d, *J* = 8.0 Hz, 2 H), 3.56-3.48 (m, 1 H), 3.44-3.37 (m, 1 H), 3.35-3.30 (m, 1 H), 2.80-2.74 (m, 1 H), 2.71-2.65 (m, 1 H), 2.55-2.52 (m, 2 H), 2.37-2.30 (m, 1 H), 2.15-2.08 (m, 1 H), 2.06-1.97 (m, 2 H), 1.96-1.88 (m, 1 H), 1.72-1.64 (m, 1 H), 1.59-1.53 (m, 2 H), 1.29-1.25 (m, 10 H), 0.87 (t, *J* = 7.0 Hz, 3 H) ppm. ^{13}C NMR ($CDCl_3$, 125 MHz), δ: 140.9, 137.2, 128.6, 128.3, 60.0, 44.8, 35.5, 34.0, 32.5, 31.9, 31.6, 30.4, 29.7, 29.5, 29.4, 29.3, 23.5, 22.7, 14.1 ppm. HRMS (ESI) calcd. for $C_{20}H_{34}N$ $(M)^+$ 288.26858, found 288.26992.

(2S)-2-(2-Methoxy-2-(4-octylphenyl)ethyl)pyrrolidine hydrochloride **(10)**

NaH (1.3 mg, 60% dispersion in mineral oil, 33 µmol, 1.2 eq.) was added to a solution of **8c diast2** (11 mg, 27 µmol, 1.0 eq.) in dry THF (1 mL) at 0 °C. The resulting mixture was stirred at the same temperature for 1 h, before adding methyl iodide (5.0 µL, 81 µmol, 3.0 eq.). Then, the reaction mixture was stirred at room temperature for 3 h, before being quenched with water (1 mL). The product was extracted with EtOAc (3 x 2 mL) and the combined organic layers were dried over $MgSO_4$, filtered and concentrated. The residue was purified by flash column chromatography

(EtOAc/hexane 1:6, R*f*: 0.16) to give the intermediate *tert*-butyl (*2S*)-2-(2-methoxy-2-(4-octylphenyl)ethyl)pyrrolidine-1-carboxylate as a colorless oil (7 mg, 64%). $[\alpha]^{25}_{D}$: -77.1 (*c* 0.35, $CHCl_3$). IR (neat), υ_{max}: 2924, 2854, 1692, 1454, 1391, 1364, 1251, 1170, 1102, 771 cm^{-1}. ^1H NMR ($CDCl_3$, 500 MHz, mixture of rotamers), δ: 7.23-7.13 (m, 4 H), 4.11 (br. s, 1 H), 4.02 (br. s, 0.5 H), 3.93 (br. s, 0.5 H), 3.39 (br. s, 0.5 H), 3.29 (br. s, 1.5 H), 3.16 (s, 3 H), 2.60-2.57 (m, 2 H), 2.27 (br. s, 1 H), 1.82-1.73 (m, 2 H), 1.62-1.56 (m, 3 H), 1.46 (s, 9 H), 1.30-1.26 (m, 10 H), 0.88 (t, *J* = 6.9 Hz, 3 H) ppm. ^{13}C NMR ($CDCl_3$, 125 MHz, mixture of rotamers), δ: 154.5, 142.2, 139.5, 128.4, 126.5, 81.6, 79.0, 78.7, 56.3, 54.7, 46.3, 46.1, 42.6, 35.7, 31.9, 31.5, 30.9, 30.3, 29.7, 29.5, 29.3, 29.2, 28.6, 23.7, 23.2, 22.6, 14.1 ppm. HRMS (ESI) calcd. for $C_{26}H_{44}NO_3$ $(M+H)^+$ 418.33210, found 418.33141.

tert-Butyl (*2S*)-2-(2-methoxy-2-(4-octylphenyl)ethyl)pyrrolidine-1-carboxylate (6.0 mg, 14 µmol) was submitted to general procedure A. The crude was purified by flash column chromatography (EtOH/CH_2Cl_2 1:10, R*f*: 0.20) to give product **10** as a white solid (3 mg, 60%). For biological testing a portion of this solid was dissolved in the minimum amount of HPLC grade water, filtered (pore size = 0.45 µm) and lyophilized. $[\alpha]^{25}_{D}$: -55.0 (*c* 0.20, $CHCl_3$). IR (neat), υ_{max}: 2921, 2851, 2766, 1459, 1107, 1033, 827, 722, 564 cm^{-1}. ^1H NMR ($CDCl_3$, 500 MHz), δ: 10.53 (br. s, 1 H), 8.54 (br. s, 1 H), 7.19 (d, *J* = 8.1 Hz, 2 H), 7.14 (d, *J* = 8.1 Hz, 2 H), 4.35 (dd, *J* = 10.2, 2.9 Hz, 1 H), 3.91 (br. s, 1 H), 3.51-3.46 (m, 1 H), 3.38-3.33 (m, 1 H), 3.20 (s, 3 H), 2.59-2.56 (m, 2 H), 2.28-2.21 (m, 2 H), 2.07-2.03 (m, 2 H), 1.95-1.92 (m, 1 H), 1.73-1.67 (m, 1 H), 1.61-1.55 (m, 2 H), 1.30-1.24 (m, 10 H), 0.87 (t, *J* = 7.0 Hz, 3 H) ppm. ^{13}C NMR ($CDCl_3$, 125 MHz), δ: 143.2, 137.3, 128.7, 126.4, 82.4, 58.9, 56.5, 44.5, 40.1, 35.7, 31.9, 31.4, 30.7, 29.7, 29.5, 29.3, 29.2, 23.1, 22.6, 14.1 ppm. HRMS (ESI) calcd. for $C_{21}H_{36}NO$ $(M)^+$ 318.27914, found 318.28009.

tert-Butyl (2S,4R)-4-((tert-butyldimethylsilyl)oxy)-2-(2-methoxy-2-oxoethyl)pyrrolidine-1-carboxylate **(11a)**

Commercially available 1-(*tert*-butyl) 2-methyl (2S,4R)-4-((*tert*-butyldimethylsilyl)oxy)pyrrolidine-1,2-dicarboxylate (0.20 g, 0.56 mmol, 1.0 eq.) was dissolved in MeOH (1 mL) and an aqueous LiOH (0.33 mL, 1.0 M, 1.5 eq.) was added. The solution was stirred at 45 °C for 3h whereby TLC analysis indicated that the reaction had gone to completion. A 5% (w/w) aqueous HCl solution was added

dropwise until pH = 2, whereby a white precipitate was formed. The mixture was extracted with Et_2O (2 x 5 mL). The resulting organic layer was collected, dried over Na_2SO_4, filtered and concentrated to afford a colorless oil which was brought to the next step without further purification.

The colorless oil (0.12 g, 0.35 mmol, 1.0 eq.) was dissolved in THF (2 mL) then Et_3N (97 µL, 0.70 mmol, 2.0 eq.) and *iso*-butylchloroformate (58 µL, 0.31 mmol, 1.6 eq.) were added. The resulting mixture was stirred at room temperature for 1 h. Afterwards, the reaction mixture was cooled to 0 °C and a freshly prepared solution of CH_2N_2 in Et_2O was added dropwise until the resulting mixture remained bright yellow. Then, the reaction mixture was stirred for 1h at 0 °C and for 30 min at room temperature, adding further CH_2N_2 any time the mixture had turned back to colorless. After a persistant yellow color remained, the flask was cooled again to 0 °C and a 0.5 M solution of acetic acid in water was slowly added until the mixture turned colorless. Then, the layers were separated and the aqueous one was extracted with EtOAc (3 x 5 mL). The combined organic layers were washed with water (5 mL) and brine (5 mL), dried over Na_2SO_4, filtered and concentrated. The residue was purified by flash column chromatography (EtOAc/hexane 1:3, R*f*: 0.21) to give the diazo intermediate as a pale yellow oil. This intermediate was redissolved in dry MeOH (2 mL) and a solution of silver benzoate (16 mg, 70 µmol, 0.2 eq.) in Et_3N (97 µL, 0.70 mmol, 2.0 eq.) was added to this mixture under an argon atmosphere. Then, the flask was wrapped in aluminum foil and the reaction mixture was refluxed for 2 h. Afterwards, the mixture was left to reach room temperature, filtered through a Celite pad washing with abundant EtOAc and concentrated. The residue was purified by flash column chromatography (hexane/EtOAc 8:2 R*f*: 0.28) to give **11a** as a colorless oil (77 mg, 59% over 2 steps). $[\alpha]^{25}_D$: -74.10 (*c* 0.78, $CHCl_3$). IR (neat), υ_{max}: 2929, 1739, 1693, 1472, 1152, 1108, 853, 774 cm^{-1}. ^1H NMR ($CDCl_3$, 500 MHz, mixture of rotamers), δ: 4.32-4.28 (p, *J* = 4.3 Hz, 1 H), 4.24-4.16 (m, 1 H), 3.65 (s, 3 H), 3.43-3.33 (m, 2 H), 2.99-2.86 (dd, *J* = 11.1, 4.6 Hz, 1 H), 2.37 (m, 1 H), 2.09 (m, 1 H), 1.84 (m, 1 H), 1.44 (s, 9 H), 0.85 (s, 9 H), 0.04 (s, 6 H) ppm. ^{13}C NMR ($CDCl_3$, 125 MHz, mixture of rotamers), δ: 172.0, 171.9, 155.0, 154.9, 79.9, 79.5, 70.2, 69.6, 55.1, 54.7, 53.0, 51.6, 41.2, 40.5, 39.6, 38.9, 28.6, 25.8, 18.1 ppm. HRMS (ESI) calcd. for $C_{25}H_{40}NO_3$ $(M+H)^+$ 374.23680, found 374.23637.

tert-Butyl (2S,4R)-4-((tert-butyldimethylsilyl)oxy)-2-(2-(methoxy(methyl)amino)-2-oxoethyl)pyrrolidine-1-carboxylate **(11b)**

Iso-propyl magnesium chloride (0.24 mL, 2.0 M in THF, 0.48 mmol, 6.0 eq.) was added dropwise to a solution of **11a** (30 mg, 80 µmol, 1.0 eq.) and N,O-dimethylhydroxylamine (23 mg, 0.24 mmol, 3.0 eq.) in dry THF (1 mL) at -20 °C. The resulting mixture was allowed to reach 0 °C over 3 h, then, it was stirred at the same temperature overnight. Afterwards, the reaction mixture was quenched by adding a few drops of water. Then, the mixture was filtered on a Celite pad washing with abundant EtOAc and concentrated. The residue was purified by flash column chromatography (hexane/EtOAc 7:3 R*f*: 0.35) to give **11b** as a colorless oil (26 mg, 81%). $[\alpha]^{25}_{D}$: -56.60 (*c* 0.58, $CHCl_3$). IR (neat), υ_{max}: 2954, 1692, 1390, 1252, 1156, 835 cm^{-1}. ^1H NMR ($CDCl_3$, 500 MHz, mixture of rotamers), δ: 4.34-4.26 (m, 2 H), 3.68 (s, 3 H), 3.43-3.32 (m, 2 H), 3.16-3.02 (m, 4 H), 2.46 (bs, 1 H), 2.12 (bs, 1 H), 1.87 (bs, 1 H), 1.45 (s, 9 H), 0.85 (s, 9 H), 0.04 (s, 6 H) ppm. ^{13}C NMR ($CDCl_3$, 125 MHz, mixture of rotamers), δ: 172.7, 172.4, 155.0, 79.7, 79.3, 70.3, 69.7, 61.4, 55.1, 54.5, 53.1, 41.4, 40.6, 37.7, 36.7, 32.1, 32.1, 28.6, 28.5, 25.9, 25.9, 18.1 ppm. HRMS (ESI) calcd. for $C_{25}H_{40}NO_3$ $(M+H)^+$ 403.26230, found 403.26277.

tert-Butyl (2S,4R)-4-hydroxy-2-(2-(4-octylphenyl)-2-oxoethyl)pyrrolidine-1-carboxylate **(11c)**

11b was submitted to general procedure C (11 mg, 20 µmol, 1.0 eq.). The crude yellow oil was submitted to general procedure B without further purification. The resulting residue was purified by flash column chromatography (hexane/EtOAc 8:2 R*f*: 0.33) to give **11c** as a yellow oil (5 mg, 63% over 2 steps). $[\alpha]^{25}_{D}$: +50.40 (*c* 0.25, $CHCl_3$). IR (neat), υ_{max}: 2953, 1856, 1783, 1251, 932, 704 cm^{-1}. ^1H NMR ($CDCl_3$, 500 MHz, mixture of rotamers), δ: 7.89 (bs, 2 H), 7.26-7.24 (m, 2 H), 4.44-4.40 (m, 2 H), 3.90-3.87 (m, 0.57 H), 3.67.3.60 (m, 1 H), 3.46 (m, 0.64 H), 2.89-2.84 (dd, *J* = 15.5, 9.6 Hz, 1 H), 2.65-2.62 (m, 2 H), 2.22 (m, 2 H), 1.90 (bs, 1 H), 1.62-1.59 (m, 2 H), 1.45 (s, 9 H), 1.32-1.23 (m, 10 H), 0.88-0.85 (t, 3 H) ppm. ^{13}C NMR ($CDCl_3$, 125 MHz, mixture of rotamers), δ: 198.9, 198.2, 171.3, 154.9, 149.3, 149.1, 134.6, 128.8, 128.5, 80.3, 79.7, 69.9, 69.4, 60.5, 54.9, 54.6, 53.3, 43.3, 40.3, 36.1, 32.0, 31.2, 29.5, 29.4, 29.3, 28.6, 22.8, 21.2, 14.3, 14.2 ppm. HRMS (ESI) calcd. for $C_{25}H_{40}NO_3$ $(M+H)^+$ 418.29519, found 418.29710.

(2S,4R)-4-Hydroxy-2-(2-(4-octylphenyl)-2-oxoethyl)pyrrolidin-1-ium chloride **(11)**

11 was synthesized in accordance with the general procedure A, starting from **11c** (21 mg, 50 mmol). **11** was obtained as a white solid (13 mg, 75%). IR (neat), υ_{max}: 3310, 2921, 1669, 1605, 1277 cm^{-1}. ^{1}H NMR ($CDCl_3$, 500 MHz, mixture of diastereomers), δ: 7.71-7.70 (d, *J* = 8.2 Hz, 2 H), 7.00-6.99 (d, *J* = 8.0 Hz, 2 H), 4.51 (s, 1 H), 4.07-4.04 (dd, *J* = 11.3, 6.4 Hz, 1 H major isomer), 3.99-3.96 (dd, *J* = 9.0, 6.2 Hz, 1 H minor isomer), 3.41-3.24 (m, 2 H), 2.37-2.05 (m, 3 H), 1.77-1.63 (m, 1 H), 1.36 (m, 2 H), 1.18-1.14 (m, 10 H), 0.78-0.76 (t, 3 H) ppm. ^{13}C NMR ($CDCl_3$, 125 MHz, mixture of diastereomers), δ: 198.5, 149.1, 133.5, 128.5, 128.5, 69.1, 69.1, 54.3, 54.0, 52.8, 38.5, 37.7, 35.6, 31.8, 30.8, 29.4, 29.4, 29.3, 22.6, 13.8 ppm. HRMS (ESI) calcd. for $C_{25}H_{40}NO_3$ $(M+H)^+$ 318.24276, found 318.24284.

1-(tert-butyl) 2-ethyl (2R,4R)-4-(((tert-butyldiphenylsilyl)oxy)methyl)-5-oxopyrrolidine-1,2-dicarboxylate **(12a3)** *and 1-(tert-butyl) 2-ethyl (2R,4S)-4-(((tert-butyldiphenylsilyl)oxy)methyl)-5-oxopyrrolidine-1,2-dicarboxylate* **(epi-12a3)** (See Schéma 8.4)

HCl (84 mL, 0.20 N in H_2O, 17 mmol, 1.0 eq.) was added dropwise to a solution of **12a1** (5.3 g, 17 mmol, 1.0 eq.) in MeOH (125 mL) and the resulting solution was stirred at room temperature for 1 h. Afterwards, a small amount of bromocresol green was added to monitor the pH of the solution and $NaBH_3CN$ (2.1 g, 34 mmol, 2.0 eq.) was added portion wise (4 portions over 2 h). Meanwhile, the pH of the solution had been corrected by adding a few drops of HCl (0.2 N in H_2O), anytime the pH indicator had turned blue. HCl is always added in the minimal amount necessary to make the indicator turn back to yellow. The reaction mixture was stirred at room temperature for 48 h, continuing monitoring and correcting the pH when needed. Eventually, a few drops of $NaHCO_3$ satd. solution were added until the indicator turned blue and the mixture was concentrated *in vacuo* to remove the organic solvent. Brine (130 mL) was added to the mixture and the product was extracted in EtOAc (3 x 130 mL). The organic layers were dried over Na_2SO_4, filtered and concentrated. The resulting residue was purified by flash column chromatography (MeOH/CH_2Cl_2 1:20, R*f*: 0.24) to give the intermediate alcohol **12a2** (3.38 g, 70%) as a 2:1 mixture of diasteroisomers. This intermediate was redissolved in dry DMF (60 mL) and imidazole (2.4 g, 35 mmol, 3.0 eq.) was added to the resulting solution. Then, this mixture was cooled to 0 °C and TBDPSCl (4.6 mL, 18 mmol, 1.5 eq.) was added dropwise. The resulting solution was stirred at room temperature for 3 h, before adding EtOH (1 mL) and stirring for additional 30 min.

Eventually, the mixture was poured into water (400 mL) and the product was extracted into Et_2O (3 x 300 mL). The organic layers were dried over Na_2SO_4, filtered and concentrated. The resulting residue was purified by flash column chromatography (Et_2O/hexane 1:2 R*f*: 0.13 and 0.06, then Et_2O/hexane 1:1) to give **12a3** (2.98 g, 48%) and **epi-12a3** (1.12 g, 18%) as colorless oils. The stereochemistry was assigned by performing NOESY experiments (through space coupling observed between 2-H and 4-H in **epi-12a3**) and in analogy with similar published products. [27] **12a3:** $[\alpha]^{25}_D$: +28.3 (*c* 2.7, $CHCl_3$). IR (neat), υ_{max}: 2931, 1792, 1746, 1718, 1472, 1428, 1369, 1313, 1278, 1188, 1151, 1111, 1007, 966, 913, 848, 822, 734, 702, 613, 504 cm^{-1}. ^1H NMR ($CDCl_3$, 500 MHz), δ: 7.66-7.62 (m, 4 H), 7.43-7.37 (m, 6 H), 4.62 (dd, *J* = 9.7, 3.2 Hz, 1 H), 4.24 (q, *J* = 7.1 Hz, 2 H), 4.03 (dd, *J* = 10.2, 4.8 Hz, 1 H), 3.80 (dd, *J* = 10.2, 3.4 Hz, 1 H), 2.82-2.77 (m, 1 H), 2.46-2.40 (m, 1H), 2.17-2.12 (m, 1 H), 1.50 (s, 9 H), 1.30 (t, *J* = 7.1 Hz, 3 H), 1.03 (s, 9 H) ppm. ^{13}C NMR ($CDCl_3$, 125 MHz), δ: 173.3, 171.6, 149.3, 135.7, 135.5, 133.2, 132.6, 129.8, 127.7, 83.4, 62.9, 61.6, 57.6, 44.5, 27.8, 26.8, 25.2, 19.2, 14.1 ppm. HRMS (ESI) calcd. for $C_{29}H_{39}NO_6SiNa$ $(M+Na)^+$ 548.24389, found 548.24492. **epi-12a3:** $[\alpha]^{25}_D$: +7.7 (*c* 3.6, $CHCl_3$). IR (neat), υ_{max}: 2931, 1791, 1746, 1718, 1473, 1428, 1369, 1318, 1151, 1109, 1032, 970, 909, 822, 781, 734, 702, 613, 504 cm^{-1}. ^1H NMR ($CDCl_3$, 500 MHz), δ: 7.66-7.61 (m, 4 H), 7.44-7.35 (m, 6 H), 4.50 (dd, *J* = 8.9, 7.5 Hz, 1 H), 4.22-4.13 (m, 2 H), 3.93 (dd, *J* = 10.3, 6.7 Hz, 1 H), 3.87 (dd, *J* = 10.3, 4.1 Hz, 1 H), 2.79 (dddd, *J* = 9.5, 8.7, 6.7, 4.1 Hz, 1 H), 2.52-2.45 (m, 1H), 2.16 (ddd, *J* = 13.2, 8.7, 7.5 Hz, 1 H), 1.49 (s, 9 H), 1.25 (t, *J* = 7.1 Hz, 3 H), 1.04 (s, 9 H) ppm. ^{13}C NMR ($CDCl_3$, 125 MHz), δ: 172.7, 171.3, 149.2, 135.6, 135.5, 133.2, 132.9, 129.7, 127.7, 83.5, 62.3, 61.5, 57.6, 45.4, 27.8, 26.7, 24.3, 19.2, 14.0 ppm. HRMS (ESI) calcd. for $C_{29}H_{39}NO_6SiNa$ $(M+Na)^+$ 548.24389, found 548.24498.

1-(tert-Butyl) 2-ethyl (2R,4S)-4-(((tert-butyldiphenylsilyl)oxy)methyl)pyrrolidine-1,2-dicarboxylate **(13a)** (See Schéma 8.4)

$LiEt_3BH$ (4.7 mL, 1.0 M in THF, 4.7 mmol, 1.2 eq.) was added dropwise to a solution of **12a3** (2.1 g, 3.9 mmol, 1.0 eq.) in anhydrous THF (70 mL) at -78 °C under an argon atmosphere and the resulting solution was stirred at the same temperature for 30 min. Afterwards, the reaction mixture was quenched with $NaHCO_3$ satd. sol. (20 mL) and allowed to reach 0 °C, then a few drops of H_2O_2 30% were added and the mixture was stirred at 0 °C for 20 min. Eventually, the organic solvent was removed under *vacuo* and the remaining aqueous layer was extracted with CH_2Cl_2 (3

x 120 mL). The combined organic layers were dried over Na_2SO_4, filtered and concentrated, affording a colorless oil. This intermediate hemiaminal was redissolved in anhydrous CH_2Cl_2 (70 mL) and Et_3SiH (1.25 mL, 7.8 mmol, 2 eq.) was added to the solution under an argon atmosphere. The resulting mixture was cooled to -78 °C and BF_3OEt_2 (481 µL, 3.90 mmol, 1 eq.) was added dropwise. The reaction mixture was stirred at -78 °C for 30 min, before adding $NaHCO_3$ satd. sol. (20 mL) and allowing the mixture to reach room temperature. The product was extracted with CH_2Cl_2 (3 x 120 mL) and the organic extracts were dried over Na_2SO_4, filtered and concentrated. The residue was purified by flash column chromatography (EtOAc/hexane 1:6, R*f*: 0.24) to give **13a** as a colorless oil (1.52 g, 76% over two steps). $[\alpha]^{25}_D$: +24.7 (*c* 1.5, $CHCl_3$). IR (neat), υ_{max}: 2931, 2858, 1744, 1699, 1473, 1427, 1389, 1365, 1257, 1188, 1110, 1030, 939, 870, 823, 741, 702, 611, 505 cm^{-1}. ^1H NMR ($CDCl_3$, 500 MHz, mixture of rotamers), δ: 7.65-7.63 (m, 4 H), 7.44-7.37 (m, 6 H), 4.34 (dd, *J* = 7.9, 4.1 Hz, 0.4 H), 4.24-4.14 (m, 2.6 H), 3.73 (dd, *J* = 10.6, 7.7 Hz, 0.6 H), 3.64-3.59 (m, 2.4 H), 3.29 (dd, *J* = 10.6, 7.4 Hz, 0.6 H), 3.23, (dd, *J* = 10.5, 7.4 Hz, 0.4 H), 2.60-2.51 (m, 1 H), 2.13-2.04 (m, 1H), 2.03-1.98 (m, 1 H), 1.47 (s, 3.6 H), 1.42 (s, 5.4 H), 1.30-1.25 (m, 3 H), 1.06 (s, 3.6 H), 1.05 (s, 5.4 H) ppm. ^{13}C NMR ($CDCl_3$, 125 MHz, mixture of rotamers), δ: 173.2, 172.9, 154.4, 153.7, 135.5, 133.4, 133.3, 129.7, 127.7, 79.8, 79.7, 64.8, 60.9, 60.8, 59.0, 58.7, 48.9, 48.8, 39.8, 38.9, 33.0, 32.2, 28.4, 28.3, 26.8, 19.2, 14.3, 14.1 ppm. HRMS (ESI) calcd. for $C_{29}H_{42}NO_5Si$ $(M+H)^+$ 512.28268, found 512.28059.

(2R,4S)-1-(tert-Butoxycarbonyl)-4-(((tert-butyldiphenylsilyl)oxy)methyl)pyrrolidine-2-carboxylic acid **(12a4)** (See Schéma 8.4)

NaOH (0.29 mL, 1.0 N in H_2O, 0.29 mmol, 1.5 eq.) was added to a solution of **13a** (99 mg, 0.19 mmol, 1.0 eq.) in MeOH (1.2 mL) and the resulting mixture was vigorously stirred for 24 h. Afterwards, the organic solvent was concentrated *in vacuo* and the residue was suspended in brine (20 mL). Afterwards, while gradually acidifying to pH=2 by adding HCl 0.2 N, the product was extracted with CH_2Cl_2 (6 x 20 mL). The organic layers were dried over Na_2SO_4, filtered and concentrated, affording **12a4** (93 mg, 99%) as a colorless solid. $[\alpha]^{25}_D$: +19.3 (*c* 0.9, MeOH). IR (neat), υ_{max}: 2929, 1699, 1390, 1366, 1162, 1108, 998, 906, 823, 739, 700, 608, 503 cm^{-1}. ^1H NMR (CD_3OD, 500 MHz, mixture of rotamers), δ: 7.74-7.66 (m, 4 H), 7.47-7.37 (m, 6 H), 4.30-4.21 (m, 1 H), 3.66-3.57 (m, 3 H), 3.37-3.33 (m, 1 H), 2.57-2.54 (m, 1 H), 2.17-2.11 (m, 1H), 2.06-2.03 (m, 1

H), 1.48 (s, 3.6 H), 1.44 (s, 5.4 H), 1.06 (s, 9 H) ppm. ^{13}C NMR (CD_3OD, 125 MHz, mixture of rotamers), δ: 175.9, 154.9, 154.6, 135.9, 135.3, 134.6, 133.1, 129.6, 129.5, 129.0, 127.5, 127.2, 80.0, 79.8, 64.8, 64.6, 59.5, 48.9, 48.6, 39.7, 38.9, 32.8, 32.1, 27.4, 27.2, 26.0, 25.8, 18.7, 18.5 ppm. HRMS (ESI) calcd. for $C_{27}H_{38}NO_5SiNa$ $(M+Na)^+$ 506.23332, found 506.23394.

tert-Butyl (2R,4S)-4-(((tert-butyldiphenylsilyl)oxy)methyl)-2-(2-methoxy-2-oxoethyl)pyrrolidine-1-carboxylate **(12a)** (See Schéma 8.4)

Et_3N (54 µL, 0.39 mmol, 2.0 eq.) and *iso*-butylchloroformate (40 µL, 0.31 mmol, 1.6 eq.) were added to a solution of **12a4** (94 mg, 0.19 mmol) in anhydrous THF (2 mL) at 0 °C and the resulting mixture was stirred at room temperature for 1 h. Afterwards, the reaction mixture was cooled to 0 °C and a freshly prepared solution of CH_2N_2 in Et_2O was added dropwise until the resulting mixture remained bright yellow. Then, the reaction mixture was stirred for 1h at 0 °C and for 30 min at room temperature, adding further CH_2N_2 any time the mixture had turned back to colorless. After a persistent yellow color remained, the flask was cooled again to 0 °C and a 0.5 M solution of acetic acid in water was slowly added until the mixture turned colorless. Then, the layers were separated and the aqueous one was extracted with EtOAc (3 x 5 mL). The combined organic layers were washed with water (5 mL) and brine (5 mL), dried over Na_2SO_4, filtered and concentrated. The residue was purified by flash column chromatography (EtOAc/hexane 1:3, R*f*: 0.21) to give the diazo intermediate as a pale yellow oil. This intermediate was redissolved in dry MeOH (2 mL) and a solution of silver benzoate (9 mg, 0.0388 mmol, 0.2 eq.) in Et_3N (54 µL, 0.388 mmol, 2 eq.) was added to this mixture under an argon atmosphere. Then, the flask was wrapped in aluminum foil and the reaction mixture was refluxed for 2 h. Afterwards, the mixture was left to reach room temperature, filtered through a Celite pad washing with abundant EtOAc and concentrated. The residue was purified by flash column chromatography (EtOAc/hexane 1:4, R*f*: 0.27) to give **12a** as a colorless oil (54 mg, 55% over two steps). $[\alpha]^{25}_D$: +21.2 (*c* 1.0, $CHCl_3$). IR (neat), υ_{max}: 2931, 2858, 1737, 1692, 1428, 1388, 1365, 1253, 1161, 1109, 823, 740, 702, 611, 504 cm^{-1}. ^{1}H NMR ($CDCl_3$, 500 MHz, mixture of rotamers), δ: 7.64-7.62 (m, 4 H), 7.44-7.37 (m, 6 H), 4.21 (br. s, 0.5 H), 4.13 (br. s, 0.5 H), 3.67 (s, 3 H), 3.63-3.60 (m, 1 H), 3.58-3.51 (m, 1.5 H), 3.43 (br. s, 0.5 H), 3.25-3.16 (m, 1 H), 2.91, (d, *J* = 14.2 Hz, 0.5 H), 2.80 (d, *J* = 14.6 Hz, 0.5 H), 2.50-2.44 (m, 1 H), 2.33 (dd, *J* = 14.6, 9.7 Hz, 1H), 1.86 (br. s, 1 H), 1.80-1.77 (m, 1 H), 1.46 (s, 9 H), 1.05 (s, 9

H) ppm. ^{13}C NMR ($CDCl_3$, 125 MHz, mixture of rotamers), δ: 171.9, 154.3, 154.1, 135.5, 133.5, 129.7, 127.9, 127.7, 79.6, 79.3, 65.3, 54.0, 51.6, 49.1, 39.3, 39.2, 38.7, 38.4, 33.7, 33.1, 28.5, 26.8, 19.2 ppm. HRMS (ESI) calcd. for $C_{29}H_{42}NO_5Si$ $(M+H)^+$ 512.28268, found 512.28235.

tert-Butyl (2R,4S)-4-(((tert-butyldiphenylsilyl)oxy)methyl)-2-(2-(methoxy(methyl)amino)-2-oxoethyl)pyrrolidine-1-carboxylate **(12b)**

12a (53 mg, 0.10 mmol, 1.0 eq.) was submitted to the procedure from **11b**. The residue was purified by flash column chromatography (EtOAc/hexane 1:1, R*f*: 0.30) to give **12b** as a colorless oil (47 mg, 84%). $[\alpha]^{25}_D$: +23.3 (*c* 0.6, $CHCl_3$). IR (neat), υ_{max}: 2931, 2857, 1690, 1385, 1364, 1256, 1162, 1109, 1000, 906, 870, 823, 739, 702, 611, 504 cm^{-1}. ^{1}H NMR ($CDCl_3$, 500 MHz, mixture of rotamers), δ: 7.65-7.62 (m, 4 H), 7.44-7.36 (m, 6 H), 4.24 (br. s, 1 H), 3.68 (s, 3 H), 3.65-3.62 (m, 1 H), 3.56 (br. s, 1.5 H), 3.45 (br. s, 0.5 H), 3.24 (br. s, 1 H), 3.17 (s, 3 H), 3.00, (d, *J* = 14.7 Hz, 0.5 H), 2.88 (d, *J* = 13.6 Hz, 0.5 H), 2.52-2.45 (m, 2 H), 1.89-1.81 (m, 2 H), 1.46 (s, 9 H), 1.04 (s, 9 H) ppm. ^{13}C NMR ($CDCl_3$, 125 MHz, mixture of rotamers), δ: 172.3, 154.2, 135.6, 135.5, 133.6, 129.7, 127.7, 79.5, 79.1, 65.4, 61.2, 54.0, 49.1, 39.2, 38.4, 36.8, 36.4, 33.8, 32.0, 28.5, 26.8, 19.2 ppm. HRMS (ESI) calcd. for $C_{30}H_{45}N_2O_5Si$ $(M+H)^+$ 541.30923, found 541.30687.

tert-Butyl (2R,4S)-4-(((tert-butyldiphenylsilyl)oxy)methyl)-2-(2-(4-octylphenyl)-2-oxoethyl)pyrrolidine-1-carboxylate **(12c)**

Prepared according to general procedure C, starting from **12b** (30 mg, 55 µmol). The crude was purified by flash column chromatography (EtOAc/hexane 1:10, R*f*: 0.17) to give **12c** as a colorless oil (25 mg, 68%). $[\alpha]^{25}_D$: +5.3 (*c* 0.3, $CHCl_3$). IR (neat), υ_{max}: 2924, 2853, 1671, 1606, 1515, 1458, 1390, 1366, 1175, 1111, 823, 739, 701, 611, 504 cm^{-1}. ^{1}H NMR ($CDCl_3$, 500 MHz, mixture of rotamers), δ: 7.95 (d, *J* = 7.3 Hz, 1 H), 7.90 (d, *J* = 6.8 Hz, 1 H), 7.64-7.61 (m, 4 H), 7.43-7.35 (m, 6 H), 7.27-7.26 (m, 2 H), 4.38-4.34 (m, 1 H), 3.72 (d, *J* = 14.8 Hz, 0.5 H), 3.61 (br. s, 1 H), 3.58-3.53 (m, 1.5 H), 3.50-3.43 (m, 1 H), 3.29-3.25 (m, 0.5 H), 3.22-3.19 (m, 0.5 H), 2.88-2.78 (m, 1 H), 2.65 (br. s, 2 H), 2.54-2.48 (m, 1 H), 1.87-1.75 (m, 2 H), 1.65-1.59 (m, 2 H), 1.47 (s, 4.5 H), 1.45 (s, 4.5 H), 1.31-1.26 (m, 10 H), 1.03 (s, 9 H), 0.88 (t, *J* = 6.9 Hz, 3 H) ppm. ^{13}C NMR ($CDCl_3$, 125 MHz, mixture of rotamers), δ: 198.7, 198.3, 154.4, 154.2, 134.6, 133.5, 129.7, 128.7, 128.5, 128.4, 127.7, 79.7, 79.3, 65.4, 65.2, 54.4, 49.2, 43.9, 43.2, 39.2, 38.4, 36.0, 33.7, 32.7, 31.8, 31.1, 29.7,

29.4, 29.3, 29.2, 28.5, 26.8, 22.6, 19.2, 14.1 ppm. HRMS (ESI) calcd. for $C_{42}H_{60}NO_4Si$ $(M+H)^+$ 670.42861, found 670.42981.

2-((2R,4S)-4-(Hydroxymethyl)pyrrolidin-2-yl)-1-(4-octylphenyl)ethan-1-one hydrochloride **(12)**

Prepared according to general procedure B, starting from **12c** (14 mg, 21 µmol). The crude was purified by flash column chromatography (EtOAc/hexane 1:1, R*f*: 0.28) to give the intermediate *tert*-butyl (*2R,4S*)-4-(hydroxymethyl)-2-(2-(4-octylphenyl)-2-oxoethyl)pyrrolidine-1-carboxylate as a colorless oil (9 mg, 99%). $[\alpha]^{25}_D$: +7.5 (*c* 0.4, $CHCl_3$). IR (neat), υ_{max}: 3439, 2924, 2854, 1673, 1606, 1394, 1366, 1255, 1173, 1123, 772, 558 cm^{-1}. ^1H NMR ($CDCl_3$, 500 MHz, mixture of rotamers), δ: 7.94 (d, *J* = 7.7 Hz, 1 H), 7.89 (d, *J* = 7.9 Hz, 1 H), 7.27-7.24 (m, 2 H), 4.42-4.37 (m, 1 H), 3.72 (d, *J* = 15.5 Hz, 0.5 H), 3.63 (br. s, 1.5 H), 3.58-3.49 (m, 1.5 H), 3.47 (br. s, 0.5 H), 3.26-3.23 (m, 0.5 H), 3.16-3.13 (m, 0.5 H), 2.91-2.80 (m, 1 H), 2.65 (br. s, 2 H), 2.55-2.46 (m, 1 H), 1.89-1.80 (m, 2 H), 1.64-1.59 (m, 2 H), 1.46-1.40 (m, 9 H), 1.31-1.25 (m, 10 H), 0.88 (t, *J* = 7.0 Hz, 3 H) ppm. ^{13}C NMR ($CDCl_3$, 125 MHz, mixture of rotamers), δ: 198.5, 198.0, 154.2, 148.8, 149.0, 134.5, 128.5, 128.4, 127.7, 79.7, 79.5, 65.2, 54.4, 49.2, 49.0, 43.9, 43.2, 39.2, 38.4, 36.0, 33.7, 32.7, 31.8, 31.1, 29.7, 29.4, 29.3, 29.2, 28.5, 26.8, 22.6, 14.1 ppm. HRMS (ESI) calcd. for $C_{26}H_{42}NO_4$ $(M+H)^+$ 432.31084, found 432.30903.

tert-Butyl (*2R,4S*)-4-(hydroxymethyl)-2-(2-(4-octylphenyl)-2-oxoethyl)pyrrolidine-1-carboxylate (8.0 mg, 19 µmol) was submitted to general procedure A. The crude was purified by flash column chromatography (EtOH/CH_2Cl_2 1:4, R*f*: 0.15) to give product **12** as a white solid (6 mg, 88%). Note: the product epimerized spontaneously on C-2 when dissolved in MeOH or H_2O, giving a 1:1 mixture of diasteroisomers. For biological testing a portion of the product was dissolved in the minimum amount of HPLC grade water, filtered (pore size = 0.45 µm) and lyophilized. IR (neat), υ_{max}: 3376, 2922, 2852, 1675, 1605, 1570, 1465, 1378, 1282, 1184, 1039, 906, 815, 722, 549 cm^{-1}. ^1H NMR (CD_3OD, 500 MHz, 1:1 mixture of diasteroisomers), δ: 7.98 (d, *J* = 8.3 Hz, 4 H), 7.38 (d, *J* = 8.3 Hz, 4 H), 4.18-4.12 (m, 1 H), 4.09-4.04 (m, 1 H), 3.76-3.65 (m, 4 H, partially deuterated), 3.63-3.58 (m, 2 H), 3.47-3.39 (m, 4 H, partially deuterated), 3.20-3.13 (m, 2 H), 2.74-2.71 (m, 4 H), 2.67-2.58 (m, 2 H), 2.44-2.38 (m, 1 H), 2.22-2.17 (m, 1 H), 1.99 (dt, *J* = 13.5, 8.4 Hz, 1 H), 1.70-1.62 (m, 5 H), 1.36-1.30 (m, 20 H), 0.91 (t, *J* = 7.0 Hz, 6 H) ppm. ^{13}C NMR (CD_3OD, 125 MHz, 1:1 mixture

of diasteroisomers), δ: 197.1, 149.7, 133.6, 128.6, 128.0, 62.4, 61.9, 56.2, 55.3, 39.6, 39.0, 35.5, 32.9, 32.6, 31.6, 30.9, 29.1, 29.0, 28.9, 22.3, 13.0 ppm. HRMS (ESI) calcd. for $C_{21}H_{34}NO_2$ $(M)^+$ 332.25841, found 332.25898.

tert-Butyl (2S,4S)-4-(((tert-butyldiphenylsilyl)oxy)methyl)-2-(3-methoxy-3-oxopropyl)pyrrolidine-1-carboxylate **(13b)**

DIBAL-H (0.76 mL, 1.0 M in CH_2Cl_2, 0.76 mmol, 2.0 eq.) was added dropwise to a solution of **13a** (0.19 g, 0.38 mmol, 1.0 eq.), in dry CH_2Cl_2 (3.5 mL) at -78 °C. The resulting mixture was stirred at the same temperature for 2 h, before quenching the reaction mixture with MeOH (100 µL). Then, the solution was allowed to reach room temperature and a 2 M solution of potassium sodium tartrate in water (3.5 mL) was added. The resulting mixture was vigorously stirred at room temperature for 30 min, before separating the layers. The aqueous one was extracted with CH_2Cl_2 (3 x 7 mL) and the combined organic layers were dried over $MgSO_4$, filtered and concentrated, affording a colorless oil. This intermediate aldehyde was redissolved in dry CH_2Cl_2 (3.5 mL) and methyl(triphenylphosphoranylidene)acetate (191 mg, 0.57 mmol, 1.5 eq.) was added at 0 °C. The resulting solution was stirred for 1 h at 0 °C and for 1 h at room temperature, before being cooled again to 0 °C and quenched with NH_4Cl satd. sol. (3.5 mL). The layers were separated and the aqueous one was extracted with CH_2Cl_2 (3 x 7 mL). The combined organic layers were washed with water (7 mL) and brine (7 mL), dried over Na_2SO4, filtered and concentrated. The residue was purified by flash column chromatography (EtOAc/hexane 1:4, R*f*: 0.30) to give the intermediate *tert*-butyl (*2R,4S*)-4-(((*tert*-butyldiphenylsilyl)oxy)methyl)-2-((E)-3-methoxy-3-oxoprop-1-en-1-yl)pyrrolidine-1-carboxylate as a colorless oil (143 mg, 72%). $[\alpha]^{25}_D$: +36.4 (*c* 1.1, $CHCl_3$). IR (neat), υ_{max}: 2931, 2858, 1725, 1693, 1428, 1387, 1364, 1265, 1162, 1107, 978, 861, 823, 740, 701, 611, 503 cm^{-1}. ^1H NMR ($CDCl_3$, 500 MHz, mixture of rotamers), δ: 7.65-7.62 (m, 4 H), 7.43-7.37 (m, 6 H), 6.87-6.97 (m, 1 H), 5.83 (t, *J* = 14.5 Hz, 1 H), 4.53 (br. s, 0.4 H), 4.37 (br. s, 0.6 H), 3.75 (s, 1.8 H), 3.73 (s, 1.2 H), 3.61 (d, *J* = 6.3 Hz, 2 H), 3.60-3.57 (m, 0.6 H), 3.50-3.46 (m, 0.4 H), 3.27 (t, *J* = 9.4 Hz, 0.6 H), 3.21-3.18 (m, 0.4 H), 2.50-2.41 (m, 1 H), 1.97-1.86 (m, 1 H), 1.80 (dd, *J* = 6.4, 2.5 Hz, 0.6 H), 1.78 (dd, *J* = 6.4, 2.5 Hz, 0.4 H), 1.46 (s, 5.4 H), 1.41 (s, 3.6 H), 1.05 (s, 9 H) ppm. ^{13}C NMR ($CDCl_3$, 125 MHz, mixture of rotamers), δ: 166.8, 154.2, 154.1, 148.7, 148.4, 135.5, 133.3, 129.7, 127.9, 127.7, 120.0, 79.7, 65.0, 64.9, 57.7, 57.4, 51.6, 49.0, 48.9, 39.3, 38.4,

34.1, 33.4, 28.4, 28.2, 26.8, 19.2 ppm. HRMS (ESI) calcd. for $C_{30}H_{42}NO_5Si$ $(M+H)^+$ 524.28270, found 524.28136.

tert-Butyl (*2R,4S*)-4-(((*tert*-butyldiphenylsilyl)oxy)methyl)-2-((E)-3-methoxy-3-oxoprop-1-en-1-yl)pyrrolidine-1-carboxylate (0.12 g, 0.23 mmol, 1.0 eq.) was dissolved in MeOH (9 mL) and Pd/C (10% w/w, 29 mg, 27 µmol, 0.12 eq.) was added to the resulting solution. The air was removed from the flask under vacuum and replaced with hydrogen (balloon). The reaction mixture was vigorously stirred overnight at room temperature. Afterwards, the mixture was filtered through a Celite pad, washing with MeOH. The collected solution was concentrated *in vacuo*, affording **13b** as a colorless oil (122 mg, 99%). $[\alpha]^{20}_D$: +20.9 (*c* 0.9, $CHCl_3$). IR (neat), υ_{max}: 2931, 2857, 1737, 1690, 1427, 1388, 1364, 1254, 1169, 1109, 823, 739, 701, 610, 504 cm^{-1}. ^1H NMR ($CDCl_3$, 500 MHz, mixture of rotamers), δ: 7.70-7.63 (m, 4 H), 7.44-7.37 (m, 6 H), 3.88 (br. s, 0.5 H), 3.80 (br. s, 0.5 H), 3.67 (s, 3 H), 3.58 (d, *J* = 6.2 Hz, 2 H), 3.49-3.43 (m, 0.5 H), 3.40-3.35 (m, 0.5 H), 3.29-3.24 (m, 0.5 H), 3.22-3.17 (m, 0.5 H), 2.54-2.48 (m, 1 H), 2.32 (br. s, 2 H), 2.04-1.92 (m, 1 H), 1.75-1.66 (m, 3 H), 1.46 (s, 9 H), 1.05 (s, 9 H) ppm. ^{13}C NMR ($CDCl_3$, 125 MHz, mixture of rotamers), δ: 173.9, 173.7, 154.7, 154.5, 135.5, 133.5, 129.7, 127.7, 79.4, 79.1, 65.6, 65.4, 56.5, 51.5, 48.9, 39.5, 38.7, 33.4, 32.8, 31.1, 30.2, 30.0, 28.5, 26.8, 19.2 ppm. HRMS (ESI) calcd. for $C_{30}H_{44}NO_5Si$ $(M+H)^+$ 526.2983, found 526.2993.

tert-Butyl (2S,4S)-4-(hydroxymethyl)-2-(3-(4-octylphenyl)-3-oxopropyl)pyrrolidine-1-carboxylate **(13c)**

13b (0.12 g, 0.23 mmol) was submitted to the procedure reported for **12b**. The crude was purified by flash column chromatography (EtOAc/hexane 1:1, R*f*: 0.28) to give the intermediate *tert*-butyl (*2S,4S*)-4-(((*tert*-butyldiphenylsilyl)oxy)methyl)-2-(3-(methoxy(methyl)amino)-3-oxopropyl)pyrrolidine-1-carboxylate as a colorless oil (111 mg, 87%). $[\alpha]^{25}_D$: +20.2 (*c* 1.1, $CHCl_3$). IR (neat), υ_{max}: 2930, 2857, 1688, 1386, 1364, 1254, 1175, 1109, 997, 823, 740, 702, 611, 504 cm^{-1}. ^1H NMR ($CDCl_3$, 500 MHz, mixture of rotamers), δ: 7.65-7.63 (m, 4 H), 7.44-7.36 (m, 6 H), 3.92 (br. s, 0.5 H), 3.83 (br. s, 0.5 H), 3.68 (s, 3 H), 3.59 (d, *J* = 6.1 Hz, 2 H), 3.51-3.45 (m, 0.5 H), 3.43-3.37 (m, 0.5 H), 3.30-3.25 (m, 0.5 H), 3.17 (br. s, 3.5 H), 2.57-2.51 (m, 1 H), 2.43 (br. s, 2 H), 1.94 (br. s, 1 H), 1.71 (br. s, 3 H), 1.45 (s, 9 H), 1.04 (s, 9 H) ppm. ^{13}C NMR ($CDCl_3$, 125 MHz, mixture of

rotamers), δ: 174.4, 174.2, 154.7, 135.5, 133.5, 129.6, 127.7, 79.2, 78.9, 65.7, 65.5, 61.1, 56.8, 48.8, 39.5, 38.7, 33.6, 33.0, 32.2, 30.0, 29.8, 29.7, 29.2 28.5, 26.8, 19.2 ppm. HRMS (ESI) calcd. for $C_{31}H_{47}N_2O_5Si$ $(M+H)^+$ 555.3249, found 555.3268.

tert-Butyl (*2S,4S*)-4-(((*tert*-butyldiphenylsilyl)oxy)methyl)-2-(3-(methoxy(methyl)amino)-3-oxopropyl)pyrrolidine-1-carboxylate (34 mg, 61 µmol) was submitted in sequence to general procedures C and B. The crude was purified by flash column chromatography (EtOAc/hexane 1:1, R*f*: 0.20) to give **13c** as a colorless oil (12 mg, 44% over two steps). $[\alpha]^{25}_D$: +6.3 (*c* 0.6, $CHCl_3$). IR (neat), υ_{max}: 3437, 2923, 2854, 1678, 1605, 1391, 1364, 1253, 1174, 1122, 770, 567 cm^{-1}. ^1H NMR ($CDCl_3$, 500 MHz, mixture of rotamers), δ: 7.87 (d, *J* = 8.3 Hz, 2 H), 7.26-7.24 (m, 2 H), 4.01 (br. s, 0.5 H), 3.95 (br. s, 0.5 H), 3.64-3.60 (m, 2 H), 3.47-3.44 (m, 1 H), 3.31-3.26 (m, 0.5 H), 3.18-3.12 (m, 0.5 H), 3.09-3.02 (m, 0.5 H), 2.96 (br. s, 1.5 H), 2.64 (t, *J* = 7.6 Hz, 2 H), 2.54 (br. s, 1 H), 2.04 (br. s, 1 H), 1.88-1.74 (m, 3 H), 1.64-1.54 (m, 2 H), 1.41 (s, 9 H), 1.30-1.25 (m, 10 H), 0.87 (t, *J* = 7.0 Hz, 3 H) ppm. ^{13}C NMR ($CDCl_3$, 125 MHz, mixture of rotamers), δ: 199.8, 199.2, 154.8, 148.8, 148.6, 134.6, 128.6, 128.2, 79.5, 79.2, 64.8, 56.8, 49.0, 48.4, 39.6, 38.8, 36.0, 35.7, 35.3, 33.8, 33.2, 31.8, 31.1, 29.7, 29.6, 29.5, 29.4, 29.2, 29.1, 28.5, 27.5, 22.6, 14.1 ppm. HRMS (ESI) calcd. for $C_{27}H_{44}NO_4$ $(M+H)^+$ 446.32650, found 446.32667.

3-((2S,4S)-4-(Hydroxymethyl)pyrrolidin-2-yl)-1-(4-octylphenyl)propan-1-one hydrochloride **(13)** *and (2S)-2-(hydroxymethyl)-5-(4-octylphenyl)-1,2,3,6,7,7a-hexahydropyrrolizin-4-ium chloride* **(13d)**

Prepared according to general procedure A, starting from **13c** (6.0 mg, 13 µmol). The crude was triturated and washed with Et_2O, affording **13** as a white solid (4 mg, 80%). Note: in CD_3OD the product was slowly but completely converted into the bicyclic salt **13d**. On the other hand, in D_2O the two species resulted in equilibrium, giving a mixture with a 2:1 constant ratio in favor of the open compound **13**. For biological testing a portion of the product was dissolved in the minimum amount of HPLC grade water, filtered (pore size = 0.45 µm) and lyophilized. **13:** ^1H NMR (CD_3OD, 500 MHz), δ: 7.94 (d, *J* = 8.3 Hz, 2 H), 7.33 (d, *J* = 8.3 Hz, 2 H), 3.75-3.67 (m, 1 H), 3.63-3.53 (m, 2 H), 3.50 (dd, *J* = 11.8, 8.2 Hz, 1 H), 3.23 (dt, *J* = 13.9, 6.9 Hz, 2 H, partially deuterated), 3.12 (dd, *J* = 11.8, 6.8 Hz, 1 H), 2.71-2.67 (m, 2 H), 2.66-2.60 (m, 1 H), 2.21-2.01 (m, 3 H), 1.91 (dt, *J* = 13.5,

9.1 Hz, 1 H), 1.68-1.61 (m, 2 H), 1.33-1.29 (m, 10 H), 0.89 (t, *J* = 6.9 Hz, 3 H) ppm. **13d:** IR (neat), υ_{max}: 3410, 2923, 2853, 1645, 1605, 1456, 1417, 1373, 1296, 1190, 1045, 811, 566 cm^{-1}. ^{1}H NMR (CD_3OD, 500 MHz), δ: 7.93 (d, *J* = 8.4 Hz, 2 H), 7.56 (d, *J* = 8.4 Hz, 2 H), 5.09-5.00 (m, 1 H), 4.23-4.17 (m, 1 H), 4.14-4.06 (m, 2 H, partially deuterated), 3.71 (dd, *J* = 6.0, 1.3 Hz, 2 H), 3.68-3.61 (m, 1 H, partially deuterated), 3.02-2.95 (m, 1 H), 2.80-2.76 (m, 2 H), 2.60 (dt, *J* = 12.7, 7.6 Hz, 1 H), 2.28 (ddd, *J* = 12.8, 7.4, 2.0 Hz, 1 H), 2.13-2.02 (m, 1 H), 1.98-1.90 (m, 1 H), 1.72-1.65 (m, 2 H), 1.35-1.29 (m, 10 H), 0.89 (t, *J* = 6.9 Hz, 3 H) ppm. ^{13}C NMR (CD_3OD, 125 MHz), δ: 178.8, 152.6, 131.2, 129.5, 123.6, 75.7, 63.2, 51.4, 43.4, 41.1, 35.6, 31.6, 31.1, 30.7, 29.1, 29.0, 28.9, 26.6, 22.3, 13.0 ppm.

((2S,5S)-5-(4-Octylphenyl)hexahydro-1H-pyrrolizin-2-yl)methanol hydrochloride **(14)**

$NaBH_4$ (0.5 mg, 12 µmol, 1.5 eq.) was added to a solution of **13d** (3.0 mg, 8.0 µmol, 1.0 eq.) in MeOH (300 µL) at 0 °C. The resulting mixture was stirred for 1 h at the same temperautre. Afterwards, the reaction mixture was quenched with HCl 1 N (20 µL) and concentrated. The crude was purified by flash column chromatography ($MeOH/CH_2Cl_2$ 1:4, R*f*: 0.58) to give product **14** as a white solid (3 mg, 99%, dr. 10:1). The stereochemistry was assigned by performing NOESY experiments (through space coupling observed between 2-H and 5-H in the major diasteroisomer). For biological testing the product was dissolved in the minimum amount of HPLC grade water, filtered (pore size = 0.45 µm) and lyophilized. $[\alpha]^{25}_{D}$: -58.7 (*c* 0.15, MeOH). IR (neat), υ_{max}: 3417, 2923, 2853, 1518, 1456, 1089, 1037, 833, 535 cm^{-1}. ^{1}H NMR (CD_3OD, 500 MHz), δ: 7.49 (d, *J* = 8.1 Hz, 2 H), 7.32 (d, *J* = 8.1 Hz, 2 H), 4.52-4.46 (m, 1 H), 4.42 (dd, *J* = 10.9, 6.7 Hz, 1 H), 3.69 (dd, *J* = 11.1, 5.2 Hz, 1 H), 3.62 (dd, *J* = 11.1, 5.9 Hz, 1 H), 3.45 (dd, *J* = 11.8, 6.6 Hz, 1 H), 3.09 (dd, *J* = 11.8, 10.5 Hz, 1 H), 2.92-2.83 (m, 1 H), 2.67-2.64 (m, 2 H), 2.54-2.51 (m, 1 H), 2.41-2.35 (m, 2 H), 2.09-2.05 (m, 2 H), 2.00-1.92 (m, 1 H), 1.65-1.59 (m, 2 H), 1.32-1.28 (m, 10 H), 0.89 (t, *J* = 6.9 Hz, 3 H) ppm. ^{13}C NMR (CD_3OD, 125 MHz), δ: 145.1, 130.2, 129.2, 127.9, 72.7, 68.6, 60.7, 54.1, 39.5, 35.2, 32.8, 32.7, 31.6, 31.2, 31.1, 29.1, 29.0, 28.9, 22.3, 13.0 ppm. HRMS (ESI) calcd. for $C_{22}H_{36}NO$ $(M)^+$ 330.2797, found 330.2793.

tert-Butyl (2R,4R)-4-((tert-butyldimethylsilyl)oxy)-2-(3-methoxy-3-oxopropyl)pyrrolidine-1-carboxylate **(15a)**

15a was submitted to the Horner-Wadsworth-Emmons extension procedure from **13b**, starting from commercially available 1-(*tert*-butyl) 2-methyl (2S,4R)-4-((*tert*-butyldimethylsilyl)oxy)pyrrolidine-1,2-dicarboxylate (0.20 g, 0.56 mmol, 1.0 eq.). The residue was purified by flash column chromatography (hexane/EtOAc 8:2 R*f*: 0.38) to give the intermediate *tert*-butyl (*2S,4R*)-4-((*tert*-butyldimethylsilyl)oxy)-2-((E)-3-methoxy-3-oxoprop-1-en-1-yl)pyrrolidine-1-carboxylate as a colorless oil (150 mg, 69% over 2 steps). $[\alpha]^{25}_{D}$: -3.03 (*c* 3.15, $CHCl_3$). IR (neat), υ_{max}: 2977, 2926, 2855, 1701, 1396, 1260, 987, 753 cm^{-1}. ^1H NMR ($CDCl_3$, 500 MHz, mixture of rotamers), δ: 6.85-6.84 (m, 1 H), 5.90-5.75 (d, *J* = 15.0 Hz, 1 H), 4.57-4.47 (m, 1 H), 4.35-4.33 (t, *J* = 7.8 Hz, 1 H), 3.75 (s, 3 H), 3.47-3.36 (m, 2 H), 2.10-2.06 (m, 1 H), 1.85-1.80 (m, 1 H), 1.45 (s, 9 H), 0.89 (s, 9 H), 0.07 (s, 6 H) ppm. ^{13}C NMR ($CDCl_3$, 125 MHz, mixture of rotamers), δ: 200.3, 200.0, 166.9, 154.7, 149.3, 148.9, 128.5, 127.6, 127.0, 120.0, 79.9, 70.0, 69.7, 69.5, 56.9, 55.3, 54.8, 51.6, 41.5, 40.6, 36.9, 28.4, 28.2, 25.7, 17.9 ppm. HRMS (ESI) calcd. for $C_{25}H_{40}NO_3$ $(M+H)^+$ 618.35301, found 618.35381.

tert-Butyl (*2S,4R*)-4-((*tert*-butyldimethylsilyl)oxy)-2-((E)-3-methoxy-3-oxoprop-1-en-1-yl)pyrrolidine-1-carboxylate (0.15 g, 0.39 mmol, 1.0 eq.) was dissolved in MeOH (15 mL) and Pd/C (10% w/w, 47 mg, 44 μmol, 0.11 eq.) was added to the resulting solution. The air was removed from the flask under vacuum and replaced with hydrogen (balloon). The reaction mixture was vigorously stirred overnight at room temperature. Afterwards, the mixture was filtered through a Celite pad, washing with MeOH. The collected solution was concentrated *in vacuo*, affording **15a** as a colorless oil (149 mg, 99%). $[\alpha]^{20}_{D}$: -29.09 (*c* 0.44, $CHCl_3$). IR (neat), υ_{max}: 2929; 1739; 1693; 1390; 1154; 833; 773 cm^{-1}. ^1H NMR ($CDCl_3$, 500 MHz, mixture of rotamers), δ: 4.33-4.32 (q, 1 H), 4.10-3.95 (m, 1 H), 3.66 (s, 3 H), 3.48-3.32 (m, 2 H), 2.30 (bs, 2 H), 2.07-1.96 (m, 2 H), 1.78-1.71 (m, 2 H), 1.45 (s, 9 H), 0.86 (s, 9 H), 0.05 (s, 6 H) ppm. ^{13}C NMR ($CDCl_3$, 125 MHz, mixture of rotamers), δ: 174.1, 155.3, 79.6,79.4, 70.5, 70.0, 55.6, 55.0, 54.7, 51.7, 40.8, 40.1, 31.0, 30.7, 30.5, 30.2, 28.6, 25.9, 18.1 ppm. HRMS (ESI) calcd. for $C_{25}H_{40}NO_3$ $(M+H)^+$ 388.25140, found 388.25200.

tert-Butyl (2R,4R)-4-hydroxy-2-(3-(4-octylphenyl)-3-oxopropyl)pyrrolidine-1-carboxylate **(15b)**

15a (0.33 g, 0.86 mmol) was submitted to the procedure from **12b**. The residue was purified by flash column chromatography (hexane/EtOAc 6:4 R*f*: 0.25) to give the intermediate *tert*-butyl

(*2R,4R*)-4-((*tert*-butyldimethylsilyl)oxy)-2-(3-(methoxy(methyl)amino)-3-oxopropyl)pyrrolidine-1-carboxylate as a colorless oil (328 mg, 92%).

tert-Butyl (*2R,4R*)-4-((*tert*-butyldimethylsilyl)oxy)-2-(3-(methoxy(methyl)amino)-3-oxopropyl)pyrrolidine-1-carboxylate (100 mg, 0.24 mmol) was submitted in sequence to general procedures C and B. The resulting residue was purified by flash column chromatography (hexane/EtOAc 4:6 R*f*: 0.33) to give **15b** as a yellow oil (61 mg, 59% over 2 steps). $[\alpha]^{25}_{D}$: -19.00 (*c* 0.40, $CHCl_3$). IR (neat), υ_{max}: 2922, 1672, 1411 cm^{-1}. ^1H NMR ($CDCl_3$, 500 MHz, mixture of rotamers), δ: 7.90-7.88 (d, J = 8.2 Hz, 2 H), 7.29-7.27 (d, *J* = 9.3 Hz, 2 H), 4.48-4.47 (m, 1 H), 4.12-4.09 (m, 1 H), 3.60-3.58 (d, *J* = 11.7 Hz, 1 H), 3.47-3.43 (dd, *J* = 12.0, 4.6 Hz, 1 H), 2.99-2.95 (m, 2 H), 2.69-2.66 (t, *J* = 6.4 Hz, 2 H), 2.21-2.11 (m, 2 H), 1.91-1.87 (m, 3 H), 1.66-1.63 (m, 2 H), 1.46 (s, 9 H), 1.33-1.28 (m, 10 H), 0.92 (t, 3 H) ppm. ^{13}C NMR ($CDCl_3$, 125 MHz, mixture of rotamers), δ: 199.4, 155.2, 148.8, 134.5, 129.5, 128.6, 128.2, 79.6, 70.0, 55.6, 54.7, 40.3, 36.0, 31.9, 31.1, 29.7, 29.6, 29.4, 29.3, 29.2, 28.5, 22.7, 14.1, 14.1 ppm. HRMS (ESI) calcd. for $C_{25}H_{40}NO_3$ $(M+H)^+$ 454.29280, found 454.29428.

(2R,4R)-4-Hydroxy-2-(3-(4-octylphenyl)-3-oxopropyl)pyrrolidin-1-ium chloride **(15)**

15 was synthesized in accordance with the general procedure A, starting from **15b** (43 mg, 0.1 mmol). **15** was obtained as a white solid (26 mg, 72%). As for **13**, **15** revealed prone to cyclize spontaneously to **15d** in protic solvent such as MeOH. IR (neat), υ_{max}: 2977, 2926, 2855, 1701, 1396, 1260, 987, 753 cm^{-1}. ^1H NMR ($CDCl_3$, 500 MHz, opened form **15**), δ: 7.96-7.94 (d, *J* = 8.3 Hz, 2 H), 7.35-7.33 (d, *J* = 8.3 Hz, 2 H), 4.54 (m, 1 H), 3.95-3.90 (m, 1 H), 3.48-3.43 (dd, *J* = 12.5, 4.1 Hz, 1 H), 3.28-3.19 (m, 3 H), 2.71-2.67 (m, 2 H), 2.26-2.10 (m, 3 H), 1.87-1.80 (m, 1 H), 1.65 (m, 2 H), 1.34-1.29 (m, 10 H), 0.91-0.88 (t, *J* = 6.85 Hz, 3 H) ppm. ^1H NMR ($CDCl_3$, 500 MHz, cyclized form **15d**), δ: 8.00-7.98 (d, *J* = 8.5 Hz, 1 H), 7.59-7.57 (d, *J* = 8.4 Hz, 2 H), 5.24 (m, 1 H), 4.93-4.90 (m, 1 H), 4.33-4.29 (m, 1 H), 4.17-4.13 (m, 2 H), 3.74 (m, 1 H), 2.83-2.79 (m, 2 H), 2.64 (m, 1 H), 2.36-2.32 (dd, *J* = 13.1, 6.1 Hz, 1 H), 2.12-2.09 (m, 1 H), 1.97-1.89 (m, 1 H), 1.71 (m, 2 H), 1.36-1.31 (m, 10 H), 0.93-0.90 (t, *J* = 6.9 Hz, 3 H) ppm. HRMS (ESI) calcd. for $C_{25}H_{40}NO_3$ $(M+H)^+$ 618.35301, found 618.35381.

(S)-tert-Butyl 2-(4-bromobenzoyl)pyrrolidine-1-carboxylate **(17b)**

BuLi (2.5 M in hexane, 11 mL, 24 mmol, 2.0 eq.) was added dropwise via syringe to a stirred and cooled to -78 °C solution of 1,4-dibromobenzene (5.88 g, 24.9 mmol, 2.06 eq.) in dry THF (42 mL) under Ar. Stirring was continued for 30 min before *N*-Boc-D-prolinal **17a** (2.2 g, 1.0 mmol) in THF (18 mL) was added via syringe over ca 5 min. Stirring was continued for a further 15 min and the mixture was quenched by addition of sat. NH_4Cl (20 mL) and H_2O (10 mL). The bulk of the THF was then removed *in vacuo* and the mixture was extracted into Et_2O (30 mL), washed once with brine (15 mL) and dried ($MgSO_4$). Evaporation of the solvent and chromatography over SiO_2 (2.5 x 40 cm) using 13% EtOAc-hexanes afforded (2*S*)-*tert*-butyl 2-((4-bromophenyl) (hydroxy)methyl) pyrrolidine-1-carboxylate as a mixture of diastereomers (2.3 g, 59%).

Dess-Martin periodinane (3.5 g, 8.2 mmol, 1.3 eq.) was added as a solid over ca 2 min to a stirred and cooled (0 °C) solution of (2*S*)-*tert*-butyl 2-((4-bromophenyl) (hydroxy)methyl)pyrrolidine-1-carboxylate (mixture of diastereomers, 2.3 g, 6.5 mmol, 1.0 eq.) in CH_2Cl_2 (24 mL). The flask was capped with a glass stopper and stirring was continued overnight. The mixture was then quenched by the addition of sat. $NaHCO_3$ (10 mL) and H_2O (5 mL) and stirring was continued for 30 min. The mixture was then filtered through Celite (2 x 3cm), washing the filter cake with CH_2Cl_2. The aqueous layer was extracted once with CH_2Cl_2 (10 mL) and the combined organic was dried ($MgSO_4$), evaporated, and chromatographed over SiO_2 (2.5 x 30 cm) using 13% EtOAc-hexanes to afford (*S*)-*tert*-butyl 2-(4-bromobenzoyl)pyrrolidine-1-carboxylate **17b** (1.6011 g, 70%). HRMS (ESI) calcd. for $C_{16}H_{20}BrNO_3$ $(M+Na)^+$ 376.05188, found 376.05202.

tert-Butyl (S)-2-((R)-1-(4-bromophenyl)-3-ethoxy-1-hydroxy-3-oxopropyl)pyrrolidine-1-carboxylate **(17c)** *and tert-butyl (S)-2-((S)-1-(4-bromophenyl)-3-ethoxy-1-hydroxy-3-oxopropyl)pyrrolidine-1-carboxylate* **(epi-17c)**

BuLi (2.5 M in hexane, 5.5 mL, 14 mmol, 3.0 eq.) was added via syringe to a stirred and cooled to -78 °C solution of *i*-Pr_2NH (1.9 mL, 14 mmol, 3.0 eq.) in THF (12 mL). The cooling bath was removed for 10 min and then replaced and stirring was continued for a further 10 min before EtOAc (1.5 mL, 15 mmol, 3.4 eq.) was added dropwise via syringe. Stirring was then continued for 45 min before (*S*)-*tert*-butyl-2-(4-bromobenzoyl)pyrrolidine-1-carboxylate **17b** (1.6 g, 4.6 mmol, 1.0 eq.) in THF (5 mL + 1 mL rinse) was added at a slow dropwise rate via syringe (ca 15 min). Stirring was

then continued for 20 min and then the mixture was quenched by the addition of sat. NH_4Cl (5 mL) and H_20 (5 mL). The reaction mixture was diluted with Et_2O (30 mL) and washed once with H_2O (20 mL), once with brine (20 mL) and dried (Na_2SO_4). Evaporation of the solvent provided (*S*)-*tert*-butyl 2-((*S*)-1-(4-bromophenyl)-3-ethoxy-1-hydroxy-3-oxopropyl)pyrrolidine-1-carboxylate **17c** and (*S*)-*tert*-butyl 2-((*R*)-1-(4-bromophenyl)-3-ethoxy-1-hydroxy-3-oxopropyl)pyrrolidine-1-carboxylate **epi-17c** as a mixture (1.54 g, 76%), which was used directly in the next step without further purification. HRMS (ESI) calcd. for $C_{25}H_{40}NO_3$ $(M+H)^+$ 464.10431, found 464.10432.

tert-Butyl (S)-2-((R)-1-(4-bromophenyl)-1-hydroxy-3-(tosyloxy)propyl)pyrrolidine-1-carboxylate **(17d)** *and (S)-tert-butyl 2-((S)-1-(4-bromophenyl)-1-hydroxy-3-(tosyloxy)propyl)pyrrolidine-1-carboxylate* **(epi-17d)**

$LiBH_4$ solution (2.0 M in THF, 1.1 mL, 2.2 mmol, 0.6 eq.) was added via syringe to a stirred and cooled to 0 °C solution of esters (*S*)-*tert*-butyl 2-((*S*)-1-(4-bromophenyl)-3-ethoxy-1-hydroxy-3-oxopropyl)pyrrolidine-1-carboxylate **17c** and (*S*)-*tert*-butyl 2-((*R*)-1-(4-bromophenyl)-3-ethoxy-1-hydroxy-3-oxopropyl)pyrrolidine-1-carboxylate **epi-17c** (mixture from previous step, 1.5 g, 3.5 mmol, 1.0 eq.) in THF (10 mL) under Ar. The ice-bath was left in place but not recharged and stirring was continued for 7 h. The mixture was then quenched by the careful addition of H_2O (3 mL) and then $NaHCO_{3\,aq}$ (sat., 5 mL). EtOAc (10 mL) was then added and the biphasic mixture was stirred for 1 h. The aqueous phase was extracted once with EtOAc (10 mL) and the combined organic was washed once with brine (10 mL) and dried (Na_2SO_4). Evaporation of the solvent and filtration of the residue through a plug of SiO_2 (2 x 4 cm) using 40% EtOAc-hexanes (ca 100 mL, TLC control) afforded the alcohols (*S*)-*tert*-butyl 2-((*R*)-1-(4-bromophenyl)-1,3-dihydroxypropyl)pyrrolidine-1-carboxylate and (*S*)-*tert*-butyl 2-((*S*)-1-(4-bromophenyl)-1,3-dihydroxypropyl)pyrrolidine-1-carboxylate as a mixture (1.38 g, 72%).

Et_3N (0.93 mL, 6.7 mmol, 1.2 eq.) followed by TsCl (1.2 g, 6.1 mmol, 1.1 eq.) were added to a stirred solution of alcohols (*S*)-*tert*-butyl-2-((*R*)-1-(4-bromophenyl)-1,3-dihydroxypropyl) pyrrolidine -1-carboxylate and (*S*)-*tert*-butyl-2-((*S*)-1-(4-bromophenyl)-1,3-dihydroxypropyl) pyrrolidine-1-carboxylate mixture from previous step (2.2 g, 5.55 mmol, 1.0 eq.) in CH_2Cl_2 (10 mL).

The flask was capped with a glass stopper and stirred for 8 h. The mixture was diluted with CH_2Cl_2 (10 mL), washed once with H_2O (25 mL), and dried ($MgSO_4$). Removal of the solvent *in vacuo* and chromatography over SiO_2 (2.5 x 35 cm) using 10% EtOAc-hexanes afforded the tosylates (*S*)-*tert*-butyl 2-((*R*)-1-(4-bromophenyl)-1-hydroxy-3-(tosyloxy)propyl)pyrrolidine-1-carboxylate **17d** and (*S*)-*tert*-butyl 2-((*S*)-1-(4-bromophenyl)-1-hydroxy-3-(tosyloxy)propyl)pyrrolidine-1-carboxylate **epi-17d** as a mixture (2.2 g, 72%).

(1R)-1-(4-Bromophenyl)-1-hydroxyoctahydropyrrolizin-4-ium 4-methylbenzenesulfonate **(17e)** *and (1S)-1-(4-bromophenyl)-1-hydroxyoctahydropyrrolizin-4-ium 4-methylbenzenesulfonate* **(epi-17e)**

A solution of tosylates (*S*)-*tert*-butyl 2-((*R*)-1-(4-bromophenyl)-1-hydroxy-3-(tosyloxy)propyl)pyrrolidine-1-carboxylate **17d** and (*S*)-*tert*-butyl 2-((*S*)-1-(4-bromophenyl)-1-hydroxy-3-(tosyloxy)propyl)pyrrolidine-1-carboxylate **epi-17d** (2.2 g, 4.0 mmol, 1.0 eq.) was stirred for 10h at 110 °C in PhMe (18 mL) under Ar. The solvent was then removed *in vacuo* and the residue was chromatographed over SiO_2 (2.5 x 35 cm) using 10-20% MeOH-$CHCl_3$ to give a faster eluting fraction ((1*R*,7a*S*)-1-(4-bromophenyl)-1-hydroxyoctahydropyrrolizin-4-ium 4-methylbenzenesulfonate) **17e** and a slower eluting fraction ((1*S*,7a*S*)-1-(4-bromophenyl)-1-hydroxyoctahydropyrrolizin-4-ium 4-methylbenzenesulfonate) **epi-17e**. Mixed fractions were discarded. After removal of the solvent, the faster eluting diastereomer was crystallized from CH_2Cl_2-*t*-BuOMe (note 1) to provide ((1*R*,7a*S*)-1-(4-bromophenyl)-1-hydroxyoctahydropyrrolizin-4-ium 4-methylbenzenesulfonate **17e** (0.7 g, 38%). The slower eluting fraction was also evaporated to dryness and the solid residue was suspended in CH_2Cl_2 (3 mL) and filtered through a syringe filter (25 mm, PTFE 0.45 µm) to remove silica washing with three portions of CH_2Cl_2 (3 ml each) (note 2). The solvent was then removed *in vacuo* and the solid residue was crystallized from CH_2Cl_2-*t*-BuOMe (note 3) to provide (1*S*,7a*S*)-1-(4-bromophenyl)-1-hydroxyoctahydropyrrolizin-4-ium 4-methylbenzenesulfonate **epi-17e** (0.3 g, 17%). **17e:** mp 143 °C. $[\alpha]^{25}_{D}$: +21 (*c* 0.65, MeOH). IR (neat), υ_{max}: 3371, 3673, 1657, 1394, 561 cm^{-1}. ^1H NMR (400 MHz, $CDCl_3$), δ: 1.74-1.83 (m, 1 H), 2.05-2.13 (m, 1 H), 2.24-2.33 (m, 2 H), 2.39 (s, 3 H), 2.45 (dd, *J* = 5.4, 13.4 Hz, 1 H), 2.81 (ddd, *J* = 7.2, 13.0, 13.0 Hz, 1 H), 3.03-3.09 (m, 1 H), 3.32 (ddd, *J* = 5.9, 12.8, 12.8 Hz, 1 H), 3.55 (ddd, *J* = 6.0, 6.0, 11.7 Hz, 1 H), 3.80-3.87 (br s, 1 H), 3.94-3.99 (m, 1 H),

4.38 (app dd, *J* = 4.5, 8.0 Hz, 1 H), 7.18 (d, *J* = 8.1 Hz, 2 H), 7.36 (d, *J* = 8.7 Hz, 2 H), 7.45 (d, *J* = 8.7 Hz, 2 H), 7.71 (d, *J* = 8.1 Hz, 2 H), 11.26 (br s, 1 H) ppm. ^{13}C NMR (100 MHz, $CDCl_3$), δ: 21.8, 22.8, 27.5, 42.6, 53.7, 55.7, 79.4, 122.3, 126.1, 127.7, 129.4, 132.0, 140.3, 141.0, 142.0 ppm. LRMS found m/z 282.0. **epi-17e:** mp = 177.5-178.5 °C. IR (neat), υ_{max}: 1234, 1185, 1009, 815, 696, 568, 478 cm^{-1}. ^{1}H NMR (400 MHz, $CDCl_3$), δ: 1.18-1.26 (m, 1 H), 1.77-1.84 (m, 1 H), 1.93-2.01 (m, 2 H), 2.39 (s, 3 H), 2.53-2.66 (overlapping m, 2 H), 2.97 (ddd, *J* = 11.4, 9.6, 6.8 Hz, 1 H), 3.26 (dd, *J* = 11.6, 6.4 Hz, 1 H), 3.98 (ddd, *J* = 11.3, 6.1, 6.1 Hz, 1 H), 4.31 (ddd, *J* = 11.9, 11.9, 7.1 Hz, 1 H), 4.61 (dd, *J* = 10.0, 8.2 Hz, 1 H), 5.80 (br s, 1 H), 7.18 (d, *J* = 7.9 Hz, 2 H), 7.33 (d, *J* = 8.6 Hz, 2 H), 7.49 (d, *J* = 8.6 Hz, 2 H), 7.73 (d, *J* = 7.9 Hz, 2 H) ppm. ^{13}C NMR (100 MHz, $CDCl_3$), δ: 4.3, 21.8, 26.0, 29.8, 33.5, 54.2, 57.2, 81.8, 123.1, 126.3, 128.6, 129.3, 132.2, 139.4, 140.9, 141.8 ppm. LRMS found m/z 282.0. Note 1: Diastereomer (1*R*,7a*S*)-1-(4-bromophenyl)-1-hydroxyoctahydropyrrolizin-4-ium 4-methylbenzenesulfonate was dissolved in ca. 10 mL of CH_2Cl_2 and was then brought to boiling with a heat gun. t-BuOMe (ca 5 mL) was then added and the solution was allowed to crystallize overnight, the flask being left completely open. The next day the flask was capped with a glass stopper and cooled at ca -15 °C (freezer section of fridge) for a further 10 h. Filtration afforded flocculent white needles of ((1*R*,7a*S*)-1-(4-bromophenyl)-1-hydroxyoctahydropyrrolizin-4-ium 4-methylbenzenesulfonate. Note 2: The syringe filter was attached to a syringe and the plunger was removed. The suspension was then transferred to this syringe via Pasteur pipette and forced through the filter by re-inserting the plunger. Note 3: Diastereomer (1*S*,7a*S*)-1-(4-bromophenyl)-1-hydroxyoctahydropyrrolizin-4-ium 4-methylbenzenesulfonate was dissolved in ca 10 mL of CH_2Cl_2 with stirring in an oil bath set at 45 °C. tBu-OMe was added (ca 3mL) and stirring was discontinued. The oil bath was shut off but left in place and the mixture was allowed to crystallize overnight, the flask being left completely open. The next day the flask was capped with a glass stopper and cooled at ca -15 °C (freezer section of fridge) for a further 10 h. Filtration afforded small needles.

(1R)-1-(4-Octylphenyl)hexahydro-1H-pyrrolizin-1-ol hydrochloride **(17)**

To a solution of catecholborane (0.14 mL, 1.0 M in THF, 0.14 mmol, 1.5 eq.) was added the octyne dropwise (20 µL, 0.14 mmol, 1.5 eq.). Gas formation was observed during the addition. The colorless solution was refluxed for 2h then cooled back to rt. In another flask, **17e** (41 mg, 90

µmol, 1.0 eq.) was dissolved in a biphasic mixture of DME (1.1 mL) and aqueous $NaHCO_3$ (1 M) solution, then the octyne/catecholborane solution was syringed into the flask. $Pd(PPh_3)_4$ (3.1 mg, 2.7 µmol, 0.03 eq.) was added and the overall white suspension was refluxed overnight. Et_2O and brine added. The aqueous layer was extracted x2 with Et_2O. The organic layers were collected, dried over Na_2SO_4, filtered through Celite, and concentrated. The crude oil was chromatographed over SiO_2 (9:1 DCM/MeOH) to deliver an orange oil (18 mg). The product was engaged in the next step without further purification. The previously obtained oil (12 mg, 38 µmol, 1.0 eq.) was dissolved in MeOH (1.2 mL) and Pd/C was added in one portion (10% w/w, 4.0 mg, 3.8 mmol, 0.1 eq.). The flask was purged x3 with H_2 and the black suspension was stirred for 1h30. Then HCl (9.5 µL, 4.0 M, 38 µmol, 1.0 eq.) was added and the solution was stirred for 2h, then filtered through a pad of Celite and concentrated. The resulting crude was chromatographed on reversed C18 column (0 to 20% MeCN in H_2O) to deliver **17** as a colorless oil (9 mg, 29% over two steps). $[\alpha]^{25}_D$: -16.00 (*c* 0.275, MeOH) IR (neat), υ_{max}: 3357, 2923, 1593, 1349 cm^{-1}. ^1H NMR ($CDCl_3$, 500 MHz, mixture of rotamers), δ: 7.14-7.08 (m, 4 H), 4.78 (bs, 1 H), 4.60-4.57 (t, *J* =, 0.47 H), 4.54-4.50 (t, *J* = 14.8, 0.53 H), 3.91-3.67 (m, 3 H), 3.54-3.47 (m, 1 H), 2.58-2.54 (m, 2 H), 2.30-2.25 (m, 0.53 H), 2.13-2.09 (m, 0.47 H), 1.84-1.81 (m, 1 H), 1.58-1.56 (m, 2 H), 1.58-1.40 (m, 25 H), 1.29-1.25 (m, 13 H), 0.89-0.86 (t, *J* = , 3 H) ppm. ^{13}C NMR ($CDCl_3$, 125 MHz, mixture of rotamers), δ: 207.1, 207.1, 154.6, 153.8, 142.2, 141.9, 130.6, 130.3, 129.7, 129.6, 129.0, 128.9, 83.1, 83.1, 83.1, 83.0, 82.9, 80.9, 80.5, 75.7, 75.6, 74.8, 74.8, 63.4, 62.5, 53.8, 53.7, 53.5, 53.5, 47.6, 46.3, 32.0, 30.0, 30.0, 29.6, 29.4, 28.5, 28.4, 22.8, 14.2 ppm. HRMS (ESI) calcd. for $C_{23}H_{37}NO_3Na$ $(M+H)^+$ 316.2635, found 316.2644.

tert-Butyl 3-hydroxy-3-(4-octylphenyl)pyrrolidine-1-carboxylate **((±)18b)**

(±)18b was synthesized in accordance with the general procedure C, starting from **18a** (0.10 g, 0.54 mmol). The resulting residue was purified by flash column chromatography (hexane/EtOAc 8:2, R*f*: 0.28) to give **(±)18b** as a pale yellow oil (123 mg, 61%). IR (neat), υ_{max}: 3392, 2923, 1670, 1412, 1134 cm^{-1}. ^1H NMR (500 MHz, $CDCl_3$, mixture of rotamers) δ 7.37 (t, *J* = 6.6 Hz, 2H), 7.18 (d, *J* = 8.0 Hz, 2H), 3.80 – 3.49 (m, 4H), 2.65 – 2.50 (m, 2H), 2.36 – 2.09 (m, 2H), 1.67 – 1.54 (m, 2H), 1.47 (d, *J* = 11.1 Hz, 9H), 1.38 – 1.11 (m, 10H), 0.88 (t, *J* = 7.0 Hz, 3H). ^{13}C NMR (125 MHz, $CDCl_3$, mixture of rotamers) δ 154.9, 154.8, 142.8, 140.1, 128.7, 125.2, 125.2, 80.7, 79.9, 79.6, 59.7, 58.8,

45.2, 44.7, 39.6, 38.9, 35.7, 32.0, 31.6, 29.9, 29.6, 29.5, 29.4, 28.7, 22.8, 14.3. HRMS (ESI) calcd. for $C_{23}H_{37}NO_3Na$ $(M+Na)^+$ 398.2666, found 398.2681.

3-Hydroxy-3-(4-octylphenyl)pyrrolidin-1-ium chloride **((±)18)**

18 was synthesized in accordance with the general procedure A, starting from **18b** (25 mg, 66 µmol). The resulting residue was triturated with a mixture of CH_2Cl_2/Et_2O (9:1) to give **18** as a pale yellow oil (9.6 mg, 45 %). R*f*: 0.18 CH_2Cl_2/MeOH 9:1, 1% Et_3N). IR (neat), υ_{max}: 3385, 2922, 1617, 1379, 1179, 1086 cm^{-1}. ^1H NMR (500 MHz, MeOD) δ 7.44 (d, *J* = 8.1 Hz, 2H), 7.22 (d, *J* = 8.0 Hz, 2H), 3.61 (d, *J* = 9.8 Hz, 2H), 3.43 (dd, *J* = 30.3, 11.5 Hz, 2H), 2.68 – 2.55 (m, 2H), 2.43 (dd, *J* = 23.4, 10.3 Hz, 1H), 2.33 (d, *J* = 11.0 Hz, 1H), 1.61 (d, *J* = 7.3 Hz, 2H), 1.40 – 1.22 (m, 10H), 0.89 (t, *J* = 6.9 Hz, 3H). ^{13}C NMR (125 MHz, MeOD) δ 142.7, 137.9, 128.3, 125.1, 79.6, 56.6, 48.1, 48.0, 47.8, 47.6, 47.4, 47.3, 47.1, 44.4, 38.1, 35.0, 31.6, 31.3, 29.2, 29.0, 28.9, 22.3, 13.0. HRMS (ESI) calcd. for $C_{18}H_{29}NO$ $(M+H)^+$ 276.2322, found 276.2326.

tert-Butyl (S)-2-(methoxy(methyl)carbamoyl)pyrrolidine-1-carboxylate **(19b)**

To a -20 °C cooled solution containing **19a** (0.32 g, 1.4 mmol, 1.0 eq.) and N,O-dimethylhydroxylamine-HCl (205 mg, 2.1 mmol, 1.5 eq.) in dry THF (1 mL) was added *i*PrMgCl (1.4 mL, 2.8 mmol, 2.0 M in THF, 2.0 eq.) dropwise. The light brown solution was stirred at -10 °C for 20 min whereby additional N,O-dimethylhydroxylamine-HCl (205 mg, 2.1 mmol, 1.5 eq.) was added in one portion followed by *i*PrMgCl (1.4 mL, 2.8 mmol, 2.0 M in THF, 2.0 eq.) dropwise. The reaction mixture was stirred for 20 additional min at -10 °C whereby TLC analysis indicated that the reaction had gone to completion. Saturated aqueous NH_4Cl solution (5 mL) was added and the resulting aqueous layer was extracted with EtOAc (2 x 5 mL). The organic layers were collected, dried over Na_2SO_4, filtered and concentrated to give **19b** as a pure colorless oil (321 mg, 89%) which was brought to the next step without further purification (R*f*: 0.34 hexanes/EtOAc 5:5). $[\alpha]^{20}_D$: -13.92 (*c* 1.25, $CHCl_3$). The spectral data matched those reported in the litterature. [6]

tert-Butyl (S)-2-(4-octylbenzoyl)pyrrolidine-1-carboxylate **(19c)**

19c was synthesized in accordance with the general procedure C, starting from **19b** (0.10 g, 0.39 mmol). The resulting residue was purified by flash column chromatography (hexane/EtOAc 8:2 R*f*: 0.32) to give **19c** as a yellow oil (98 mg, 65%). $[\alpha]^{20}_{D}$: -78.05 (*c* 0.21, $CHCl_3$). IR (neat), υ_{max}: 2925, 2584, 1687, 1391, 1160 cm^{-1}. ^1H NMR (500 MHz, $CDCl_3$) δ 7.88 (dd, *J* = 19.0, 8.2 Hz, 2H), 7.25 (dd, *J* = 15.6, 7.8 Hz, 2H), 5.37 – 5.16 (m, 1H), 3.76 – 3.41 (m, 2H), 2.64 (dt, *J* = 11.2, 7.8 Hz, 2H), 2.37 – 2.22 (m, 1H), 1.99 – 1.85 (m, 3H), 1.67 – 1.55 (m, 2H), 1.46 (s, 4H), 1.36 – 1.20 (m, 16H), 0.87 (t, *J* = 7.0 Hz, 3H). ^{13}C NMR ($CDCl_3$, 125 MHz, mixture of rotamers), δ: 198.7, 198.2, 154.6, 154.0, 149.1, 149.1, 133.0, 132.9, 128.8, 128.8, 128.8, 128.4, 79.8, 79.7, 61.4, 61.1, 46.9, 46.8, 36.1, 32.0, 31.2, 29.5, 29.4, 29.3, 28.6, 28.3, 23.7, 22.8, 14.2 ppm. HRMS (ESI) calcd. for $C_{24}H_{37}NO_3$ $(M+Na)^+$ 410.26660, found 410.26710.

(S)-2-(4-Octylbenzoyl)pyrrolidin-1-ium chloride **(19)**

19 was synthesized in accordance with the general procedure A, starting from **19c** (27 mg, 70 µmol). The resulting residue was triturated with EtOAc to give **19** as a white powder (14 mg, 64%). $[\alpha]^{20}_{D}$: -38.71 (*c* 0.16, $CHCl_3$). IR (neat), υ_{max}: 2923, 2853, 1686, 1397, 1250, 997 cm^{-1}. ^1H NMR (500 MHz, MeOD) δ 8.00 (d, *J* = 8.3 Hz, 2H), 7.43 (d, *J* = 8.3 Hz, 2H), 5.34 (dd, *J* = 9.3, 7.1 Hz, 1H), 3.45 (dt, *J* = 15.3, 6.1 Hz, 2H), 2.79 – 2.61 (m, 1H), 2.24 – 1.90 (m, 2H), 1.73 – 1.58 (m, 2H), 1.42 – 1.23 (m, 10H), 0.90 (t, *J* = 7.0 Hz, 3H). ^{13}C NMR ($CDCl_3$, 125 MHz, mixture of rotamers), δ: 194.9, 152.9, 132.1, 130.8, 130.7, 64.8, 47.8, 37.3, 33.3, 32.6, 31.4, 30.9, 30.7, 30.6, 25.5, 24.0, 14.7 ppm. HRMS (ESI) calcd. for $C_{19}H_{30}NO$ $(M+H)^+$ 288.23219, found 288.23192.

tert-Butyl (2S,4R)-4-((tert-butyldimethylsilyl)oxy)-2-(methoxy(methyl)carbamoyl)pyrrolidine-1-carboxylate **(20b)**

20b was synthesized in accordance with the procedure from **19b**, starting from **20a** (50 mg, 0.14 mmol). The crude colorless oil of **20b** (54 mg, 95%) was brought to the next step without further purification (R*f*: 0.25 hexanes/EtOAc 7:3). $[\alpha]^{25}_{D}$: -14.00 (*c* 0.50, $CHCl_3$). The spectral data matched those reported in the litterature.[7]

tert-Butyl (2R,4S)-4-((tert-butyldimethylsilyl)oxy)-2-(methoxy(methyl)carbamoyl)pyrrolidine-1-carboxylate **(21b)**

21b was synthesized in accordance with the procedure of its enantiomer **20b,** starting from **21a** (0.30 mg, 0.84 mmol). **21b** was obtained as a colorless oil (298 mg, 91 %) which was brought to the next step without further purification (R*f*: 0.25 hexanes/EtOAc 7:3). $[\alpha]^{25}_{D}$: +13.00 (*c* 1.00, $CHCl_3$). The spectral data matched those reported for its enantiomer.

tert-Butyl (2S,4R)-4-hydroxy-2-(4-octylbenzoyl)pyrrolidine-1-carboxylate **(20c)**

20b (0.20 g, 0.52 mmol) was submitted in sequence to general procedures C and B. The resulting residue was purified by flash column chromatography (hexane/EtOAc 4:6 R*f*: 0.35) to give **20c** as a yellow oil (135 mg, 65% over 2 steps). $[\alpha]^{25}_{D}$: -6.66 (*c* 0.27, $CHCl_3$). IR (neat), υ_{max}: 2924, 1686, 1605, 1399, 1158 cm^{-1}. ^1H NMR ($CDCl_3$, 500 MHz, mixture of rotamers), δ: 7.95-7.90 (m, 2 H), 7.31-7.27 (m, 2 H), 5.51-5.48 (t, J = 7.6 Hz, 0.45 H), 5.42-5.39 (t, *J* = 8.1 Hz, 0.55 H), 4.55 (s, 1 H), 3.80-3.56 (m, 2 H), 2.71-2.68 (m, 2 H), 2.41-2.37 (m, 1 H), 2.09-2.04 (m, 1 H), 1.74-1.62 (m, 3 H), 1.49 (s, 3 H), 1.32-1.26 (m, 15 H), 0.92-0.89 (t, *J* = 7.0 Hz, 3 H) ppm. ^{13}C NMR ($CDCl_3$, 125 MHz, mixture of rotamers), δ: 199.0, 198.5, 154.9, 154.4, 149.7, 149.6, 133.4, 133.3, 129.2, 129.1, 129.1, 128.7, 80.7, 80.4, 71.0, 70.3, 60.0, 59.7, 55.6, 40.1, 39.3, 36.4, 32.2, 31.5, 31.4, 29.8, 29.6, 29.6, 28.8, 28.5, 23.0, 14.5 ppm. HRMS (ESI) calcd. for $C_{25}H_{40}NO_3$ $(M+H)^+$ 426.26150, found 426.26245.

tert-Butyl (2R,4S)-4-hydroxy-2-(4-octylbenzoyl)pyrrolidine-1-carboxylate **(21c)**

21b (0.30 g, 0.77 mmol) was submitted in sequence to general procedures C and B. The resulting residue was purified by flash column chromatography (hexane/ EtOAc 4:6 R*f*: 0.35) to give **21c** as a yellow oil (205 mg, 62% over 2 steps). $[\alpha]^{25}_{D}$: +38.18 (*c* 1.65, $CHCl_3$). The spectral data matched those reported for its enantiomer.

(2S,4R)-4-Hydroxy-2-(4-octylbenzoyl)pyrrolidin-1-ium chloride **(20)**

20 was synthesized in accordance with the general procedure A, starting from **20c** (18 mg, 70 µmol). **20** was obtained as a white solid (18 mg, 86%). $[\alpha]^{25}_{D}$: -30.69 (*c* 0.80, $CHCl_3$). IR (neat), υ_{max}: 2923, 2470, 2070, 1596, 1463, 1119, 973 cm^{-1}. ^1H NMR ($CDCl_3$, 500 MHz), δ: 7.99-7.98 (d, *J* = 8.2 Hz, 1 H), 7.43-7.42 (d, *J* = 7.9 Hz, 2 H), 5.51-5.47 (dd, J = 10.3, 8.2 Hz, 1 H), 4.61-4.60 (m, 1 H), 3.39 (s, 2 H), 2.73-2.71 (m, 2 H), 2.66-2.62 (dd, J = 12.9, 8.2 Hz, 1 H), 2.07-2.02 (ddd, *J* = 13.8, 10.4, 4.2 Hz, 1 H), 1.68-1.65 (m, 2 H), 1.34-1.28 (m, 10 H), 0.91-0.88 (t, *J* = 7.0 Hz, 3 H) ppm. ^{13}C NMR ($CDCl_3$,

125 MHz), δ: 194.6, 162.8, 152.6, 131.8, 130.4, 130.4, 71.3, 63.3, 55.0, 40.5, 37.0, 33.0, 32.2, 30.5, 30.4, 30.3, 23.7, 14.4 ppm. HRMS (ESI) calcd. for $C_{25}H_{40}NO_3$ $(M+H)^+$ 304.22770, found 304.22860.

(2R,4S)-4-Hydroxy-2-(4-octylbenzoyl)pyrrolidin-1-ium chloride **(21)**

21 was synthesized in accordance with the general procedure A, starting from **21c** (30 mg, 70 µmol). **21** was obtained as a white solid (16 mg, 64%). $[\alpha]^{25}_D$: +25.63 (*c* 0.34, $CHCl_3$). The spectral data matched those reported for its enantiomer.

(3R,5R)-5-(4-Octylbenzyl)pyrrolidin-3-ol **(16)**

20c (20 mg, 50 µmol) was dissolved in EtOH (5 mL) and Pd/C (10% w/w, 24 mg, 22 µmol, 0.4 eq.) was added to the resulting solution. The air was removed from the flask under vacuum and replaced with hydrogen (balloon). The reaction mixture was vigorously stirred for 24 h at room temperature. Afterwards, the mixture was filtered through a Celite pad, washing with abundant EtOH, and the collected solution was concentrated *in vacuo.* The crude was purified by flash column chromatography (EtOAc/hexane 1:1, R*f*: 0.35) to give the intermediate *tert*-butyl (*2R,4R*)-4-hydroxy-2-(4-octylbenzyl)pyrrolidine-1-carboxylate as a colorless oil (6 mg, 32%). $[\alpha]^{25}_D$: -32.7 (*c* 0.30, $CHCl_3$). IR (neat), υ_{max}: 3408, 2923, 2853, 1694, 1668, 1513, 1455, 1393, 1365, 1253, 1153, 1116, 981, 858, 770, 553 cm^{-1}. ^1H NMR ($CDCl_3$, 500 MHz, mixture of rotamers), δ: 7.11-7.04 (m, 4 H), 4.22-4.14 (m, 2 H), 3.50 (br. s, 0.6 H), 3.35 (br. s, 0.4 H), 3.30 (br. s, 1 H), 3.09 (br. s, 1 H), 2.68 (br. s, 0.4 H), 2.63 (br. s, 0.6 H), 2.57-2.54 (m, 2 H), 1.87 (br. s, 2 H), 1.60-1.55 (m, 2 H), 1.52 (s, 9 H), 1.31-1.26 (m, 10 H), 0.87 (t, *J* = 7.0 Hz, 3 H) ppm. ^{13}C NMR ($CDCl_3$, 125 MHz, mixture of rotamers), δ: 154.9, 141.0, 135.3, 129.3, 128.4, 79.7, 69.7, 69.4, 57.3, 54.5, 40.3, 39.4, 35.6, 31.9, 31.6, 29.5, 29.3, 29.2, 28.6, 22.6, 14.1 ppm. HRMS (ESI) calcd. for $C_{24}H_{39}NO_3Na$ $(M+Na)^+$ 412.28222, found 412.28110.

tert-Butyl (*2R,4R*)-4-hydroxy-2-(4-octylbenzyl)pyrrolidine-1-carboxylate (6.0 mg, 15 µmol) was submitted to general procedure A. The crude was triturated in Et_2O to give product **16** as a white solid (5 mg, 100%). For biological testing a portion of the product was dissolved in the minimum amount of HPLC grade water, filtered (pore size = 0.45 µm) and lyophilized. $[\alpha]^{25}_D$: +4.0 (*c* 0.25, MeOH). IR (neat), υ_{max}: 3318, 2920, 2851, 1515, 1437, 1394, 1314, 1266, 1159, 1080, 1063, 1031, 961, 772, 720, 615, 531, 450 cm^{-1}. ^1H NMR (CD_3OD, 500 MHz), δ: 7.25 (d, *J* = 8.1 Hz, 2 H), 7.21 (d,

J = 8.1 Hz, 2 H), 4.56 (t, *J* = 4.2 Hz, 1 H), 4.12-4.05 (m, 1 H), 3.50 (dd, *J* = 12.4, 4.2 Hz, 1 H), 3.19 (d, *J* = 12.4 Hz, 1 H), 3.05 (d, *J* = 7.6 Hz, 2 H), 2.63-2.60 (m, 2 H), 2.13 (dd, *J* = 13.7, 5.8 Hz, 1 H), 1.90 (ddd, *J* = 13.7, 11.6, 4.2 Hz, 1 H), 1.65-1.59 (m, 2 H), 1.34-1.31 (m, 10 H), 0.92 (t, *J* = 7.0 Hz, 3 H) ppm. ^{13}C NMR (CD_3OD, 125 MHz), δ: 141.9, 133.6, 128.7, 128.4, 69.0, 60.3, 53.0, 39.5, 37.1, 35.1, 31.6, 31.3, 29.2, 29.0, 28.9, 22.3, 13.0 ppm.

tert-Butyl (2R,4S)-4-(((tert-butyldiphenylsilyl)oxy)methyl)-2-(methoxy(methyl)carbamoyl)pyrrolidine-1-carboxylate **(22b)**

Iso-propyl magnesium chloride (0.59 mL, 2.0 M in THF, 1.2 mmol, 6.0 eq.) was added dropwise to a solution of **13a** (100 mg, 0.195 mmol, 1.0 eq.) and N,O-dimethylhydroxylamine (87 mg, 0.89 mmol, 4.5 eq.) in dry THF (1 mL) at -20 °C. The resulting mixture was kept at the same temperature and stirred for 1 h. Afterwards, the reaction mixture was quenched at -20 °C by adding NH_4Cl satd. sol. (5 mL) and the product was extracted with EtOAc (3 x 5 mL). The organic layers were washed with brine (5 mL), dried over Na_2SO_4, filtered and concentrated. The residue was purified by flash column chromatography (EtOAc/hexane 1:2, R*f*: 0.09) to give **22b** as a colorless oil (102 mg, 99%). $[\alpha]^{25}_D$: +13.6 (*c* 1.7, $CHCl_3$). IR (neat), υ_{max}: 2931, 2858, 1696, 1472, 1427, 1388, 1365, 1319, 1256, 1164, 1109, 999, 940, 909, 879, 823, 741, 702, 613, 504, 489 cm^{-1}. ^{1}H NMR ($CDCl_3$, 500 MHz, mixture of rotamers), δ: 7.65-7.63 (m, 4 H), 7.43-7.37 (m, 6 H), 4.75 (d, *J* = 6.5, 0.5 H), 4.65 (d, *J* = 6.2, 0.5 H), 3.80-3.78 (m, 0.5 H), 3.77 (s, 1.5 H), 3.70 (s, 1.5 H), 3.69-3.65 (m, 0.5 H), 3.59 (dd, *J* = 6.1, 1.7 Hz, 2 H), 3.35 (dd, *J* = 10.5, 7.0 Hz, 0.5 H), 3.29 (dd, *J* = 10.5, 7.1 Hz, 0.5 H), 3.20 (s, 3 H), 2.69-2.55 (m, 1 H), 2.11 (dt, *J* = 12.9, 8.8 Hz, 0.5 H), 2.03 (dt, *J* = 12.9, 9.5 Hz, 0.5 H), 1.95-.1.90 (m, 1 H), 1.46 (s, 4.5 H), 1.42 (s, 4.5 H), 1.05 (s, 4.5 H), 1.04 (s, 4.5 H) ppm. ^{13}C NMR ($CDCl_3$, 125 MHz, mixture of rotamers), δ: 173.1, 154.5, 153.8, 135.5, 133.4, 133.3, 129.6, 127.7, 79.5, 79.4, 65.0, 61.3, 61.2, 56.7, 56.4, 49.3, 49.1, 39.5, 38.6, 32.7, 32.0, 28.5, 28.4, 26.8, 26.7, 19.2 ppm. HRMS (ESI) calcd. for $C_{29}H_{43}N_2O_5Si$ $(M+H)^+$ 527.29358, found 527.29360.

tert-Butyl (2R,4S)-4-(((tert-butyldiphenylsilyl)oxy)methyl)-2-(4-octylbenzoyl)pyrrolidine-1-carboxylate **(22c)**

Prepared by applying in sequence general procedures C and B, starting from **22b** (85 mg, 0.16 mmol). The crude was purified by flash column chromatography (EtOAc/hexane 1:1, R*f*: 0.16) to

give **22c** as a colorless oil (32 mg, 48% over two steps). $[\alpha]^{25}_{D}$: +16.6 (*c* 0.65, $CHCl_3$). IR (neat), υ_{max}: 3434, 2924, 2854, 1687, 1605, 1394, 1365, 1223, 1161, 1129, 998, 882, 769 cm^{-1}. ^1H NMR ($CDCl_3$, 500 MHz, mixture of rotamers), δ: 7.89 (d, *J* = 8.1 Hz, 0.8 H), 7.85 (d, *J* = 8.1 Hz, 1.2 H), 7.27 (d, *J* = 8.1 Hz, 1.2 H), 7.24 (d, *J* = 8.1 Hz, 0.8 H), 5.37 (dd, *J* = 9.4, 2.4 Hz, 0.4 H), 5.24 (dd, *J* = 9.3, 3.6 Hz, 0.6 H), 3.82-3.75 (m, 1 H), 3.66-3.57 (m, 2 H), 3.33 (dd, *J* = 10.7, 6.9 Hz, 0.6 H), 3.27 (dd, *J* = 10.6, 7.8 Hz, 0.4 H), 2.67-2.62 (m, 2 H), 2.57-2.46 (m, 1 H), 2.20 (dt, *J* = 12.9, 9.0 Hz, 0.6 H), 2.12 (dt, *J* = 12.2, 9.6 Hz, 0.4 H), 2.03-1.99 (m, 1 H), 1.93 (br. s, 0.4 H), 1.76 (br. s, 0.6 H), 1.66-1.58 (m, 2 H), 1.45 (s, 3.6 H), 1.30-1.27 (m, 10 H), 1.26 (s, 5.4 H), 0.87 (t, *J* = 6.9 Hz, 3 H) ppm. ^{13}C NMR ($CDCl_3$, 125 MHz, mixture of rotamers), δ: 198.3, 197.8, 154.5, 153.9, 149.1, 132.6, 132.4, 128.7, 128.6, 128.3, 79.9, 79.8, 64.1, 64.0, 61.0, 60.9, 49.3, 48.9, 39.7, 38.8, 36.0, 33.1, 32.2, 31.8, 31.1, 31.0, 29.4, 29.2, 28.5, 28,2, 22.6, 14.1 ppm. HRMS (ESI) calcd. for $C_{25}H_{39}NO_4Na$ $(M+Na)^+$ 440.27713, found 440.27771.

((2R,4S)-4-(Hydroxymethyl)pyrrolidin-2-yl)(4-octylphenyl)methanone hydrochloride **(22)**

Prepared according to general procedure A, starting from **22c** (6.0 mg, 14 µmol). The crude was triturated in Et_2O to give product **22** as a white solid (5 mg, 100%). For biological testing a portion of the product was dissolved in the minimum amount of HPLC grade water, filtered (pore size = 0.45 µm) and lyophilized. $[\alpha]^{25}_{D}$: +46.4 (*c* 0.25, $CHCl_3$). IR (neat), υ_{max}: 3370, 2922, 2852, 1683, 1605, 1570, 1464, 1416, 1400, 1373, 1350, 1310, 1263, 1182, 1164, 1092, 1060, 1013, 989, 967, 901, 722, 528 cm^{-1}. ^1H NMR (CD_3OD, 500 MHz), δ: 8.01 (d, *J* = 8.3 Hz, 2 H), 7.45 (d, *J* = 8.3 Hz, 2 H), 5.43 (t, *J* = 7.9 Hz, 1 H), 3.70 (dd, *J* = 10.9, 4.7 Hz, 1 H), 3.65 (dd, *J* = 10.9, 5.0 Hz, 1 H), 3.62 (dd, *J* = 11.2, 6.8 Hz, 1 H), 3.34-3.30 (m, 1 H), 2.77-2.73 (m, 2 H), 2.60-2.52 (m, 2 H), 2.19-2.13 (m, 1 H), 1.71-1.65 (m, 2 H), 1.37-1.31 (m, 10 H), 0.91 (t, *J* = 7.0 Hz, 3 H) ppm. ^{13}C NMR (CD_3OD, 125 MHz), δ: 193.1, 151.1, 130.2, 129.0, 63.2, 61.7, 48.0, 39.5, 35.6, 32.3, 31.6, 30.8, 29.1, 29.0, 28.9, 22.3, 13.0 ppm. HRMS (ESI) calcd. for $C_{20}H_{32}NO_2$ $(M)^+$ 318.24276, found 318.24265.

tert-Butyl (2S,4R)-4-hydroxy-2-(2-(4-octylphenyl)acetyl)pyrrolidine-1-carboxylate **(23a)**

Prepared by applying in sequence general procedures C using octyl benzyl bromide [635] then B starting from **20b** (500 mg, 1.24 mmol). The resulting residue was purified by flash column

chromatography (hexane/EtOAc 4:6, R*f*: 0.40) to give **23a** as a yellow oil (303 mg, 59% over 2 steps). $[\alpha]^{25}_{D}$: -66.58 (*c* 1.55, $CHCl_3$). IR (neat), υ_{max}: 3433, 2923, 1676, 1394, 1159 cm^{-1}. ^1H NMR ($CDCl_3$, 500 MHz, mixture of rotamers), δ: 7.14-7.09 (m, 4 H), 4.61-4.54 (m, 1 H), 4.35 (bs, 1 H), 3.81 (s, 0.75 H), 3.74-3.67 (m, 1.25 H), 3.63-3.61 (m, 0.63 H), 3.53-3.44 (m, 1.37 H), 2.58-2.55 (t, *J* = 7.7 Hz, 2 H), 2.08-1.79 (m, 2 H), 1.59-1.56 (m, 2 H), 1.46 (s, 3.51 H), 1.39 (s, 5.19 H), 1.30-1.26 (m, 10 H), 0.89-0.86 (t, *J* = 7.0 Hz, 3 H) ppm. ^{13}C NMR ($CDCl_3$, 125 MHz, mixture of rotamers), δ: 207.9, 207.2, 154.8, 154.2, 142.0, 141.7, 130.6, 130.3, 129.6, 129.5, 128.8, 128.7, 80.7, 80.3, 70.4, 69.5, 63.4, 62.7, 55.2, 55.2, 47.1, 46.1, 35.6, 31.9, 31.5, 29.5, 29.3, 29.3, 28.3, 22.7, 14.1 ppm. HRMS (ESI) calcd. for $C_{25}H_{40}NO_3$ $(M+H)^+$ 318.24276, found 318.24270.

tert-Butyl (2R,4S)-4-hydroxy-2-(2-(4-octylphenyl)acetyl)pyrrolidine-1-carboxylate **(24a)**

Prepared by applying in sequence general procedures C using octyl benzyl bromide [635] then B starting from **21b** (484 mg, 1.20 mmol). The resulting residue was purified by flash column chromatography (hexane/EtOAc 4:6, R*f*: 0.40) to give **24a** as a yellow oil (340 mg, 68% over 2 steps). $[\alpha]^{25}_{D}$: +65.30 (*c* 0.19, $CHCl_3$). The spectral data matched those reported for its enantiomer.

(2S,4R)-4-Hydroxy-2-(2-(4-octylphenyl)acetyl)pyrrolidin-1-ium chloride **(23)**

23 was synthesized in accordance with the general procedure A, starting from **23a** (25 mg, 60 µmol). **23** was obtained as a white powder (18 mg, 86%). $[\alpha]^{25}_{D}$: +91.9 (*c* 0.09, $CHCl_3$). IR (neat), υ_{max}: 3364, 3191, 2953, 2703, 1716, 1332, 1071, 763, 682 cm^{-1}. ^1H NMR ($CDCl_3$, 500 MHz), δ: 7.19-7.16 (s, 4 H), 4.79-4.75 (dd, *J* = 7.5 Hz, 1 H), 4.56 (m, 1 H), 3.92 (s, 2 H), 3.32-3.26 (m, 2H), 2.61 (dd, *J* = 10.8, 7.8 Hz, 2 H), 2.49-2.45 (dd, *J* = 13.4, 7.7 Hz, 1 H), 2.06-2.00 (ddd, *J* = 13.5, 11.1, 4.0 Hz, 1 H), 1.61-1.59 (m, 2 H), 1.32-1.28 (m, 10 H), 0.93-0.88 (t, *J* = 6.98 Hz, 3 H) ppm. ^{13}C NMR ($CDCl_3$, 125 MHz), δ: 202.3, 201.9, 145.0, 142.0, 129.6, 129.4, 128.5, 128.4, 128.2, 69.6, 68.7, 64.6, 64.2, 53.4, 63.1, 35.1, 31.6, 31.3, 29.2, 29.0, 28.9, 22.3, 13.0 ppm. HRMS (ESI) calcd. for $C_{25}H_{40}NO_3$ $(M+H)^+$ 318.24276, found 318.24750.

(2R,4S)-4-Hydroxy-2-(2-(4-octylphenyl)acetyl)pyrrolidin-1-ium chloride **(24)**

24 was synthesized in accordance with the general procedure A, starting from **24a** (17 mg, 40 µmol). **24** was obtained as a white powder (15 mg, 98%). $[\alpha]^{25}_{D}$: -80.04 (*c* 0.04, $CHCl_3$). The spectral data matched those reported for its enantiomer.

(2S,4R)-4-Hydroxy-2-(1-hydroxy-2-(4-octylphenyl)ethyl)pyrrolidin-1-ium chloride **(25)**

$NaBH_4$ (2.2 mg, 58 µmol, 1.2 eq.) was added in one portion to a solution of **23a** (20 mg, 50 µmol, 1.0 eq.) in dry MeOH (0.8 mL). The solution was stirred at rt for 2h. Saturated aqueous NH_4Cl solution was added and the resulting aqueous layer was extracted with EtOAc (1 x 2 mL). The organic layers were combined, washed with brine (1 x 2 mL), dried over Na_2SO_4, filtered and concentrated. The resulting residue was purified by flash column chromatography (hexane/EtOAc 4:6, R*f*: 0.38) to give the intermediate *tert*-butyl (*2S,4R*)-4-hydroxy-2-(1-hydroxy-2-(4-octylphenyl)ethyl)pyrrolidine-1-carboxylate as a colorless oil (15 mg, 75%). $[\alpha]^{20}_{D}$: -11.76 (*c* 1.02, $CHCl_3$). IR (neat), υ_{max}: 3409, 2923, 1664, 1403, 1160, 990, 771 cm^{-1}. ^1H NMR ($CDCl_3$, 500 MHz, mixture of rotamers), δ: 7.17-7.15 (d, *J* = 7.8 Hz, 2 H), 7.11-7.09 (d, *J* = 7.9 Hz, 2 H), 4.40 (bs, 1 H), 4.11-4.09 (m, 1 H), 3.83 (bs, 1 H), 3.65 (bs, 1 H), 3.39-3.36 (dd, *J* = 12.1, 4.2 Hz, 1 H), 2.82-2.78 (m , 1 H), 2.57-2.54 (m, 3 H), 2.09-2.06 (m, 1 H), 1.89-1.77 (m, 2 H), 1.65 (bs, 1 H), 1.60-1.55 (m, 2 H), 1.46 (s, 9 H), 1.31-1.25 (m, 10 H), 0.89-0.86 (t, *J* = 7.0 Hz, 3 H), ppm. ^{13}C NMR ($CDCl_3$, 125 MHz, mixture of rotamers), δ: 158.1, 157.9, 141.1, 135.6, 129.5, 128.6, 80.9, 80.3, 73.0, 70.0, 55.6, 35.7, 32.0, 31.7, 29.6, 29.5, 29.4, 28.6, 28.5, 22.8, 14.2 ppm. HRMS (ESI) calcd. for $C_{25}H_{40}NO_3$ $(M+H)^+$ 442.29278, found 442.29415.

tert-Butyl (*2S,4R*)-4-hydroxy-2-(1-hydroxy-2-(4-octylphenyl)ethyl)pyrrolidine-1-carboxylate (6.0 mg, 14 µmol) was submitted to the general procedure A. **25** was obtained as a white powder (5 mg, 98%). IR (neat), υ_{max}: 3363, 2955, 1315, 968, 557 cm^{-1}. ^1H NMR ($CDCl_3$, 500 MHz, mixture of diastereomers), δ: 7.20-7.19 (d, *J* = 8.1 Hz, 2 H), 7.15-7.13 (d, *J* = 8.1 Hz, 2 H), 4.55-4.53 (m, 1 H), 3.92-3.88 (m, 1 H), 3.79-3.74 (m, 1 H), 3.30-3.29 (m, 2 H), 3.22-3.19 (m, 1 H), 2.83-2.80 (m, 2 H), 2.60-2.57 (t, *J* = , 2 H), 2.08-2.04 (m, 1 H), 1.97-1.91 (m, 1 H), 1.61-1.58 (m, 2 H), 1.33-1.29 (m, 10 H), 0.91-0.89 (t, *J* = 7.0 Hz, 3 H) ppm. ^{13}C NMR ($CDCl_3$, 125 MHz, mixture of diastereomers), δ: 142.7, 135.8, 130.7, 129.8, 72.8, 71.2, 63.9, 54.4, 42.2, 38.1, 36.7, 33.2, 33.0, 30.8, 30.6, 30.5, 23.9, 14.6 ppm. HRMS (ESI) calcd. for $C_{25}H_{40}NO_3$ $(M+H)^+$ 320.25835, found 320.25841.

(2R,4S)-4-Hydroxy-2-(1-hydroxy-2-(4-octylphenyl)ethyl)pyrrolidin-1-ium chloride **(26)**

24a (14 mg, 30 µmol) was submitted to the procedure of its enantiomer **23a**. The resulting residue was purified by flash column chromatography (hexane/EtOAc 4:6, R*f*: 0.38) to give the intermediate *tert*-Butyl (*2R,4S*)-4-hydroxy-2-(1-hydroxy-2-(4-octylphenyl)ethyl)pyrrolidine-1-carboxylate as a colorless oil (10 mg, 71 %). The spectral data matched those reported for its enantiomer.

tert-Butyl (*2R,4S*)-4-hydroxy-2-(1-hydroxy-2-(4-octylphenyl)ethyl)pyrrolidine-1-carboxylate (10 mg, 24 µmol) was submitted to the general procedure A. **26** was obtained as a white powder (8 mg, 95 %). The spectral data matched those reported for its enantiomer.

(2S,4R)-2-(4-Octylbenzoyl)-4-(phosphonooxy)pyrrolidin-1-ium chloride **(29)**

Di-*tert*-butyl diethylphosphoramidite (93%, 44 µL, 0.15 mmol, 2.0 eq.) and tetrazole (0.45 M in ACN, 0.22 mmol, 3.0 eq.) were added dropwise to a solution of **20c** (30 mg, 74 µmol, 1.0 eq.) in dry THF (1 mL) at 0°. The resulting mixture was stirred for 1.5 h, allowing it to warm up to room temperature. The reaction mixture was cooled to -30 °C whereby tBuOOH (5.0 M, 60 µL, 0.30 mmol, 4.0 eq.) was added dropwise. The resulting mixture was stirred at -30 °C for 15 min and at rt for 15 additional min. Afterwards, the reaction mixture was cooled back to 0 °C whereby an aqueous $NaHSO_3$ solution (10% w/w, 2 mL) was added dropwise. The aqueous layer was extracted with EtOAc (3 x 2 mL). The resulting organic layer was washed with brine (2 mL), dried over Na_2SO_4, filtered and concentrated. The residue was purified by flash column chromatography (EtOAc/hexane 5:5 + 0.5% Pyridine, R*f*: 0.32) to give the intermediate *tert*-butyl (*2S,4R*)-4-((di-*tert*-butoxyphosphoryl)oxy)-2-(4-octylbenzoyl)pyrrolidine-1-carboxylate as a colorless oil (26 mg, 62%). $[\alpha]^{25}_D$: -11.76 (*c* 1.02, $CHCl_3$). IR (neat), υ_{max}: 2977, 2926, 2855, 1701, 1396, 1260, 987, 753 cm^{-1}. ^1H NMR ($CDCl_3$, 500 MHz, mixture of rotamers), δ: 7.91-7.90 (d, *J* = 8.2 Hz, 0.85 H), 7.87-7.86 (d, *J* = 8.2 Hz, 1.15 H), 7.28-7.26 (d, *J* = 8.7 Hz, 1.15 H), 7.25-7.24 (d, *J* = 8.7 Hz, 0.85 H), 5.47-5.43 (t, *J* = 8.0 Hz, 0.4 H), 5.37-5.33 (t, *J* = 8.2 Hz, 0.6 H), 4.91 (m, 1 H), 3.93-3.90 (dd, *J* = 12.2 Hz, 0.6 H), 3.87-3.85 (m, 0.4 H), 3.75-3.69 (m, 1 H), 2.67-2.62 (m, 2 H), 2.62-2.54 (m, 1 H), 2.09-2.01 (m, 1 H), 1.62 (m, 2 H), 1.50-1.48 (m, 18 H), 1.44 (s, 4 H), 1.30-1.22 (m, 15 H), 0.87 (t, *J* = 7.4 Hz, 3 H). ^{13}C NMR ($CDCl_3$, 125 MHz, mixture of rotamers), δ: 198.5, 198.0, 154.3, 153.7, 149.5, 149.4, 133.1,

133.0, 128.9, 128.9, 128.8, 128.5, 83.1, 83.0, 83.0 83.0, 80.4, 80.2, 75.8, 75.8, 75.2, 75.2, 59.5, 59.2, 53.7, 53.7, 53.4, 53.3, 36.2, 32.0, 31.2, 30.1, 30.0, 29.5, 59.3, 28.5, 28.2, 22.8, 14.2 ppm. HRMS (ESI) calcd. for $C_{25}H_{40}NO_3$ $(M+H)^+$ 618.35301, found 618.35381.

tert-Butyl (*2S,4R*)-4-((di-*tert*-butoxyphosphoryl)oxy)-2-(4-octylbenzoyl)pyrrolidine-1-carboxylate (25 mg, 40 µmol) was submitted to general procedure A. **29** was obtained as a white solid (12 mg, 66%). $[\alpha]^{25}_D$: -29.39 (*c* 0.37, $CHCl_3$). IR (neat), υ_{max}: 2923, 1685, 1165, 1032, 922, 513 cm^{-1}. ^1H NMR ($CDCl_3$, 500 MHz, mixture of rotamers), δ: 8.01-7.99 (d, *J* = 7.4 Hz, 2 H), 7.42-7.40 (d, *J* = 7.8 Hz, 2 H), 5.53 (bs, 1 H), 4.98 (bs, 1 H), 3.70 (bs, 1 H), 3.44 (bs, 1 H), 2.99 (bs, 1 H), 2.73-2.70 (t, *J* = 7.6, 2 H), 2.08 (m, 1 H), 1.67-1.64 (m, 2 H), 1.34-1.25 (m, 10 H), 0.90-0.87 (t, *J* = 7.0 Hz, 3 H) ppm. ^{13}C NMR ($CDCl_3$, 125 MHz, mixture of rotamers), δ: 193.0, 151.2, 130.3, 129.1, 129.0, 74.2, 61.9, 52.7, 38.0, 35.6, 31.6, 30.8, 29.1, 29.0, 28.9, 22.3, 13.0 ppm. HRMS (ESI) calcd. for $C_{25}H_{40}NO_3$ $(M+H)^+$ 384.19344, found 384.19257.

(2S,4R)-2-(4-Octylbenzoyl)-4-(phosphonooxy)pyrrolidin-1-ium chloride **(30)**

21c (50 mg, 0.12 mmol) was submitted to the procedure of its enantiomer. The residue was purified by flash column chromatography (EtOAc/hexane 5:5 + 0.5% Pyridine, R*f*: 0.32) to give the intermediate *tert*-butyl (*2R,4S*)-4-((di-*tert*-butoxyphosphoryl)oxy)-2-(4-octylbenzoyl)pyrrolidine-1-carboxylate as a colorless oil (71 mg, 63%). $[\alpha]^{25}_D$: +11.04 (*c* 0.53, $CHCl_3$). The spectral data matched those reported for its enantiomer. *tert*-Butyl (*2R,4S*)-4-((di-*tert*-butoxyphosphoryl)oxy)-2-(4-octylbenzoyl)pyrrolidine-1-carboxylate (27 mg, 0.05 mmol) was submitted to general procedure A. **30** was obtained as a white solid (14 mg, 78%). $[\alpha]^{25}_D$: +27.27 (*c* 0.55, $CHCl_3$). The spectral data matched those reported for its enantiomer.

(2S,4R)-2-(2-(4-Octylphenyl)acetyl)-4-(phosphonooxy)pyrrolidin-1-ium chloride **(31)**

23a (68 mg, 0.16 mmol) was submitted to the procedure from **31**. The resulting residue was purified by flash column chromatography (hexane/EtOAc 6:4, R*f*: 0.37) to give the intermediate *tert*-butyl (*2S,4R*)-4-((di-*tert*-butoxyphosphoryl)oxy)-2-(2-(4-octylphenyl)acetyl)pyrrolidine-1-carboxylate as a colorless oil (65 mg, 67 %). $[\alpha]^{25}_D$: -45.23 (*c* 0.65, $CHCl_3$). IR (neat), υ_{max}: 2925, 1696, 1393, 1262, 1160, 989 cm^{-1}. ^1H NMR ($CDCl_3$, 500 MHz, mixture of rotamers), δ: 7.14-7.08 (m, 4 H), 4.78 (bs, 1 H), 4.60-4.57 (t, *J* = 8.9, 7.4 Hz, 0.47 H), 4.54-4.50 (t, *J* = 9.1, 7.7 Hz, 0.53 H),

3.91-3.67 (m, 3 H), 3.54-3.47 (ddd, *J* = 16.6, 13.4, 3.3 Hz, 1 H), 2.58-2.54 (m, 2 H), 2.30-2.25 (m, 0.53 H), 2.13-2.09 (m, 0.47 H), 1.84-1.81 (m, 1 H), 1.58-1.56 (m, 2 H), 1.58-1.40 (m, 25 H), 1.29-1.25 (m, 13 H), 0.89-0.86 (t, *J* = 7.0 Hz, 3 H) ppm. ^{13}C NMR ($CDCl_3$, 125 MHz, mixture of rotamers), δ: 207.1, 207.1, 154.6, 153.8, 142.2, 141.9, 130.6, 130.3, 129.7, 129.6, 129.0, 128.9, 83.1, 83.1, 83.1, 83.0, 82.9, 80.9, 80.5, 75.7, 75.6, 74.8, 74.8, 63.4, 62.5, 53.8, 53.7, 53.5, 53.5, 47.6, 46.3, 32.0, 30.0, 30.0, 29.6, 29.4, 28.5, 28.4, 22.8, 14.2 ppm. HRMS (ESI) calcd. for $C_{25}H_{40}NO_3$ $(M+H)^+$ 610.38672, found 610.38470.

tert-Butyl (*2S,4R*)-4-((di-*tert*-butoxyphosphoryl)oxy)-2-(2-(4-octylphenyl)acetyl)pyrrolidine-1-carboxylate (30 mg, 50 µmol) was submitted to general procedure A. **31** was obtained as a purple paste (12 mg, 57%). $[\alpha]^{25}_D$: +4.72 (*c* 1.35, $CHCl_3$). IR (neat), υ_{max}: 2922, 1724, 1514, 1173, 1009 cm^{-1}. ^{1}H NMR ($CDCl_3$, 500 MHz), δ: 7.17 (m, 4 H), 5.00 (bs, 1 H), 4.82-4.77 (m, 1 H), 3.98-3.92 (s, 2 H), 3.60-3.57 (d, *J* = 12.7 Hz, 1 H), 3.42-3.39 (d, *J* = 9.4 Hz, 1 H), 2.83-2.78 (m, 1 H), 2.62-2.58 (m, 2 H), 2.18-2.13 (m, 1 H), 1.60 (m, 2 H), 1.33-1.29 (m, 10 H), 0.92-0.88 (t, *J* = 10.7 Hz, 3 H) ppm. ^{13}C NMR ($CDCl_3$, 125 MHz), δ: 201.7, 142.0, 141.6, 129.5, 129.5, 129.4, 129.4, 128.5, 128.4, 128.2, 75.0, 74.4, 74.4, 64.5, 64.1, 63.8, 63.3, 52.4, 52.3, 45.1, 35.1, 31.6, 31.3, 29.2, 29.0, 28.9, 22.3, 13.0 ppm. HRMS (ESI) calcd. for $C_{25}H_{40}NO_3$ $(M+H)^+$ 398.20909, found 398.20750.

(2R,4S)-2-(2-(4-Octylphenyl)acetyl)-4-(phosphonooxy)pyrrolidin-1-ium chloride **(32)**

24a (68 mg, 0.16 mmol) was submitted to the procedure of its enantiomer. The resulting residue was purified by flash column chromatography (hexane/EtOAc 6:4, R*f*: 0.37) to give the intermediate *tert*-butyl (*2R,4S*)-4-((di-*tert*-butoxyphosphoryl)oxy)-2-(2-(4-octylphenyl)acetyl)pyrrolidine-1-carboxylate as a colorless oil (66 mg, 68 %). $[\alpha]^{25}_D$: +53.18 (*c* 0.85, $CHCl_3$). The spectral data matched those reported for its enantiomer.

tert-Butyl (*2R,4S*)-4-((di-*tert*-butoxyphosphoryl)oxy)-2-(2-(4-octylphenyl)acetyl)pyrrolidine-1-carboxylate (35 mg, 60 µmol) was submitted to general procedure A. **32** was obtained as a purple paste (15 mg, 60%). $[\alpha]^{25}_D$: -5.03 (*c* 1.20, $CHCl_3$). The spectral data matched those reported for its enantiomer.

8.2.2 Biology methods

8.2.2.1 Compounds.

Compound stocks (2.5-50 mM) were prepared in water with the exception of **5**, **6**, **15**, **20**, **21**, **23**, **24**, **27**, **28**, **29**, and **30,** which were prepared in DMSO. FTY720 (S)-Phosphate was purchased from Cayman Chemical Company (cat# 10006408) and prepared in DMSO immediately before use. Vorinostat (suberoylanilide hydroxamic acid, SAHA) was purchased from LC Labs (cat# V-8477) and prepared in DMSO.

8.2.2.2 Cell Culture Studies.

FL5.12 cells (murine hematopoietic stem cells originally obtained from Craig Thompson, Memorial Sloan Kettering Cancer Center) were maintained at 5-750,000 cells/mL, with a density of 400-600,000 cells/mL the day of treatment. FL5.12 cells were cultured in RPMI 1640 (Mediatech) supplemented with 500 pg/mL recombinant murine IL-3 (cat# 575502, Biolegend), 10% Fetal Bovine Serum (Sigma-Aldrich), 1% HEPES buffer (Mediatech), 2 mM L-Glutamine (Mediatech), 55 μM β-mercaptoethanol (Sigma-Aldrich), and antibiotics. MEFs (murine embryonic fibroblasts generated in-house or obtained from Ashley Snider, Stony Brook School of Medicine) were maintained in DMEM with 4.5 g/L glucose and L-glutamine (Mediatech) supplemented with 10% Fetal Bovine Serum (Sigma-Aldrich) and antibiotics. Cells were screened for Mycoplasma every 3 months using the Look-Out Mycoplasma PCR Detection kit (cat# MP0035, Sigma-Aldrich).

8.2.2.3 Viability Assays.

FL5.12 cells were treated at 25,000/mL. Viability was determined at 48 h by vital dye exclusion (4'6-diamidino-2-phenylindole (DAPI) or propidium iodide) using flow cytometry. IC_{50} values were calculated using GraphPad Prism (GraphPad Software, Inc., La Jolla, CA)

8.2.2.4 Nutrient Transporter Expression.

Surface CD98 (4F2hc, SLC3A2) expression in FL5.12 cells plated at 225-250,000/mL was measured after a 3 h treatment using phycoerythrin (PE)-conjugated anti-mouse CD98 antibody (Biolegend). PE-conjugated rat IgG2a κ antibody (Biolegend) was used as an isotype control. 150-200,000 cells were stained in triplicate in 100 μL FACS block (PBS with 10% FBS and 0.05% NaN_3) containing

0.25 µL antibody on ice for 30 min, washed twice with 1 mL FACS wash (PBS containing 2% FCS and 0.05% NaN_3), and analyzed on a BD LSR II or FACS Calibur flow cytometer. Data was processed using FlowJo (Treestar), where analysis was limited to viable cells as determined by vital dye exclusion (DAPI) or forward/side scatter.

8.2.2.5 Vacuolation Assay.

FL5.12 cells were treated at a density of 200,000/mL for 3 h before being imaged at 100X using brightfield microscopy on a Nikon TE2000-S fluorescence microscope equipped with DIC filters. Vacuoles in at least 5 images were qualitatively evaluated for at least 2 biological replicates in each experimental condition. Scores were assigned as follows: 0 = no vacuoles, + = some cells vacuolated, ++ = most cells have at least 1 vacuole, +++ = all cells heavily vacuolated. Two researchers scored each replicate independently to mitigate any potential biases.

8.2.2.6 HDAC activity assays.

HDAC activity was measured for recombinant HDAC1 (Cayman, cat# 10011617) or HeLa extract (Enzo, cat# BML-KI137) using the Enzo COLOR DE LYS HDAC colorimetric activity assay kit (cat# BML-AK501-0001) or the Cayman HDAC Fluorometric Activity Assay Kit (cat# 10011563). Reaction mixtures containing acetylated lysine substrate were incubated at 37˚C for 15-30 min. After developer was added, plates were incubated for 10-15 min at 37˚C and absorbance at 405 nm measured with an Epoch microplate spectrophotometer (BioTek) or 15 min at rt and fluorescence measured with a SpectraMax Gemini XS plate reader (Molecular Devices) with excitation at 355 nm and emission at 460 nm. For fluorescence measurements, each reaction was conducted ± trichostatin A to generate corrected fluorescence values per the Cayman protocol.

8.2.2.7 Western blot.

Cell lysates were prepared in RIPA lysis buffer (10 mM Tris-Cl (pH 8.0), 1% Triton X-100, 1% sodium deoxycholate, 0.1% SDS, 140 mM NaCl) containing 1X complete protease inhibitor (Pierce cat# 88265). Where indicated, histones were acid extracted in 0.2 N HCl overnight at 4˚C. Protein concentration was quantified using Pierce BCA protein assay (Thermo Scientific cat# 23223) and samples prepared in 1X NuPage sample buffer (Invitrogen cat#NP0007) with 5 mM DTT. Samples were run on 4-12% NuPAGE gels (cat# NP0336BOX), transferred to BioTrace NT nitrocellulose

membranes (Pall cat# 66485), incubated 1 h in blocking solution (5% bovine serum albumin, 7.7 µM NaN_3 in 1X TBST), incubated with primary antibodies (H3K9, cat#9649; H3K18, cat#13998; H3, cat#4499; H4K5, cat#8647; H4K8, cat#2594; H4, cat#2935, all) overnight at 4˚C in blocking solution, and with secondary antibodies (IRDye 800 or 680 conjugates, cat# 926-3211 or 926-6802, LI-COR) for 1 h at RT. Membranes were analyzed on a LI-COR Odyssey SA Imager and analyzed using Image Studio software (LI-COR).

8.2.2.8 Statistics.

IC_{50} values are shown with the 95% confidence interval as calculated in GraphPad Prism. CD98 loss is given as the mean of at least 2 biological replicates.

8.3 Partie expérimentale de l'article 2

8.3.1 Chemistry

8.3.1.1 Synthetic schemes

Schéma 8.5 SMAPS synthesis.

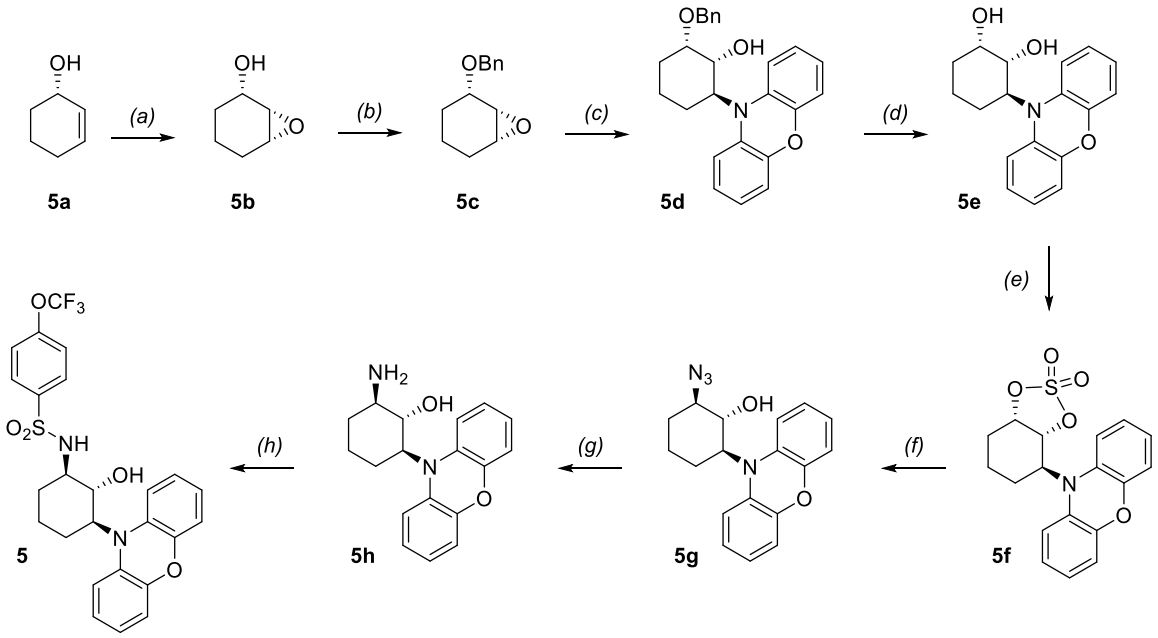

Conditions: (a) $VO(acac)_2$, TBHP, Toluene, Rx, 65%. *(b)* NaH, BnBr, THF, 50 °C, 68%. *(c)* 10H-P, $Yb(OTf)_3$, 1,2-DCE, 93%. *(d)* H_2, Pd/C, THF/MeOH (1:1), 96%. *(e)* SO_2Cl_2, Et_3N, CH_2Cl_2, -78 °C, 58%. *(f)* NaN_3, DMF, 94%. *(g)* PPh_3, H_2O, THF, 96%. *(h)* Sulfonyl chloride, Et_3N, DCM, 0 °C to rt, 74-93%.

Schéma 8.6 Hybrid phenoxazine/phenothiazine synthesis.

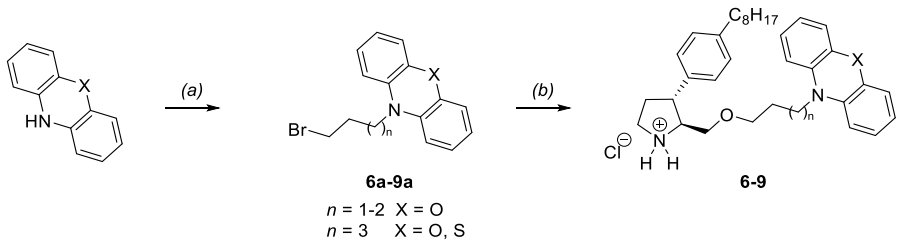

n = 1-2 X = O
n = 3 X = O, S

Conditions: (a) **1.** Bromoacetyl chloride, $MeCN/Et_2O$ (10:1), rt; **2.** $BH_3.Me_2S$, THF, 0 °C, 42-69% over 2 steps. *(b)* **1.** *tert*-butyl (2*S*,3*R*)-2-(hydroxymethyl)-3-(4-octylphenyl)pyrrolidine-1-carboxylate, NaH, DMF, rt; **2.** HCl (4M), dioxane, rt, 62-71% over 2 steps.

Schéma 8.7 Hybrid sphingolipid-N-heteroaromatic synthesis.

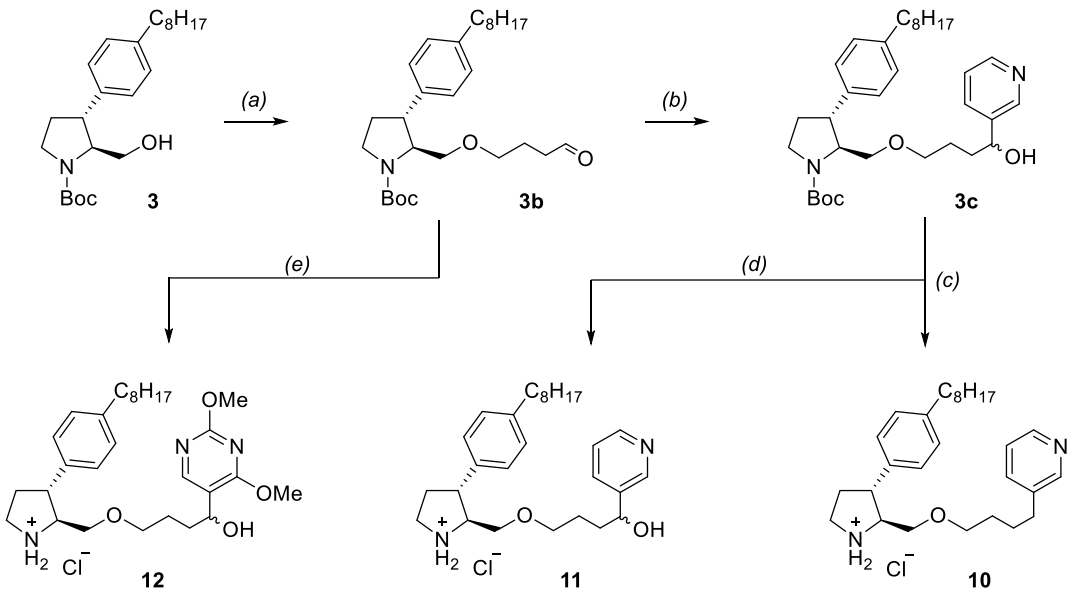

Conditions: (a) **1.** 5-bromopent-1-ene, TBAI, NaOH (50% w/w), rt, 85%; **2.** O_3, CH_2Cl_2, -78 °C *then* PPh_3, 95%. *(b)* 3-iodopyridine, EtMgBr, THF, 0 °C, 91%. *(c)* **1.** Ac_2O, pyridine, 0 °C to rt, 87%; **2.** H_2, Pd/C, MeOH; **3.** HCl (4M), dioxane, 38% over 2 steps. *(d)* HCl (4M), dioxane, rt, 96%. *(e)* **1.** 5-iodo-2,4-dimethoxypyrimidine, EtMgBr, THF, 0 °C 88%; **2.** HCl (4M), dioxane, rt, 93% over 2 steps.

8.3.1.2 Adapted synthesis of SMAP

(1S,2S,6R)-7-Oxabicyclo[4.1.0]heptan-2-ol **5b** [636]

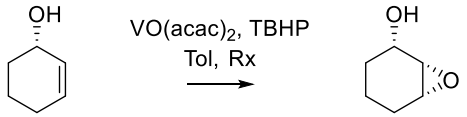

(S)-cyclohex-2-en-1-ol **5a** was synthesized in accordance with the procedure from Nicolaou *et al.* [637] To a solution of **5a** (50 mg, 0.51 mmol, 1.0 eq.) in dry toluene (1 mL) was added $VO(acac)_2$ (1.9 mg, 7.0 µmol, 0.014 eq.). The solution was refluxed and TBHP (63 µL, 0.56 mmol, 1.1 eq) was added dropwise. The reaction mixture was stirred for 1.5 h whereby TLC analysis indicated that the reaction went to completion. The solution was cooled to rt and a solution of acetic anhydride (200 µL) and dry pyridine (275 µL) was added. The resulting solution was stirred overnight and then poured onto ice. Et_2O (4 mL) was added and the organic layer was washed with water (2 mL), HCl aq (2 mL, 1.0 M), $NaHSO_3$ satd. aq. sol. (2mL), $NaHCO_3$ satd. aq. sol. (2 mL) and brine (2 mL), dried over Na_2SO_4, filtered and concentrated. The crude was purified by flash column

chromatography (8:2 hexane/EtOAc, R*f*: 0.28) to afford **5b** as a colorless oil (38 mg, 65%). $[\alpha]^{25}_{D}$: -67.8 (*c* 1.02, $CHCl_3$). The spectral data matched those reported in the literature. [638]

(1R,2S,6R)-2-(Benzyloxy)-7-oxabicyclo[4.1.0]heptane **5c** [639]

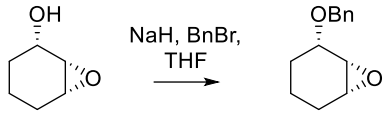

5b **5c**

To a suspension of NaH (14 mg, 60% in mineral oil, 0.35 mmol, 2.0 eq.) in dry THF (750 μL) was added BnBr (21 μL, 0.17 mmol, 0.96 eq.) and the suspension was warmed up to 50 °C. A solution of **5b** (50 mg, 0.18 mmol, 1.0 eq.) in dry THF (500 μL) was added and the resulting solution was stirred at 55 °C for 18 h whereby TLC analysis indicated that the reaction went to completion. The solution was cooled to rt and quenched with water. Et_2O (2 mL) was added, the organic layer was collected, washed with water (2 mL), dried over Na_2SO_4, filtered and concentrated. The crude was purified by flash column chromatography (85:15 hexane/EtOAc, R*f*: 0.34) to afford **5c** as a colorless oil (25 mg, 68%). $[\alpha]^{25}_{D}$: -39.4 (*c* 0.95, $CHCl_3$). ^{1}H NMR (500 MHz, $CDCl_3$) δ 6.98 – 6.81 (m, 8H), 5.32 (dd, *J* = 5.7, 3.7 Hz, 1H), 5.25 (dd, *J* = 9.9, 4.8 Hz, 1H), 4.11 (ddd, *J* = 12.5, 9.9, 4.4 Hz, 1H), 2.39 (dd, *J* = 12.2, 2.1 Hz, 1H), 2.23 – 2.14 (m, 1H), 1.83 – 1.60 (m, 4H). ^{13}C NMR (126 MHz, $CDCl_3$) δ 138.8, 128.4, 127.8, 127.6, 74.7, 70.2, 54.1, 53.5, 25.0, 23.1, 19.8. HRMS (ESI) calcd. for $C_{13}H_{16}O$ $(M+H)^+$ 204.11503, found 204.11524.

(1R,2S,6S)-2-(Benzyloxy)-6-(10H-phenoxazin-10-yl)cyclohexan-1-ol **5d** [640]

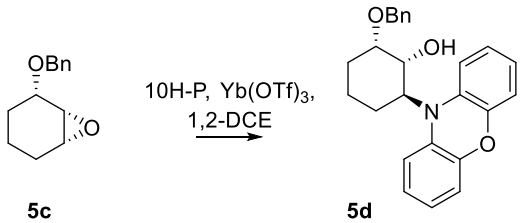

5c **5d**

To a solution of phenoxazine (0.22 mg, 1.2 mmol, 2.4 eq.) in dry 1,2-dichloroethane (1.65 mL) was added **5c** (100 mg, 0.49 mmol, 1.0 eq.) followed by $Yb(OTf)_3$ (91 mg, 0.15 mmol, 0.3 eq.). The reaction mixture was stirred overnight whereby TLC analysis indicated that the reaction went to completion. The suspension was filtered over Celite and washed thoroughly with EtOAc then concentrated. The crude was purified by flash column chromatography (85:15 hexane/EtOAc, R*f*:

0.34) to afford **5d** as a silver foam (175 mg, 93%). $[\alpha]^{25}_{D}$: +19.9 (*c* 0.93, $CHCl_3$). ^{1}H NMR (400 MHz, $CDCl_3$) δ 7.43 – 7.27 (m, 5H), 7.00 – 6.73 (m, 8H), 4.68 (q, *J* = 12.0 Hz, 2H), 4.04 (s, 1H), 3.98 (dd, *J* = 10.7, 3.0 Hz, 1H), 3.89 (t, *J* = 11.0 Hz, 1H), 2.78 (bs, 1H), 2.16 – 1.95 (m, 2H), 1.63 (m, 3H), 1.37 – 1.27 (m, 1H). ^{13}C NMR (126 MHz, $CDCl_3$) δ 150.2, 138.9, 135.2, 128.5, 127.8, 127.7, 127.6, 123.7, 123.3, 119.8, 116.2, 77.6, 73.1, 71.7, 67.0, 28.7, 28.3, 19.7. HRMS (ESI) calcd. for $C_{25}H_{25}NO_3$ $(M+H)^+$ 388.18344, found 388.18362.

(1S,2R,3S)-3-(10H-Phenoxazin-10-yl)cyclohexane-1,2-diol **5e** [293]

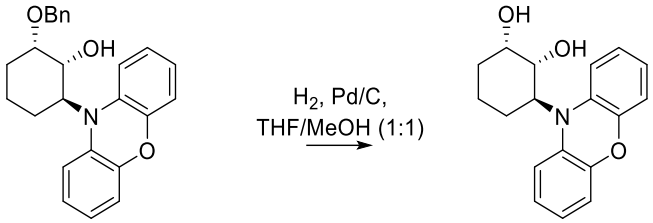

5d **5e**

To a solution of **5d** (143 mg, 0.37 mmol, 1.0 eq.) in dry THF/MeOH (4 mL, 1:1) was added Pd/C (7.5 mg, 37 µmol, 0.1 eq.) and the flask was purged with H_2. The reaction mixture was stirred at rt for 5h whereby TLC analysis indicated that the reaction went to completion. The suspension was filtered over Celite, and concentrated to afford **5e** as a brown powder (129 mg, 92%). R*f*: 0.29 (6:4 hexane/EtOAc) $[\alpha]^{25}_{D}$: -25.8 (*c* 0.67, $CHCl_3$). ^{1}H NMR (500 MHz, $CDCl_3$) δ 6.99 – 6.81 (m, 8H), 4.27 (q, *J* = 2.9 Hz, 1H), 3.96 (dd, *J* = 10.6, 3.0 Hz, 1H), 3.82 – 3.74 (m, 1H), 3.19 (bs, 1H), 2.47 (bs, 1H), 1.96 (m, 2H), 1.78 – 1.66 (m, 1H), 1.57 – 1.37 (m, 3H). ^{13}C NMR (126 MHz, $CDCl_3$) δ 150.6, 134.7, 124.1, 123.9, 120.6, 116.4, 72.9, 69.4, 67.1, 30.0, 27.5, 19.5. HRMS (ESI) calcd. for $C_{18}H_{19}NO_3$ $(M+H)^+$ 298.13649, found 298.13656.

(3aR,4S,7aS)-4-(10H-Phenoxazin-10-yl)hexahydrobenzo[d][1,3,2]dioxathiole 2,2-dioxide **5f** [641]

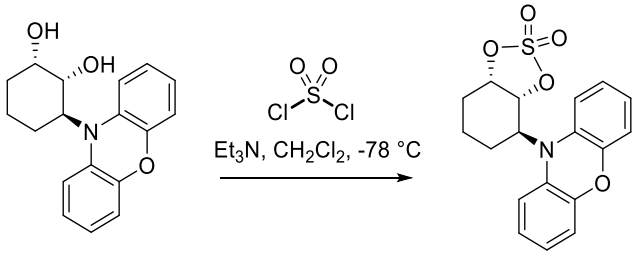

5e **5f**

To a suspension of **5e** (20 mg, 67 µmol, 1.0 eq.) in dry CH_2Cl_2 (1.2 mL) was added dry Et_3N (93 µL, 0.67 mmol, 10.0 eq.) and the resulting solution was cooled to -78 °C whereupon SO_2Cl_2 (0.80 mL, 0.5 M in CH_2Cl_2, 0.40 mmol, 6.0 eq.) was added dropwise. The solution was stirred at -78 °C for 2 h, then cannulated to another flask containing CH_2Cl_2 (5 mL) with a $NaHCO_3$ satd. aq. sol. (5 mL). The aqueous layer was extracted with CH_2Cl_2 (5 mL). The combined organic layers were washed with brine (5 mL), dried over Na_2SO_4, filtered and concentrated. The crude was purified by flash column chromatography (7:3 hexane/EtOAc, R*f*: 0.25) to afford **5f** as a brown oil (24 mg, 58% of yield, 75% of conversion). $[\alpha]^{25}_D$: +48.9 (*c* 0.43, $CHCl_3$). ^{1}H NMR (500 MHz, $CDCl_3$) δ 6.98 – 6.81 (m, 8H), 5.32 (dd, *J* = 5.7, 3.7 Hz, 1H), 5.25 (dd, *J* = 9.9, 4.8 Hz, 1H), 4.11 (ddd, *J* = 12.5, 9.9, 4.4 Hz, 1H), 2.39 (dd, *J* = 12.2, 2.1 Hz, 1H), 2.23 – 2.14 (m, 1H), 1.83 – 1.60 (m, 4H). ^{13}C NMR (126 MHz, $CDCl_3$) δ 150.4, 133.7, 124.2, 123.8, 119.9, 116.4, 84.0, 82.3, 65.2, 29.6, 26.7, 19.0. HRMS (ESI) calcd. for $C_{18}H_{17}NO_5S$ $(M+H)^+$ 360.09002, found 360.08953.

(1R,2R,6S)-2-Azido-6-(10H-phenoxazin-10-yl)cyclohexan-1-ol **5g**

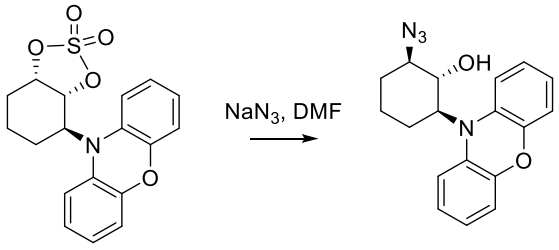

5f **5g**

To a solution of **5f** (36 mg, 0.10 mmol, 1.0 eq.) in dry DMF (2.0 mL) was added NaN_3 (12 mg, 0.18 mmol, 1.8 eq.) and the reaction mixture was stirred at 80 °C for 3.5 h whereby TLC analysis indicated that the reaction went to completion. The solution was concentrated and diluted with Et_2O (7 mL). A H_2SO_4 aq. (7mL, 20% w/w) was added and the biphasic mixture was stirred for 1 h whereby TLC analysis showed no more sulfonate. $NaHCO_3$ was slowly added dropwise to the solution until no more gas formation was observed. The aqueous layer was extracted with Et_2O (7 mL). The combined organic layers were washed with brine (1 x 7 mL), dried over Na_2SO_4, filtered and concentrated. The crude was purified by flash column chromatography (9:1 hexane/EtOAc, R*f*: 0.3) to afford **5g** as a colorless oil (30 mg, 94%). $[\alpha]^{25}_D$: -9.3 (*c* 0.30, $CHCl_3$). ^{1}H NMR (500 MHz, $CDCl_3$) δ 7.00 – 6.82 (m, 8H), 3.84 (t, *J* = 9.7 Hz, 1H), 3.39 (m, 1H), 3.35 – 3.26 (m, 1H), 3.24 (s, 1H),

1.96 (m, 2H), 1.78 (m, 1H), 1.54 (m, 1H), 1.31 (m, 2H). ^{13}C NMR (126 MHz, $CDCl_3$) δ 150.6, 134.4, 124.3, 123.9, 120.9, 116.4, 75.7, 71.8, 65.4, 29.9, 27.1, 22.2. HRMS (ESI) calcd. for $C_{18}H_{18}N_4O_2$ $(M+H)^+$ 323.15025, found 323.15050.

(1S,2R,6S)-2-Amino-6-(10H-phenoxazin-10-yl)cyclohexan-1-ol **5h** [642]

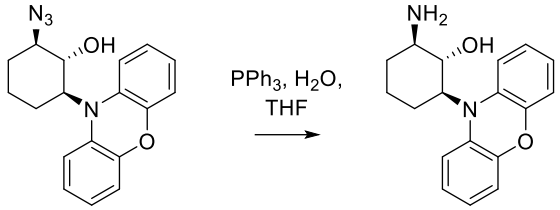

5g **5h**

To a solution of **5g** (26 mg, 81 µmol, 1.0 eq.) in dry THF (1 mL) cooled to 0 °C was added water (7.3 µL, 0.81 mmol, 10.0 eq.) followed by PPh_3 (53 mg, 0.20 mmol, 2.5 eq.). The solution was stirred at 0 °C for 5 min then warmed to 50 °C for 6h whereby TLC/mass analyses indicated that the reaction went to completion. The mixture was concentrated. The crude was purified by flash column chromatography (9:1 CH_2Cl_2 /MeOH, R*f*: 0.45) to afford **5h** as orange crystals (23 mg, 96%). $[\alpha]^{25}_D$: -4.7 (*c* 0.43, $CHCl_3$). ^{1}H NMR (400 MHz, MeOD) δ 7.09 – 6.70 (m, 8H), 3.86 (t, *J* = 9.7 Hz, 1H), 3.48 (td, *J* = 12.1, 4.2 Hz, 1H), 2.88 – 2.74 (m, 1H), 2.03 – 1.74 (m, 4H), 1.56 – 1.24 (m, 2H). ^{13}C NMR (126 MHz, MeOD) δ 151.0, 136.5, 124.7, 123.9, 120.0, 116.8, 75.1, 70.4, 57.3, 31.2, 29.5, 23.5. HRMS (ESI) calcd. for $C_{18}H_{20}N_2O_2$ $(M+H)^+$ 297.1598, found 297.1592.

N-((1R,2R,3S)-2-Hydroxy-3-(10H-phenoxazin-10-yl)cyclohexyl)-4-(trifluoromethoxy)benzenesulfonamide **5**

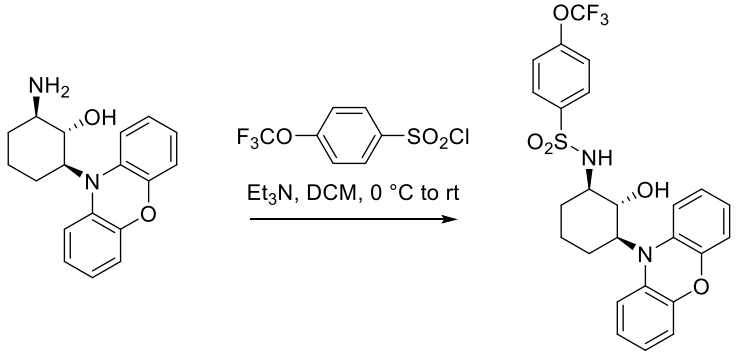

5h **5**

To a solution of **5h** (5.0 mg, 17 µmol, 1.0 eq.) in dry CH_2Cl_2 (135 µL) cooled to 0 °C was added dry Et_3N (95 µL, 68 µmol, 4.0 eq.). A solution of 4-(trifluoromethoxy)benzenesulfonyl chloride (38 µL,

19 µmol, 1.1 eq.) was then added over 1h. The solution was allowed to reach rt and stirred for an additional 1 h whereby TLC analysis indicated that the reaction went to completion. Water (300 µL) was added and the biphasic solution was diluted with CH_2Cl_2 (300 µL). The aqueous layer was extracted with CH_2Cl_2 (1 mL). The organic layers were combined, washed with brine, dried over Na_2SO_4, filtered and concentrated. The crude was purified by flash column chromatography (8:2 hexane/EtOAc, R*f*: 0.23) to afford **5** as a colorless oil (10 mg, 81%). $[\alpha]^{25}_D$: +11.2 (*c* 0.1, CH_2Cl_2) / -10.0 (*c* 0.1, MeOH). ^{1}H NMR (500 MHz, MeOD) δ 8.09 – 7.93 (m, 2H), 7.48 – 7.39 (m, 2H), 7.02 – 6.65 (m, 8H), 3.83 (t, *J* = 9.8 Hz, 1H), 3.39 (ddd, *J* = 12.7, 10.3, 4.2 Hz, 1H), 3.10 (m, 1H), 1.93 (m, 1H), 1.83 – 1.73 (m, 2H), 1.73 – 1.61 (m, 1H), 1.37 – 1.27 (m, 2H). ^{13}C NMR (126 MHz, MeOD) δ 151.5, 149.5, 140.8, 135.1, 129.1, 123.2, 122.4, 120.7, 118.5, 115.3, 72.8, 69.1, 59.1, 32.2, 28.4, 22.1. ^{19}F NMR (376 MHz, MeOD) δ -59.37. HRMS (ESI) calcd. for $C_{25}H_{23}F_3N_2O_5S$ $(M+H)^+$ 521.1353, found 521.1353.

8.3.1.3 General procedure for the synthesis of hybrid derivatives of **3**

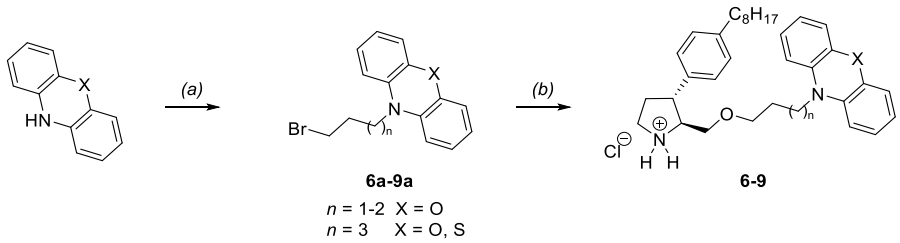

Conditions: (a) **1.** Bromoacetyl chloride, MeCN/Et_2O (10:1), rt; **2.** $BH_3.Me_2S$, THF, 0 °C, 42-69% over 2 steps. *(b)* **1.** *tert*-butyl (2*S*,3*R*)-2-(hydroxymethyl)-3-(4-octylphenyl)pyrrolidine-1-carboxylate, NaH, DMF, rt; **2.** HCl (4M), dioxane, rt, 62-71% over 2 steps.

1. The product was synthesized according to the procedure reported by Houghton *et al.* [643] Phenoxazine or phenothiazine (2.0 mmol, 1.0 eq.) was dissolved in a mixture of dry acetonitrile/diethyl ether (5 mL:0.5 mL). Bromoacetyl chloride (6.0 mmol, 3.0 eq.) was then added dropwise with constant stirring. The resulting mixture was stirred at rt for 18h whereby TLC analysis indicated that the reaction went to completion. The solution was then quenched with water (1 mL) and diluted with an aqueous NaOH solution (50 mL, 1.0 M) and EtOAc (50 mL). The aqueous layer was extracted with EtOAc (2 x 50 mL). The combined organic layers were collected, dried over Na_2SO_4, filtered and concentrated under reduced pressure to afford the amide derivative as a colorless oil. The product was engaged in the next step without further purification.

2. The crude residue (2.0 mmol, 1.0 eq.) was dissolved in dry THF (5.0 mL) and the resulting solution was cooled to 0 °C. A solution of BH_3•Me_2S (6.0 mL, 6.0 mmol, 3.0 eq., C = 1.0 M) was then added dropwise and the solution was stirred at rt for 24h whereby TLC analysis indicated that the reaction went to completion. The solution was quenched with distilled water (1 mL) and the aqueous layer was extracted with EtOAc (3 x 5 mL). The organic layers were combined, washed with brine (1 x 5 mL), dried over Na_2SO_4, filtered and concentrated under reduced pressure. The residue was chromatographed on silica gel to afford the titled compound.

3. To a solution of *tert*-butyl (2S,3R)-2-(hydroxymethyl)-3-(4-octylphenyl)pyrrolidine-1-carboxylate [255] **3** (0.53 mmol, 1.0 eq.) in dry DMF (3.0 mL) was added NaH (60% in mineral oil, 0.80 mmol, 1.5 eq.) in 2 portions. The reaction mixture was stirred at rt until gas formation ceased (e.g. 10 mins). The bromo tricyclic derivative (0.66 mmol, 1.3 eq.) was then added in 3 portions and the resulting solution was stirred at rt for 2h whereby TLC analysis indicated that the reaction went to completion. MeOH (3.0 mL) was added followed by distilled water (3.0 mL). The aqueous layer was extracted with Et_2O (3.0 mL) and the organic layers were collected, washed with distilled water (3.0 mL), brine (3.0 mL), dried over Na_2SO_4, filtered and concentrated. The residue was chromatographed on silica gel (85:15 hexane/EtOAc) and brought to the next step without further purification.

4. The compound (0.21 mmol, 1.0 eq.) was dissolved in HCl (1.0 mL, XS, 4M in dioxane) and stirred at rt for 1h30 whereby TLC analysis indicated that the reaction went to completion. The solution was concentrated and the residue was chromatographed on silica gel to afford the titled compound.

8.3.1.4 Library of hybrid derivatives of **3**

10-(3-Bromopropyl)-10H-phenoxazine **(6a)**

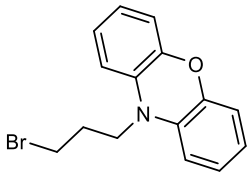

6a

Chromatographed on silica gel with hexane/EtOAc (95:5 hexane/EtOAc, R*f*: 0.28). Pale green oil, 54% yield over 2 steps; ^{1}H NMR (500 MHz, Chloroform-*d*) δ 6.81 (ddd, *J* = 8.0, 7.0, 2.1 Hz, 2H), 6.72 – 6.59 (m, 4H), 6.55 (dd, *J* = 8.0, 1.3 Hz, 2H), 3.77 – 3.65 (m, 2H), 3.54 (t, *J* = 6.1 Hz, 2H), 2.23 (tt, *J* = 7.4, 6.0 Hz, 2H).; ^{13}C NMR (126 MHz, $CDCl_3$) δ 145.1, 133.2, 123.8, 121.2, 115.6, 111.3, 42.3, 30.9, 27.8; HRMS calcd for $C_{15}H_{14}Br^{79}NO$ $(M+NH_4)^+$: 304.033315, found: 304.03299.

(2S,3R)-2-((3-(10H-Phenoxazin-10-yl)propoxy)methyl)-3-(4-octylphenyl)pyrrolidin-1-ium chloride **(6)**

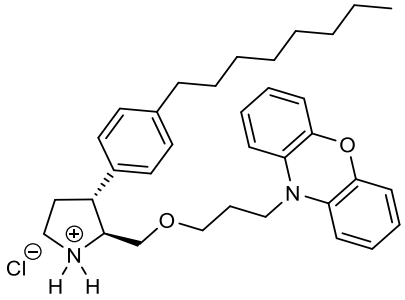

6

Chromatographed on silica gel with hexane/EtOAc (95:5 CH_2Cl_2/MeOH, R*f*: 0.28). Colorless oil, 62% yield over 2 steps; $[\alpha]^{25}_{D}$ + 7.3 (*c* 0.17, MeOH); ^{1}H NMR (500 MHz, Methanol-d_4) δ 7.23 – 7.09 (m, 4H), 6.70 (m, 2H), 6.64 – 6.49 (m, 6H), 3.65 – 3.53 (m, 4H), 3.50 (m, 2H), 3.43 (m, 1H), 3.29 (m, 1H), 3.20 (ddd, *J* = 11.2, 8.7, 7.2 Hz, 1H), 3.06 (q, *J* = 8.0 Hz, 1H), 2.62 – 2.50 (m, 2H), 2.39 – 2.28 (m, 1H), 2.06 (ddt, *J* = 12.8, 10.3, 8.6 Hz, 1H), 1.87 (qd, *J* = 7.3, 5.7 Hz, 2H), 1.58 (m, 2H), 1.35 – 1.19 (m, 10H), 0.88 (t, *J* = 7.0 Hz, 3H); ^{13}C NMR (126 MHz, MeOD) δ 146.3, 143.0, 139.5, 134.6, 130.0, 128.5, 124.8, 121.8, 116.2, 112.9, 71.6, 69.6, 66.8, 48.3, 46.5, 41.5, 36.5, 35.6, 33.0, 32.7, 30.6, 30.4, 30.4, 26.5, 23.7, 14.4; HRMS calcd for $C_{34}H_{45}N_2O_2$ $(M+H)^+$: 513.34756 and $C_{34}H_{45}N_2O_2$ $(M+Na)^+$: 535.3295, found: 513.34913 and 535.32443.

10-(4-Bromobutyl)-10H-phenoxazine **(7a)**

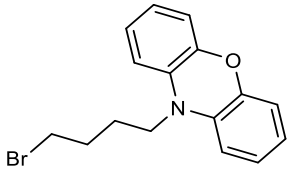

7a

Chromatographed on silica gel with hexane/EtOAc (95:5 hexane/EtOAc, R*f*: 0.29). blue solid, 42% yield over 2 steps; ^{1}H NMR (500 MHz, Chloroform-*d*) δ 6.80 (m, 2H), 6.72 – 6.58 (m, 4H), 6.48 (dd, *J* = 8.0, 1.2 Hz, 2H), 3.57 – 3.50 (m, 2H), 3.47 (t, *J* = 6.6 Hz, 2H), 2.05 – 1.94 (m, 2H), 1.92 – 1.78 (m, 2H); ^{13}C NMR (126 MHz, $CDCl_3$) δ 145.2, 133.3, 123.8, 121.1, 115.6, 111.4, 43.3, 33.1, 30.1, 23.9; HRMS calcd for $C_{16}H_{16}BrNO$ $(M+H)^+$: 318.04880, found: 318.04889.

(2S,3R)-2-((4-(10H-Phenoxazin-10-yl)butoxy)methyl)-3-(4-octylphenyl)pyrrolidin-1-ium chloride **(7)**

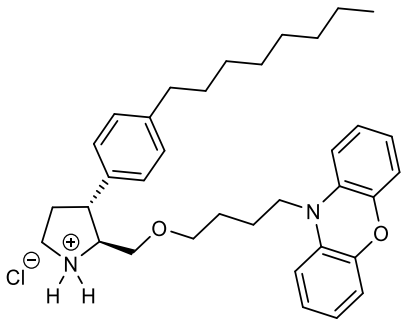

7

Chromatographed on silica gel with hexane/EtOAc (95:5 CH_2Cl_2/MeOH, R*f*: 0.28). Colorless oil, 64% yield over 2 steps; $[\alpha]^{25}_{D}$ + 9.8° (*c* 0.22, MeOH); ^{1}H NMR (500 MHz, Methanol-d_4) δ 7.19 – 7.04 (m, 4H), 6.75 (ddd, *J* = 8.0, 7.3, 1.7 Hz, 2H), 6.71 – 6.51 (m, 6H), 3.59 – 3.42 (m, 6H), 3.36 (ddd, *J* = 9.9, 6.3, 3.7 Hz, 1H), 3.24 (ddd, *J* = 11.1, 8.5, 4.2 Hz, 1H), 3.15 (m, 1H), 3.02 (td, *J* = 9.8, 8.1 Hz, 1H), 2.59 – 2.50 (m, 2H), 2.34 – 2.23 (m, 1H), 2.01 (ddt, *J* = 12.8, 10.1, 8.5 Hz, 1H), 1.76 – 1.62 (m, 4H), 1.57 (m, 2H), 1.39 – 1.20 (m, 10H), 0.89 (t, *J* = 7.0 Hz, 3H); ^{13}C NMR (126 MHz, MeOD) δ 146.3, 142.8, 139.7, 134.6, 129.9, 128.5, 124.9, 121.8, 116.2, 112.8, 72.0, 71.5, 67.0, 48.2, 46.5, 44.4, 36.5, 35.6, 33.0, 32.7, 30.6, 30.4, 30.3, 27.7, 23.7, 22.9, 14.4; HRMS calcd for $C_{35}H_{46}N_2O_2$ $(M+H)^+$: 527.36321, found: 527.36457.

10-(5-Bromopentyl)-10H-phenoxazine **(8a)**

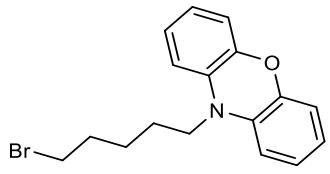

8a

Chromatographed on silica gel with hexane/EtOAc (gradient: 98:2 to 80:20). Pale violet oil, 66% yield over 2 steps; ^{1}H NMR (400 MHz, $CDCl_3$) δ: 6.88–6.80 (m, 2H), 6.75–6.65 (m, 4H), 6.46–6.50 (m, 2H), 3.42 – 3.54 (m, 4H), 1.92–2.00 (m, 2H), 1.65–1.75 (m, 2H), 1.54–1.63 (m, 2H); ^{13}C NMR (100 MHz, $CDCl_3$) δ: 145.0, 133.3, 123.7, 120.9, 115.4, 111.3, 43.8, 33.6, 32.4, 25.5, 24.2; HRMS calcd for $C_{17}H_{19}Br^{79}NO$ $(M+H)^+$: 332.0645 and $C_{17}H_{18}Br^{81}NO$ $(M+H)^+$ 334.0624, found: 332.0640 and 334.0627.

(2S,3R)-2-(((5-(10H-Phenoxazin-10-yl)pentyl)oxy)methyl)-3-(4-octylphenyl)pyrrolidin-1-ium chloride **(8)**

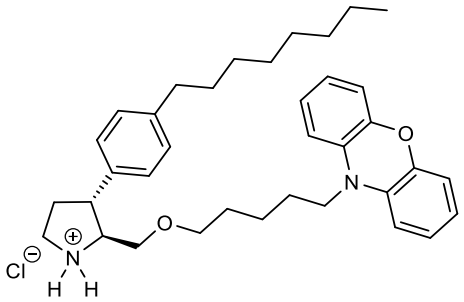

8

Chromatographed on silica gel with CH_2Cl_2/MeOH (gradient: 98:2 to 90:10). Brown solid, 71% yield over 2 steps; $[\alpha]^{25}_{D}$ + 12.1° (*c* 0.3, MeOH); ^{1}H NMR (500 MHz, DMSO-d_6) δ: 9.96 (br s, 1H), 9.23 (br s, 1H), 7.23 (d, *J* = 8.0 Hz, 2H), 7.14 (d, *J* = 8.0 Hz, 2H), 6.83–6.77 (m, 2H), 6.67–6.59 (m, 6H), 3.65 – 3.57 (m, 2H), 3.53–3.38 (m, 3H), 3.27–3.18 (m, 1H), 3.15–3.07 (m, 1H), 2.53 – 2.50 (m, 2H), 2.33–2.24 (m, 1H), 2.08–1.98 (m, 1H), 1.58–1.46 (m, 6H), 1.43–1.36 (m, 2H), 1.28–1.16 (m, 10 H), 0.83 (t, *J* = 8.0 Hz, 3H); ^{13}C NMR (100 MHz, $CDCl_3$) δ: 144.1, 141.4, 136.3, 132.8, 128.7, 127.4, 124.1, 120.7, 115.0, 111.9, 70.4, 67.7, 63.9, 45.1, 44.2, 42.9, 34.7, 32.6, 31.3, 30.9, 28.8, 28.7, 28.6, 24.1, 22.7, 22.1, 13.9; HRMS calcd for $C_{36}H_{48}N_2O_2$ $(M+H)^+$: 541.7995, found: 541.3810.

10-(5-Bromopentyl)-10H-phenothiazine **(9a)**

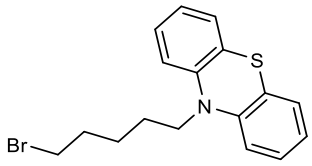

9a

Chromatographed on silica gel with hexane/EtOAc (gradient: 98:2 to 80:20).Pale gray oil, 69% yield over 2 steps; ^{1}H NMR (400 MHz, $CDCl_3$) δ: 7.19–7.12 (m, 4H), 6.92 (t, *J* = 7.6 Hz, 2H), 6.86 (d, *J* = 8.2 Hz, 2H), 3.88 (t, *J* = 7.0 Hz, 2H), 3.38 (t, *J* = 6.8 Hz, 2H), 1.92–1.79 (m, 4H), 1.63–1.54 (m, 2H); ^{13}C NMR (125 MHz, $CDCl_3$) δ: 145.4, 127.7, 127.4, 125.4, 122.6, 115.6, 47.2, 33.8, 32.5, 26.2, 25.7; HRMS calcd for $C_{17}H_{18}Br^{79}NS$ $(M+H)^+$: 348.0416 and $C_{17}H_{18}Br^{81}NS$ $(M+H)^+$ 350.0396, found: 348.0410 and 350.0391.

(2S,3R)-2-(((5-(10H-Phenothiazin-10-yl)pentyl)oxy)methyl)-3-(4-octylphenyl)pyrrolidin-1-ium **(9)**

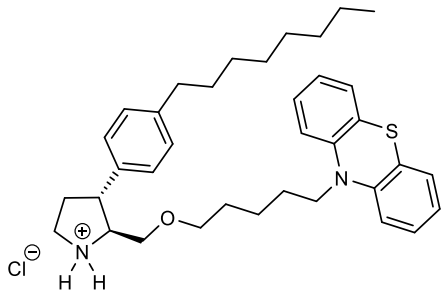

9

Chromatographed on silica gel with CH_2Cl_2/MeOH (gradient: 98:2 to 90:10). Yellow solid, 68% yield over 2 steps; $[\alpha]^{25}_{D}$ + 14.6° (*c* 0.2, MeOH); ^{1}H NMR (500 MHz, DMSO-d_6) δ: 7.18 (t, *J* = 7.4 Hz, 4H), 7.13 (d, *J* = 7.6 Hz, 4H), 7.00 (d = *J* = 8.2 Hz, 2H), (t, *J* = 7.4 Hz, 2H), 3.84 (t, *J* = 6.6 Hz, 2H), 3.50–3.34 (m, 2H), 3.17–3.09 (m, 2H), 3.04–2.97 (m, 2H), 2.54–2.50 (m, 1H), 2.29–2.20 (m, 1H), 2.00–1.90 (m, 1H), 1.70–1.63 (m, 2H), 1.56–1.43 (m, 4H), 1.42–1.35 (m, 2H), 1.30–1.17 (m, 10H), 0.84 (t, *J* = 6.8 Hz, 3H); ^{13}C NMR (125 MHz, $CDCl_3$) δ: 144.8, 141.1, 128.6, 127.6, 127.4, 127.1, 123.7, 122.4, 115.8, 70.4, 68.8, 64.4, 46.4, 45.4, 44.7, 34.7,33.1, 31.3, 31.0, 28.8,28.7, 28.7, 28.5, 26.0, 22.9, 22.1, 14.0; HRMS calcd for $C_{36}H_{48}N_2OS$ $(M+H)^+$: 557.3560, found: 541.3543.

8.3.1.5 Synthesis of heteroaromatic linker analogs of **3**

tert-Butyl (2S,3R)-3-(4-octylphenyl)-2-((pent-4-en-1-yloxy)methyl)pyrrolidine-1-carboxylate **3a** [644]

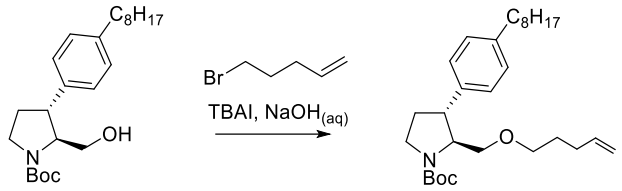

3 **3a**

A solution of 5-bromo-1-pentene (30 µL, 0.27 mmol, 5.2 eq) and tetrabutylammonium iodide (19 mg, 50 µmol, 1.0 eq) was stirred at rt for 20 min. **3** (20 mg, 50 µmol, 1.0 eq) was added followed by a 50% w/w aqueous solution of NaOH (0.07 mL) and the mixture was stirred overnight. The mixture was extracted with CH_2Cl_2 and the organic layer was washed with brine, dried over $MgSO_4$, filtered and evaporated to dryness. The crude product was purified by column chromatography (9:1 hexane/EtOAc) to give **3b** (20 mg, 85%) as a colorless oil. $[\alpha]^{25}_D$ +12.7° (*c* 0.15, MeOH); ^{1}H NMR (500 MHz, $CDCl_3$): δ 7.11 (s, 4H), 5.80 (ddt, *J* = 17.0, 10.5, 6.5 Hz, 1H), 5.02-4.98 (m, 1H), 4.96-4.94 (m, 1H), 3.99-3.81 (m, 1H), 3.73-3.64 (m, 1H), 3.62-3.50 (m, 2H), 3.46-3.43 (m, 3H), 3.39-3.31 (m, 1H), 2.59-2.54 (m, 2H), 2.29-2.21 (m, 1H), 2.12-2.06 (m, 2H), 1.93-1.83 (m, 1H), 1.64-1.58 (m, 4H), 1.48 (s, 9H), 1.31-1.26 (m, 10H), 0.88 (t, *J* = 7.0 Hz, 3H). ^{13}C NMR (125 MHz, $CDCl_3$): δ 154.5, 141.3, 138.4, 131.0, 128.7, 127.2, 114.8, 79.6, 70.7, 63.8, 46.7, 46.2, 45.7, 35.7, 32.0, 31.8, 31.7, 30.5, 29.9, 29.6, 29.5, 29.4, 29.1, 22.8, 14.3**;** HRMS calcd for $C_{29}H_{47}NO_3Na$: 480.3448. Found: 480.3464.

tert-Butyl (2S,3R)-3-(4-octylphenyl)-2-((4-oxobutoxy)methyl)pyrrolidine-1-carboxylate **(3b)**

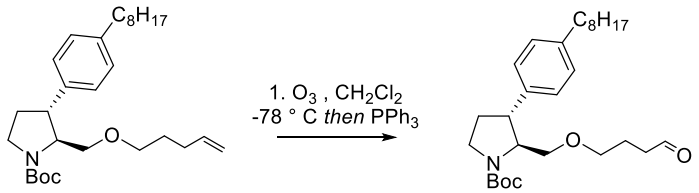

3a **3b**

O_3 was bubbled through a solution of **3a** (0.41 g, 0.90 mmol) in CH_2Cl_2 (40 mL) at -78 °C until the solution was saturated (blue color). Then, argon was bubbled through the solution for 15 min to

remove the excess of O_3 and Ph_3P (2.4 g, 9.0 mmol, 10 eq.) was added. The mixture was allowed to reach room temperature and stirred for 1 h. Finally, the solution was concentrated *in vacuo*. The crude was purified by flash column chromatography (EtOAc/hexane 1:4, R*f*: 0.24) to give **3b** as a colorless oil (393 mg, 95%). $[\alpha]^{25}_{D}$ +21.1 (*c* 0.95, $CHCl_3$); ^{1}H NMR ($CDCl_3$, 500 MHz, mixture of rotamers), δ 9.74 (t, *J* = 1.5 Hz, 1 H), 7.12 (d, *J* = 8.5 Hz, 2 H), 7.10 (d, *J* = 8.5 Hz, 2 H), 3.94 (br. s, 0.45 H), 3.82 (br. s, 0.55 H), 3.70 (br. s, 1 H), 3.59 (br. s, 0.55 H), 3.53 (br. s, 1.45 H), 3.48-3.45 (m, 2 H), 3.40-3.36 (m, 1 H), 3.33 (br. s, 1 H), 2.58-2.55 (m, 2 H), 2.47 (br. s, 2 H), 2.26-2.19 (m, 1 H), 1.89-1.86 (m, 3 H), 1.62-1.56 (m, 2 H), 1.48 (s, 9 H), 1.30-1.26 (m, 10 H), 0.87 (t, *J* = 6.9 Hz, 3 H); ^{13}C NMR ($CDCl_3$, 125 MHz, mixture of rotamers), δ 202.4, 202.2, 154.3, 141.2, 140.6, 140.3, 128.6, 127.1, 79.5, 79.3, 70.8, 70.1, 69.6, 63.6, 63.3, 46.8, 46.5, 46.1, 45.8, 40.9, 35.5, 32.6, 31.9, 31.5, 29.7, 29.4, 29.2, 28.5, 22.6, 14.1; HRMS (ESI) calcd. for $C_{28}H_{45}NO_4Na$ $(M+Na)^+$ 482.3241, found 482.3241.

tert-Butyl (2S,3R)-2-((4-hydroxy-4-(pyridin-3-yl)butoxy)methyl)-3-(4-octylphenyl)pyrrolidine-1-carboxylate **(3c)**

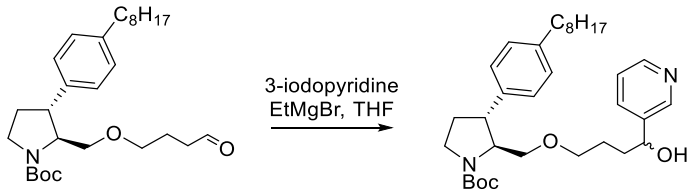

3b **3c**

EtMgBr (0.37 mL, 1.0 M in THF, 0.37 mmol, 4.4 eq.) was added dropwise to a solution of 3-iodopyridine (68 mg, 0.33 mmol, 4.0 eq.) in dry THF (2 mL). The resulting mixture was stirred for 30 min at room temperature, before being cooled to 0 °C. Then, a solution of **3b** (38 mg, 83 µmol, 1.0 eq.) in dry THF (1 mL), was added dropwise and the resulting mixture was stirred for 1 h at 0 °C. Afterwards, the reaction mixture was quenched with NH_4Cl satd. aq. sol. (3 mL) and the product was extracted with EtOAc (3 x 15 mL). The combined organic layers were washed with $NaHCO_3$ satd. aq. sol. (3 mL) and brine (3 mL), dried over Na_2SO_4, filtered and concentrated. The crude was purified by flash column chromatography (pure EtOAc, R*f*: 0.25) to give **3c** as a pale yellow oil (41 mg, 91%, containing a residual inseparable impurity). ^{1}H NMR ($CDCl_3$, 500 MHz, mixture of rotamers and diasteroisomers), δ 8.58 (s, 1 H), 8.50 (dd, *J* = 4.8, 1.4 Hz, 1 H), 7.74-7.71

(m, 1 H), 7.30-7.27 (m, 1 H), 7.11 (s, 4 H), 4.75 (dd, *J* = 8.0, 4.6 Hz, 1 H), 3.96 (br. s, 0.5 H), 3.84 (br. s, 0.5 H), 3.81 (br. s, 0.5 H), 3.71 (br. s, 0.5 H), 3.61 (br. s, 1 H), 3.58-3.54 (m, 2 H), 3.53 (br. s, 1 H), 3.40-3.36 (m, 2 H), 2.57-2.54 (m, 2 H), 2.24-2.19 (m, 1 H), 1.91-1.83 (m, 3 H), 1.71-1.69 (m, 2 H), 1.61-1.55 (m, 2 H), 1.47 (s, 9 H), 1.30-1.25 (m, 10 H), 0.87 (t, *J* = 7.0 Hz, 3 H); ^{13}C NMR ($CDCl_3$, 125 MHz, mixture of rotamers and diasteroisomers), δ 154.5, 154.1, 148.3, 147.5, 141.4, 133.8, 128.7, 127.1, 124.5, 79.7, 79.5, 71.7, 71.2, 70.8, 69.6, 63.6, 63.3, 46.9, 46.5, 46.2, 45.9, 37.0, 36.9, 35.5, 32.7, 31.9, 31.5, 29.7, 29.5, 29.4, 29.2, 28.5, 26.1, 22.7, 14.1; HRMS (ESI) calcd. for $C_{33}H_{51}N_2O_4$ $(M+H)^+$ 539.3843, found 539.3852.

tert-Butyl (2S,3R)-2-((4-acetoxy-4-(pyridin-3-yl)butoxy)methyl)-3-(4-octylphenyl)pyrrolidine-1-carboxylate **(3d)**

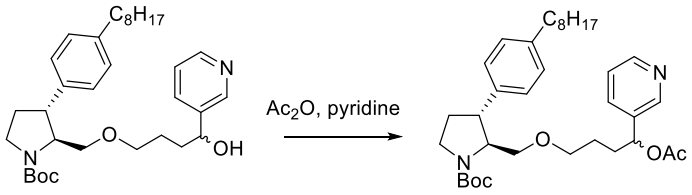

3c **3d**

Acetic anhydride (200 µL) was added to a solution of **3c** (35 mg, 65 µmol, 1.0 eq.) in pyridine (1 mL) at 0 °C and the resulting mixture was stirred overnight at room temperature. Afterward, the reaction mixture was diluted with Et_2O (5 mL) and washed with $NaHCO_3$ satd. aq. sol. (2 mL), H_2O (2 mL) and brine (2 mL). The organic layer was dried over Na_2SO_4, filtered and concentrated. The crude was purified by flash column chromatography (EtOAc/hexane 1:1, R*f*: 0.30) to give **3d** as a colorless oil (33 mg, 87%); ^{1}H NMR ($CDCl_3$, 500 MHz, mixture of rotamers and diasteroisomers), δ 8.59 (s, 1 H), 8.54 (d, *J* = 4.3 Hz, 1 H), 7.63-7.61 (m, 1 H), 7.28-7.25 (m, 1 H), 7.10 (d, *J* = 8.3 Hz, 2 H), 7.08 (d, *J* = 8.3 Hz, 2 H), 5.77-5.74 (m, 1 H), 3.95 (br. s, 0.45 H), 3.83 (br. s, 0.55 H), 3.66 (br. s, 1 H), 3.57 (br. s, 0.55 H), 3.51 (br. s, 1.45 H), 3.44-3.43 (m, 2 H), 3.41-3.37 (m, 1 H), 3.32 (br. s, 1 H), 2.57-2.54 (m, 2 H), 2.24-2.19 (m, 1 H), 2.07 (s, 3 H), 2.00-1.93 (m, 1 H), 1.88-1.81 (m, 2 H), 1.61-1.55 (m, 3 H), 1.46 (s, 10 H), 1.30-1.25 (m, 10 H), 0.87 (t, *J* = 7.0 Hz, 3 H); ^{13}C NMR ($CDCl_3$, 125 MHz, mixture of rotamers and diasteroisomers), δ 170.1, 154.4, 154.3, 149.3, 148.3, 141.2, 136.1, 134.2, 128.6, 127.0, 123.4, 79.5, 79.3, 73.7, 70.9, 70.5, 69.6, 63.6, 63.2, 46.6, 46.5, 46.0, 45.6,

35.5, 32.8, 32.6, 32.5, 31.9, 31.7, 31.5, 29.7, 29.5, 29.4, 29.2, 28.5, 25.8, 22.6, 21.1, 14.1; HRMS (ESI) calcd. for $C_{35}H_{53}N_2O_5$ $(M+H)^+$ 581.3949, found 581.39623.

3-(4-(((2S,3R)-3-(4-Octylphenyl)pyrrolidin-2-yl)methoxy)butyl)pyridine hydrochloride **(10)**

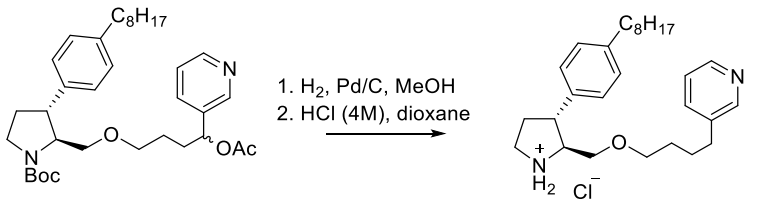

3d **10**

3d (17 mg, 29 µmol, 1.0 eq.) was dissolved in MeOH (4 mL) and Pd/C (10%, 10 mg, 9.3 µmol, 0.3 eq.) was added to the resulting solution. The air was removed from the flask under vacuum and replaced with hydrogen (balloon). The reaction mixture was vigorously stirred for 2 h at room temperature. Afterwards, the mixture was filtered through a celite pad, washing with MeOH and the collected solution was concentrated *in vacuo*. The crude was purified by flash column chromatography (EtOAc/hexane 1:1, R*f*: 0.27) to give a colorless oil. This intermediate was dissolved in dry dioxane (120 µL) and HCl (120 µL, 4 M in dioxane) was added to the solution. The reaction mixture was stirred at r.t. for 2 h. The solution was then concentrated *in vacuo* in several cycles co-distilling with dry dioxane. The crude was triturated three times in Et_2O affording **10** as a white solid (5 mg, 38%). $[\alpha]^{25}_D$ +12.5 (*c* 1.03, MeOH); (NMR spectra were recorded using the free amine form) ^{1}H NMR (CD_3OD, 500 MHz), δ 8.40 (s, 1 H), 8.37 (d, *J* = 4.9 Hz, 1 H), 7.71 (d, *J* = 7.8 Hz, 1 H), 7.37 (dd, *J* = 7.8, 4.9 Hz, 1 H), 7.21 (d, *J* = 8.2 Hz, 2 H), 7.17 (d, *J* = 8.2 Hz, 2 H), 3.56-3.46 (m, 5 H), 3.39-3.33 (m, 1 H), 3.28-3.23 (m, 1 H), 3.14-3.09 (m, 1 H), 2.69 (t, J = 7.6 Hz, 2 H), 2.62-2.59 (m, 2 H), 2.38-2.33 (m, 1 H), 2.14-2.08 (m, 1 H), 1.76-1.70 (m, 2 H), 1.66-1.60 (m, 4 H), 1.34-1.30 (m, 10 H), 0.91 (t, *J* = 7.0 Hz, 3 H); ^{13}C NMR (CD_3OD, 125 MHz), δ 148.6, 146.1, 141.7, 138.6, 137.4, 136.9, 128.6, 127.1, 123.7, 70.7, 69.1, 65.4, 46.3, 44.9, 35.1, 33.6, 32.1, 31.6, 31.3, 29.2, 29.0, 28.9, 28.7, 27.3, 22.3, 13.0; HRMS (ESI) calcd. for $C_{28}H_{43}N_2O$ $(M)^+$ 423.33699, found 423.33859.

4-(((2S,3R)-3-(4-Octylphenyl)pyrrolidin-2-yl)methoxy)-1-(pyridin-3-yl)butan-1-ol hydrochloride **(11)**

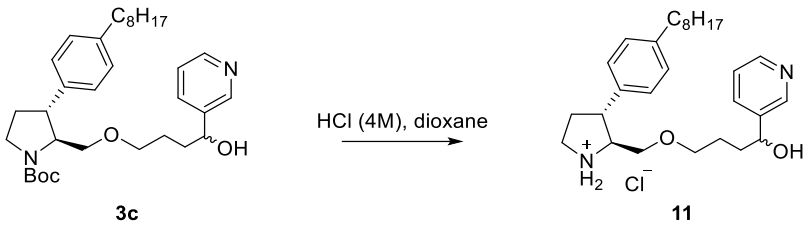

An amount of **3c** (6.0 mg, 11 µmol, 1.0 eq.) was dissolved in dry dioxane (120 µL) and HCl (120 µL, 4.0 M in dioxane) was added to the solution. The solution was stirred at rt for 2h and concentrated. The crude was triturated three times in Et_2O, then dissolved in CH_2Cl_2, filtering away the insoluble residue, and concentrated again, affording **11** as a colorless residue (5 mg, 96%). ^{1}H NMR ($CDCl_3$, 500 MHz, mixture of diasteroisomers), δ 8.58 (s, 1 H), 8.49 (d, *J* = 3.7 Hz, 1 H), 7.73-7.70 (m, 1 H), 7.27-7.24 (m, 1 H), 7.16-7.10 (m, 4 H), 4.79 (td, *J* = 8.4, 5.1 Hz, 1 H), 3.57-3.46 (m, 3 H), 3.37 (dd, *J* = 16.8, 7.7 Hz, 1 H), 3.28-3.23 (m, 1 H), 3.20-3.16 (m, 1 H), 3.14-3.07 (m, 1 H), 2.89-2.80 (m, 1 H), 2.58-2.55 (m, 2 H), 2.29-2.22 (m, 1 H), 1.97-1.90 (m, 1 H), 1.87-1.82 (m, 2 H), 1.80-1.76 (m, 0.5 H), 1.75-1.70 (m, 1 H), 1.69-1.64 (m, 0.5 H), 1.62-1.56 (m, 2 H), 1.31-1.25 (m, 10 H), 0.88 (t, *J* = 6.9 Hz, 3 H); ^{13}C NMR ($CDCl_3$, 125 MHz, mixture of diasteroisomers), δ 148.5, 147.8, 141.2, 140.6, 140.4, 140.1, 133.4, 128.6, 127.4, 123.3, 72.4, 71.5, 71.2, 66.1, 66.0, 47.5, 47.3, 46.2, 37.4, 37.1, 35.7, 35.5, 31.9, 31.5, 29.7, 29.5, 29.4, 29.2, 25.9, 25.6, 22.7, 14.1; HRMS (ESI) calcd. for $C_{28}H_{43}N_2O_2$ $(M)^+$ 439.3325, found 439.3321.

tert-Butyl (2S,3R)-2-((4-(2,4-dimethoxypyrimidin-5-yl)-4-hydroxybutoxy)methyl)-3-(4-octylphenyl)pyrrolidine-1-carboxylate **(3e)**

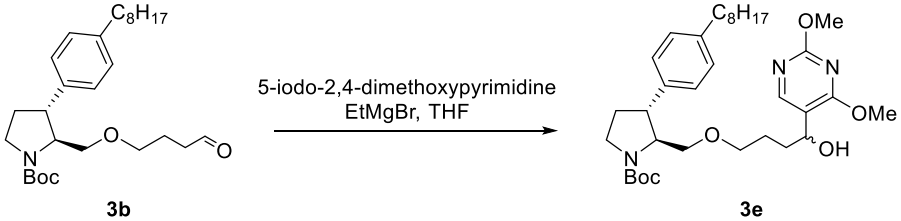

EtMgBr (0.37 mL, 1.0 M in THF, 0.37 mmol, 4.4 eq.) was added dropwise to a solution of 5-iodo-2,4-pyrimidine (88 mg, 0.33 mmol, 4.0 eq.) in dry THF (2 mL). The resulting mixture was stirred for 30 min at room temperature, before being cooled to 0 °C. Then, a solution of **3b** (38 mg, 83 µmol, 1.0 eq.) in dry THF (1 mL) was added dropwise and the resulting mixture was stirred for 1 h at 0 °C. Afterwards, the reaction mixture was quenched with NH_4Cl satd. aq. sol. (3 mL) and the product was extracted with EtOAc (3 x 15 mL). The combined organic layers were washed with $NaHCO_3$ sat. aq. sol. (3 mL) and brine (3 mL), dried over Na_2SO_4, filtered and concentrated. The crude was purified by flash column chromatography (EtOAc/hexane 1:1, R*f*: 0.16) to give **3e** as a colorless oil (44 mg, 88%); ^{1}H NMR ($CDCl_3$, 500 MHz, mixture of rotamers and diasteroisomers), δ 8.26 (s, 1 H), 7.10 (s, 4 H), 4.77-4.75 (m, 1 H), 3.99 (s, 3 H), 3.98 (s, 3.5 H), 3.83 (br. s, 0.5 H), 3.80 (br. s, 0.5 H), 3.70 (br. s, 0.5 H), 3.61-3.53 (m, 2 H), 3.51 (br. s, 2 H), 3.40-3.34 (m, 2 H), 2.57-2.54 (m, 2 H), 2.26-2.20 (m, 1 H), 1.92-1.83 (m, 2 H), 1.81-1.73 (m, 1 H), 1.71-1.63 (m, 2 H), 1.61-1.55 (m, 2 H), 1.47 (s, 9 H), 1.30-1.25 (m, 10 H), 0.87 (t, *J* = 7.0 Hz, 3 H); ^{13}C NMR ($CDCl_3$, 125 MHz, mixture of rotamers and diasteroisomers), δ 168.2, 164.5, 155.7, 154.5, 154.3, 141.3, 128.6, 127.1, 117.8, 117.6, 79.6, 79.4, 71.3, 70.8, 69.6, 69.4, 67.6, 63.7, 63.4, 54.7, 53.9, 46.7, 46.6, 46.1, 45.8, 35.5, 34.2, 32.6, 31.9, 31.7, 31.5, 29.7, 29.4, 29.2, 28.5, 26.2, 22.6, 14.1; HRMS (ESI) calcd. for $C_{34}H_{54}N_3O_6$ $(M+H)^+$ 600.40071, found 600.40059.

1-(2,4-Dimethoxypyrimidin-5-yl)-4-(((2S,3R)-3-(4-octylphenyl)pyrrolidin-2-yl)methoxy)butan-1-ol hydrochloride **(12)**

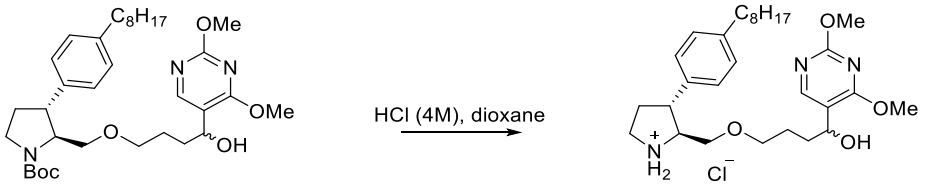

3e **12**

An amount of **3e** (18 mg, 30 µmol, 1.0 eq.) was dissolved in dry dioxane (360 µL) and HCl (4.0 M in dioxane, 0.36 mL, 1.4 mmol, excess) was added to the solution. The solution was stirred at rt for 2h and concentrated. The crude was triturated three times in Et_2O, then dissolved in CH_2Cl_2, filtering away the insoluble residue, and concentrated again, affording **12** as a white solid (14 mg, 93%); ^{1}H NMR ($CDCl_3$, 500 MHz, mixture of diasteroisomers), δ 8.29 (s, 0.5 H), 8.27 (s, 0.5 H), 7.14-

7.10 (m, 4 H), 4.80 (td, *J* = 8.7, 3.9 Hz, 1 H), 3.99 (s, 3 H), 3.98 (s, 3 H), 3.55-3.46 (m, 3 H), 3.38-3.34 (m, 1 H), 3.23 (ddd, *J* = 9.7, 7.7, 3.0 Hz, 1 H), 3.18-3.13 (m, 1 H), 3.12-3.07 (m, 1 H), 2.89-2.80 (m, 1 H), 2.58-2.55 (m, 2 H), 2.28-2.21 (m, 1 H), 1.96-1.89 (m, 1 H), 1.88-1.82 (m, 1 H), 1.81-1.75 (m, 1 H), 1.74-1.64 (m, 2 H), 1.62-1.56 (m, 2 H), 1.31-1.25 (m, 10 H), 0.87 (t, *J* = 7.0 Hz, 3 H); ^{13}C NMR ($CDCl_3$, 125 MHz, mixture of diasteroisomers), δ 168.1, 164.5, 164.4, 155.7, 141.1, 140.3, 128.5, 127.4, 118.2, 118.0, 72.3, 71.2, 67.4, 67.1, 66.2, 54.7, 53.9, 47.4, 47.2, 46.3, 46.2, 35.6, 35.5, 34.6, 34.4, 31.9, 31.5, 29.7, 29.5, 29.4, 29.2, 26.0, 25.8, 22.6, 14.1; HRMS (ESI) calcd. for $C_{29}H_{46}N_3O_4$ $(M)^+$ 500.34828, found 500.35031.

8.3.2 Biology methods

8.3.2.1 Compounds.

Compounds **3** and **5** – **9** were made up at 50 mM in DMSO. Compound **4** (perphenazine) was purchased from Sigma (P6402-1G) and made up in EtOH. Compounds **10** – **12** were made up at 5 mM in H_2O. Calyculin A was purchased from VWR (89157-750) and made up in EtOH.

8.3.2.2 Cell culture.

FL5.12 cells were originally obtained from Craig Thompson (Memorial Sloan Kettering). Cells were cultured in RPMI 1640 (Mediatech) supplemented with 500 pg/mL recombinant murine IL-3 (cat# 575502, Biolegend), 10% Fetal Bovine Serum (Sigma-Aldrich), 1% HEPES buffer (Mediatech), 2 mM L-Glutamine (Mediatech), 55 μM β-mercaptoethanol (Sigma-Aldrich), and antibiotics at 5-750,000 cells/mL. Density was limited to 400-600,000 cells/mL the day of an experiment. Cells were screened for Mycoplasma every 3 months using the Look-Out Mycoplasma PCR Detection kit (cat# MP0035, Sigma-Aldrich).

8.3.2.3 Viability assays.

FL5.12 cells were plated at 25,000/mL with the indicated compounds for 48 h. Viability was determined by exclusion of propidium iodide using flow cytometry. IC_{50} values were calculated using GraphPad Prism (GraphPad Software, Inc., La Jolla, CA).

8.3.2.4 Surface nutrient transporter quantification.

FL5.12 cells were treated with the indicated compounds for 3 h at a density of 250,000/mL. Where indicated, cells were pre-treated with 5 nM calyculin A for 60 min before the addition of compound **3**, **4**, **5**, or **10** at 2x IC_{50} concentrations for an additional 2 h. Surface CD98 (4F2hc, SLC3A2) expression was measured in triplicate by staining 200,000 cells with 0.5 µg/mL phycoerythrin (PE)-conjugated anti-mouse CD98 antibody or isotype control PE-conjugated rat IgG2a κ antibody (Biolegend) and analyzed on a BD LSR II. Data was processed using FlowJo (Treestar), where analysis was limited to viable cells as determined by forward/side scatter.

8.3.2.5 Vacuolation assays.

FL5.12 cells were treated with the indication compounds at a density of 250-300,000/mL for 3 h before being imaged at 100X using brightfield microscopy on a Nikon TE2000-S fluorescence microscope equipped with DIC filters. Where indicated, cells were pre-treated with 10 nM calyculin A for 60 min before the addition of 2.5 µM **3** for an additional 2 h. Vacuoles were evaluated in at least 30 cells in at least 3 biological replicates per experimental condition. Individual scores were assigned as follows: 0 = no vacuoles, 1 = some small vacuoles, 2 = multiple vacuoles, 3 = multiple large vacuoles. Individual scores were combined into a vacuolation score using the equation vacuolation score = [(3 x % cells in category 3) + (2 x % cells in category 2) + (1 x % cells in category 1)]/3. Biological replicates were performed by at least two researchers to mitigate any potential biases.

8.3.2.6 Statistics.

Data shown are means of at least 3 biological replicates shown ± standard deviation, except for Figure 2.17 – B, where the mean of 2 biological replicates with range is shown.

8.4 Partie expérimentale de l'article 3

8.4.1 Synthetic Scheme

Schéma 8.8 General synthetic approach toward 2-Oxa-5-azabicyclo[2.2.1]heptane structures

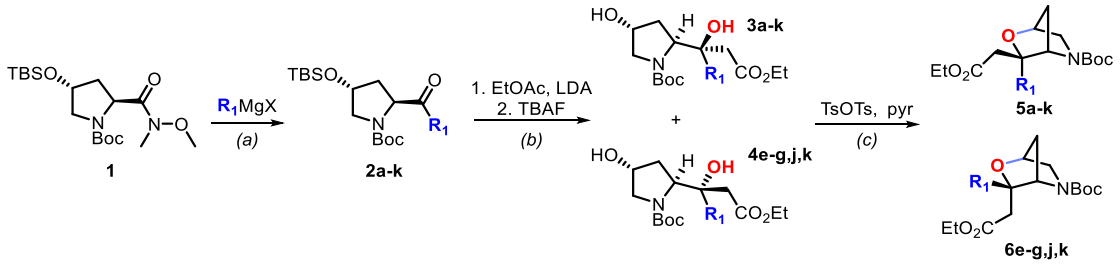

8.4.2 General Procedures

*General procedure A for ketone formation (**2a**-**2k**).* To a 1-neck round-bottomed flask was dissolved *tert*-butyl (2*S*,4*R*)-4-((*tert*-butyldimethylsilyl)oxy)-2-(methoxy(methyl)carbamoyl)pyrrolidine-1-carboxylate **1** [316] in Et_2O/THF (C = 0.10 M unless otherwise stated). The solution was cooled to 0 °C whereupon RMgBr/RMgCl was added dropwise. The solution was stirred at 0 °C for 5 min then at rt until TLC analysis indicated that the reaction went to completion. The reaction mixture was quenched by addition of a saturated aqueous solution of NH_4Cl. The aqueous layer was extracted with three times with EtOAc. The organic layers were collected, washed with saturated aqueous solution of NH_4Cl, distilled water, brine, dried over Na_2SO_4, filtered, and concentrated under reduced pressure.

*General procedure B for EtOAc addition followed by silyl ether removal (**3a**-**3k**, **4e**-**4h**,**j**,**k**).* To a 2-neck round-bottomed flask equipped with a low temperature thermometer was added THF (C = 0.50 M) followed by EtOAc (3.4 eq). The solution was cooled to -78 °C and LDA (1.0 M in THF/Hexane, 3.0 eq.) was added dropwise. The solution was stirred at -78 °C for 40 min then a solution of the ketone (C = 0.50 M in THF, 1.0 eq.) was added dropwise over 20 min. The solution was kept at -78 °C for an additional 20 min whereby TLC analysis indicated that the reaction went to completion. The reaction mixture was quenched by addition of a saturated aqueous solution of NH_4Cl, and the suspension was allowed to reach rt. The aqueous layer was extracted with three times with EtOAc. The organic layers were collected, washed with NH_4Cl saturated aqueous solution, distilled water, brine, dried over Na_2SO_4, filtered, and concentrated under reduced

pressure. The residual oil was transferred to a 1-neck round-bottomed flask and THF (C = 0.10 M) was added. The solution was cooled to 0 °C then TBAF (C = 1.0 M in THF, 1.1 eq.) was added. The reaction mixture was stirred 5 min at 0 °C then at rt overnight whereby TLC analysis indicated that the reaction went to completion. The reaction mixture was quenched by addition of a saturated aqueous solution of $NaHCO_3$. The aqueous layer was extracted with three times with EtOAc. The organic layers were collected, washed with $NaHCO_3$ saturated aqueous solution, distilled water, brine, dried over Na_2SO_4, filtered, and concentrated under reduced pressure.

*General procedure C for 2-oxa-5-azabicyclo[2.2.1]heptane formation (**5a**-**5k**, **6e**-**6g**,**j**,**k**).* To a 2-neck round-bottomed flask equipped with a condenser was dissolved the starting material (1.0 eq.) in dry pyridine (C = 0.10 M). TsOTs (3.0 eq.) was added, and the reaction mixture was stirred at rt until complete disappearance of the starting material was observed by TLC. A reference sample was taken out of the reaction mixture and the solution was heated to 100 °C in an oil bath and stirred for 8h whereby TLC or LC-MS analysis indicated complete consumption of the tosyl intermediate. The reaction mixture was allowed to reach rt and quenched by addition of an aqueous solution of $CuSO_4$ (10%w/w). The aqueous layer was extracted with EtOAc. The organic layers were collected, washed two times with an aqueous solution of $CuSO_4$ (10%w/w), distilled water, brine, dried over Na_2SO_4, filtered and concentrated under reduced pressure.

8.4.3 Library of 2-Oxa-5-azabicyclo[2.2.1]heptane

*tert-Butyl (2S,4R)-4-((tert-butyldimethylsilyl)oxy)-2-(2-phenylacetyl)pyrrolidine-1-carboxylate (**2a**).* Prepared according to general procedure A starting from *tert*-butyl (2*S*,4*R*)-4-((*tert*-butyldimethylsilyl)oxy)-2-(methoxy(methyl)carbamoyl)pyrrolidine-1-carboxylate **1** (1.0 g, 2.6 mmol, 1.0 eq.) in THF, using benzylmagnesium chloride (7.7 mL, C = 1.0 M in Et_2O, 7.7 mmol, 3.0 eq.). Chromatographed over SiO_2 (100% Hexanes to 9:1 Hexanes/EtOAc) to afford **2a** as a colorless oil (636 mg, 59%). $[\alpha]^{25}_D$: -55.5 (*c* 1.0, $CHCl_3$). ^1H NMR (500 MHz, $CDCl_3$, mixture of rotamers) δ 7.26 (dt, *J* = 51.5, 7.1 Hz, 5H), 4.56 (t, *J* = 7.7 Hz, 0.5H), 4.47 (t, *J* = 8.1 Hz, 0.5H), 4.22 (m, 1H), 3.89 – 3.80 (m, 1H), 3.80 – 3.70 (m, 1H), 3.49 (m, 1H), 3.41 (dd, *J* = 11.1, 4.6 Hz, 0.5H), 3.33 – 3.28 (m, 0.5H), 1.95 (m, 0.5H), 1.87 – 1.80 (m, 0.5H), 1.80 – 1.72 (m, 1H), 1.47 (s, 4H), 1.41 (s, 5H), 0.84 (m, 9H), 0.00 (m, 6H). $^{13}C\{^1H\}$ NMR (126 MHz, $CDCl_3$, mixture of rotamers) δ 207.9,

207.6, 155.1, 154.3, 133.9, 133.6, 129.8, 129.7, 128.8, 128.7, 127.3, 127.1, 80.6, 80.2, 70.6, 69.8, 64.1, 63.3, 55.4, 55.3, 47.5, 46.1, 39.7, 38.7, 28.6, 28.4, 25.8, 18.0, 18.0, -4.7, -4.7, -4.8, -4.8. HRMS (ESI-TOF) m/z: [M + Na]+ Calcd for $C_{23}H_{37}NO_4SiNa$ 442.2384; Found 442.2388; [M + K]+ Calcd for $C_{23}H_{37}NO_4SiK$ 458.2123; Found 458.2124.

*tert-Butyl (2S,4R)-2-((R)-4-ethoxy-2-hydroxy-4-oxo-1-phenylbutan-2-yl)-4-hydroxypyrrolidine-1-carboxylate (**3a**) and tert-butyl (2S,4R)-2-((S)-4-ethoxy-2-hydroxy-4-oxo-1-phenylbutan-2-yl)-4-hydroxypyrrolidine-1-carboxylate (**4a**).* Prepared according to general procedure B starting from *tert*-butyl (2*S*,4*R*)-4-((*tert*-butyldimethylsilyl)oxy)-2-(2-phenylacetyl)pyrrolidine-1-carboxylate **2a** (0.51 mg, 1.2 mmol, 1.0 eq.). Chromatographed over SiO_2 (100% Hexanes to 5:5 Hexanes/EtOAc) to afford an inseparable mixture of **3a** (366 mg, 76% over 2 steps) and **4a** (32 mg, 7% over 2 steps) (92:8) as a pale-yellow oil. $[\alpha]^{25}_D$: -5.7 (*c* = 1.9, MeOH). ^{1}H NMR (500 MHz, $CDCl_3$, mixture of isomers) δ 7.35 (d, m, 2H), 7.28 – 7.24 (m, 2H), 7.23 – 7.19 (m, 1H), 4.37 (bs, 1H), 4.19 (t, *J* = 7.9 Hz, 1H), 4.11 – 3.98 (m, 2H), 3.78 – 3.67 (bs, 1H), 3.30 (dd, *J* = 12.3, 3.8 Hz, 1H), 3.02 (d, *J* = 13.9 Hz, 0.92H, major isomer), 2.86 (d, *J* = 13.7 Hz, 0.08H, minor isomer), 2.74 (d, *J* = 13.9 Hz, 0.92H, major isomer), 2.65 (d, *J* = 13.8 Hz, 0.08H, minor isomer), 2.44 (d, *J* = 14.6 Hz, 1H), 2.34 (d, *J* = 14.6 Hz, 1H), 2.14 – 2.00 (m, 2H), 1.90 (bs, 1H), 1.45 (s, 9H), 1.23 (t, *J* = 7.1 Hz, 3H). ^{13}C{^{1}H} NMR (126 MHz, $CDCl_3$, mixture of isomers) δ 172.0, 158.1, 137.0, 131.1, 128.1, 126.6, 81.1, 77.0, 70.2, 63.8, 60.6, 56.7, 43.3, 40.3, 36.9, 28.5, 14.2. HRMS (ESI-TOF) m/z: [M + Na]+ Calcd for $C_{21}H_{31}NO_6Na$ 416.2044; Found 416.2054; [M + K]+ Calcd for $C_{21}H_{31}NO_6K$ 432.1783; Found 432.1787.

*tert-Butyl (1S,3R,4S)-3-benzyl-3-(2-ethoxy-2-oxoethyl)-2-oxa-5-azabicyclo[2.2.1]heptane-5-carboxylate (**5a**).* Prepared according to general procedure C starting from *tert*-butyl (2*S*,4*R*)-2-((*R*)-4-ethoxy-2-hydroxy-4-oxo-1-phenylbutan-2-yl)-4-hydroxypyrrolidine-1-carboxylate **3a** and (2*S*,4*R*)-*tert*-butyl 2-((S)-4-ethoxy-2-hydroxy-4-oxo-1-phenylbutan-2-yl)-4-hydroxypyrrolidine-1-carboxylate **4a** (92:8) (34 mg, 86 μmol, 1.0 eq.). Chromatographed over SiO_2 (100% Hexanes to 7:3 Hexanes/EtOAc) to afford **5a** as a light-yellow oil (24 mg, 74%). $[\alpha]^{25}_D$: +8.6 (*c* = 1.1, MeOH). ^{1}H NMR (500 MHz, $CDCl_3$, mixture of rotamers) δ 7.35 (m, 1H), 7.32 – 7.26 (m, 3H), 7.22 (m, 1H), 4.78 – 4.65 (m, 1H), 4.58 (m, 1H), 4.14 (m, 2H), 3.45 – 3.26 (m, 2H), 3.11 (dd, *J* = 13.9, 7.5 Hz, 1H), 2.94 (m, 1H), 2.35 (m, 1H), 2.28 – 2.21 (m, 1H), 2.19 – 2.10 (m, 1H), 1.80 – 1.70 (m, 1H), 1.50 (m, 9H), 1.29 – 1.24 (m, 3H). ^{13}C{^{1}H} NMR (126 MHz, $CDCl_3$, mixture of rotamers) δ 170.0, 169.7, 154.7,

154.5, 137.7, 137.6, 131.1, 130.9, 130.8, 128.2, 126.6, 126.6, 86.2, 85.8, 80.2, 79.8, 62.5, 61.5, 60.6, 60.6, 53.8, 53.1, 40.9, 40.7, 40.5, 40.4, 36.0, 35.8, 28.6, 28.5, 14.4. HRMS (ESI-TOF) m/z: [M + Na]+ Calcd for $C_{21}H_{29}NO_5Na$ 398.1938; Found 398.1946; [M + K]+ Calcd for $C_{21}H_{29}NO_5K$ 414.1677; Found 414.1681.

*tert-Butyl (2S,4R)-4-((tert-butyldimethylsilyl)oxy)-2-(2-(3,5-dimethoxyphenyl)acetyl)pyrrolidine-1-carboxylate (**2b**).* Prepared according to general procedure A starting from *tert*-butyl (2*S*,4*R*)-4-((*tert*-butyldimethylsilyl)oxy)-2-(methoxy(methyl)carbamoyl)pyrrolidine-1-carboxylate **1** (52 mg, 0.13 mmol, 1.0 eq.) in THF, using (3,5-dimethoxybenzyl)magnesium chloride (2.0 mL, C = 0.20 M in THF, 0.40 mmol, 3.0 eq.). Chromatographed over SiO_2 (100% Hexanes to 85:15 Hexanes/EtOAc) to afford **2b** as a colorless oil (51 mg, 82%). $[\alpha]^{25}_D$: -50.9 (*c* = 2.1, $CHCl_3$). ^{1}H NMR (500 MHz, $CDCl_3$, mixture of rotamers) δ 6.43 – 6.27 (m, 3H), 4.56 (t, *J* = 7.7 Hz, 0.5H), 4.47 (t, *J* = 8.0 Hz, 0.5H), 4.29 – 4.14 (m, 1H), 3.76 (m, 7H), 3.73 – 3.62 (q, *J* = 15.0 Hz, 1H), 3.48 (m, 1H), 3.42 (dd, *J* = 11.1, 4.6 Hz, 0.5H), 3.30 (ddd, *J* = 11.1, 3.1, 1.4 Hz, 0.5H), 1.96 (ddd, *J* = 11.8, 7.9, 3.5 Hz, 0.5H), 1.83 (ddd, *J* = 8.0, 4.1, 1.3 Hz, 0.5H), 1.80 – 1.72 (m, 1H), 1.47 (s, 4H), 1.41 (s, 5H), 0.83 (m, 9H), 0.00 (m, 6H). ^{13}C{^{1}H} NMR (126 MHz, $CDCl_3$, mixture of rotamers) δ 207.9, 207.5, 161.1, 161.0, 155.1, 154.2, 136.0, 135.6, 107.8, 107.8, 99.4, 99.2, 80.6, 80.2, 70.6, 69.8, 64.1, 63.2, 55.4, 55.4, 55.4, 55.3, 47.8, 46.5, 39.8, 38.9, 28.6, 28.4, 25.8, 25.8, 25.7, 18.0, 18.0, -4.8, -4.8, -4.8. HRMS (ESI-TOF) m/z: [M + Na]+ Calcd for $C_{25}H_{41}NO_6SiNa$ 502.2595; Found 502.2595.

*tert-Butyl (2S,4R)-2-((R)-1-(3,5-dimethoxyphenyl)-4-ethoxy-2-hydroxy-4-oxobutan-2-yl)-4-hydroxypyrrolidine-1-carboxylate (**3b**) and tert-butyl (2S,4R)-2-((S)-1-(3,5-dimethoxyphenyl)-4-ethoxy-2-hydroxy-4-oxobutan-2-yl)-4-hydroxypyrrolidine-1-carboxylate (**4b**).* Prepared according to general procedure B starting from *tert*-butyl (2*S*,4*R*)-4-((*tert*-butyldimethylsilyl)oxy)-2-(2-(3,5-dimethoxyphenyl)acetyl)pyrrolidine-1-carboxylate **2b** (48 mg, 0.10 mmol, 1.0 eq.). Chromatographed over SiO_2 (100% Hexanes to 5:5 Hexanes/EtOAc) to afford an inseparable mixture of **3b** (33 mg, 73% over 2 steps) and **4b** (2 mg, 3% over 2 steps) (94:6) as a colorless oil. $[\alpha]^{25}_D$: -12.1 (*c* = 1.5, $CHCl_3$). ^{1}H NMR (500 MHz, $CDCl_3$, mixture of isomers) δ 6.54 (s, 2H), 6.33 (t, *J* = 2.3 Hz, 1H), 4.38 (bs, 1H), 4.22 (t, *J* = 7.9 Hz, 1H), 4.14 – 3.96 (m, 2H), 3.76 (m, 7H), 3.30 (dd, *J* = 12.2, 3.9 Hz, 1H), 2.98 (d, *J* = 13.8 Hz, 0.94H, major isomer), 2.79 (d, *J* = 13.6 Hz, 0.06H, minor isomer), 2.68 (d, *J* = 13.9 Hz, 0.94H, major isomer), 2.58 (d, *J* = 13.6 Hz, 0.06H, minor isomer), 2.45

(d, *J* = 14.6 Hz, 1H), 2.36 (d, *J* = 14.6 Hz, 1H), 2.13 – 2.02 (m, 2H), 1.83 (bs, 2H), 1.45 (s, 9H), 1.24 (t, *J* = 7.1 Hz, 3H). $^{13}C\{^{1}H\}$ NMR (126 MHz, $CDCl_3$, mixture of isomers) δ 172.0, 160.4, 139.3, 109.0, 98.8, 81.1, 77.0, 70.3, 63.7, 60.7, 56.6, 55.4, 43.6, 40.4, 36.9, 28.5, 14.2. HRMS (ESI-TOF) m/z: [M + Na]+ Calcd for $C_{23}H_{35}NO_8Na$ 476.2255; Found 476.2272; [M + K]+ Calcd for $C_{23}H_{35}NO_8K$ 492.1994; Found 492.2010.

*tert-Butyl (1S,3R,4S)-3-(3,5-dimethoxybenzyl)-3-(2-ethoxy-2-oxoethyl)-2-oxa-5-azabicyclo[2.2.1] heptane-5-carboxylate (**5b**).* Prepared according to general procedure C starting from *tert*-butyl (2*S*,4*R*)-2-((*R*)-1-(3,5-dimethoxyphenyl)-4-ethoxy-2-hydroxy-4-oxobutan-2-yl)-4-hydroxypyrrolidine-1-carboxylate **3b** and *tert*-butyl (2*S*,4*R*)-2-((*S*)-1-(3,5-dimethoxyphenyl)-4-ethoxy-2-hydroxy-4-oxobutan-2-yl)-4-hydroxypyrrolidine-1-carboxylate **4b** (94:6) (20 mg, 40 mmol, 1.0 eq.). Chromatographed over SiO_2 (100% Hexanes to 7:3 Hexanes/EtOAc) to afford **5b** as an orange oil (13 mg, 66%). $[\alpha]^{25}_{D}$: +8.0 (*c* = 0.5, $CHCl_3$). ^{1}H NMR (500 MHz, $CDCl_3$, mixture of rotamers) δ 6.56 (d, *J* = 2.3 Hz, 1H), 6.46 (d, *J* = 2.3 Hz, 1H), 6.33 (t, *J* = 2.3 Hz, 1H), 4.70 (m, 1H), 4.57 (m, 1H), 4.18 – 4.05 (m, 2H), 3.77 (m, 6H), 3.41 – 3.25 (m, 2H), 3.05 (m, 1H), 2.95 (m, 0.4H), 2.82 (m, 0.6H), 2.44 (d, *J* = 15.9 Hz, 0.5H), 2.37 – 2.23 (m, 1.5H), 2.20 – 2.11 (m, 1H), 1.74 (m, 1H), 1.52 (s, 5H), 1.47 (s, 4H), 1.32 – 1.20 (m, 3H). $^{13}C\{^{1}H\}$ NMR (126 MHz, $CDCl_3$, mixture of rotamers) δ 170.1, 169.8, 160.7, 160.6, 154.7, 154.6, 140.0, 139.8, 109.0, 108.7, 99.1, 98.5, 86.2, 85.7, 80.2, 79.9, 77.1, 62.6, 61.6, 60.6, 55.5, 55.4, 53.9, 53.1, 40.8, 40.7, 40.7, 35.9, 35.8, 28.6, 14.4. HRMS (ESI-TOF) m/z: [M + Na]+ Calcd for $C_{23}H_{33}NO_7Na$ 458.2149; Found 458.2138; [M + K]+ Calcd for $C_{23}H_{33}NO_7K$ 474.1887; Found 474.1880.

*tert-Butyl (2S,4R)-2-(2-(3-bromophenyl)acetyl)-4-((tert-butyldimethylsilyl)oxy)pyrrolidine-1-carboxylate (**2c**).* Prepared according to general procedure A starting from *tert*-butyl (2*S*,4*R*)-4-((*tert*-butyldimethylsilyl)oxy)-2-(methoxy(methyl)carbamoyl)pyrrolidine-1-carboxylate **1** (100 mg, 0.26 mmol, 1.0 eq.) in Et_2O, using (3-bromobenzyl)magnesium bromide (3.1 mL, C = 0.25 M in Et_2O, 0.78 mmol, 3.0 eq.). Chromatographed over SiO_2 (100% Hexanes to 9:1 Hexanes/EtOAc) to afford **2c** as a pale-brown oil (95 mg, 74%). $[\alpha]^{25}_{D}$: -43.3 (*c* = 1.2, $CHCl_3$). ^{1}H NMR (400 MHz, $CDCl_3$, mixture of rotamers) δ 7.44 – 7.33 (m, 2H), 7.24 – 7.10 (m, 2H), 4.55 (t, *J* = 7.7 Hz, 0.5H), 4.47 (t, *J* = 8.1 Hz, 0.5H), 4.32 – 4.22 (m, 1H), 3.82 (q, *J* = 16.2 Hz, 1H), 3.72 (s, 1H), 3.59 – 3.46 (m, 1H), 3.42 (dd, *J* = 11.2, 4.6 Hz, 0.5H), 3.34 (m, 0.5H), 2.08 – 1.99 (m, 0.5H), 1.97 – 1.88 (m, 0.5H),

1.81 (m, 1H), 1.48 (s, 4.5H), 1.40 (s, 4.5H), 0.85 (m, 9H), 0.03 (m, 6H). $^{13}C\{^{1}H\}$ NMR (126 MHz, $CDCl_3$, mixture of rotamers) δ 207.2, 206.8, 155.2, 154.3, 136.2, 135.9, 132.9, 132.7, 130.4, 130.3, 130.2, 130.2, 128.5, 128.4, 122.8, 122.7, 80.8, 80.4, 70.6, 69.8, 64.4, 63.4, 55.4, 46.5, 45.0, 39.6, 38.5, 28.6, 28.4, 28.3, 25.9, 25.8, 18.1, -4.7, -4.7, -4.7, -4.8. HRMS (ESI-TOF) m/z: [M + Na]+ Calcd for $C_{23}H_{36}BrNO_4SiNa$ 520.1489; Found 520.1489.

*tert-Butyl (2S,4R)-2-((R)-1-(3-bromophenyl)-4-ethoxy-2-hydroxy-4-oxobutan-2-yl)-4-hydroxypyrrolidine-1-carboxylate (**3c**) and tert-butyl (2S,4R)-2-((S)-1-(3-bromophenyl)-4-ethoxy-2-hydroxy-4-oxobutan-2-yl)-4-hydroxypyrrolidine-1-carboxylate (**4c**).* Prepared according to general procedure B starting from *tert*-butyl (2*S*,4*R*)-2-(2-(3-bromophenyl)acetyl)-4-((*tert*-butyldimethylsilyl)oxy)pyrrolidine-1-carboxylate **2c** (45 mg, 90 µmol, 1.0 eq.). Chromatographed over SiO_2 (100% Hexanes to 5:5 Hexanes/EtOAc) to afford an inseparable mixture of **3c** (29 mg, 68% over 2 steps) and **4c** (1 mg, 3% over 2 steps) (96:4) as a colorless oil. $[\alpha]^{25}_D$: -15.0 (*c* = 1.5, $CHCl_3$). ^{1}H NMR (500 MHz, $CDCl_3$, mixture of isomers) δ 7.52 (m, 1H), 7.39 – 7.29 (m, 2H), 7.13 (t, *J* = 7.8 Hz, 1H), 4.38 (m, 1H), 4.17 (t, *J* = 8.0 Hz, 1H), 4.13 – 3.98 (m, 2H), 3.75 (bs, 1H), 3.30 (dd, *J* = 12.3, 3.7 Hz, 1H), 3.00 (d, *J* = 13.9 Hz, 0.96H, major isomer), 2.82 (d, *J* = 13.7 Hz, 0.04H, minor isomer), 2.70 (d, *J* = 13.9 Hz, 0.96H, major isomer), 2.60 (d, *J* = 13.7 Hz, 0.04H, minor isomer), 2.44 (d, *J* = 14.6 Hz, 1H), 2.34 (d, *J* = 14.6 Hz, 1H), 2.10 – 2.00 (m, 2H), 1.84 (bs, 1H), 1.45 (s, 9H), 1.25 (t, *J* = 7.1 Hz, 3H). $^{13}C\{^{1}H\}$ NMR (126 MHz, $CDCl_3$, mixture of isomers) δ 171.9, 158.1, 139.5, 133.9, 129.8, 129.7, 129.6, 122.1, 81.3, 76.9, 70.2, 63.9, 60.8, 56.7, 42.9, 40.2, 36.9, 28.5, 14.3, 13.9. HRMS (ESI-TOF) m/z: [M + Na]+ Calcd for $C_{21}H_{30}BrNO_6Na$ 494.1149; Found 494.1158; [M + K]+ Calcd for $C_{21}H_{30}BrNO_6K$ 510.0888; Found 510.0898.

*tert-Butyl (1S,3R,4S)-3-(3-bromobenzyl)-3-(2-ethoxy-2-oxoethyl)-2-oxa-5-azabicyclo[2.2.1]heptane-5-carboxylate (**5c**).* Prepared according to general procedure C starting from *tert*-butyl (2*S*,4*R*)-2-((*R*)-1-(3-bromophenyl)-4-ethoxy-2-hydroxy-4-oxobutan-2-yl)-4-hydroxypyrrolidine-1-carboxylate **3c** and *tert*-butyl (2*S*,4*R*)-2-((*S*)-1-(3-bromophenyl)-4-ethoxy-2-hydroxy-4-oxobutan-2-yl)-4-hydroxypyrrolidine-1-carboxylate **4c** (96:4) (31 mg, 66 µmol, 1.0 eq.). Chromatographed over SiO_2 (100% Hexanes to 8:2 Hexanes/EtOAc) to afford **5c** as a colorless oil (18 mg, 60%). $[\alpha]^{25}_D$: -2.5 (*c* = 0.7, $CHCl_3$). ^{1}H NMR (500 MHz, $CDCl_3$, mixture of rotamers) δ 7.53 (s, 0.4H), 7.45 (m, 0.6H), 7.40 – 7.35 (m, 1H), 7.31 (d, *J* = 7.6 Hz, 0.4H), 7.27 (d, *J* = 7.7 Hz, 0.6H),

7.17 (m, 1H), 4.77 (s, 0.4H), 4.72 (s, 0.6H), 4.61 (m, 1H), 4.17 (m, 2H), 3.43 (m, 0.6H), 3.35 (m, 1.4H), 3.11 (m, 1H), 2.91 (m, 1H), 2.39 – 2.24 (m, 2H), 2.18 (m, 1H), 1.83 – 1.74 (m, 1H), 1.55 (s, 5.5H), 1.50 (s, 3.5H), 1.35 – 1.26 (m, 3H). $^{13}C\{^{1}H\}$ NMR (126 MHz, $CDCl_3$, mixture of rotamers) δ 169.9, 169.6, 154.7, 140.0, 133.9, 133.7, 129.8, 129.8, 129.5, 122.3, 85.9, 85.6, 80.3, 80.0, 77.6, 62.5, 61.5, 60.7, 53.8, 53.1, 40.9, 40.7, 40.2, 35.9, 35.7, 29.8, 28.6, 14.4. HRMS (ESI-TOF) m/z: [M + Na]+ Calcd for $C_{21}H_{28}BrNO_5Na$ 476.1043; Found 476.1026; [M + K]+ Calcd for $C_{21}H_{28}BrNO_5K$ 492.0782; Found 492.0765.

*tert-Butyl (2S,4R)-4-((tert-butyldimethylsilyl)oxy)-2-(2-(4-fluorophenyl)acetyl)pyrrolidine-1-carboxylate (**2d**).* Prepared according to general procedure A starting from *tert*-butyl (2*S*,4*R*)-4-((*tert*-butyldimethylsilyl)oxy)-2-(methoxy(methyl)carbamoyl)pyrrolidine-1-carboxylate **1** (0.20 g, 0.52 mmol, 1.0 eq.) in Et_2O, using (4-fluorobenzyl)magnesium bromide (2.4 mL, C = 0.65 M in Et_2O, 1.5 mmol, 3.0 eq.). Chromatographed over SiO_2 (100% Hexanes to 9:1 Hexanes/EtOAc) to afford **2d** as a colorless oil (148 mg, 65%). $[\alpha]^{25}_D$: -56.1 (*c* = 0.44, $CHCl_3$). ^{1}H NMR (500 MHz, $CDCl_3$, mixture of rotamers) δ 7.16 (m, 2H), 7.01 (q, *J* = 8.7 Hz, 2H), 4.56 (t, *J* = 7.7 Hz, 0.5H), 4.46 (t, *J* = 8.1 Hz, 0.5H), 4.27 (m, 1H), 3.87 – 3.78 (m, 1H), 3.73 (m, 1H), 3.52 (m, 0.5H), 3.49 (m, 0.5H), 3.44 (m, 0.5H), 3.34 (m, 0.5H), 2.01 (dddd, *J* = 12.7, 7.8, 3.4, 1.6 Hz, 0.5H), 1.90 (dddd, *J* = 11.9, 8.0, 4.0, 1.4 Hz, 0.5H), 1.78 (m, 1H), 1.47 (s, 4.4H), 1.40 (s, 4.6H), 0.84 (s, 9H), 0.02 (m, 6H). $^{13}C\{^{1}H\}$ NMR (126 MHz, $CDCl_3$, mixture of rotamers) δ 207.8, 207.4, 163.1, 163.0, 161.2, 161.1, 155.1, 154.3, 131.4, 131.3, 131.3, 131.2, 129.6, 129.6, 129.3, 129.3, 115.8, 115.6, 115.6, 115.5, 80.7, 80.3, 77.4, 77.2, 76.9, 70.6, 69.8, 64.2, 63.3, 55.4, 55.4, 46.2, 44.8, 39.6, 38.6, 28.6, 28.4, 25.8, 18.1. HRMS (ESI-TOF) m/z: [M + Na]+ Calcd for $C_{23}H_{37}FNO_4SiNa$ 461.2290; Found 461.2311.

*tert-Butyl (2S,4R)-2-((R)-4-ethoxy-1-(4-fluorophenyl)-2-hydroxy-4-oxobutan-2-yl)-4-hydroxypyrrolidine-1-carboxylate (**3d**) and tert-butyl (2S,4R)-2-((S)-4-ethoxy-1-(4-fluorophenyl)-2-hydroxy-4-oxobutan-2-yl)-4-hydroxypyrrolidine-1-carboxylate (**4d**).* Prepared according to general procedure B starting from *tert*-butyl (2*S*,4*R*)-4-((*tert*-butyldimethylsilyl)oxy)-2-(2-(4-fluorophenyl)acetyl)pyrrolidine-1-carboxylate **2d** (0.18 g, 0.34 mmol, 1.0 eq.). Chromatographed over SiO_2 (100% Hexanes to 6:4 Hexanes/EtOAc) to afford an inseparable mixture of **3d** (104 mg, 75% over 2 steps) and **4d** (3 mg, 2% over 2 steps) (97:3) as a colorless oil. $[\alpha]^{25}_D$: -20.0 (*c* = 1.1, $CHCl_3$). ^{1}H NMR (500 MHz, $CDCl_3$, mixture of isomers) δ 7.33 (m, 2H), 6.98 – 6.91 (m, 2H), 4.38 (m,

1H), 4.16 (t, *J* = 8.1 Hz, 1H), 4.13 – 3.98 (m, 2H), 3.74 (m, 1H), 3.31 (dd, *J* = 12.3, 3.7 Hz, 1H), 3.00 (d, *J* = 14.0 Hz, 0.97H, major isomer), 2.82 (d, *J* = 13.9 Hz, 0.03H, minor isomer), 2.70 (d, *J* = 14.0 Hz, 0.97H, major isomer), 2.61 (d, *J* = 13.9 Hz, 0.03H, minor isomer), 2.43 (d, *J* = 14.5 Hz, 1H), 2.33 (d, *J* = 14.5 Hz, 1H), 2.05 (m, 2H), 1.71 (bs, 1H), 1.45 (s, 9H), 1.24 (t, *J* = 7.1 Hz, 3H). $^{13}C\{^{1}H\}$ NMR (126 MHz, $CDCl_3$, mixture of isomers) δ 171.7, 162.7, 160.7, 157.9, 132.4, 132.4, 132.2, 132.2, 114.7, 114.5, 81.0, 77.2, 76.9, 76.7, 69.9, 63.6, 60.4, 56.5, 42.2, 40.0, 36.7, 29.6, 28.2, 14.0. HRMS (ESI-TOF) m/z: [M + Na]+ Calcd for $C_{21}H_{30}FNO_6Na$ 434.1949; Found 434.1953.

*tert-Butyl (1S,3R,4S)-3-(2-ethoxy-2-oxoethyl)-3-(4-fluorobenzyl)-2-oxa-5-azabicyclo[2.2.1]heptane-5-carboxylate (**5d**).* Prepared according to general procedure C starting from *tert*-butyl (2*S*,4*R*)-2-((*R*)-4-ethoxy-1-(4-fluorophenyl)-2-hydroxy-4-oxobutan-2-yl)-4-hydroxypyrrolidine-1-carboxylate **3d** and *tert*-butyl (2*S*,4*R*)-2-((*S*)-4-ethoxy-1-(4-fluorophenyl)-2-hydroxy-4-oxobutan-2-yl)-4-hydroxypyrrolidine-1-carboxylate **4d** (97:3) (32 mg, 77 µmol, 1.0 eq.). Chromatographed over SiO_2 (100% Hexanes to 7:3 Hexanes/EtOAc) to afford **5d** as a light-yellow oil (18 mg, 60%). $[\alpha]^{25}_{D}$: -33.0 (*c* = 0.6, $CHCl_3$). ^{1}H NMR (500 MHz, $CDCl_3$, mixture of rotamers) δ 7.40 – 7.28 (m, 1H), 7.26 (m, 1H), 6.96 (t, *J* = 8.7 Hz, 2H), 4.74 – 4.65 (m, 1H), 4.58 (m, 1H), 4.14 (m, 2H), 3.43 – 3.23 (m, 2H), 3.08 (m, 1H), 2.90 (m, 1H), 2.35 – 2.20 (m, 2H), 2.16 (m, 1H), 1.76 (m, 1H), 1.50 (m, 9H), 1.30 – 1.23 (m, 3H). $^{13}C\{^{1}H\}$ NMR (126 MHz, $CDCl_3$, mixture of rotamers) δ 169.9, 169.6, 162.9, 160.9, 154.7, 154.5, 133.3, 133.2, 132.4, 132.3, 132.2, 115.1, 114.9, 86.1, 85.7, 80.2, 79.9, 77.4, 77.2, 76.9, 62.5, 61.4, 60.6, 53.8, 53.1, 40.8, 40.6, 39.6, 39.6, 36.0, 35.8, 29.8, 28.6, 14.4. HRMS (ESI-TOF) m/z: [M + Na]+ Calcd for $C_{21}H_{28}FNO_5Na$ 416.1844; Found 416.1840.

*tert-Butyl (2S,4R)-2-benzoyl-4-((tert-butyldimethylsilyl)oxy)pyrrolidine-1-carboxylate (**2e**).* Prepared according to general procedure A starting from *tert*-butyl (2*S*,4*R*)-4-((*tert*-butyldimethylsilyl)oxy)-2-(methoxy(methyl)carbamoyl)pyrrolidine-1-carboxylate **1** (500 mg, 1.29 mmol, 1.0 eq.) in Et_2O, using phenylmagnesium bromide (3.9 mL, C = 1.0 in THF, 3.9 mmol, 3.0 eq.). Chromatographed over SiO_2 (100% Hexanes to 8:2 Hexanes/EtOAc) to afford **2e** as a colorless oil (277 mg, 53%). $[\alpha]^{25}_{D}$: -13.1 (*c* = 1.1, $CHCl_3$). ^{1}H NMR (500 MHz, $CDCl_3$, mixture of rotamers) δ 8.03 – 7.97 (m, 0.8H), 7.97 – 7.93 (m, 1.2H), 7.57 (m, 1H), 7.46 (m, 2H), 5.44 (dd, *J* = 8.6, 6.3 Hz, 0.4H), 5.31 (t, *J* = 7.6 Hz, 0.6H), 4.44 (m, 1H), 3.75 (dd, *J* = 11.1, 4.9 Hz, 0.6H), 3.69 (dd, *J* = 11.0, 5.1 Hz, 0.4H), 3.53 – 3.45 (m, 0.6H), 3.41 (dd, *J* = 11.0, 3.1 Hz, 0.4H), 2.30 – 2.19 (m, 1H),

2.06 – 1.91 (m, 1H), 1.45 (s, 3.8H), 1.23 (s, 5.2H), 0.88 (m, 9H), 0.10 – 0.04 (m, 6H). $^{13}C\{^{1}H\}$ NMR (126 MHz, $CDCl_3$, mixture of rotamers) δ 199.3, 198.8, 154.7, 153.9, 135.5, 135.4, 133.5, 133.4, 128.9, 128.8, 128.7, 128.3, 80.2, 80.0, 70.7, 70.0, 60.1, 59.8, 55.2, 55.0, 40.3, 39.3, 28.6, 28.3, 25.9, 25.8, 18.2, 18.1, -4.7, -4.7, -4.7. The spectral data matched those of the literature. [645]

*tert-Butyl (2S,4R)-2-((S)-3-ethoxy-1-hydroxy-3-oxo-1-phenylpropyl)-4-hydroxypyrrolidine-1-carboxylate (**3e**) and tert-butyl (2S,4R)-2-((R)-3-ethoxy-1-hydroxy-3-oxo-1-phenylpropyl)-4-hydroxypyrrolidine-1-carboxylate (**4e**).* Prepared according to general procedure B starting from *tert*-butyl (2*S*,4*R*)-2-benzoyl-4-((*tert*-butyldimethylsilyl)oxy)pyrrolidine-1-carboxylate **2e** (0.25 g, 0.62 mmol, 1.0 eq.). Chromatographed over SiO_2 (100% Hexanes to 6:4 Hexanes/EtOAc) to afford **3e** (109 mg, 46% over 2 steps) as a white solid and **4e** (47 mg, 20% over 2 steps) as a white solid (ratio: 2:1). *Diastereomer **3e*** **:** $[\alpha]^{25}_{D}$: -64.6 (*c* = 0.7, $CHCl_3$). ^{1}H NMR (500 MHz, $CDCl_3$, mixture of rotamers) δ 7.47 – 7.42 (m, 2H), 7.32 – 7.28 (m, 2H), 7.27 – 7.22 (m, 1H), 4.43 (bs, 1H), 3.97 (m, 2H), 3.62 (bs, 1H), 3.41 (bs, 1H), 3.22 (bs, 1H), 2.94 (m, 1H), 2.69 (bs, 1H), 2.22 – 2.09 (m, 1H), 1.84 (bs, 1H), 1.47 (s, 9H), 1.05 (t, *J* = 7.1 Hz, 3H). $^{13}C\{^{1}H\}$ NMR (126 MHz, $CDCl_3$, mixture of rotamers) δ 173.3, 156.8, 142.1, 128.1, 127.5, 126.6, 80.5, 76.9, 70.3, 64.6, 60.8, 56.0, 43.4, 36.1, 28.5, 14.0. HRMS (ESI-TOF) m/z: [M + Na]+ Calcd for $C_{20}H_{29}NO_6Na$ 402.1887; Found 402.1891; [M + K]+ Calcd for $C_{20}H_{29}NO_6K$ 418.1627; Found 418.1629. *Diastereomer **4e*** **:** $[\alpha]^{25}_{D}$: +15.0 (*c* = 0.2, $CHCl_3$). ^{1}H NMR (500 MHz, $CDCl_3$, mixture of rotamers) δ 7.49 – 7.37 (m, 2H), 7.32 (t, *J* = 7.6 Hz, 2H), 7.25 – 7.21 (m, 1H), 4.97 (bs, 1H), 4.51 (m, 2H), 4.01 – 3.86 (m, 2H), 3.60 (m, 1H), 3.42 (m, 1H), 3.14 (m, 1H), 2.90 (m, 1H), 2.06 (m, 1H), 1.54 (m, 11H), 0.99 (t, *J* = 7.1 Hz, 3H). $^{13}C\{^{1}H\}$ NMR (126 MHz, $CDCl_3$, mixture of rotamers) δ 173.7, 157.1, 143.4, 128.3, 127.2, 125.8, 80.3, 78.5, 77.9, 76.9, 71.4, 64.8, 64.6, 60.8, 56.3, 43.6, 35.7, 28.6, 14.0. HRMS (ESI-TOF) m/z: [M + Na]+ Calcd for $C_{20}H_{29}NO_6Na$ 402.1887; Found 402.1880.

*tert-Butyl (1S,3S,4S)-3-(2-ethoxy-2-oxoethyl)-3-phenyl-2-oxa-5-azabicyclo[2.2.1]heptane-5-carboxylate (**5e**).* Prepared according to general procedure C starting from *tert*-butyl (2*S*,4*R*)-2-((*S*)-3-ethoxy-1-hydroxy-3-oxo-1-phenylpropyl)-4-hydroxypyrrolidine-1-carboxylate **3e** (34 mg, 90 µmol, 1.0 eq.). Chromatographed over SiO_2 (100% Hexanes to 7:3 Hexanes/EtOAc) to afford **5e** as a colorless oil (16 mg, 49%). $[\alpha]^{25}_{D}$: +7.7 (*c* = 0.7, $CHCl_3$). ^{1}H NMR (500 MHz, $CDCl_3$, mixture of rotamers) δ 7.47 (m, 1H), 7.44 – 7.41 (m, 1H), 7.27 (m, 2H), 7.19 (m, 1H), 4.93 (s, 0.5H), 4.85 (s,

0.5H), 4.79 (s, 0.5H), 4.76 (s, 0.5H), 3.92 (m, 2H), 3.22 (dd, *J* = 10.5, 1.7 Hz, 0.5H), 3.13 (dd, *J* = 10.5, 1.8 Hz, 0.5H), 3.07 (d, *J* = 10.8 Hz, 0.5H), 3.03 (d, *J* = 10.5 Hz, 0.5H), 2.87 – 2.74 (m, 1H), 2.66 (m, 1H), 2.28 (m, 1H), 1.86 (m, 1H), 1.30 (s, 4.5H), 1.12 (s, 4.5H), 1.01 (m, 3H). $^{13}C\{^{1}H\}$ NMR (126 MHz, $CDCl_3$, mixture of rotamers) δ 169.4, 169.2, 153.3, 153.2, 142.0, 141.8, 127.8, 127.5, 127.2, 127.1, 126.3, 126.1, 88.5, 88.2, 79.7, 79.2, 78.2, 77.8, 63.4, 62.3, 60.6, 60.5, 52.4, 51.9, 47.1, 46.8, 36.5, 36.2, 28.4, 28.2, 14.0. HRMS (ESI-TOF) m/z: [M + Na]+ Calcd for $C_{20}H_{27}NO_5Na$ 384.1781; Found 384.1769; [M + K]+ Calcd for $C_{20}H_{27}NO_5K$ 400.1521; Found 400.1515.

*tert-Butyl (1S,3R,4S)-3-(2-ethoxy-2-oxoethyl)-3-phenyl-2-oxa-5-azabicyclo[2.2.1]heptane-5-carboxylate (**6e**).* Procedure 1: Prepared according to general procedure C starting from *tert*-butyl (2*S*,4*R*)-2-((*R*)-3-ethoxy-1-hydroxy-3-oxo-1-phenylpropyl)-4-hydroxypyrrolidine-1-carboxylate **4e** (20 mg, 53 µmol, 1.0 eq.). Chromatographed over SiO_2 (100% Hexanes to 7:3 Hexanes/EtOAc) to afford **6e** as a colorless oil (8 mg, 42%). $[\alpha]^{25}_{D}$: +20.0 (*c* = 0.2, $CHCl_3$). ^{1}H NMR (500 MHz, $CDCl_3$, mixture of rotamers) δ 7.38 (m, 1H), 7.35 – 7.29 (m, 3H), 7.26 – 7.18 (m, 1H), 4.73 (m, 1H), 4.65 (bs, 0.5H), 4.57 (bs, 0.5H), 3.93 – 3.81 (m, 2H), 3.43 (m, 1H), 3.38 (dd, *J* = 10.5, 1.5 Hz, 0.5H), 3.33 (dd, *J* = 10.4, 1.5 Hz, 0.5H), 3.08 (d, *J* = 14.7 Hz, 0.5H), 2.98 (d, *J* = 14.9 Hz, 0.5H), 2.76 (d, *J* = 15.0 Hz, 0.5H), 2.71 (d, *J* = 14.7 Hz, 0.5H), 1.80 (m, 1H), 1.55 (s, 4.5H), 1.50 (s, 4.5H), 0.92 (m, 3H). $^{13}C\{^{1}H\}$ NMR (126 MHz, $CDCl_3$, mixture of rotamers) δ 170.3, 170.0, 154.7, 154.5, 142.6, 128.2, 128.2, 127.2, 127.2, 125.6, 125.6, 87.9, 87.6, 80.3, 80.1, 77.8, 64.5, 63.6, 60.3, 60.3, 54.0, 53.4, 44.0, 43.9, 35.4, 34.9, 28.7, 28.6, 14.0, 14.0. HRMS (ESI-TOF) m/z: [M + Na]+ Calcd for $C_{20}H_{27}NO_5Na$ 384.1781; Found 384.1795; [M + K]+ Calcd for $C_{20}H_{27}NO_5K$ 400.1521; Found 400.1531.

*tert-Butyl (2S,4R)-4-((tert-butyldimethylsilyl)oxy)-2-(4-chlorobenzoyl)pyrrolidine-1-carboxylate (**2f**).* Prepared according to general procedure A starting from *tert*-butyl (2*S*,4*R*)-4-((*tert*-butyldimethylsilyl)oxy)-2-(methoxy(methyl)carbamoyl)pyrrolidine-1-carboxylate **1** (2.4 g, 6.1 mmol, 1.0 eq.) in Et_2O (19 mL, C = 0.32 mol/L), using freshly prepared (4-chlorophenyl)magnesium bromide (24 mL, C = 1.0 in Et_2O, 24 mmol, 4.0 eq.). Chromatographed over SiO_2 (100% Hexanes to 10:1 Hexanes/EtOAc) to afford **2f** as a colorless oil (1.8 g, 68%). $[\alpha]_D^{25}$ -11.0 (*c* 4.0 g/L, $CHCl_3$). ^{1}H NMR (700 MHz, $CDCl_3$, mixture of rotamers) δ 7.97 – 7.86 (m, 2H), 7.50 – 7.39 (m, 2H), 5.38 (dd, *J* = 8.6, 6.5 Hz, 0.45H), 5.26 (t, *J* = 7.7 Hz, 0.55H), 4.44 (m, 1H), 3.73 (dd, *J* = 11.2, 4.9 Hz, 0.55H), 3.67 (dd, *J* = 11.0, 5.0 Hz, 0.45H), 3.50 (m, 0.55H), 3.43 – 3.38 (m, 0.45H), 2.26 – 2.18 (m,

1H), 2.01 – 1.91 (m, 1H), 1.45 (s, 4.25H), 1.23 (s, 4.75H), 0.88 (m, 9H), 0.07 (m, 6H). $^{13}C\{^{1}H\}$ NMR (176 MHz, $CDCl_3$, mixture of rotamers) δ 198.2, 197.9, 154.8, 153.8, 140.0, 139.9, 133.8, 130.1, 129.7, 129.3, 129.2, 129.1, 80.3, 80.2, 70.8, 70.1, 60.1, 59.7, 55.2, 55.0, 40.3, 39.3, 28.6, 28.3, 25.9, 25.9, 18.2, 18.1, -4.6, -4.6, -4.7, -4.7. HRMS (ESI-TOF) m/z: [M + Na]+ Calcd for $C_{22}H_{34}ClNO_4SiNa$ 462.1838; Found 462.1834; [M + K]+ Calcd for $C_{22}H_{34}ClNO_4SiK$ 478.1577; Found 478.1583.

*tert-Butyl (2S,4R)-4-((tert-butyldimethylsilyl)oxy)-2-((S)-1-(4-chlorophenyl)-3-ethoxy-1-hydroxy-3-oxopropyl)pyrrolidine-1-carboxylate (**3f**) and tert-butyl (2S,4R)-4-((tert-butyldimethylsilyl)oxy)-2-((R)-1-(4-chlorophenyl)-3-ethoxy-1-hydroxy-3-oxopropyl)pyrrolidine-1-carboxylate (**4f**).* Prepared according to general procedure B starting from *tert*-butyl (2*S*,4*R*)-2-benzoyl-4-((*tert*-butyldimethylsilyl)oxy)pyrrolidine-1-carboxylate **2f** (0.23 g, 0.52 mmol, 1.0 eq.). Chromatographed over SiO_2 (100% Hexanes to 6:4 Hexanes/EtOAc) to afford **3f** (84 mg, 39%) as a white solid and **4f** (34 mg, 16%) as a white solid (ratio: 2:1). *Diastereomer **3f***: $[\alpha]_D^{25}$ -65.9 (*c* 4.4 g/L, $CHCl_3$). ^{1}H NMR (700 MHz, $CDCl_3$, mixture of rotamers) δ 7.40 – 7.33 (m, 2H), 7.28 (m, 2H), 5.33 – 4.55 (m, 1H), 4.38 (bs, 1H), 3.98 (m, 2H), 3.75 (bs, 1H), 3.40 (m, 1H), 3.15 (m, 1H), 2.91 (m, 1H), 2.72 (bs, 1H), 2.06 (m, 1H), 1.81 (m, 2H), 1.44 (s, 9H), 1.08 (t, *J* = 7.2 Hz, 3H). $^{13}C\{^{1}H\}$ NMR (176 MHz, $CDCl_3$, mixture of rotamers) δ 173.0, 156.7, 140.9, 133.6, 128.2, 128.1, 80.6, 76.8, 70.2, 64.5, 60.9, 56.1, 43.4, 42.8, 36.1, 28.6, 28.5, 14.1. HRMS (ESI-TOF) m/z: [M + Na]+ Calcd for $C_{20}H_{28}ClNO_6Na$ 436.1497; Found 436.1485; [M + K]+ Calcd for $C_{20}H_{28}ClNO_6K$ 452.1237; Found 452.1231. *Diastereomer **4f***: *Rf* = 0.31 (6:4 hexanes/EtOAc). $[\alpha]_D^{25}$ +18.5 (*c* 4.0 g/L, $CHCl_3$). ^{1}H NMR (700 MHz, $CDCl_3$, mixture of rotamers) δ 7.42 – 7.27 (m, 4H), 5.18 – 4.58 (m, 1H), 4.58 – 4.21 (m, 2H), 3.95 (m, 2H), 3.68 (m, 1H), 3.38 (bs, 1H), 3.10 (m, 1H), 2.88 (m, 1H), 2.07 – 1.95 (m, 1H), 1.48 (m, 11H), 1.03 (t, *J* = 7.1 Hz, 3H). $^{13}C\{^{1}H\}$ NMR (176 MHz, $CDCl_3$, mixture of rotamers) δ 173.5, 142.1, 133.2, 128.5, 128.2, 127.3, 80.4, 78.3, 71.2, 70.3, 64.5, 60.9, 56.3, 43.4, 35.5, 28.6, 28.5, 14.0. HRMS (ESI-TOF) m/z: [M + Na]+ Calcd for $C_{20}H_{28}ClNO_6Na$ 436.1497; Found 436.1491; [M + K]+ Calcd for $C_{20}H_{28}ClNO_6K$ 452.1237; Found 452.1237.

*tert-Butyl (1S,3S,4S)-3-(4-chlorophenyl)-3-(2-ethoxy-2-oxoethyl)-2-oxa-5-azabicyclo[2.2.1]heptane-5-carboxylate (**5f**).* Prepared according to general procedure C starting from (2*S*,4*R*)-*tert*-butyl 4-((*tert*-butyldimethylsilyl)oxy)-2-((*S*)-1-(4-chlorophenyl)-3-ethoxy-1-

hydroxy-3-oxopropyl)pyrrolidine-1-carboxylate ***3f*** (10 mg, 25 µmol, 1.0 eq.). Chromatographed over SiO_2 (100% Hexanes to 8:2 Hexanes/EtOAc) to afford **5f** as a colorless oil (3 mg, 31%). $[\alpha]_D^{25}$ -14.29 (*c* 2.8 g/L, MeOH). ^{1}H NMR (500 MHz, $CDCl_3$, mixture of rotamers) δ 7.46 (m, 1H), 7.41 (m, 1H), 7.29 (m, 2H), 4.94 – 4.89 (m, 0.5H), 4.85 (m, 0.5H), 4.82 (m, 0.5H), 4.79 (m, 0.5H), 4.01 – 3.94 (m, 2H), 3.26 (dd, *J* = 10.6, 1.8 Hz, 0.5H), 3.17 (dd, *J* = 10.6, 1.7 Hz, 0.5H), 3.07 (m, 0.5H), 3.03 (m, 0.5H), 2.82 (dd, *J* = 14.2, 2.1 Hz, 1H), 2.68 (dd, *J* = 14.1, 5.0 Hz, 1H), 2.30 (m, 1H), 1.90 (m, 1H), 1.36 (s, 4.5H), 1.19 (s, 4.5H), 1.08 (dt, *J* = 7.1, 5.0 Hz, 3H). $^{13}C\{^1H\}$ NMR (176 MHz, $CDCl_3$, mixture of rotamers) δ 169.2, 169.1, 153.3, 153.2, 140.6, 140.4, 133.0, 132.9, 128.3, 128.0, 127.9, 127.7, 127.6, 127.3, 88.2, 87.8, 80.0, 79.5, 78.3, 77.9, 77.3, 63.3, 62.3, 60.7, 60.7, 52.4, 51.9, 46.7, 46.4, 36.6, 36.2, 28.4, 28.2, 14.1. HRMS (ESI-TOF) m/z: [M + Na]+ Calcd for $C_{20}H_{26}ClNO_5Na$ 418.1392; Found 418.1412.

*tert-Butyl (1S,3R,4S)-3-(4-chlorophenyl)-3-(2-ethoxy-2-oxoethyl)-2-oxa-5-azabicyclo[2.2.1]heptane-5-carboxylate (**6f**).* Prepared according to general procedure C starting from (2*S*,4*R*)-*tert*-butyl 4-((*tert*-butyldimethylsilyl)oxy)-2-((*R*)-1-(4-chlorophenyl)-3-ethoxy-1-hydroxy-3-oxopropyl)pyrrolidine-1-carboxylate **4f** (22 mg, 53 µmol, 1.0 eq.). The residual oil was chromatographed over SiO_2 (8:2 hexanes/EtOAc, Ninhydrin /CAM/ $KMnO_4$) to afford **6f** as a colorless oil (7.4 mg, 35%). $[\alpha]_D^{25}$: + 45.6 (*c* 8.3 g/L, $CHCl_3$). ^{1}H NMR (500 MHz, $CDCl_3$, mixture of rotamers) δ 7.35 – 7.27 (m, 4H), 4.72 (m, 1H), 4.63 – 4.60 (bs, 0.55H), 4.55 (bs, 0.45H), 3.95 – 3.85 (m, 2H), 3.45 – 3.29 (m, 2H), 3.04 (d, *J* = 14.9 Hz, 0.55H), 2.93 (d, *J* = 15.2 Hz, 0.45H), 2.73 (dd, *J* = 26.4, 15.1 Hz, 1H), 1.75 (m, 1H), 1.52 (m, 10H), 0.98 (dt, *J* = 17.6, 7.2 Hz, 3H). $^{13}C\{^1H\}$ NMR (176 MHz, $CDCl_3$, mixture of rotamers) δ 170.1, 169.8, 154.7, 154.4, 141.2, 133.1, 133.1, 128.4, 128.4, 127.1, 127.1, 87.5, 87.2, 80.4, 80.2, 77.9, 77.5, 64.3, 63.5, 60.5, 60.4, 53.9, 53.3, 43.7, 43.6, 35.4, 34.9, 28.6, 28.6, 14.1, 14.0. HRMS (ESI-TOF) m/z: [M + Na]+ Calcd for $C_{20}H_{26}ClNO_5Na$ 418.1392; Found 418.1412.

*tert-Butyl (2S,4R)-4-((tert-butyldimethylsilyl)oxy)-2-(4-methoxybenzoyl)pyrrolidine-1-carboxylate (**2g**).* Prepared according to general procedure A starting from *tert*-butyl (2*S*,4*R*)-4-((*tert*-butyldimethylsilyl)oxy)-2-(methoxy(methyl)carbamoyl)pyrrolidine-1-carboxylate **1** (0.95 g, 2.4 mmol, 1.0 eq.) in Et_2O, using (4-methoxyphenyl)magnesium bromide (15 mL, C = 0.5 M, 7.3 mmol, 3.0 eq.). Chromatographed over SiO_2 (100% Hexanes to 98:2 $CHCl_3$/EtOAc) to afford **2g** as a pale-

yellow oil (788 mg, 74%). $[\alpha]^{25}_{D}$: -18.8 (*c* = 0.8, MeOH). ^{1}H NMR (500 MHz, $CDCl_3$, mixture of rotamers) δ 8.00 – 7.91 (m, 2H), 6.96 – 6.89 (m, 2H), 5.40 (dd, *J* = 8.7, 6.1 Hz, 0.4H), 5.32 – 5.22 (dd, *J* = 15.0, 5.1 Hz, 1H), 4.42 (m, 1H), 3.85 (m, 3H), 3.76 – 3.71 (dd, *J* = 10.3, 5.2 Hz, 0.6H), 3.67 (dd, *J* = 10.1, 5.4 Hz, 0.4H), 3.46 (dd, *J* = 11.1, 3.3Hz, 0.6H), 3.39 (dd, *J* = 11.0, 3.7 Hz, 0.4H), 2.26 – 2.16 (m, 1H), 1.97 (m, 1H), 1.44 (s, 4H), 1.22 (s, 5H), 0.87 (m, 9H), 0.07 – 0.02 (m, 6H). ^{13}C{^{1}H} NMR (126 MHz, $CDCl_3$, mixture of rotamers) δ 197.7, 197.1, 163.8, 163.8, 154.7, 153.9, 130.9, 130.6, 128.4, 128.3, 114.0, 113.9, 80.0, 79.8, 70.7, 70.0, 59.7, 59.5, 55.6, 55.1, 54.9, 40.3, 39.4, 28.6, 28.2, 25.9, 25.8, 18.1, 18.0, -4.7, -4.7, -4.8. HRMS (ESI-TOF) m/z: [M + Na]+ Calcd for $C_{23}H_{37}NO_5SiNa$ 458.2333; Found 458.2332; [M + K]+ Calcd for $C_{23}H_{37}NO_5SiK$ 474.2073; Found 474.2079.

*tert-Butyl (2S,4R)-2-((S)-3-ethoxy-1-hydroxy-1-(4-methoxyphenyl)-3-oxopropyl)-4-hydroxypyrrolidine-1-carboxylate (**3g**) and tert-butyl (2S,4R)-2-((R)-3-ethoxy-1-hydroxy-1-(4-methoxyphenyl)-3-oxopropyl)-4-hydroxypyrrolidine-1-carboxylate (**4g**).* Prepared according to general procedure B starting from *tert*-butyl (2*S*,4*R*)-4-((*tert*-butyldimethylsilyl)oxy)-2-(4-methoxybenzoyl)pyrrolidine-1-carboxylate **2g** (98 mg, 0.23 mmol, 1.0 eq.). Chromatographed over SiO_2 (100% Hexanes to 7:3 Hexanes/EtOAc) to afford **3g** (33 mg, 36%) as a colorless oil and **4g** (17 mg, 18%) as a colorless oil (ratio: 2:1). *Diastereomer **3g*** **:** $[\alpha]^{25}_{D}$: -79.1 (*c* = 1.6, $CHCl_3$). ^{1}H NMR (500 MHz, $CDCl_3$, mixture of rotamers) δ 7.37 – 7.31 (m, 2H), 6.92 – 6.76 (m, 2H), 4.37 (bs, 1H), 4.05 – 3.93 (m, 2H), 3.78 (s, 3H), 3.62 (bs, 1H), 3.39 (bs, 1H), 3.17 (bs, 1H), 2.90 (m, 1H), 2.68 (bs, 1H), 2.11 (m, 1H), 1.77 (m, 2H), 1.46 (s, 9H), 1.07 (t, *J* = 7.1 Hz, 3H). ^{13}C{^{1}H} NMR (126 MHz, $CDCl_3$, mixture of rotamers) δ 173.3, 159.0, 156.7, 134.0, 127.8, 113.4, 80.4, 76.6, 70.2, 64.6, 60.7, 56.0, 55.3, 43.3, 36.0, 28.5, 14.1. HRMS (ESI-TOF) m/z: [M + Na]+ Calcd for $C_{21}H_{31}NO_7Na$ 432.1993; Found 432.1971; [M + K]+ Calcd for $C_{21}H_{31}NO_7K$ 448.1732; Found 448.1715. *Diastereomer **4g*** **:** $[\alpha]^{25}_{D}$: +28.6 (*c* = 0.7, $CHCl_3$). ^{1}H NMR (500 MHz, $CDCl_3$, mixture of rotamers) δ 7.32 (m, 2H), 6.84 (d, *J* = 8.8 Hz, 2H), 4.79 (m, 1H), 4.46 (m, 2H), 4.01 – 3.89 (m, 2H), 3.79 (s, 3H), 3.61 (bs, 1H), 3.40 (m, 1H), 3.10 (m, 1H), 2.87 (m, 1H), 2.06 (bs, 1H), 1.51 (m, 10H), 1.02 (t, *J* = 7.1 Hz, 3H). ^{13}C{^{1}H} NMR (126 MHz, $CDCl_3$, mixture of rotamers) δ 173.7, 158.7, 135.4, 126.9, 113.6, 80.2, 78.2, 71.3, 64.7, 60.8, 56.3, 55.3, 43.7, 35.6, 28.6, 14.0. HRMS (ESI-TOF) m/z: [M + Na]+ Calcd for $C_{21}H_{31}NO_7Na$ 432.1993; Found 432.1979.

*tert-Butyl (1S,3S,4S)-3-(2-ethoxy-2-oxoethyl)-3-(4-methoxyphenyl)-2-oxa-5-azabicyclo[2.2.1]heptane-5-carboxylate (**5g**).* Prepared according to general procedure C starting from *tert*-butyl (2*S*,4*R*)-2-((*S*)-3-ethoxy-1-hydroxy-1-(4-methoxyphenyl)-3-oxopropyl)-4-hydroxypyrrolidine-1-carboxylate **3g** (18 mg, 44 µmol, 1.0 eq.). Chromatographed over SiO_2 (100% Hexanes to 6:4 Hexanes/EtOAc) to afford **5g** as a colorless oil (8.0 mg, 47%). $[\alpha]^{25}_{D}$: -8.5 (*c* = 0.2, $CHCl_3$). ^{1}H NMR (500 MHz, $CDCl_3$, mixture of rotamers) δ 7.39 (m, 1H), 7.33 (m, 1H), 6.81 (m, 2H), 4.89 (s, 0.5H), 4.82 (s, 1H), 4.77 (s, 0.5H), 4.74 (s, 0.5H), 3.95 (m, 2H), 3.76 (d, *J* = 5.6 Hz, 3H), 3.22 (dd, *J* = 10.5, 1.8 Hz, 0.5H), 3.13 (dd, *J* = 10.5, 1.8 Hz, 0.5H), 3.06 (d, *J* = 10.8 Hz, 0.5H), 3.02 (d, *J* = 10.7 Hz, 0.5H), 2.79 (dd, *J* = 13.9, 2.2 Hz, 1H), 2.65 (dd, *J* = 13.9, 5.1 Hz, 1H), 2.30 – 2.23 (m, 1H), 1.86 (m, 1H), 1.33 (s, 4.5H), 1.15 (s, 4.5H), 1.05 (dt, *J* = 14.3, 4.7 Hz, 3H). ^{13}C{^{1}H} NMR (126 MHz, $CDCl_3$, mixture of rotamers) δ 169.5, 169.4, 158.7, 153.4, 134.2, 134.0, 127.5, 127.3, 113.2, 112.9, 88.3, 87.9, 79.7, 79.3, 78.1, 77.7, 63.5, 62.4, 60.6, 60.5, 55.4, 52.5, 51.9, 47.1, 46.9, 36.6, 36.2, 28.5, 28.3, 14.1. HRMS (ESI-TOF) m/z: [M + Na]+ Calcd for $C_{21}H_{29}NO_6Na$ 414.1887; Found 414.1890; [M + K]+ Calcd for $C_{21}H_{29}NO_6K$ 430.1627; Found 430.1629.

*tert-Butyl (1S,3R,4S)-3-(2-ethoxy-2-oxoethyl)-3-(4-methoxyphenyl)-2-oxa-5-azabicyclo[2.2.1]heptane-5-carboxylate (**6g**).* Prepared according to general procedure C starting from *tert*-butyl (2*S*,4*R*)-2-((*R*)-3-ethoxy-1-hydroxy-1-(4-methoxyphenyl)-3-oxopropyl)-4-hydroxypyrrolidine-1-carboxylate **4g** (15 mg, 37 µmol, 1.0 eq.). Chromatographed over SiO_2 (100% Hexanes to 75:25, Hexanes/EtOAc) to afford **6g** as an orange oil. (8 mg, 56%) $[\alpha]^{25}_{D}$: +27.0 (*c* = 0.4, $CHCl_3$). ^{1}H NMR (500 MHz, $CDCl_3$, mixture of rotamers) δ 7.31 – 7.19 (m, 2H), 6.85 (m, 2H), 4.71 (m, 1H), 4.621 (bs, 0.5H), 4.54 (bs, 0.5H), 3.93 – 3.84 (m, 2H), 3.78 (m, 3H), 3.45 – 3.27 (m, 2H), 3.04 (d, *J* = 14.7 Hz, 0.5H), 2.94 (d, *J* = 15.0 Hz, 0.5H), 2.74 (d, *J* = 15.0 Hz, 0.5H), 2.69 (d, *J* = 14.8 Hz, 0.5H), 1.84 – 1.78 (m, 1H), 1.62 – 1.56 (m, 1H), 1.54 (s, 4.5H), 1.49 (s, 4.5H), 0.96 (dt, *J* = 16.3, 7.2 Hz, 3H). ^{13}C{^{1}H} NMR (126 MHz, $CDCl_3$, mixture of rotamers) δ 170.4, 170.1, 158.7, 154.7, 154.5, 134.7, 127.8, 126.7, 126.7, 113.6, 113.5, 87.7, 87.4, 80.3, 80.0, 64.4, 63.6, 60.3, 60.3, 55.4, 54.0, 53.4, 44.0, 43.9, 35.4, 34.9, 28.6, 28.6, 14.1, 14.1. HRMS (ESI-TOF) m/z: [M + H]+ Calcd for $C_{21}H_{29}NO_6H$ 392.2068; Found 392.2055; [M + Na]+ Calcd for $C_{21}H_{29}NO_6Na$ 414.1887; Found 414.1873.

*tert-Butyl (2S,4R)-4-((tert-butyldimethylsilyl)oxy)-2-propionylpyrrolidine-1-carboxylate (**2h**).* Prepared according to general procedure A starting from *tert*-butyl (2*S*,4*R*)-4-((*tert*-butyldimethylsilyl)oxy)-2-(methoxy(methyl)carbamoyl)pyrrolidine-1-carboxylate **1** (50 mg, 0.13 mmol, 1.0 eq.) in THF, using ethylmagnesium bromide (0.39 mL, C = 1.0 M in THF, 0.39 mmol, 3.0 eq.). Chromatographed over SiO_2 (100% Hexanes to 85:15 Hexanes/EtOAc) to afford **2h** as a colorless oil (34 mg, 73%). $[\alpha]^{25}_D$: -44.5(*c* = 0.9, $CHCl_3$). ^1H NMR (500 MHz, $CDCl_3$, mixture of rotamers) δ 4.48 (t, *J* = 7.7 Hz, 0.4H), 4.41 – 4.32 (m, 1.6H), 3.58 – 3.47 (m, 1.6H), 3.35 (ddd, *J* = 11.1, 3.1, 1.5 Hz, 0.4H), 2.60 – 2.39 (m, 2H), 2.14 – 2.01 (m, 1H), 1.82 (m, 1H), 1.44 (s, 4H), 1.39 (s, 5H), 1.06 (m, 3H), 0.86 (s, 9H), 0.05 (s, 6H). $^{13}C\{^1H\}$ NMR (126 MHz, $CDCl_3$, mixture of rotamers) δ 210.9, 210.9, 155.0, 154.2, 80.4, 80.1, 70.6, 69.9, 64.0, 63.3, 55.4, 55.3, 39.4, 38.3, 32.9, 31.7, 28.6, 28.4, 25.8, 18.1, 18.1, 7.6, 7.5, -4.6, -4.7, -4.7. HRMS (ESI-TOF) m/z: [M + Na]+ Calcd for $C_{18}H_{35}NO_4SiNa$ 380.2238; Found 380.2246; [M + K]+ Calcd for $C_{18}H_{35}NO_4SiK$ 396.1967; Found 396.1981.

*tert-Butyl (2S,4R)-2-((R)-1-ethoxy-3-hydroxy-1-oxopentan-3-yl)-4-hydroxypyrrolidine-1-carboxylate (**3h**).* Prepared according to general procedure B starting from *tert*-butyl (2*S*,4*R*)-4-((*tert*-butyldimethylsilyl)oxy)-2-propionylpyrrolidine-1-carboxylate **2h** (0.43 g, 1.2 mmol, 1.0 eq.). Chromatographed over SiO_2 (100% Hexanes to 5:5 Hexanes/EtOAc) to afford **3h** as a pale-yellow oil (358 mg, 90% over 2 steps). $[\alpha]^{25}_D$: -48.6 (*c* = 1.9, MeOH). ^1H NMR (500 MHz, $CDCl_3$) δ 4.32 (m, 1H), 4.24 (t, *J* = 8.4 Hz, 1H), 4.14 – 4.06 (m, 2H), 3.74 (d, *J* = 11.8 Hz, 1H), 3.27 (dd, *J* = 12.2, 3.0 Hz, 1H), 2.42 (d, *J* = 13.9 Hz, 1H), 2.33 (d, *J* = 13.9 Hz, 1H), 2.17 (bs, 1H), 2.05 – 1.99 (m, 1H), 1.85 (m, 1H), 1.70 (m, 1H), 1.46 (m, 10H), 1.24 (t, *J* = 7.1 Hz, 3H), 0.98 (t, *J* = 7.4 Hz, 3H). $^{13}C\{^1H\}$ NMR (126 MHz, $CDCl_3$) δ 172.0, 158.3, 81.2, 76.4, 69.7, 63.8, 60.5, 56.8, 40.4, 37.1, 30.5, 28.5, 14.3, 7.6. HRMS (ESI-TOF) m/z: [M + Na]+ Calcd for $C_{16}H_{29}NO_6Na$ 354.1887; Found 354.1896; [M + K]+ Calcd for $C_{16}H_{29}NO_6K$ 370.1626; Found 370.1632.

*tert-Butyl (1S,3R,4S)-3-(2-ethoxy-2-oxoethyl)-3-ethyl-2-oxa-5-azabicyclo[2.2.1]heptane-5-carboxylate (**5h**).* Prepared according to general procedure C starting from *tert*-butyl (2*S*,4*R*)-2-(1-ethoxy-3-hydroxy-1-oxopentan-3-yl)-4-hydroxypyrrolidine-1-carboxylate **3h** (59 mg, 0.18 mmol, 1.0 eq.). Chromatographed over SiO_2 (100% Hexanes to 7:3 Hexanes/EtOAc) to afford **5h** as a light-orange oil (35 mg, 63%). $[\alpha]^{25}_D$: +3.3 (*c* = 1.2, MeOH). ^1H NMR (500 MHz, $CDCl_3$, mixture of

rotamers) δ 4.55 – 4.46 (m, 2H), 4.13 (m, 2H), 3.28 (dd, *J* = 10.6, 1.6 Hz, 0.6H), 3.23 (dd, *J* = 10.5, 1.5 Hz, 0.4H), 3.12 (m, 1H), 2.54 – 2.33 (m, 2H), 2.16 (d, *J* = 10.3 Hz, 1H), 1.82 – 1.66 (m, 2H), 1.59 (m, 1H), 1.45 (m, 9H), 1.30 – 1.22 (m, 3H), 0.97 (m, 3H). $^{13}C\{^{1}H\}$ NMR (126 MHz, $CDCl_3$, mixture of rotamers) δ 170.0, 169.8, 154.4, 154.2, 86.8, 86.4, 79.9, 79.6, 76.8, 62.0, 60.9, 60.6, 53.5, 52.8, 41.1, 41.0, 36.5, 36.1, 35.8, 28.6, 28.5, 28.4, 28.1, 27.7, 14.3, 13.9, 9.1, 9.0. HRMS (ESI-TOF) m/z: [M + Na]+ Calcd for $C_{16}H_{27}NO_5Na$ 336.1781; Found 336.1777; [M + K]+ Calcd for $C_{16}H_{27}NO_5K$ 352.1521; Found 352.1514.

*tert-Butyl (2S,4R)-4-((tert-butyldimethylsilyl)oxy)-2-(3-methylbutanoyl)pyrrolidine-1-carboxylate (**2i**).* Prepared according to general procedure A starting from *tert*-butyl (2*S*,4*R*)-4-((*tert*-butyldimethylsilyl)oxy)-2-(methoxy(methyl)carbamoyl)pyrrolidine-1-carboxylate **1** (0.51 g, 1.3 mmol, 1.0 eq.) in Et_2O, using *iso*-butylmagnesium bromide (2.0 mL, C = 2.0 M in Et_2O, 4.0 mmol, 3.0 eq.). Chromatographed over SiO_2 (100% Hexanes to 85:15 Hexanes/EtOAc) to afford **2i** as a colorless oil (135 mg, 27%). $[\alpha]^{25}_D$: -36.0 (*c* = 0.3, $CHCl_3$). ^{1}H NMR (500 MHz, $CDCl_3$, mixture of rotamers) δ 4.46 (t, *J* = 7.6 Hz, 0.45H), 4.38 – 4.31 (m, 1.55H), 3.58 – 3.49 (m, 1.55H), 3.35 (m, 0.45H), 2.42 (dd, *J* = 17.0, 6.6 Hz, 0.45H), 2.38 – 2.29 (m, 1.55H), 2.24 – 2.01 (m, 2H), 1.89 – 1.78 (m, 1H), 1.45 (s, 4H), 1.41 (s, 5H), 0.91 (m, 6H), 0.86 (m, 9H), 0.05 (m, 6H). $^{13}C\{^{1}H\}$ NMR (126 MHz, $CDCl_3$, mixture of rotamers) δ 209.6, 154.9, 154.4, 80.4, 80.0, 70.6, 69.8, 64.4, 63.7, 55.3, 55.3, 48.6, 47.4, 39.0, 37.8, 28.6, 28.5, 25.9, 25.8, 25.6, 23.8, 23.6, 22.9, 22.8, 22.7, 22.7, 18.1, -4.6, -4.7, -4.7. HRMS (ESI-TOF) m/z: [M + Na]+ Calcd for $C_{20}H_{39}NO_4SiNa$ 408.2541; Found 408.2536.

*tert-Butyl (2S,4R)-2-((R)-1-ethoxy-3-hydroxy-5-methyl-1-oxohexan-3-yl)-4-hydroxypyrrolidine-1-carboxylate (**3i**).* Prepared according to general procedure B starting from *tert*-butyl (2*S*,4*R*)-4-((*tert*-butyldimethylsilyl)oxy)-2-(3-methylbutanoyl)pyrrolidine-1-carboxylate **2i** (115 mg, 0.30 mmol, 1.0 eq.). Chromatographed over SiO_2 (100% Hexanes to 6:4 Hexanes/EtOAc) to afford **3i** as a pale-yellow oil (85 mg, 79%). $[\alpha]^{25}_D$: -62.2 (*c* = 0.6, $CHCl_3$). ^{1}H NMR (500 MHz, $CDCl_3$) δ 4.34 – 4.27 (m, 2H), 4.08 (m, 2H), 3.71 (m, 1H), 3.28 – 3.20 (m, 1H), 2.52 (bs, 1H), 2.40 (d, *J* = 14.0 Hz, 1H), 2.32 (d, *J* = 14.0 Hz, 1H), 2.02 (ddt, *J* = 13.9, 7.9, 2.1 Hz, 1H), 1.93 – 1.77 (m, 2H), 1.52 (dd, *J* = 14.4, 6.8 Hz, 1H), 1.43 (s, 9H), 1.33 – 1.27 (dd, *J* = 15.3, 5.4 Hz, 1H), 1.22 (t, *J* = 7.1 Hz, 3H), 0.99 (d, *J* = 6.6 Hz, 3H), 0.91 (d, *J* = 6.6 Hz, 3H). $^{13}C\{^{1}H\}$ NMR (126 MHz, $CDCl_3$) δ 171.9, 158.3, 81.2, 77.3, 76.5, 69.6, 64.4, 60.4, 56.8, 46.0, 41.1, 37.2, 28.5, 28.4, 25.2, 24.8, 23.9, 14.3, 14.2. HRMS (ESI-

TOF) m/z: [M + Na]+ Calcd for $C_{18}H_{33}NO_6Na$ 382.2200; Found 382.2181; [M + K]+ Calcd for $C_{18}H_{33}NO_6K$ 398.1940; Found 398.1924.

*tert-Butyl (1S,3R,4S)-3-(2-ethoxy-2-oxoethyl)-3-isobutyl-2-oxa-5-azabicyclo[2.2.1]heptane-5-carboxylate (**5i**).* Prepared according to general procedure C starting from *tert*-butyl (2*S*,4*R*)-2-((*R*)-1-ethoxy-3-hydroxy-5-methyl-1-oxohexan-3-yl)-4-hydroxypyrrolidine-1-carboxylate **3i** (36 mg, 0.10 mmol, 1.0 eq.). Chromatographed over SiO_2 (100% Hexanes to 8:2 Hexanes/EtOAc) to afford **5i** as a colorless oil (22 mg, 65%). $[\alpha]^{25}_D$: +14.1 (*c* = 0.9, $CHCl_3$). ^{1}H NMR (500 MHz, $CDCl_3$, mixture of rotamers) δ 4.64 – 4.60 (bs, 0.35H), 4.59 – 4.56 (bs, 0.65H), 4.47 (m, 1H), 4.17 – 4.08 (m, 2H), 3.28 (dd, *J* = 10.5, 1.7 Hz, 0.65H), 3.23 (dd, *J* = 10.5, 1.7 Hz, 0.35H), 3.15 (dd, *J* = 10.5, 1.4 Hz, 0.65H), 3.11 (d, *J* = 10.5 Hz, 0.35H), 2.64 (d, *J* = 15.0 Hz, 0.65H), 2.59 (d, *J* = 14.6 Hz, 0.35H), 2.44 (dd, *J* = 14.5, 1.2 Hz, 0.35H), 2.40 (dd, *J* = 15.0, 1.5 Hz, 0.65H), 2.15 – 2.05 (m, 1H), 1.85 (m, 1H), 1.77 – 1.63 (m, 2H), 1.46 (m, 9H), 1.41 – 1.31 (m, 0.35H), 1.29 – 1.24 (m, 3.65H), 0.95 (m, 3H), 0.90 (d, *J* = 6.7 Hz, 3H). ^{13}C{^{1}H} NMR (126 MHz, $CDCl_3$, mixture of rotamers) δ 170.0, 169.8, 154.7, 154.4, 86.2, 85.9, 79.8, 79.5, 76.8, 63.1, 62.1, 60.7, 60.6, 53.5, 52.8, 43.3, 43.2, 41.8, 41.5, 35.5, 35.4, 28.6, 28.6, 24.9, 24.9, 24.8, 24.7, 23.8, 23.4, 14.4. HRMS (ESI-TOF) m/z: [M + Na]+ Calcd for $C_{18}H_{31}NO_5Na$ 364.2094; Found 364.2090; [M + K]+ Calcd for $C_{18}H_{31}NO_5K$ 380.1834; Found 380.1828.

*tert-Butyl (2S,4R)-4-((tert-butyldimethylsilyl)oxy)-2-(thiophene-2-carbonyl)pyrrolidine-1-carboxylate (**2j**).* Prepared according to general procedure A starting from *tert*-butyl (2*S*,4*R*)-4-((*tert*-butyldimethylsilyl)oxy)-2-(methoxy(methyl)carbamoyl)pyrrolidine-1-carboxylate **1** (100 mg, 0.26 mmol, 1.0 eq.) in THF, using thiophen-2-ylmagnesium bromide (1.3 mL, 1.0 M in THF, 1.3 mmol, 5.0 eq.). Chromatographed over SiO_2 (100% Hexanes to 85:15 Hexanes/EtOAc) to afford **2j** as a brown oil (57 mg, 54%). $[\alpha]^{25}_D$: -7.2 (*c* = 2.8, $CHCl_3$). ^{1}H NMR (500 MHz, $CDCl_3$, mixture of rotamers) δ 7.82 (dd, *J* = 3.8, 1.2 Hz, 0.35H), 7.78 (dd, *J* = 3.8, 1.1 Hz, 0.65H), 7.64 (m, 1H), 7.13 (m, 1H), 5.20 (dd, *J* = 8.3, 6.7 Hz, 0.35H), 5.00 (t, *J* = 7.9 Hz, 0.65H), 4.45 (m, 1H), 3.72 (dd, *J* = 11.3, 4.5 Hz, 0.65H), 3.66 (dd, *J* = 11.0, 4.9 Hz, 0.35H), 3.51 (dt, *J* = 11.3, 2.5 Hz, 0.65H), 3.40 (ddd, *J* = 11.1, 3.4, 1.3 Hz, 0.35H), 2.23 (m, 1H), 2.09 – 1.97 (m, 1H), 1.43 (s, 3H), 1.22 (s, 6H), 0.87 (m, 9H), 0.06 (m, 6H). ^{13}C{^{1}H} NMR (126 MHz, $CDCl_3$, mixture of rotamers) δ 192.5, 191.9, 154.7, 154.0, 141.5, 141.0, 134.1, 133.9, 132.6, 132.2, 128.2, 80.5, 80.1, 70.7, 70.1, 62.0, 61.1, 55.3, 55.3, 40.6,

39.7, 28.5, 28.1, 25.9, 25.8, 18.1, 18.1, -4.6, -4.7, -4.7. HRMS (ESI-TOF) m/z: [M + Na]+ Calcd for $C_{20}H_{33}NO_4SSiNa$ 434.1792; Found 434.1773; [M + K]+ Calcd for $C_{20}H_{33}NO_4SSiK$ 450.1531; Found 450.1513.

*tert-Butyl (2S,4R)-2-((R)-3-ethoxy-1-hydroxy-3-oxo-1-(thiophen-2-yl)propyl)-4-hydroxypyrrolidine-1-carboxylate (**3j**) and tert-butyl (2S,4R)-2-((S)-3-ethoxy-1-hydroxy-3-oxo-1-(thiophen-2-yl)propyl)-4-hydroxypyrrolidine-1-carboxylate (**4j**).* Prepared according to general procedure B starting from *tert*-butyl (2*S*,4*R*)-4-((*tert*-butyldimethylsilyl)oxy)-2-(thiophene-2-carbonyl)pyrrolidine-1-carboxylate **2j** (122 mg, 300 µmol, 1.0 eq.). Chromatographed over SiO_2 (100% Hexanes to 6:4 Hexanes/EtOAc) to afford an inseparable mixture of **3j** (58 mg, 51% over 2 steps) and **4j** (19 mg, 17% over 2 steps) (3:1) as a brown oil. ^{1}H NMR (500 MHz, $CDCl_3$, mixture of isomers and rotamers) δ 7.22 (dd, *J* = 5.0, 1.2 Hz, 0.75H), 7.19 (dd, *J* = 5.0, 1.2 Hz, 0.25H), 6.93 (m, 1H), 6.89 (m, 1H), 6.12 – 4.85 (m, 1H), 4.45 (m, 1H), 4.04 (m, 2H), 3.75 (bs, 1H), 3.52 (m, 1H), 3.25 – 2.70 (m, 3H), 2.24 (m, 1H), 1.86 (m, 2H), 1.47 (m, 9H), 1.11 (m, 3H). ^{13}C{^{1}H} NMR (126 MHz, $CDCl_3$, mixture of isomers and rotamers) δ 172.9, 157.0, 148.7, 147.0, 126.9, 125.4, 124.8, 124.6, 123.5, 80.6, 70.9, 70.1, 64.7, 60.9, 56.3, 44.5, 36.1, 28.5, 28.5, 14.1. HRMS (ESI-TOF) m/z: [M + Na]+ Calcd for $C_{18}H_{27}NO_6SNa$ 408.1451; Found 408.1445; [M + K]+ Calcd for $C_{18}H_{27}NO_6SK$ 424.1191; Found 424.1185.

*tert-Butyl (1S,3R,4S)-3-(2-ethoxy-2-oxoethyl)-3-(thiophen-2-yl)-2-oxa-5-azabicyclo[2.2.1]heptane-5-carboxylate (**5j**) and (1S,3S,4S)-tert-butyl 3-(2-ethoxy-2-oxoethyl)-3-(thiophen-2-yl)-2-oxa-5-azabicyclo[2.2.1]heptane-5-carboxylate (**6j**).* Prepared according to general procedure C starting from *tert*-butyl (2*S*,4*R*)-2-((*R*)-3-ethoxy-1-hydroxy-3-oxo-1-(thiophen-2-yl)propyl)-4-hydroxypyrrolidine-1-carboxylate **3j**/**4j** (32 mg, 83 µmol, 1.0 eq.). Chromatographed over SiO_2 (100% Hexanes to 7:3 Hexanes/EtOAc) to afford **5j** (4.5 mg, 15%) and **6j** (1.5 mg, 5%) (3:1) as a yellow oil. ^{1}H NMR (500 MHz, $CDCl_3$, mixture of rotamers and isomers) δ 7.15 (m, 0.6H), 7.11 (dd, *J* = 5.0, 1.2 Hz, 0.4H), 6.98 (dd, *J* = 3.6, 1.2 Hz, 0.4H), 6.95 – 6.90 (m, 1.4H), 6.87 – 6.86 (m, 0.2H), 4.89 (m, 1H), 4.75 (m, 1H), 4.08 – 3.99 (m, 2H), 3.38 – 3.15 (m, 2H), 2.87 – 2.71 (m, 2H), 2.31 – 2.23 (m, 1H), 1.92 (m, 1H), 1.31 (s, 4.2H), 1.25 (s, 1.4H), 1.21 (s, 3.4H), 1.12 (dt, *J* = 10.2, 7.1 Hz, 3H). ^{13}C{^{1}H} NMR (126 MHz, $CDCl_3$, mixture of rotamers and isomers) δ 169.1, 168.9, 153.4, 146.3, 146.0, 129.7, 127.7, 127.1, 127.0, 126.8, 124.2, 124.1, 123.8, 123.5,

87.4, 87.0, 79.7, 79.4, 78.5, 78.3, 78.0, 66.0, 63.9, 62.8, 60.9, 60.8, 60.8, 54.0, 52.8, 52.3, 47.0, 47.0, 36.8, 36.4, 36.0, 29.8, 28.4, 28.3, 14.2. HRMS (ESI-TOF) m/z: [M + Na]+ Calcd for $C_{18}H_{25}NO_5SNa$ 390.1346; Found 390.1355; [M + K]+ Calcd for $C_{18}H_{25}NO_5SK$ 406.1085; Found 406.1092.

*tert-Butyl (2S,4R)-4-((tert-butyldimethylsilyl)oxy)-2-nicotinoylpyrrolidine-1-carboxylate (**2k**).* To a 2-neck round-bottomed flask equipped with a low temperature thermometer was dissolved 3-bromopyridine (483 µL, d = 1.64, 5.0 mmol, 4.0 eq.) in Et_2O (6.7 mL). The solution was cooled to -78 °C and *n*-BuLi (2.0 mL, C = 2.5 M in Hexane, 5.0 mmol, 4.0 eq.) was added dropwise. The mixture was stirred at -78 °C for 1h (turned into a milky solution) and *tert*-butyl (2*S*,4*R*)-4-((*tert*-butyldimethylsilyl)oxy)-2-(methoxy(methyl)carbamoyl)pyrrolidine-1-carboxylate **1** (0.49 g, 1.3 mmol, 1.0 eq.) in Et_2O (2.5 mL) was added dropwise. Stirred at -78 °C for 3h then allowed to reach rt and kept stirred for 15 min. MeOH was added (solution turned clear) followed by H_2O and Et_2O. The aqueous layer was extracted with Et_2O (x3). The organic layers were collected, washed with distilled water (x1) brine (x1), dried over Na_2SO_4, filtered and concentrated under reduced pressure. Chromatographed over SiO_2 (100% Hexanes to 7:3 Hexanes/EtOAc) to afford **2k** as a pale-yellow oil (260 mg, 51%). $[\alpha]^{25}_D$: -12.1 (*c* = 0.7, $CHCl_3$). ^{1}H NMR (500 MHz, $CDCl_3$, mixture of rotamers) δ 9.16 (ddd, *J* = 6.7, 2.3, 0.9 Hz, 1H), 8.78 (dd, *J* = 4.8, 1.7 Hz, 0.5H), 8.74 (dd, *J* = 4.8, 1.7 Hz, 0.5H), 8.25 (dt, *J* = 8.0, 2.0 Hz, 0.5H), 8.21 (dt, *J* = 8.0, 2.0 Hz, 0.5H), 7.42 (ddd, *J* = 7.9, 4.8, 0.9 Hz, 0.5H), 7.39 (ddd, *J* = 8.0, 4.8, 0.9 Hz, 0.5H), 5.40 – 5.31 (m, 0.5H), 5.24 (m, 0.5H), 4.48 – 4.34 (m, 1H), 3.70 (dd, *J* = 11.2, 4.7 Hz, 0.5H), 3.64 (dd, *J* = 11.1, 4.8 Hz, 0.5H), 3.50 (m, 0.5H), 3.40 (ddd, *J* = 11.1, 3.3, 1.3 Hz, 0.5H), 2.28 – 2.18 (m, 1H), 1.96 (dddd, *J* = 19.8, 12.5, 7.3, 4.9 Hz, 1H), 1.41 (s, 4.5H), 1.20 (s, 4.5H), 0.85 (s, 9H), 0.04 (m, 6H). ^{13}C{^{1}H} NMR (126 MHz, $CDCl_3$, mixture of rotamers) δ 198.4, 198.1, 154.7, 153.9, 153.7, 153.7, 149.8, 149.6, 136.0, 135.6, 130.9, 130.9, 123.9, 123.8, 80.4, 80.2, 70.7, 70.0, 60.4, 60.0, 55.2, 55.0, 40.1, 39.1, 28.5, 28.2, 25.8, 25.8, 18.1, 18.0, -4.7, -4.7, -4.8. HRMS (ESI-TOF) m/z: [M + H]+ Calcd for $C_{21}H_{34}N_2O_4SiH$ 407.2361; Found 407.2349; [M + Na]+ Calcd for $C_{21}H_{34}N_2O_4SiNa$ 429.2180; Found 429.2183.

*tert-Butyl (2S,4R)-2-((S)-3-ethoxy-1-hydroxy-3-oxo-1-(pyridin-3-yl)propyl)-4-hydroxypyrrolidine-1-carboxylate (**3k**) and tert-butyl (2S,4R)-2-((R)-3-ethoxy-1-hydroxy-3-oxo-1-(pyridin-3-yl)propyl)-4-hydroxypyrrolidine-1-carboxylate (**4k**).* Prepared according to general procedure B starting from

tert-butyl (2*S*,4*R*)-4-((*tert*-butyldimethylsilyl)oxy)-2-nicotinoylpyrrolidine-1-carboxylate **2k** (100 mg, 0.25 mmol, 1.0 eq.). Chromatographed over SiO_2 (100% Hexanes to 100% EtOAc) to afford an inseparable mixture of **3k** (49 mg, 52%) and **4k** (16 mg, 17%) (3:1) as a white foam (65 mg, 69% over 2 steps). ^{1}H NMR (500 MHz, $CDCl_3$, mixture of isomers and rotamers) δ 8.61 (m, 1H), 8.42 (m, 1H), 7.79 (d, *J* = 8.0 Hz, 0.75H), 7.74 (d, *J* = 8.0 Hz, 0.25H), 7.23 (dd, *J* = 8.0, 4.8 Hz, 1H), 4.37 (m, 1H), 4.05 – 3.87 (m, 2H), 3.71 (bs, 1H), 3.50 (m, 1H), 3.31 – 3.03 (m, 2H), 2.92 (m, 1H), 2.85 – 2.64 (m, 1H), 2.14 – 1.72 (m, 2H), 1.46 (bs, 2.25H) 1.39 (s, 6.75H), 1.05 (t, *J* = 7.1 Hz, 2.25H), 0.99 (t, *J* = 7.1 Hz, 0.75H). ^{13}C{^{1}H} NMR (126 MHz, $CDCl_3$, mixture of isomers and rotamers) δ 172.9, 172.6, 156.9, 148.3, 147.8, 147.3, 139.0, 138.2, 134.7, 134.0, 123.2, 123.0, 80.6, 76.2, 70.4, 69.7, 64.6, 60.9, 56.2, 43.2, 42.1, 36.2, 35.6, 28.5, 28.4, 14.0, 13.9. HRMS (ESI-TOF) m/z: [M + H]+ Calcd for $C_{19}H_{28}N_2O_6H$ 381.2020; Found 381.2034.

*tert-Butyl (1S,3S,4S)-3-(2-ethoxy-2-oxoethyl)-3-(pyridin-3-yl)-2-oxa-5-azabicyclo[2.2.1]heptane-5-carboxylate (**5k**) and tert-butyl (1S,3R,4S)-3-(2-ethoxy-2-oxoethyl)-3-(pyridin-3-yl)-2-oxa-5-azabicyclo[2.2.1]heptane-5-carboxylate (**6k**).* Prepared according to general procedure C starting from *tert*-butyl (2*S*,4*R*)-2-((*S*)-3-ethoxy-1-hydroxy-3-oxo-1-(pyridin-3-yl)propyl)-4-hydroxypyrrolidine-1-carboxylate **3k**/**4k** (27 mg, 71 µmol, 1.0 eq.). Chromatographed over SiO_2 (100% Hexanes to 2:8 Hexanes/EtOAc) to afford a mixture of **5k** (10.5 mg, 41%) as a colorless oil and **6k** (3.5 mg, 13%) (3:1) as a colorless oil. The isomers were separated by preparative HPLC (Sunfire C18, 19 x 100mm, 5um; 21.6 ml/min; H_2O (+0.1% Formic acid)/MeOH 20% to 80%). $[\alpha]^{25}_D$: -22.0 (*c* = 5.0, MeOH). *Diastereomer **5k*** : ^{1}H NMR (700 MHz, $CDCl_3$, mixture of rotamers) δ 8.81 (bs, 0.5H), 8.65 (bs, 0.5H), 8.48 (bs, 1H), 7.87 (m, 0.5H), 7.80 (m, 0.5H), 7.23 (m, 1H), 4.97 – 4.92 (m, 0.5H), 4.92 – 4.88 (m, 0.5H), 4.81 (m, 1H), 3.95 (m, 2H), 3.25 (dd, *J* = 10.7, 1.7 Hz, 0.5H), 3.17 (dd, *J* = 10.6, 1.7 Hz, 0.5H), 3.04 (m, 1H), 2.85 – 2.79 (m, 1H), 2.69 (dd, *J* = 14.3, 8.9 Hz, 1H), 2.33 – 2.25 (m, 1H), 1.91 (m, 1H), 1.33 (s, 4.5H), 1.14 (s, 4.5H), 1.04 (dt, *J* = 8.6, 7.2 Hz, 3H). ^{13}C{^{1}H} NMR (176 MHz, $CDCl_3$, mixture of rotamers) δ 168.9, 168.8, 163.7, 153.3, 153.1, 148.2, 147.7, 138.1, 137.6, 134.7, 134.3, 122.9, 122.4, 87.5, 86.9, 80.4, 79.7, 78.4, 77.9, 77.4, 63.2, 62.1, 60.8, 60.8, 52.6, 52.1, 46.6, 46.4, 36.4, 35.9, 29.8, 28.4, 28.3, 28.2, 28.2, 14.1. HRMS (ESI-TOF) m/z: [M + H]+ Calcd for $C_{19}H_{26}N_2O_5H$ 363.1915; Found 363.1929. *Diastereomer **6k*** : $[\alpha]^{25}_D$: +76.0 (*c* = 1.0, MeOH). ^{1}H NMR (700 MHz, $CDCl_3$, mixture of rotamers) δ 8.63 (m, 1H), 8.50 (bs, 1H), 7.73 (m,

1H), 7.28 (bs, 1H), 4.75 (m, 1H), 4.69 (bs, 0.5H), 4.63 (bs, 0.5H), 3.90 (m, 2H), 3.45 – 3.32 (m, 2H), 3.06 (d, *J* = 15.1 Hz, 0.5H), 2.97 (d, *J* = 15.5 Hz, 0.5H), 2.81 (d, *J* = 15.5 Hz, 0.5H), 2.76 (d, *J* = 15.2 Hz, 0.5H), 1.75 (m, 1H), 1.66 (m, 1H), 1.54 (s, 4.5H), 1.50 (s, 4.5H), 1.00 (t, *J* = 7.1 Hz, 1.5H), 0.96 (t, *J* = 7.0 Hz, 1.5H). $^{13}C\{^{1}H\}$ NMR (176 MHz, $CDCl_3$, mixture of rotamers) δ 169.9, 169.6, 154.6, 154.4, 148.6, 147.3, 133.9, 133.6, 86.5, 86.1, 80.6, 80.4, 78.0, 77.6, 64.1, 63.2, 60.6, 60.6, 54.0, 53.4, 43.7, 43.6, 35.5, 35.1, 28.6, 28.6, 14.1, 14.0. HRMS (ESI-TOF) m/z: [M + H]+ Calcd for $C_{19}H_{26}N_2O_5H$ 363.1915; Found 363.1927.

(1S,3R,4S)-3-(carboxymethyl)-3-(4-chlorophenyl)-2-oxa-5-azabicyclo[2.2.1]heptan-5-ium ***7f****.* A solution of *tert*-Butyl (1S,3R,4S)-3-(4-chlorophenyl)-3-(2-ethoxy-2-oxoethyl)-2-oxa-5-azabicyclo[2.2.1]heptane-5-carboxylate **6f** (34 mg, 87 µmol, 1.0 eq.) in EtOH/H_2O (1:1, 580 µL) was treated with solid LiOH (12.2 mg, 511 µmol, 5.9 eq.) and stirred vigorously overnight. The mixture was diluted with water, washed with dichloromethane and the organic layer was discarded. The aqueous layer was acidified to pH = 4 using an aqueous solution of HCl (1 M). The aqueous layer was extracted with dichloromethane twice. The organic layers were combined, dried over Na_2SO_4, filtered, and evaporated under reduced pressure to give the crude carboxylic acid which was dissolved in a solution of HCl in dioxane (84.3 µL, C = 4.0 mol/L, 0.34 mmol, 8.0 eq.) and stirred for 24h. The reaction mixture was concentrated under reduced pressure and two additional cycles of evaporation were performed in water to afford **7f** as a light-yellow amorphous powder (3.8 mg, 34%). A small amount of the zwitterion **7f'** was obtained by elution on a Dowex 50WX8 column (mesh 200). Crystals of both HCl salt **7f** and zwitterion **7f'** were obtained after slow evaporation in EtOH. $[\alpha]^{25}_{D}$: + 8.9 (c= 6.1, MeOH). ^{1}H NMR (500 MHz, D_2O) δ 7.47 – 7.40 (m, 2H), 7.39 – 7.32 (m, 2H), 4.96 (m, 1H), 4.79 (m, 1H), 3.61 – 3.54 (m, 1H), 3.43 (m, 1H), 3.16 (dd, *J* = 14.8, 5.4 Hz, 1H), 2.98 (dd, *J* = 15.2, 5.5 Hz, 1H), 2.15 – 2.06 (m, 1H), 1.89 (m, 1H). $^{13}C\{^{1}H\}$ NMR (126 MHz, D_2O) δ 172.6, 138.9, 133.6, 128.6, 126.4, 83.7, 75.7, 71.5, 70.6, 66.5, 63.7, 60.2, 51.6, 43.1, 34.0. *Persistent impurity from HCl in dioxane was observed by ^{1}H (3.86-3.62 ppm) and ^{13}C (71.5, 70.6, 66.5 and 60.2 ppm) NMR.* HRMS (ESI-TOF) m/z: [M + H]+ Calcd for $C_{13}H_{14}ClNO_3H$ 268.0735; Found 268.0725.

8.5 Partie expérimentale de l'article 4

8.5.1 Synthetic schemes

Schéma 8.9 Synthesis of **9**/**10**.

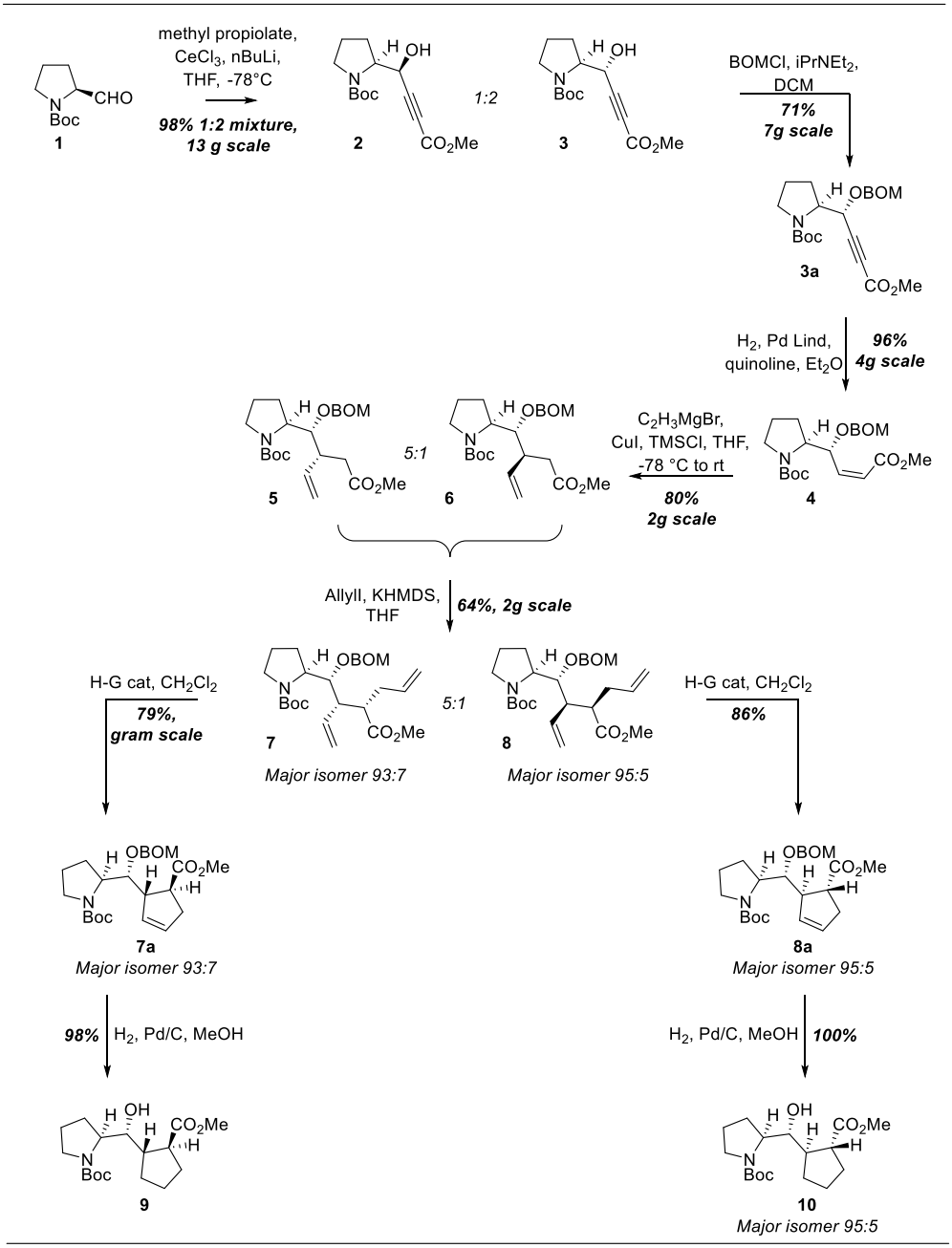

Schéma 8.10 Synthesis of **15**.

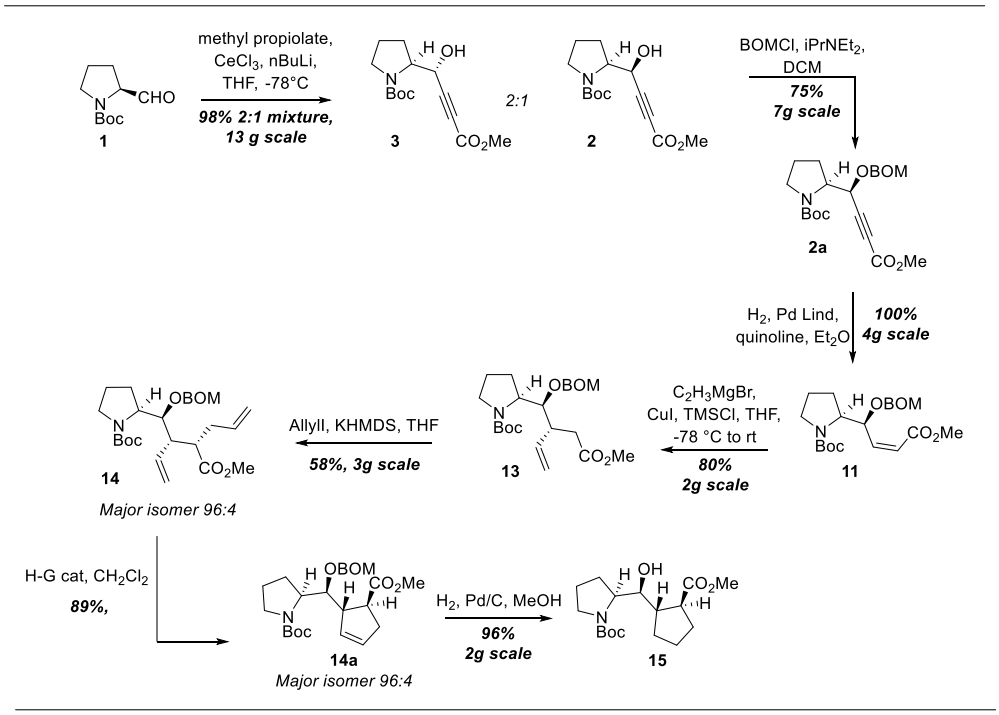

Schéma 8.11 Synthesis of **16**.

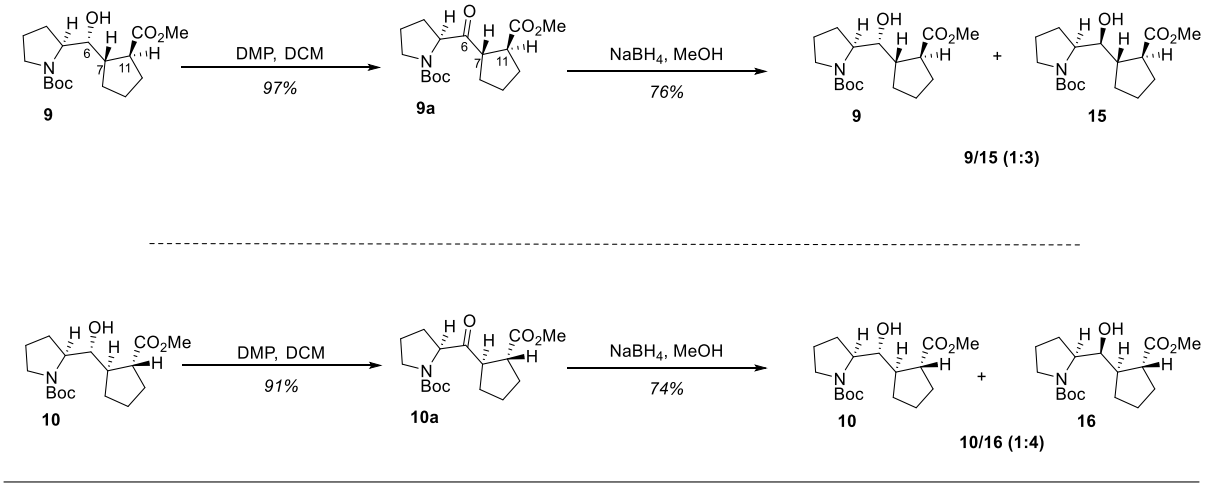

Schéma 8.12 Synthesis of **A**-**D**.

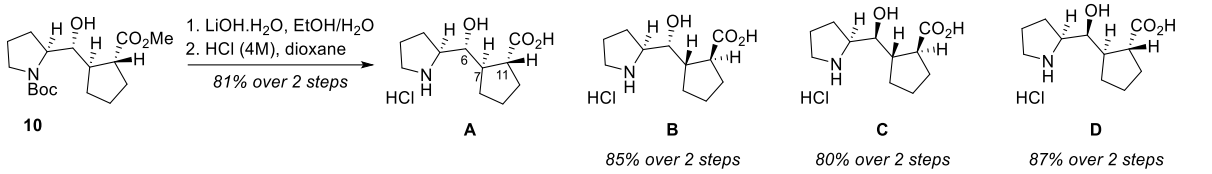

8.5.2 Experimental section

tert-Butyl (S)-2-((S)-1-hydroxy-4-methoxy-4-oxobut-2-yn-1-yl)pyrrolidine-1-carboxylate ***2*** *and tert-butyl (S)-2-((R)-1-hydroxy-4-methoxy-4-oxobut-2-yn-1-yl)pyrrolidine-1-carboxylate* ***3****.*[442]

Anhydrous $CeCl_3$ (24 g, 99 mmol, 1.5 eq.) was added to a 500 mL 1-neck round-bottomed flask and the flask was purged with Ar. THF (198 mL) was added and the white suspension was vigorously stirred at rt for 2h. To another 1L 2-neck round-bottomed flask equipped with a thermometer and purged with Ar was dissolved dry *i*-Pr_2NH (16.7 mL, 119 mmol, 1.8 eq.) in THF (95 mL). The solution was cooled to -78 °C and *n*-BuLi (40 mL, C = 2.5 M in hexanes, 99 mmol, 1.5 eq.) was added dropwise. The solution was stirred at -78 °C for 5 min, at 0 °C for 25 additional min and then cooled back to -78 °C whereby methyl propiolate (10.6 mL, 119 mmol, 1.8 eq.) was added dropwise. The resulting yellow solution was stirred at -78 °C for 30 min. The $CeCl_3$ suspension was cooled to -78 °C and added via a cannula in one portion to the methyl propiolate solution. The resulting orange milky solution was stirred at -78 °C for 1 h. A solution of **1a** (13 g, 66 mmol, 1.0 eq.) in THF (57 mL) was added and the solution was stirred at -78 °C for 30 min whereby TLC analysis (8:2 hexanes/EtOAc, *p*-anisaldehyde) indicated that the reaction had gone to completion. A mixture of glacial acetic acid/THF (1:4, 100 mL) was added dropwise at -78 °C. The suspension was allowed to reach rt and diluted with Et_2O (500 mL). An aqueous citric acid solution (500 mL, 10% w/w) was added, and the aqueous layer was extracted with Et_2O (200 mL). The organic layers were combined, washed with an aqueous citric acid solution (1 x 500 mL, 10% w/w), $NaHCO_3$ sat. aq. sol. (3 x 300 mL), brine (1 x 300 mL), dried over Na_2SO_4, filtered, and concentrated under reduced pressure. The resulting orange oil was chromatographed over silica gel (100% hexanes to 8:2 hexanes/EtOAc, *p*-anisaldehyde/ninhydrin) to deliver **2** and **3** in a 1:2 ratio of diastereomers (**2** = 6.2 g, **3** = 12.3 g, 98%). A small amount of **3** was crystallized by slow

evaporation of Et_2O. *Diastereomer* **2**: *Rf* = 0.25 (75 :25 hexanes/EtOAc). $[\alpha]_D^{25}$ -112 (*c* 0.22 g/L, $CHCl_3$). ^1H NMR ($CDCl_3$, 500 MHz), δ: 5.42 (m, 1H), 4.43 (m, 1H), 4.13 – 4.09 (m, 1H), 3.78 (s, 3H), 3.45 – 3.35 (m, 2H), 2.13 – 2.08 (m, 1H), 1.92 – 1.84 (m, 3H), 1.47 (s, 9H). $^{13}C\{^1H\}$ NMR ($CDCl_3$, 125 MHz), δ: 157.8, 153.9, 86.8, 81.2, 76.5, 67.1, 62.1, 52.9, 47.8, 28.7, 28.5, 24.0. HRMS (ESI) for $C_{14}H_{21}NO_5$ $(M+Na)^+$: Calc: 306.1312; Found: 306.1304. *Diastereomer* **3**: Melting point: 55 °C. *Rf* = 0.27 (75:25 hexanes/EtOAc). $[\alpha]_D^{25}$ -120 (*c* 0.45 g/L, $CHCl_3$). ^1H NMR ($CDCl_3$, 500 MHz), δ: 6.43 (d, *J* = 9.0 Hz, 1H), 4.52 (d, *J* = 8.9 Hz, 1H), 4.10 (m, 1H), 3.76 (s, 3H), 3.56 (m, 1H), 3.36 (m, 1H), 2.17 (m, 1H), 2.00 (m, 1H), 1.78 – 1.72 (m, 2H), 1.48 (s, 9H). $^{13}C\{^1H\}$ NMR ($CDCl_3$, 125 MHz), δ: 157.6, 153.9, 86.4, 81.3, 76.7, 67.5, 63.1, 52.8, 48.5, 29.4, 28.5, 24.0. HRMS (ESI) for $C_{14}H_{21}NO_5$ $(M+Na)^+$: Calc: 306.1312; Found: 306.1311, for $C_{14}H_{21}NO_5$ $(M+K)^+$: Calc: 322.1051; Found: 322.1048.

tert-Butyl (S)-2-((R)-1-((benzyloxy)methoxy)-4-methoxy-4-oxobut-2-yn-1-yl)pyrrolidine-1-carboxylate ***3a***.[646] *(see Schéma 8.8)*

Procedure adapted from ref [646]. An amount of **3** (7.0 g, 25 mmol, 1.0 eq.) was added to a 500 mL 3-neck round-bottomed flask equipped with a thermometer and the flask was purged with Ar. CH_2Cl_2 (123 mL) was added and the solution was cooled to 0 °C. Dry *i*-$PrNEt_2$ (17 mL, 99 mmol, 4.0 eq.) was added followed by BOMCl (15 mL, 70% purity, 74 mmol, 3.0 eq.). The resulting solution was allowed to reach rt after 5 min and then refluxed with an oil bath for 24 h whereby TLC analysis (8:2 hexanes/EtOAc, ninhydrin) indicated that the reaction had gone to completion. DCM (400 mL) was added, and the organic layer was washed with water (1 x 200 mL), brine (1 x 200 mL), dried over Na_2SO_4, filtered and concentrated under reduced pressure. The orange residue was chromatographed over silica gel (100% hexanes to 85:15 hexanes/EtOAc, ninhydrin /$KMnO_4$) to afford **3a** as a colorless oil (7.1 g, 71%). *Rf* = 0.28 (85:15 hexanes/EtOAc). $[\alpha]_D^{25}$ -5.7 (*c* 2.6 g/L, $CHCl_3$). ^1H NMR ($CDCl_3$, 500 MHz, mixture of rotamers), δ: 7.34 – 7.26 (m, 5H), 5.17 (s, 0.4H), 4.92 (s, 0.6H), 4.89 (d, *J* = 7.0 Hz, 1H), 4.70 (d, *J* = 7.0 Hz, 1H), 4.59 (d, *J* = 11.9 Hz, 1H), 4.54 – 4.50 (m, 1H), 4.09 – 4.06 (m, 0.5H), 4.00 – 3.98 (m, 0.5H), 3.77 – 3.74 (m, 3H), 3.53 – 3.49 (m, 0.5H) 3.42 – 3.37 (m, 1.5H), 2.20 (m, 1H), 2.09 – 1.92 (m, 2H), 1.87 – 1.73 (m, 1H), 1.46 – 1.41 (m, 9H). $^{13}C\{^1H\}$ NMR ($CDCl_3$, 125 MHz, mixture of rotamers), δ: 154.5, 154.0, 153.6, 137.4, 137.2, 128.5, 128.5, 128.1, 128.1, 128.0, 127.9, 92.9, 92.8, 85.0, 84.9, 80.2, 79.6, 77.8, 77.7, 69.7, 69.4, 67.2, 66.3,

60.3, 52.9, 52.8, 47.7, 47.4, 28.7, 28.5, 27.3, 26.5, 24.5, 23.8. HRMS (ESI) for $C_{22}H_{29}NO_6$ $(M+Na)^+$: Calc: 426.1887; Found: 426.1883, for $C_{22}H_{29}NO_6$ $(M+K)^+$: Calc: 442.1627; Found: 442.1628.

*tert-Butyl (S)-2-((R,Z)-1-((benzyloxy)methoxy)-4-methoxy-4-oxobut-2-en-1-yl)pyrrolidine-1-carboxylate **4**.*[647]

Procedure adapted from ref [647]. Lindlar catalyst ((Pd on $CaCO_3$), 2.1 g, 5.0% w/w, 1.0 mmol, 0.1 eq.) was added to a 250 mL 1-neck round-bottomed flask and the flask was purged with Ar. Et_2O (50 mL) was added followed by quinoline (0.22 mL, 2.0 mmol, 0.20 eq.) and the resulting grey suspension was stirred at rt for 10 min. A solution of **3a** (4.0 g, 9.9 mmol, 1.0 eq.) in Et_2O (50 mL) was added and the flask was purged with five alternating cycles of vacuum/H_2. The reaction mixture was stirred for 24h under an H_2 atmosphere whereby TLC analysis (8:2 hexanes/EtOAc, CAM) indicated that the reaction had gone to completion. The grey suspension was filtered through a pad of Celite, washed with abundant Et_2O and concentrated under reduced pressure. The residue was dissolved in EtOAc (250 mL) and an aqueous HCl solution (200 mL, C = 0.5 M) was added. The aqueous layer was extracted with EtOAc (3 x 150 mL). The organic layers were collected, washed with water (1 x 150 mL), brine (1 x 150 mL), dried over Na_2SO_4, filtered and concentrated under reduced pressure to afford **4** as an orange oil (3.85 g, 96%). *Rf* = 0.32 (8:2 hexanes/EtOAc). $[\alpha]_D^{25}$ -106.6 (*c* 2.1 g/L, $CHCl_3$). ^1H NMR ($CDCl_3$, 500 MHz, mixture of rotamers), δ: 7.35 – 7.27 (m, 5H), 6.25 – 6.11 (m, 1H), 5.88 (m, 1H), 5.47 – 5.44 (t, *J* = 11.2 Hz, 1H), 4.73 – 4.70 (dd, *J* = 5.2, 14.8 Hz, 2H), 4.64 – 4.56 (dd, *J* = 16.1, 32.8 Hz, 2H), 4.00 - 3.92 (m, 1H), 3.77 – 3.68 (m, 3H), 3.47 - 3.30 (m, 2H), 2.07 – 1.99 (m, 2H), 1.87 – 1.79 (m, 2H), 1.48 – 1.40 (m, 9H). $^{13}C\{^1H\}$ NMR ($CDCl_3$, 125 MHz, mixture of rotamers), δ: 166.3, 165.8, 154.7, 148.6, 147.8, 137.8, 128.5, 128.5, 128.1, 127.9, 127.8, 127.7, 121.9, 121.4, 93.7, 79.9, 79.1, 74.5, 74.1, 69.7, 60.3, 59.7, 59.6, 51.5, 51.4, 46.8, 28.6, 28.0, 27.4, 23.7, 23.0. HRMS (ESI) for $C_{22}H_{31}NO_6$ $(M+H)^+$: Calc: 406.2224; Found: 406.2210, for $C_{22}H_{31}NO_6$ $(M+Na)^+$: Calc: 428.2044; Found: 428.2033.

*tert-Butyl (S)-2-((1R,2R)-1-((benzyloxy)methoxy)-2-(2-methoxy-2-oxoethyl)but-3-en-1-yl)pyrrolidine-1-carboxylate **5** and tert-Butyl (S)-2-((1R,2S)-1-((benzyloxy)methoxy)-2-(2-methoxy-2-oxoethyl)but-3-en-1-yl)pyrrolidine-1-carboxylate **6**.*

CuI (5.6 g, 30 mmol, 6.0 eq.) was added to a 500 mL 2-neck round-bottomed flask equipped with a thermometer and the flask was purged with Ar. THF (99 mL) was added and the resulting

suspension was cooled to -78 °C whereupon vinylmagnesium bromide (59.2 mL, C = 1.00 M in THF, 59.2 mmol, 12.0 eq.) was added slowly (Caution: To ensure the reproducibility of the reaction, vinylmagnesium bromide should be freshly made or coming from recent/new reagent). The resulting milky brown solution was stirred at -78 °C for 30 min then TMSCl (11.3 mL, 88.8 mmol, 18.0 eq.) was added followed by a solution of **4** (2.0 g, 4.9 mmol, 1.0 eq.) in THF (55 mL). The mixture was stirred for 30 min at -78 °C then was allowed to reach 0 °C and stirred for an additional 5 min (turned black). An aqueous NH_4OH (30% w/w in water)/NH_4Cl sat. aq. sol. solution (1:1, 690 mL) was added dropwise and the reaction mixture was stirred for 10 min. The mixture was diluted with EtOAc (690 mL) and the layers were separated. The aqueous layer was further extracted with EtOAc (2 x 300 mL). The organic layers were collected, washed with aqueous NH_4OH (30% w/w in water)/NH_4Cl sat. aq. sol. (1:1, 1 x 600 mL), NH_4Cl sat. aq. sol. (1 x 600 mL), brine (1 x 300 mL), dried over Na_2SO_4, filtered, and concentrated under reduced pressure. The residue was chromatographed over silica gel (100% hexanes to 85:15 hexanes/EtOAc, $KMnO_4$) to afford **5** and **6** as a mixture of diastereomers (5:1 determined at the next step, 1.7 g, 80%) which was brought to the next step without further purification. *(Characterization over 2 steps)*

tert-Butyl (S)-2-((1R,2S,3S)-1-((benzyloxy)methoxy)-3-(methoxycarbonyl)-2-vinylhex-5-en-1-yl)pyrrolidine-1-carboxylate ***7*** *and tert-Butyl (S)-2-((1R,2R,3R)-1-((benzyloxy)methoxy)-3-(methoxycarbonyl)-2-vinylhex-5-en-1-yl)pyrrolidine-1-carboxylate* ***8****.*[449]

The mixture of **5** and **6** (1.7 g, 3.9 mmol, 1.0 eq.) was added to a 50 mL 1-neck round-bottomed flask and the flask was purged with Ar. THF (16 mL) was added and the solution was cooled to -78 °C whereby KHMDS (9.3 mL, C = 0.50 M in toluene, 4.7 mmol, 1.2 eq.) was added dropwise. The reaction mixture was stirred at -78 °C for 30 min then allyl iodide (1.8 mL, 19 mmol, 5.0 eq.) was added and the solution was stirred at -78 °C for 4h whereby LRMS analysis indicated that the reaction had gone to completion. NH_4Cl sat. aq. sol. (60 mL) was added, and the reaction mixture was left to reach rt. EtOAc (60 mL) was added and the aqueous layer was extracted with EtOAc (2 x 60 mL). The organic layers were combined, washed with NH_4Cl sat. aq. sol. (1 x 100 mL), ater (1 x 100 mL) brine (1 x 100 mL), dried over Na_2SO_4, filtered, and concentrated under reduced pressure. The residue was chromatographed over silica gel (100% hexanes to 85:15

hexanes/EtOAc, $KMnO_4$) to afford **7** (m = 981 mg, 53%) and **8** as orange oils (m = 203 mg, 11%). *Diastereomer* **7**: *Rf* = 0.34 (85:15 hexanes/EtOAc). $[\alpha]_D^{25}$ -46.6 (*c* 2.25 g/L, $CHCl_3$). ^1H NMR ($CDCl_3$, 500 MHz, mixture of rotamers) δ 7.34 – 7.27 (m, 5H), 5.74 – 5.71 (m, 2H), 5.18 – 4.97 (m, 4H), 4.72 – 4.57 (m, 4H), 4.18 (bs, 0.4H), 4.07 (bs, 0.5H), 3.86 – 3.81 (m, 1H), 3.67 – 3.54 (m, 3.5H), 3.42 – 3.38 (bs, 0.5H), 3.20 (dt, *J* = 10.7, 6.8 Hz, 1H), 2.69 – 2.65 (ddd, *J* = 10.6, 8.2, 3.7 Hz, 1H), 2.63 – 2.58 (m, 1H), 2.35 – 2.22 (m, 2H), 2.15 – 2.00 (m, 1H), 1.96 – 1.85 (m, 2H), 1.72 – 1.68 (m, 1H), 1.49 – 1.43 (m, 9H). $^{13}C\{^1H\}$ NMR ($CDCl_3$, 125 MHz, mixture of rotamers) δ 174.7, 154.6, 138.2, 136.1, 135.9, 135.6, 128.5, 128.5, 128.3, 127.9, 127.8, 127.7, 119.0, 118.2, 116.8, 96.5, 96.0, 80.1, 79.6, 79.2, 70.4, 60.3, 60.1, 51.5, 50.1, 47.4, 47.1, 46.5, 33.7, 33.4, 29.8, 28.7, 26.8, 25.7, 24.8, 24.3. HRMS (ESI) for $C_{27}H_{39}NO_6$ $(M+H)^+$: Calc: 474.2850; Found: 474.2848, for $C_{27}H_{39}NO_6$ $(M+Na)^+$: Calc: 496.2670; Found: 496.2661, for $C_{22}H_{29}NO_6$ $(M+K)^+$: Calc: 512.2409; Found: 512.2411. *Diastereomer* **8**: *Rf* = 0.29 (85:15 hexanes/EtOAc). $[\alpha]_D^{25}$ -44.7 (*c* 2.3 g/L, $CHCl_3$). ^1H NMR ($CDCl_3$, 500 MHz, mixture of rotamers), 7.34 – 7.26 (m, 5H), 5.71 – 5.50 (m, 2H), 5.15 – 5.12 (dd, *J* = 10.1, 1.8 Hz, 1H), 5.07 – 5.03 (dd, *J* = 17.1, 1.8 Hz, 1H), 5.03 – 4.97 (m, 1H), 4.95 – 4.90 (m, 1H), 4.72 – 4.67 (m, 2H), 4.66 – 4.56 (m, 2H), 4.30 (d, *J* = 10.2 Hz, 0.5H), 4.14 (d, *J* = 10.4 Hz, 0.5H), 3.88 (m, 0.5H), 3.81 (m, 0.5H), 3.64 (d, *J* = 1.7 Hz, 3H), 3.54 (m, 0.5H), 3.44 (m, 0.5H), 3.22 (m, 1H), 2.87 – 2.83 (m, 1H), 2.62 – 2.59 (m, 1H), 2.29 – 2.26 (m, 2H), 2.05 (m, 1H), 1.91 – 1.78 (m, 2H), 1.69 – 1.62 (m, 1H), 1.48 – 1.42 (m, 9H). $^{13}C\{^1H\}$ NMR ($CDCl_3$, 125 MHz, mixture of rotamers), δ: 175.0, 174.9, 154.7, 154.4, 138.2, 138.0, 136.1, 136.0, 135.4, 128.5, 127.8, 127.7, 127.7, 118.9, 118.9, 116.6, 116.4, 96.9, 96.5, 79.7, 79.3, 78.3, 78.1, 70.7, 70.6, 59.6, 59.6, 51.4, 51.4, 50.2, 50.0, 47.7, 47.3, 46.2, 46.0, 32.1, 32.0, 28.7, 28.6, 25.1, 24.7, 24.4, 24.2. HRMS (ESI) for $C_{27}H_{39}NO_6$ $(M+Na)^+$: Calc: 496.2670; Found: 496.2663, for $C_{22}H_{29}NO_6$ $(M+K)^+$: Calc: 512.2409; Found: 512.2409.

*tert-Butyl (S)-2-((R)-((benzyloxy)methoxy)((1S,5S)-5-(methoxycarbonyl)cyclopent-2-en-1-yl)methyl)pyrrolidine-1-carboxylate **7a**. (see Schéma 8.8)*

An amount of **7** (1.1 g, 2.4 mmol, 1.0 eq.) was added to a 25 mL 1-neck round-bottomed flask and the flask was purged with Ar. CH_2Cl_2 (24 mL) was added followed by Hoveyda-Grubbs second generation catalyst (0.16 g, 0.24 mmol, 0.1 eq.) and the reaction mixture was stirred at rt for 3h whereby LRMS analysis indicated that the reaction had gone to completion. Ethyl vinyl ether (15 mL) was added, and the solution was stirred for 1h and concentrated under reduced pressure.

The crude residue was chromatographed over silica gel (100% hexanes to 85:15 hexanes/EtOAc, ninhydrin) to afford **7a** as a colorless oil (850 mg, 79%) (The minor isomer was separated). *Rf* = 0.26 (85:15 hexanes/EtOAc). $[\alpha]_D^{25}$ +46.9 (*c* 1.25 g/L, $CHCl_3$). ^1H NMR ($CDCl_3$, 500 MHz, mixture of rotamers), δ: δ 7.33 (m, 4H), 7.29 – 7.26 (m, 1H), 5.78 (m, 1H), 5.71 (m, 1H), 4.76 – 4.68 (m, 2H), 4.65 – 4.52 (m, 2H), 4.07 (d, *J* = 9.1 Hz, 0.45H), 3.96 (m, 1H), 3.85 (m, 0.55H), 3.69 (m, 3H), 3.56 (s, 0.55H), 3.43 (m, 0.45H), 3.32 – 3.24 (m, 1H), 3.19 (bs, 1H), 3.08 (m, 0.45H), 2.97 (m, 0.55H), 2.69 (m, 2H), 2.13 (m, 1H), 2.01 – 1.82 (m, 2H), 1.75 (m, 1H), 1.44 (m, 9H). $^{13}C\{^1H\}$ NMR ($CDCl_3$, 125 MHz, mixture of rotamers), δ: 176.3, 176.1, 154.7, 154.4, 138.1, 137.9, 131.1, 131.0, 129.7, 129.6, 128.4, 127.8, 127.7, 96.1, 95.7, 81.5, 81.4, 79.8, 79.2, 70.1, 70.0, 59.6, 59.4, 52.8, 52.7, 52.1, 52.0, 47.5, 47.1, 44.9, 44.4, 37.0, 36.7, 28.6, 26.0, 25.2, 24.8, 24.2. HRMS (ESI) for $C_{25}H_{35}NO_6$ $(M+H)^+$: Calc: 446.2537; Found: 446.2530, for $C_{25}H_{35}NO_6$ $(M+Na)^+$: Calc: 468.2357; Found: 468.2347.

*tert-Butyl (S)-2-((R)-hydroxy((1S,2S)-2-(methoxycarbonyl)cyclopentyl)methyl)pyrrolidine-1-carboxylate **9**.*

An amount of **7a** (0.29 g, 0.64 mmol, 1.0 eq.) was added to a 10 mL 1-neck round-bottomed flask and the flask was purged with Ar. Dry MeOH (6.4 mL) was added followed by Pd/C (675 mg, 10% w/w, 63 µmol, 0.1 eq.) and the flask was purged with five alternating cycles of vacuum/H_2. The black suspension was stirred at rt for 24h under a H_2 atmosphere whereby MS analysis showed that the reaction had gone to completion. The suspension was filtered over a pad of Celite washing with abundant MeOH and concentrated under reduced pressure to afford **9** as a colorless oil (206 mg, 98%). A small amount was crystallized by slow diffusion (Et_2O/ hexanes) *Rf* = 0.4 (6:4 hexanes/EtOAc). Melting point: 83 °C. $[\alpha]_D^{25}$ -8.7 (*c* 2.35 g/L, $CHCl_3$). ^1H NMR ($CDCl_3$, 700 MHz, mixture of rotamers) δ 4.52 (bs, 0.7H), 4.06 (m, 0.7H), 3.85 – 3.78 (m, 1.3H), 3.66 (s, 3H), 3.58 – 3.50 (m, 1H), 3.24 – 3.21 (m, 1H), 2.85 – 2.55 (m, 1H), 2.25 – 2.23 (m, 1H), 2.00 (bs, 1H), 1.96 – 1.60 (m, 9.3H), 1.46 (s, 9H). $^{13}C\{^1H\}$ NMR ($CDCl_3$, 176 MHz, mixture of rotamers) δ 177.2, 176.9, 156.9, 154.9, 80.3, 80.1, 75.2, 75.0, 62.2, 61.0, 51.9, 51.7, 48.2, 47.5, 47.4, 46.8, 46.2, 44.8, 31.1, 30.3, 29.1, 28.6, 27.8, 26.0, 25.8, 25.6, 24.5. HRMS (ESI) for $C_{17}H_{29}NO_5$ $(M+Na)^+$: Calc: 350.1938; Found: 350.1930, for $C_{17}H_{29}NO_5$ $(M+K)^+$: Calc: 366.1677; Found: 366.1677. HPLC: 100%.

*tert-Butyl (S)-2-((R)-((benzyloxy)methoxy)((1R,5R)-5-(methoxycarbonyl)cyclopent-2-en-1-yl)methyl)pyrrolidine-1-carboxylate **8a**. (see Schéma 8.8)*

An amount of **8a** was synthesized in accordance with the procedure of its diastereomer **7a** starting from **8** (0.45 g, 0.94 mmol, 1.0 eq.). The residue was chromatographed over silica gel (100% hexanes to 85:15 hexanes/EtOAc, ninhydrin) to afford **8a** as a colorless oil (360 mg, 86%). *Rf* = 0.29 (85:15 hexanes/EtOAc). $[\alpha]_D^{25}$ -100.9 (*c* 1.1 g/L, $CHCl_3$). ^1H NMR ($CDCl_3$, 500 MHz, mixture of rotamers) δ 7.36 – 7.28 (m, 5H), 5.72 (bs, 1H), 5.62 (bs, 1H), 4.79 – 4.66 (m, 3H), 4.55 – 4.51 (m, 1H), 4.11 (m, 0.4H), 4.00 (m, 0.5H), 3.90 (m, 0.5H), 3.81 (m, 0.5H), 3.70 – 3.66 (m, 3H), 3.56 – 3.53 (m, 0.55H), 3.46 – 3.43 (m, 0.45H), 3.25 – 3.20 (m, 3H), 2.76 – 2.60 (m, 1H), 2.57 – 2.54 (m, 1H), 2.18 – 2.05 (m, 1H), 1.97 – 1.88 (m, 2H), 1.75 – 1.72 (m, 1H), 1.43 (m, 9H). $^{13}C\{^1H\}$ NMR ($CDCl_3$, 125 MHz, mixture of rotamers), δ: 176.7, 176.4, 154.7, 154.4, 138.1, 138.0, 130.8, 130.4, 130.2, 130.0, 128.4, 128.3, 127.8, 127.7, 127.6, 96.0, 95.6, 81.3, 81.0, 79.8, 79.3, 70.0, 70.0, 59.8, 59.6, 52.9, 52.7, 51.9, 51.9, 47.4, 47.0, 44.7, 36.5, 36.2, 28.6, 25.9, 25.1, 24.9, 24.4. HRMS (ESI) for $C_{25}H_{35}NO_6$ $(M+H)^+$: Calc: 446.2537; Found: 446.2531, for $C_{25}H_{35}NO_6$ $(M+Na)^+$: Calc: 468.2357; Found: 468.2347, for $C_{25}H_{35}NO_6$ $(M+K)^+$: Calc: 484.2096, Found: 484.2102.

*tert-Butyl (S)-2-((R)-hydroxy((1R,2R)-2-(methoxycarbonyl)cyclopentyl)methyl)pyrrolidine-1-carboxylate **10**.*

An amount of **10** was synthesized in accordance with the procedure of its diastereomer **9** starting from **8a** (0.15 g, 0.34 mmol, 1.0 eq.). The crude residue was chromatographed over silica gel (100% hexanes to 6:4 hexanes/EtOAc, $KMnO_4$/ ninhydrin) to afford **10** as a colorless oil (110 mg, 100%). *Rf* = 0.28 (6:4 hexanes/EtOAc). $[\alpha]_D^{25}$ -85.7 (*c* 1.2 g/L, $CHCl_3$). ^1H NMR ($CDCl_3$, 700 MHz, mixture of rotamers) δ 3.93 – 3.78 (m, 2H), 3.68 (s, 3H), 3.59 (bs, 0.4H), 3.46 (bs, 0.6H), 3.22 (bs, 1H), 2.92 (bs, 0.5H), 2.69 (bs, 1H), 2.26 (m, 1H), 2.11 (bs, 0.3H), 2.04 – 1.74 (m, 6H), 1.72 – 1.66 (m, 3H), 1.51 – 1.46 (m, 9.6H), 1.32 (s, 0.4H). $^{13}C\{^1H\}$ NMR ($CDCl_3$, 176 MHz, mixture of rotamers) δ 178.0, 177.7, 155.7, 154.9, 79.7, 76.0, 61.4, 60.8, 52.0, 49.0, 48.0, 47.5, 46.8, 46.4, 31.3, 30.8, 30.0, 29.3, 28.7, 28.6, 25.5, 25.3, 25.0, 24.8, 24.5. HRMS (ESI) for $C_{17}H_{29}NO_5$ $(M+H)^+$: Calc: 328.2119; Found: 328.2107, for $C_{17}H_{29}NO_5$ $(M+Na)^+$: Calc: 350.1938; Found: 350.1926. HPLC: 96% as a 95:5 mixture.

*tert-Butyl (S)-2-((S)-1-((benzyloxy)methoxy)-4-methoxy-4-oxobut-2-yn-1-yl)pyrrolidine-1-carboxylate **2a**. (see Schéma 8.9)*

An amount of **2a** was synthesized in accordance with the procedure of its diastereomer **3a** starting from **2** (7.2 g, 25 mmol, 1.0 eq.). The crude residue was chromatographed over silica gel (100% hexanes to 85:15 hexanes/EtOAc, *p*-anisaldehyde / ninhydrin) to afford **2a** as a pale-yellow oil (7.7 g, 75%). *Rf* = 0.29 (85:15 hexanes/EtOAc). $[\alpha]_D^{25}$ -163 (*c* 2.80 g/L, $CHCl_3$). ^1H NMR ($CDCl_3$, 500 MHz, mixture of rotamers), δ: 7.38 – 7.28 (m, 5H), 5.13 (bs, 0.5H), 4.99 (bs, 0.5H), 4.95 – 4.91 (m, 1H), 4.80 (m, 0.5H), 4.76 (m, 0.5H), 4.69 – 4.58 (m, 2H), 4.09 (bs, 0.5H), 3.98 (bs, 0.5H), 3.75 (s, 3H), 3.56 – 3.53 (bs, 0.5H), 3.43-3.38 (m, 1.5H), 2.18 – 2.05 (m, 3H), 1.83 – 1.79 (m, 1H), 1.47 – 1.41 (m, 9H). $^{13}C\{^1H\}$ NMR ($CDCl_3$, 125 MHz, mixture of rotamers), δ: 154.9, 154.3, 153.6, 153.4, 137.5, 137.4, 128.5, 128.3, 127.9, 93.4, 93.1, 85.4, 84.6, 80.2, 79.8, 78.0, 77.9, 69.9, 67.4, 67.2, 59.7, 59.5, 52.9, 47.3, 47.0, 28.5, 27.7, 26.9, 24.3, 23.5 ppm. HRMS (ESI) for $C_{22}H_{29}NO_6$ $(M+Na)^+$: Calc.: 426.1887; Found: 426.1888, for $C_{22}H_{29}NO_6$ $(M+K)^+$: Calc.: 442.1627; Found: 442.1630.

*tert-Butyl (S)-2-((S,Z)-1-((benzyloxy)methoxy)-4-methoxy-4-oxobut-2-en-1-yl)pyrrolidine-1-carboxylate **11**.*

An amount of **11** was synthesized in accordance with the procedure of its diastereomer **4** starting from **2a** (4.8 g, 12 mmol, 1.0 eq) to afford **11** as an orange oil (4.8 g, 100%). *Rf* = 0.3 (8:2 hexanes/EtOAc). $[\alpha]_D^{25}$ +15 (*c* 2.35 g/L, $CHCl_3$). ^1H NMR ($CDCl_3$, 500 MHz, mixture of rotamers), δ: 7.34 – 7.27 (m, 5H), 6.16 – 6.12 (m, 1H), 5.95 – 5.92 (d, *J* = 11.8 Hz, 1H), 5.53 – 5.44 (m, 1H), 4.73 (m, 2H), 4.66 – 4.64 (d, *J* = 11.9 Hz, 1H), 4.62 – 4.54 (d, *J* = 11.9 Hz, 1H), 4.15 (bs, 1H), 3.68 (s, 3H), 3.48 – 3.41 (m, 1H), 3.30 (bs, 1H), 2.01 – 1.74 (m, 4H), 1.46 (s, 9H). $^{13}C\{^1H\}$ NMR ($CDCl_3$, 125 MHz, mixture of rotamers), δ: 166.2, 166.0, 155.0, 146.9, 146.6, 138.0, 128.5, 128.4, 128.3, 127.9, 127.7, 127.7, 122.5, 122.2, 93.4, 79.7, 79.2, 73.8, 69.7, 69.6, 60.3, 60.1, 59.7, 51.5, 51.4, 47.0, 46.8, 28.5, 27.5, 24.4, 23.8. HRMS (ESI) for $C_{22}H_{31}NO_6$ $(M+Na)^+$: Calc.: 428.2044; Found: 428.2053, for $C_{22}H_{31}NO_6$ $(M+K)^+$: Calc.: 444.1783; Found: 444.1792.

*(S)-tert-Butyl 2-((S,E)-1-((benzyloxy)methoxy)-4-methoxy-4-oxobut-2-en-1-yl)pyrrolidine-1-carboxylate **12**.*

An amount of **2** (31.0 mg, 109 µmol, 1.0 eq.) was added to a 5 mL 1-neck round-bottomed flask and the flask was purged with Ar. THF (995 µL) was added and the solution was cooled to 78 °C

whereby Red-Al (68.2 µL, 219 µmol, 2.0 eq., 65% w/w in toluene) was added slowly. The mixture was stirred at -78 °C for 30 min then quenched with an aqueous HCl solution (1 mL) and left to reach rt. The biphasic mixture was diluted with EtOAc (1 mL) and separated. The aqueous layer was extracted with EtOAc (2 x 1 mL). The organic layers were collected, washed with $NaHCO_3$ sat. aq. sol. (1 x 2 mL), water (1 x 2 mL), brine (1 x 2 mL), dried over Na_2SO_4, filtered and concentrated under reduced pressure to afford a mixture of (S)-*tert*-butyl 2-((*S,E*)-1-hydroxy-4-methoxy-4-oxobut-2-en-1-yl)pyrrolidine-1-carboxylate and **2** (75:25 ratio, determined by ^{1}H NMR). The crude oil was transferred to a 5 mL 1-neck round-bottomed flask and the flask was purged with Ar. CH_2Cl_2 (911 µL) was added and the solution was cooled to 0 °C. *i*PrNEt$_2$ (63.5 µL, 364 µmol, 4.0 eq.) and benzyl chloromethyl ether (63.4 µL, 273 µmol, 3.0 eq., 60% technical grade) were added successively and the reaction mixture was maintained at 0 °C for 5 min, then heated at 45 °C for 24h whereby TLC analysis (75:25 hexanes/EtOAc, ninhydrin) indicated that the reaction had gone to completion. The reaction mixture was left to reach rt and diluted with CH_2Cl_2 (1 mL). The organic layer was washed with water (1 x 1 mL), brine (1 x 1 mL), dried over Na_2SO_4, filtered and concentrated under reduced pressure. The crude residue was chromatographed over silica gel (100% hexanes to 85:15 hexanes/EtOAc, ninhydrin) to afford **14a** as a colorless oil (24 mg, 55%) and **2a** as a colorless oil (8 mg, 18%). *Rf* = 0.29 (85:15 hexanes/EtOAc). $[\alpha]_D^{25}$ -56.0 (*c* 4.0 g/L, $CHCl_3$). ^{1}H NMR ($CDCl_3$, 700 MHz, mixture of rotamers), δ 7.36 – 7.31 (m, 4H), 7.28 (m, 1H), 6.90 – 6.84 (m, 1H), 6.06 (dd, *J* = 15.7, 1.7 Hz, 1H), 4.89 – 4.71 (m, 3H), 4.66 (m, 1H), 4.58 (d, *J* = 11.9 Hz, 1H), 4.17 (m, 0.5H), 4.07 (m, 1H), 3.74 (s, 3H), 3.46 (m, 0.5H), 3.35 (m, 0.5H), 3.27 (m, 1H), 1.94 – 1.89 (m, 2H), 1.76 – 1.72 (m, 2H), 1.46 (m, 9H). ^{13}C{^{1}H} NMR ($CDCl_3$, 176 MHz, mixture of rotamers), δ 166.7, 166.5, 154.9, 154.6, 145.6, 145.0, 137.8, 137.6, 128.6, 128.5, 128.1, 128.0, 128.0, 127.9, 127.9, 127.8, 127.8, 122.6, 122.5, 93.8, 93.4, 80.2, 79.7, 76.2, 76.1, 69.9, 59.8, 59.6, 51.8, 47.3, 47.0, 28.6, 28.6, 26.6, 25.8, 24.4, 23.6. HRMS (ESI) for $C_{22}H_{31}NO_6$ $(M+Na)^+$: Calc: 428.2044; Found: 428.2054.

*tert-Butyl (S)-2-((1S,2R)-1-((benzyloxy)methoxy)-2-(2-methoxy-2-oxoethyl)but-3-en-1-yl)pyrrolidine-1-carboxylate **13**.*

An amount of **13** was synthesized in accordance with the procedure of their diastereomers **5/6** starting from **11** (2.5 g, 6.2 mmol, 1.0 eq). The crude residue was chromatographed over silica gel

(100% hexanes to 8:2 hexanes/EtOAc, CAM/ ninhydrin) to afford **13** as an orange oil (2.1 g, 80%). (*Characterization over 2 steps)*

*tert-Butyl (S)-2-((1S,2S,3S)-1-((benzyloxy)methoxy)-3-(methoxycarbonyl)-2-vinylhex-5-en-1-yl)pyrrolidine-1-carboxylate **14**.*

An amount of **14** was synthesized in accordance with the procedure of their diastereomers **7/8** starting from **13** (3.4 g, 7.8 mmol, 1.0 eq). The crude residue was chromatographed over silica gel (100% hexanes to 85:15 hexanes/EtOAc, $KMnO_4$/ ninhydrin) to afford **14** as a colorless oil (2.2 g, 58%). *Rf* = 0.28 (85:15 hexanes/EtOAc). $[\alpha]_D^{25}$ -13.1 (*c* 2.85 g/L, $CHCl_3$). ^1H NMR ($CDCl_3$, 500 MHz, mixture of rotamers) δ 7.34 – 7.28 (m, 5H), 5.79 – 5.67 (m, 1H), 5.52 – 5.46 (m, 1H), 5.11 – 4.83 (m, 4H), 4.81 – 4.63 (m, 3H), 4.57 – 4.53 (m, 1H), 4.33 – 4.29 (m, 0.5H), 4.27 – 4.24 (m, 0.5H), 4.15 – 4.09 (m, 1H), 3.64 – 3.62 (m, 3H), 3.42 – 3.39 (m, 0.6H), 3.37 – 3.32 (m, 0.4H), 3.07 – 3.04 (m, 1H), 2.78 – 2.60 (m, 2H), 2.30 – 2.25 (m, 1H), 2.25 – 2.16 (m, 1H), 2.05 – 1.88 (m, 2H), 1.82 – 1.68 (m, 2H), 1.47 – 1.43 (m, 9H). $^{13}C\{^1H\}$ NMR ($CDCl_3$, 125 MHz, mixture of rotamers), δ: 175.4, 175.2, 154.6, 154.4, 138.1, 137.9, 136.1, 136.0, 135.9, 135.4, 128.5, 128.5, 127.8, 127.8, 127.7, 116.7, 116.5, 116.4, 115.9, 96.1, 80.4, 79.7, 79.5, 79.0, 70.1, 59.1, 59.0, 51.3, 47.8, 47.7, 47.3, 47.0, 33.3, 33.1, 28.7, 28.7, 26.7, 25.9, 24.3, 23.6. HRMS (ESI) for $C_{27}H_{39}NO_6$ $(M+Na)^+$: Calc.: 496.2670; Found: 496.2655, for $C_{27}H_{39}NO_6$ $(M+K)^+$: Calc.: 512.2409; Found: 512.2396.

*tert-Butyl (S)-2-((S)-((benzyloxy)methoxy)((1S,5S)-5-(methoxycarbonyl)cyclopent-2-en-1-yl)methyl)pyrrolidine-1-carboxylate **14a**. (see Schéma 8.9)*

An amount of **14a** was synthesized in accordance with the procedure of its diastereomer **7a** starting from **14** (101 mg, 214 µmol, 1.0 eq.). The crude residue was chromatographed over silica gel (100% hexanes to 85:15 hexanes/EtOAc, ninhydrin) to afford **14a** as a colorless oil (84 mg, 89%). *Rf* = 0.34 (8:2 hexanes/EtOAc). $[\alpha]_D^{25}$ +76 (*c* 0.75 g/L, $CHCl_3$). ^1H NMR ($CDCl_3$, 500 MHz, mixture of rotamers), δ: 7.34 – 7.27 (m, 5H), 5.71 – 5.98 (m, 1H), 5.53 – 5.51 (m, 1H), 4.78 – 4.71 (m, 2H), 4.63 – 4.53 (dd, *J* = 11.6, 20.2 Hz, 2H), 4.20 (bs, 0.4H), 4.06 (bs, 0.6H), 3.81 (m, 0.4H) 3.71 (m, 3.5H), 3.52 – 3.45 (m, 1H), 3.29 – 3.21 (m, 3H), 2.77 – 2.73 (m, 1H), 2.57 – 2.53 (m, 1H), 2.01 – 1.75 (m, 4H), 1.45 (s, 9H) ppm. $^{13}C\{^1H\}$ NMR ($CDCl_3$, 125 MHz, mixture of rotamers), δ: 177.0, 155.1, 138.1, 131.3, 130.3, 128.5, 127.8, 127.8, 127.7, 95.5, 95.3, 80.5, 80.3, 79.6, 79.3, 69.8, 59.2, 59.0, 52.0, 51.5, 47.1, 46.7, 44.3, 43.7, 36.8, 28.7, 28.6, 27.8, 27.2, 24.2, 23.4. HRMS (ESI) for

$C_{25}H_{35}NO_6$ $(M+Na)^+$: Calc.: 468.2357; Found: 468.2377, for $C_{25}H_{35}NO_6$ $(M+K)^+$: Calc.: 484.2096; Found: 484.2112.

*tert-Butyl (S)-2-((S)-hydroxy((1S,2S)-2-(methoxycarbonyl)cyclopentyl)methyl)pyrrolidine-1-carboxylate **15**.*

An amount of **15** was synthesized in accordance with the procedure of its diastereomer **9** starting from **14a** (64 mg, 0.14 mmol, 1.0 eq.). The crude residue was chromatographed over silica gel (8:2 hexanes/EtOAc, ninhydrin) to afford **15** as a colorless oil (44 mg, 96%). *Rf* = 0.25 (8:2 hexanes/EtOAc). $[\alpha]_D^{25}$ -26 (*c* 0.95 g/L, $CHCl_3$). ^{1}H NMR ($CDCl_3$, 500 MHz, mixture of rotamers) δ 5.05 (bs, 1H), 3.88 – 3.83 (ddd, *J* = 9.2, 7.8, 3.6 Hz, 1H), 3.66 (s, 3H), 3.51 – 3.45 (m, 2H), 3.30 – 3.25 (ddd, *J* = 10.9, 7.3, 5.2 Hz, 1H), 3.00 – 2.75 (m, 1H), 2.42 – 2.38 (m, 1H), 1.97 – 1.57 (m, 10H), 1.46 (s, 9H). ^{13}C{^{1}H} NMR ($CDCl_3$, 125 MHz, mixture of rotamers) δ 178.1, 158.5, 80.7, 78.1, 61.6, 51.8, 47.4, 46.2, 43.1, 32.3, 31.1, 28.8, 28.6, 26.3, 24.3. HRMS (ESI) for $C_{17}H_{29}NO_5$ $(M+H)^+$: Calc.: 328.2119; Found: 328.2132, for $C_{17}H_{29}NO_5$ $(M+Na)^+$: Calc.: 350.1938; Found: 350.1950. HPLC: 98%.

*tert-Butyl (S)-2-((1S,2S)-2-(methoxycarbonyl)cyclopentane-1-carbonyl)pyrrolidine-1-carboxylate **9a**. (see Schéma 8.10)*

An amount of **9** (100 mg, 305 µmol, 1.0 eq.) was added to a 5 mL 1-neck round-bottomed flask and the flask was purged with Ar. CH_2Cl_2 (680 µL) was added followed by Dess-Martin periodinane (3-oxo-1λ^5-benzo[d][1,2]iodaoxole-1,1,1(*3H*)-triyl triacetate) (194 mg, 458 µmol, 1.5 eq.). The reaction mixture was stirred at rt for 2h whereby TLC analysis (5:5 hexanes/EtOAc, ninhydrin) indicated that the reaction had gone to completion. The solvent was removed under reduced pressure. The residue was dissolved with Et_2O (2 mL) and a sat. aq. $Na_2S_2O_3$ solution (2 mL) was added. The phases were separated and the aqueous layer was extracted with Et_2O (2 x 3 mL). The organic layers were collected, washed with a sat. aq. $Na_2S_2O_3$ solution (2 x 3 mL), a sat. aq. $NaHCO_3$ solution (3 x 3 mL), water (1 x 3 mL), brine (1 x 3 mL), dried over Na_2SO_4, filtered, and concentrated under reduced pressure to afford **9a** as a colorless oil (96.0 mg, 97%). *Rf* = 0.35, (8:2 hexanes/EtOAc). $[\alpha]_D^{25}$ +4.9 (*c* 4.5 g/L, $CHCl_3$). ^{1}H NMR ($CDCl_3$, 400 MHz, mixture of rotamers) δ 4.42 – 4.34 (m, 1H), 3.66 (s, 3H), 3.57 – 3.42 (m, 2H), 3.41 – 3.32 (m, 1H), 3.24 – 3.20 (q, *J* = 7.8 Hz, 0.4H), 3.15 – 3.05 (q, *J* = 7.8 Hz, 0.6H), 2.26 – 1.64 (m, 10.8H), 1.43 (s, 4H), 1.38 (s, 5H). ^{13}C{^{1}H}

NMR ($CDCl_3$, 101 MHz, mixture of rotamers) δ 211.8, 211.1, 175.9, 175.6, 154.7, 154.2, 80.2, 79.8, 65.2, 64.7, 52.0, 52.0, 50.4, 50.3, 47.2, 47.0, 46.9, 30.7, 30.7, 30.6, 29.9, 29.9, 28.9, 28.5, 28.4, 26.1, 26.0, 24.5, 23.7. HRMS (ESI) for $C_{17}H_{27}NO_5$ $(M+Na)^+$: Calc.: 348.1781; Found: 348.1772, for $C_{17}H_{27}NO_5$ $(M+K)^+$: Calc.: 364.1521; Found: 364.1522.

tert-Butyl (S)-2-((R)-hydroxy((1S,2S)-2-(methoxycarbonyl)cyclopentyl)methyl)pyrrolidine-1-carboxylate ***9*** *and tert-butyl (S)-2-((S)-hydroxy((1S,2S)-2-(methoxycarbonyl)cyclopentyl)methyl)pyrrolidine-1-carboxylate* ***15****.*

An amount of **9a** (22 mg, 67 µmol, 1.0 eq.) was added to a 5 mL 1-neck round-bottomed flask and the flask was purged with Ar. MeOH (338 µL) was added followed by $NaBH_4$ (5.6 mg, 0.15 mmol, 2.2 eq.). The reaction mixture was stirred at rt for 40 min whereby MS analysis indicated that the reaction had gone to completion. The reaction mixture was stopped by slow addition of a sat. aq. NH_4Cl solution (500 µL) and the mixture was diluted with EtOAc (2 mL) and a sat. aq. NH_4Cl solution (1.5 mL). The phases were separated, and the aqueous layer was extracted with EtOAc (2 x 2 mL). The organic layers were collected, washed with a sat. aq. NH_4Cl solution (1 x 2 mL), water (1 x 2 mL), brine (1 x 2 mL), dried over Na_2SO_4, filtered, and concentrated under reduced pressure to afford a 1:3 mixture of **9/15** as a colorless oil (96.0 mg, 97%). (Ratio determined by ^1H NMR, see. I.3.4. section in Supp. Info.)

tert-Butyl (S)-2-((1R,2R)-2-(methoxycarbonyl)cyclopentane-1-carbonyl)pyrrolidine-1-carboxylate ***10a****. (see Schéma 8.10)*

An amount of **10a** was synthesized in accordance with the procedure of its diastereomer **9a** starting from **10** (20 mg, 61 µmol, 1.0 eq.) to afford **10a** as a colorless oil (18.0 mg, 91%). *Rf* = 0.35, (8:2 hexanes/EtOAc). $[\alpha]_D^{25}$ -72.3 (*c* 6.0 g/L, $CHCl_3$). ^1H NMR ($CDCl_3$, 400 MHz, mixture of rotamers) δ 4.50 – 4.42 (m, 1H), 3.64 – 3.62 (m, 3H), 3.54 – 3.21 (m, 4H), 2.24 – 1.90 (m, 4H), 1.86 – 1.62 (m, 6H), 1.39 (m, 9H). $^{13}C\{^1H\}$ NMR ($CDCl_3$, 101 MHz, mixture of rotamers) δ 209.6, 208.8, 175.7, 175.5, 154.4, 154.0, 80.0, 79.5, 64.6, 64.2, 51.9, 51.8, 51.1, 50.7, 47.0, 46.8, 45.2, 45.0, 30.9, 30.6, 30.3, 30.2, 29.3, 28.5, 28.5, 28.3, 25.8, 25.7, 24.0, 23.0. HRMS (ESI) for $C_{17}H_{27}NO_5$ $(M+Na)^+$: Calc.: 348.1781; Found: 348.1765, for $C_{17}H_{27}NO_5$ $(M+K)^+$: Calc.: 364.1521; Found: 364.1507.

*tert-Butyl (S)-2-((R)-hydroxy((1R,2R)-2-(methoxycarbonyl)cyclopentyl)methyl)pyrrolidine-1-carboxylate **10** and tert-butyl (S)-2-((R)-hydroxy((1S,2S)-2-(methoxycarbonyl)cyclopentyl)methyl)pyrrolidine-1-carboxylate **16**.*

An amount of **10/16** was synthesized in accordance with the procedure of its diastereomer **9/15** starting from **10a** (73 mg, 0.23 mmol, 1.0 eq.). The crude residue was chromatographed over silica gel (100% hexanes to 8:2 to 6:4 hexanes/EtOAc, $KMnO_4$/ ninhydrin) to afford **10** as a colorless oil (11 mg, 15%) and **16** as white crystals (43 mg, 59%). **16** was recrystallized by slow evaporation of $CHCl_3$. Melting point: 60 °C. **16**: *Rf* = 0.35, (8:2 hexanes/EtOAc). $[\alpha]_D^{25}$ -129.3 (*c* 0.8 g/L, $CHCl_3$). ^1H NMR ($CDCl_3$, 500 MHz) δ 5.15 (bs, 1H), 3.84 – 3.81 (m, 1H), 3.66 (s, 3H), 3.58 – 3.52 (m, 1H), 3.51 – 3.47 (m, 1H), 3.29 – 3.26 (dt, *J* = 15.0, 5.0 Hz, 1H), 2.98 – 2.94 (q, *J* = 9.0 Hz, 1H), 2.27 – 2.16 (q, *J* = 8.5 Hz, 1H), 1.99 – 1.81 (m, 2H), 1.81 – 1.62 (m, 8H), 1.46 (s, 9H). $^{13}C\{^1H\}$ NMR ($CDCl_3$, 125 MHz), δ: 177.2, 158.5, 80.8, 75.6, 61.8, 51.7, 47.3, 46.6, 46.0, 30.4, 28.5, 25.4, 24.3, 24.0 ppm. HRMS (ESI) for $C_{17}H_{29}NO_5$ $(M+Na)^+$: Calc.: 350.1938; Found: 350.1939, for $C_{17}H_{29}NO_5$. HPLC: 97% as 94:6 mixture.

*(1R,2R)-2-((R)hydroxy((S)-pyrrolidin-2-yl)methyl)cyclopentane-1-carboxylic acid hydrochloride **A**.*

An amount of **10** (13 mg, 41 µmol, 1.0 eq.) was added to a 5 mL 1-neck round-bottomed flask and the flask was purged with Ar. The residue was dissolved in EtOH (136 µL) then water (136 µL) was added. The mixture was cooled to 0 °C and $LiOH.H_2O$ (6.9 mg, 0.16 mmol, 4.0 eq.) was added in one portion. The reaction mixture was stirred at 0 °C for 5 min then was allowed to reach rt. The stirring was continued for 3h30 whereby TLC analysis (7:3 hexanes/EtOAc, ninhydrin) indicated that the reaction had gone to completion. CH_2Cl_2 (400 µL) was added, and the reaction mixture was transferred to a sintered funnel. The layers were separated, and the aqueous layer was washed with CH_2Cl_2 (2 x 400 µL). The aqueous layer was collected and a 10% w/w $KHSO_4$ aqueous solution was slowly added dropwise until pH = 3-4 (monitored with pH paper). The aqueous layer was extracted with CH_2Cl_2 (3 x 500 µL). The organic layers were collected, dried with Na_2SO_4, filtered, and concentrated under reduced pressure to afford the carboxylic acid as a colorless oil (structure confirmed by ^1H NMR/LRMS, yield over 2 steps). The crude oil was transferred to a 5 mL 1-neck round-bottomed flask and the flask was purged with Ar. A solution of HCl (410 µL, 1.64 mmol, 40.0 eq., 4M in dioxane) was added and the reaction mixture was stirred at rt for 30 min

whereby TLC analysis (94:6 CH_2Cl_2/MeOH, ninhydrin) indicated that the reaction had gone to completion. The reaction mixture was concentrated under reduced pressure to afford a colorless oil. The residue was washed with CH_2Cl_2 and the filtrate was syringed out of the vial, then concentrated under reduced pressure. Five cycles were performed isolating **A** for each cycle as the substrate. Isolated fractions were analyzed by ^{1}H NMR then collected together to afford **A** as a colorless oil (8.3 mg, 81% over two steps). *Rf* = 0.3, (8:2 DCM/MeOH +1% formic acid). $[\alpha]_D^{25}$ -58.0 (*c* 5.5 g/L, MeOH). ^{1}H NMR (CD_3OD, 700 MHz, mixture of isomers) δ 3.77 (dd, *J* = 7.7, 3.4 Hz, 0.08H), 3.70 (dd, *J* = 8.8, 3.5 Hz, 0.92H), 3.63 (m, 1H), 3.28 (m, 2H), 2.80 – 2.76 (dt, *J* = 9.2, 7.0 Hz, 0.92H), 2.57 (q, *J* = 7.8 Hz, 0.07H), 2.34 – 2.31 (p, *J* = 8.4 Hz, 0.92H), 2.30 – 2.26 (m, 0.08H), 2.12 – 2.05 (m, 2H), 2.03 – 1.97 (m, 3H), 1.87 – 1.83 (m, 2H), 1.80 – 1.64 (m, 2H), 1.40 – 1.35 (dq, *J* = 12.5, 8.4 Hz, 1H). ^{13}C{^{1}H} NMR (CD_3OD, 176 MHz, mixture of isomers) δ 180.5, 179.5, 73.3, 72.5, 64.5, 64.2, 48.5, 48.4, 48.0, 46.8, 46.8, 32.2, 32.0, 30.5, 30.0, 26.4, 26.3, 24.8, 24.7, 24.7, 24.2. HRMS (ESI) for $C_{11}H_{19}NO_3$ $(M+H)^+$: Calc.: 214.1438; Found: 214.1438. HPLC: 93% as 95:5 mixture.

*(1S,2S)-2-((R)-Hydroxy((S)-pyrrolidin-2-yl)methyl)cyclopentane-1-carboxylic acid hydrochloride **B**.*

An amount of **B** was synthesized in accordance with the procedure of its diastereomer **A** starting from **9** (11 mg, 34 µmol, 1.0 eq.) to afford **B** as a colorless oil (7.2 mg, 85%). *Rf* = 0.38, (8:2 DCM/MeOH +1% formic acid). $[\alpha]_D^{25}$ +26.3 (*c* 7.0 g/L, MeOH). ^{1}H NMR (CD_3OD, 500 MHz) δ 3.78 – 3.76 (dd, *J* = 7.7, 3.4 Hz, 1H), 3.68 – 3.64 (m, 1H), 3.27 (m, 2H), 2.57 – 2.54 (m, 1H), 2.29 – 2.23 (p, *J* = 7.9 Hz, 1H), 2.10 – 1.83 (m, 7H), 1.74 – 1.62 (m, 3H). ^{13}C{^{1}H} NMR (CD_3OD, 125 MHz) δ 179.7, 72.5, 64.5, 48.5, 47.8, 46.8, 32.3, 30.0, 26.3, 24.8, 24.7. HRMS (ESI) for $C_{11}H_{19}NO_3$ $(M+H)^+$: Calc.: 214.1438; Found: 214.1436. HPLC: 94% as a 99:1 mixture.

*(1S,2S)-2-((S)hydroxy((S)-pyrrolidin-2-yl)methyl)cyclopentane-1-carboxylic acid hydrochloride **C**.*

An amount of **C** was synthesized in accordance with the procedure of its diastereomer **A** starting from **15** (9.7 mg, 30 µmol, 1.0 eq.) to afford **C** as a colorless oil (6.4 mg, 80%). *Rf* = 0.31, (8:2 DCM/MeOH +1% formic acid). $[\alpha]_D^{25}$ +17.93 (*c* 3.5 g/L, MeOH). ^{1}H NMR (CD_3OD, 700 MHz) δ 3.64 – 3.62 (t, *J* = 5.9 Hz, 1H), 3.58 – 3.55 (m, 1H), 3.29 – 3.23 (m, 2H), 2.80 (m, 1H), 2.38 – 2.35 (m, 1H), 2.18 – 2.15 (m, 1H), 2.06 (m, 1H), 2.03 – 1.78 (m, 5H), 1.77 – 1.64 (m, 2H), 1.52 – 1.47 (dq, *J* = 12.4, 8.3 Hz, 1H). ^{13}C{^{1}H} NMR (CD_3OD, 176 MHz) δ 180.6, 73.9, 64.8, 48.0, 46.6, 46.5, 32.6, 31.0,

28.3, 26.7, 24.9. HRMS (ESI) for $C_{11}H_{19}NO_3$ $(M+H)^+$: Calc.: 214.1438; Found: 214.1441. HPLC: 100%.

*(1R,2R)-2-((S)-Hydroxy((S)-pyrrolidin-2-yl)methyl)cyclopentane-1-carboxylic acid hydrochloride **D**.* An amount of **D** was synthesized in accordance with the procedure of its diastereomer **A** starting from **16** (8.5 mg, 26 µmol, 1.0 eq.) to afford **D** as a colorless oil (5.6 mg, 87%). *Rf* = 0.35, (8:2 DCM/MeOH +1% formic acid). $[\alpha]_D^{25}$ -89.5 (*c* 6.8 g/L, MeOH). ^{1}H NMR (CD_3OD, 700 MHz) δ 3.79 – 3.77 (dd, *J* = 7.6, 3.7 Hz, 1H), 3.52 – 3.50 (dt, *J* = 9.6, 7.4 Hz, 1H), 3.27 – 3.24 (dd, *J* = 8.1, 6.5 Hz, 2H), 2.76 – 2.74 (m, 1H), 2.28 – 2.25 (m, 1H), 2.16 (m, 1H), 2.09 (m, 1H), 2.06 – 1.94 (m, 2H), 1.92 – 1.85 (m, 1H), 1.80 – 1.72 (m, 2H), 1.72 – 1.65 (m, 3H). $^{13}C\{^1H\}$ NMR (CD_3OD, 176 MHz) δ 179.4, 72.5, 65.4, 47.7, 47.1, 46.4, 31.3, 28.2, 26.4, 26.1, 24.8. HRMS (ESI) for $C_{11}H_{19}NO_3$ $(M+H)^+$: Calc.: 214.1438; Found: 214.1434. HPLC: 98% as 98:2 mixture.

8.6 Partie expérimentale de l'article 5

8.6.1 Synthetic schemes

Schéma 8.13 Synthesis of compound **I**.

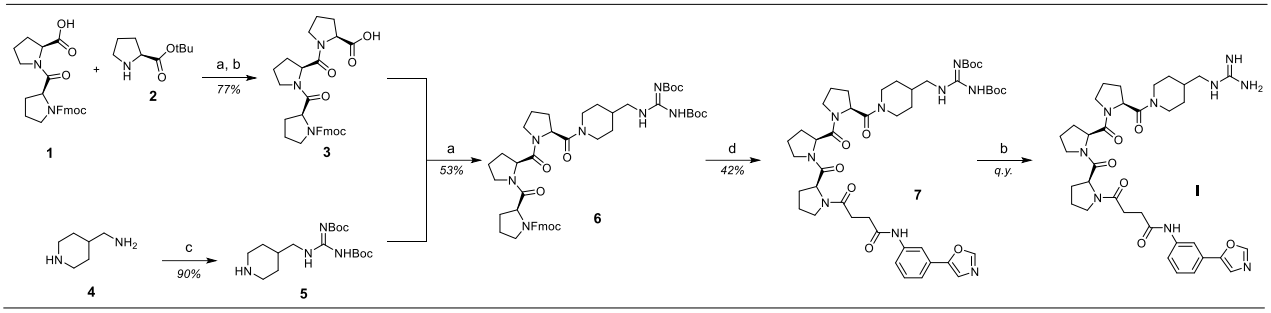

[a]Reagents and conditions: (a) TBTU, DIPEA, DMF, rt, 2h; (b) 1,2-DCE, TFA, 2h, reflux; (c) 1,3-di-Boc-2-methylisothiourea, CH_2Cl_2, 1h, rt; (d) DBU, DMF, 10 min, 50 °C *then* succinic anhydride, DIPEA, 20 min, rt *then* TBTU, 3-oxazol-5-ylaniline, 2h, rt ;

Schéma 8.14 Synthesis of compound **II**.

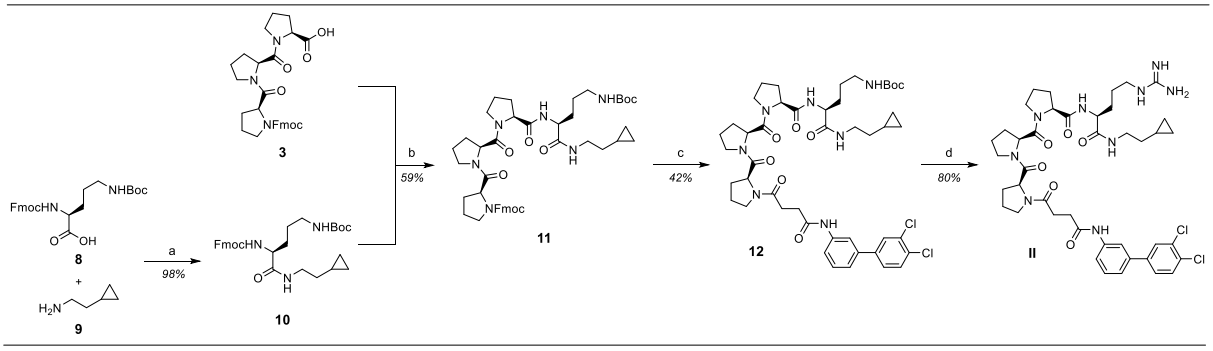

[a]Reagents and conditions: (a) TBTU, DIPEA, DMF, 1h, rt; (b) DBU, DMF, 50 °C *then* TBTU, DIPEA, DMF, 1h, rt; (c) DBU, DMF, 10 min, 50 °C *then* succinic anhydride, DIPEA, 20 min, rt *then* TBTU, 3-(3,4-dichlorophenyl)aniline, 2h, rt (d) HCl/1,4-dioxane, MeOH, 1h, rt *then* pyrazole-1-carboxamidine hydrochloride, DIPEA, DMA, 1h, 60 °C;

Schéma 8.15 Synthesis of compound **III**.

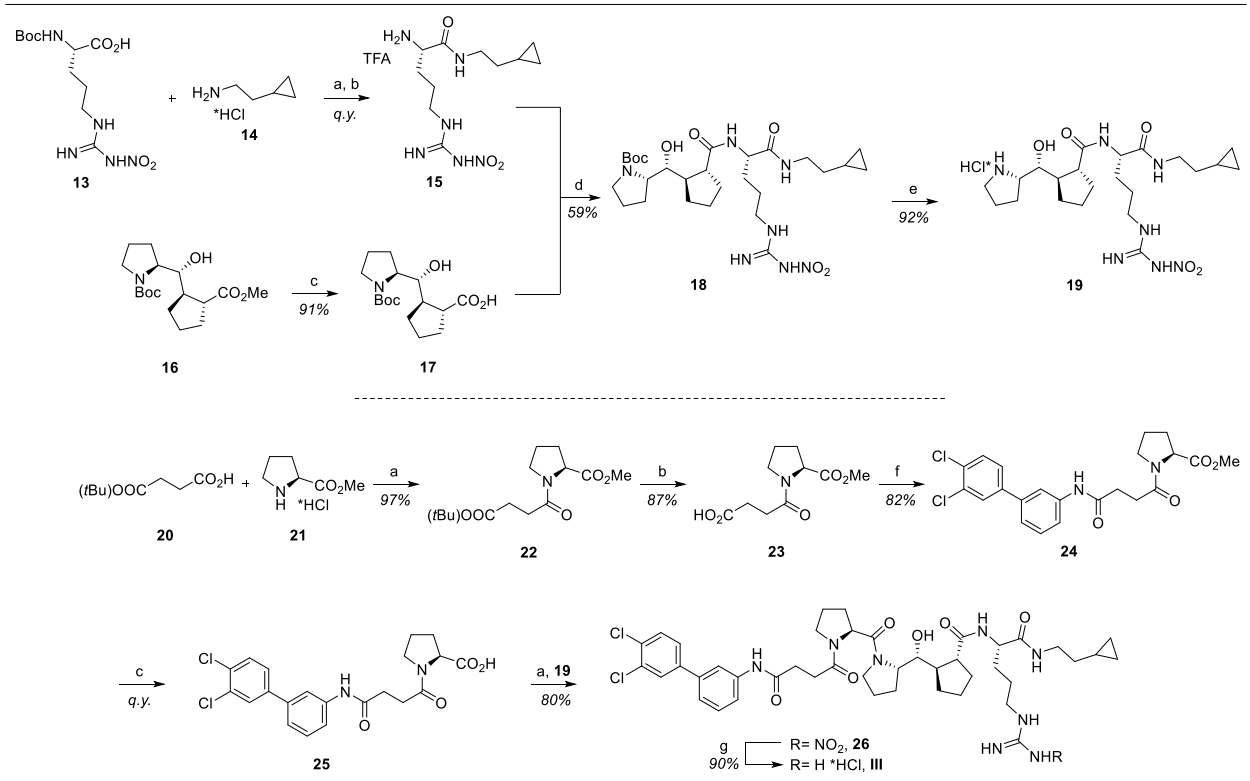

(a) EDC, HOBt, DIPEA, CH_2Cl_2, rt, 16h; (b) TFA/CH_2Cl_2, rt, 2h; (c) 1:1 1 M aq. LiOH/THF, rt, 1h; (d) DIPEA, PyBOP, CH_2Cl_2, rt, 16h; (e) HCl (4M), dioxane, rt, 30 min; (f) 3',4'-dichloro-[1,1'-biphenyl]-3-amine, HATU, DIPEA, CH_2Cl_2, rt, 7h; (g) H_2, 10% Pd/C, 1:1 MeOH/EtOAc, 6M aq. HCl (2 drops), rt, 4h.

Schéma 8.16 Synthesis of compound **IV**.

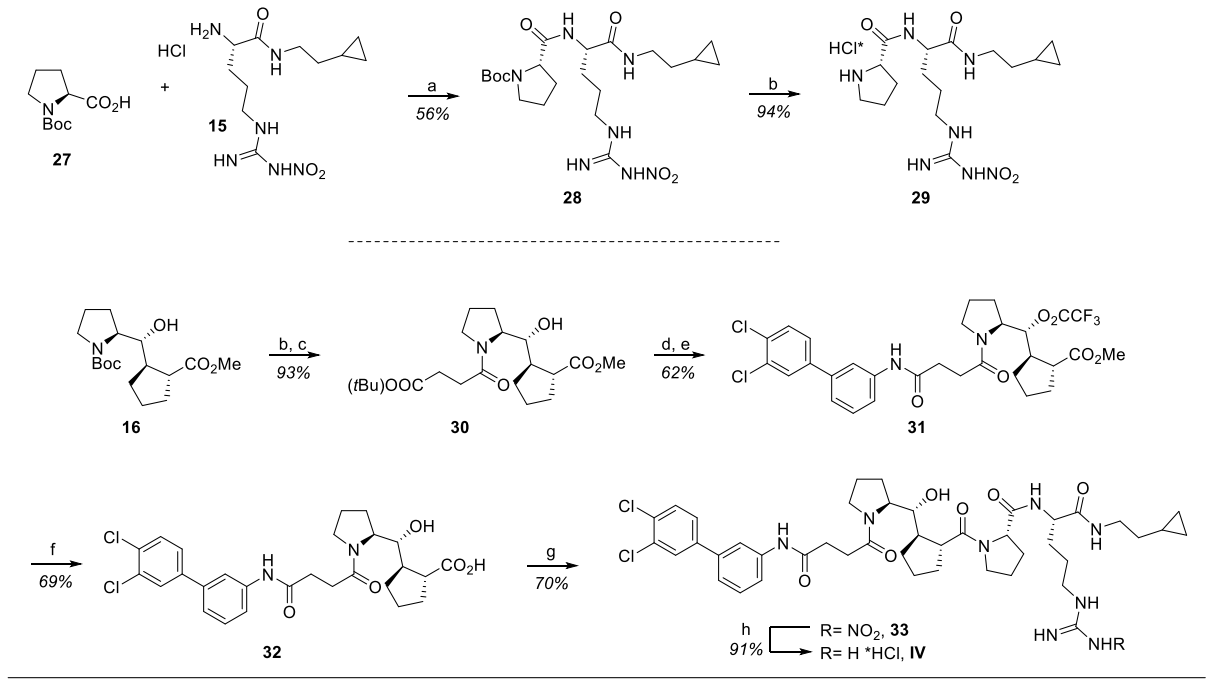

(a) DIPEA, PyBOP, CH_2Cl_2, rt, 16h; (b) HCl (4M), dioxane, rt, 30 min; (c) **20**, EDC, HOBt, DIPEA, CH_2Cl_2, rt, 16h; (d) TFA/CH_2Cl_2, rt, 2h; (e) 3',4'-dichloro-[1,1'-biphenyl]-3-amine, HATU, DIPEA, CH_2Cl_2, rt, 7h; (f) LiOH, THF, rt, 1h; (g) **29**, EDC, HOBt, DIPEA, CH_2Cl_2, rt, 16h; (h) H2, 10% Pd/C, 1:1 MeOH/EtOAc, 6M aq. HCl (2 drops), rt, 4h.

8.6.2 Synthesis and characterization of peptidomimetics

8.6.2.1 General procedures

General Procedure A: Amide coupling

Carboxylic acid (1.0 eq), TBTU (1.05 – 1.1 eq) and DIPEA (1.1 – 1.2 eq) were combined in a DMF solution (1.25 – 5.0 mL/mmol acid). After stirring at rt for 10 min, the amine (1.0 – 1.2 eq) was added and the mixture was stirred for another 1h. Work-up and purification (unless otherwise specified): the reaction mixture was filtered, injected onto an RP C18 column and purified via preparative reversed phase chromatography. The appropriate fractions were combined, concentrated under reduced pressure to approximately 25 mL then extracted with CH_2Cl_2 (2 × 20 mL). The combined organic extracts were dried over Na_2SO_4 and concentrated to furnish the targeted amide product.

General Procedure B: Fmoc deprotection

Fmoc protected amine (1.0 eq) and DBU (0.1 eq) were combined in a DMF solution (1.0 – 5.5 mL/mmol acid). After 20 min to 1h of stirring at 50 °C the solution was used in the next amide coupling step.

General Procedure C: Sequential amide coupling

To a solution of amine (1.0 eq) and DIPEA (2.8 – 3.0 eq) in DMF, succinic anhydride (1.1 eq) was added and the reaction mixture was stirred for 20 min at rt. TBTU (1.2 – 1.6 eq) followed by the substituted aniline (1.3 – 1.6 eq, dissolved in 1 mL DMF) were added and the mixture was stirred for 2h. Work-up and purification: same as described in General Procedure A (unless otherwise specified).

General Procedure D: Boc deprotection 1

Boc-protected amine (1.0 eq) was dissolved in an appropriate solvent and the acid (13 – 95 eq) was added. The mixture was stirred for 0.5 – 1h at rt then concentrated under reduced pressure.

General procedure E: Ester hydrolysis

To the ester substrate (1.0 eq.) dissolved in THF (0.7 M) was added LiOH (1.5 eq., 1.0 M in H_2O) at 0 °C. The reaction mixture was stirred at 0 °C for 5 min then at rt for 1h. The mixture was diluted with water, washed with Et_2O, acidified (pH = 3) with 10% aq. citric acid and extracted twice with EtOAc. The pooled organic phase was dried over anhydrous Na_2SO_4, filtered and the solvent removed under reduced pressure.

General procedure F: Boc deprotection 2

The protected compound was dissolved in HCl/dioxane (4.0 M, 10 eq.) and the solution was stirred at rt for 2h. The solvent was removed under reduced pressure.

General procedure G: *tert*-butyl ester deprotection

The protected compound was dissolved in CH_2Cl_2 (0.65 M). The solution was cooled at 0 °C and TFA (20 eq.) was added. The solution was stirred at rt for 4h then the solvent was removed under reduced pressure.

8.6.2.2 Synthesis of **I**

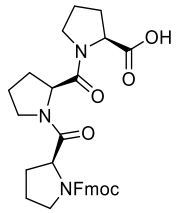

(2S)-1-[(2S)-1-[(2S)-1-(9H-Fluoren-9-ylmethoxycarbonyl)pyrrolidine-2-carbonyl]pyrrolidine-2-carbonyl]pyrrolidine-2-carboxylic acid **(3)**

Performed according to **General Procedure A.** Carboxylic acid **1** (1.3 g, 3.0 mmol, 1.0 eq.), TBTU (1.0 g, 3.1 mmol, 1.03 eq.), DIPEA (0.6 mL, 3.5 mmol, 1.2 eq.) and *tert*-butyl (2S)-pyrrolidine-2-carboxylate **2** (0.60 g, 3.5 mmol, 1.2 eq.) were reacted in DMF (10 mL). Exception to the general procedure: the reaction mixture was quenched by the addition of saturated aqueous solution of Na_2CO_3 then extracted with CH_2Cl_2 (2 × 50 mL). The combined organic extracts were dried over Na_2SO_4 and concentrated to give a brown syrup which was dissolved in 1,2-DCE (5 mL). TFA (3.0 mL, 39.20 mmol, 13 eq.) was added and the reaction mixture was refluxed for 2h. The reaction

mixture was cooled to rt, concentrated and the crude residue was purified by flash column chromatography over silica (eluent: CH_2Cl_2 /acetone 10-40%) to provide the title compound **3** as a white foam (1.2 g, 77%).

^{1}H NMR (500 MHz, DMSO-d6) δ 7.93-7.86 (m, 2H), 7.69-7.62 (m, 1H), 7.60+7.57 (2d, J=7.7 Hz, 1H). 7.46-7.28 (m, 4H), 4.65-4.11 (m, 6H), 3.71-3.07 (m, 6H), 2.24-1.58 (m, 12H).
HRMS (ESI-TOF) m/z: $[M+H]^+$ calcd for $C_{30}H_{33}N_3O_6$ 532.2448, found 532.2439.

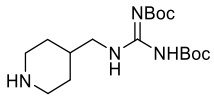

tert-Butyl (NE)-N-[(tert-butoxycarbonylamino)-(4-piperidylmethylamino)methylene]carbamate **(5)**

To the solution of **4** (1.8 g, 15.4 mmol, 1.5 eq.) in CH_2Cl_2 (40 mL) *tert*-butyl (NZ)-N-[(*tert*-butoxycarbonylamino)-methylsulfanyl-methylene]carbamate (2.9 g, 10 mmol, 1.0 eq.) was added over 5 min. The reaction mixture was stirred for 1h then the volatiles were removed under reduced pressure and water (20 mL) was added to the residue. A white precipitate was formed and filtered off. The precipitate was dissolved in CH_2Cl_2 (50 mL), the organic solution was dried over $MgSO_4$ and concentrated to afford the title compound **5** as white crystals (3.2 g, 90%).
^{1}H NMR (500 MHz, DMSO-d6) δ 8.28 (t, J=5.5 Hz, 1H), 3.16 (t, J=5.5 Hz, 2H), 2.90 (brd, J=12.0 Hz, 2H), 2.39 (td, J=12.0, 2.2 Hz, 2H), 1.64-1.53 (m, 1H), 1.52 (d, J=11.8 Hz, 2H), 1.47 (s, 9H), 1.39 (s, 9H), 1.01 (qd, J=11.8, 3.8 Hz, 2H).
HRMS (ESI-TOF) m/z: $[M+H]^+$ calcd for $C_{17}H_{32}N_4O_4$ 357.2502, found 357.2491.

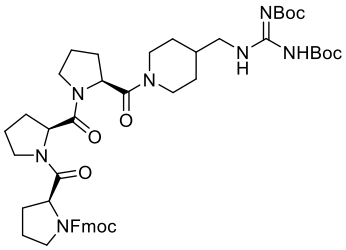

9H-Fluoren-9-ylmethyl (2S)-2-[(2S)-2-[(2S)-2-[4-[[[(E)-N,N'-bis(tert-butoxycarbonyl)carbamimidoyl] amino]methyl]piperidine-1-carbonyl]pyrrolidine-1-carbonyl]pyrrolidine-1-carbonyl]pyrrolidine-1-carboxylate **(6)**

Following **General Procedure A,** carboxylic acid **3** (2.7 g, 5.0 mmol, 1.0 eq.), TBTU (1.8 g, 5.5 mmol, 1.1 eq.), DIPEA (1.1 mL, 6.3 mmol, 1.3 eq.) and amine **5** (2.1 g, 6.0 mmol, 1.2 eq.) were reacted in DMF (10 mL) to afford the title product **6** as a white foam (2.3 g, 53%).

^{1}H NMR (500 MHz, DMSO-d6) δ 11.50 (s, 1H), 8.40-8.27 (m, 1H), 7.94-7.82 (m, 2H), 7.69-7.62 (m, 1H), 7.60+7.57 (2d, J=7.7 Hz, 1H), 7.45-7.28 (m, 4H), 4.88-4.10 (m, 8H), 4.04-3.87 (m, 1H), 3.72-3.35 (m, 4H), 3.32-3.09 (m, 4H), 3.05-2.87 (m, 1H), 2.21-2.00 (m, 3H), 1.97-1.55 (m, 12H), 1.47 (s, 9H), 1.39 (s, 9H) 1.19-0.87 (m, 2H).

HRMS (ESI-TOF) m/z: $[M+H]^+$ calcd for $C_{47}H_{63}N_7O_9$ 870.4766, found 870.4746.

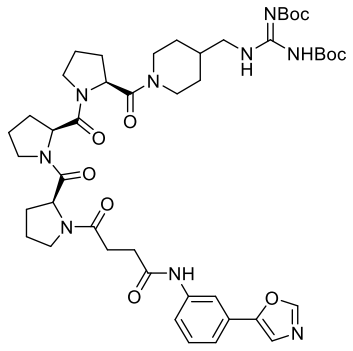

tert-Butyl (NE)-N-[(tert-butoxycarbonylamino)-[[1-[(2S)-1-[(2S)-1-[(2S)-1-[4-(3-oxazol-5-ylanilino)-4-oxo-butanoyl]pyrrolidine-2-carbonyl]pyrrolidine-2-carbonyl]pyrrolidine-2-carbonyl]-4-piperidyl]methylamino] methylene]carbamate **(7)**

Step I. Following **General Procedure B,** Fmoc-amine **6** (0.21 g, 0.25 mmol, 1.0 eq.) and DBU (2.5 µL, 17 µmol, 0.07 eq.) were reacted in DMF (3.0 mL) for 20 min. Step II. Following **General Procedure C,** DIPEA (0.12 mL, 0.70 mmol, 2.8 eq.), succinic anhydride (27 mg, 0.27 mmol, 1.1 eq.), TBTU (95 mg, 0.30 mmol, 1.2 eq.) and 3-oxazol-5-ylaniline (98 mg, 0.39 mmol, 1.6 eq.) were added successively to the solution of amine prepared in Step I. After purification and work-up the title compound **7** was isolated as a white foam (102 mg, 42%).

^{1}H NMR (500 MHz, DMSO-d6) δ 11.52+11.50 (2s, 1H), 10.1 (s, 1H), 8.45 (s, 1 H), 8.37-8.30 (m, 1H), 8.05 (brs, 1H), 7.62 (s, 1H), 7.54-7.48 (m, 1H), 7.42-7.36 (m, 2H), 4.87-4.49 (m, 3H), 4.36-2.90 (m, 11H), 2.74-1.54 (m, 20H), 1.47 (s, 9H), 1.39 (s, 9H), 1.19-0.86 (m, 2H).

HRMS (ESI-TOF) m/z: $[M+H]^+$ calcd for $C_{47}H_{63}N_7O_9$ 890.4776, found 890.4776.

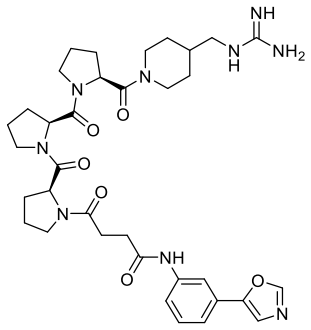

4-[(2S)-2-[(2S)-2-[(2S)-2-[4-(Guanidinomethyl)piperidine-1-carbonyl]pyrrolidine-1-carbonyl]pyrrolidine-1-carbonyl]pyrrolidin-1-yl]-N-(3-oxazol-5-ylphenyl)-4-oxo-butanamide trifluoroacetic acid salt **(I)**

Following **General Procedure D** deprotection step**,** Boc-guanidine **7** (100 mg, 0.11 mmol, 1.0 eq.) and TFA (0.8 mL, 10 mmol, 95 eq.) were reacted in DCE (2.0 mL) for 1h at 50 °C. Methanol (5.0 mL) was added and the solution was concentrated under reduced pressure at rt. The residue was dissolved in acetonitrile/water (1:2 mL) and freeze-dried to furnish the title compound **I** as a white foam (94.0 mg, quantitative yield).

^{1}H NMR (500 MHz, DMSO-d_6) δ 10.11 (s, 1H), 8.45 (s, 1H), 8.05 (bs, 1H), 7.62 (s, 1H), 7.59 (m, 1H), 7.54 – 7.49 (m, 1H), 7.39 (m, 2H), 7.25 – 6.68 (m, 4H), 4.86 – 4.51 (m, 3H), 4.34 – 4.24 (m, 1H), 4.00 (m, 1H), 3.79 – 3.58 (m, 2H), 3.56 – 3.32 (m, 4H), 3.02 (m, 2H), 2.72 – 2.63 (m, 1H), 2.60 – 2.55 (m, 1H), 2.55 – 2.52 (m, 3H), 2.20 – 1.59 (m, 14H), 1.17 – 0.88 (m, 2H).

^{13}C NMR (126 MHz, DMSO) δ 170.9, 169.5, 169.2, 158.4, 158.2, 151.9, 150.5, 140.1, 129.6, 127.8, 122.0, 118.9, 118.8, 117.0, 114.1, 57.7, 57.4, 56.4, 46.7, 46.5, 46.5, 46.3, 45.6, 44.1, 41.1, 35.5, 31.0, 29.5, 28.8, 28.4, 27.9, 27.3, 24.4, 24.3, 24.1.

HRMS (ESI-TOF) m/z: $[M+H]^+$ calcd for $C_{35}H_{47}N_9O_6$ 690.3728, found 690.3725.

HPLC: 94%

8.6.2.3 Synthesis of **II**

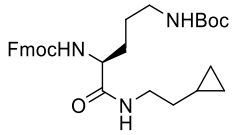

9H-Fluoren-9-ylmethyl N-[(1S)-4-(tert-butoxycarbonylamino)-1-(2-cyclopropylethylcarbamoyl) butyl] carbamate **(10)**

Following **General Procedure A**, carboxylic acid **8** (5.0 g, 11 mmol, 1.0 eq.), TBTU (3.9 g, 12 mmol, 1.1 eq.), DIPEA (3.8 mL, 22 mmol, 2.0 eq.) and 2-cyclopropylethanamine **9** (1.2 mL, 13 mmol, 1.2 eq.) were reacted in DMF (20.0 mL) then the reaction mixture was poured into ice/water (300 mL). The precipitated product was collected by filtration, washed with water and dried in high vacuum at 40 °C to provide the title compound **10** as a white solid (5.6 g, 98%).

^{1}H NMR (500 MHz, DMSO-d6) δ 7.89 (dm, J=7.4 Hz, 2H), 7.84 (dm, J=7.4 Hz, 2H), 7.82-7.70 (m, 1H), 7.41 (td, J=7.4, 1.1 Hz, 2H), 7.34 (td, J=7.4, 1.1 Hz, 2H), 6.84-6.75 (m, 1H), 6.54-6.31 (br, 1H), 4.32-3.00 (m, 5H), 2.94-2.80 (m, 2H), 1.64-1.18 (m, 16H), 0.73-0.58 (m, 1H), 0.42-0.29 (m, 2H), 0.08- -0.05 (m, 2H).

HRMS (ESI-TOF) m/z: $[M+H]^+$ calcd for $C_{30}H_{39}N_3O_5$ 522.2968, found 522.2961.

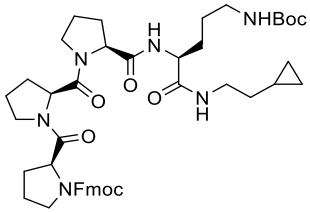

9H-Fluoren-9-ylmethyl (2S)-2-[(2S)-2-[(2S)-2-[[(1S)-4-(tert-butoxycarbonylamino)-1-(2-cyclopropylethylcarbamoyl) butyl]carbamoyl]pyrrolidine-1-carbonyl]pyrrolidine-1-carbonyl]pyrrolidine-1-carboxylate **(11)**

Step I. Following **General Procedure B**, Fmoc-amine **10** (2.2 g, 4.3 mmol, 1.2 eq.) and DBU (65 µL, 0.43 mmol, 0.12 eq.) were reacted in DMF (10 mL) for 1h. Step II. Following **General Procedure**

A, carboxylic acid **3** (1.9 g, 3.6 mmol, 1.0 eq.), TBTU (1.3 g, 3.9 mmol, 1.1 eq.), DIPEA (0.7 mL, 4.3 mmol, 1.2 eq.) and the solution of amine **10** prepared in Step I were reacted in DMF (10 mL) then the reaction mixture was concentrated to give a brown syrup. The crude product was dissolved in CH_2Cl_2 (50 mL) and washed with water (2 × 30 mL). The organic phase was dried over Na_2SO_4 and concentrated to provide the title compound **11** as a white foam which was used in the next step without further purification (1.7 g, 59%).

^{1}H NMR (500 MHz, DMSO-d6) δ 7.92-7.87 (m, 2H), 7.77-7.71 (m, 2H), 7.68-7.63 (m, 1H), 7.61-7.55 (m, 1H), 7.45-7.28 (m, 4H), 6.78-6.71 (m, 1H), 4.59-4.03 (m, 7H), 3.72-2.96 (m, 8H), 2.93-2.79 (m, 2H), 2.22-1.21 (m, 27H), 0.72-0.59 (m, 1H), 0.41-0.32 (m, 2H), 0.05- -0.05 (m, 2H);

HRMS (ESI-TOF) m/z: $[M+H]^+$ calcd for $C_{45}H_{60}N_6O_8$ 813.4551, found 813.4542.

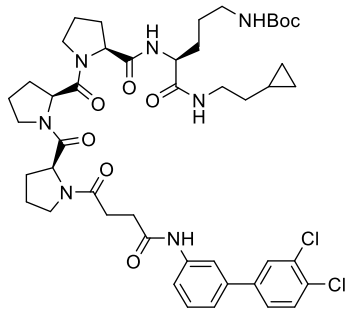

tert-Butyl N-[(4S)-5-(2-cyclopropylethylamino)-4-[[(2S)-1-[(2S)-1-[(2S)-1-[4-[3-(3,4-dichlorophenyl)anilino]-4-oxo-butanoyl]pyrrolidine-2-carbonyl]pyrrolidine-2-carbonyl]pyrrolidine-2-carbonyl]amino]-5-oxo-pentyl]carbamate **(12)**

Step I. Following **General Procedure B**, Fmoc-amine **11** (0.15 g, 0.19 mmol, 1.0 eq.) and DBU (3.0 µL, 0.02 mmol, 0.1 eq.) were reacted in DMF (2.0 mL) for 20 min. Step II. Following **General Procedure C,** DIPEA (90 µL, 0.53 mmol, 2.8 eq.), succinic anhydride (21 mg, 0.21 mmol, 1.1 eq.), TBTU (72 mg, 0.22 mmol, 1.2 eq,) and 3-(3,4-dichlorophenyl)aniline hydrochloride (82 mg, 0.30 mmol, 1.6 eq.) were added successively to the solution of amine prepared in Step I. After purification and work-up the title compound **12** was isolated as a white foam (102.0 mg, 42%).

^{1}H NMR (500 MHz, DMSO-d6) δ 10.11-9.99 (s, 1H), 7.98-7.93 (m, 1H), 7.85-7.81 (m, 1H), 7.78-7.69 (m, 3H), 7.63-7.55 (m, 2H), 7.43-7.33 (m, 2H), 6.75 (t, J=5.7 Hz, 1H), 4.89-4.02 (m, 4H), 3.83-

3.25 (m, 7H), 3.19-2.98 (m, 2H), 2.91-2.82 (m, 2H), 2.80-1.18 (m, 31H), 0.71-0.59 (m, 1H), 0.40-0.31 (m, 2H), 0.05- -0.04 (m, 2H);

HRMS (ESI-TOF) m/z: $[M+H]^+$ calcd for $C_{46}H_{61}Cl_2N_7O_8$: 910.4037, found 910.4025.

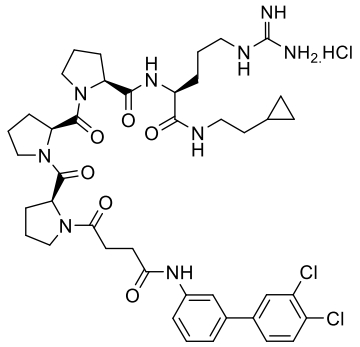

(2S)-N-[(1S)-1-(2-Cyclopropylethylcarbamoyl)-4-guanidino-butyl]-1-[(2S)-1-[(2S)-1-[4-[3-(3,4-dichlorophenyl) anilino]-4-oxo-butanoyl]pyrrolidine-2-carbonyl]pyrrolidine-2-carbonyl]pyrrolidine-2-carboxamide trifluoroacetic acid salt **(II)**

Following **General Procedure D**, Boc-amine **12** (33 mg, 36 µmol, 1.0 eq.) and HCl (0.8 mL, 3.2 mmol, 4.0 M in 1,4-dioxane, 90 eq) were reacted in 1,4-dioxane (3.0 mL) and methanol (1.0 mL) for 1h then concentrated under reduced pressure. The residue was then dissolved in DMA (1.0 mL), and DIPEA (50 µL, 0.30 mmol, 8.0 eq.) followed by pyrazole-1-carboxamidine hydrochloride (42 mg, 0.30 mmol, 8.0 eq.) were added. After stirring for 16 h at 60 °C the reaction mixture was concentrated under reduced pressure. The residue was dissolved in acetonitrile/water (2:2 mL) then directly injected onto a preconditioned 40 g silica column and purified via HILIC to afford compound **II** as a white powder (28.0 mg, 80%).

^{1}H NMR (500 MHz, DMSO-d_6) δ 10.09 (m, 1H), 7.96 (bs, 1H), 7.89 – 7.79 (m, 3H), 7.73 (d, *J* = 8.4 Hz, 1H), 7.59 (m, 2H), 7.48 (m, 1H), 7.42 – 7.35 (m, 2H), 7.01 (m, 4H), 4.65 – 4.50 (m, 1H), 4.30 (m, 1H), 4.14 – 4.10 (m, 1H), 3.70 – 3.32 (m, 7H), 3.18 – 3.01 (m, 4H), 2.72 – 2.52 (m, 3H), 2.20 – 1.83 (m, 9H), 1.81 – 1.63 (m, 5H), 1.55 – 1.36 (m, 3H), 1.29 (q, *J* = 7.0 Hz, 2H), 0.66 (m, 1H), 0.37 (dd, *J* = 8.0, 1.4 Hz, 2H), 0.01 (m, 2H).

^{13}C NMR (126 MHz, DMSO) δ 171.4, 170.8, 170.4, 169.6, 169.2, 156.6, 140.8, 140.1, 138.0, 131.1, 129.8, 129.5, 129.3, 129.1, 128.3, 126.8, 121.3, 118.7, 117.0, 58.1, 58.1, 57.6, 52.7, 46.6, 46.5, 40.5, 39.3, 33.9, 31.0, 29.0, 28.8, 28.4, 27.9, 27.7, 25.0, 24.5, 24.4, 24.1, 22.0, 8.5, 4.1, 4.1.

HRMS (ESI-TOF) m/z: $[M+H]^+$ calcd for $C_{42}H_{55}Cl_2N_9O_6$ 852.3731, found 852.3716.

HPLC: 98%

8.6.2.4 Synthesis of **III**

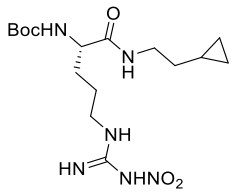

(S)-tert-Butyl (1-((2-cyclopropylethyl)amino)-5-(3-nitroguanidino)-1-oxopentan-2-yl)carbamate **(13a)**

2-Cyclopropylethanamine hydrochloride **14** (0.10 g, 0.82 mmol, 1.0 eq.) was dissolved in CH_2Cl_2 (2.7 mL) and the solution was cooled to 0 °C. BocArg(NO_2)OH **13** (0.33 g, 0.99 mmol, 1.2 eq.) and DIPEA (501 µL, 2.88 mmol, 3.5 eq.) were added, followed by HOBt (0.13 g, 0.99 mmol, 1.2 eq.) and EDC (378 mg, 1.97 mmol, 2.4 eq.). The reaction mixture was stirred at 0 °C for 10 min, then at rt for 14h. The reaction mixture was diluted with CH_2Cl_2, washed with 10% aq. citric acid, 10% aq. $NaHCO_3$, and brine. The organic phase was dried over anhydrous Na_2SO_4, filtered and the solvent removed under reduced pressure. The crude was purified by column chromatography on SiO_2 gel with 95:5 to 92.5:7.5 CH_2Cl_2/MeOH obtaining the title compound as a white foam (318.0 mg, q.y.).

^{1}H NMR (500 MHz, Chloroform-*d*) δ 8.66 (bs, 1H), 8.10 – 7.42 (bs, 2H), 6.96 (bs, 1H), 5.64 (bs, 1H), 4.34 – 3.96 (m, 1H), 3.46 – 3.19 (m, 4H), 1.87 – 1.55 (m, 4H), 1.41 (m, 11H), 0.64 (m, 1H), 0.47 – 0.34 (m, 2H), 0.08 – -0.04 (m, 2H).

HRMS (ESI-TOF) m/z: $[M+H]^+$ calcd for $C_{16}H_{30}N_6O_5$: 387.23504; found 387.23440. $[M+Na]^+$ calcd for $C_{16}H_{30}N_6O_5$: 409.21699; found 409.21668.

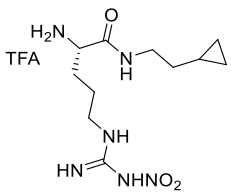

(S)-2-Amino-N-(2-cyclopropylethyl)-5-(3-nitroguanidino)pentanamide trifluoroacetate **(15)**

The title compound was obtained from **13a** (0.32 g, 0.82 mmol, 1.0 eq.) following general procedure **G** as an orange foam (236.0 mg, q.y.).

^{1}H NMR (500 MHz, Methanol-d_4) δ 3.87 (m, 1H), 3.33 – 3.25 (m, 4H), 1.90 (m, 2H), 1.68 (m, 2H), 1.42 (m, 2H), 0.77 – 0.65 (m, 1H), 0.50 – 0.39 (m, 2H), 0.08 (m, 2H).

HRMS (ESI-TOF) m/z: $[M+H]^+$ calcd for $C_{11}H_{22}N_6O_3$: 287.18262; found 287.18198. $[M+Na]^+$ calcd for $C_{11}H_{22}N_6O_3$: 309.16456; found 309.16415.

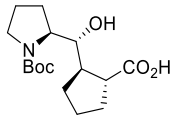

(1R,2R)-2-((R)-((S)-1-(tert-Butoxycarbonyl)pyrrolidin-2-yl)(hydroxy)methyl)cyclopentanecarboxylic acid **(17)**

The title compound was synthetised from **16**[511] (54 mg, 0.16 mmol, 1.0 eq.) following general procedure **E**. The reaction mixture was acidified with 10% aq. citric acid, then extracted twice with EtOAc. The pooled organic phase was dried over anhydrous Na_2SO_4, filtered and the solvent removed under reduced pressure to afford **17** as a colourless oil (46.4 mg, 91%).

^{1}H NMR (400 MHz, Methanol-d_4) δ 3.94 – 3.77 (m, 2H), 3.47 (m, 1H), 3.27 (m, 1H), 2.71 (m, 1H), 2.27 – 2.15 (m, 1H), 2.09 – 1.79 (m, 6H), 1.71 (m, 3H), 1.47 (m, 10H).

HRMS (ESI-TOF) m/z: $[M+Na]^+$ calcd for $C_{16}H_{27}NO_5$: 336.17814; found 336.17916. $[M+K]^+$ calcd for $C_{16}H_{27}NO_5$: 352.15208; found 352.15194.

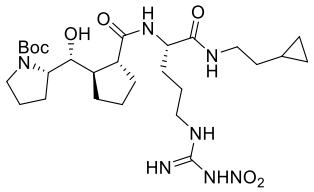

(S)-tert-Butyl 2-((R)-((1R,2R)-2-(((S)-1-((2-cyclopropylethyl)amino)-5-(3-nitroguanidino)-1-oxopentan-2-yl)carbamoyl)cyclopentyl)(hydroxy)methyl)pyrrolidine-1-carboxylate **(18)**

An amount of **17** (46 mg, 0.15 mmol, 1.0 eq.) was dissolved in CH_2Cl_2 (740 µL) and the solution was cooled to 0 °C. **15** (71 mg, 0.18 mmol, 1.2 eq.) and DIPEA (0.11 mL, 0.64 mmol, 4.3 eq.) were added, followed by PyBOP (0.12 g, 0.22 mmol, 1.5 eq.). The reaction mixture was stirred at 0 °C for 10 min, then at rt for 14h. The reaction mixture was diluted with CH_2Cl_2, washed with 10% aq. citric acid, 10% aq. $NaHCO_3$, and brine. The organic phase was dried over anhydrous Na_2SO_4, filtered and the solvent removed under reduced pressure. The crude was purified by column chromatography on SiO_2 gel with 95:5 to 92:8 CH_2Cl_2/MeOH to afford **18** as a white foam (51.2 mg, 59%).

^{1}H NMR (500 MHz, Chloroform-*d*) δ 8.55 (bs, 1H), 7.67 (m, 2H), 7.22 (m, 1H), 4.56 (m, 1H), 3.91 (m, 2H), 3.47 (m, 2H), 3.29 – 3.17 (m, 4H), 2.67 (m, 1H), 2.06 – 1.56 (m, 14H), 1.43 (s, 11H), 1.35 (q, *J* = 7.1 Hz, 2H), 0.61 (m, 1H), 0.43 – 0.34 (m, 2H), 0.01 (m, 2H).

HRMS (ESI-TOF) m/z: $[M+H]^+$ calcd for $C_{27}H_{47}N_7O_7$: 582.36097; found 582.36248. $[M+Na]^+$ calcd for $C_{27}H_{47}N_7O_7$: 604.34292; found 604.34452.

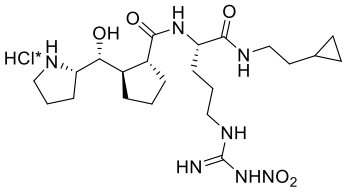

(1R,2R)-N-((S)-1-((2-Cyclopropylethyl)amino)-5-(3-nitroguanidino)-1-oxopentan-2-yl)-2-((R)-hydroxy((S)-pyrrolidin-2-yl)methyl)cyclopentanecarboxamide hydrochloride **(19)**

The title compound was obtained from **18** (51 mg, 88 µmol, 1.0 eq.) following general procedure **F** as a white foam (42 mg, 92%).

^{1}H NMR (500 MHz, Chloroform-*d*) δ 4.41 (m, 1H), 3.83 (dd, *J* = 9.5, 2.8 Hz, 1H), 3.69 (m, 1H), 3.40 – 3.26 (m, 6H), 2.77 (q, *J* = 8.1 Hz, 1H), 2.28 (p, *J* = 8.7 Hz, 1H), 2.13 – 1.96 (m, 5H), 1.81 (m, 9H), 1.44 – 1.40 (m, 3H), 0.73 (m, 1H), 0.51 – 0.41 (m, 2H), 0.09 (m, 2H).

HRMS (ESI-TOF) m/z: $[M+H]^+$ calcd for $C_{22}H_{39}N_7O_5$: 482.30854; found 482.30957.

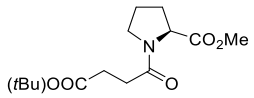

(S)-methyl 1-(4-(tert-Butoxy)-4-oxobutanoyl)pyrrolidine-2-carboxylate **(22)**

ProOMe*HCl **21** (0.15 g, 0.90 mmol, 1.0 eq.) was dissolved in CH_2Cl_2 (3.0 mL) and the solution was cooled to 0 °C. Mono-*tert*-butyl succinate **20** (187 mg, 1.10 mmol, 1.2 eq.) and DIPEA (545 µL, 3.13 mmol, 3.5 eq.) were added, followed by HOBt (145 mg, 1.07 mmol, 1.2 eq.) and EDC (412 mg, 2.15 mmol, 2.4 eq.). The reaction mixture was stirred at 0 °C for 10 min, then at rt for 14h. The reaction mixture was diluted with CH_2Cl_2, washed with 10% aq. citric acid, 10% aq. $NaHCO_3$, and brine. The organic phase was dried over anhydrous Na_2SO_4, filtered and the solvent removed under reduced pressure. The crude was purified by column chromatography on SiO_2 gel with 1:1 to 4:6 hexanes/EtOAc obtaining the title compound as a colorless oil (247.0 mg, 97%).

^{1}H NMR (500 MHz, Chloroform-*d*, mixture of rotamers) δ 4.49 (dd, *J* = 8.7, 3.5 Hz, 1H), 3.75 (s, 0.6H), 3.70 (s, 2.4H), 3.68 – 3.59 (m, 1H), 3.55 (m, 1H), 2.69 – 2.47 (m, 4H), 2.27 (m, 0.4H), 2.17 (m, 1H), 2.11 – 1.94 (m, 2.3H), 1.89 (m, 0.3H), 1.43 (s, 9H).

HRMS (ESI-TOF) m/z: $[M+H]^+$ calcd for $C_{14}H_{23}NO_5$ 286.16490; found 286.16513. $[M+Na]^+$ calcd for $C_{14}H_{23}NO_5$: 308.14684; found 308.14760.

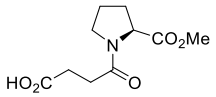

(S)-4-(2-(Methoxycarbonyl)pyrrolidin-1-yl)-4-oxobutanoic acid **(23)**

The title compound was obtained from **22** (0.23 g, 0.80 mmol, 1.0 eq.) following general procedure **G** as a colorless oil (184 mg, 87%).

^{1}H NMR (500 MHz, Chloroform-*d*, mixture of rotamers) δ 8.44 (bs, 1H), 4.48 (m, 1H), 3.75 (s, 0.6H), 3.70 (s, 2.4H), 3.64 (m, 1H), 3.53 (m, 1H), 2.79 – 2.51 (m, 4H), 2.40 – 2.15 (m, 1.4H), 2.07 – 1.86 (m, 2.6H).

HRMS (ESI-TOF) m/z: $[M+H]^+$ calcd for $C_{10}H_{15}NO_5$: 230.10230; found 230.10259. $[M+Na]^+$ calcd for $C_{10}H_{15}NO_5$: 252.08424; found 252.08483.

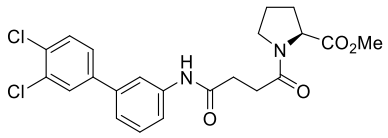

(S)-methyl 1-(4-((3',4'-Dichloro-[1,1'-biphenyl]-3-yl)amino)-4-oxobutanoyl)pyrrolidine-2-carboxylate **(24)**

An amount of **23** (0.11 g, 0.46 mmol, 1.0 eq.) was dissolved in CH_2Cl_2 (2.4 mL) and the solution was cooled to 0 °C. 3',4'-dichloro-[1,1'-biphenyl]-3-amine (0.13 g, 0.55 mmol, 1.2 eq.) and DIPEA (239 µL, 1.37 mmol, 3.0 eq.) were added, followed by HATU (0.26 g, 0.69 mmol, 1.5 eq.). The reaction mixture was stirred at 0 °C for 10 min, then at rt for 7h. The reaction mixture was diluted with CH_2Cl_2, washed with 10% aq. citric acid, 10% aq. $NaHCO_3$, and brine. The organic phase was dried over anhydrous Na_2SO_4, filtered and the solvent removed under reduced pressure. The crude was purified by column chromatography on SiO_2 gel with 1:9 hexanes/EtOAc to afford **24** as a white foam (168.0 mg, 82%).

^{1}H NMR (500 MHz, Chloroform-*d*, mixture of rotamers) δ 8.97 (m, 1H), 7.78 (s, 0.14H), 7.75 (s, 0.86H), 7.62 (m, 1H), 7.47 – 7.42 (m, 2H), 7.36 (m, 1H), 7.32 – 7.27 (m, 1H), 7.19 – 7.13 (m, 1H), 4.50 (ddd, *J* = 12.6, 8.5, 3.1 Hz, 1H), 3.77 (s, 0.4H), 3.66 (s, 3.6H), 3.56 (dt, *J* = 9.8, 7.0 Hz, 1H), 2.88 – 2.56 (m, 3.86H), 2.52 – 2.44 (m, 0.14H), 2.33 – 2.25 (m, 0.14H), 2.19 (m, 0.86H), 2.12 – 2.04 (m, 1H), 2.03 – 1.97 (m, 1.7H), 1.90 (m, 0.3H).

HRMS (ESI-TOF) m/z: $[M+H]^+$ calcd for $C_{22}H_{22}Cl_2N_2O_4$: 449.10294; found 449.10399. $[M+Na]^+$ calcd for $C_{22}H_{22}Cl_2N_2O_4$: 471.08488; found 471.08561.

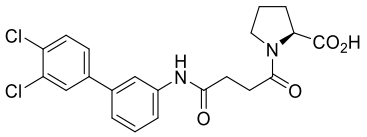

(S)-1-(4-((3',4'-Dichloro-[1,1'-biphenyl]-3-yl)amino)-4-oxobutanoyl)pyrrolidine-2-carboxylic acid **(25)**

The title compound was obtained from **24** (0.10 g, 0.23 mmol, 1.0 eq.) following general procedure **E**. The reaction mixture was acidified with 10% aq. citric acid, then extracted twice with EtOAc. The pooled organic phase was dried over anhydrous Na_2SO_4, filtered and the solvent removed under reduced pressure to afford **25** as a white foam (98.8 mg, q.y.).

^{1}H NMR (500 MHz, Chloroform-*d*, mixture of rotamers) δ 10.03 (bs, 1H), 9.32 (m, 0.2H), 9.22 (m, 0.8H), 7.72 (m, 1H), 7.52 (s, 1H), 7.42 (m, 1H), 7.34 (m, 1H), 7.18 (t, *J* = 7.9 Hz, 1H), 7.07 (m, 1H), 4.49 (dd, *J* = 8.3, 2.9 Hz, 0.16H), 4.40 (m, 0.84H), 3.56 (m, 1H), 3.41 (m, 1H), 2.89 – 2.56 (m, 4H), 2.14 – 1.77 (m, 4H).

HRMS (ESI-TOF) m/z: $[M+H]^+$ calcd for $C_{21}H_{20}Cl_2N_2O_4$: 435.08729; found 435.08776. $[M+H]^+$ calcd for $C_{21}H_{20}Cl_2N_2O_4$: 457.06923; found 457.06938.

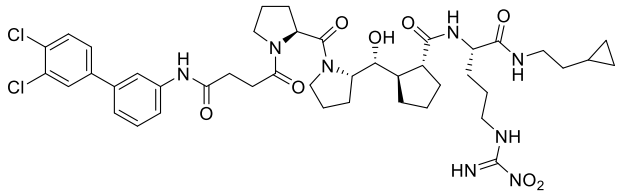

(1R,2R)-N-((S)-1-((2-Cyclopropylethyl)amino)-5-(3-nitroguanidino)-1-oxopentan-2-yl)-2-((R)-((S)-1-((S)-1-(4-((3',4'-dichloro-[1,1'-biphenyl]-3-yl)amino)-4-oxobutanoyl)pyrrolidine-2-carbonyl)pyrrolidin-2-yl)(hydroxy)methyl)cyclopentanecarboxamide **(26)**

An amount of **25** (49 mg, 94 µmol, 1.0 eq.) and **19** (41 mg, 94 µmol, 1.0 eq.) were dissolved in CH_2Cl_2 (314 µL) and the solution was cooled to 0 °C. DIPEA (57 µL, 0.33 mmol, 3.5 eq.) was added, followed by HOBt (15 mg, 0.11 mmol, 1.2 eq.) and EDC (43 mg, 0.23 mmol, 2.4 eq.). The reaction mixture was stirred at 0 °C for 10 min, then at rt for 14h. The reaction mixture was diluted with CH_2Cl_2, washed with 10% aq. citric acid, 10% aq. $NaHCO_3$, and brine. The organic phase was dried

over anhydrous Na_2SO_4, filtered and the solvent removed under reduced pressure. The crude was purified by column chromatography on SiO_2 gel with 93:7 CH_2Cl_2/MeOH to afford **26** as an amorphous solid (68 mg, 80%).

^{1}H NMR (500 MHz, Methanol-d_4, mixture of rotamers) δ 7.89 (m, 0.15H), 7.86 (m, 0.15H), 7.83 (m, 0.7H), 7.72 (t, *J* = 2.0 Hz, 0.3H), 7.71 (m, 0.7H), 7.56 – 7.45 (m, 3H), 7.35 (m, 1H), 7.28 (m, 1H), 4.91 (dd, *J* = 8.7, 3.1 Hz, 0.3H), 4.64 (m, 0.85H), 4.53 – 4.45 (m, 0.15H), 4.34 (m, 1H), 4.17 (m, 0.15H), 4.10 – 4.04 (m, 0.85H), 3.93 (m, 1H), 3.79 – 3.65 (m, 3H), 3.48 (m, 0.15H), 3.42 (m, 0.85H), 3.29 – 3.19 (m, 4H), 2.90 – 2.72 (m, 2H), 2.72 – 2.53 (m, 3H), 2.37 (m, 0.3H), 2.30 – 1.95 (m, 7.7H), 1.87 – 1.60 (m, 10H), 1.41 – 1.34 (m, 3H), 0.72 – 0.60 (m, 1H), 0.42 (m, 2H), 0.10 – -0.02 (m, 2H).

HRMS (ESI-TOF) m/z: $[M+H]^+$ calcd for $C_{43}H_{57}Cl_2N_9O_8$: 898.37799; found 898.38163.

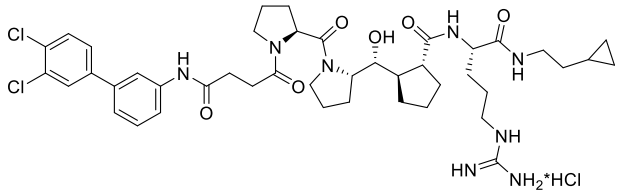

(1R,2R)-N-((S)-1-((2-Cyclopropylethyl)amino)-5-guanidino-1-oxopentan-2-yl)-2-((R)-((S)-1-((S)-1-(4-((3',4'-dichloro-[1,1'-biphenyl]-3-yl)amino)-4-oxobutanoyl)pyrrolidine-2-carbonyl)pyrrolidin-2-yl)(hydroxy)methyl)cyclopentanecarboxamide hydrochloride **(III)**

Pd/C (10% w/w, 33 mg, 31 µmol, 0.8 eq.) was added to a solution of **26** (33 mg, 37 µmol, 1.0 eq.) in 1:1 MeOH/EtOAc (20 mM) and 6.0 M aq. HCl (2 drops), and the mixture was stirred under H_2 (atmospheric pressure) at rt for 4 h. The catalyst was removed by filtration and the solution was dried under reduced pressure to afford **III** as an amorphous solid (30 mg, 90%). The residue was purified by preparative HPLC (Atlantis dC18, 19x100m, 5µm – flow: 24 mL/min – gradient: A. H_2O (+0.1% formic acid)/ B. MeCN. 0min: 15%B, 10min: 75%B, 11.5min: 15%B, 15min: 15%B).

^{1}H NMR (700 MHz, Methanol-d_4) δ 8.55 (bs, 2H), 7.91 (m, 1H), 7.76 (d, *J* = 2.1 Hz, 1H), 7.59 (d, *J* = 8.4 Hz, 1H), 7.56 – 7.50 (m, 2H), 7.39 (m, 1H), 7.34 (m, 1H), 4.94 (dd, *J* = 8.7, 3.0 Hz, 0.2H), 4.71 – 4.61 (m, 0.8H), 4.34 – 4.26 (m, 1H), 4.20 – 4.07 (m, 1H), 3.93 (m, 1H), 3.85 – 3.58 (m, 3H), 3.57 – 3.42 (m, 1H), 3.24 (m, 3H), 3.19 – 3.13 (m, 1H), 2.91 – 2.73 (m, 2H), 2.71 – 2.54 (m, 3H), 2.25 (m,

1H), 2.20 – 1.99 (m, 6H), 1.90 – 1.75 (m, 6H), 1.67 (m, 5H), 1.46 (m, 1H), 1.39 (m, 2H), 0.71 – 0.64 (m, 1H), 0.47 – 0.40 (m, 2H), 0.05 (m, 2H).

^{13}C NMR (176 MHz, MeOD) δ 179.2, 179.1, 173.9, 173.8, 173.4, 173.3, 173.3, 173.0, 172.9, 172.8, 172.7, 172.3, 170.2, 158.6, 158.6, 142.7, 142.6, 140.8, 140.8, 140.8, 140.5, 140.4, 133.8, 133.8, 132.5, 132.4, 132.0, 132.0, 130.6, 130.6, 129.8, 129.8, 127.8, 127.8, 123.5, 123.4, 120.7, 120.7, 120.6, 119.4, 119.4, 119.3, 78.5, 76.1, 75.9, 62.6, 62.4, 61.6, 60.8, 60.0, 59.9, 54.0, 54.0, 54.0, 51.4, 51.3, 51.3, 42.0, 40.7, 40.7, 35.5, 35.5, 32.6, 32.3, 32.2, 31.9, 31.4, 31.3, 31.2, 30.9, 30.8, 30.7, 30.4, 30.4, 30.3, 30.3, 30.3, 30.1, 30.0, 26.8, 26.8, 26.7, 26.5, 26.4, 26.4, 26.3, 26.2, 25.7, 25.7, 24.5, 24.4, 24.3, 23.6, 9.5, 9.4, 4.7, 4.7.

HRMS (ESI-TOF) m/z: $[M+H]^+$ calcd for $C_{43}H_{58}Cl_2N_8O_6$: 853.39291; found 853.39191. $[M+Na]^+$ calcd for $C_{43}H_{58}Cl_2N_8O_6$: 875.37486; found 875.37126.

HPLC: 99% with by-products:

- 94% (**III**) (96:4 mixture of isomer)
- 4% (**III**) as a mono-chlorinated analog
- 1% (**III**) as a dechlorinated analog

8.6.2.5 Synthesis of **IV**

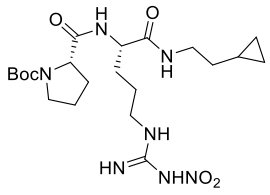

(S)-tert-Butyl 2-(((S)-1-((2-cyclopropylethyl)amino)-5-(3-nitroguanidino)-1-oxopentan-2-yl)carbamoyl)pyrrolidine-1-carboxylate **(28)**

BocProOH **27** (65 mg, 0.30 mmol, 1.2 eq.) was dissolved in CH_2Cl_2 (1.3 mL) and the solution was cooled to 0 °C. **15** (0.10 g, 0.25 mmol, 1.0 eq.) and DIPEA (187 µL, 1.07 mmol, 4.3 eq.) were added, followed by PyBOP (195 mg, 0.38 mmol, 1.5 eq.). The reaction mixture was stirred at 0 °C for 10 min, then at rt for 14h. The reaction mixture was diluted with CH_2Cl_2, washed with 10% aq. citric acid, 10% aq. $NaHCO_3$, and brine. The organic phase was dried over anhydrous Na_2SO_4, filtered and the solvent removed under reduced pressure. The crude was purified by column

chromatography on SiO_2 gel with 97:3 to 92:8 CH_2Cl_2/MeOH to afford **28** as a white foam (68.4 mg, 56%).

^{1}H NMR (500 MHz, Chloroform-*d*) δ 8.67 (m, 1H), 8.24 – 7.33 (m, 3.5H), 6.81 (m, 0.5H), 4.75 (bs, 0.25H), 4.56 (m, 0.75H), 4.33 (bs, 0.75H), 4.15 (bs, 0.25H), 3.52 – 3.33 (m, 3H), 3.30 – 3.08 (m, 3H), 2.10 (m, 1H), 2.04 – 1.53 (m, 7H), 1.41 (m, 9H), 1.37 – 1.30 (m, 2H), 0.62 (m, 1H), 0.39 (dd, *J* = 7.8, 5.4 Hz, 2H), 0.01 (m, 2H).

HRMS (ESI-TOF) m/z: $[M+H]^+$ calcd for $C_{21}H_{37}N_7O_6$: 484.28781; found 484.28746. $[M+Na]^+$ calcd for $C_{21}H_{37}N_7O_6$: 506.26975; found 506.27039.

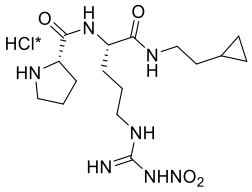

(S)-N-((S)-1-((2-Cyclopropylethyl)amino)-5-(3-nitroguanidino)-1-oxopentan-2-yl)pyrrolidine-2-carboxamide hydrochloride **(29)**

The title compound was obtained from **28** (52 mg, 0.11 mmol, 1.0 eq.) following general procedure **F** as a white powder (42 mg, 94%).

^{1}H NMR (500 MHz, Methanol-d_4) δ 4.38 (dd, *J* = 8.5, 5.3 Hz, 2H), 3.46 – 3.33 (m, 2H), 3.28 – 3.18 (m, 3H), 2.47 (h, *J* = 7.6 Hz, 1H), 2.06 (m, 3H), 1.93 – 1.65 (m, 4H), 1.40 – 1.36 (m, 2H), 0.75 – 0.65 (m, 1H), 0.46 – 0.39 (m, 2H), 0.06 (td, *J* = 4.9, 3.0 Hz, 2H).

HRMS (ESI-TOF) m/z: $[M+H]^+$ calcd for $C_{16}H_{29}N_7O_4$: 384.23538; found 384.23579. $[M+Na]^+$ calcd for $C_{16}H_{29}N_7O_4$: 406.21732; found 406.21743.

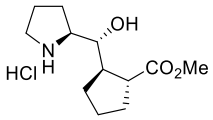

(1R,2R)-Methyl 2-((R)-hydroxy((S)-pyrrolidin-2-yl)methyl)cyclopentanecarboxylate hydrochloride **(16a)**

The title compound was obtained from **16**[511] (71 mg, 0.22 mmol, 1.0 eq.) following the general procedure **F** as a colorless oil (57 mg, q.y.).

^{1}H NMR (400 MHz, Methanol-d_4) δ 3.71 – 3.59 (m, 5H), 3.27 (m, 2H), 2.79 (dt, *J* = 9.3, 7.3 Hz, 1H), 2.38 – 2.27 (m, 1H), 2.12 – 1.94 (m, 5H), 1.91 – 1.66 (m, 4H), 1.37 (m, 1H).

HRMS (ESI-TOF) m/z: $[M+H]^+$ calcd for $C_{12}H_{21}NO_3$: 228.15942; found 228.16012.

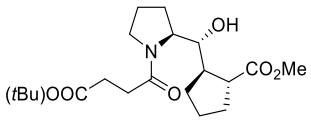

(1R,2R)-Methyl 2-((R)-((S)-1-(4-(tert-butoxy)-4-oxobutanoyl)pyrrolidin-2-yl)(hydroxy)methyl)cyclopentanecarboxylate **(30)**

An amount of **16a** (57 mg, 0.22 mmol, 1.0 eq.) was dissolved in CH_2Cl_2 (723 µL) and the solution was cooled to 0 °C. Mono-*tert*-butyl succinate **20** (45 mg, 0.26 mmol, 1.2 eq.) and DIPEA (132 µL, 0.76 mmol, 3.5 eq.) were added, followed by HOBt (35 mg, 0.26 mmol, 1.2 eq.) and EDC (0.10 g, 0.52 mmol, 2.4 eq.). The reaction mixture was stirred at 0 °C for 10 min, then at rt for 14h. The reaction mixture was diluted with CH_2Cl_2, washed with 10% aq. citric acid, 10% aq. $NaHCO_3$, and brine. The organic phase was dried over anhydrous Na_2SO_4, filtered and the solvent removed under reduced pressure. The crude was purified by column chromatography on SiO_2 gel with 4:6 to 3:7 hexanes/EtOAc to afford **30** as a white solid (77.4 mg, 93%) which was recrystallized from 1:3 EtOAc/hexanes as colourless needles.

m.p. = 110.6-111.4 °C

^{1}H NMR (500 MHz, Chloroform-*d*) δ 4.11 (ddd, *J* = 8.1, 5.8, 1.9 Hz, 1H), 4.03 (dd, *J* = 9.4, 1.9 Hz, 1H), 3.66 (s, 3H), 3.54 (m, 1H), 3.44 (dt, *J* = 10.0, 7.3 Hz, 1H), 2.67 – 2.60 (m, 2H), 2.59 – 2.43 (m, 3H), 2.27 – 2.19 (q, *J* = 8.2 Hz, 1H), 2.02 (m, 2H), 1.96 – 1.84 (m, 2H), 1.83 – 1.72 (m, 3H), 1.70 – 1.62 (m, 2H), 1.49 (dq, *J* = 12.3, 8.5 Hz, 1H), 1.43 (s, 9H).

HRMS (ESI-TOF) m/z: $[M+H]^+$ calcd for $C_{20}H_{33}NO_6$: 384.23806; found 384.24013. $[M+Na]^+$ calcd for $C_{20}H_{33}NO_6$: 406.22001, found 406.21972.

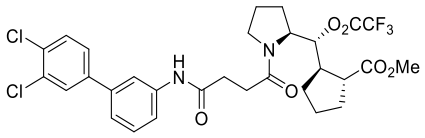

(1R,2R)-Methyl 2-((R)-((S)-1-(4-((3',4'-dichloro-[1,1'-biphenyl]-3-yl)amino)-4-oxobutanoyl)pyrrolidin-2-yl)(trifluoroacetoxy)methyl)cyclopentanecarboxylate **(31)**

An amount of **30** (70.0 mg, 0.21 mmol, 1.0 eq.) was submitted to general procedure **G**. The crude contained a mixture of 4-((*S*)-2-((*R*)-hydroxy((1*R*,2*R*)-2-(methoxycarbonyl)cyclopentyl)methyl)pyrrolidin-1-yl)-4-oxobutanoic acid and 4-((S)-2-((R)-trifluoroacetoxy((1*R*,2*R*)-2-(methoxycarbonyl)cyclopentyl)methyl)pyrrolidin-1-yl)-4-oxobutanoic acid and was submitted to the next step without further purification.

The mixture of acids (0.21 mmol, 1.0 eq.) was dissolved in CH_2Cl_2 (1.1 mL) and the solution was cooled to 0 °C. 3',4'-dichloro-[1,1'-biphenyl]-3-amine (61 mg, 0.26 mmol, 1.2 eq.) and DIPEA (0.11 mL, 0.64 mmol, 3.0 eq.) were added, followed by HATU (0.12 g, 0.32 mmol, 1.5 eq.). The reaction mixture was stirred at 0 °C for 10 min, then at rt for 7h. The reaction mixture was diluted with CH_2Cl_2, washed with 10% aq. citric acid, 10% aq. $NaHCO_3$, and brine. The organic phase was dried over anhydrous Na_2SO_4, filtered and the solvent removed under reduced pressure. The crude was purified by column chromatography on SiO_2 gel with 2:8 hexanes/EtOAc to 100% EtOAc, and then 95:5 CH_2Cl_2/MeOH to afford **31** as a white foam (84.9 mg, 62%) and a fraction containing tetramethylurea byproduct in mixture with (1*R*,2*R*)-methyl 2-((*R*)-((*S*)-1-(4-((3',4'-dichloro-[1,1'-biphenyl]-3-yl)amino)-4-oxobutanoyl)pyrrolidin-2-yl)(hydroxy)methyl)cyclopentanecarboxylate (17.0 mg, 14%, calculated by ^{1}H NMR).

^{1}H NMR (500 MHz, Methanol-d_4) δ 7.90 (t, *J* = 2.0 Hz, 1H), 7.75 (d, *J* = 2.1 Hz, 1H), 7.59 – 7.50 (m, 3H), 7.38 (t, *J* = 7.9 Hz, 1H), 7.32 (dt, *J* = 7.9, 1.3 Hz, 1H), 5.73 (dd, *J* = 10.6, 2.0 Hz, 0.9H), 5.60 – 5.53 (m, 0.1H), 4.30 (ddd, *J* = 7.7, 5.5, 1.9 Hz, 1H), 3.74 – 3.64 (m, 1H), 3.61 (m, 3H), 3.51 – 3.45 (m, 0.1H), 3.37 (ddd, *J* = 10.3, 7.4, 6.1 Hz, 1H), 2.81 – 2.46 (m, 6H), 2.12 – 2.04 (m, 2H), 2.04 – 1.90 (m, 4H), 1.79 – 1.72 (m, 3H), 1.63 – 1.54 (m, 1H).

HRMS (ESI-TOF) m/z: $[M+H]^+$ calcd for $C_{30}H_{31}Cl_2F_3N_2O_6$: 643.15840; found 643.15949. $[M+Na]^+$ calcd for $C_{30}H_{31}Cl_2F_3N_2O_6$: 665.14035; found 665.14106.

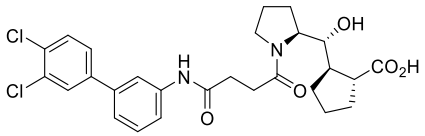

(1R,2R)-2-((R)-((S)-1-(4-((3',4'-Dichloro-[1,1'-biphenyl]-3-yl)amino)-4-oxobutanoyl)pyrrolidin-2-yl)(hydroxy)methyl)cyclopentanecarboxylic acid **(32)**

An amount of **31** (86 mg, 0.13 mmol, 1.0 eq.) was dissolved in THF (389 µL) and LiOH (0.39 mL, 1.0 M in H_2O, 3.0 eq.) was added at 0 °C. The reaction was stirred at 0 °C for 5 min then at rt for 1h. The reaction mixture was acidified with 10% aq. citric acid, then extracted twice with EtOAc. The pooled organic phase was dried over anhydrous Na_2SO_4, filtered and the solvent removed under reduced pressure. The obtained crude was purified by column chromatography on SiO_2 gel with 95:5 CH_2Cl_2/MeOH to afford **32** as a colourless oil (48 mg, 69%).

^{1}H NMR (500 MHz, Chloroform-*d*) δ 9.18 (s, 0.9H), 8.99 (s, 0.1H), 7.69 – 7.61 (m, 1H), 7.56 (d, *J* = 2.1 Hz, 0.1H), 7.52 (d, *J* = 2.2 Hz, 0.9H), 7.49 – 7.44 (m, 1H), 7.40 (d, *J* = 8.3 Hz, 1H), 7.27 (m, 0.5H), 7.25 (m, 0.5H), 7.23 (m, 1H), 7.13 (m, 1H), 4.15 – 4.06 (m, 1.8H), 3.97 (m, 0.1H), 3.84 (d, *J* = 10.2 Hz, 0.1H), 3.73 (m, 0.1H), 3.72 (m, 0.1H), 3.50 (m, 1.8.H), 3.29 (m, 0.1H), 2.91 – 2.73 (m, 1.8H), 2.67 (m, 1.2H), 2.57 (m, 1H), 2.46 (td, *J* = 8.7, 6.2 Hz, 1H), 2.08 – 1.92 (m, 4H), 1.88 – 1.65 (m, 3H), 1.59 (m, 1H), 1.49 (m, 2H), 1.26 (m, 2H).

HRMS (ESI-TOF) m/z: $[M+H]^+$ calcd for for $C_{27}H_{30}Cl_2N_2O_5$: 533.16045; found 533.16090. $[M+Na]^+$ calcd for for $C_{27}H_{30}Cl_2N_2O_5$: 555.14240; found 555.14295.

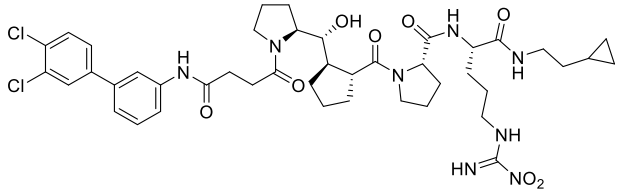

(S)-N-((S)-1-((2-Cyclopropylethyl)amino)-5-(3-nitroguanidino)-1-oxopentan-2-yl)-1-((1R,2R)-2-((R)-((S)-1-(4-((3',4'-dichloro-[1,1'-biphenyl]-3-yl)amino)-4-oxobutanoyl)pyrrolidin-2-yl)(hydroxy)methyl)cyclopentanecarbonyl)pyrrolidine-2-carboxamide **(33)**

An amount of **32** (48 mg, 90 µmol, 1.0 eq.) and **29** (38 mg, 90 µmol, 1.0 eq.) were dissolved in CH_2Cl_2 (299 µL) and the solution was cooled to 0 °C. DIPEA (55 µL, 0.31 mmol, 3.5 eq.) was added, followed by HOBt (15 mg, 0.11 mmol, 1.2 eq.) and EDC (41 mg, 0.22 mmol, 2.4 eq.). The reaction mixture was stirred at 0 °C for 10 min, then at rt for 14h. The reaction mixture was diluted with CH_2Cl_2, washed with 10% aq. citric acid, 10% aq. $NaHCO_3$, and brine. The organic phase was dried over anhydrous Na_2SO_4, filtered and the solvent removed under reduced pressure. The crude was purified by column chromatography on SiO_2 gel with 93:7 CH_2Cl_2/MeOH to afford **33** as an amorphous solid (56 mg, 70%).

^{1}H NMR (500 MHz, Methanol-d_4) δ 7.89 (t, *J* = 1.9 Hz, 0.1H), 7.84 (m, 0.9H), 7.72 (m, 0.3H), 7.70 (d, *J* = 2.1 Hz, 0.7H), 7.56 – 7.46 (m, 3H), 7.39 – 7.33 (m, 1H), 7.30 (m, 1H), 4.51 (dd, *J* = 8.6, 2.5 Hz, 0.1H), 4.42 – 4.35 (m, 0.9H), 4.32 (dd, *J* = 8.8, 4.8 Hz, 1H), 4.12 – 4.05 (m, 1H), 3.98 (dd, *J* = 10.2, 1.9 Hz, 1H), 3.84 (m, 0.1H), 3.80 – 3.44 (m, 4H), 3.29 – 3.16 (m, 4H), 2.91 (q, *J* = 8.1 Hz, 0.1H), 2.86 – 2.63 (m, 4.9H), 2.33 – 2.24 (m, 1H), 2.16 – 1.59 (m, 17H), 1.45 – 1.34 (m, 3H), 0.74 – 0.62 (m, 1H), 0.48 – 0.37 (m, 2H), 0.04 (m, 2H).

HRMS (ESI-TOF) m/z: $[M+H]^+$ calcd for $C_{43}H_{57}Cl_2N_9O_8$ 898.37799; found 898.37767. $[M+Na]^+$ calcd for $C_{43}H_{57}Cl_2N_9O_8$: 920.35994; found 920.35885.

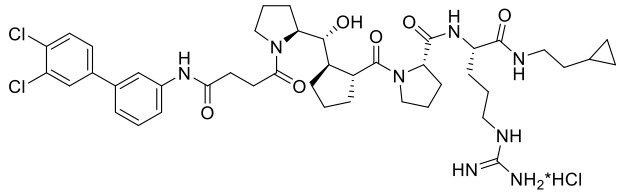

(S)-N-((S)-1-((2-Cyclopropylethyl)amino)-5-guanidino-1-oxopentan-2-yl)-1-((1R,2R)-2-((R)-((S)-1-(4-((3',4'-dichloro-[1,1'-biphenyl]-3-yl)amino)-4-oxobutanoyl)pyrrolidin-2-yl)(hydroxy)methyl)cyclopentanecarbonyl)pyrrolidine-2-carboxamide hydrochloride **(IV)**

10% Pd/C (38 mg, 0.36 µmol, 0.9 eq.) was added to a solution of **33** (38 mg, 42 µmol, 1.0 eq.) in 1:1 MeOH/EtOAc and 6 M aq. HCl (2 drops), and the mixture was stirred under H_2 (atmospheric pressure) at rt for 4 h. The catalyst was removed by filtration and the solution was concentrated under reduced pressure to afford **IV** as an amorphous solid (34 mg, 91%). The residue was purified

by preparative HPLC (Atlantis dC18, 19x100m, 5µm – flow: 24 mL/min – gradient: A. H_2O (+0.1% formic acid)/ B. MeCN. 0min: 25%B, 10min: 65%B, 11.5min: 25%B, 15min: 25%B).

^{1}H NMR (500 MHz, Methanol-d_4) δ 7.93 – 7.82 (m, 1H), 7.76 (m, 1H), 7.67 – 7.48 (m, 3H), 7.40 (m, 1H), 7.35 (m, 1H), 4.38 (dd, *J* = 8.3, 4.4 Hz, 1H), 4.31 (dd, *J* = 8.8, 4.6 Hz, 1H), 4.09 (m, 1H), 4.00 (m, 0.8H), 3.86 (m, 0.2H), 3.81 – 3.58 (m, 3H), 3.51 (m, 1H), 3.28 – 3.15 (m, 4H), 2.99 – 2.61 (m, 5H), 2.33 – 2.25 (m, 1H), 2.19 – 1.79 (m, 11.5H), 1.68 (, 5.5H), 1.54 – 1.46 (m, 1H), 1.42 – 1.35 (m, 2H), 0.69 (m, 1H), 0.47 – 0.40 (m, 2H), 0.06 (d, *J* = 4.8 Hz, 2H).
^{13}C NMR (126 MHz, MeOD) δ 178.7, 174.9, 173.8, 173.5, 173.1, 158.5, 142.5, 140.5, 140.3, 133.7, 132.4, 132.0, 130.6, 129.8, 127.8, 123.6, 120.9, 119.6, 75.4, 62.7, 61.9, 54.1, 49.8, 49.7, 42.0, 40.7, 35.4, 32.7, 32.4, 31.9, 30.8, 30.7, 30.4, 30.2, 26.6, 26.3, 25.9, 24.7, 23.6, 14.4, 9.4, 4.7, 4.7.
HRMS (ESI-TOF) m/z: $[M+H]^+$ calcd for $C_{43}H_{58}Cl_2N_8O_6$ 853.39291; found 853.39359. $[M+Na]^+$ calcd for $C_{43}H_{58}Cl_2N_8O_6$: 875.37486; found 875.37496.
HPLC: 95% with by-products:

- 92% (**IV**)
- 3% (**IV**) as a mono-chlorinated analog

8.6.3 Biological and structural data

8.6.3.1 Alanine scan

The binding constant of the alanine modified peptides was determined by SPR. **ΔG_{bind}** is computed from **K_D**. **ΔΔG** is the binding free energy difference between the unmodified peptide and the a alanine derivatives.

Name	K_D	EC_{50}	ΔG_{bind} (kj/mol)	ΔΔG (kj/mol)	Sequence
Unmodified	2.14E-07	1.33E-07	-39.58	0	PPSNPPPRPPAEARKK
Ala(153)	2.35E-07	1.99E-07	-39.34	0.24	PPANPPPRPPAEARKK
Ala(154)	2.76E-07	3.23E-07	-38.93	0.66	PPSAPPPRPPAEARKK
Ala(155)	4.48E-06	1.18E-06	-31.74	7.84	PPSNAPPRPPAEARKK

Ala(156)	3.33E-05	2.33E-05	-26.57	13.01	PPSNPAPRPPAEARKK
Ala(157)	1.64E-06	1.47E-06	-34.33	5.25	PPSNPPARPPAEARKK
Ala(158)	1.99E-04	1.64E-04	-21.96	17.62	PPSNPPPAPPAEARKK
Ala(159)	1.02E-07	5.14E-08	-41.49	-1.91	PPSNPPPRAPAEARKK
Ala(160)	2.62E-06	1.52E-06	-33.12	6.46	PPSNPPPRPAAEARKK
Ala(161)	1.97E-07	8.40E-08	-39.79	-0.21	PPSNPPPRPPAAARKK
I	5.71E-06	1.91E-06	-29.91	-9.67	n/a
II	4.25E-08	6.69E-7	-42.06	2.48	n/a
III	3.12E-07	nd	-37.12	-2.46	n/a
IV	nd	nd	nd	nd	n/a

8.6.3.2 X-Ray

PDB access code: 7YXW

Protein-peptide complex was prepared by mixing the protein with 5x molar excess of the peptide followed by overnight incubation at 4 °C and subsequent filtration using Durapore PVDF 0.1 µm centrifugal filters (Millipore).

Crystallization screening was performed using sitting drop vapor diffusion technique, 96-well 3-drop (or 2-drop) conical crystallization plates, Crystal Gryphon Nanodispender (Art Robbins Instruments) and commercially available crystallization kits (Molecular Dimensions, Hampton Research). Typically 100 nL of the prepared complex was mixed with 100 nL of the reservoir solution and equilibrated against the reservoir solution at 20 or 4 °C. The initial hits were further optimized using grid screening approach by systematic variation of pH, salt concentration and/or precipitant concentration. The diffracting crystals were obtained in 0.1 M HEPES pH 7.5, 1.2 M sodium citrate tribasic dihydrate at 4 °C and 1 : 1 complex : reservoir solution ratio. The crystals were cryoprotected in mother liquor supplemented with 0.3 M sodium malonate pH 7.0 and flash-frozen in liquid nitrogen. All crystallographic data were collected at 100 K at the SOLEIL Synchrotron (Gif-sur-Yvette, France).

Data were indexed and integrated using XDS and scaled and merged in Aimless from the CCP4 package. The crystal structure of protein-peptide complex was determined by molecular replacement with two separate ensembles as search models (Ensemble 1 = residues 157-199 and Ensemble 2 = residues 226-283,

both derived from PDB entry 1ng2). The solution contained one complex per asymmetric unit and had R_{work}/R_{free} values of 0.37/0.43. Upon obtaining the MR solution, alternate cycles of model building and refinement were performed using WinCoot and Refmac5, respectively, with 5% randomly selected reflections to monitor Rfree.

8.6.3.3 Modelling

Schrödinger Glide and LiveDesign was used to perform docking.[648] In-house X-ray structure of p47-inhibitor complex was used to construct docking grid in the rigid Glide SP docking protocol without constrains. The ligands were prepared by LigPrep at pH 7.4+/- 2.0. The docking yielded 3 poses per ligand. For gas phase optimization all atom EHT forcefield was used, in MOE. Visualizations were prepared with MOE.[649]

8.6.3.4 Surface plasmon resonance

Binding assay to p47 was performed by Surface Plasmon Resonance (SPR) on a Biacore T200 (GE Healthcare) at 20 °C using CM5 chip (GE Healthcare). h-p47 6His-Thr-Tev-(151-285)(N166D), clived form acquired from Selvita was immobilized covalently by amine coupling using standard wizard protocol, at a concentration of 23 µg/mL in sodium acetate pH 4 (GE Healthcare Life Sciences). The ligand is injected for 300s at 5µl/min to obtain about 400 immobilized RU. Amine blank is used as the reference flow cell. Binding of analytes to the ligand was monitored in real time with associations of 60 seconds and a dissociation of 300 seconds. Association (ka) and dissociation (kd) rates were fitted with a simple 1:1 kinetic interaction model using Biacore T200 Evaluation Software (GE Healthcare). The equilibrium constant (KD=kd/ka) was calculated from these fitted parameters. In the experiment, a half-log dilution of analytes was injected over p47 in Single Cycle Kinetics (SCK) with 5 increasing concentrations of 100nM, 300nM, 1µM, 3µM and 10µM per cycle. The direct binding assay (DBA) was performed with a flow rate of 50µL/min using a running buffer of Bis Tris 25mM pH 6.5, 150mM NaCl, 0.05% P20, 5% DMSO. Double subtraction was used by subtracting both reference flow cell and previous blank cycle (with running buffer). Solvent correction is applied to correct DMSO bulk effect.

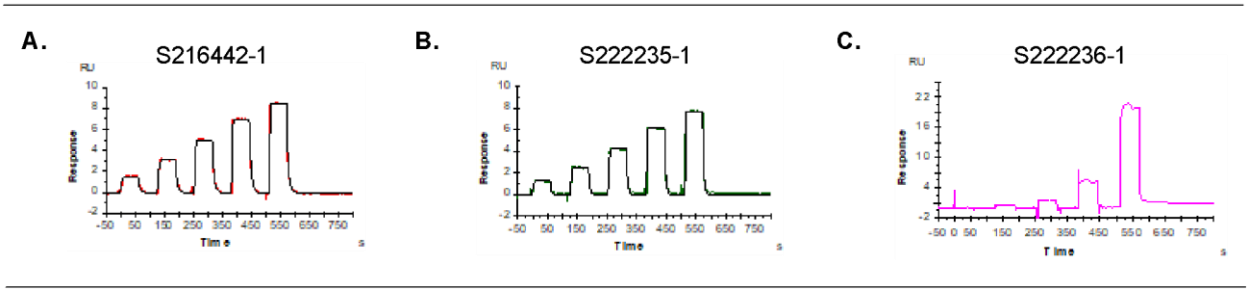

Figure 8.1 Direct binding assay to p47 by SPR on Biacore T200 (GE Healthcare).

p47 was immobilized by amine coupling on a CM5 chip at a level of about 400 RU. Five concentrations of analytes were injected in a single kinetic cycle for 60s per concentration and with a dissociation of 300s at a flow rate of 50µl/min. All the experiments were performed in Bis Tris 25mM pH 6.5, 150mM NaCl, 0.05% P20, 5% DMSO as running buffer.

The analysis was double subtracted with a reference flow cell (blank immobilization) and the previous blank cycle with buffer, a solvent correction was applied. The fit used is a 1:1 kinetic interaction model with the Biacore T200 Evaluation Software. **A. II** (S216442-1) was used as the control (100% binding at Cmax). The range studied was 10nM, 30nM, 100nM, 300nM and 1µM. **B. III** (S222235-1) was injected at 30nM, 100nM, 300nM, 1µM and 3µM. It showed a binding similar to control. **C. IV** (S222236-1) was injected at 1µM, 3µM, 10µM, 30µM and 100µM. S222236-1 was not considered as a binder as it showed bad behavior at equilibrium and no saturation.

8.7 Partie expérimentale des composés peptidomimétiques inhibiteurs de PPEP-1

8.7.1 Synthesis of fragment A

Methyl N-[[[(9H-fluoren-9-yl)methoxy]carbonyl]-L-valyl]-N-trityl-L-asparaginate **5-23a .**

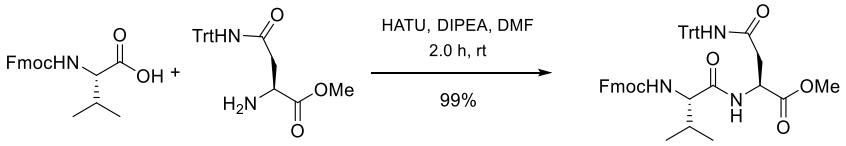

5-22 **5-23** **5-23a**

99% over two steps from Fmoc-Asn(Trt)-OH, 13 mmol scale

Methyl *N*-trityl-*L*-asparaginate **5-23** [650] (2.3 g, 6.1 mmol, 1.0 eq.), *N*-Fmoc-*L*-Valine **5-22** (2.3 g, 7.3 mmol, 1.2 eq) and HATU (2.7 g, 7.3 mmol, 1.2 eq.) were added to a round bottom flask, and the flask was purged with Ar. Dry DMF (60 mL) was added and the reaction mixture was stirred until all solids were dissolved. Afterward, DIPEA (2.3 mL, 13 mmol, 2.2 eq.) was added dropwise and the yellow solution was then stirred at rt for 2.0 h, monitored by TLC (92:08, CH_2Cl_2/MeOH, *p*-anisaldehyde/UV). The reaction mixture was quenched with NH_4Cl sat. aq. sol. (60 mL) and diluted with EtOAc (120 mL), the layers were separated, and the aqueous layer was extracted with EtOAc (2 X 60 mL). The organic layers were combined and washed with 1 M HCl aq. (6 X 120 mL), $NaHCO_3$ sat. aq. sol. (120 mL) and brine (120 mL), dried over Na_2SO_4, filtered, and concentrated under reduced pressure. The resulting solid was purified over silica gel (100% CH_2Cl_2 to 98:02, CH_2Cl_2/MeOH, *p*-anisaldehyde) to afford **5-23a** (4.2 g, 99%) as a white solid. *Rf* = 0.2 (98:02 CH_2Cl_2/MeOH). $[\alpha]^{25}_D$: +11.4 (*c* = 1.0, $CHCl_3$). ^{1}H NMR ($CDCl_3$, 400 MHz), δ: 7.76 (d, *J* = 7.5 Hz, 2H), 7.60 (t, *J* = 7.1 Hz, 2H), 7.39 (t, *J* = 7.5 Hz, 2H), 7.35-7.21 (m, 12H), 7.1-7.3 (m, 6H), 7.03 (d, *J* = 8.7 Hz, 1H), 6.73 (s, 1H), 5.49 (d, *J* = 8.8, 1H), 4.889 (dt, *J* = 8.7, 4.2, 1H), 4.44-4.27 (m, 2H), 4.22 (t, *J* = 7.1 Hz, 1H), 4.06 (dd, *J* = 8.8, 5.2 Hz, 1H), 3.65 (s, 3H), 3.12 (dd, *J* = 16.2 Hz, 4.1 Hz, 1H), 2.75 (dd, *J* = 16.1, 4.1 Hz, 1H), 2.15-2.04 (m, 1H), 0.97 (d, *J* = 6.8 Hz, 3H), 0.91 (d, *J* = 6.8 Hz, 3H). ^{13}C NMR ($CDCl_3$, 100 MHz), δ: 171.2, 171.1, 169.7, 156.4, 144.3, 144.1, 143.9, 141.4, 128.7, 128.2, 127.8,

127.3, 125.3, 125.3, 120.1, 120.0, 71.1, 67.1, 59.9, 52.7, 48.8, 47.3, 38.2, 31.8, 19.2, 17.4. HRMS (ESI) for $C_{44}H_{44}N_3O_6$ $(M+H)^+$: Calc.: 732.3044, Found: 732.3067.

Methyl N^2-(L-valyl)-N^4-trityl-L-asparaginate **5-25.**

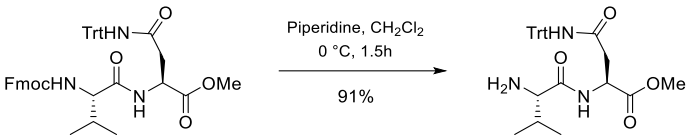

5-23a **5-25**

An amount of **5-23a** (8.1 g, 11 mmol 1.0 eq) was added to a round bottom flask, and the flask was purged with Ar. Dry CH_2Cl_2 (95 mL) was added and the solution was cooled to 0 °C followed by the addition of piperidine dropwise (19 mL) over 18 min. The reaction mixture was then stirred at 0 °C for 1.5 h, monitored by TLC (95:05, CH_2Cl_2/MeOH, *p*-anisaldehyde/UV). The reaction mixture was quenched by the slow addition of NH_4Cl sat. aq. sol. (240 mL), always keeping the temperature at 0 °C. Afterward, the mixture was diluted with CH_2Cl_2 (240 mL), the layers were separated, and the aqueous layer was extracted with CH_2Cl_2 (2 X 240 mL). The combined organic phases were washed with NH_4Cl sat. aq. sol. (240 mL), $NaHCO_3$ sat. aq. sol. (240 mL), water (240 mL) and brine (240 mL), dried over Na_2SO_4, filtered, and concentrated under reduced pressure. The resulting solid was finely crushed, suspended in hexanes (500 mL) and vigorously stirred for 2.0 h. Then, the suspension was filtered, and the solid residue was washed with hexanes. The resulting white solid was then collected in another round bottom flask and concentrated to afford **5-25** (5.0 g, 91%) as a white solid. *Rf* = 0.4 (95:05 CH_2Cl_2/MeOH, *p*-anisaldehyde/UV). $[\alpha]^{25}_D$: +25.3 (*c* = 0.3, $CHCl_3$). ^{1}H NMR ($CDCl_3$, 400 MHz), δ: 7.94 (d, *J* = 8.3 Hz, 1H), 7.33-7.21 (m, 9H), 7.19-7.12 (m, 6H), 6.68 (s, 1H), 4.78 (dt, 8.5, 4.4 Hz, 1H), 3.65 (s, 3H), 3.15 (br, 1H), 3.10 (dd, *J* = 16.0, 4.6 Hz, 1H), 2.80 (dd, *J* = 16.0, 4.2 Hz, 1H), 2.23-2.09 (m, 1H) 1.32 (br, 2H), 0.96 (d, *J* = 6.9 Hz, 3H), 0.81 (d, *J* = 6.8 Hz, 3H). ^{13}C NMR ($CDCl_3$, 100 MHz), δ: 174.7, 171.5, 169.2, 144.5, 128.8, 128.1, 127.3, 71.0, 60.4, 52.7, 48.9, 38.7, 31.5, 19.7, 16.4. HRMS (ESI) for $C_{29}H_{34}N_3O_4$ $(M+H)^+$: Calc.: 488.2543, Found: 488.2555.

Methyl (5S,8S,11S)-5-(3-(tert-butoxy)-3-oxopropyl)-1-(9H-fluoren-9-yl)-8-isopropyl-3,6,9-trioxo-11-(2-oxo-2-(tritylamino)ethyl)-2-oxa-4,7,10-triazadodecan-12-oate **5-25a.**

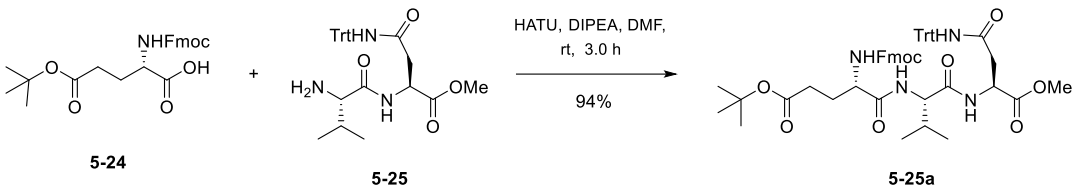

An amount of **5-25** (4.7 g, 9.6 mmol, 1.0 eq.), Fmoc-Glu(O*t*Bu)-OH **5-24** (4.9 g, 12 mmol, 1.2 eq) and HATU (4.4 g, 12 mmol, 1.2 eq.) were added to a round bottom flask, and the flask was purged with Ar. Dry DMF (96 mL) was added and the reaction mixture was stirred until all solids were dissolved. Afterward, DIPEA (3.7 mL, 21 mmol, 2.2 eq.) was added dropwise and the yellow solution was then stirred at rt for 3.0 h, monitored by TLC (9:1, CH_2Cl_2/MeOH, CAM). The reaction mixture was quenched with 1 M HCl aq. (96 mL) and diluted with EtOAc (300 mL), the layers were separated, and the aqueous layer was extracted with EtOAc (2 X 100 mL). The organic layers were combined and washed with 1 M HCl aq. (3 x 200 mL), $NaHCO_3$/brine (600 mL + 400 mL), brine (250 mL), dried over Na_2SO_4, filtered, and concentrated under reduced pressure. The resulting solid was purified over silica gel (100% CH_2Cl_2 to 96:04, CH_2Cl_2/MeOH, CAM/$KMnO_4$/UV) to afford **5-25a** (8.1 g, 94%) as a beige solid. *Rf* = 0.4 (96:04 CH_2Cl_2/MeOH, CAM). $[\alpha]^{25}_D$: +7.2 (*c* = 0.5, $CHCl_3$). ^{1}H NMR ($CDCl_3$, 500 MHz), δ: 7.76 (d, *J* = 7.6 Hz, 2H), 7.61-7.56 (m, 2H), 7.39 (t, *J* = 7.5 Hz, 2H), 7.32-7.27 (m, 9H), 7.26-7.23 (m, 6H), 7.0 (d, *J* = 8.7 Hz,1H), 9.96 (d, *J* = 8.4 Hz, 1H), 6.76 (s, 1H), 5.79 (d, *J* = 7.7 Hz, 1H), 4.91-4.81 (m, 1H), 4.42-4.31 (m, 2H), 4.29-4.23 (m, 2H), 4.21 (t, *J* = 7.1 Hz, 1H), 3.63 (s, 3H), 3.08 (d, *J* = 16.1, 4.2 Hz, 1H), 2.75 (d, *J* = 16.0, 4.1 Hz, 1H), 2.43-2.33 (m, 2H), 2.13-2.03 (m, 2H), 1.97-1.89 (m, 1H), 1.45 (s, 9H), 0.94 (d, *J* = 6.8 Hz, 3H), 0.90 (d, *J* = 6.8 Hz, 3H). ^{13}C NMR ($CDCl_3$, 125 MHz), δ: 173.2, 171.4, 171.2, 170.6, 169.7, 156.3, 144.3, 144.1, 143.8, 141.4, 141.4, 128.8, 128.2, 127.8, 127.3, 127.2, 125.3, 120.1, 81.2, 71.1, 67.2, 58.3, 54.5, 52.7, 48.8, 47.2, 38.2, 31.9, 31.4, 28.4, 28.2, 19.3, 17.5. HRMS (ESI) for $C_{53}H_{58}N_4O_9Na$ $(M+Na)^+$: Calc.: 917.4096, Found: 917.4087.

tert-Butyl (S)-4-amino-5-(((S)-1-(((S)-1-methoxy-1,4-dioxo-4-(tritylamino)butan-2-yl)amino)-3-methyl-1-oxobutan-2-yl)amino)-5-oxopentanoate **5-26.**

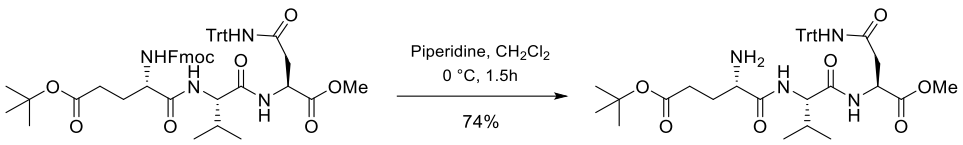

5-25a **5-26**

An amount of **5-25a** (8.1 g, 9.1 mmol) was added to a round bottom flask, and the flask was purged with Ar. Dry CH_2Cl_2 (165 mL) was added and the solution was cooled to 0 °C, then piperidine (16.5 mL) was added dropwise. The reaction mixture was then stirred at 0 °C for 1.5 h (monitored by MS). The reaction mixture was quenched with NH_4Cl sat. aq. sol. (400 mL). Afterward, the mixture was diluted with CH_2Cl_2 (400 mL), the layers were separated, and the aqueous layer was extracted with CH_2Cl_2 (165 mL). The organic layers were combined and washed with NH_4Cl sat. aq. sol. (165 mL), $NaHCO_3$ sat. aq. sol. (165 mL), and brine (50 mL), dried over Na_2SO_4, filtered, and concentrated under reduced pressure. The resulting solid was finely crushed, suspended in hexanes (500 mL) and vigorously stirred for 40 min, later, the suspension was filtered through a pad of celite, and the solid residue was washed with hexanes. The filtrate was then dissolved with CH_2Cl_2/MeOH (1:1), collected in another round bottom flask and concentrated under reduced pressure. The resulting solid was purified over silica gel (100% CH_2Cl_2 to 94:06, CH_2Cl_2/MeOH, UV/CAM/$KMnO_4$) to afford **5-26** (4.5 g, 74%) as a white solid. $[\alpha]^{25}_D$: -50.91 (*c* = 0.55, $CHCl_3$). ^{1}H NMR ($CDCl_3$, 400 MHz), δ: 7.8 (d, *J* = 9.1 Hz, 1H), 7.35-7.23 (m, 10H), 7.20-7.10 (m, 7H), 6.77 (s, 1H), 4.85 (dt, *J* = 8.7, 4.2 Hz, 1H), 4.28 (dd, *J* = 8.9, 5.0 Hz, 1H), 3.66 (s, 3H), 3.42-3.32 (m, 1H), 3.09 (dd, *J* = 15.9, 4.4 Hz, 1H), 2.74 (dd, *J* = 15.8, 4.2 Hz, 1H), 2.34 (t, *J* = 7.4 Hz, 2H), 2.24-2.01 (m, 2H), 1.87-1.74 (m, 1H), 1.63 (bs, 2H), 1.45 (s, 9H), 0.95 (dd, *J* = 6.8 Hz, 3H), 0.91 (dd, *J* = 6.8 Hz, 3H). ^{13}C NMR ($CDCl_3$, 100 MHz), δ: 174.7, 172.9, 171.3, 171.1, 169.7, 144.3, 128.7, 128.7, 128.2, 127.4, 80.7, 71.1, 57.8, 52.8, 48.9, 38.2, 32.2, 31.1, 30.3, 28.2, 19.4, 17.5. HRMS (ESI) for $C_{38}H_{49}N_4O_7$ $(M+H)^+$: Calc.: 673.3595, Found: 673.3590.

tert-Butyl (S)-4-acetamido-5-(((S)-1-(((S)-1-methoxy-1,4-dioxo-4-(tritylamino)butan-2-yl)amino)-3-methyl-1-oxobutan-2-yl)amino)-5-oxopentanoate **5-26a.**

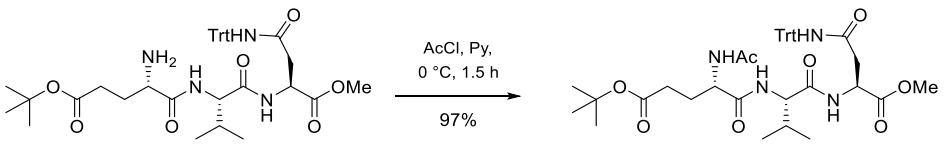

5-26 **5-26a**

An amount of **5-26** (1.0 g, 1.5 mmol, 1.0 eq) was added to a round bottom flask, and the flask was purged with Ar. Pyridine (30 mL) was added and the solution was cooled to 0 °C then AcCl (159 µL, 2.23 mmol, 1.5 eq) was added dropwise. After AcCl addition a white precipitate was formed that dissolved over time. The reaction mixture was then stirred at 0 °C for 2.0 h (monitored by TLC, 92:08, CH_2Cl_2/MeOH, *p*-anisaldehyde/UV). The reaction mixture was quenched with a 10% $CuSO_4$ solution (150 mL) and water (150 mL). The phases were separated and the aqueous layer was extracted with EtOAc (3 x 150 mL). The organic layers were combined and washed with a 10% $CuSO_4$ solution (5 x 60 mL), water (3 x 60 mL), and brine (3 x 60 mL), dried over Na_2SO_4, filtered, and concentrated under reduced pressure to afford **5-26a** (1.0 g, 97%) as a white solid. $[\alpha]^{25}_D$: +5.29 (*c* = 0.34, $CHCl_3$). ^{1}H NMR ($CDCl_3$, 500 MHz), δ: 7.33-7.26 (m, 9H), 7.20-7.14 (m, 6H) 7.09 (d, *J* = 8.2 Hz, 1H), 6.83 (s, 1H), 6.7 (bs, 1H), 4.92-4.84 (m, 1H), 4.54-4.44 (m, 1H), 4.31 (dd, *J* = 8.3, 5.2 Hz, 1H), 3.66 (s, 3H), 3.09 (dd, *J* = 16.1, 4.1 Hz, 1H), 2.8 (dd, *J* = 16.0, 4.0 Hz, 1H), 2.47-2.24 (m, 2H), 2.17-2.08 (m, 1H), 2.06-1.86 (m, 2H), 1.97 (s, 3H), 1.46 (s, 9H), 0.96 (d, *J* = 6.7 Hz, 3H), 0.93 (d, *J* = 6.7 Hz). ^{13}C NMR ($CDCl_3$, 125 MHz), δ: 173.4, 171.4, 171.2, 170.7, 170.4, 169.7, 144.4, 128.8, 128.2, 127.3, 81.2, 71.1, 58.3, 52.9, 52.7, 48.9, 38.2, 32.0, 31.4, 28.2, 28.0, 23.2, 19.2, 17.5. HRMS (ESI) for $C_{40}H_{50}N_4O_8Na$ $(M+Na)^+$: Calc.: 737.3520, Found: 737.3505.

N^2-(((S)-2-acetamido-5-(tert-butoxy)-5-oxopentanoyl)-L-valyl)-N^4-trityl-L-asparagine **5-27-A.**

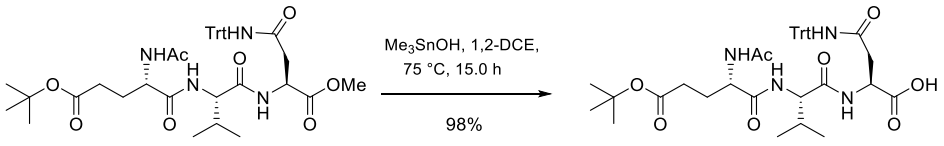

5-26a **5-27-A**

An amount of **5-26a** (0.30 g, 0.42 mmol, 1.0 eq) and Me_3SnOH (0.27 g, 1.5 mmol, 3.5 eq) were added to a vial and the vial was purged with Ar. Dry 1,2-DCE (4.2 mL) was added and the vial was sealed. The reaction mixture was stirred at 75 °C for 15.0 h. After TLC (92:08, CH_2Cl_2/MeOH, *p*-anisaldehyde/CAM) indicated a complete reaction, the mixture was partitioned between water

(30 mL) and EtOAc (30 mL). The aqueous phase was acidified to pH 3 with a 10% $KHSO_4$ solution. The aqueous layer was extracted with EtOAc (2 x 30 mL). The organic layers were combined and washed with a pH 3 $KHSO_4$ solution (3 x 20 mL), and brine (2 x 20 mL), dried over Na_2SO_4, filtered, and concentrated under reduced pressure to afford **5-27-A** (289 mg, 98%) as a beige solid. $[\alpha]^{25}_D$: -20.8 (*c* = 0.25, CH_3OH). ^1H NMR (CD_3OD, 500 MHz), δ: 7.3-7.18 (m, 15H), 4.71 (dd, *J* = 5.8, 5.8 Hz, 1H), 4.38 (dd, *J* = 9.0, 5.5 Hz, 1H), 4.28 (d, *J* = 6.3 Hz, 1H), 2.94-2.84 (m, 2H), 2.36-2.22 (m, 2H), 2.15-2.07 (m, 1H), 2.05-1.95 (m, 1H), 1.97 (s, 3H), 1.83 (dtd, *J* = 14.0, 8.7, 6.5 Hz), 1.43 (s, 9H), 0.96 (d, *J* = 6.8 Hz, 3H), 0.93 (d, = 6.8 Hz, 3H). ^{13}C NMR (CD_3OD, 125 MHz), δ: 172.6, 172.6, 172.3, 172.0, 171.6, 170.3, 144.5, 128.7, 127.3, 126.4, 80.4, 70.4, 58.2, 52.7, 49.1, 37.7, 31.4, 31.1, 27.0, 26.8, 21.0, 18.4, 16.9. HRMS (ESI) for $C_{39}H_{48}N_4O_8Na$ $(M+Na)^+$: Calc.: 723.3364, Found: 723.3343.

8.7.2 Synthesis of fragment C

(9H-fluoren-9-yl)methyl (S)-2-(tritylcarbamoyl)pyrrolidine-1-carboxylate **S5-3.**

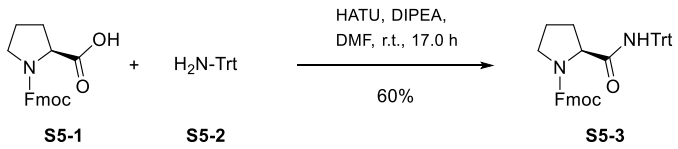

S5-1 **S5-2** **S5-3**

Fmoc-Pro-OH **S5-1** (4.6 g, 14 mmol, 1.0 eq.), triphenylmethylamine **S5-2** (3.9 g, 15 mmol, 1.1 eq) and HATU (5.8 g, 15 mmol, 1.0 eq.) were added to a round bottom flask, and the flask was purged with Ar. Dry DMF (137 mL) was added and the reaction mixture was stirred until all solids were dissolved. Afterward, DIPEA (5.3 mL, 30 mmol, 2.2 eq.) was added dropwise and the yellow solution was then stirred at rt for 21.0 h, monitored by TLC (7:3, hexanes/EtOAc, UV/$KMnO_4$). The reaction mixture was quenched with 1 M HCl aq. (140 mL) and diluted with CH_2Cl_2 (400 mL), the layers were separated, and the aqueous layer was extracted with CH_2Cl_2 (2 X 140 mL). The organic layers were combined and washed with 1 M HCl aq. (4 X 280 mL), $NaHCO_3$ sat. aq. sol. (2 x 280 mL) and brine (2 x 280 mL), dried over Na_2SO_4, filtered, and concentrated under reduced pressure. The resulting solid was purified with CombiFlash chromatography system (100% hexanes to 7:3, hexanes/EtOAc in 45 min, full run: 85 min, UV/KMnO4). The resulting solid was finely crushed, suspended in hexanes (500 mL) and vigorously stirred for 2.0 h. Then, the suspension was filtered, and the solid residue was washed with hexanes. The resulting white solid was then dissolved with

CH_2Cl_2, collected in another round bottom flask, and concentrated under reduced pressure to afford **S5-3** (4.8 g, 60%) as a white solid. *Rf* = 0.33 (7:3 hexanes/EtOAc, UV/KMnO4). $[\alpha]^{25}_D$: -68.6 (*c* = 0.37, $CHCl_3$). ^{1}H NMR (DMSO-d6, 500 MHz, mixture of rotamers), δ: 8.99 (s, 0.7H), 8.70 (s, 0.6H), 7.97-7.89 (m, 4.8H), 7.82 (d, *J* = 7.5 Hz, 1H), 7.68 (t, *J* = 7.65 Hz, 1.7H), 7.50-7.31 (m, 7.9H), 7.29-7.13 (m, 29H), 4.76 (dd, *J* = 8.5, 3.4 Hz, 1H), 4.53 (dd, *J* = 8.3, 3.2 Hz, 0.8H), 4.36-4.17 (m, 5.7H), 3.35-3.27 (m, 3.4H), 2.24-2.14 (m, 1H), 2.08-1.96 (m, 0.9H), 1.78-1.53 (m, 5.8H). ^{13}C NMR (DMSO-d6, 125 MHz, mixture of rotamers), δ: 171.4, 171.0, 154.2, 153.7, 144.6, 144.6, 144.1, 143.9, 143.7, 143.3, 140.7, 140.6, 128.5, 127.8, 127.7, 127.4, 127.4, 127.3, 127.2, 126.4, 125.7, 125.3, 125.1, 120.2, 69.4, 69.3, 66.7, 66.6, 59.9, 59.4, 47.2, 46.8, 46.7, 46.5, 30.6, 29.0, 23.8, 22.7. HRMS (ESI) for $C_{39}H_{34}N_2O_3Na$ $(M+Na)^+$: Calc.: 601.2462, Found: 601.2485.

(S)-N-tritylpyrrolidine-2-carboxamide **S5-4.**

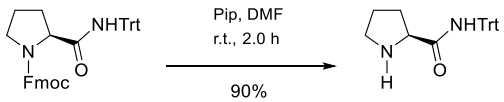

S5-3 **5-28**

An amount of **S5-3** (5.9 g, 10 mmol, 1.0 eq.) was added to a round bottom flask, and the flask was purged with Ar. Dry DMF (85 mL) was added, followed by the addition of piperidine dropwise (19 mL) over 15 min. The reaction mixture was then stirred at rt for 2.0 h monitored by TLC (7:3, hexanes/EtOAc, UV/*p*-Anisaldehyde). The reaction mixture was quenched by the slow addition of NH_4Cl sat. aq. sol. (241 mL). Afterward, the mixture was diluted with CH_2Cl_2 (210 mL), the layers were separated, and the aqueous layer was extracted with CH_2Cl_2 (2 X 85 mL). The combined organic phases were washed with NH_4Cl sat. aq. sol. (2 x 170 mL), $NaHCO_3$ sat. aq. sol. (2 x 170 mL), and brine (2 x 170 mL), dried over Na_2SO_4, filtered, and concentrated under reduced pressure. The crude oil was dissolved in EtOAc and washed with water to remove the remaining DMF. Once again, the organic phase was dried over Na_2SO_4, filtered, and concentrated under reduced pressure. The resulting solid was finely crushed, suspended in hexanes (500 mL) and vigorously stirred for 40 min. Then, the suspension was filtered, and the solid residue was washed with hexanes. The resulting white solid was then collected in another round bottom flask and concentrated to afford **5-28** (3.3 g, 90%) as a beige solid. *Rf* = 0.37 (9:1 CH_2Cl_2/MeOH, UV/*p*-Anisaldehyde). $[\alpha]^{25}_D$: -36.2 (*c* = 0.26, $CHCl_3$). ^{1}H NMR ($CDCl_3$, 500 MHz), δ: 9.19 (s, 1H), 7.35-7.21

(m, 15H), 3.78 (dd, *J* = 8.9, 5.1 Hz, 1H), 3.08 (dt, *J* = 10.3, 6.9 Hz, 1H), 2.99 (dt, *J* = 10.3, 6.4 Hz, 1H), 2.31 (bs, 1H), 2.10 /ddt, *J* = 12.9, 9.0, 7.6 Hz, 1H), 2.04-1.95 (m, 1H), 1.85-1.69 (m, 2H). ^{13}C NMR ($CDCl_3$, 125 MHz), δ: 173.9, 145.2, 128.7, 128.0, 127.0, 69.6, 61.5, 47.5, 30.6, 26.4. HRMS (ESI) for $C_{24}H_{25}N_2O$ $(M+H)^+$: Calc.: 357.1961, Found: 357.1978.

(9H-fluoren-9-yl)methyl ((S)-3-methyl-1-oxo-1-((S)-2-(tritylcarbamoyl)pyrrolidin-1-yl)butan-2-yl)carbamate **5-28a.**

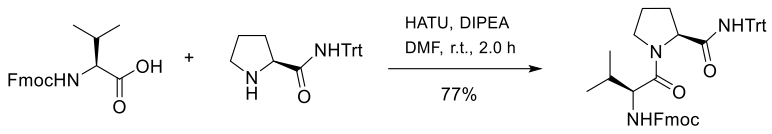

5-19 **5-28** **5-28a**

An amount of the amide **5-28** (3.2 g, 9.0 mmol, 1.0 eq.), Fmoc-Val-OH **5-19** (3.7 g, 11 mmol, 1.2 eq) and HATU (4.1 g, 11 mmol, 1.2 eq.) were added to a round bottom flask, and the flask was purged with Ar. Dry DMF (90 mL) was added and the reaction mixture was stirred until all solids were dissolved, afterward, DIPEA (3.4 mL, 20 mmol, 2.2 eq.) was added dropwise and the yellow solution was then stirred at rt for 2.0 h monitored by TLC (9:1, CH_2Cl_2/MeOH, UV/*p*-Anisaldehyde). The reaction mixture was quenched with 1 M HCl aq. (90 mL) and diluted with EtOAc (180 mL), the layers were separated, and the aqueous layer was extracted with EtOAc (2 X 90 mL). The organic layers were combined and washed with 1 M HCl aq. (5 X 180 mL), $NaHCO_3$ sat. aq. sol. (2 x 180 mL) and brine (180 mL), water (180 mL) dried over Na_2SO_4, filtered, and concentrated under reduced pressure. The resulting solid was purified over silica gel (100% Hexanes to 7:3, Hexanes/EtOAc, UV/*p*-anisaldehyde) to afford **5-28a** (4.7 g, 77%) as a white solid. *Rf* = 0.14 (7:3, Hexanes/EtOAc, UV/*p*-anisaldehyde)). $[\alpha]^{25}_D$: -93.0 (*c* = 0.23, $CHCl_3$). ^{1}H NMR ($CDCl_3$, 500 MHz), δ: 8.03 (s, 1H), 7.80 (d, *J* = 7.6 Hz, 2H), 7.63 (dd, *J* = 7.6 Hz, 2H), m (2H), 7.38-7.18 (m, 20H), 5.58 (d, *J* = 9.3 Hz, 1H), 4.72 (dd, 8.0, 2.7 Hz, 1H), 4.48-4.33 (m, 3H), 4.25 (t, *J* = 7.2 Hz, 1H), 3.75 (ddd, *J* = 9.3, 9.1, 7.1 Hz, 1H), 3.63 (ddd, *J* = 9.9, 9.1, 3.8 Hz, 1H), 2.36-2.27 (m, 1H), 2.13-2.04 (m, 1H), 2.04-1.93 (m, 2H), 1.93-1.83 (m, 1H), 0.91 (d, *J* = 6.8 Hz, 3H), 0.83 (d, *J* = 6.7 Hz, 3H). ^{13}C NMR ($CDCl_3$, 125 MHz), δ: 172.3, 169.7, 156.4, 144.7, 143.9, 143.8, 141.3, 128.7, 127.9, 127.7, 127.1, 127.0, 125.2, 120.0, 70.5, 67.1, 61.0, 57.3, 47.8, 47.2, 31.5, 27.1, 25.1, 19.5, 17.2. HRMS (ESI) for $C_{44}H_{43}N_3O_4Na$ $(M+Na)^+$: Calc.: 700.3146, Found: 700.3178.

(S)-1-(L-valyl)-N-tritylpyrrolidine-2-carboxamide **5-29-C.**

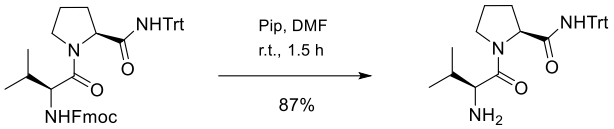

5-28a **5-29-C**

An amount of **5-28a** (4.5 g, 6.6 mmol, 1.0 eq.) was added to a round bottom flask, and the flask was purged with Ar. Dry DMF (55 mL) was added, followed by the addition of piperidine dropwise (10.9 mL) over 15 min. The reaction mixture was then stirred at rt for 1.5 h monitored by TLC (7:3, hexanes/EtOAc, UV/*p*-anisaldehyde). The reaction mixture was quenched by the slow addition of NH_4Cl sat. aq. sol. (138 mL). Afterward, the mixture was diluted with CH_2Cl_2 (138 mL), the layers were separated, and the aqueous layer was extracted with CH_2Cl_2 (2 X 55 mL). The combined organic phases were washed with NH_4Cl sat. aq. sol. (110 mL), $NaHCO_3$ sat. aq. sol. (110 mL), and brine (110 mL), dried over Na_2SO_4, filtered, and concentrated under reduced pressure. The resulting solid was purified over silica gel (100% CH_2Cl_2 to 9:1, CH_2Cl_2/MeOH, UV/*p*-anisaldehyde) to afford **5-29-C** (4.7 g, 87%) as a white solid. *Rf* = 0.37 (100% CH_2Cl_2 to 9:1, CH_2Cl_2/MeOH UV/*p*-anisaldehyde). $[\alpha]^{25}_D$: -95.2 (*c* = 0.21, $CHCl_3$). ^{1}H NMR ($CDCl_3$, 500 MHz), δ: 8.29 (s, 1H), 7.34-716 (m, 15H), 4.77 (dd, *J* = 8.1, 2.3 Hz, 1H), 3.59 (m, 2H), 3.38 (d, *J* = 5.2 Hz, 1H), 2.35 (dddd, *J* = 12.4, 6.7, 3.3, 2.3 Hz, 1H), 2.10-1.99 (m, 1H), 1.99-1.91 (m, 1H), 1.91-1.76 (m, 2H), 1.66 (bs, 2H), 0.91 (d, *J* = 6.8 Hz, 3H), 0.76 (d, *J* = 6.8 Hz, 3H). ^{13}C NMR ($CDCl_3$, 125 MHz), δ: 175.6, 169.9, 144.8, 128.7, 127.9, 126.9, 70.5, 60.9, 58.2, 47.4, 32.2, 26.8, 25.2, 20.0, 16.4. HRMS (ESI) for $C_{29}H_{34}N_3O_2$ $(M+H)^+$: Calc.: 456.2645, Found: 456.2665.

8.7.3 Synthesis of heptapeptide 5-32

(1S,2S)-methyl 2-((R)-((S)-1-((S)-2-((S)-2-((S)-2-acetamido-5-(tert-butoxy)-5-oxopentanamido)-3-methylbutanamido)-4-oxo-4-(tritylamino)butanoyl)pyrrolidin-2-yl)(hydroxy)methyl)cyclopentanecarboxylate **5-30a-*S*** *and (1S,2S)-methyl 2-((R)-((S)-1-((R)-2-((S)-2-((S)-2-acetamido-5-(tert-butoxy)-5-oxopentanamido)-3-methylbutanamido)-4-oxo-4-(tritylamino)butanoyl)pyrrolidin-2-yl)(hydroxy)methyl)cyclopentanecarboxylate* **5-30a-*R*.**

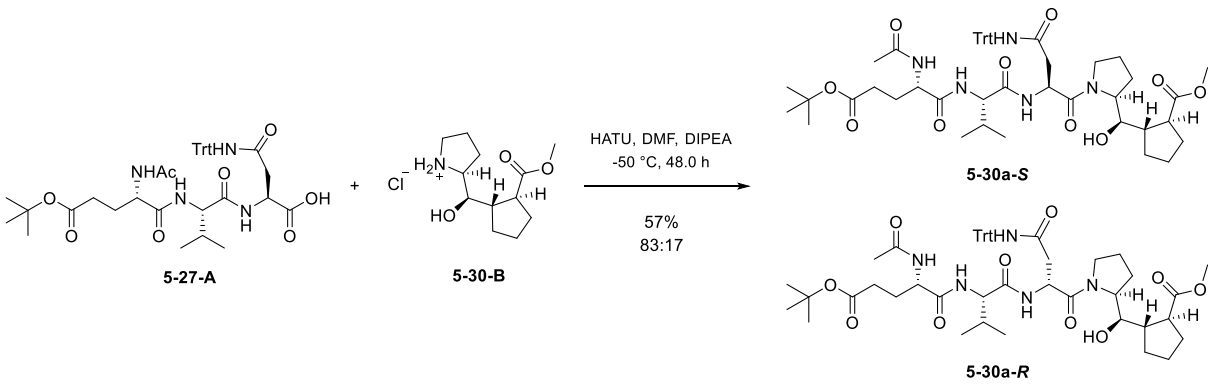

An amount of **5-30-B** [511] (45 mg, 0.17 mmol, 1.0 eq), the acid **5-27-A** (144 mg, 0.20 mmol, 1.2 eq.), and HATU (81 mg, 0.20 mmol, 1.2 eq.) were added to a round bottom flask, and the flask was purged with Ar. Dry DMF (1.7 mL) was added and the reaction mixture was stirred until all solids were dissolved, afterward, DIPEA (66 µL, 0.37 mmol, 2.2 eq.) was added dropwise at -50 °C and the yellow solution was then stirred at -50 °C for 48.0 h, monitored by TLC (85:15, CH_2Cl_2/MeOH, ninhydrin). The reaction mixture was quenched using 1 M HCl aq. (10 mL) and diluted with EtOAc (10 mL), the layers were separated, and the aqueous layer was extracted with EtOAc (2 X 10 mL). The organic layers were combined and washed with 1 M HCl aq. (4 X 10 mL), $NaHCO_3$/brine (8 x 10 mL + 10 mL), brine (2 X 10 mL), dried over Na_2SO_4, filtered, and concentrated under reduced pressure. The resulting solid was purified over silica gel (100% CH_2Cl_2 to 95:05, CH_2Cl_2/MeOH, UV/CAM) to afford an inseparable mixture of **5-30a-*S*** and **5-30a-*R*** (dr 83:17, 89 mg, 57%) as a solid. ^{1}H NMR (CD_3OD, 700 MHz, mixture of isomers and rotamers), δ: 7.30-7.17 (m, 21H), 5.08 (dd, *J* = 8.8, 6.1 Hz, 0.1H), 4.96 (dd, *J* = 8.6, 5.6 Hz, 0.1H), 4.83 (dd, *J* = 9.0, 5.3 Hz, 1H), 4.35 (dd, *J* = 8.9, 5.6 Hz, 1.2H), 4.26-4.18 (m, 1.4H), 4.14-4.09 (m, 0.3H), 4.09-4.05 (m, 1H), 3.94 (dd, *J* = 8.8, 2.2 Hz, 0.1H), 3.89 (dd, *J* = 9.3, 2.1 Hz, 1H), 3.70-3.65 (m, 2H), 3.65 (s, 3H), 3.56-3.50 (m, 0.4H), 3.48-3.43 (m, 0.2H), 3.38-3.34 (m, 0.1H), 3.24-3.19 (m, 1H), 2.97-2.89 (m, 0.2H), 2.94 (dd, *J* = 15.3, 9.0 Hz, 1H), 2.8 (m, 0.3H), 2.73 (dt, *J* = 8.9, 7.0 Hz, 1H), 2.58 (dd, *J* = 15.4, 5.3 Hz, 1H), 2.67-2.58 (m, 0.3H), 2.35-2.24 (m, 3H), 2.23-2.17 (m, 1.2H), 2.10-1.92 (m, 11.2H), 1.91-1.77 (m, 4.1H), 1.77-1.59 (m, 5.9H), 1.59-1.51 (m, 1.3H), 1.47-1.41 (m, 12.7H), 0.97-0.88 (m, 8.6H). ^{13}C NMR (CD_3OD, 176 MHz, mixture of isomers and rotamers), δ: 178.6, 178.6, 178.6, 174.1, 173.9, 173.9, 173.8, 173.8, 173.5, 173.4, 173.1, 172.9, 172.5, 171.6, 171.4, 171.4, 170.9, 170.7, 170.3, 146.1, 145.9, 145.8, 130.1, 130.1, 130.0, 128.7, 128.7, 128.6, 127.8, 127.8, 127.7, 81.9, 81.8, 81.8, 78.5, 74.3,

74.0, 71.6, 71.6, 62.4, 62.3, 62.2, 60.3, 59.9, 59.8, 54.3, 54.1, 54.1, 52.5, 52.4, 52.3, 49.9, 49.8, 48.8, 48.2, 48.1, 47.7, 47.7, 47.6, 47.6, 47.4, 40.9, 39.3, 39.1, 32.8, 32.8, 32.7, 32.7, 32.6, 32.6, 32.3, 32.1, 31.5, 31.4, 31.2, 31.0, 25.0, 24.9, 24.2, 22.5, 22.4, 20.0, 19.9, 19.8, 18.8, 18.5, 18.5. HRMS (ESI) for $C_{51}H_{68}N_5O_{10}$ $(M+H)^+$: Calc.: 910.4960, Found: 910.4952.

(1S,2S)-2-((R)-((S)-1-(N^2-(((S)-2-acetamido-5-(tert-butoxy)-5-oxopentanoyl)-L-valyl)-N^4-trityl-L-asparaginyl)pyrrolidin-2-yl)(hydroxy)methyl)cyclopentane-1-carboxylic acid **5-31.**

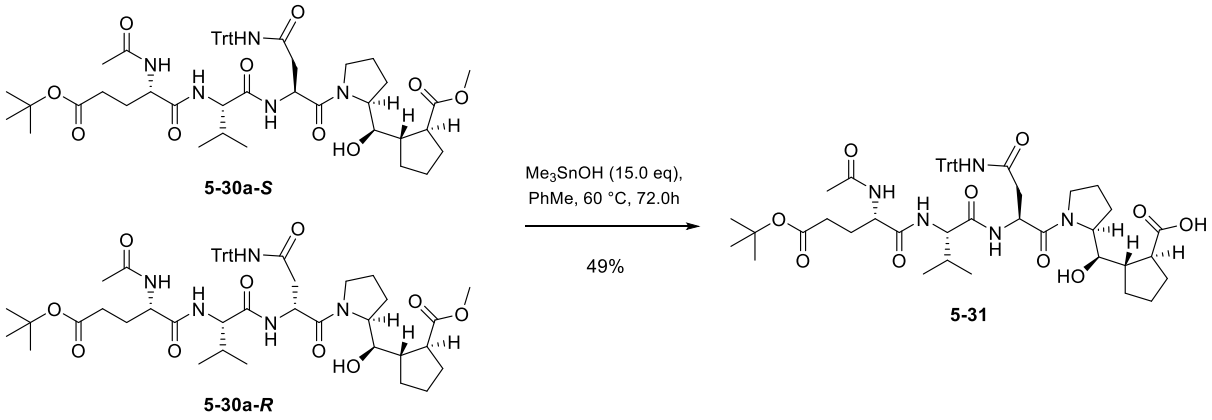

An 83:17 mixture of **5-30a** (28 mg, 31 µmol, 1.0 eq) and Me_3SnOH (28 mg, 0.154 mmol, 5.0 eq) were added to a vial and the vial was purged with Ar. Dry PhMe (0.3 mL) was added and the vial was sealed. The reaction mixture was stirred at 60 °C. Every 24.0 h, 5.0 eq of Me_3SnOH were added. After 72.0 h, the reaction mixture was partitioned between water (5 mL) and EtOAc (5 mL). The aqueous phase was acidified to pH 3 with a 10% $KHSO_4$ aq. solution and the phases were separated. The aqueous layer was extracted with EtOAc (2 x 5 mL) and the combined organic phases were washed with a pH 3 $KHSO_4$ solution (3 x 5 mL), and brine (2 x 5 mL), dried over Na_2SO_4, filtered, and concentrated under reduced pressure. The resulting solid was purified over silica gel (100% CH_2Cl_2 to 88:12, CH_2Cl_2/MeOH, CAM) to afford **5-31** (12.7 mg 46%) and 1.6 mg (5.8%) of the minor diastereoisomer. *Rf* = 0.37 (98:02 CH_2Cl_2/MeOH). $[\alpha]^{25}_D$: -3.33(*c* = 0.18, $CHCl_3$). ^1H NMR (CD_3OD, 500 MHz), δ: 7.30-7.17 (m, 15H), 4.84 (dd, *J* = 9.0, 5.4 HZ, 1H), 4.36 (dd, *J* = 8.9, 5.6 Hz, 1H), 4.20 (d, *J* = 6.9 Hz, 1H), 4.17-4.10 (m, 1H), 3.92 (dd, *J* = 9.3, 1.9 Hz, 1H), 3.70-3.63 (m, 1H), 3.21 (dt, *J* = 9.9, 7.2 Hz, 1H), 2.95 (dd, *J* = 15.3, 9.0 Hz, 1H), 2.69 (d, *J* = 15.4, 5.4 Hz, 1H), 2.72-2.62 (m, 1H), 2.37-2.17 (m, 2H), 2.08-1.75 (m, 12H), 1.72-1.61 (m, 3H), 1.60-1.50 (m, 1H), 1.43 (s, 9H), 0.93 (d, *J* = 5.1 Hz, 3H), 0.91 (d, *J* = 5.1 Hz, 3H). ^{13}C NMR (CD_3OD, 125 MHz), δ: 173.9, 173.8,

173.4, 172.9, 171.6, 170.7, 145.8, 130.0, 128.7, 127.8, 81.8, 74.2, 71.6, 62.3, 59.8, 54.1, 49.8, 47.3, 39.3, 33.1, 32.7, 32.3, 31.5, 28.4, 28.2, 26.7, 25.9, 24.9, 22.4, 19.7, 18.5. HRMS (ESI) for $C_{50}H_{66}N_5O_{10}$ $(M+H)^+$: Calc.: 896.4804, Found: 896.4836.

tert-butyl (S)-4-acetamido-5-(((S)-1-(((S)-1-((S)-2-((R)-hydroxy((1S,2S)-2-(((S)-3-methyl-1-oxo-1-((S)-2-(tritylcarbamoyl)pyrrolidin-1-yl)butan-2-yl)carbamoyl)cyclopentyl)methyl)pyrrolidin-1-yl)-1,4-dioxo-4-(tritylamino)butan-2-yl)amino)-3-methyl-1-oxobutan-2-yl)amino)-5-oxopentanoate **5-31a.**

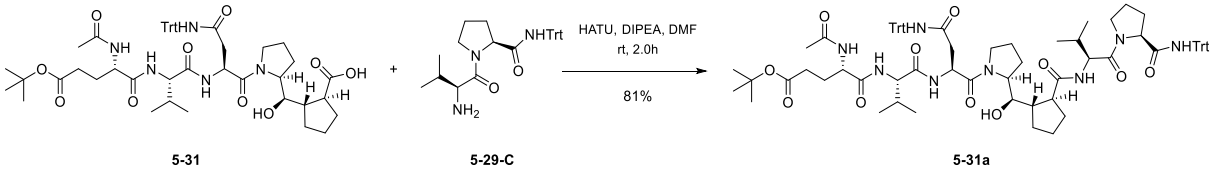

An amount of **5-31** (42 mg, 47 µmol, 1.0 eq.), the amine **5-29-C** (26 mg, 56 µmol, 1.2 eq) and HATU (22 mg, 56 µmol, 1.2 eq) were added to a round bottom flask, and the flask was purged with Ar. Dry DMF (940 µL) was added and the reaction mixture was stirred until all solids were dissolved, afterward, DIPEA (9.8 µL, 56 µmol, 1.2 eq) was added dropwise and the yellow solution was then stirred at rt for 2.0 h, monitored by TLC (9:1, CH_2Cl_2/MeOH, CAM). The reaction mixture was quenched with 1 M HCl aq. (5 mL) and diluted with EtOAc (10 mL), the layers were separated, and the aqueous layer was extracted with EtOAc (2 X 10 mL). The organic layers were combined and washed with 1 M HCl aq./brine (5 x 10 mL + 10 mL), $NaHCO_3$/brine (3 x 10 mL + 10 mL), brine (2 x 10 mL), dried over Na_2SO_4, filtered, and concentrated under reduced pressure. The resulting solid was purified over silica gel (100% EtOAc to 9:1, EtOAc/*i*-PrOH, UV/CAM) to afford **5-31a** (51 mg, 82%) as a white solid. *Rf* = 0.28 (9:1 EtOAc/*i*-PrOH). $[\alpha]^{25}_D$: -31.7 (*c* = 0.12, CH_2Cl_2). ^{1}H NMR (CD_3OD, 700 MHz, Mixture of rotamers), δ: 7.29-7.18 (m, 51H), 4.82 (dd, *J* = 7.9, 6.0 Hz, 1H), 4.76 (d, *J* = 10.7 Hz, 0.6), 4.59 (dd, *J* = 8.2, 4.6 Hz, 1H), 4.56 (dd, *J* = 7.8, 4.5 Hz, 0.6H), 4.42-4.37 (m, 1.2H), 4.37-4.32 (m, 2H), 4.20-4.16 (m, 1.6H), 4.14-4.11 (m, 0.6H), 4.07-4.03 (m, 1H), 4.01-3.99 (m, 0.6), 3.95 (dt, *J* = 9.9, 6.8 Hz, 0.6H), 3.90-3.84 (m, 2H), 3.65-3.53 (m, 3.3H), 3.38-3.34 (m, 0.6H), 3.24 (dt, *J* = 10.0, 7.5 Hz, 1H), 3.02-2.98 (m, 0.7H), 2.87-2.81 (m, 1.1H), 2.74-2.62 (m, 2.6H), 2.34-2.25 (m, 2H), 2.24-2.17 (m, 2.5H), 2.16-2.05 (m, 3H), 2.04-1.80 (m, 23.2H), 1.80-1.66 (m, 7.5H), 1.66-1.57 (m, 3.6H), 1.57-1.49 (m, 2.5H), 1.43 (s, 9H), 1.42 (s, 5.6H), 0.98 (d, *J* = 6.8 Hz, 1.8H), 0.96 (d, *J*

= 6.7 Hz, 3H), 0.92 (d, *J* = 6.7 Hz, 1.9H), 0.90 (d, *J* = 6.7 Hz, 3H), 0.87 (d, *J* = 6.8 Hz, 3H), 0.83 (d, *J* = 6.8 Hz, 3H), 0.75 (d, *J* = 6.8 Hz, 1.8H), 0.47 (d, *J* = 6.6 Hz, 1.8H). ^{13}C NMR (CD_3OD, 176 MHz, Mixture of rotamers), δ: 178.9, 178.9, 178.6, 178.6, 174.0, 173.8, 173.8, 173.5, 173.5, 173.4, 173.4, 173.3, 173.1, 172.9, 172.8, 172.7, 172.7, 171.7, 171.6, 171.5, 171.3, 170.7, 146.0, 146.0, 145.9, 145.9, 145.8, 145.8, 145.6, 145.6, 130.2, 130.1, 130.1, 130.1, 128.9, 128.7, 128.7, 127.9, 127.9, 127.9, 127.8, 81.9, 81.7, 78.2, 73.7, 72.1, 71.8, 71.8, 71.7, 71.7, 62.2, 62.0, 61.9, 61.0, 59.9, 59.1, 58.5, 58.4, 58.3, 58.2, 54.1, 53.9, 51.6, 50.0, 48.3, 48.1, 47.3, 40.3, 40.3, 39.6, 39.5, 34.5, 34.0, 33.6, 32.8, 32.8, 32.5, 32.1, 31.6, 31.6, 31.3, 31.3, 31.2, 29.6, 29.3, 28.4, 28.4, 28.2, 27.9, 27.0, 26.6, 26.0, 25.9, 25.8, 25.1, 24.5, 23.2, 22.4, 22.4, 19.9, 19.9, 19.7, 19.5, 19.5, 18.9, 18.5, 18.3. HRMS (ESI) for $C_{79}H_{96}N_8O_{11}Na$ $(M+Na)^+$: Calc.: 1355.7091, Found: 1355.7157.

(S)-4-acetamido-5-(((S)-1-(((S)-4-amino-1-((S)-2-((R)-((1S,2S)-2-(((S)-1-((S)-2-carbamoylpyrrolidin-1-yl)-3-methyl-1-oxobutan-2-yl)carbamoyl)cyclopentyl)(hydroxy)methyl)pyrrolidin-1-yl)-1,4-dioxobutan-2-yl)amino)-3-methyl-1-oxobutan-2-yl)amino)-5-oxopentanoic acid **5-32.**

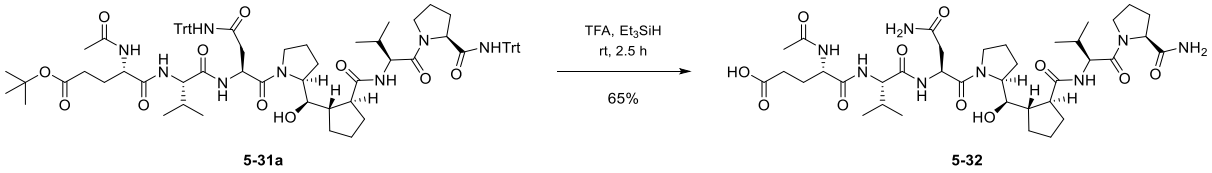

5-31a **5-32**

An amount of **5-31a** (13 mg, 9.8 µmol, 1.0 eq) was added to a round bottom flask, and the flask was purged with Ar. Neat TFA (130 µL) was added and after 10 min at stirring, Et_3SiH (9.3 µL, 59 µmol, 6.0 eq) was added. The reaction mixture was stirred for 2.5 h. After MS analysis indicated full conversion TFA was evaporated under reduced pressure. The resulting solid was finely crushed, suspended in Et_2O (5 mL) and vigorously stirred for 40 min. Then, the suspension was filtered, and the solid residue was washed with hexanes. The filtrate was then dissolved in THF (2.0 mL), treated with 0.1 M NaOH (83 µL, 9.8 µmol, 1.0 eq), and stirred for 2.5 h. After this time, the reaction mixture was acidified to pH 3 with 0.1 M HCl. The solvent was evaporated under reduced pressure and the resulting crude was purified by preparative reverse-phase high-performance liquid chromatography (Sunfire C18, H_2O-0.1% FA/ACN 5-30% in 9 min, 24 mL/min) to give **5-32** (5.0 mg, 65%). $[\alpha]^{25}_D$: -27.6 (*c* = 0.29, MeOH). ^{1}H NMR (CD_3OD, 700 MHz, Mixture of rotamers), δ: 5.18 (dd, *J* = 10.5, 3.4 Hz, 0.8H), 4.99 (t, *J* = 6.7 Hz, 1H), 4.41-4.34 (m, 4.7H), 4.31 (d,

J = 9.2 Hz, 0.8H), 4.25 (d, *J* = 6.9 Hz, 0.8H), 4.16 (d, *J* = 7.1 Hz, 1H), 4.14-4.07 (m, 1.8H), 4.05-3.97 (m, 2.8H), 3.92-3.88 (m, 1H), 3.87-3.82 (m, 1H), 3.69 (dt, *J* = 9.8, 6.6 Hz, 2H), 3.67-3.61 (m, 1H), 3.5 (q, *J* = 8.4 Hz, 1H), 3.36-3.32 (m, 1.1H), 3.01 (dd, *J* = 14.3, 3.4 Hz, 0.8H), 2.80-2.73 (m, 1.8H), 2.63-2.56 (m, 2.1H), 2.55-2.48 (m, 1.1), 2.42 (br, 2.6H), 2.30-2.23 (m, 1H), 2.23-2.14 (m, 3.5H), 2.14-2-03 (m, 9H), 2.03-1.88 (m, 19.5H), 1.81-1.67 (m, 7H), 1.67-1.54 (m, 5.2H), 1.06-1.00 (m, 6H), 1.00-0.89 (m, 18H). ^{13}C NMR (CD_3OD, 176 MHz, Mixture of rotamers), δ: 179.0, 178.9, 176.8, 176.7, 175.6, 174.9, 174.2, 174.0, 173.5, 173.4, 173.2, 173.1, 173.0, 172.6, 171.4, 170.6, 79.0, 73.5, 62.0, 61.3, 61.3, 61.2, 60.5, 59.9, 58.6, 58.3, 54.5, 54.4, 50.6, 49.9, 49.4, 48.4, 48.3, 47.4, 39.4, 38.5, 34.6, 34.0, 32.8, 32.1, 31.7, 31.6, 31.4, 31.4, 30.9, 30.9, 26.8, 26.6, 26.0, 26.0, 25.9, 25.8, 25.1, 24.5, 22.4, 22.4, 19.9, 19.8, 19.6, 19.5, 19.3, 19.1, 18.7, 18.4. HRMS (ESI) for $C_{37}H_{61}N_8O_{11}$ $(M+H)^+$: Calc.: 793.4454, Found: 793.4484.

8.7.4 Synthesis of heptapeptide 5-35

Methyl (1R,2R)-2-((R)-((S)-1-(N^2-(((S)-2-acetamido-5-(tert-butoxy)-5-oxopentanoyl)-L-valyl)-N^4-trityl-L-asparaginyl)pyrrolidin-2-yl)(hydroxy)methyl)cyclopentane-1-carboxylate 5-33a-S and methyl (1R,2R)-2-((R)-((S)-1-(N^2-(((S)-2-acetamido-5-(tert-butoxy)-5-oxopentanoyl)-L-valyl)-N^4-trityl-D-asparaginyl)pyrrolidin-2-yl)(hydroxy)methyl)cyclopentane-1-carboxylate **5-33a-*R*.**

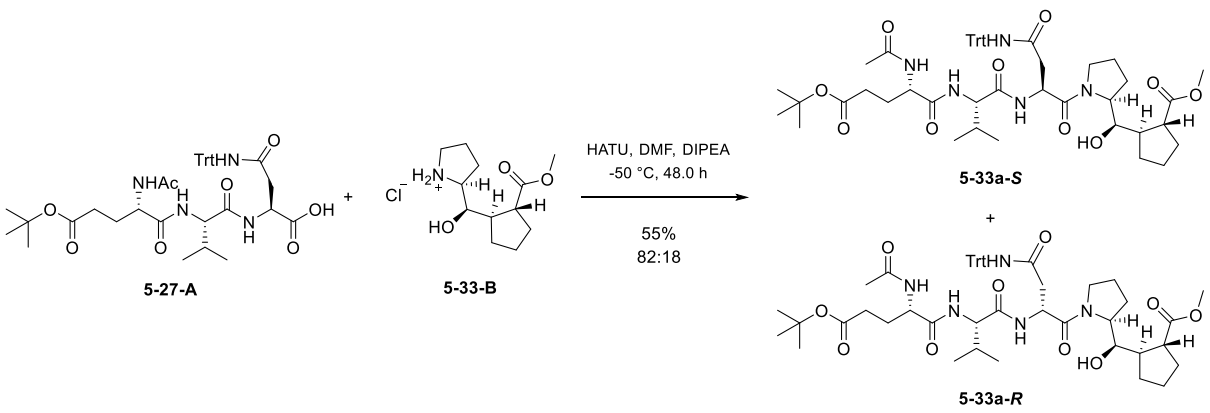

An amount of **5-33-B** [511] (26 mg, 0.10 mmol, 1.0 eq), the acid **5-27-A** (83 mg, 0.12 mmol, 1.2 eq.), and HATU (47 mg, 0.12 mmol, 1.2 eq.) were added to a round bottom flask, and the flask was purged with Ar. Dry DMF (1 mL) was added and the reaction mixture was stirred until all solids were dissolved, afterward, DIPEA (38 µL, 0.22 mmol, 2.2 eq.) was added dropwise at -50 °C and the yellow solution was then stirred at -50 °C for 48.0 h, monitored by TLC (85:15, DCM/MeOH,

ninhydrin). The reaction mixture was quenched using 1 M HCl aq. (5 mL) and diluted with EtOAc (5 mL), the layers were separated, and the aqueous layer was extracted with EtOAc (2 X 5 mL). The organic layers were combined and washed with 1 M HCl aq. (5 mL X 4), $NaHCO_3$/brine (8 x 5 mL + 5 mL), brine (2 X 5 mL), dried over Na_2SO_4, filtered, and concentrated under reduced pressure. The resulting solid was purified over silica gel (100% DCM to 95:05, DCM/MeOH, CAM/UV) to afford an inseparable mixture of **5-33a-*S*** and **5-33a-*R*** (dr 82:18, 50 mg, 55%) as a white solid. ^{1}H NMR (CD_3OD, 700 MHz, mixture of isomers and rotamers), δ: 7.31-7.17 (m, 25H), 5.0 (dd, *J* = 8.6, 6.0 Hz, 0.1H), 4.93 (dd, *J* = 8.4, 5.7 Hz, 0.2H), 4.84 (dd, *J* = 9.6, 4.9 Hz, 1H), 4.34 (dd, *J* = 8.9, 5.7 Hz, 1.3H), 4.26-4.22 (m, 0.3H), 4.20-4.17 (m, 0.2H), 4.16 (d, *J* = 7.0 Hz, 1H), 4.08-4.03 (m, 1.4H), 3.98 (dd *J* = 10.1, 1.9 Hz, 0.2H), 3.90 (dd, *J* = 10.3, 1.9 Hz, 1H), 3.71-3.64 (m, 2.4H), 3.62 (s, 0.4H), 3.62 (s, 3H), 3.60-3.49 (m, 0.5H), 3.43-3.38 (m, 0.3H), 3.20 (dt, *J* = 10.0, 7.5 Hz, 1H), 3.00 (dd, *J* = 15.5, 9.6 Hz, 1H), 2.96-2.87 (m, 0.4H), 2.75-2.55 (m, 2.8H), 2.36-2.17 (m, 4.7H), 2.11-1.91 (m, 13H), 1.87-1.78 (m, 4.3H), 1.77-1.59 (m, 6.6H), 1.56-1.46 (m, 1.6H), 1.45-1.44 (m, 4.4H), 1.43 (s, 9H), 0.98-0.89 (m, 10H). ^{13}C NMR data is reported for the major isomer and rotamer. (CD_3OD, 176 MHz), δ: 79.4, 173.9, 173.9, 173.4, 172.9, 171.7, 170.4, 145.8, 130.0, 128.7, 127.8, 81.8, 74.5, 62.2, 60.0, 54.1, 52.1, 50.1, 49.7, 48.3, 39.3, 32.7, 32.2, 32.2, 30.0, 28.4, 26.4, 25.9, 24.2, 22.4, 19.7, 18.5. HRMS (ESI) for $C_{51}H_{67}N_5O_{10}Na$ $(M+Na)^+$: Calc.: 932.4780, Found: 932.4816.

(1R,2R)-2-((R)-((S)-1-(N^2-(((S)-2-acetamido-5-(tert-butoxy)-5-oxopentanoyl)-L-valyl)-N^4-trityl-L-asparaginyl)pyrrolidin-2-yl)(hydroxy)methyl)cyclopentane-1-carboxylic acid **5-34-*S*** *and (1R,2R)-2-((R)-((S)-1-(N^2-(((S)-2-acetamido-5-(tert-butoxy)-5-oxopentanoyl)-L-valyl)-N^4-trityl-D-asparaginyl)pyrrolidin-2-yl)(hydroxy)methyl)cyclopentane-1-carboxylic acid* **5-34-*R*.**

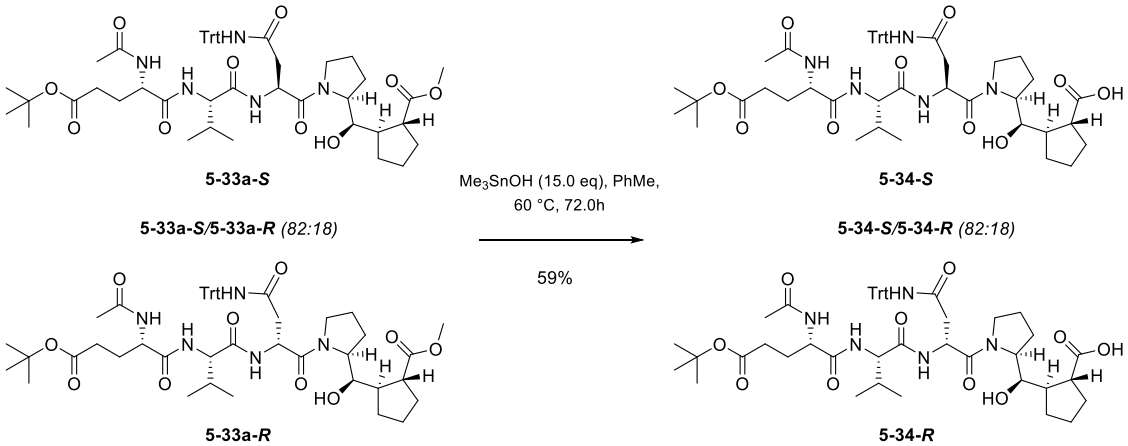

An 82:18 mixture of **5-33a** (65 mg, 71 µmol, 1.0 eq) and Me_3SnOH (65 mg, 0.36 mmol, 5.0 eq) were added to a vial and the vial was purged with Ar. Dry PhMe (0.71 mL) was added and the vial was sealed. The reaction mixture was stirred at 60 °C. Every 24.0 h, 5.0 eq of Me_3SnOH were added. After 72.0 h, the reaction mixture was partitioned between water (10 mL) and EtOAc (10 mL). The aqueous phase was acidified to pH 3 with a 10% $KHSO_4$ aq. solution and the phases were separated. The aqueous layer was extracted with EtOAc (2 x 15 mL) and the combined organic phases were washed with a pH 3 $KHSO_4$ aq. solution (3 x 15 mL), and brine (2 x 15 mL), dried over Na_2SO_4, filtered, and concentrated under reduced pressure. The resulting solid was purified over silica gel (100% CH_2Cl_2 to 88:12, CH_2Cl_2/MeOH, CAM) to afford a mixture of **5-34-*S*** and **5-34-*R*** (dr 82:18, 38 mg, 59%) as a white solid. ^1H NMR (CD_3OD, 700 MHz, mixture of isomers and rotamers), δ: 7.29-7.18 (m, 20H), 5.01 (dd, *J* = 8.7, 6.0 Hz, 0.1H), 4.94 (dd, *J* = 8.4, 5.6 Hz, 0.2H), 4.84 (dd, *J* = 8.7, 4.9 Hz, 1H), 4.35 (dd, *J* = 8.9, 5.6 Hz, 1H), 4.33-4.30 (m, 0.2H), 4.24 (dd, *J* = 86, 5.5 Hz, 0.2H), 4.19 (d, *J* = 6.9 Hz, 0.1H), 4.17 (d, *J* = 7.0 Hz, 1H), 4.11-4-06 (m, 1.2H), 4.03 (dd, *J* = 10.2, 1.8 Hz, 0.1H), 3.95 (dd, *J* = 10.3, 1.9 Hz, 1H), 3.75-3.69 (m, 1.8H), 3.61-3.55 (m, 0.2H), 3.55-3.49 (m, 0.4H), 3.45-3.39 (m, 0.4H), 3.25-3.39 (m, 1H), 3.01 (dd, *J* = 15.5, 9.7 Hz, 1H), 2.94-2.89 (m, 0.2H), 2.70 (dd, *J* = 15.5, 4.8 Hz, 1H), 2.67-2.61 (m, 0.4H), 2.58 (dt, *J* = 8.8, 7.0 Hz, 1H), 2.35-2.24 (m, 2.8H), 2.23-2.24 (m, 0.3H), 2.17-2.07 (m, 1.4H), 2.07-1.79 (m, 16H), 1.78-1.57 (m, 4.5H), 1.54-1.47 (m, 1.3H), 1.45-1.42 (m, 11.8H), 0.97-0.88 (m, 10.5H). ^{13}C NMR (CD_3OD, 176 MHz, Mixture of isomers and rotamers), δ: 180.5, 180.0, 175.3, 174.2, 174.0, 173.9, 173.9, 173.9, 173.8, 173.5, 173.4, 173.2, 172.9, 172.7, 171.8, 171.5, 171.1, 170.9, 170.8, 170.5, 145.9, 145.9, 145.8, 130.1, 130.0, 130.0, 128.8, 128.7, 128.7, 127.8, 127.8, 81.9, 81.8, 81.8, 81.8, 79.3, 75.2, 74.8, 72.0, 71.6, 62.4, 62.1, 62.0, 60.4, 60.1, 60.0, 59.5, 59.1, 56.5, 56.0, 54.2, 54.2, 54.1, 52.7, 49.8, 49.7, 47.4, 40.8, 40.7, 40.0, 39.3, 39.1, 32.8, 32.7, 32.6, 32.2, 32.0, 31.7, 31.4, 31.4, 31.2, 28.7, 28.5, 28.4, 28.4, 28.2, 28.1, 26.8, 26.7, 26.2, 26.2, 26.0, 24.3, 24.3, 22.5, 22.4, 22.4, 20.0, 19.9, 19.7, 18.9, 18.6, 18.5. HRMS (ESI) for $C_{50}H_{66}N_5O_{10}$ $(M+H)^+$: Calc.: 896.4804, Found: 896.4817.

tert-butyl (S)-4-acetamido-5-(((S)-1-(((S)-1-((S)-2-((R)-hydroxy((1R,2R)-2-(((S)-3-methyl-1-oxo-1-((S)-2-(tritylcarbamoyl)pyrrolidin-1-yl)butan-2-yl)carbamoyl)cyclopentyl)methyl)pyrrolidin-1-yl)-1,4-dioxo-4-(tritylamino)butan-2-yl)amino)-3-methyl-1-oxobutan-2-yl)amino)-5-oxopentanoate **5-34a-*S*.**

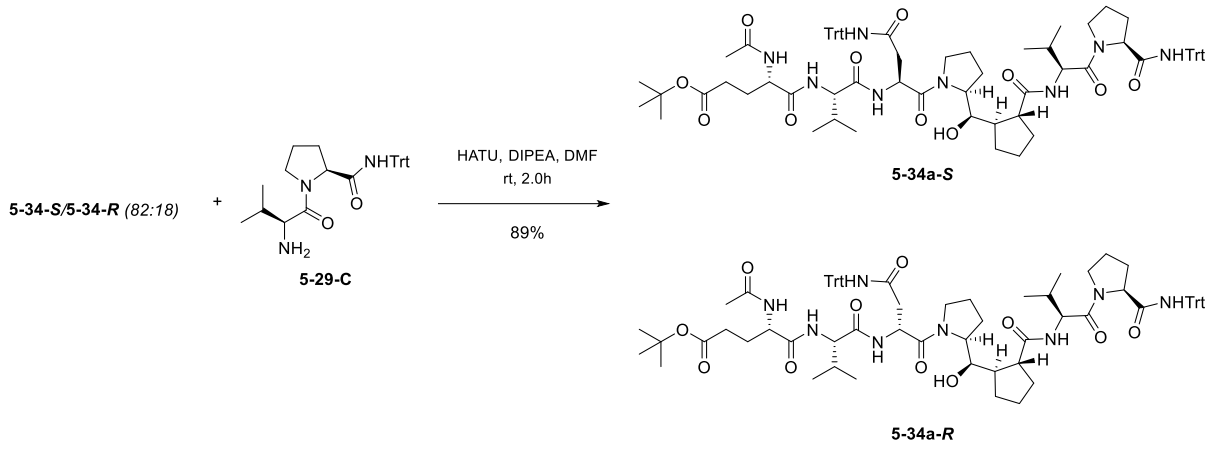

A 82:18 mixture of **5-34** (38 mg, 42 µmol, 1.0 eq.), the amine **5-29-C** (23 mg, 51 µmol, 1.2 eq) and HATU (20 mg, 51 µmol, 1.2 eq) were added to a round bottom flask, and the flask was purged with Ar. Dry DMF (850 µL) was added and the reaction mixture was stirred until all solids were dissolved, afterward, DIPEA (8.9 µL, 51 µmol, 1.2 eq) was added dropwise and the yellow solution was then stirred at rt for 2.0 h (monitored by MS analysis). The reaction mixture was quenched with 1 M HCl aq. (4 mL) and diluted with EtOAc (8 mL), the layers were separated, and the aqueous layer was extracted with EtOAc (2 X 8 mL). The organic layers were combined and washed with 1 M HCl/brine (5 x 8 mL + 8 mL), $NaHCO_3$/brine (3 x 5 mL + 5 mL), brine (2 x 8 mL), dried over Na_2SO_4, filtered, and concentrated under reduced pressure. The resulting crude was purified by preparative reverse-phase high-performance liquid chromatography (Atlantis dC18, H_2O-0.1% FA/ACN 65-90% in 9 min) to give **5-34a-*S*** (40 mg, 71%) and **5-34a-*R*** (10 mg, 18%) both as white solids. The minor isomer **5-34a-*R*** was discarded. $[\alpha]^{25}_D$: -56.2 (*c* = 0.21, CH_2Cl_2). NMR data are reported for the major rotamers. ^{1}H NMR (CD_3OD, 700 MHz), δ: 8.80 (s, 1H), 8.70 (s, 1H), 7.93 (d, *J* = 7.5 Hz, 1H), 7.30-7.18 (m, 30H), 4.84 (dd, *J* = 10.2, 4.6 Hz, 1H), 4.66 (dd, *J* = 8.2, 4.8 Hz, 1H), 4.40-4.37 (m, 1H), 4.35 (dd, *J* = 8.8, 5.7 Hz, 1H), 4.16 (d, *J* = 7.1 Hz, 1H), 4.10-4.07 (m, 1H), 3.98 (dd, *J* = 10.7, 1.8 Hz, 1H), 3.83 (dt, *J* = 9.8, 6.9 Hz, 1H), 3.69 (ddd, *J* = 9.9, 7.7, 4.3 Hz, 1H), 3.56 (dt, *J* = 9.6, 6.6 Hz, 1H), 3.18 (dt, *J* = 9.9, 7.4 Hz, 1H), 3.03 (dd, *J* = 15.3, 10.3 Hz, 1H), 2.71 (dd, *J* = 15.5, 4.4 Hz, 1H), 2.69-2.66 (m, 1H), 2.36-2.27 (m, 2H), 2.13-1.95 (m, 11H), 1.94-1.89 (m, 2H), 1.89-1.76 (m, 4H), 1.75-1.65 (m, 3H), 1.61-1.55 (m, 1H), 1.49-1.45 (m, 1H), 1.44 (s, 9H), 0.94-0.89 (m, 9H), 0.83 (d, *J* = 6.7 Hz, 3H). ^{13}C NMR (CD_3OD, 176 MHz), δ: 78.8, 173.9, 173.9, 173.5, 173.4, 173.2, 172.9, 171.6, 170.5, 145.9, 130.1, 130.1, 128.8, 128.7, 127.8, 127.8, 62.1, 62.1, 62.0, 60.0, 57.7,

57.6, 54.1, 39.5, 32.7, 32.1, 31.6, 31.5, 29.9, 29.3, 28.4, 28.2, 27.8, 26.1, 25.9, 24.4, 22.4, 20.2, 19.7, 18.6, 18.2. HRMS (ESI) for $C_{79}H_{96}N_8O_{11}Na$ $(M+Na)^+$: Calc.: 1355.7091, Found: 1355.7078.

(S)-4-acetamido-5-(((S)-1-(((S)-4-amino-1-((S)-2-((R)-((1R,2R)-2-(((S)-1-((S)-2-carbamoylpyrrolidin-1-yl)-3-methyl-1-oxobutan-2-yl)carbamoyl)cyclopentyl)(hydroxy)methyl)pyrrolidin-1-yl)-1,4-dioxobutan-2-yl)amino)-3-methyl-1-oxobutan-2-yl)amino)-5-oxopentanoic acid **5-35.**

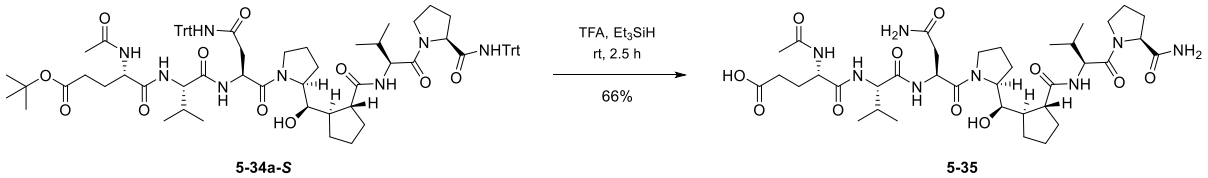

5-34a-*S* **5-35**

An amount of **5-34a-*S*** (25 mg, 19 µmol, 1.0 eq) was added to a round bottom flask, and the flask was purged with Ar. Neat TFA (187 µL) was added and after 13 min at stirring, Et_3SiH (18 µL, 0.11 mmol, 6.0 eq) was added. The reaction mixture was stirred for 2.5 h. After MS analysis indicated full conversion TFA was evaporated under reduced pressure. The resulting solid was finely crushed, suspended in Et_2O (5 mL) and vigorously stirred for 40 min. Then, the suspension was filtered, and the solid residue was washed with hexanes. The filtrate was then dissolved in THF (2.0 mL) and concentrated under reduced pressure. The resulting crude was purified by preparative reverse-phase high-performance liquid chromatography (XBridge Phenyl, H_2O-0.1% FA/ACN 15-80% in 8.5 min, then to ACN 95% in 0.3 min, then stay at ACN 90%) to give **5-35** (9.8 mg, 66%). $[\alpha]^{25}_D$: -104 (*c* = 0.2, MeOH). NMR data are reported for the major rotamer. ^{1}H NMR (CD_3OD, 700 MHz), δ: 4.98 (dd, *J* = 6.6, 6.6 Hz, 1H), 4.44-4.36 (m, 3H), 4.17 (d, *J* = 7.0 Hz, 1H), 4.14-4.10 (m, 1H), 4.07 (d, *J* = 10.4 Hz, 1H), 3.95-3.89 (m, 2H), 3.71-3.65 (m, 1H), 3.56-3.51 (m, 1H), 2.83 (dd, *J* = 14.9, 8.3 Hz, 1H), 2.76-2.69 (m, 1H), 2.61 (dd, *J* = 15.0, 5.2 Hz, 1H), 2.46 (bs, 1H), 2.26-2.18 (m, 1H), 2.14-2.02 (m, 7H), 2.02-1.85 (m, 9H), 1.83-1.73 (m, 2H), 1.72-1.63 (m, 2H), 1.62-1.54 (m, 1H), 1.49-1.40 (m, 1H), 1.04 (d, *J* = 6.7 Hz, 3H), 1.01 (d, *J* = 6.6 Hz, 3H), 0.95-0.92 (m, 6H). ^{13}C NMR (CD_3OD, 176 MHz), δ: 178.8, 177.0, 174.9, 174.0, 173.4, 173.0, 173.0, 170.8, 74.9, 62.2, 61.3, 60.1, 57.9, 54.2, 50.0, 49.9, 38.5, 31.9, 31.7, 31.1, 30.8, 30.3, 27.5, 26.1, 26.0, 24.5, 22.4, 19.9, 19.7, 18.7, 18.6. HRMS (ESI) for $C_{37}H_{60}N_8O_{11}Na$ $(M+Na)^+$: Calc.: 815.4274, Found: 815.4302.

8.7.5 Synthesis of ProCyp isomer 5-14

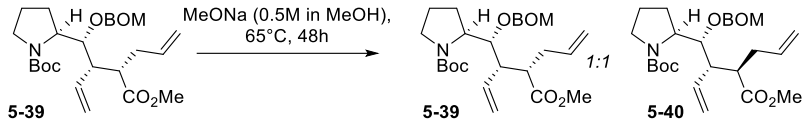

(S)-tert-butyl 2-((1R,2S)-1-((benzyloxy)methoxy)-2-(2-methoxy-2-oxoethyl)but-3-en-1-yl)pyrrolidine-1-carboxylate 5-39 and (S)-tert-butyl 2-((1R,2R)-1-((benzyloxy)methoxy)-2-(2-methoxy-2-oxoethyl)but-3-en-1-yl)pyrrolidine-1-carboxylate **5-40.**

An amount of **5-39** [511] (390 mg, 823 µmol, 1.0 eq.) was added to a sealed flask, and the flask was purged with vacuum/Ar. Sodium methoxide (24.7 mL, 12.4 mmol, 500 mM in MeOH, 15.0 eq.) was added and the flask was sealed. The reaction mixture was at 65 °C for 15h, monitored by ^{1}H NMR by comparing between integral ratios found at 4.4 ppm (**5-39**) and 4.05 ppm (**5-40**). The reaction mixture was cooled to rt, then it was quenched with NH_4Cl sat. aq. sol. (30 mL) and diluted with EtOAc (60 mL). The layers were separated, and the aqueous layer was extracted with EtOAc (2 X 60 mL). The organic layers were combined and washed with NH_4Cl sat. aq. sol. (30 mL), water (30 mL), and brine (300 mL), dried over Na_2SO_4, filtered, and concentrated under reduced pressure to afford a mixture of **5-39** and **5-40** which was brought to the next step without further purification (390 mg, 95%). *Characterization over two steps, ^{1}H NMR provided, see section 9.5.1.1.*

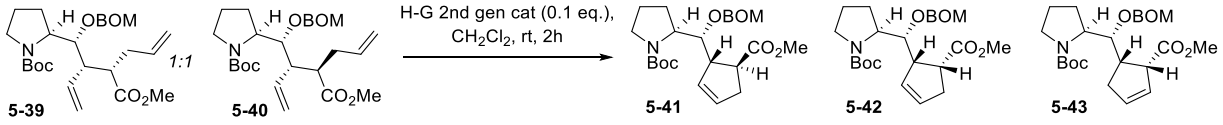

(S)-tert-butyl 2-((R)-((benzyloxy)methoxy)((1S,5S)-5-(methoxycarbonyl)cyclopent-2-en-1-yl)methyl)pyrrolidine-1-carboxylate **5-41***, (S)-tert-butyl 2-((R)-((benzyloxy)methoxy)((1S,5R)-5-(methoxycarbonyl)cyclopent-2-en-1-yl)methyl)pyrrolidine-1-carboxylate* **5-42***, and (S)-tert-butyl 2-((R)-((benzyloxy)methoxy)((1S,2R)-2-(methoxycarbonyl)cyclopent-3-en-1-yl)methyl)pyrrolidine-1-carboxylate* **5-43.**

An amount of **5-39** and **5-40** (0.30 g, 0.62 mmol, 1.0 eq.) was added to a round-bottomed flask, and the flask was purged with vacuum/Ar. CH_2Cl_2 (6.3 mL) was added followed by Hoveyda-Grubbs second generation catalyst (40 mg, 62 µmol, 0.1 eq.) and the solution was stirred at rt for 2h, monitored by mass spectrometry. Ethyl vinyl ether (3 mL) was added and the solution was stirred at rt for 1h then concentrated under reduced pressure. The residual black oil was chromatographed over silica gel (100% hexanes to 85:15 hexanes/EtOAc, *p*-anisaldehyde/ninhydrin/UV) to afford **5-41** (116 mg, 42%), **5-42** (114 mg, 41%), and **5-43** (11 mg, 4%) as colorless oils. Diastereomer **5-41** : (See reference [511]). Diastereomer **5-42**: *Rf* = 0.28 (85:15 hexanes/EtOAc). $[\alpha]^{25}_D$: +0.7 (*c* = 3.0, $CHCl_3$). ^{1}H NMR (500 MHz, Chloroform-*d*) δ 7.35 – 7.26 (m, 5H), 5.81 (m, 1H), 4.70 – 4.55 (m, 4H), 4.29 (bs, 1H), 3.87 – 3.62 (m, 4H), 3.56 (m, 0.5H), 3.42 (m, 0.5H), 3.24 – 3.16 (m, 2H), 3.11 (bs, 1H), 2.74 (m, 1H), 2.53 (m, 1H), 2.10 (m, 1H), 1.87 (m, 2H), 1.71 (m, 1H), 1.45 (m, 9H). ^{13}C NMR (126 MHz, $CDCl_3$) δ 174.6, 173.9, 154.6, 138.3, 131.0, 130.8, 130.6, 130.4, 128.4, 127.8, 127.6, 96.45, 79.0, 78.9, 78.0, 70.5, 60.9, 60.7, 51.9, 51.7, 51.1, 50.6, 47.3, 46.9, 45.7, 36.1, 35.5, 28.7, 26.9, 25.6, 24.7, 24.0. HRMS (ESI) for $C_{25}H_{35}NO_6$ $(M+H)^+$: Calc.: 446.25371, Found: 446.25352, for $C_{25}H_{35}NO_6$ $(M+Na)^+$: Calc.: 468.23566, Found: 468.23524. Diastereomer **5-43**: *Rf* = 0.3 (85:15 hexanes/EtOAc). $[\alpha]^{25}_D$: -126.8 (*c* = 5.0, $CHCl_3$). ^{1}H NMR (500 MHz, Chloroform-*d*) δ 7.36 – 7.32 (m, 4.15H), 7.28 (m, 0.85H), 6.05 (m, 1H), 5.73 (m, 1H), 4.75 (m, 2H), 4.67 (d, *J* = 12.2 Hz, 1H), 4.58 (d, *J* = 12.1 Hz, 1H), 4.50 (m, 1H), 3.80 (m, 2.6H), 3.72 – 3.61 (m, 1.8H), 3.44 (m, 0.6H), 3.35 (m, 1H), 3.20 (dt, *J* = 10.7, 7.0 Hz, 1H), 2.73 – 2.62 (m, 1H), 2.62 – 2.51 (m, 1H), 2.45 (m, 1H), 2.12 – 2.01 (m, 1H), 1.90 (m, 2H), 1.75 – 1.67 (m, 1H), 1.45 (m, 9H). ^{13}C NMR (126 MHz, $CDCl_3$) δ 173.7, 173.2, 154.7, 154.3, 138.3, 135.6, 129.4, 128.5, 128.4, 127.8, 127.6, 96.3, 95.9, 80.3, 79.0, 78.9, 78.4, 70.2, 60.3, 52.3, 52.0, 51.0, 47.5, 46.7, 36.6, 28.6, 26.5, 24.9, 24.0. HRMS (ESI) for $C_{25}H_{35}NO_6$ $(M+H)^+$: Calc.: 446.25371, Found: 446.25326, for $C_{25}H_{35}NO_6$ $(M+Na)^+$: Calc.: 468.23566, Found: 468.23511.

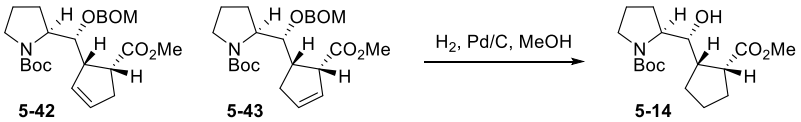

(S)-tert-butyl 2-((R)-hydroxy((1S,2R)-2-(methoxycarbonyl)cyclopentyl)methyl)pyrrolidine-1-carboxylate **5-14**

An amount of **5-42** (100 mg, 224 µmol, 0.84 eq.) and **5-43** (19 mg, 43 µmol, 0.16 eq.) were added to a round-bottomed flask, and the flask was purged with vacuum/Ar. Dry MeOH (2.7 mL) was added followed by Pd/C (28 mg, 0.26 mmol, 1.0 eq.). The flask was purged with vacuum/H_2 and the reaction mixture was stirred at rt for 3h, monitored by mass spectrometry. The suspension was filtered over a pad of Celite and washed with abundant MeOH, then concentrated under reduced pressure. The residual oil was chromatographed over silica gel (100% hexanes to 7:3 hexanes/EtOAc, Ninhydrin) to afford **5-14** (75 mg, 86%) as a colorless oil. *Rf* = 0.28 (7:3 hexanes/EtOAc). $[\alpha]^{25}_D$: -46.9 (*c* 5.5, $CHCl_3$). ^{1}H NMR (500 MHz, Chloroform-*d*, mixture of rotamers) δ 3.96 (m, , 2H), 3.68 (s, 3H), 3.50 (m, 1.5H), 3.21 (m, 1H), 2.84 – 2.77 (m, 1H), 2.15 (m, 1H), 2.02 – 1.68 (m, 9.5H), 1.58 (m, 1H), 1.45 (s, 9H). ^{13}C NMR (126 MHz, $CDCl_3$, mixture of rotamers) δ 177.0, 155.9, 155.3, 79.8, 72.4, 71.7, 62.0, 61.5, 51.9, 47.8, 47.2, 46.1, 30.8, 29.9, 28.6, 26.8, 26.0, 25.4, 24.3, 23.7. HRMS (ESI) for $C_{17}H_{29}NO_5$ $(M+H)^+$: Calc.: 328.21185, Found: 328.21057, for $C_{17}H_{29}NO_5$ $(M+Na)^+$: Calc.: 350.19379, Found: 350.19338.

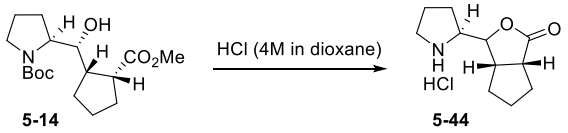

(3aS,6aR)-3-((S)-pyrrolidin-2-yl)hexahydro-1H-cyclopenta[c]furan-1-one hydrochloride **5-44.**

An amount of **5-14** (20 mg, 61 µmol, 1.0 eq.) was added to a round-bottomed flask, and the flask was purged with vacuum/Ar. HCl (0.31 mL, 1.2 mmol, 4.0 M in dioxane, 20 eq.) was added and the reaction mixture was stirred at rt for 30 min, monitored by TLC (75:25 hexanes/EtOAc, ninhydrin). The reaction mixture was concentrated at 15 °C under reduced pressure. The pressure was gradually decreased to remove HCl gases slowly. The residual oil was chromatographed over silica gel (100% CH_2Cl_2 to 88:12 CH_2Cl_2/MeOH, ninhydrin) to afford **5-44** (12.0 mg, 85%) as colorless crystals. *Rf* = 0.29 (88:12 CH_2Cl_2/MeOH). $[\alpha]^{25}_D$: -33.3 (*c* 6.0, MeOH). ^{1}H NMR (500 MHz, Methanol-d_4, mixture of rotamers) δ 4.51 (dd, *J* = 8.3, 6.0 Hz, 1H), 3.53 (q, *J* = 7.7 Hz, 1H), 3.24 (dt, *J* = 8.9, 3.4 Hz, 1H), 3.10 (ddt, *J* = 10.9, 7.5, 3.7 Hz, 2H), 2.96 (qd, *J* = 8.3, 5.9 Hz, 1H), 2.16 (m, 1H), 2.05 – 1.88 (m, 4H), 1.86 – 1.79 (m, 2H), 1.70 – 1.62 (m, 2H), 1.57 (m, 1H). ^{13}C NMR (126 MHz, MeOD, mixture of rotamers) δ 182.1, 174.1, 82.6, 76.2, 64.6, 59.9, 47.9, 47.3, 47.2, 46.4, 46.2, 44.4, 32.6, 31.5, 31.4, 29.8, 29.6, 27.7, 27.4, 25.7, 25.6, 23.8. HRMS (ESI) for $C_{11}H_{17}NO_2$ $(M+H)^+$: Calc.: 196.13321, Found: 196.13300.

8.7.6 Synthesis of heptapeptide 5-52

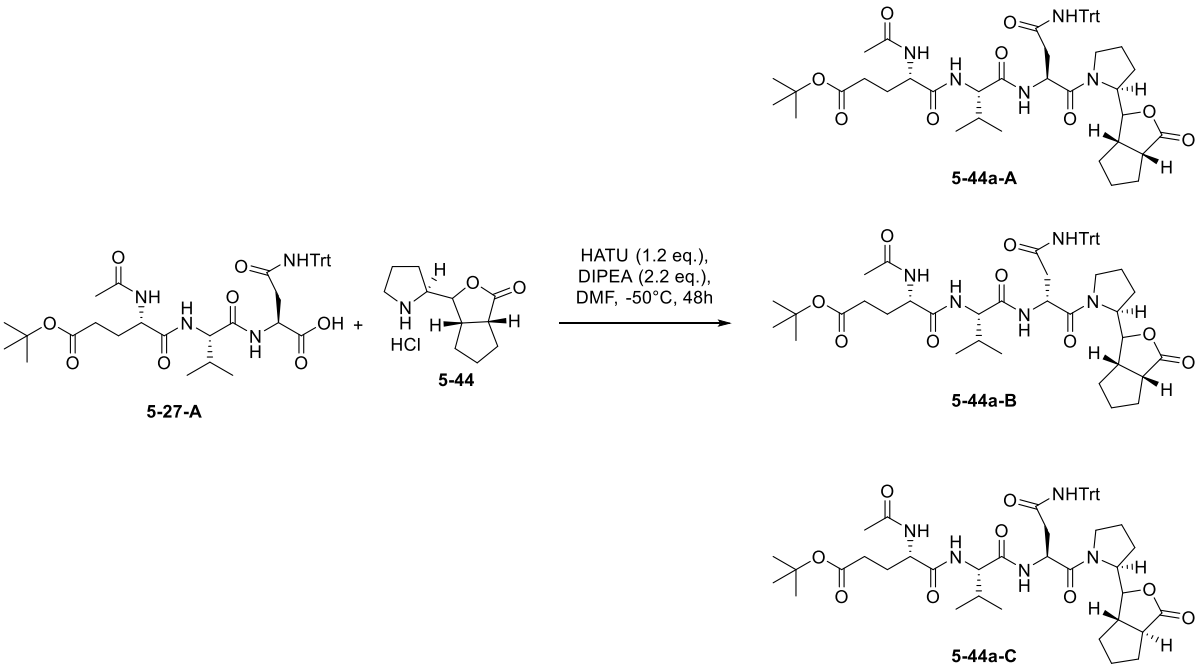

(4S)-tert-butyl 4-acetamido-5-(((2S)-1-(((2S)-1,4-dioxo-1-((2S)-2-((3aR,6aS)-3-oxohexahydro-1H-cyclopenta[c]furan-1-yl)pyrrolidin-1-yl)-4-(tritylamino)butan-2-yl)amino)-3-methyl-1-oxobutan-2-yl)amino)-5-oxopentanoate **5-44a-A***, (4S)-tert-butyl 4-acetamido-5-(((2S)-1-(((2R)-1,4-dioxo-1-((2S)-2-((3aR,6aS)-3-oxohexahydro-1H-cyclopenta[c]furan-1-yl)pyrrolidin-1-yl)-4-(tritylamino)butan-2-yl)amino)-3-methyl-1-oxobutan-2-yl)amino)-5-oxopentanoate* **5-44a-B** *and (4S)-tert-butyl 4-acetamido-5-(((2S)-1-(((2S)-1,4-dioxo-1-((2S)-2-((3aS,6aS)-3-oxohexahydro-1H-cyclopenta[c]furan-1-yl)pyrrolidin-1-yl)-4-(tritylamino)butan-2-yl)amino)-3-methyl-1-oxobutan-2-yl)amino)-5-oxopentanoate* **5-44a-C.**

An amount of **5-27-A** (51 mg, 73 µmol, 1.2 eq.), **5-44** (14 mg, 61 µmol, 1.0 eq) and HATU (29 mg, 73 µmol, 1.2 eq.) were added to a round-bottomed flask, and the flask was purged with Ar. Dry DMF (607 µL) was added and the reaction mixture was stirred until all solids were dissolved. The reaction mixture was cooled to -50 °C and DIPEA (23 µL, 134 µmol, 2.2 eq.) was added dropwise and the yellow solution was then stirred at -50 °C for 48 h, monitored by mass spectrometry. The reaction mixture was quenched with NH_4Cl sat. aq. sol. (1 mL) and allowed to reach rt. EtOAc (1 mL) was added, the layers were separated, and the aqueous layer was extracted with EtOAc (2 X 2 mL). The organic layers were combined and washed with NH_4Cl sat. aq. sol. (3 X 3 mL), $NaHCO_3$

sat. aq. sol. (3 X 3 mL), water (3 X 3 mL), and brine (3 mL), dried over Na_2SO_4, filtered, and concentrated under reduced pressure. The resulting solid was chromatographed over silica gel (100% CH_2Cl_2 to 94:06, CH_2Cl_2/MeOH, CAM) to afford a mixture of **5-44a-A**, **5-44a-B**, and **5-44a-C** (35 mg, 66%, 75:21:4) as a white solid. *Rf* = 0.3 (94:06 CH_2Cl_2/MeOH). ^{1}H NMR (700 MHz, CD_3OD, mixture of rotamers and diastereomers) δ 7.29 – 7.18 (m, 15H), 4.96 (dd, *J* = 9.1, 5.6 Hz, 0.15H), 4.90 (dd, *J* = 8.3, 5.6 Hz, 0.85H), 4.82 (d, *J* = 6.4 Hz, 0.14H), 4.74 (dd, *J* = 6.0, 3.4 Hz, 0.1H), 4.64 (dd, *J* = 6.1, 2.8 Hz, 0.75H), 4.50 – 4.48 (m, 0.15H), 4.40 – 4.24 (m, 1.85H), 4.21 (d, *J* = 6.8 Hz, 0.7H), 4.15 (dd, *J* = 14.2, 7.1 Hz, 0.25H), 3.69 (m, 0.75H), 3.61 – 3.36 (m, 1.3H), 3.14 (m, 0.25H), 3.10 – 3.05 (m, 0.15H), 3.03 – 2.96 (m, 1.05H), 2.91 (m, 1.5H), 2.71 – 2.61 (m, 1H), 2.34 – 2.23 (m, 2H), 2.10 – 1.73 (m, 13H), 1.60 (m, 3H), 1.44 (m, 9H), 0.97 – 0.88 (m, 6H). ^{13}C NMR (176 MHz, CD_3OD, mixture of rotamers and diastereomers) δ 182.8, 182.7, 182.6, 173.9, 173.8, 173.8, 173.8, 173.8, 173.6, 173.4, 173.4, 173.1, 173.0, 172.9, 171.4, 171.4, 171.3, 171.2, 171.2, 171.0, 145.9, 145.9, 145.8, 130.1, 130.0, 130.0, 128.7, 128.7, 128.7, 128.7, 127.8, 127.8, 86.1, 83.0, 82.9, 81.8, 81.8, 79.5, 79.3, 79.1, 71.7, 71.6, 60.3, 60.0, 59.8, 59.5, 59.0, 58.9, 54.2, 54.1, 53.9, 49.8, 49.6, 49.5, 48.1, 48.0, 47.8, 47.8, 47.7, 47.3, 45.1, 44.9, 44.5, 40.5, 39.3, 39.0, 32.7, 32.7, 32.6, 32.2, 32.0, 31.6, 30.2, 30.0, 29.9, 28.4, 28.4, 28.2, 28.1, 28.1, 27.9, 27.7, 27.6, 27.4, 26.6, 26.6, 25.9, 25.7, 24.3, 22.5, 22.4, 22.4, 19.8, 19.8, 19.7, 18.7, 18.5. HRMS (ESI) for $C_{50}H_{63}N_5O_9$ $(M+Na)^+$: Calc.: 900.45180, Found: 900.45398.

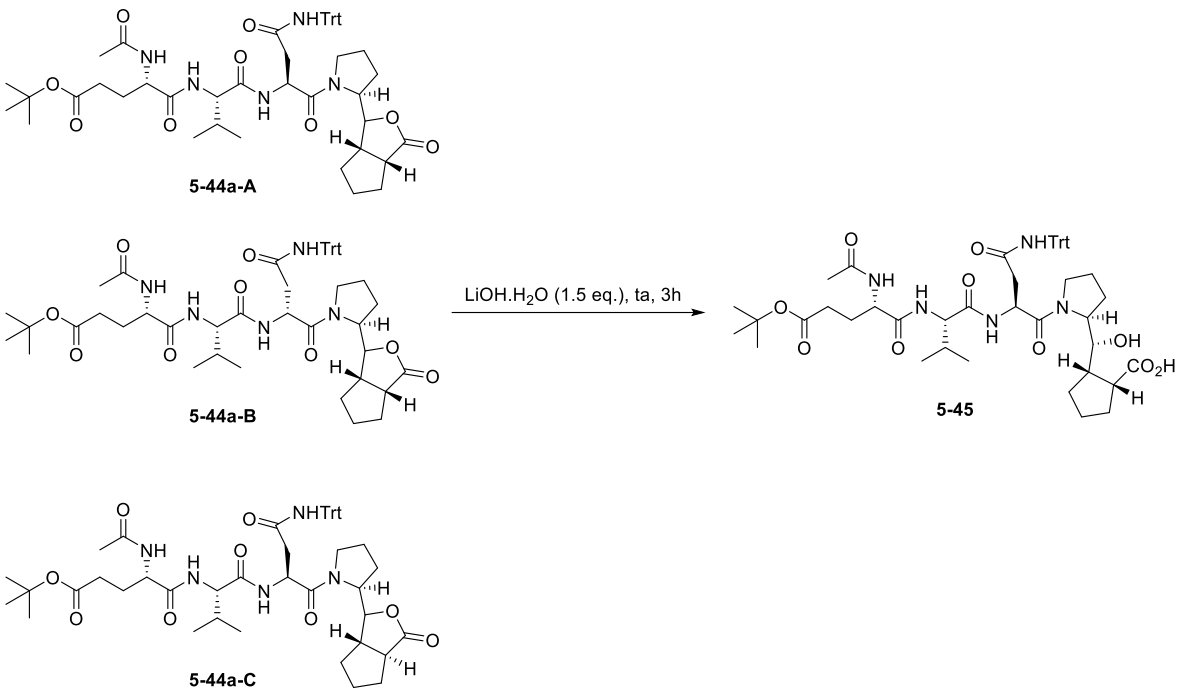

(1R,2S)-2-((R)-((S)-1-((S)-2-((S)-2-((S)-2-acetamido-5-(tert-butoxy)-5-oxopentanamido)-3-methylbutanamido)-4-oxo-4-(tritylamino)butanoyl)pyrrolidin-2-yl)(hydroxy)methyl)cyclopentanecarboxylic acid **5-45**

An amount of **5-44a-A**, **5-44a-B**, and **5-44a-C** (12.0 mg, 13.7 µmol, 1.0 eq.) was added to a round-bottomed flask, and the flask was purged with Ar. A solution of EtOH/H_2O (4:1, 1.4 mL) was added followed by LiOH (137 µL, 13.7 µmol, C = 100 mM in H_2O, 1.0 eq.). The reaction mixture was stirred at rt for 3h, monitored by TLC analysis (94:06 DCM, MeOH, CAM). LiOH (69 µL, 6.9 µmol, C = 0.10 M in H_2O, 0.5 eq.) was added and the reaction mixture was stirred for an additional 2h. The reaction mixture was diluted with water (1.0 mL) and CH_2Cl_2 (1.0 mL) and the pH of the aqueous layer was acidified to pH = 3-4 with a 10% w/w $KHSO_4$ aq. sol. The aqueous layer was extracted with CH_2Cl_2 (3 x 2 mL). The organic layers were collected, dried over Na_2SO_4, filtered, and concentrated under reduced pressure. The resulting white solid was chromatographed over silica gel (100% CH_2Cl_2 to 93:07 CH_2Cl_2/MeOH, CAM) to afford **5-45** as a white solid (9.0 mg, 73%). *Rf* = 0.3 (94:06 CH_2Cl_2/MeOH). $[\alpha]^{25}_D$: -33.3 (*c* 6.0, MeOH). ^{1}H NMR (700 MHz, CD_3OD, mixture of rotamers) δ 7.31 – 7.16 (m, 15H), 4.36 – 4.24 (m, 3H), 4.19 (d, *J* = 6.7 Hz, 1H), 3.71 (m, 1H), 3.13 (m, 1H), 2.96 (dd, *J* = 15.1, 9.1 Hz, 1H), 2.68 (m, 2H), 2.36 – 2.24 (m, 2H), 2.10 – 1.77 (m, 17H),

1.69 (m, 1H), 1.60 (m, 1H), 1.43 (m, 9H), 0.93 – 0.87 (m, 6H). ^{13}C NMR (176 MHz, CD_3OD, mixture of rotamers) δ 173.9, 173.9, 173.6, 172.9, 171.6, 170.6, 170.5, 145.8, 130.6, 130.0, 130.0, 128.8, 128.7, 127.8, 127.8, 81.9, 71.6, 62.8, 60.0, 54.2, 39.6, 32.7, 32.2, 31.8, 28.4, 28.3, 28.1, 25.9, 24.7, 24.7, 24.5, 22.4, 19.8, 18.5. HRMS (ESI) for $C_{50}H_{63}N_5O_9$ $(M+Na)^+$: Calc.: 900.45180, Found: 900.45398.

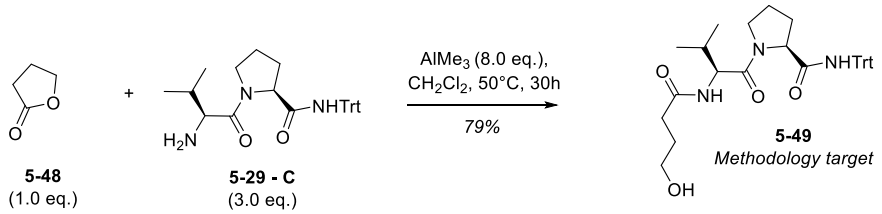

(S)-1-((S)-2-(4-hydroxybutanamido)-3-methylbutanoyl)-N-tritylpyrrolidine-2-carboxamide **5-49**

An amount of **5-29-C** (79 mg, 0.17 mmol, 3.0 eq.) was added to a 1-neck round-bottomed flask dried and flushed under Ar and the flask was purged with Ar. CH_2Cl_2 (290 µL) was added and the solution **A** was cooled to 0 °C whereby $AlMe_3$ (232 µL, 465 µmol, C = 2.0 M in CH_2Cl_2, 8.0 eq.) was added (gas formation observed). The mixture was stirred at 0 °C for 50 min. In a sealing flask dried and flushed under Ar was dissolved **5-48** (4.4 µL, 58 µmol, 1.0 eq.) in CH_2Cl_2 (290 µL). The solution **A** was then transferred to the sealing flask. The flask was sealed and heated at 50 °C (gas formation observed at first) for 30h, monitored by TLC analysis (4:6 Hexanes/EtOAc, $KMnO_4$/*p*-anisaldehyde). The reaction mixture was cooled to rt and quenched with HCl aq. (1.0 M, 500 µL) and diluted with CH_2Cl_2 (500 µL). The layers were separated, and the aqueous layer was extracted with CH_2Cl_2 (3 x 500 µL). The organic layers were collected washed with HCl aq. (1.0 M, 3 x 2 mL), $NaHCO_3$ (1 x 2 mL), brine (1 x 2 mL), dried over Na_2SO_4, filtered and concentrated under reduced pressure. The residual oil was chromatographed over silica gel (95:05 CH_2Cl_2/MeOH, *p*-anisaldehyde) to afford an inseparable mixture of **5-49** and **5-29-C** (1:1.2, 47 mg, 79%) as a white solid. *No characterization reported, ^{1}H NMR provided, see section 9.5.1.2.*

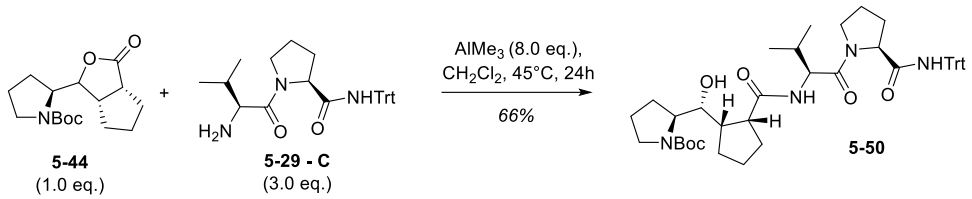

(S)-tert-butyl 2-((R)-hydroxy((1S,2R)-2-(((S)-3-methyl-1-oxo-1-((S)-2-(tritylcarbamoyl)pyrrolidin-1-yl)butan-2-yl)carbamoyl)cyclopentyl)methyl)pyrrolidine-1-carboxylate **5-50**

An amount of **5-29-C** (21 mg, 46 µmol, 3.0 eq.) was added to a 1-neck round-bottomed flask dried and flushed under Ar and the flask was purged with Ar. CH_2Cl_2 (76 µL) was added and the solution **A** was cooled to 0 °C whereupon $AlMe_3$ (61 µL, 0.12 mmol, C = 2.0 M in CH_2Cl_2, 8.0 eq.) was added (gas formation observed). The mixture was stirred at 0 °C for 50 min. In a sealing flask dried and flushed under Ar was dissolved **5-44** (4.5 mg, 15 µmol, 1.0 eq.) in CH_2Cl_2 (76 µL). The solution **A** was then transferred to the sealing flask. The flask was sealed and heated at 50 °C (gas formation observed at first) for 24h, monitored by TLC analysis (95:05 CH_2Cl_2/MeOH, ninhydrin). The reaction mixture was cooled to rt and quenched with NH_4Cl sat. aq. sol. (300 µL) and diluted with CH_2Cl_2 (300 µL). The layers were separated, and the aqueous layer was extracted with CH_2Cl_2 (1 x 300 µL). The organic layers were collected washed with HCl aq. (1.0 M, 2 x 1 mL), $NaHCO_3$ (1 x 1 mL), brine (1 x 1 mL), dried over Na_2SO_4, filtered and concentrated under reduced pressure. The residual oil was chromatographed over silica gel (95:05 CH_2Cl_2/MeOH, ninhydrin) to afford **5-50** as a white solid (7.5 mg, 66%). *Rf* = 0.3 (94:06 CH_2Cl_2/MeOH). $[\alpha]^{25}_D$: -124.8 (*c* 8.0, MeOH). ^{1}H NMR (700 MHz, CD_3OD, mixture of rotamers) δ 8.73 (m, 1H), 7.27 – 7.19 (m, 15H), 4.66 – 4.59 (m, 1.1H), 4.48 (m, 0.4H), 4.38 (m, 0.5H), 3.96 – 3.80 (m, 2.6H), 3.73 (m, 0.4H), 3.58 (m, 1H), 3.44 (m, 1H), 3.26 (m, 1H), 2.64 – 2.54 (m, 1H), 2.24 (m, 1H), 2.14 – 1.56 (m, 16H), 1.49 (m, 9H), 0.94 (m, 3H), 0.90 (m, 3H). ^{13}C NMR (176 MHz, CD_3OD, mixture of rotamers) δ 179.0, 178.3, 173.4, 173.4, 172.8, 156.8, 156.5, 145.9, 145.9, 130.1, 128.7, 127.8, 81.1, 80.7, 75.4, 74.6, 71.8, 71.7, 62.1, 62.1, 62.0, 61.7, 58.0, 57.7, 47.9, 47.9, 47.7, 34.0, 33.3, 31.7, 31.6, 31.3, 30.3, 29.5, 29.4, 29.0, 28.9, 26.8, 26.7, 26.3, 26.0, 25.9, 25.6, 25.6, 24.8, 19.8, 19.8, 18.7, 18.6. HRMS (ESI) for $C_{45}H_{58}N_4O_6$ $(M+Na)^+$: Calc.: 773.42486, Found: 773.42700.

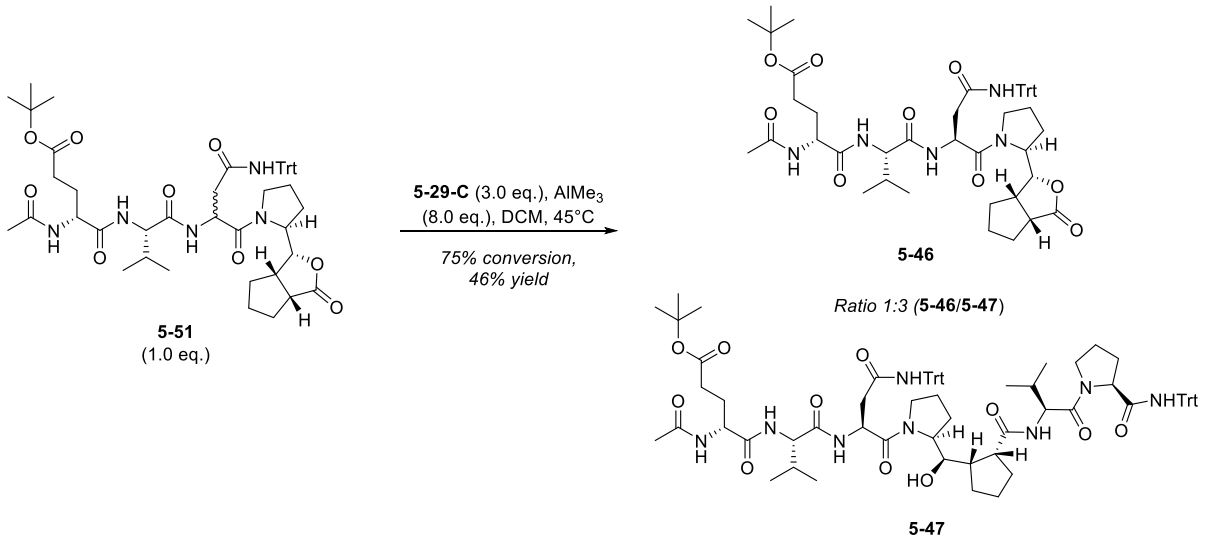

(4R)-tert-butyl 4-acetamido-5-(((2S)-1-(((2S)-1,4-dioxo-1-(2-((1R,3aR,6aS)-3-oxohexahydro-1H-cyclopenta[c]furan-1-yl)pyrrolidin-1-yl)-4-(tritylamino)butan-2-yl)amino)-3-methyl-1-oxobutan-2-yl)amino)-5-oxopentanoate **5-46** *and (R)-tert-butyl 4-acetamido-5-(((S)-1-(((S)-1-((S)-2-((R)-hydroxy((1S,2R)-2-(((S)-3-methyl-1-oxo-1-((S)-2-(tritylcarbamoyl)pyrrolidin-1-yl)butan-2-yl)carbamoyl)cyclopentyl)methyl)pyrrolidin-1-yl)-1,4-dioxo-4-(tritylamino)butan-2-yl)amino)-3-methyl-1-oxobutan-2-yl)amino)-5-oxopentanoate* **5-47**

An amount of **5-29-C** (36 mg, 79 µmol, 3.0 eq.) was added to a 1-neck round-bottomed flask dried and flushed under Ar and the flask was purged with Ar. CH_2Cl_2 (131 µL) was added and the solution **A** was cooled to 0 °C whereby $AlMe_3$ (105 µL, 210 µmol, C = 2.0 M in CH_2Cl_2, 8.0 eq.) was added (gas formation observed). The mixture was stirred at 0 °C for 50 min. In a sealing flask dried and flushed under Ar was dissolved **5-51** (23 mg, 26 µmol, 1.0 eq.) in CH_2Cl_2 (262 µL). The solution **A** was then transferred to the sealing flask. The flask was sealed and heated at 50 °C (gas formation observed at first) for 19h, monitored by TLC analysis (94:06 CH_2Cl_2/MeOH, CAM). The reaction mixture was cooled to rt and quenched with NH_4Cl sat. aq. sol. (500 µL) and diluted with CH_2Cl_2 (300 µL). The layers were separated, and the aqueous layer was extracted with CH_2Cl_2 (3 x 1 mL). The organic layers were collected, then washed with NH_4Cl sat. aq. sol. (3 x 1 mL), water (1 x 1 mL), brine (1 x 1 mL), dried over Na_2SO_4, filtered and concentrated under reduced pressure. The white solid was purified by reverse-phase high performance liquid chromatography chromatography (Sunfire C18, 19 x100 mm, 5 µm; H_2O-0.1% FA/ACN 50-90% 0-10 min → 90% 10-11 min → 90-50% 11-11.5 min → 50% 11.5-15 min; Flow: 24 mL/min (2.4 mL/min at column

dilution)) to afford **5-47** as a white solid (16 mg, 46%) and **5-46** as a white solid (4 mg, 17%). *Rf* = 0.3 (94:06 CH_2Cl_2/MeOH). $[\alpha]^{25}_D$: -94.3 (*c* 2.8, MeOH). ^{1}H NMR (700 MHz, CD_3OD, mixture of rotamers) δ 7.32 – 7.15 (m, 30H), 4.84 (dd, *J* = 8.8, 5.6 Hz, 1H), 4.66 (dd, *J* = 8.2, 5.2 Hz, 1H), 4.38 (d, *J* = 7.2 Hz, 1H), 4.35 (dd, *J* = 9.0, 5.6 Hz, 1H), 4.28 (m, 2H), 4.20 (d, *J* = 6.9 Hz, 1H), 4.14 (m, 1H), 4.03 (m, 1H), 3.79 – 3.74 (m, 1H), 3.52 (dt, *J* = 9.9, 6.9 Hz, 1H), 3.08 (q, *J* = 8.7 Hz, 1H), 2.91 (dd, *J* = 15.2, 8.9 Hz, 1H), 2.78 (m, 1H), 2.65 (dd, *J* = 15.1, 5.5 Hz, 1H), 2.29 (m, 2H), 2.10 – 1.73 (m, 20H), 1.67 (m, 1H), 1.49 (m, 1H), 1.43 (s, 9H), 0.93 – 0.89 (m, 12H). ^{13}C NMR (176 MHz, CD_3OD, mixture of rotamers) δ 178.2, 173.9, 173.7, 173.6, 173.6, 173.4, 172.6, 171.5, 170.4, 167.1, 145.9, 145.8, 135.6, 130.6, 130.2, 130.1, 130.1, 130.0, 128.8, 128.7, 128.7, 127.8, 127.8, 81.8, 71.7, 71.6, 71.3, 68.7, 62.4, 62.1, 59.6, 58.2, 54.1, 46.7, 40.3, 39.8, 32.7, 32.4, 32.2, 31.7, 31.2, 30.8, 30.3, 30.2, 29.4, 28.4, 28.4, 28.1, 26.1, 25.8, 25.1, 25.1, 24.9, 24.0, 22.4, 19.9, 19.8, 19.3, 18.6, 14.4, 11.4. HRMS (ESI) for $C_{79}H_{96}N_8O_{11}$ $(M+Na)^+$: Calc.: 1333.72713, Found: 1333.72609.

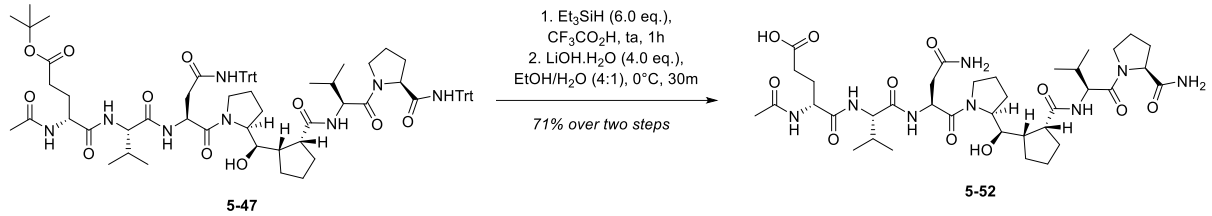

(R)-4-acetamido-5-(((S)-1-(((S)-4-amino-1-((S)-2-((R)-((1S,2R)-2-(((S)-1-((S)-2-carbamoylpyrrolidin-1-yl)-3-methyl-1-oxobutan-2-yl)carbamoyl)cyclopentyl)(hydroxy)methyl)pyrrolidin-1-yl)-1,4-dioxobutan-2-yl)amino)-3-methyl-1-oxobutan-2-yl)amino)-5-oxopentanoic acid **5-52**

An amount of **5-47** (17 mg, 12 µmol, 1.0 eq) was added to a round bottom flask, and the flask was purged with Ar. Neat TFA (123 µL) was added and after 10 min of stirring, Et_3SiH (12 µL, 74 µmol, 6.0 eq) was added. The reaction mixture was stirred for 1 h, monitored by mass spectrometry. The reaction mixture was diluted with CH_2Cl_2 (500 µL) and TFA was slowly evaporated under reduced pressure. The resulting solid was finely crushed, suspended in Et_2O (2.5 mL) and vigorously stirred for 40 min. Et_2O was removed and the process was repeated 2 times. The white solid was transferred to a 1-neck round-bottomed flask and dissolved in EtOH/H_2O (4:1, 206 µL). The solution was cooled to 0 °C and LiOH (99 µL, 50 µL, C = 0.50 M in H_2O, 4.0 eq.) was added dropwise. The reaction mixture was stirred at 0 °C for 1h then at rt for 12h, monitored by mass

spectrometry. The reaction mixture was quenched by dropwise addition of a 10% w/w $KHSO_4$ aq. sol. until pH = 3-4, then it was concentrated at rt under reduced pressure. The crude material was purified by reverse-phase high performance liquid chromatography chromatography (Sunfire C18, 19 x100 mm, 5 µm; H_2O-0.1% FA/ACN 0-80% 0-10 min → 80% 10-11 min → 80-0% 11-11.5 min → 0% 11.5-15 min; Flow: 24 mL/min (2.4 mL/min at column dilution)) to afford **5-52** (7.0 mg, 71% over two steps) as a white solid. *Rf* = 0.3 (94:06 CH_2Cl_2/MeOH). $[\alpha]^{25}_D$: -136.5 (*c* 4.0, MeOH). ^{1}H NMR (700 MHz, CD_3OD, mixture of rotamers) δ 7.99 (dd, *J* = 18.2, 7.5 Hz, 1H), 5.00 (dd, *J* = 8.3, 5.9 Hz, 1H), 4.58 – 4.54 (m, 0.1H), 4.48 (m, 0.1H), 4.43 – 4.36 (m, 2.7H), 4.22 (m, 3H), 4.06 (dt, *J* = 10.0, 6.7 Hz, 1H), 4.01 – 3.88 (m, 1H), 3.66 (dt, *J* = 9.9, 6.9 Hz, 1H), 3.48 (dt, *J* = 10.2, 7.6 Hz, 1H), 2.92 – 2.75 (m, 2H), 2.63 – 2.53 (m, 1H), 2.39 (m, 2H), 2.28 – 2.19 (m, 1H), 2.12 – 1.75 (m, 20H), 1.54 (m, 1H), 1.07 – 0.88 (m, 12H). ^{13}C NMR (176 MHz, CD_3OD, mixture of rotamers) δ 178.3, 178.2, 178.1, 177.1, 177.0, 176.6, 176.5, 174.9, 174.7, 174.0, 173.9, 173.9, 173.4, 173.4, 173.3, 173.3, 172.9, 172.8, 172.8, 172.7, 170.7, 170.2, 71.3, 71.2, 62.3, 62.3, 61.3, 60.1, 59.9, 59.9, 58.6, 58.5, 58.3, 54.1, 54.1, 54.0, 49.7, 49.6, 49.5, 47.8, 47.7, 47.6, 47.5, 47.4, 38.7, 38.6, 32.5, 32.2, 32.1, 32.1, 32.0, 32.0, 31.9, 31.7, 31.6, 31.3, 31.3, 31.2, 30.8, 30.8, 30.1, 29.6, 29.5, 28.5, 28.2, 28.2, 27.7, 27.4, 26.1, 26.1, 25.7, 25.6, 25.5, 25.3, 25.3, 25.2, 25.1, 25.1, 24.0, 23.4, 23.0, 22.4, 22.4, 19.9, 19.8, 19.8, 19.7, 19.7, 19.6, 19.5, 19.3, 18.9, 18.7, 18.5. HRMS (ESI) for $C_{37}H_{60}N_8O_{11}$ $(M+H)^+$: Calc.: 793.44543, Found: 793.44268. HPLC: 99%.

Chapitre 9. Annexes

9.1 Annexes de l'article 1

9.1.1 Supplemental figures

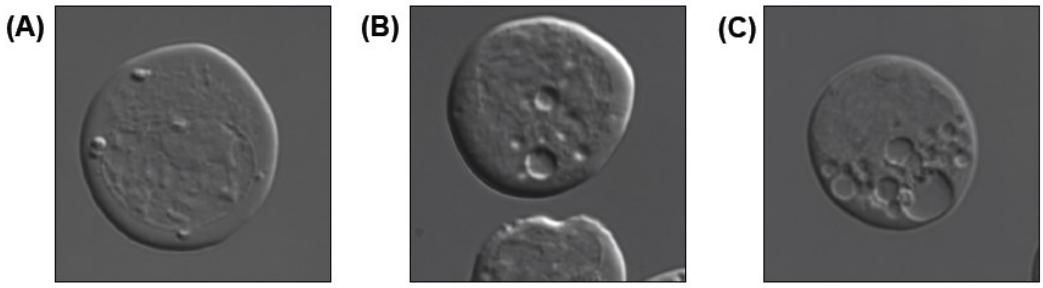

Figure 9.1 Supplemental Figure 1: Representative vacuolation images. (A) Vehicle-treated FL5.12 cells showing no vacuolation (score of 0). (B – C) FL5.12 cells that exemplify a vacuolation score of + (B) and maximal vacuolation score of +++ (C).

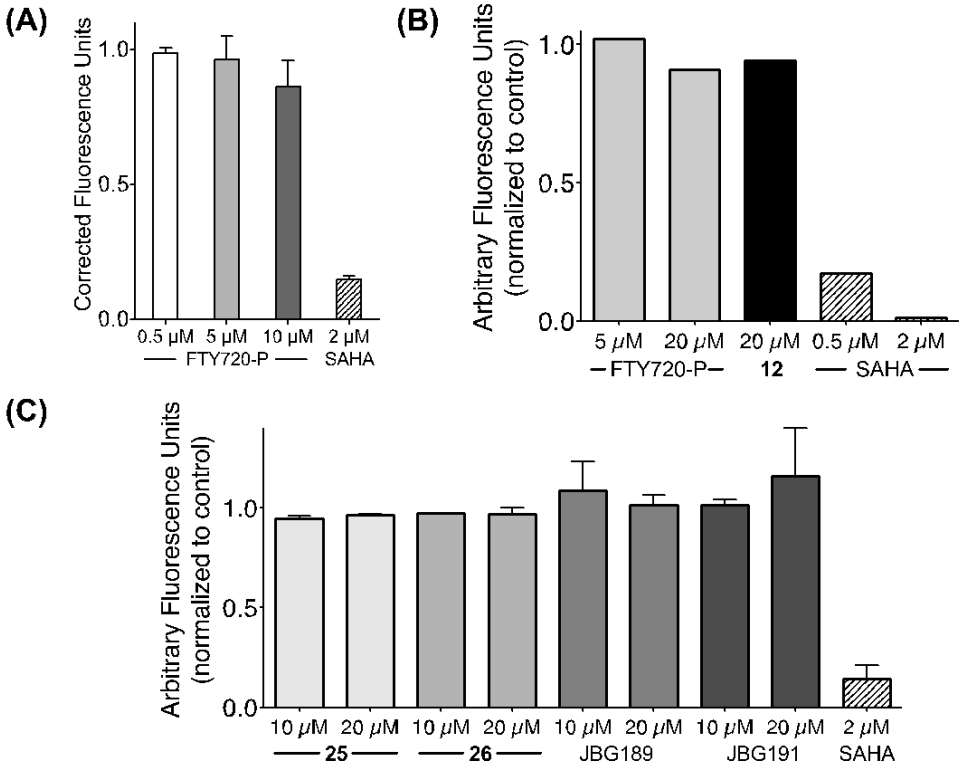

Figure 9.2 Supplemental Figure 2: FTY720-P and intended dual-action inhibitors do not reduced HDAC activity in vitro. The activity of recombinant HDAC1 (A, B) or HDACs present in HeLa extract (C) measured with Cayman HDAC Fluorometric Activity Assay Kit (A) or Enzo COLOR DE LYS HDAC Colorimetric activity assay kit (B, C). HDAC activity in the presence of FTY720-P, select compounds described in the text, or the known HDAC inhibitor SAHA is shown. The mean and the range of 2 biological replicates (2 technical replicates each) is shown in (A) and (C) and the mean of 2 technical replicates shown in (B).

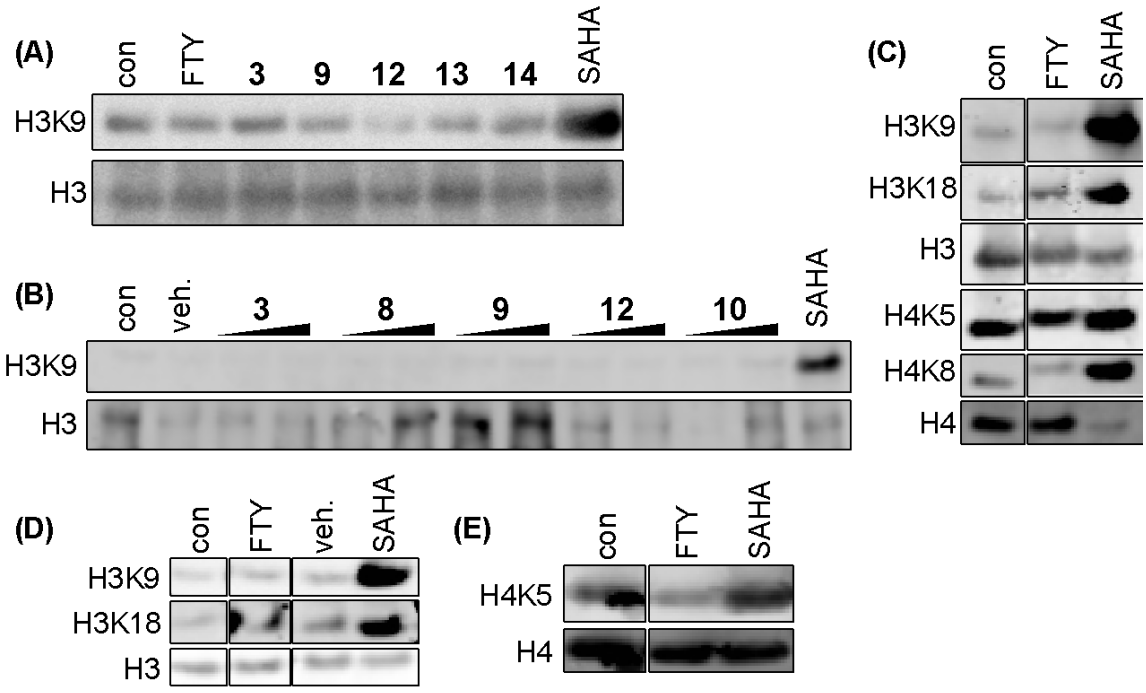

Figure 9.3 Supplemental Figure 3: FTY720 does not inhibit HDACs in cells. (A-B) FL5.12 (A) or WT MEF (B) cells treated with 10 µM FTY720, 10 (A) or 10 and 20 µM intended dual-action inhibitors, or 5 µM SAHA for 6 h. (C – E) WT MEFs treated with 5 µM (C), the IC50 concentration (6.1µM, D), or 10 µM (E) FTY720 or 2 µM SAHA for 24 (D) or 6 h (C, E). Whole-cell lysates are shown in (A – D) and acid-extracted histones in (E). In all images, treatments not relevant to the conclusions have been excluded where marked with a vertical black line.

9.1.2 X-rays

9.1.2.1 Data for **21c**

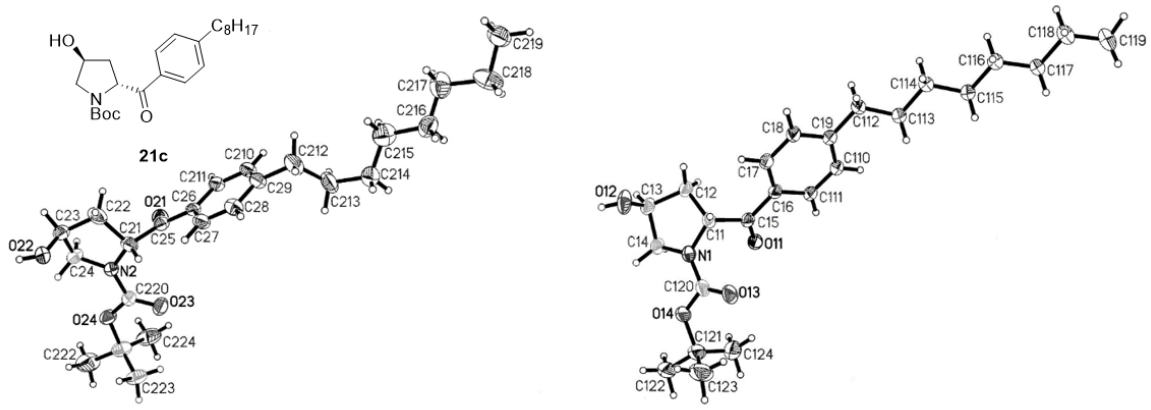

Tableau 9.1 Crystal data and structure refinement for **21c**.

Identification code	han532
Empirical formula	$C_{24}H_{37}NO_4$
Formula weight	403.54
Temperature/K	150
Crystal system	triclinic
Space group	P1
a/Å	6.9670(4)
b/Å	11.0868(6)
c/Å	15.7123(9)
α/°	85.490(3)
β/°	89.120(3)
γ/°	82.256(3)
Volume/Å^3	1198.84(12)
Z	2
ρ_{calc}g/cm^3	1.118
μ/mm^{-1}	0.383
F(000)	440.0
Crystal size/mm^3	0.36 × 0.15 × 0.03
Radiation	GaKα (λ = 1.34139)
2Θ range for data collection/°	4.908 to 122.296
Index ranges	-9 ≤ h ≤ 9, -14 ≤ k ≤ 14, -20 ≤ l ≤ 20
Reflections collected	67725

Independent reflections	10647 [R_{int} = 0.0595, R_{sigma} = 0.0381]
Data/restraints/parameters	10647/182/557
Goodness-of-fit on F^2	1.027
Final R indexes [I>=2σ (I)]	R_1 = 0.0549, wR_2 = 0.1451
Final R indexes [all data]	R_1 = 0.0682, wR_2 = 0.1564
Largest diff. peak/hole / e $Å^{-3}$	0.58/-0.26
Flack parameter	0.25(7)

9.1.2.2 Data for **24b1**

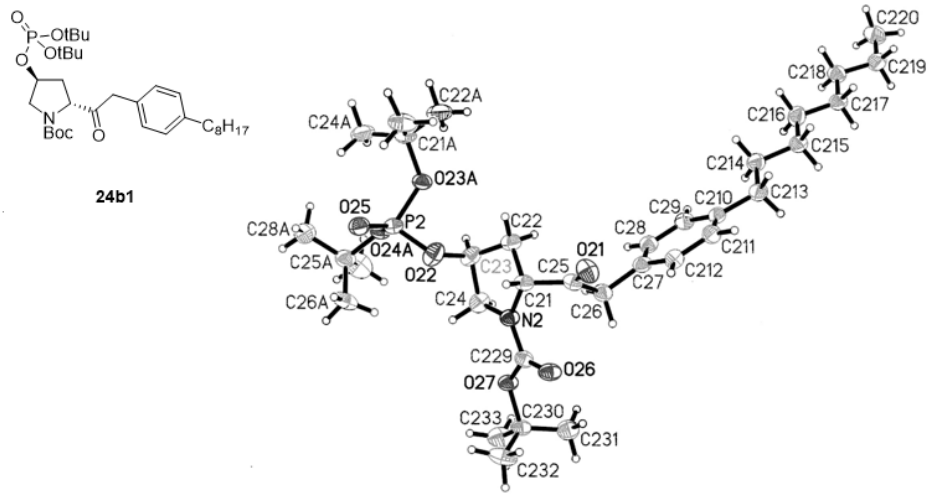

Tableau 9.2 Crystal data and structure refinement for **24b1**.

Identification code	han530
Empirical formula	$C_{33}H_{56}NO_7P$
Formula weight	609.75
Temperature/K	150
Crystal system	triclinic
Space group	P1
a/Å	6.0167(5)
b/Å	10.1227(8)
c/Å	30.232(2)
α/°	95.061(4)
β/°	92.640(4)
γ/°	103.259(4)
Volume/$Å^3$	1781.0(3)
Z	2
$\rho_{calc}g/cm^3$	1.137

μ/mm^{-1}	0.666
F(000)	664.0
Crystal size/mm^3	0.09 × 0.06 × 0.03
Radiation	GaKα (λ = 1.34139)
2Θ range for data collection/°	5.118 to 121.842
Index ranges	-7 ≤ h ≤ 7, -13 ≤ k ≤ 13, -39 ≤ l ≤ 39
Reflections collected	63607
Independent reflections	15722 [R_{int} = 0.0806, R_{sigma} = 0.0701]
Data/restraints/parameters	15722/24/815
Goodness-of-fit on F^2	1.042
Final R indexes [I>=2σ (I)]	R_1 = 0.0854, wR_2 = 0.2078
Final R indexes [all data]	R_1 = 0.1103, wR_2 = 0.2296
Largest diff. peak/hole / e $Å^{-3}$	0.42/-0.30
Flack parameter	0.05(5)

9.2 Annexes de l'article 2

9.2.1 Supplemental figures

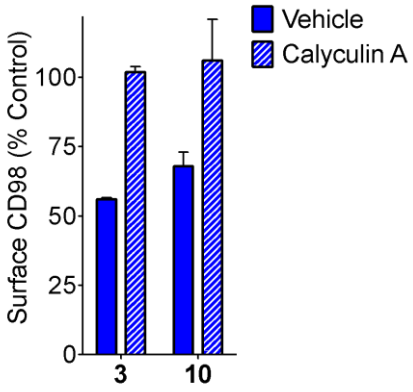

Figure 9.4 Supplementary Figure 1. Nutrient transporter loss at 2x IC_{50} of compound **10** ± pretreatment with 5 nM Calyculin A. Values for **3** are repeated from Figure 5B to allow for comparison. Data shown are means ± range.

9.2.2 X-ray data for 5f

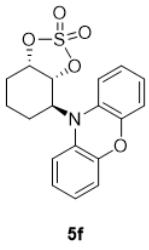

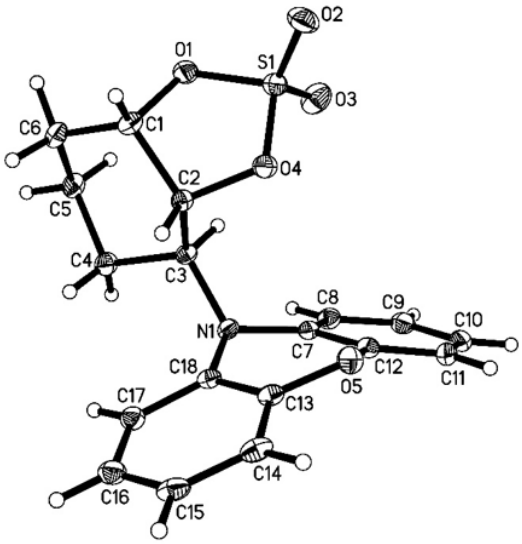

Tableau 9.3 Crystal data and structure refinement for **5f**.

Identification code	han535

Empirical formula	$C_{18}H_{17}NO_5S$
Formula weight	359.38
Temperature/K	150
Crystal system	orthorhombic
Space group	$P2_12_12_1$
a/Å	6.3229(2)
b/Å	11.5095(4)
c/Å	21.6812(8)
α/°	90
β/°	90
γ/°	90
Volume/Å^3	1577.81(9)
Z	4
ρ_{calc}g/cm^3	1.513
μ/mm^{-1}	1.362
F(000)	752.0
Crystal size/mm^3	0.22 × 0.08 × 0.08
Radiation	GaKα (λ = 1.34139)
2Θ range for data collection/°	7.094 to 121.236
Index ranges	-7 ≤ h ≤ 8, -14 ≤ k ≤ 14, -28 ≤ l ≤ 28
Reflections collected	29324
Independent reflections	3616 [R_{int} = 0.0371, R_{sigma} = 0.0185]
Data/restraints/parameters	3616/0/227
Goodness-of-fit on F^2	1.164
Final R indexes [I>=2σ (I)]	R_1 = 0.0351, wR_2 = 0.0900
Final R indexes [all data]	R_1 = 0.0353, wR_2 = 0.0904
Largest diff. peak/hole / e Å^{-3}	0.32/-0.40
Flack parameter	-0.014(3)

9.3 Annexes de l'article 3

9.3.1 Supplemental figures

9.3.1.1 Modeling

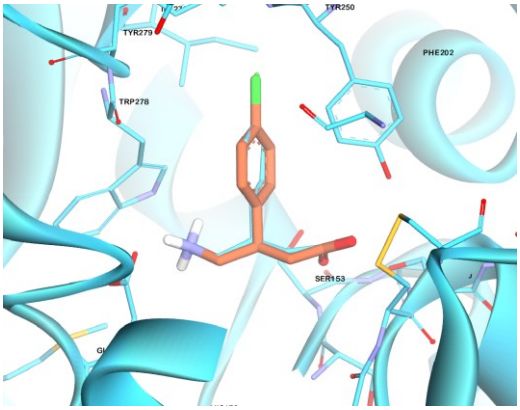

Figure 9.5 Supplemental Figure 1. Superposition of crystal structure of baclofen (blue) and docked pose obtained for baclofen (orange) in the active site of GABA(B) using Autodock4. [361]

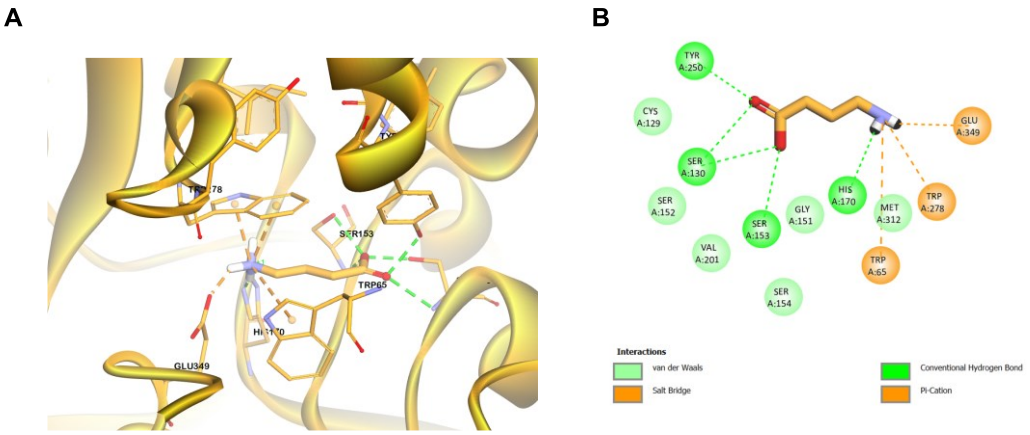

Figure 9.6 Supplemental Figure 2. A. X-ray visualization of GABA inside the GABA-B receptor. B. GABA interactions with proximal residues inside the active site of GABA-B.

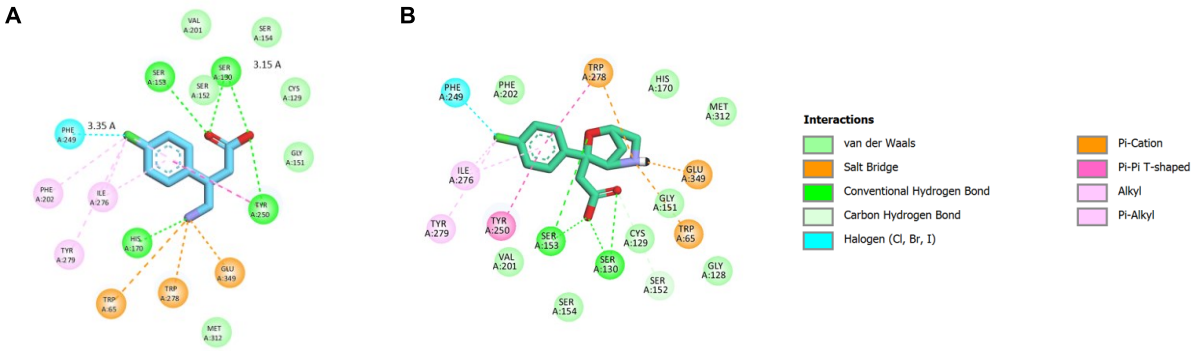

Figure 9.7 Supplemental Figure 3. A. (R)-baclofen interactions with proximal residues inside the active site of GABA-B. B. constrained baclofen analogue F interactions with proximal residues inside the active site of GABA-B.

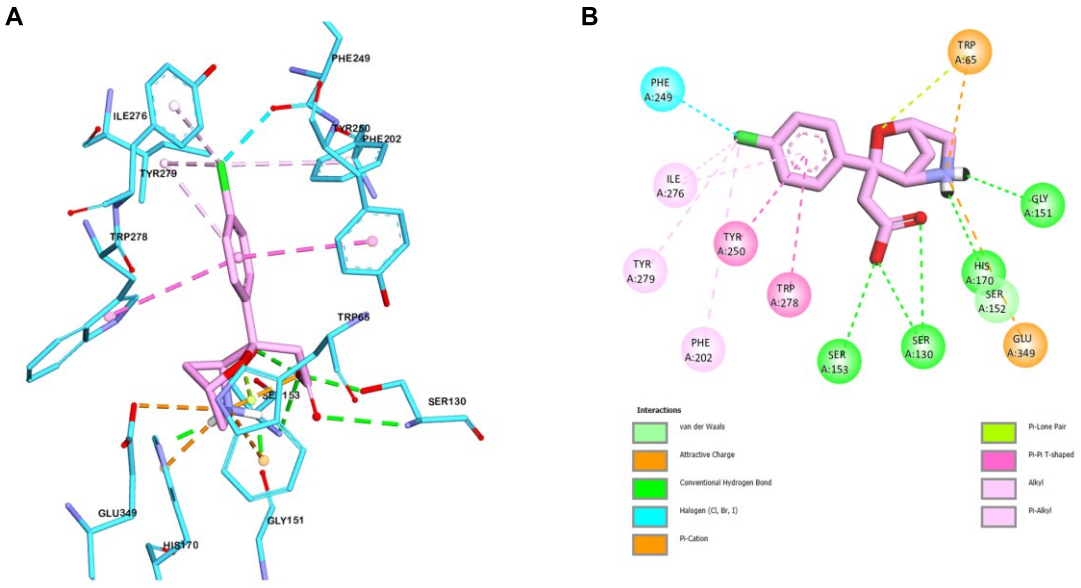

Figure 9.8 Supplemental Figure 4. A. Docking pose of constrained baclofen analogue G inside the GABA-B receptor. B. Interactions of G with proximal residues inside the active site of GABA-B.

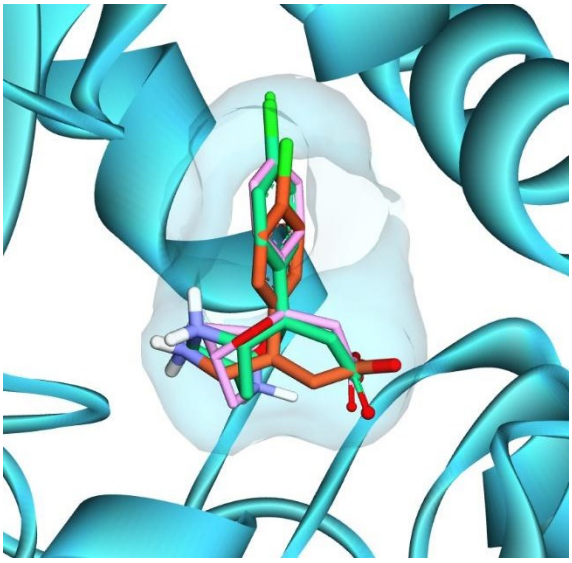

Figure 9.9 Supplemental Figure 5. Superposition of the docking pose for baclofen and the 2 constrained analogues inside the GABA-B receptor.

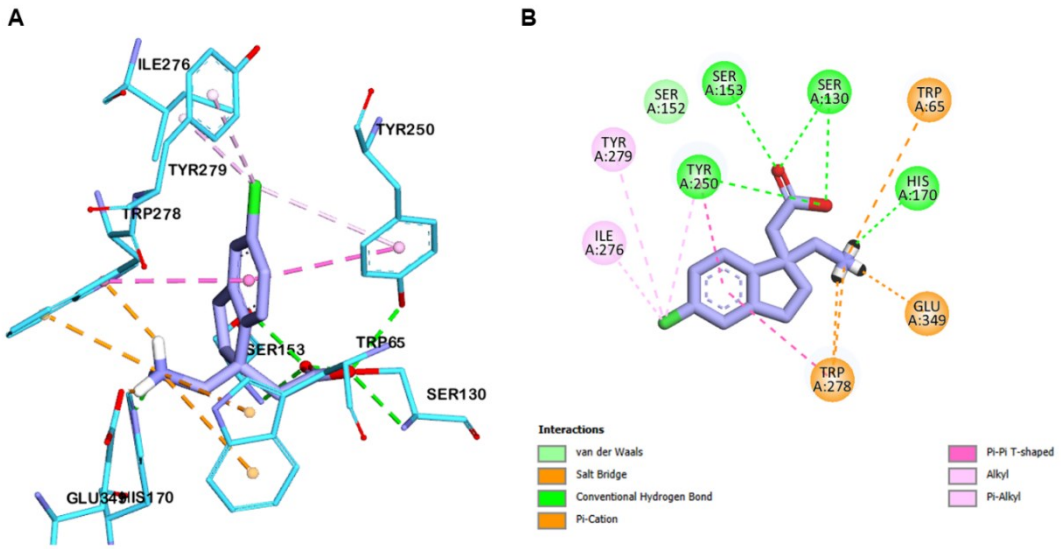

Figure 9.10 Supplemental Figure 6. A. Docking pose of the branched indane baclofen mimetic J inside the GABA-B receptor. B. Interactions of J with proximal residues inside the active site of GABA-B. [351]

9.3.1.2 LLAMA

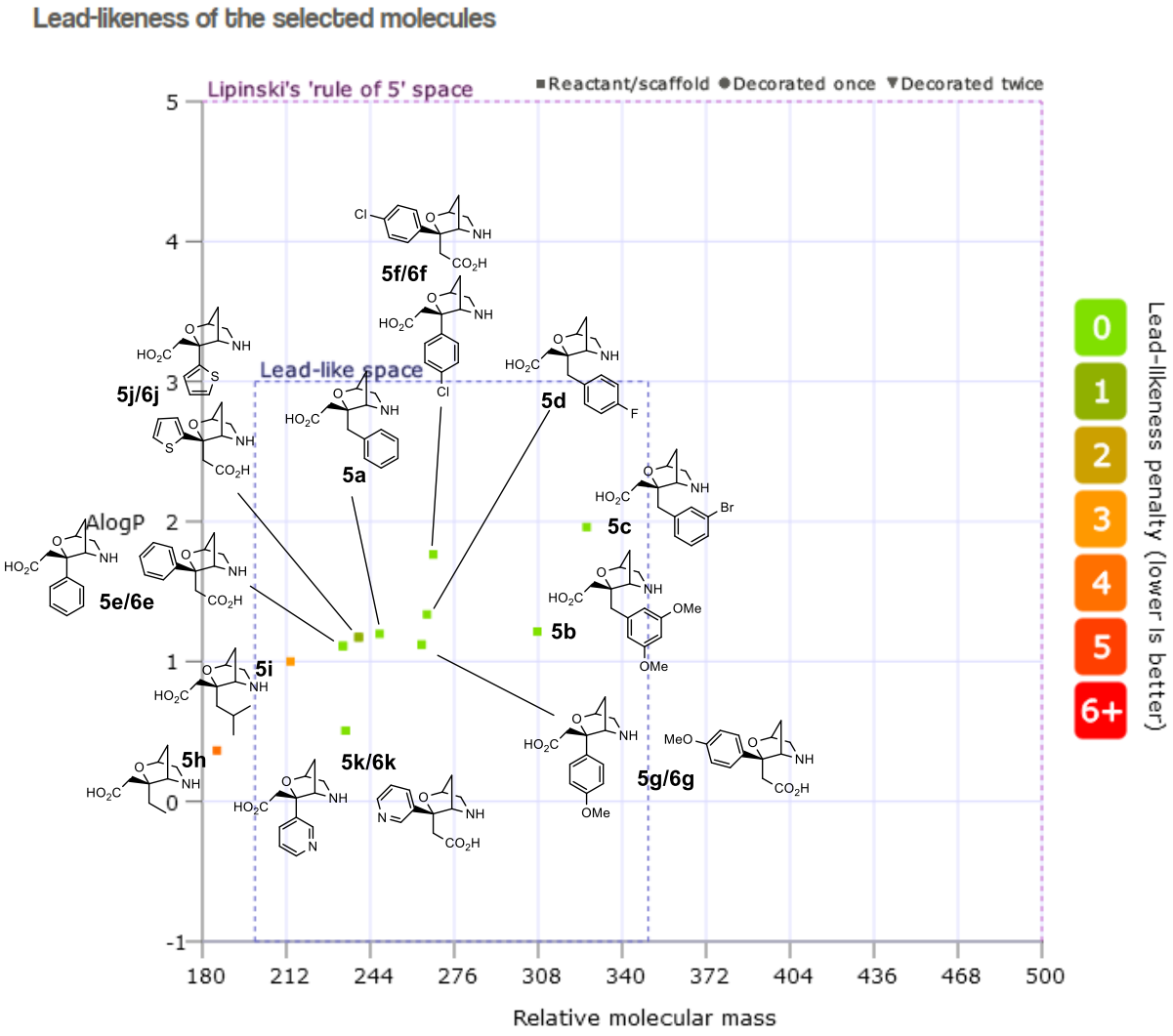

Figure 9.11 Supplemental Figure 7. Lead-likeness diagram of the ϒ-amino acid-morpholine analogues using the open-access database LLAMA.

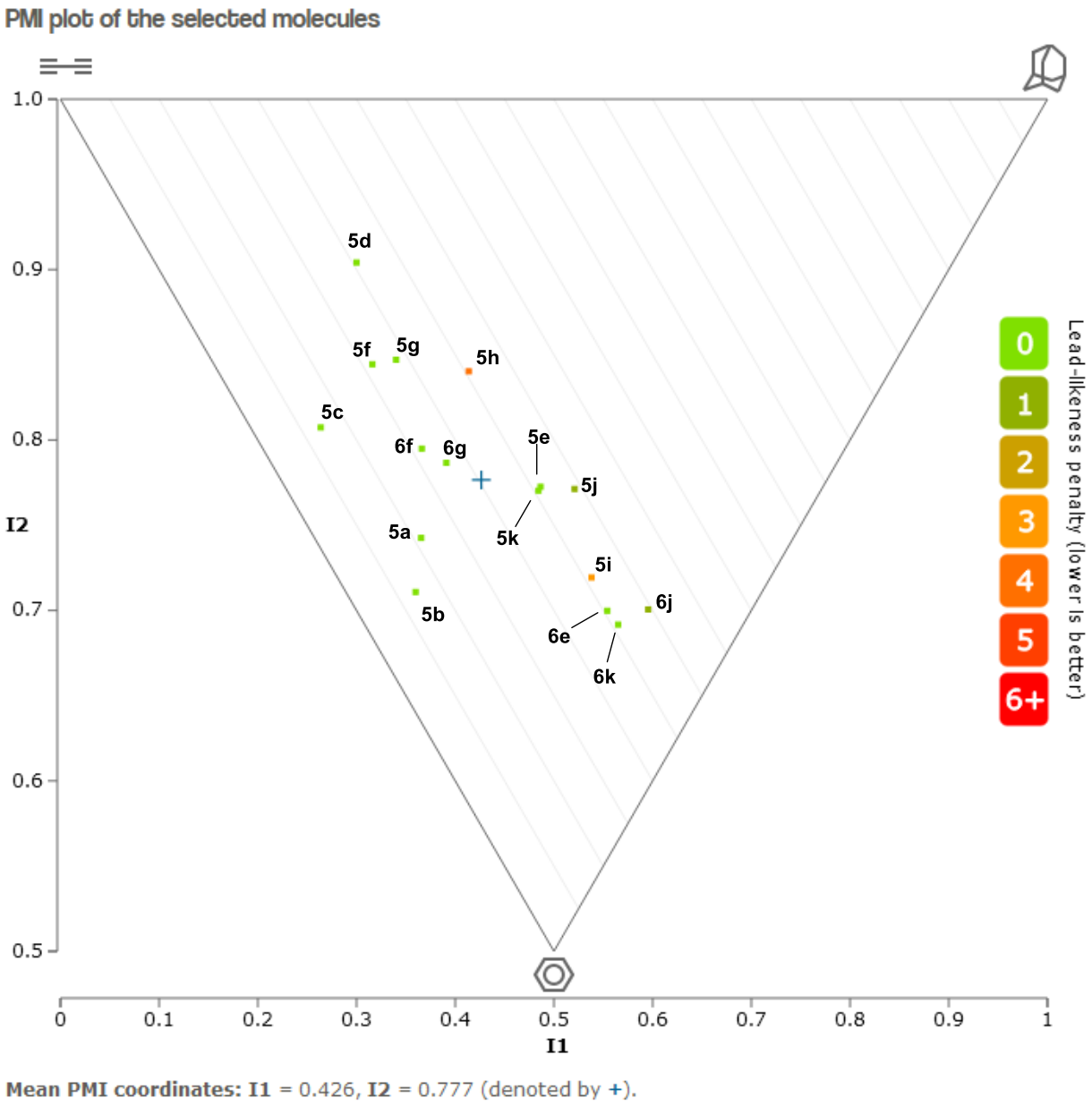

Figure 9.12 Supplemental Figure 8. Principal Moment of Inertia (PMI) plot of the ϒ-amino acid-morpholine analogues using the open-access database LLAMA.

9.3.2 X-rays

9.3.2.1 Data for **7f**

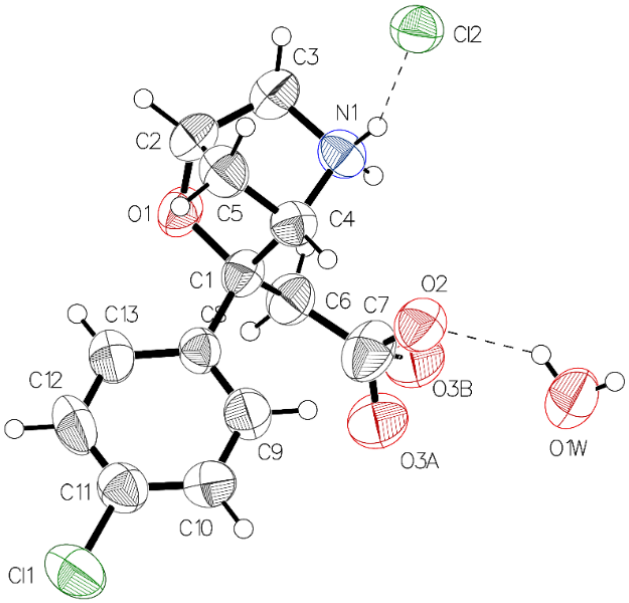

Tableau 9.4 Crystal data and structure refinement for **7f**.

Empirical formula	$C_{13}H_{16}Cl_2NO_4$
Formula weight	321.17
Temperature [K]	150
Crystal system	monoclinic
Space group (number)	$P2_1$ (4)
a [Å]	5.6473(6)
b [Å]	8.6449(10)
c [Å]	15.3759(16)
α [°]	90
β [°]	96.078(4)
γ [°]	90
Volume [Å^3]	746.44(14)
Z	2
ρ_{calc} [gcm^{-3}]	1.429
μ [mm^{-1}]	2.669
F(000)	334
Crystal size [mm^3]	0.045×0.048×0.065
Crystal colour	clear light colourless
Crystal shape	Fragment
Radiation	Ga K_α (λ=1.34139 Å)

2Θ range [°]	5.03 to 115.49 (0.79 Å)
Index ranges	-7 ≤ h ≤ 7 -10 ≤ k ≤ 10 -3 ≤ l ≤ 18
Reflections collected	2962
Independent reflections	2962 R_{int} = 0.0939 R_{sigma} = 0.0680
Completeness to θ = 53.594°	99.5 %
Data / Restraints / Parameters	2962 / 7 / 188
Goodness-of-fit on F^2	1.079
Final *R* indexes [$I \geq 2\sigma(I)$]	R_1 = 0.0654 wR_2 = 0.1781
Final *R* indexes [all data]	R_1 = 0.1030 wR_2 = 0.2060
Largest peak/hole [eÅ^{-3}]	0.42/−0.37
Flack X parameter	0.147(18)

9.3.2.2 Data for **7f'**

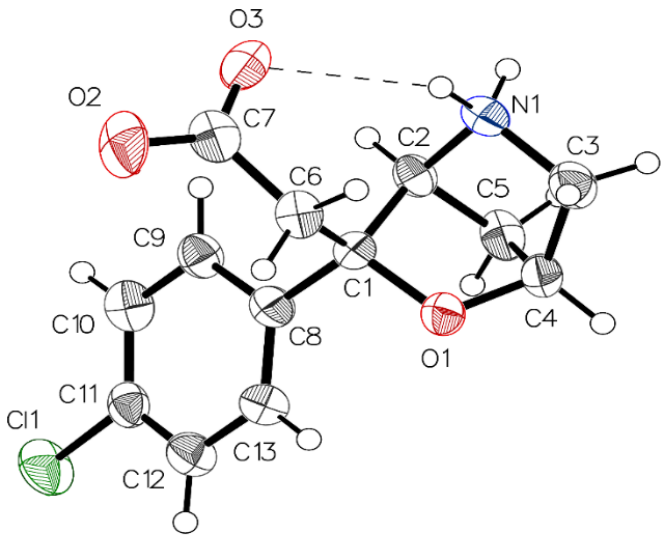

Tableau 9.5 Crystal data and structure refinement for **7f'**.

Empirical formula	$C_{13}H_{14}ClNO_3$
Formula weight	267.70
Temperature [K]	150

Crystal system	monoclinic
Space group (number)	$P2_1$ (4)
a [Å]	5.7671(6)
b [Å]	8.3185(8)
c [Å]	12.8468(13)
α [°]	90
β [°]	102.808(7)
γ [°]	90
Volume [Å^3]	600.97(11)
Z	2
ρ_{calc} [gcm^{-3}]	1.479
μ [mm^{-1}]	1.865
F(000)	280
Crystal size [mm^3]	0.04×0.06×0.1
Crystal colour	clear light colourless
Crystal shape	Fragment
Radiation	Ga K_α (λ=1.34139 Å)
2Θ range [°]	6.14 to 111.35 (0.81 Å)
Index ranges	-7 ≤ h ≤ 7 -10 ≤ k ≤ 9 -14 ≤ l ≤ 15
Reflections collected	4258
Independent reflections	2090 R_{int} = 0.0628 R_{sigma} = 0.1066
Completeness to θ = 53.594°	99.3 %
Data / Restraints / Parameters	2090 / 4 / 172
Goodness-of-fit on F^2	1.044
Final *R* indexes [I≥2σ(I)]	R_1 = 0.0634 wR_2 = 0.1226
Final *R* indexes [all data]	R_1 = 0.1086 wR_2 = 0.1408
Largest peak/hole [eÅ^{-3}]	0.26/−0.29
Flack X parameter	0.10(6)

9.4 Annexes de l'article 4

9.4.1 NMR experiments for stereoisomers determination

9.4.1.1 Structural studies

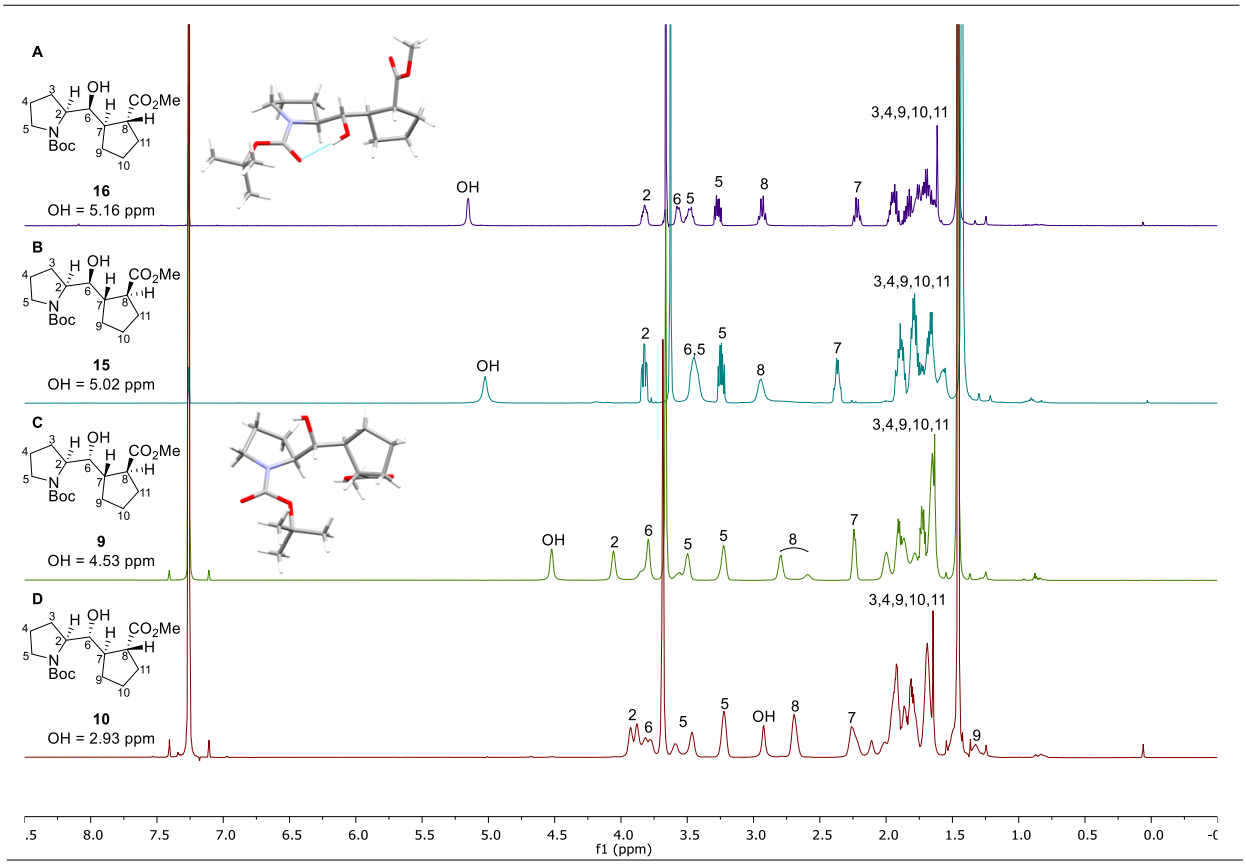

Figure 9.13 ^{1}H NMR in $CDCl_3$ at 25 °C (500 MHz).

Comments:

- δ(OH) **10** = 2,9 ppm (No H-bond)
- δ(OH) **9**, **15**, **16** = 4.5, 5.0, 5.1 ppm (H-bond)
- Rotamers observed
- δ(OH) minor rotamers = 1.5 – 2.0 ppm

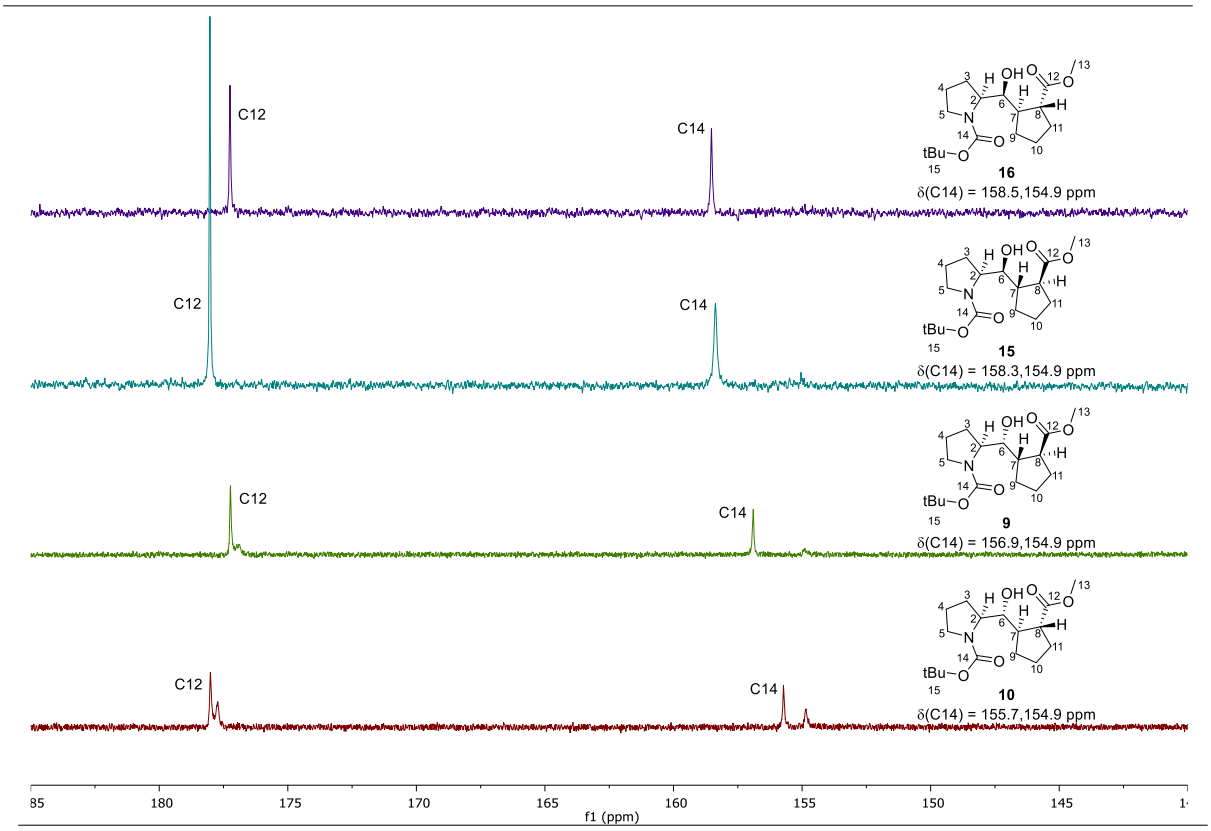

Figure 9.14 $^{13}C\{^{1}H\}$ NMR in $CDCl_3$ at 25 °C (500 MHz).

Comments:

- δ(C12) equivalent for all isomers
- δ(C14) are increasingly downfield in the series **10**<**9**<**15**<**16**
- δ(C14) following the trend observed for OH (p.2)
- δ(C14) minor rotamers = 154.9 ppm

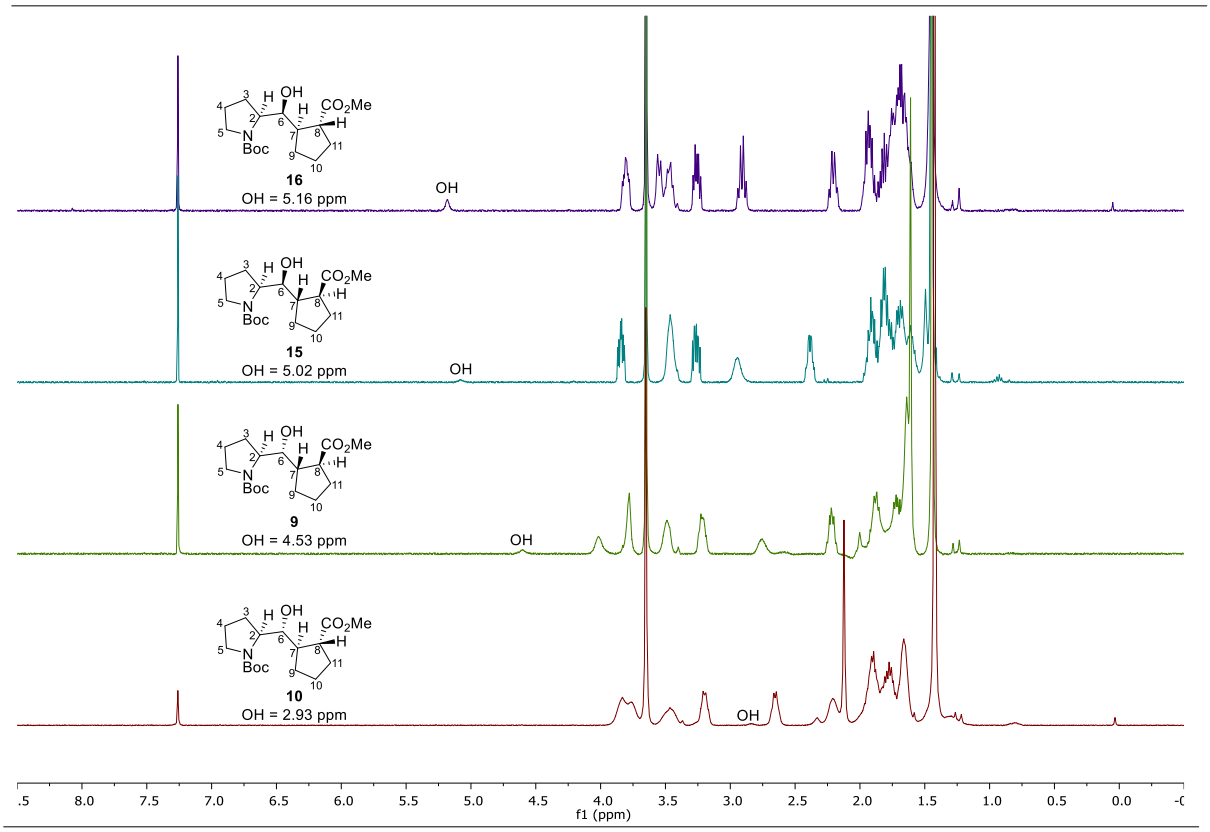

Figure 9.15 ^{1}H NMR in $CDCl_3$ at 25 °C (+5% D_2O, t = 5 min) (500 MHz).

Comments:

- OH fully exchange after 10 min
- Weak H-bond due to unstable 7-membered ring

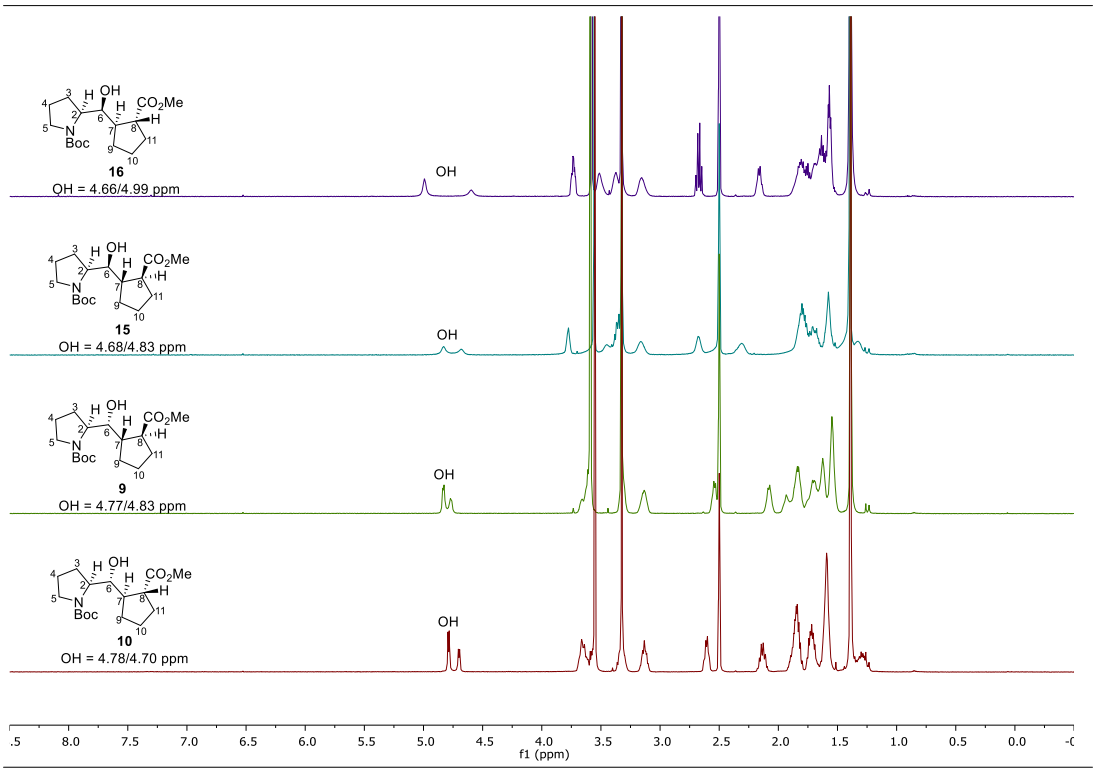

Figure 9.16 ^{1}H NMR in d6-DMSO at 25 °C (500 MHz).

A Values

	δ(DMSO)	*δ($CDCl_3$)*	*Δδ(OH)*	*A(NMR)*		
NBoc series						
*R1 (**10**)*	*4.79*	*2.92*	*1.87*	*0.25521*	*Major rotamer*	
*R2 (**10**)*	*4.71*	*2.11*	*2.6*	*0.3523*	*Minor rotamer*	
*R1 (**9**)*	*4.84*	*4.53*	*0.31*	***0.04773***	*Major rotamer*	
*R2 (**9**)*	*4.77*	*1.92*	*2.85*	*0.38555*	*Minor rotamer*	
15	*4.76*	*5.02*	*-0.26*	***-0.02808***		
16	*4.8*	*5.16*	*-0.36*	***-0.04138***		

Comments:

- A value is related to the difference in chemical shift between spectra recorded in $CDCl_3$/d6-DMSO [651]
- Presence of H-bond can be determined based on A
- H-bond observed for major rotamer **9**, **15** and **16**

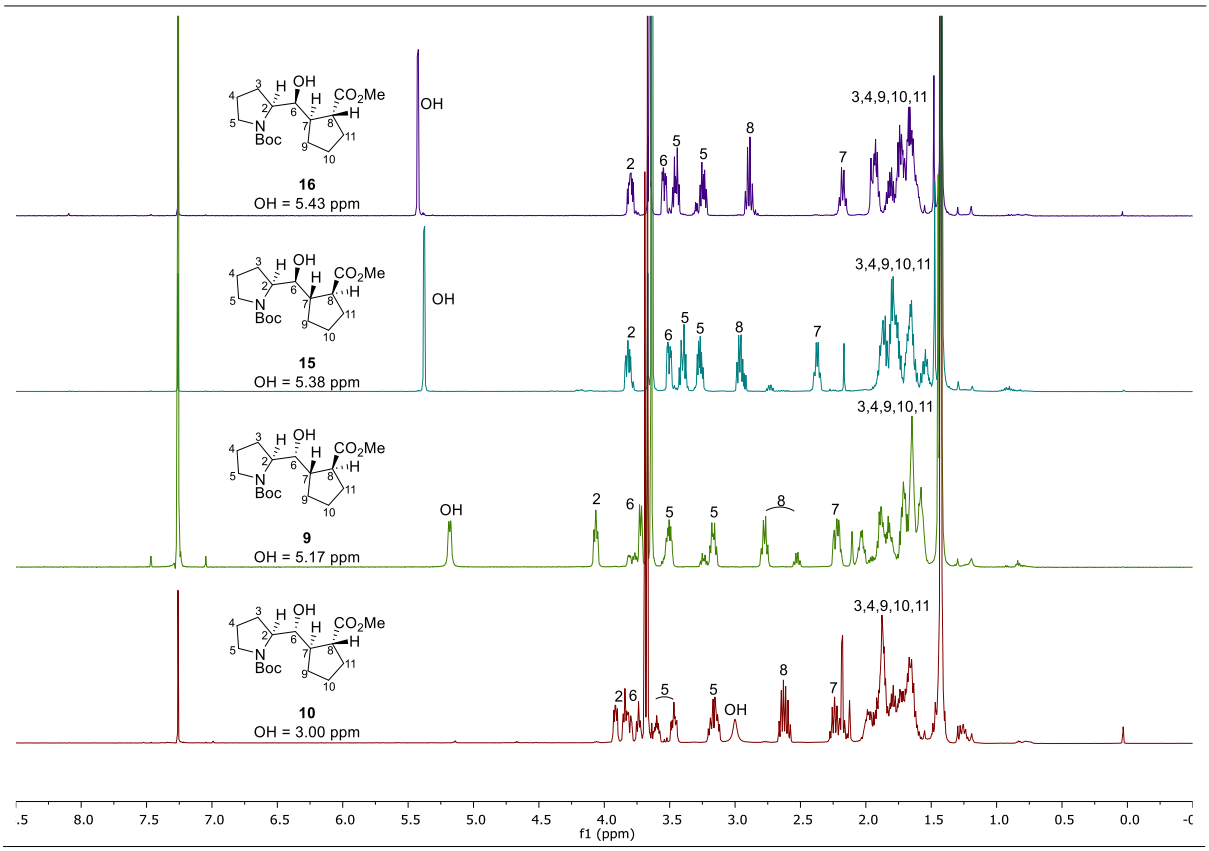

Figure 9.17 ^{1}H NMR in $CDCl_3$ at -50 °C (500 MHz).

Comments:

- At -50 °C:

δ(OH) **10** = 3,0 ppm (No H-bonding)

δ(OH) **9**/**15**/**16** = 5.2, 5.4, 5.4 ppm (H-bond)

- At 25 °C (cf. Figure 9.13):

δ(OH) **10** = 2,9 ppm (No H-bond)

δ(OH) **9**/**15**/**16** = 4.5, 5.0, 5.1 ppm (H-bond)

- δ(OH) **9**/**15**/**16** shift downfield with lower temp

=> H-bond is strengthened at low temp

- J-coupling of OH **9**/**15**/**16** can be observed at -50 °C (H-bond behavior)

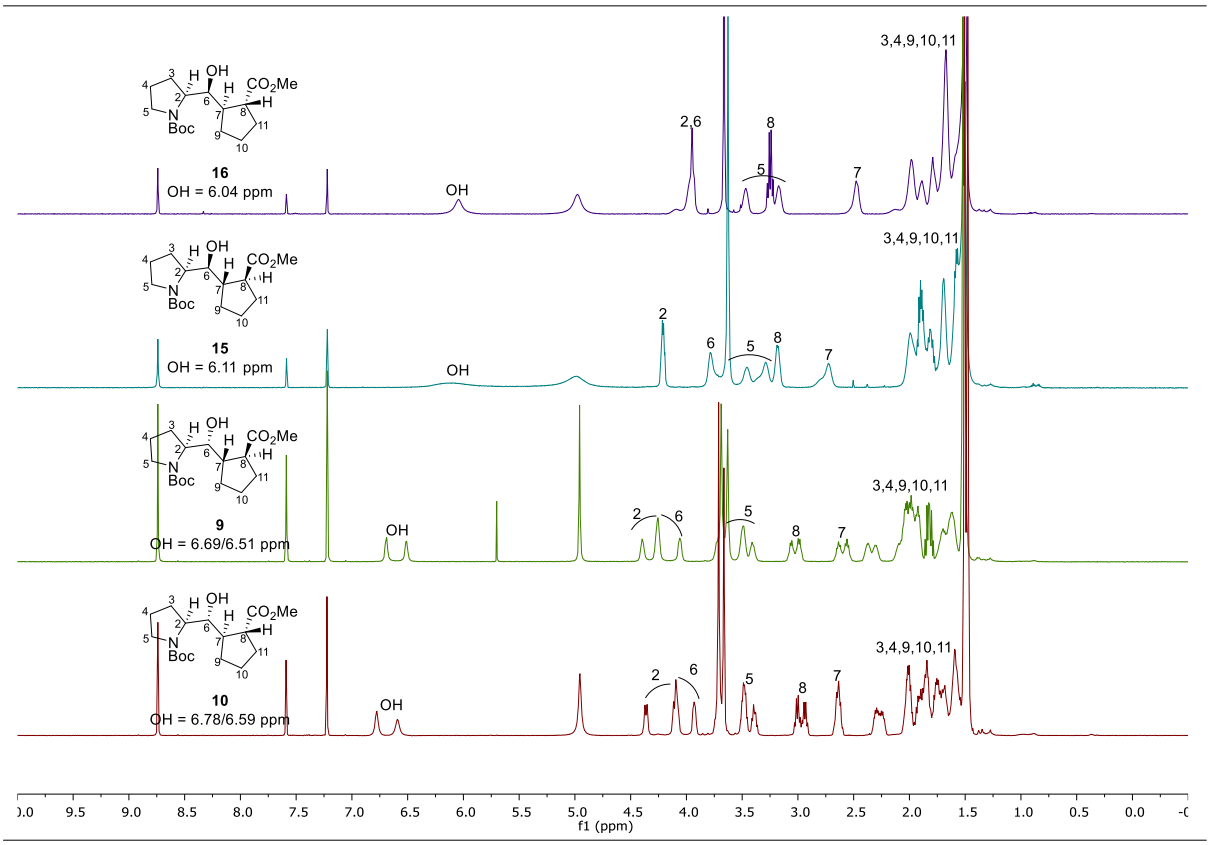

Figure 9.18 ^{1}H NMR in pyridine-d5 at 25 °C (500 MHz).

Comments:

- Loss of intramolecular H-bond
- δ(OH) are shifted downfield => H-bond with Pyr-d5
- δ(OH) 6.0 – 6.5 for all isomers

9.4.1.2 NOE experiments (500 MegaHertz)

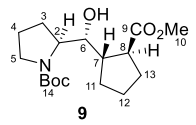

9

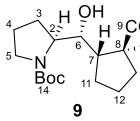

9

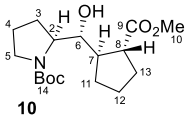
OH
H
H
$^{9}CO_2Me$
10
N
Boc
14
10

H_8
No Correlation with H_7
4.5
4.0
3.5
3.0
2.5
2.0
1.5
1.0
0.5
0.0
ppm

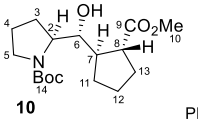
OH
H
H
$^{9}CO_2Me$
10
N
Boc
14
10

H_7
Phase cancelled correlation with H_8
4.5
4.0
3.5
3.0
2.5
2.0
1.5
1.0
0.5
0.0
ppm

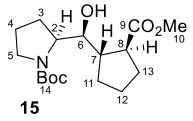
H
OH
H
9CO2Me
10
N
Boc
14
15

H8
Phase cancelled correlation with H7
8.0
7.5
7.0
6.5
6.0
5.5
5.0
4.5
4.0
3.5
3.0
2.5
2.0
1.5
1.0
0.5
0.0
ppm

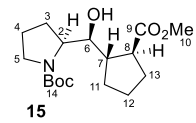
H
OH
H
9CO2Me
10
N
Boc
14
15

H7
Phase cancelled correlation with H8
8.0
7.5
7.0
6.5
6.0
5.5
5.0
4.5
4.0
3.5
3.0
2.5
2.0
1.5
1.0
0.5
0.0
ppm

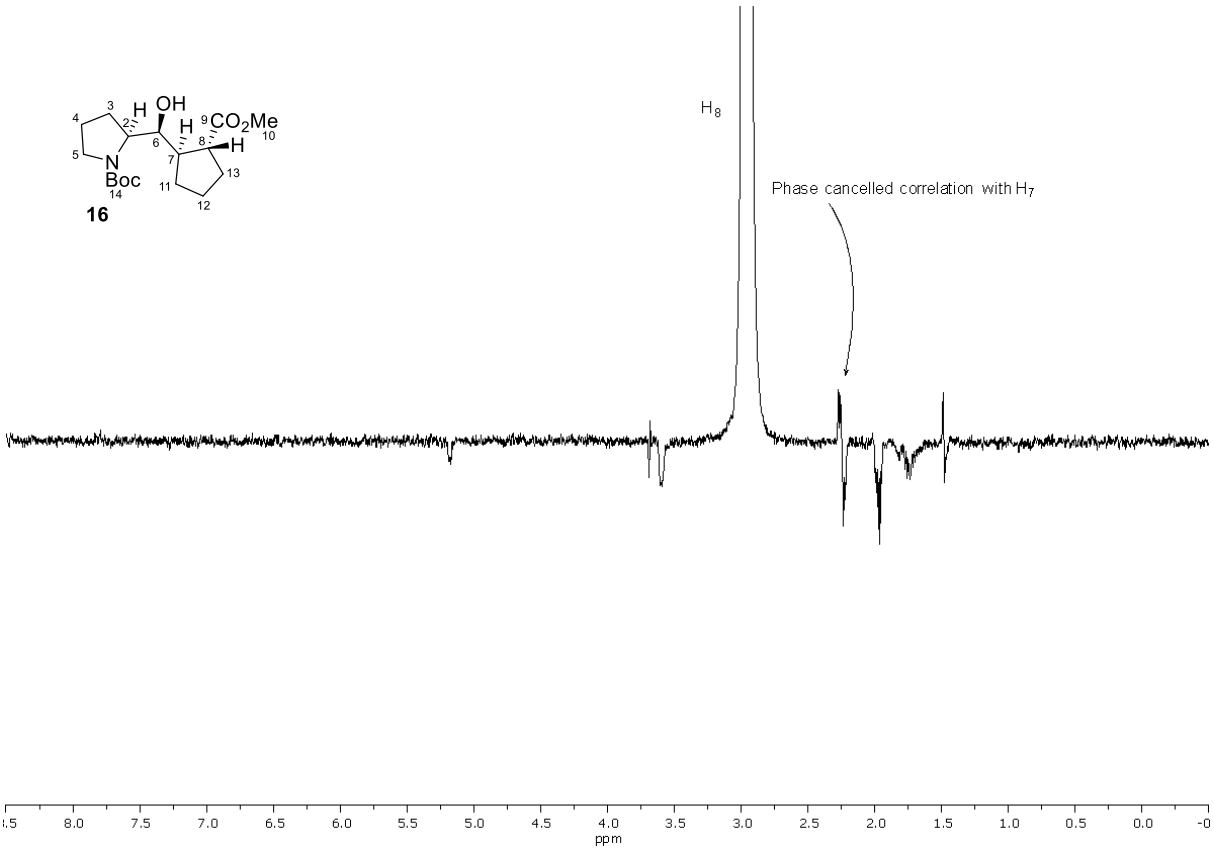
H8
Phase cancelled correlation with H7
ppm

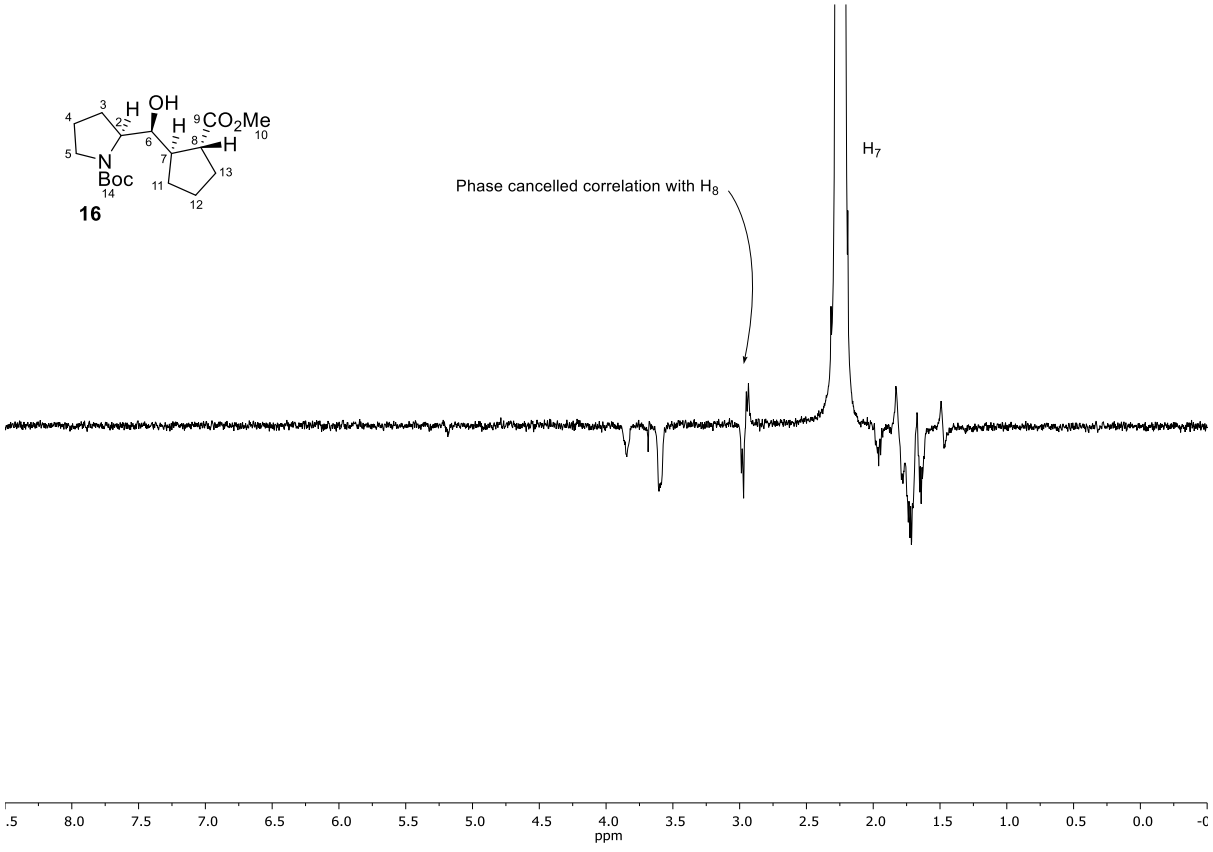
H7
Phase cancelled correlation with H8
ppm

16

9.4.2 X-rays

9.4.2.1 Data for **2a**

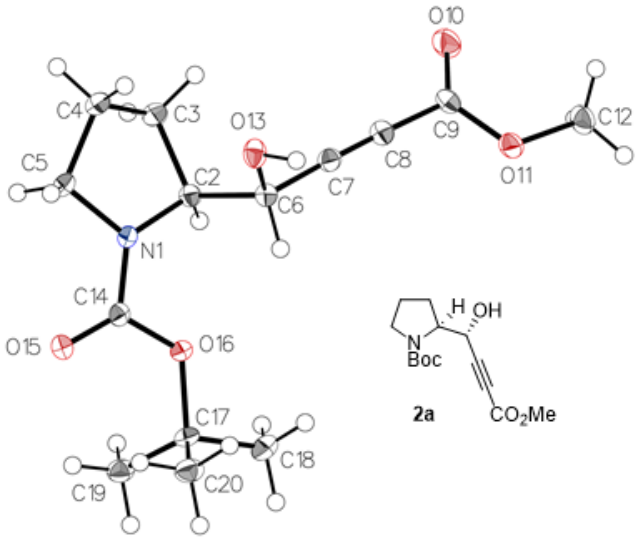

Tableau 9.6 Crystal data and structure refinement for **2a**.

Identification code	han549
Empirical formula	$C_{14}H_{21}NO_5$
Formula weight	283.32
Temperature/K	100
Crystal system	orthorhombic
Space group	$P2_12_12_1$
a/Å	6.7265(2)
b/Å	14.6897(5)
c/Å	15.0222(5)
α/°	90
β/°	90
γ/°	90
Volume/Å^3	1484.35(8)
Z	4
ρ_{calc}g/cm^3	1.268
μ/mm^{-1}	0.799
F(000)	608.0
Crystal size/mm^3	0.39 × 0.39 × 0.33
Radiation	CuKα (λ = 1.54178)
2Θ range for data collection/°	12.05 to 140.228

Index ranges	-8 ≤ h ≤ 8, -17 ≤ k ≤ 17, -18 ≤ l ≤ 18
Reflections collected	38883
Independent reflections	2774 [R_{int} = 0.0224, R_{sigma} = 0.0083]
Data/restraints/parameters	2774/0/189
Goodness-of-fit on F^2	1.090
Final R indexes [I>=2σ (I)]	R_1 = 0.0247, wR_2 = 0.0629
Final R indexes [all data]	R_1 = 0.0247, wR_2 = 0.0629
Largest diff. peak/hole / e $Å^{-3}$	0.20/-0.14
Flack parameter	0.03(2)

9.4.2.2 Data for **9**

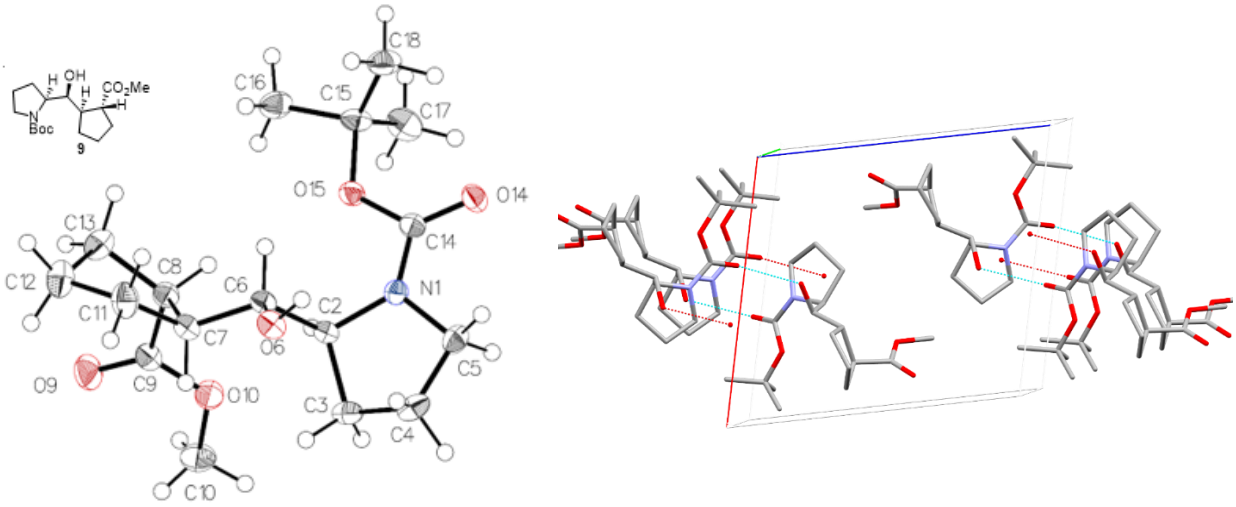

Tableau 9.7 Crystal data and structure refinement for **9**.

Identification code	han552
Empirical formula	$C_{17}H_{29}NO_5$
Formula weight	327.41
Temperature/K	100
Crystal system	monoclinic
Space group	$P2_1$
a/Å	10.8993(2)
b/Å	7.1434(2)
c/Å	11.7383(2)
α/°	90
β/°	102.9370(10)
γ/°	90

Volume/Å^3	890.72(3)
Z	2
ρ_{calc}g/cm^3	1.221
μ/mm^{-1}	0.728
F(000)	356.0
Crystal size/mm^3	0.38 × 0.08 × 0.08
Radiation	CuKα (λ = 1.54178)
2Θ range for data collection/°	7.728 to 140.122
Index ranges	-13 ≤ h ≤ 13, -8 ≤ k ≤ 7, -14 ≤ l ≤ 14
Reflections collected	17568
Independent reflections	3055 [R_{int} = 0.0266, R_{sigma} = 0.0191]
Data/restraints/parameters	3055/1/216
Goodness-of-fit on F^2	1.047
Final R indexes [I>=2σ (I)]	R_1 = 0.0373, wR_2 = 0.0998
Final R indexes [all data]	R_1 = 0.0377, wR_2 = 0.1009
Largest diff. peak/hole / e Å^{-3}	0.25/-0.22
Flack parameter	0.15(12)

9.4.2.3 Data for **16**

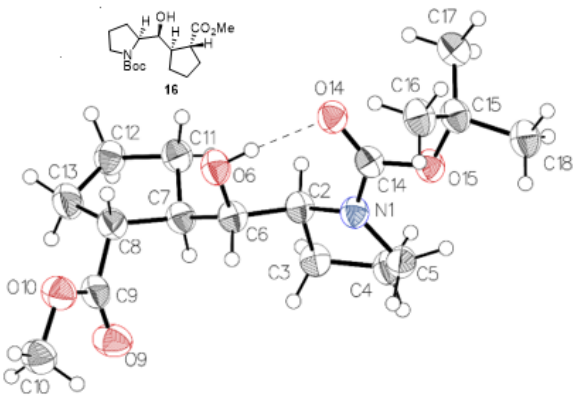

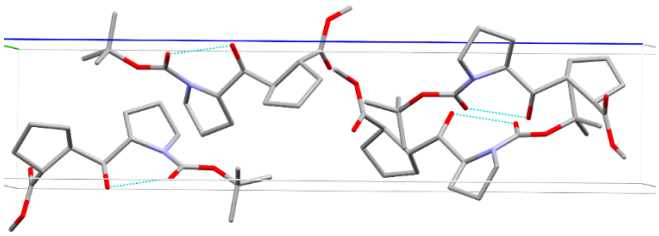

Tableau 9.8 Crystal data and structure refinement for **16**.

Identification code	han560
Empirical formula	$C_{17}H_{29}NO_5$
Formula weight	327.41
Temperature/K	100

Crystal system	orthorhombic
Space group	$P2_12_12_1$
a/Å	5.7711(2)
b/Å	11.2060(5)
c/Å	27.7817(10)
α/°	90
β/°	90
γ/°	90
Volume/Å^3	1796.67(12)
Z	4
ρ_{calc}g/cm^3	1.210
μ/mm^{-1}	0.721
F(000)	712.0
Crystal size/mm^3	0.14 × 0.12 × 0.1
Radiation	CuKα (λ = 1.54178)
2Θ range for data collection/°	6.362 to 144.37
Index ranges	-7 ≤ h ≤ 7, -13 ≤ k ≤ 13, -34 ≤ l ≤ 34
Reflections collected	24660
Independent reflections	3518 [R_{int} = 0.0558, R_{sigma} = 0.0322]
Data/restraints/parameters	3518/0/216
Goodness-of-fit on F^2	1.050
Final R indexes [I>=2σ (I)]	R_1 = 0.0401, wR_2 = 0.1070
Final R indexes [all data]	R_1 = 0.0456, wR_2 = 0.1125
Largest diff. peak/hole / e Å^{-3}	0.19/-0.14
Flack parameter	-0.17(15)

9.5 Annexes des composés peptidomimétiques inhibiteurs de PPEP-1

9.5.1 RMN ^{1}H supplémentaires

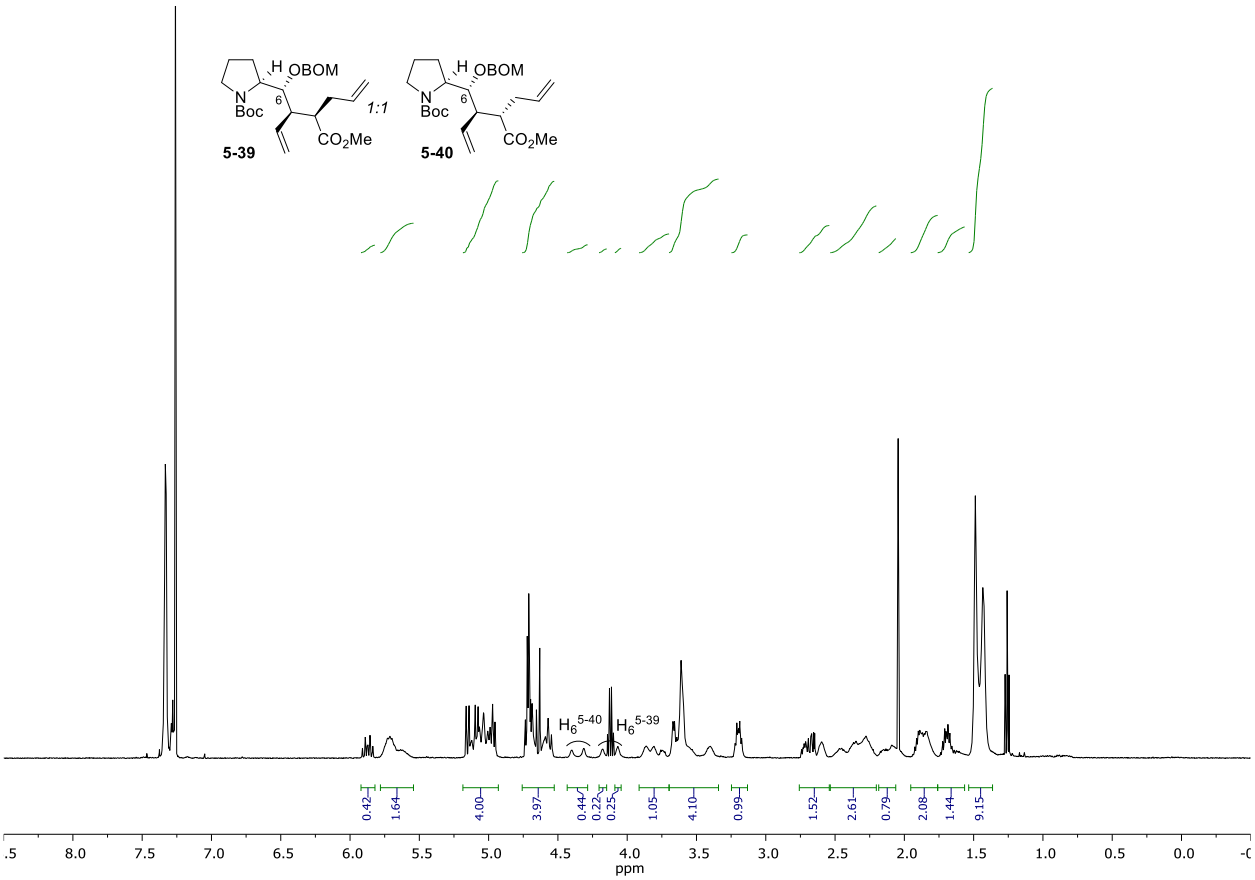

Figure 9.19 RMN ^{1}H de l'épimérisation de **5-39**

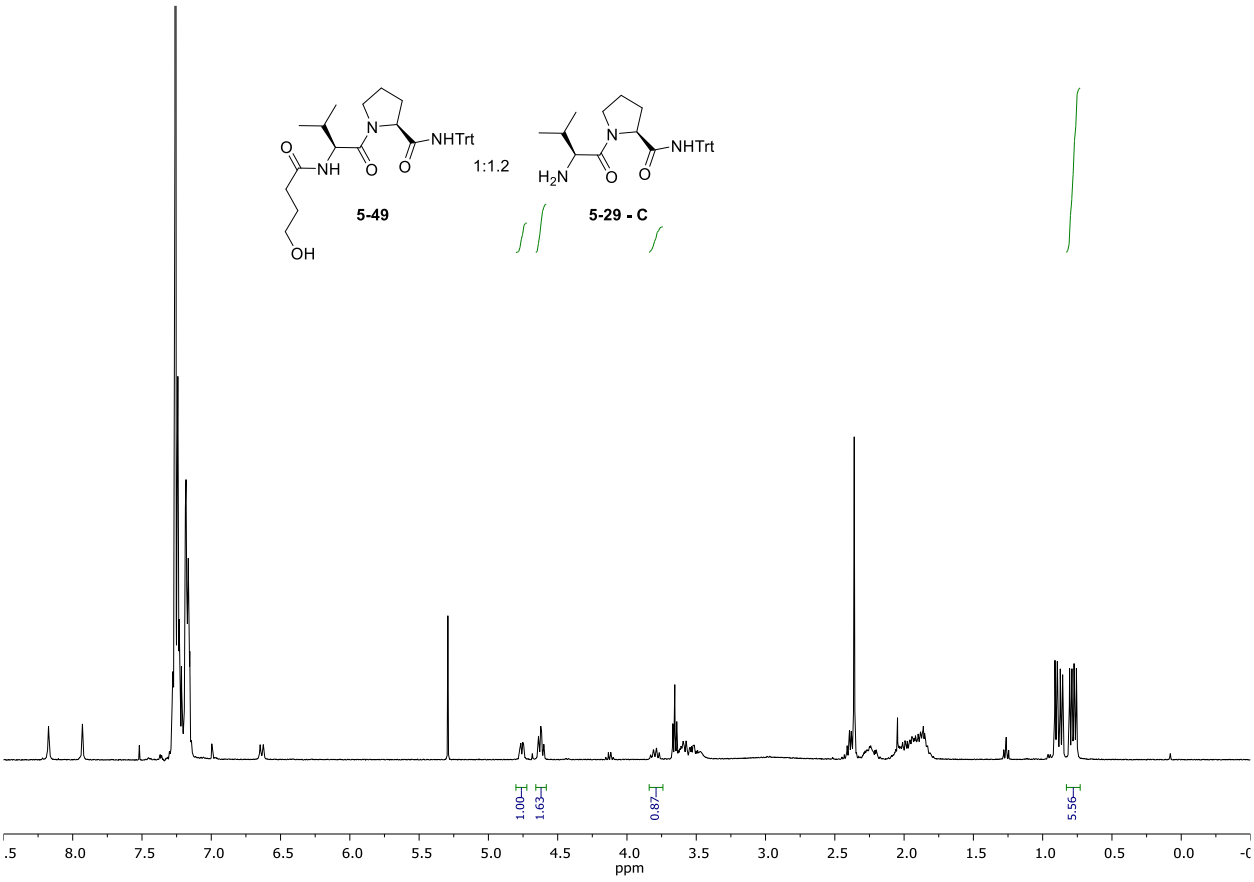

Figure 9.20 RMN ^{1}H de la réaction méthodologique d'ouverture de la γ-butyrolactone